

Mechanisms and Machine Science 6

Zhen Huang
Qinchuan Li
Huafeng Ding

Theory of Parallel Mechanisms

 Springer

Theory of Parallel Mechanisms

MECHANISMS AND MACHINE SCIENCE

Volume 6

Series Editor

MARCO CECCARELLI

For further volumes:
<http://www.springer.com/series/8779>

Zhen Huang • Qinchuan Li • Huafeng Ding

Theory of Parallel Mechanisms

 Springer

Zhen Huang
Robotics Research Center
Yanshan University
Qinhuangdao, Hebei, China

Qinchuan Li
Mechatronic Department
Zhejiang Sci-Tech University
Hangzhou, China

Huafeng Ding
Robotics Research Center
Yanshan University
Qinhuangdao, China

ISSN 2211-0984
ISBN 978-94-007-4200-0
DOI 10.1007/978-94-007-4201-7
Springer Dordrecht Heidelberg New York London

ISSN 2211-0992 (electronic)
ISBN 978-94-007-4201-7 (eBook)

Library of Congress Control Number: 2012942326

© Springer Science+Business Media Dordrecht 2013

This work is subject to copyright. All rights are reserved by the Publisher, whether the whole or part of the material is concerned, specifically the rights of translation, reprinting, reuse of illustrations, recitation, broadcasting, reproduction on microfilms or in any other physical way, and transmission or information storage and retrieval, electronic adaptation, computer software, or by similar or dissimilar methodology now known or hereafter developed. Exempted from this legal reservation are brief excerpts in connection with reviews or scholarly analysis or material supplied specifically for the purpose of being entered and executed on a computer system, for exclusive use by the purchaser of the work. Duplication of this publication or parts thereof is permitted only under the provisions of the Copyright Law of the Publisher's location, in its current version, and permission for use must always be obtained from Springer. Permissions for use may be obtained through RightsLink at the Copyright Clearance Center. Violations are liable to prosecution under the respective Copyright Law.

The use of general descriptive names, registered names, trademarks, service marks, etc. in this publication does not imply, even in the absence of a specific statement, that such names are exempt from the relevant protective laws and regulations and therefore free for general use.

While the advice and information in this book are believed to be true and accurate at the date of publication, neither the authors nor the editors nor the publisher can accept any legal responsibility for any errors or omissions that may be made. The publisher makes no warranty, express or implied, with respect to the material contained herein.

Printed on acid-free paper

Springer is part of Springer Science+Business Media (www.springer.com)

Preface

In the past decades, parallel mechanisms (PMs) have attracted a lot of attention from the academic and industrial communities. Compared with the more commonly used serial robots, the parallel one has attractive advantages in accuracy, rigidity, capacity, and load-to-weight ratio. The PMs have been and are being used in a wide variety of applications such as motion simulators, parallel manipulators, nano-manipulators, and micro-manipulators. In recent years, the research and application have evolved from general six-DOF PMs to lower-mobility PMs. The essential reason is that lower-mobility PMs have similar applications to general six-DOF PMs, while they are much simpler in structure and cheaper in cost. The research of lower-mobility PMs has become new hot point. A great deal of research on lower-mobility PM has been carried out all over the world, and a large number of new mechanisms, such as Delta, Tricept, and medical robots, have been built for various applications.

This book introduces our original research efforts on PMs for the 30 years. The contents include mechanism analyses and syntheses.

In mechanism analysis, the unified mobility methodology is first systematically presented. The search for a general and valid mobility methodology has been ongoing for about 150 years. Our methodology is proposed based on the screw theory, whose generality and validity have only been recently proven. This is a very important progress. The principle of the kinematic influence coefficient and its new development are described. This principle fits the kinematic analysis of various parallel manipulators including both 6-DOF and lower-mobility ones. The singularities are classified from a new point of view, and new progresses in singularity are introduced. The concept of the over-determinate input is researched, and in practice, there are many machines that work with over-determinate input, i.e., their input number is much bigger than their mobility number. To set the inputs to be accordance and optimum distribute and to obtain the expectant motion acceleration is introduced here. A new method of force analysis of PMs is presented. This method based on screw theory can remarkably reduce the number of unknowns and keep the number of simultaneous equilibrium equations not more than six on every occasion. In mechanism synthesis, the synthesis of spatial

symmetrical PMs is discussed. The synthesis method of difficult four- and five-DOF symmetrical mechanisms, which has first been put forward by our group in 2002, is emphatically introduced. The three-order screw system and its space distribution of kinematic screws for infinite possible motions of lower-mobility mechanisms are also analyzed. In the last chapter, a new theory for the topological structure analysis and synthesis of kinematic chains is represented. Based on the array representation of loops in topological graphs of kinematic chains, the basic loop operation algebra and a unique representation are introduced. Addressing the problem of isomorphism identification by finding a unique representation of graphs is presented. This process makes isomorphism identification very easy and remains efficient even when the kinematic chain links increase up to the thirties. The unique numerical atlas database is established and developed for use in the numerical synthesis of mechanisms.

Given that many of the abovementioned research are based on the screw theory, the basic screw theory is first introduced in the beginning of this book.

Using the screw theory to analyze some issues on spatial mechanisms is quite facile and convenient. This theory is also a good one for various mathematical instruments. A pair of spatial vectors or dual vectors can be used to construct a screw. The screw can then be applied to express the following: (1) position and orientation of a spatial straight line in geometry, (2) line and angular velocities of a rigid body in kinematics, (3) force and moment in statics, (4) constraint force and couple, and (5) rotational and translational mobilities in freedom analysis. The concept of a screw with six scalars is then easily used in kinematics and dynamic analysis. The screw can be facilely transformed into various mathematic forms, such as for vector, matrix, algebraic, and geometrical analyses. The screw has a clear geometrical concept, an explicit physical meaning, a simple expressing form, and convenient algebraic calculation. For these reasons, the screw concept is widely applied in mechanisms, especially recently, to resolve numerous difficult foreland issues. Students, engineers, and practically anyone who has studied linear algebra can easily understand the theory.

The authors gratefully acknowledge the continuous financial support of the National Natural Science Foundation of China for more than 20 years. This book can be a textbook for postgraduate students and general scientific technique personnel. Some more profound chapters can be suitable for doctoral students in the field of mechanical engineering.

Yanshan University
Qinhuangdao beachfront

Zhen Huang

Contents

1	Basics of Screw Theory	1
1.1	Introduction	1
1.2	Equation of a Line	2
1.3	Mutual Moment of Two Lines	5
1.4	Line Vectors and Screws	6
1.4.1	The Line Vector	6
1.4.2	The Screw	8
1.5	Screw Algebra	10
1.5.1	Screw Sum	10
1.5.2	Product of a Scalar and a Screw	11
1.5.3	Reciprocal Product	11
1.6	Instantaneous Kinematics of a Rigid Body	11
1.6.1	Instantaneous Rotation	12
1.6.2	Instantaneous Translation	13
1.6.3	Instantaneous Screw Motion	13
1.7	Statics of a Rigid Body	14
1.7.1	A Force Acting on a Body	14
1.7.2	A Couple Acting on a Body	15
1.7.3	A Twist Acting on a Body	15
	References	16
2	Dependency and Reciprocity of Screws	17
2.1	Concept of Screw Systems	17
2.2	Second-Order Screw System	19
2.2.1	Linear Combination of Two Screws	19
2.2.2	Special Two-Screw System	21
2.3	Third-Order Screw System	24
2.3.1	Principal Screws	25
2.3.2	Special Three-Screw Systems	26
2.4	Grassmann Line Geometry	28

2.5	Screw Dependency in Different Geometrical Spaces	30
2.5.1	Basic Concepts	30
2.5.2	Different Geometrical Spaces	31
2.6	Reciprocal Screws	36
2.6.1	Concept of a Reciprocal Screw	36
2.6.2	Dualism in the Physical Meaning of Reciprocal Screws	38
2.7	Reciprocal Screw System	39
2.8	Reciprocal Screw and Constrained Motion	41
2.8.1	Three Skew Lines in Space	42
2.8.2	Three Lines Parallel to a Plane Without a Common Normal	43
2.8.3	Three Non-concurrent Coplanar Lines	44
2.8.4	Three Coplanar and Concurrent Line Vectors	44
2.8.5	Three Line Vectors Concurrent in Space	44
2.8.6	Three Line Vectors Parallel in Space	45
	References	45
3	Mobility Analysis Part-1	47
3.1	The Concept and Definition of Mobility	47
3.2	Mobility Open Issue	49
3.2.1	Grübler-Kutzbach Criterion	49
3.2.2	Mobility Open Issue	52
3.3	Mobility Principle Based on Reciprocal Screw	53
3.3.1	Mechanism Can Be Expressed as a Screw System	53
3.3.2	Development of Our Unified Mobility Principle	54
3.3.3	The Modified G-K Formulas	55
3.4	Constraint Analysis Based on Reciprocal Screw	57
3.4.1	The Common Constraint	57
3.4.2	Parallel Constraint	58
3.4.3	Over-Constraint	59
3.4.4	The Generalized Kinematic Pair	59
3.5	Mobility Property Analyses	60
3.5.1	Translation and Rotation	60
3.5.2	Rotational Axis	62
3.5.3	Instantaneous Mobility and Full-Cycle Mobility	63
3.5.4	Full-Field Mobility	63
3.5.5	Parasitic Motion	65
3.5.6	Self-motion	65
	References	65
4	Mobility Analysis Part-2	71
4.1	Mobility Analysis of Simple Mechanisms	71
4.1.1	Open Chain Linkage	71
4.1.2	Roberval Mechanism	73

4.1.3	RUPUR Mechanism	76
4.1.4	Hervé Six-Bar Mechanism	77
4.1.5	Spatial 4P Mechanism	78
4.1.6	Delassus H-H-H-H Mechanism	79
4.1.7	Hervé 's CCC Mechanism	80
4.2	Mobility Analysis of Classical Mechanisms	81
4.2.1	Bennett Mechanism	81
4.2.2	Five-Bar Goldberg Linkage	84
4.2.3	Six-Bar Goldberg Linkage	86
4.2.4	Myard Linkage with Symmetrical Plane	87
4.2.5	Bricard with Symmetrical Plane	88
4.2.6	Altmann Abb.34 Mechanism	91
4.2.7	Altmann Six-Bar Linkage	94
4.2.8	Waldron Six-Bar Linkage	95
4.3	Mobility Analysis of Modern Parallel Mechanisms	97
4.3.1	4-DOF 4-URU Mechanism	97
4.3.2	3-CRR Mechanism	99
4.3.3	Zlatanov and Gosselin's Mechanism	100
4.3.4	Carricato's Mechanism	101
4.3.5	Delta Mechanism	103
4.3.6	H4 Manipulator	108
4.3.7	Yang's Mechanism	112
4.4	Mobility Analysis of Hoberman Switch-Pitch Ball	114
4.4.1	Structure Analysis	115
4.4.2	Three-Link Chain	117
4.4.3	Eight-Link Loop	118
4.4.4	Double Loop	119
4.4.5	Three-Loop Chain	121
4.4.6	The Whole Mechanism	122
4.5	Six-Hole Cubiform Mechanism	123
4.5.1	Double-Hole Linkage	124
4.5.2	Four-Hole Linkage	125
4.5.3	Five-Hole Linkage	130
4.5.4	The Whole Six-Hole Mechanism	132
	References	132
5	Kinematic Influence Coefficient and Kinematics Analysis	135
5.1	Concept of KIC	136
5.2	KIC and Kinematic Analysis of Serial Chains	138
5.2.1	Position Analysis	138
5.2.2	First-Order KIC	140
5.2.3	Second-Order KIC	142
5.3	Kinematic Analysis of Parallel Mechanism	144
5.3.1	First-Order KIC and Mechanism Velocity Analysis	146
5.3.2	Second-Order KIC and Mechanism Accelerations	150

5.4	Virtual Mechanism Principle of Lower-Mobility Parallel Mechanisms	155
5.4.1	Virtual Mechanism Principle	155
5.4.2	Kinematic Analysis Based on Virtual Mechanism Principle	157
	References	162
6	Full-Scale Feasible Instantaneous Screw Motion	163
6.1	Introduction	163
6.2	Determination of Principal Screws	165
6.2.1	The Representation of Pitch and Axes	165
6.2.2	Principal Screws of a Third-Order Screw System	167
6.3	Full-Scale Feasible Instantaneous Screws of the 3-RPS Mechanism	171
6.3.1	Virtual Mechanism and Jacobian Matrix	171
6.3.2	Upper Platform Is Parallel to the Base	173
6.3.3	The Upper Platform Rotates by an Angle α About Line a_2a_3	175
6.3.4	General Configuration of the 3-RPS Mechanism	177
6.4	Full-Scale Feasible Instantaneous Screw of a 3-UPU Mechanism	180
6.4.1	Mobility Analysis	181
6.4.2	First-Order Influence Matrices and Kinematic Analysis	184
6.4.3	Initial Configuration	185
6.4.4	The Second Configuration	186
6.5	Full-Scale Feasible Instantaneous Screw of a 3-RPS Pyramid Mechanism	189
6.5.1	First-Order Influence Coefficient Matrix	189
6.5.2	Principal Screws and Full-Scale Feasible Motions	191
6.6	A 3-DOF Rotational Parallel Manipulator Without Intersecting Axes	200
6.6.1	An Open Problem of the PMs with Intersecting Axes	201
6.6.2	A 3-D Revolute Mechanism Without Intersecting Axes	203
6.6.3	The Orientation Workspace	207
6.6.4	Examples	213
6.6.5	Discussions About the Differences Between the SPMs and the 3-RPS Cubic PM	214
	References	215
7	Special Configuration of Mechanisms	217
7.1	Introduction	217
7.2	Classification of the Special Configuration	219
7.2.1	Singular Kinematics Classification	220
7.2.2	Classification of the Singularity via a Linear Complex	223

7.3 Singular Kinematic Principle 224

7.4 Singularity Loci of 3/6-Stewart for Special Orientations 227

 7.4.1 Typical Singularity Structures of 3/6-SP 227

 7.4.2 Hyperbolic Singularity Equation Derived
 in an Oblique Plane 230

 7.4.3 Singularity Equation Derived in 3D Space 234

 7.4.4 Singularity Distribution in 3D Space 242

7.5 Structure and Property of The Singularity Loci of 3/6-Stewart
for General Orientations ($\phi \neq \pm 30^\circ, \pm 90^\circ, \pm 150^\circ$) 243

 7.5.1 Singularity Equation Based on Theorem 7.2 for General
 Orientations 243

 7.5.2 Singularity Analysis Using Singularity-Equivalent-
 Mechanism 245

 7.5.3 General Case 248

 7.5.4 Five Special Cases of the Singularity Equation 251

7.6 Structure and Property of the Singularity Loci
of the 6/6-Stewart 256

 7.6.1 Jacobian Matrix 258

 7.6.2 Singularity Analysis in 3D Space 258

 7.6.3 Singularity Analysis in Parallel Principal-Sections 259

7.7 Singularity of a 3-RPS Manipulator 270

 7.7.1 3-RPS Mechanism 270

 7.7.2 Singularity and Its Spatial Distribution 273

 7.7.3 Geometry and Constraint Analysis 278

Appendix A 284

References 285

8 Dynamic Problems of Parallel Mechanisms 289

 8.1 Over-Determine Inputs 289

 8.1.1 Influence Coefficient Matrices and Inertia Forces 290

 8.1.2 The Accordant Equation for Over-Determinate Inputs 292

 8.1.3 Optimization of Over-Determinate Input 294

 8.1.4 The Weight Distribution of the Input Torques 297

 8.2 Kinetostatic Analysis of 4-UPU Parallel Mechanisms 297

 8.2.1 Main-Pair Reaction Forces 300

 8.2.2 Numerical Example 308

 8.3 Kinetostatic Analysis of 4-R(CRR) Parallel Manipulator 309

 8.3.1 4-R(CRR) Parallel Manipulator 309

 8.3.2 Main-Pair Reaction 312

 8.3.3 Active Moments and Reactions of Other
 Pairs in Limbs 318

 8.3.4 Numerical Example 321

 8.3.5 Discussion 322

References 323

9	Constraint Screw-Based Method for Type Synthesis	325
9.1	Description of Constraints Acting on a Rigid Body	326
9.2	Limb Twist and Limb Constraint Systems	328
9.2.1	Limb Twist System	328
9.2.2	Limb Constraint System	329
9.3	Platform Twist and Platform Constraint Systems	329
9.3.1	Platform Twist System	329
9.3.2	Platform Constraint System and Classification of Lower-Mobility PMs	330
9.4	Constraint-Screw Based Synthesis Method	331
9.4.1	Procedure of the Constraint-Screw Based Synthesis Method	331
9.4.2	Generation of Different Architectures of PM	334
9.4.3	Discrimination for Instantaneous PMs	334
9.5	Examples	334
9.5.1	Type Synthesis of a 3R2T 5-DOF PM	335
9.5.2	Type Synthesis of 2R3T 5-DOF PMs	337
9.5.3	Type Synthesis of 1R3T 4-DOF PMs	340
9.5.4	Type Synthesis of 3R1T 4-DOF PMs	341
9.5.5	Type Synthesis of 2R2T 4-DOF PMs	344
9.5.6	Type Synthesis of a 2R1T 3-DOF PM	350
9.5.7	Type Synthesis of a 3T 3-DOF PM	352
9.5.8	Type Synthesis of a 3R 3-DOF PM	357
9.5.9	Type Synthesis of a 1R2T 3-DOF PM	361
9.6	Type Synthesis of Non-symmetrical PMs	361
	References	363
10	Digital Topology Theory of Kinematic Chains and Atlas Database	365
10.1	Topology Modeling of Mechanisms	365
10.1.1	Modeling of Simple Joint Kinematic Chains	365
10.1.2	Modeling of Multiple Joint Kinematic Chains	368
10.1.3	Modeling of Geared (cam) Kinematic Chains	371
10.2	Loop Operation Algebra of Kinematic Chains	376
10.2.1	Loop and Its Representation	376
10.2.2	“ \ominus ” Operation of Loops	378
10.2.3	“ \otimes ” Operation of Loops	379
10.2.4	“ \oplus ” Operation of Loops	380
10.2.5	Loop Analysis	385
10.2.6	Edge-Based Operations of Loops	388
10.3	Isomorphism Identification	390
10.3.1	Perimeter Topological Graph	390
10.3.2	Canonical Perimeter Topological Graph	392
10.3.3	Characteristic Perimeter Topological Graph	395

10.3.4	Examples of Isomorphism Identification	397
10.3.5	Analysis of Computational Complexity	406
10.4	Detection of Rigid Sub-chains	407
10.5	Digital Atlas Database and Synthesis	408
	References	416
Index	419

Chapter 1

Basics of Screw Theory

1.1 Introduction

Screw theory is a powerful mathematical tool for the analysis of spatial mechanisms. A screw consists of two three-dimensional vectors. A screw can be used to denote the position and orientation of a spatial vector, the linear velocity and angular velocity of a rigid body, or a force and a couple, respectively. Therefore, the concept of a screw is convenient in kinematics and dynamics, while the transformation between the screw-based method and vector and matrix methods is straightforward. When applied in mechanism analysis, screw theory has the advantages of clear geometrical concepts, explicit physical meaning, simple expression and convenient algebraic calculation. It is worth noting that the preliminary requirements for screw theory are only linear algebra and basic dynamics in undergraduate level. Thus, screw theory has been widely applied and researchers have used screw theory to make great contribution to many frontier problems in mechanism theory.

Screw theory was established in the nineteenth century. First, Chasles (1830) proposed the concept of twist motion of a rigid body, which was further developed by Poincot (1848). Then Plücker gave his research and proposed his screw expression [1]. Then, in his classic book *Screw theory* (1875), Ball discussed the kinematics and dynamics of a rigid body under complex constraints using screw theory [2]. In the last 60 years, many researchers, such as Dimentberg [3], Yang and Freudenstein [4], Waldron [5], Roth [6], Hunt [7], Phillips [8], Duffy [9] and Angeles [10] etc, have made important contributions to screw theory.

This chapter first addresses the expression of a straight line and its Plücker line coordinates in three-dimensional space. The line vector and screw as well as their characteristics and the screw algebra are introduced. In the last part, this chapter

also introduces the expression for the instantaneous motion of a rigid body and the statics of the body using screw theory.¹

1.2 Equation of a Line

Two distinct points $A(x_1, y_1, z_1)$ and $B(x_2, y_2, z_2)$ determine a line, as shown in Fig. 1.1. The vector \mathbf{S} denoting the direction of the line can be expressed as

$$\mathbf{S} = (x_2 - x_1)\mathbf{i} + (y_2 - y_1)\mathbf{j} + (z_2 - z_1)\mathbf{k}, \quad (1.1)$$

where \mathbf{i} , \mathbf{j} , and \mathbf{k} are unit vectors corresponding to each coordinate axis.

If we let

$$\begin{aligned} x_2 - x_1 &= L \\ y_2 - y_1 &= M \\ z_2 - z_1 &= N, \end{aligned} \quad (1.2)$$

then substituting Eq. (1.2) into Eq. (1.1), we have

$$\mathbf{S} = L\mathbf{i} + M\mathbf{j} + N\mathbf{k}, \quad (1.3)$$

where L , M , and N are direction ratios.

The distance between the two points is given by

$$|\mathbf{S}| = \sqrt{L^2 + M^2 + N^2}. \quad (1.4)$$

Let

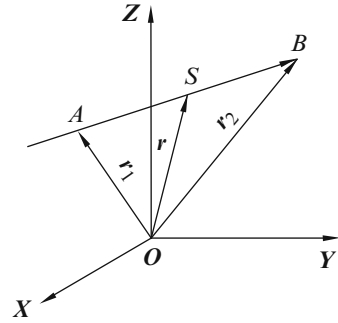
$$\begin{aligned} l &= L/|\mathbf{S}| \\ m &= M/|\mathbf{S}| \\ n &= N/|\mathbf{S}|, \end{aligned} \quad (1.5)$$

where l , m and n are direction cosines of the line. Then Eq. (1.4) reduces to

$$l^2 + m^2 + n^2 = 1. \quad (1.6)$$

¹ The content of screw theory in this book is based on the teaching material presented by Dr. Duffy at Florida University in 1982. At that time, the first author of this book listened attentively to the lectures and was deeply inspired by the course content. The author wishes to express here once again his acknowledgments to Dr. Duffy.

Fig. 1.1 Plücker Coordinates of a line



Note that a line can be determined by its direction and a point on it. We can write the vector equation of the line as

$$(\mathbf{r} - \mathbf{r}_1) \times \mathbf{S} = \mathbf{0}. \quad (1.7)$$

Equation (1.7) can also be expressed as

$$\mathbf{r} \times \mathbf{S} = \mathbf{S}_0, \quad (1.8)$$

where

$$\mathbf{S}_0 = \mathbf{r}_1 \times \mathbf{S} \quad (1.9)$$

is the moment of the line about the origin O.

The vectors $(\mathbf{S}; \mathbf{S}_0)$ are called the Plücker coordinates of the line and satisfy the orthogonality condition

$$\mathbf{S} \cdot \mathbf{S}_0 = 0. \quad (1.10)$$

Note that $(\mathbf{S}; \mathbf{S}_0)$ is homogeneous, since multiplying both sides of Eq. (1.8) by a scalar λ yields the same line.

Expanding Eq. (1.9) leads to

$$\mathbf{S}_0 = \begin{vmatrix} \mathbf{i} & \mathbf{j} & \mathbf{k} \\ x_1 & y_1 & z_1 \\ L & M & N \end{vmatrix}. \quad (1.11)$$

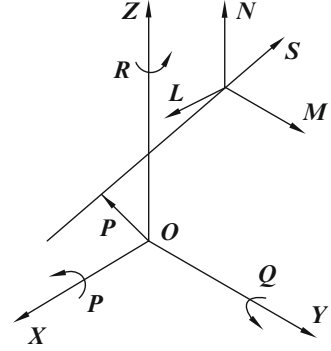
Equation (1.11) can be expressed in the form

$$\mathbf{S}_0 = P\mathbf{i} + Q\mathbf{j} + R\mathbf{k}, \quad (1.12)$$

where

$$\begin{aligned} P &= y_1N - z_1M \\ R &= x_1M - y_1L. \end{aligned} \quad (1.13)$$

Fig. 1.2 Distance between the line and origin



Expanding Eq. (1.8) and considering Eq. (1.12), we have

$$\begin{aligned} yN - zM - P &= 0 \\ zL - xN - Q &= 0 \\ xM - yL - R &= 0. \end{aligned} \quad (1.14)$$

From Eqs. (1.3), (1.12) and (1.10), the orthogonality condition can be written as

$$LP + MQ + NR = 0. \quad (1.15)$$

The six Plücker coordinates of the line $(L, M, N; P, Q, R)$ are illustrated in Fig. 1.2.

(L, M, N) consists of the direction ratios of the line and (P, Q, R) are the x, y and z components of the moment of the line about the origin. The coordinates $(S; S_0)$ are related by Eqs. (1.6) and (1.11). Therefore only four of the six scalars $(L, M, N; P, Q, R)$ are independent, and there are ∞^4 lines in space.

The distance of the line from the origin is determined by the length of a vector P from O and perpendicular to the line. From Eq. (1.8), we have $P \times S = S_0$, and therefore

$$S \times (P \times S) = S \times S_0.$$

Expanding the left side of the above equation, we have

$$S \times (P \times S) = (S \cdot S)P - (S \cdot P)S = (S \cdot S)P,$$

and so solving equation for P gives

$$P = \frac{S \times S_0}{S \cdot S}. \quad (1.16)$$

This can be expressed in the form

$$\mathbf{P} = \frac{|\mathbf{S}||\mathbf{S}_0|}{|\mathbf{S}||\mathbf{S}|} \mathbf{e} = \frac{|\mathbf{S}_0|}{|\mathbf{S}|} \mathbf{e}, \tag{1.17}$$

where \mathbf{e} is a unit vector perpendicular to $\mathbf{S} \times \mathbf{S}_0$. Therefore

$$|\mathbf{P}| = \frac{|\mathbf{S}_0|}{|\mathbf{S}|}. \tag{1.18}$$

When $\mathbf{S}_0 = 0$, the line passes through the origin and the Plücker line coordinates are $(\mathbf{S}; 0)$ or $(l \ m \ n; 0 \ 0 \ 0)$. When $\mathbf{S} = 0$, the line lies in a plane at infinity and the Plücker coordinates are $(0; \mathbf{S}_0)$ or $(0 \ 0 \ 0; l \ m \ n)$.

1.3 Mutual Moment of Two Lines

The vector equations of two skew lines separated by a perpendicular distance of a_{12} and a twist angle of α_{12} (see Fig. 1.3) are given by

$$\mathbf{r}_1 \times \mathbf{S}_1 = \mathbf{S}_{01} \tag{1.19}$$

$$\mathbf{r}_2 \times \mathbf{S}_2 = \mathbf{S}_{02}. \tag{1.20}$$

The projection of the moment vector $a_{12}\mathbf{a}_{12} \times \mathbf{S}_2$ on the line \mathbf{S}_1 is given by $a_{12} \mathbf{a}_{12} \times \mathbf{S}_2 \cdot \mathbf{S}_1$ and is called the moment of \mathbf{S}_2 about the line \mathbf{S}_1 . This scalar quantity is usually called the mutual moment of the two lines and can also be obtained by projecting the moment vector $-a_{12}\mathbf{a}_{12} \times \mathbf{S}_1$ on the line \mathbf{S}_2 , namely,

$$M_m = a_{12}\mathbf{a}_{12} \times \mathbf{S}_2 \cdot \mathbf{S}_1 = a_{12}\mathbf{a}_{21} \times \mathbf{S}_1 \cdot \mathbf{S}_2. \tag{1.21}$$

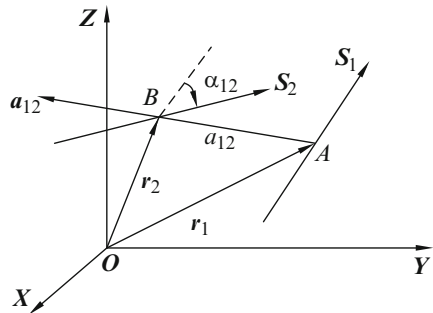


Fig. 1.3 Mutual moment of two lines

Expanding the scalar triple product and considering $\mathbf{r}_2 - \mathbf{r}_1 = a_{12}\mathbf{a}_{12}$, we have

$$(\mathbf{r}_2 - \mathbf{r}_1) \cdot \mathbf{S}_2 \times \mathbf{S}_1 = \mathbf{r}_2 \times \mathbf{S}_2 \cdot \mathbf{S}_1 + \mathbf{r}_1 \times \mathbf{S}_1 \cdot \mathbf{S}_2. \quad (1.22)$$

Substituting Eqs. (1.19) and (1.20) into Eq. (1.22) yields

$$\mathbf{M}_m = \mathbf{S}_1 \cdot \mathbf{S}_{02} + \mathbf{S}_2 \cdot \mathbf{S}_{01}. \quad (1.23)$$

Since both \mathbf{S}_1 and \mathbf{S}_2 are unit vectors, $\mathbf{S}_1 \cdot \mathbf{S}_1 = \mathbf{S}_2 \cdot \mathbf{S}_2 = 1$, and so

$$\mathbf{S}_2 \times \mathbf{S}_1 = -a_{12} \sin \alpha_{12}. \quad (1.24)$$

The mutual moment of the two lines is then given by

$$\mathbf{M}_m = (\mathbf{r}_2 - \mathbf{r}_1) \cdot \mathbf{S}_2 \times \mathbf{S}_1 = -a_{12} \sin \alpha_{12}. \quad (1.25)$$

From this expression, it is clear that the mutual moment of two lines is independent of the coordinate-frame.

Alternatively, Eq. (1.23) can be written as

$$\mathbf{M}_m = l_1 p_2 + m_1 q_2 + n_1 r_2 + p_1 l_2 + q_1 m_2 + r_1 n_2. \quad (1.26)$$

If the lines are parallel or intersect at infinity, we have $\alpha_{12} = 0$ and their mutual moment is zero. If the two lines intersect, which means the perpendicular distance between the two lines is zero, we have $a_{12} = 0$. Therefore, when two lines are coplanar, the mutual moment of the two lines is always zero:

$$\mathbf{S}_1 \cdot \mathbf{S}_{02} + \mathbf{S}_2 \cdot \mathbf{S}_{01} = 0. \quad (1.27)$$

1.4 Line Vectors and Screws

1.4.1 The Line Vector

This section will introduce two important concepts. One is the line vector and the other is the screw. Recall that in Sect. 1.2 we established the equation of a line:

$$\mathbf{r} \times \mathbf{S} = \mathbf{S}_0. \quad (1.28)$$

The dual vector $(\mathbf{S}; \mathbf{S}_0)$, which denotes a straight line in space, is also called a line vector. When $|\mathbf{S}| = 1$, \mathbf{S} is a unit vector and $(\mathbf{S}; \mathbf{S}_0)$ is a unit line vector. However, \mathbf{S}_0 is in general not a unit vector. The two vectors \mathbf{S} and \mathbf{S}_0 are orthogonal,

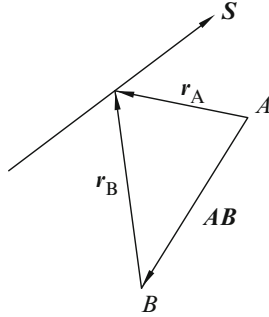


Fig. 1.4 Line moment is not origin-dependent

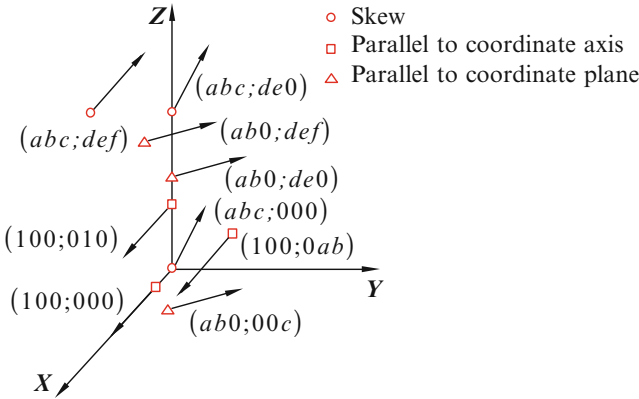


Fig. 1.5 Various forms of line vector

so that $S \cdot S_0 = 0$. The unit line vectors $(S; S_0)$ stand in one-to-one correspondence with the ∞^4 lines in space.

The vector S is not origin-dependent. The vector S_0 , which remains constant as S is being moved along the line, is the moment of S about the origin O . Clearly, S_0 is origin-dependent, and if the origin is shifted from point O to point A , then the moment of S about A can be written as (Fig. 1.4)

$$S_A = r_A \times S = (AB + r_B) \times S. \tag{1.29}$$

Substituting $S_B = r_B \times S$ into Eq. (1.29), we have

$$S_A = S_B + AB \times S. \tag{1.30}$$

When the line vectors are in different positions in space, the Plücker coordinates are different. In particular, when the line vector is located in certain special positions with respect to the coordinate system, many of the components are zero, as shown in Fig. 1.5. This is convenient for screw analysis.

1.4.2 The Screw

When the two vectors of a dual vector do not satisfy the orthogonality condition $\mathbf{S} \cdot \mathbf{S}^0 \neq 0$,² which is the more general case, the dual vector is called a screw and is denoted by

$$\mathcal{S} = (\mathbf{S}; \mathbf{S}^0), \mathbf{S} \cdot \mathbf{S}^0 \neq 0. \quad (1.31)$$

When $|\mathbf{S}| = 1$, \mathcal{S} is a unit screw.

The vector \mathbf{S} of a screw is also not origin-dependent. The vector \mathbf{S}^0 is origin-dependent and if the origin is shifted from point O to point A , the moment of \mathbf{S} about A can be obtained as

$$\mathbf{S}^A = \mathbf{S}^0 + \mathbf{AO} \times \mathbf{S}. \quad (1.32)$$

Multiplying both sides of this equation by \mathbf{S} , we have

$$\mathbf{S} \cdot \mathbf{S}^A = \mathbf{S} \cdot \mathbf{S}^0. \quad (1.33)$$

Equation (1.33) shows that $\mathbf{S} \cdot \mathbf{S}^0$ is not origin-dependent. If $\mathbf{S} \neq 0$, we can obtain the origin-independent variable

$$h = \frac{\mathbf{S} \cdot \mathbf{S}^0}{\mathbf{S} \cdot \mathbf{S}} = \frac{lp + mq + nr}{l^2 + m^2 + n^2}, \quad (1.34)$$

which is called the pitch of a screw. The line vector is a special screw with a zero pitch. A screw with an infinite pitch is called a couple and is denoted by $(\mathbf{0}; \mathbf{S})$.

The number of the unit screws in 3D space is ∞^5 , and the number of screws in 3D space is ∞^6 .

A line vector corresponds to a straight line in space, and a screw also has its axis line. To determine the axis line that the screw lies on, \mathbf{S}^0 is decomposed into two parts, which are parallel and perpendicular to \mathbf{S} , respectively, as shown in Fig. 1.6:

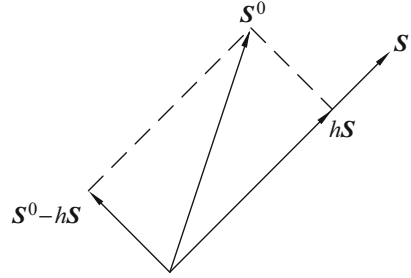
$$(\mathbf{S}; \mathbf{S}^0) = (\mathbf{S}; \mathbf{S}^0 - h\mathbf{S} + h\mathbf{S}). \quad (1.35)$$

Obviously, $\mathbf{S}^0 - h\mathbf{S}$ is normal to \mathbf{S} , and $\mathbf{S}^0 - h\mathbf{S} = \mathbf{S}_0$. The equation of the axis of the screw is given by

$$\mathbf{r} \times \mathbf{S} = \mathbf{S}^0 - h\mathbf{S}. \quad (1.36)$$

² For the convenience of readers, to distinguish between line vector and screw, the dual component of screw is expressed as \mathbf{S}^0 .

Fig. 1.6 Axis of a screw



The Plücker coordinates of the line are $(\mathbf{S}; \mathbf{S}^0 - h\mathbf{S})$. From Eq. (1.25), a screw can be expressed as

$$\mathcal{S} = (\mathbf{S}; \mathbf{S}^0) = (\mathbf{S}; \mathbf{S}^0 - h\mathbf{S}) + (0; h\mathbf{S}), \quad (1.37)$$

or

$$\mathcal{S} = (\mathbf{S}; \mathbf{S}^0) = (\mathbf{S}; \mathbf{r} \times \mathbf{S} + h\mathbf{S}) = (\mathbf{S}; \mathbf{S}_0 + h\mathbf{S}) = (\mathbf{S}; \mathbf{S}_0) + (0; h\mathbf{S}). \quad (1.38)$$

This indicates that a line vector and a couple can combine to form a screw, or that any screw with non-zero finite pitch can be considered the summation of a line vector and a couple. There are four factors that determine a screw: position and direction of the axis, and the magnitude and pitch of the screw.

$$\begin{aligned} \text{Screw: } (\mathbf{S}; \mathbf{S}^0) : \mathbf{S} \neq 0, \quad \mathbf{S} \cdot \mathbf{S}^0 \neq 0, \quad \infty \neq h \neq 0 \\ \text{Line vector: } (\mathbf{S}; \mathbf{S}_0) : \mathbf{S} \neq 0, \quad \mathbf{S} \cdot \mathbf{S}_0 = 0, \quad h = 0 \\ \text{Couple: } (0; \mathbf{S}) : \mathbf{S} \neq 0, \quad h = \infty \end{aligned}$$

Example 1.1. $(l \ m \ n; \ hl \ hm \ hn)$ is a screw with pitch h and passing through the origin.

Example 1.2. $(1 \ 0 \ 0; \ 1 \ 0 \ 0)$ is a screw with pitch $h = 1$ and passing through the origin, since

$$\begin{aligned} h &= (\mathbf{S} \cdot \mathbf{S}^0) / (\mathbf{S} \cdot \mathbf{S}) = 1, \\ \mathbf{r} \times \mathbf{S} &= \mathbf{S}^0 - h\mathbf{S} = 0. \end{aligned}$$

Example 1.3. $(1 \ 1 \ 1; \ 1 \ 1 \ 1) / \sqrt{3}$ is also a unit screw with pitch $h = 1$ that passes through the origin and points in the direction $(1 \ 1 \ 1)$.

Example 1.4. Identify $\mathcal{S} = (\mathbf{S}; \mathbf{S}^0) = (1 \ 1 \ 0; \ 1 \ 0 \ 0)$ and determine its axis.

Solution. The pitch of the screw is $h = (\mathbf{S} \cdot \mathbf{S}^0) / (\mathbf{S} \cdot \mathbf{S}) = 1/2$. Considering that $\mathbf{S}^0 = \mathbf{S}_0 + h\mathbf{S} = \mathbf{r} \times \mathbf{S} + h\mathbf{S}$, the equation of the axis is $\mathbf{r} \times \mathbf{S} = \mathbf{S}^0 - h\mathbf{S}$.

Thus we have

$$\mathbf{r} \times \mathbf{S} = (1/2 - 1/2 \ 0)^T.$$

1.5 Screw Algebra

Screws obey the following algebraic operations [11], and these operations have special meanings.

1.5.1 Screw Sum

The sum of two screws $\mathcal{S}_1 = (\mathbf{S}_1; \mathbf{S}_1^0)$, and $\mathcal{S}_2 = (\mathbf{S}_2; \mathbf{S}_2^0)$ is defined as follows

$$\mathcal{S}_1 + \mathcal{S}_2 = (\mathbf{S}_1 + \mathbf{S}_2; \mathbf{S}_1^0 + \mathbf{S}_2^0) \quad (1.39)$$

Equation (1.39) shows that the sum of two screws is still a screw.

Theorem 1.1. *The sum of two line vectors is a line vector only if their axes are coplanar and the sum of their first vectors is non-zero, namely $\mathbf{S}_1 + \mathbf{S}_2 \neq \mathbf{0}$.*

Proof. If \mathcal{S}_1 and \mathcal{S}_2 are two line vectors, then $\mathbf{S}_1 \cdot \mathbf{S}_{01} = 0$ and $\mathbf{S}_2 \cdot \mathbf{S}_{02} = 0$. If the two line vectors are coplanar, then their mutual moment is equal to zero. That is, $\mathbf{S}_{01} \cdot \mathbf{S}_2 + \mathbf{S}_{02} \cdot \mathbf{S}_1 = 0$. Therefore, we obtain

$$(\mathbf{S}_1 + \mathbf{S}_2) \cdot (\mathbf{S}_{01} + \mathbf{S}_{02}) = 0. \quad (1.40)$$

Equation (1.40) shows that the sum of two line vectors is still a line vector and its pitch is zero.

Theorem 1.2. *If two line vectors intersect, their sum is a line vector passing the intersection point.*

Proof. Since the sum of two line vectors is still a line vector, it can be expressed as

$$\mathbf{r} \times (\mathbf{S}_1 + \mathbf{S}_2) = \mathbf{S}_{01} + \mathbf{S}_{02}. \quad (1.41)$$

If r_1 denotes the position vector of the intersection point, r_1 lies on both of the lines and satisfies the equations of both lines:

$$\mathbf{r}_1 \times \mathbf{S}_1 = \mathbf{S}_{01}, \quad \mathbf{r}_1 \times \mathbf{S}_2 = \mathbf{S}_{02}. \quad (1.42)$$

Thus we have

$$\mathbf{r}_1 \times (\mathbf{S}_1 + \mathbf{S}_2) = \mathbf{S}_{01} + \mathbf{S}_{02}. \quad (1.43)$$

Equation (1.43) shows that the point r_1 lies on the line determined by the sum of the two line vectors.

Note that when two lines are not coplanar, the sum of the two line vectors is a screw with non-zero pitch instead of a line vector. Further, the sum of a line vector and a couple is not a line vector.

Theorem 1.3. *The sum of two couples, if not zero, is another couple.*

1.5.2 Product of a Scalar and a Screw

The product of a scalar λ and a screw $\$$ is defined by

$$\lambda\$ = (\lambda\mathbf{S}; \lambda\mathbf{S}^0). \quad (1.44)$$

1.5.3 Reciprocal Product

The reciprocal product of two screws, say $\$1 = (\mathbf{S}_1; \mathbf{S}_1^0)$, $\$2 = (\mathbf{S}_2; \mathbf{S}_2^0)$, is defined by

$$\$1 \circ \$2 = \mathbf{S}_1 \cdot \mathbf{S}_2^0 + \mathbf{S}_2 \cdot \mathbf{S}_1^0 \quad (1.45)$$

where the symbol \circ denotes the reciprocal product of two screws.

When the origin of the coordinate system shifts from point O to point A , the two screws $\$1$ and $\$2$ become

$$\begin{aligned} \$1^A &= (\mathbf{S}_1; \mathbf{S}_1^A) = (\mathbf{S}_1; \mathbf{S}_1^0 + \mathbf{A}\mathbf{O} \times \mathbf{S}_1), \\ \$2^A &= (\mathbf{S}_2; \mathbf{S}_2^A) = (\mathbf{S}_2; \mathbf{S}_2^0 + \mathbf{A}\mathbf{O} \times \mathbf{S}_2). \end{aligned} \quad (1.46)$$

The reciprocal product of the two new screws is

$$\$1^A \circ \$2^A = \mathbf{S}_1 \cdot (\mathbf{S}_2^0 + \mathbf{A}\mathbf{O} \times \mathbf{S}_2) + \mathbf{S}_2 \cdot (\mathbf{S}_1^0 + \mathbf{A}\mathbf{O} \times \mathbf{S}_1) = \$1 \circ \$2. \quad (1.47)$$

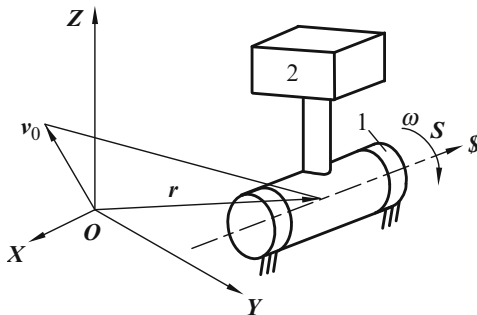
This result indicates that the reciprocal product of two screws is not origin-dependent.

The reciprocal product of two screws represents the work produced by a wrench acting on a rigid body undergoing an infinitesimal twist.

1.6 Instantaneous Kinematics of a Rigid Body

The most general motion in three-dimensional space is screw motion, which means simultaneous translational and rotational motion. Pure translation and pure rotation are special cases of screw motion. In this section, we will discuss pure rotation,

Fig. 1.7 Instantaneous rotation of a body



translation, and screw motion, including how to determine the Plücker coordinates, pitch, and the equation of axis.

1.6.1 Instantaneous Rotation

In Fig. 1.7, the rigid body labeled by 2 is rotating about another rigid body labeled by 1. The axis of rotation is S . Such a rotation can be described by the angular velocity line vector

$$\omega\mathcal{S} = \omega(S; S_0) = (\omega S; \omega S_0), \tag{1.48}$$

where ω is the amplitude of the rotation and S is the unit vector in the direction of the line.

The equation of the axis of rotation is given by

$$r \times S = S_0. \tag{1.49}$$

The second component of Eq. (1.48) is

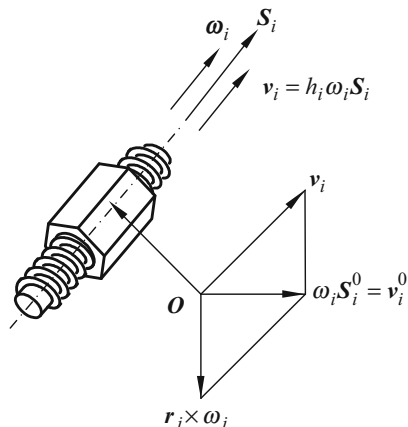
$$\omega S_0 = \omega r \times S = r \times \omega = v_0, \tag{1.50}$$

which is the velocity of a point coincident with the origin, or the tangent velocity of the point coincident with the origin. Equation (1.48) can also be rewritten as follows:

$$\omega\mathcal{S} = (\omega; v_0). \tag{1.51}$$

Therefore, the dual vectors denoting the rotation of a rigid body include the angular velocity, ω , and the linear velocity, v_0 , of the point coincident with the origin. The Plücker coordinates of a rotating rigid body are $\omega(S; S_0)$ or $(\omega; v_0)$. When the rotational axis passes through the origin, the Plücker coordinates of the rotational axis are $\omega\mathcal{S} = (\omega; 0)$ or $(\omega; 0)$.

Fig. 1.8 Twist motion of a body



1.6.2 Instantaneous Translation

An instantaneous translation of one rigid body relative to another one can be conveniently modeled by connecting the two bodies by a prismatic or sliding pair (as illustrated in Fig. 1.7). The translational velocity v can be expressed as a scalar multiple of the instantaneous linear displacement v and a unit vector S parallel to the direction of motion. The vector S is for convenience drawn through the center line of the joint. However, all points in the moving body have the same linear velocity $v = vS$, and a self-parallel displacement of the vector S does not affect the motion. The same motion is obtained when the joint is reconnected parallel to its original attachment and the body is given the same instantaneous translational displacement v . For this reason, S is called a free vector and the motion can be quantified by taking a scalar multiple of the free vector $v(\theta; S)$ or $(\theta; v)$. Some readers may prefer to consider instantaneous translation to be an instantaneous rotation about an axis that is orthogonal to S and that lies in the plane at infinity. The Plücker coordinates of this axis are $(\theta; S)$, and the instantaneous rotation about this axis can be expressed as the scalar multiple $v(\theta; S)$.

1.6.3 Instantaneous Screw Motion

When the motion of one body 2 relative to another includes rotation about the axis S_1 and translation in the direction S_1 , the situation is more complex, as shown in Fig. 1.8. The body rotates about the axis S_1 , with the instantaneous wrench $\omega_1(S_1; S_{01})$, where $(S_1; S_{01})$ is unit screw. The body also translates with screw $v_2(\theta; S_1)$ along the axis S_1 at the same time. The absolute motion of the body is the sum of the two parts.

That is,

$$\begin{aligned}\omega_i \mathcal{S}_i &= (\omega_1 \mathcal{S}_1; \omega_1 \mathcal{S}_{01}) + (\mathbf{0}; v_1 \mathcal{S}_1) = (\omega_1 \mathcal{S}_1; \omega_1 \mathcal{S}_{01} + h \omega_1 \mathcal{S}_1) \\ &= \omega_1 (\mathcal{S}_1; \mathcal{S}_1^0),\end{aligned}\tag{1.52}$$

or

$$\omega_i \mathcal{S}_i = \omega_1 (\mathcal{S}_1; \mathcal{S}_1^0) = (\boldsymbol{\omega}_1; \mathbf{v}^0),\tag{1.53}$$

where $\boldsymbol{\omega}_1$ is the angular velocity of the body and \mathbf{v}^0 is the velocity of a point in the body coincident with the origin. Note that the directions of \mathbf{v}^0 and $\boldsymbol{\omega}_1$ are different in general, unless the axis of the screw passes the origin. The pitch is

$$h = \frac{\mathcal{S}_1 \cdot \mathcal{S}_1^0}{\mathcal{S}_1 \cdot \mathcal{S}_1} = \frac{\boldsymbol{\omega}_1 \cdot \mathbf{v}^0}{\boldsymbol{\omega}_1 \cdot \boldsymbol{\omega}_1}.\tag{1.54}$$

1.7 Statics of a Rigid Body

1.7.1 A Force Acting on a Body

Analogous to instantaneous rotation, unit line vectors can be used to express the action of a force on a body, as shown in Fig. 1.9. A force \mathbf{f} can be expressed as a scalar multiple $f\mathcal{S}$ of the unit vector \mathcal{S} bound to the line. The moment of the force \mathbf{C}_O about a reference point O can be expressed as a scalar multiple $f\mathcal{S}_0$ of the moment vector $\mathcal{S}_0 = \mathbf{r} \times \mathcal{S}$. The action of the force upon the body can thus be elegantly expressed as a scalar multiple $f\mathcal{S}$ of the unit line vector

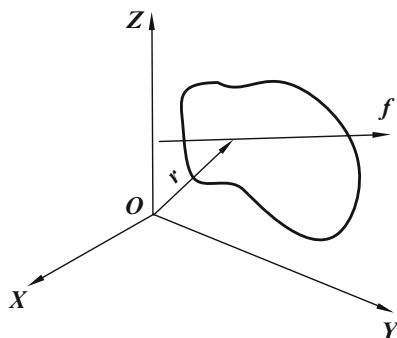
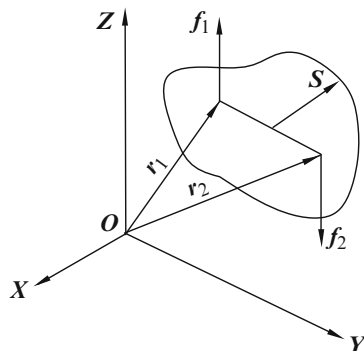


Fig. 1.9 Force acting on a body

Fig. 1.10 A couple acting on a body



$$f\$\ = (f; fS_0) = (f; C_0), \tag{1.55}$$

where $\$$ is unit line vector, $S \cdot S = 1$ and $S \cdot S_0 = 0$. The line vector can be used to express the magnitude, direction and the acting line in space.

The Plücker coordinates of the force line vector are $f(S; S_0)$, $(fS; fS_0)$ or $(f; C_0)$, where C_0 is the moment of force f about the origin, that is, $C_0 = fS_0 = fr \times S_0$. When the force f passes through the origin, the moment vanishes ($C_0 = 0$), and the Plücker coordinates of the force are $(f; 0)$.

1.7.2 A Couple Acting on a Body

Figure 1.10 illustrates a rigid body subjected to two equal and opposite forces f_1 and f_2 . These two forces constitute a couple, the moment of which is given by

$$C = (r_2 - r_1) \times f_2 = (r_1 - r_2) \times f_1 \tag{1.56}$$

The vector C is clearly normal to the plane containing the forces, and C can thus be expressed as a scalar multiple CS of any unit vector normal to the plane. The vector S is therefore a free vector and the couple vector C can be given a self-parallel displacement without altering the statics of the body.

The couple C can thus be expressed as a scalar multiple $C(0; S)$ of the free vector $(0; S)$. Alternatively, the couple can be considered a force acting upon the body along a line that is orthogonal to S and that lies in the plane at infinity. The Plücker coordinates of this line are $(0; S)$, and the force acting upon the body can be expressed as the scalar multiple $C(0; S)$.

1.7.3 A Twist Acting on a Body

A general system of forces and couples acting upon a rigid body can be reduced to a single force $f_1(S_i; S_i^0)$ and a single couple $C(0; S)$. This force couple combination

was called a dynamy by Plücker and Hunt. The above mentioned force screw f_1 ($\mathbf{S}_i; \mathbf{S}_i^0$) can be expressed as the sum of a force f_1 ($\mathbf{S}_i; \mathbf{S}_i^0$) and a couple $\mathbf{C}(0; \mathbf{S})$ with the same direction as the force. When the origin is located on the axis \mathbf{S}_1 , this force screw can be expressed as

$$f_1(\mathbf{S}_1; \mathbf{S}_1^0) = (f_1; \mathbf{C}_0). \quad (1.57)$$

When the origin does not lie on the axis \mathbf{S}_1 , the force screw is

$$f_1(\mathbf{S}_1; \mathbf{S}_1^0) = (f_1; \mathbf{C}^0), \quad (1.58)$$

where \mathbf{C}^0 is the moment about the origin.

References

1. Plücker J (1865) On a new geometry of space. *Philos Trans* 155:725–791
2. Ball RA (1900) *Treatise on the theory of screws*. Cambridge University Press, Cambridge, pp 1–30
3. Dimentberg FM (1950) Determination of the motion of spatial mechanisms. Akad Nauk, Moscow (Russian)
4. Yang AT, Freudenstein F (1964) Application of dual-number quaternion algebra to the analysis of spatial mechanisms. *Trans ASME* 86E:300–308 (*J Appl Mech* 31)
5. Waldron KJ (1966) The constraint analysis of mechanisms. *J Mech* 1:101–114
6. Roth B (1967) On the screw axes and other special lines associated of a rigid body. *J Eng Ind* 89:102–109
7. Hunt KH (1978) *Kinematic geometry of mechanisms*. Oxford University Press, Oxford
8. Phillips J (1990) *Freedom in machinery*. Cambridge University Press, Sydney, pp 147–168
9. Duffy J (1982). *The screw theory and its application*. Class note of University of Florida, Gainesville
10. Angeles J (1994) On twist and wrench generators and annihilators. In: Seabra Pereira MFO, Ambrosio JAC (eds) *Computer-aided analysis of rigid and flexible mechanical system*. Kluwer Academic, Dordrecht
11. Brand L (1947) *Vector and tensor analysis*. Wiley, New York, pp 51–83

Chapter 2

Dependency and Reciprocity of Screws

This chapter introduces the concept of a screw system and focuses on second-order and third-order screw systems, especially their various special forms. The linear dependency of screws is discussed. The principle of Grassmann line geometry and screw dependency for different geometrical spaces are also introduced. Near the end of the chapter, the concept and analysis of the reciprocal screw and constraint motion are presented.

2.1 Concept of Screw Systems

The concept of a screw system is deduced from kinematics. For an open chain or a serial robot, the motion of the end-effector can be expressed as the summation of the motions of all links. When the motions of all the links of the serial chain are expressed as screws, the motion of the end-effector is the linear combination of all screws. All the screws which determine the motions of all the links of a serial chain form a screw system. More generally, when all the kinematic pairs of a mechanism are expressed as screws, all the screws in the mechanism construct a screw system [1, 2], which is denoted as $\hat{\mathcal{S}}$.

On the basis of the number of linearly independent screws, screw systems can be classified into six categories. The first is called the first-order screw system or one-screw system, which contains only one screw. The second is called the second-order screw system or two-screw system or two-system, which contains two linearly independent screws. The third category is called the third-order screw system or three-screw system comprising three linearly independent screws. The fourth category is called the fourth-order screw system or four-screw system, which contains four linearly independent screws. The fifth category contains five linearly independent screws and is called the fifth-order screw system or five-screw system.

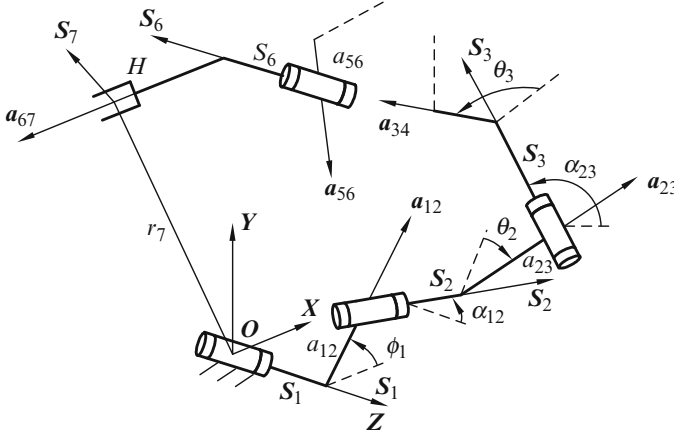


Fig. 2.1 Serial robot

Finally, the sixth category is called the sixth-order screw system or six-screw system, which contains six linearly independent screws.

Example 2.1. Screw system of a serial robot

For a serial robot, when all the kinematic pairs are associated with screws, the motion of the end-effector is the linear combination of all the screws. These screws construct a typical screw system.

A serial kinematic chain is composed of links successively connected by kinematic pairs. The mobility of the chain is only the number of the kinematic pairs when all kinematic pairs are single-DOF types. Generally, an n -DOF serial robot consists of $n+1$ links connected by n kinematic pairs, Fig. 2.1.

The relative motion between any two neighboring links can be expressed as a product of a relative scalar angular speed and a unit screw, $\omega\mathcal{S}$. If the serial chain consists of n kinematic pairs, the corresponding screw system is expressed as follows

$$\mathcal{S}_i = [\mathcal{S}_1, \mathcal{S}_2, \dots, \mathcal{S}_n] \quad (2.1)$$

When all the relative motions between any two neighboring links are expressed as $\omega_1\mathcal{S}_1, \omega_2\mathcal{S}_2, \dots, \omega_n\mathcal{S}_n$, the motion of the end-effector can be expressed as follows

$$\omega_i\mathcal{S}_i = \omega_1\mathcal{S}_1 + \omega_2\mathcal{S}_2 + \dots + \omega_n\mathcal{S}_n = \sum \omega_j\mathcal{S}_j \quad (j = 1, 2, \dots, n) \quad (2.2)$$

where

$$\begin{aligned} \omega_i\mathcal{S}_i &= \omega_i(\mathcal{S}_i; \mathcal{S}_i^0) = (\omega_i; v_i^0) \\ \omega_j\mathcal{S}_j &= \omega_j(\mathcal{S}_j; \mathcal{S}_{0j}) \end{aligned} \quad (2.3)$$

2.2 Second-Order Screw System

A second-order screw system contains all the linear combinations of two linearly independent screws. A third-order screw system comprises all the linear combinations of three linearly independent screws. The second-order and third-order screw systems are fundamentals and are introduced in this chapter.

2.2.1 Linear Combination of Two Screws

Consider two screws, $\$A = (S_A; S_A^0)$ and $\$B = (S_B; S_B^0)$. Their common normal is a_{AB} . The Z-axis is assumed to be aligned along the common normal of axes S_A and S_B , and then S_A and S_B intersect at Z_A and Z_B . The angles from the X-axis to S_A and S_B are θ_A and θ_B , Fig. 2.2.

The sum screw after the linear combination of the two screws is given by

$$\lambda_i \$i = \lambda_i (S_i; S_i^0), \quad i = 1, 2 \tag{2.4}$$

where

$$\lambda_i S_i = S_A + \lambda S_B \tag{2.5}$$

$$\lambda_i S_i^0 = S_A^0 + \lambda S_B^0 \tag{2.6}$$

The pitch of the sum screw is

$$h = \frac{S_i \cdot S_i^0}{S_i \cdot S_i} \tag{2.7}$$

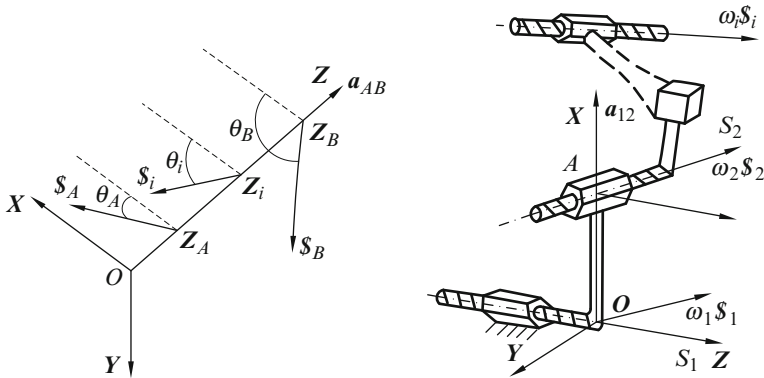
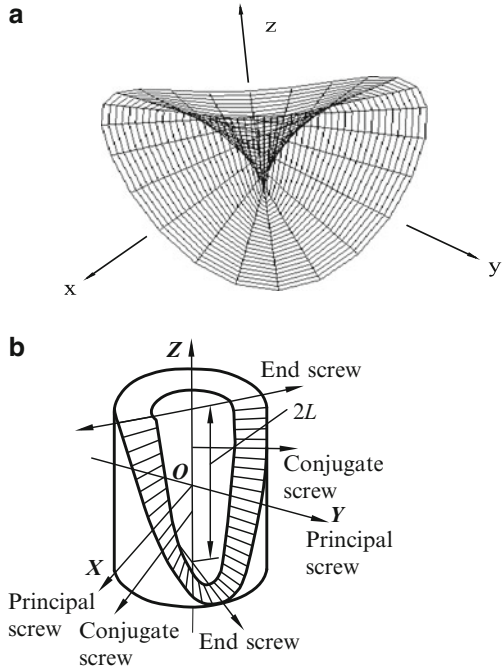


Fig. 2.2 Summation of two screws

Fig. 2.3 Cylindroid
 (a) cylindroid given by Ball
 (b) cylindroid given by Phillips



The Plücker coordinate of the axis of the sum screw is $(S_i; S_i^0 - hS_i)$ and its axis equation is

$$r_i \times S_i = S_i^0 - hS_i \tag{2.8}$$

When λ is given, the sum screw is determined, and when λ is associated with different values, the sum screws are also different. Thus, there are infinite sum screws in a three-dimensional (3-D) space for a two-screw system.

References [1] and [3] show the surface of a two-screw system (Fig. 2.3).

The surface in Fig. 2.3a was discovered in 1870 and is called cylindroid by Ball[1]. The illustration in Fig. 2.3b was suggested by Phillips [3], and this illustration is easier to understand and is analyzed in the following paragraph.

The linear-combination screws of any two linearly independent screws with different pitches constitute a special closed ruled surface, the cylindroid. Each radial from the center axis of the cylindroid denotes a screw axis, which is also normal to the center line. The mid-section of the cylindroid is the XY plane. The X - and Y -axes correspond to two orthogonal screws with the extremum pitches h_x and h_y of the two-screw system. The two screws, which are aligned with the X - and Y -axes, are the two principal screws of the two-screw system. The coordinate frame coincident with two principal screws is called a principal coordinate system. The ruled surface is closed and has a determinate length. When the pitches h_x and h_y of the two principal screws are unequal and non-zero, the cylindroid is in a general form. When the pitches

of the two principal screws are equal or have infinite values, they make up the special two-screw system. The general two-screw system is discussed below.

1. **Principal screw** The two-screw system has two principal screws, whose pitches have the extremum in the system. The angle between these screws is $\theta = 90^\circ$.
2. **End screw** The end screw is located at the end of the cylindroid, and a cylindroid has two end screws.
3. **Conjugate screw** Two screws with identical pitches are called conjugate screws. Any screw in a cylindroid has its own conjugate except the principal screws. Conjugate screws are located on different sides of the XY plane at the same distances.
4. **Zero-pitch screw** In the infinite screws of a two-screw system, there are only two screws with zero pitch, and that is only when the signs of two principal screws are opposite. The two screws with zero pitch are always located on the two sides of the XY plane of the principal coordinate system.

From the analysis above, we can deduce that the linear combination of any two screws may yield infinite screws with different pitches, which form a cylindroid in space. In the infinite screws, there are at most two line vectors with zero pitch.

2.2.2 Special Two-Screw System

In the principal coordinate frame, the two principal screws are expressed as follows

$$\begin{aligned} \$\alpha &= (1 \quad 0 \quad 0; \quad h_\alpha \quad 0 \quad 0) \\ \$\beta &= (0 \quad 1 \quad 0; \quad 0 \quad h_\beta \quad 0) \end{aligned} \quad (2.9)$$

1. **When $h_\alpha = h_\beta = h$, it is the first special two-screw system¹.**

In this case, the pitches of both screws are equal. The two principal screws can be expressed as

$$\begin{aligned} \$\alpha &= (1 \quad 0 \quad 0; \quad h \quad 0 \quad 0) \\ \$\beta &= (0 \quad 1 \quad 0; \quad 0 \quad h \quad 0) \end{aligned} \quad (2.10)$$

The linear combination of the two principal screws is

$$\$_\Sigma = \$\alpha + \lambda \$\beta = (1 \quad \lambda \quad 0; \quad h \quad \lambda h \quad 0)$$

¹The definition is provided by Hunt.

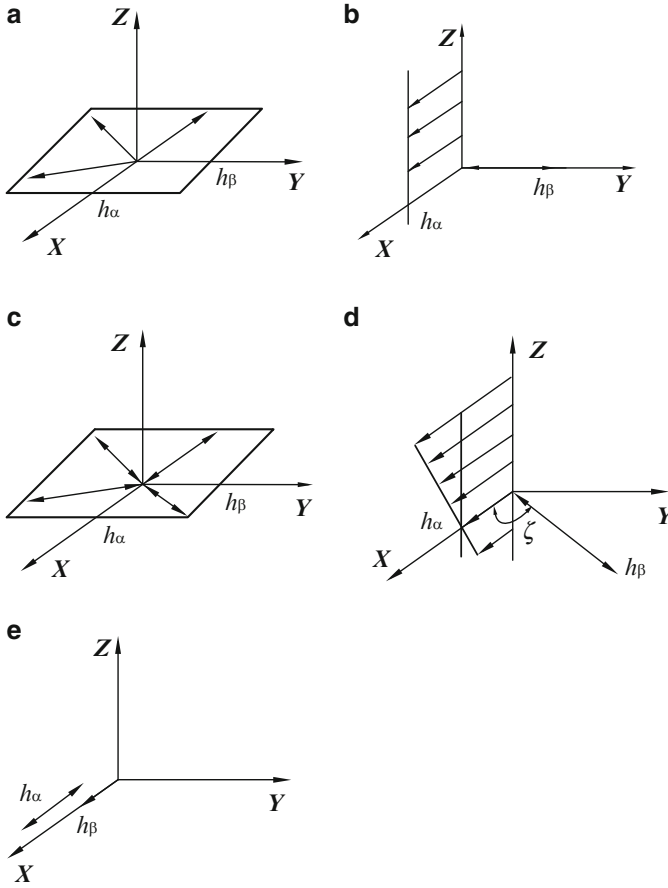


Fig. 2.4 Special two-screw systems (a) first special two-system (b) second special two-system (The bi-directional arrow denotes the screw with infinite pitch (i.e., a couple).) (c) third special two-system (d) fourth special two-system (e) fifth special two-system

where λ is a constant and the pitch of the sum screw is expressed as

$$h_{\Sigma} = \frac{S \cdot S^0}{S \cdot S} = h \tag{2.11}$$

Since $S^0 = hS$, and $r \times S = 0$, it indicates that the sum screw also passes the origin. As shown in Fig. 2.4a, all the sum screws with identical pitch h pass the origin, and the cylindroid degenerates into a coplanar and concurrent flat pencil.

2. **When h_{α} is finite, and $h_{\beta} = \infty$, $\alpha \perp \beta$, $\zeta = 90^\circ$ (the second special two-screw system).** ζ is the angle between vectors α and β .

The two principal screws are expressed as

$$\begin{aligned}\$ _{\alpha} &= (1 \quad 0 \quad 0; \quad h_{\alpha} \quad 0 \quad 0) \\ \$ _{\beta} &= (0 \quad 0 \quad 0; \quad 0 \quad 1 \quad 0)\end{aligned}\quad (2.12)$$

The linear combination of the two principal screws yields

$$\$ _{\Sigma} = \$ _{\alpha} + \lambda \$ _{\beta} = (1 \quad 0 \quad 0; \quad h_{\alpha} \quad \lambda \quad 0) \quad (2.13)$$

The pitch of the sum screw is $h_{\Sigma} = h_{\alpha}$ and the equation of its axis is

$$\mathbf{r} \times \mathbf{S} = \mathbf{S}^0 - h_{\Sigma} \mathbf{S} = (0 \quad \lambda \quad 0) \quad (2.14)$$

The result indicates that the sum screw lies in the ZX plane and is parallel to the X -axis, Fig. 2.4b.

3. **When h_{α} is finite, $h_{\beta} = \infty$ and $0 < \zeta < 90^{\circ}$ (the fourth special two-screw system).** The two principal screws are

$$\begin{aligned}\$ _{\alpha} &= (1 \quad 0 \quad 0; \quad h_{\alpha} \quad 0 \quad 0) \\ \$ _{\beta} &= (0 \quad 0 \quad 0; \quad c\zeta \quad s\zeta \quad 0)\end{aligned}\quad (2.15)$$

where $c\zeta$ and $s\zeta$ denote the sine and cosine of angle ζ , respectively. The linear combination of the two principal screws yields

$$\$ _{\Sigma} = \$ _{\alpha} + \lambda \$ _{\beta} = (1 \quad 0 \quad 0; \quad h_{\alpha} + \lambda c\zeta \quad \lambda s\zeta \quad 0) \quad (2.16)$$

The result shows that the direction of the sum screw is identical to that of screw $\$ _{\alpha}$, and the pitch of the sum screw is $h_{\Sigma} = h_{\alpha} + \lambda c\zeta$ with the axis equation written as

$$\mathbf{r} \times \mathbf{S} = \mathbf{S}^0 - h_{\Sigma} \mathbf{S} = (0 \quad \lambda s\zeta \quad 0) \quad (2.17)$$

The sum screw intersects at the Z -axis at $(0, 0, z)$, $z = \lambda s c\zeta$. Hence, the pitch of the sum screw is

$$h_{\Sigma} = h_{\alpha} + z c\zeta / s\zeta \quad (2.18)$$

The gradient of the pitch with respect to Z is

$$\frac{dh_{\Sigma}}{dz} = \frac{dh}{dz} = \text{ctg}\zeta \quad (2.19)$$

Therefore, all the sum screws are parallel to X -axis and intersect at Z -axis, as shown in Fig. 2.4d.

4. **When h_α is finite and $h_\beta = \infty$ and $\zeta = 0^\circ$** , the system is the fifth special two-screw system.

The two principal screws are

$$\begin{aligned} \mathcal{S}_\alpha &= (1 \ 0 \ 0; \ h_\alpha \ 0 \ 0) \\ \mathcal{S}_\beta &= (0 \ 0 \ 0; \ 1 \ 0 \ 0) \end{aligned} \quad (2.20)$$

The sum screw is in the form

$$\mathcal{S}_\Sigma = \mathcal{S}_\alpha + \lambda \mathcal{S}_\beta = (1 \ 0 \ 0; \ h_\alpha + \lambda \ 0 \ 0), \quad h_\Sigma = h_\alpha + \lambda \quad (2.21)$$

As shown in Fig. 2.4e, all the sum screws are in the X direction and their pitches can be of any value.

5. **When $h_\alpha = h_\beta = \infty$, the directions of two screws are perpendicular** (the third special two-screw system)

In this system, the two principal screws are

$$\begin{aligned} \mathcal{S}_\alpha &= (0 \ 0 \ 0; \ 1 \ 0 \ 0) \\ \mathcal{S}_\beta &= (0 \ 0 \ 0; \ 0 \ 1 \ 0) \end{aligned} \quad (2.22)$$

Their arbitrary linear combination is

$$\mathcal{S}_\Sigma = \mathcal{S}_\alpha + \lambda \mathcal{S}_\beta = (0 \ 0 \ 0 \ ; \ 1 \ \lambda \ 0) \quad (2.23)$$

The sum screw also indicates a couple being parallel to the same plane, Fig. 2.4c

2.3 Third-Order Screw System

All screws produced by the linear combination of three linearly independent screws form a third-order screw system or three-screw system. A three-screw system has ∞^2 screws. Generally, a three-screw system comprises three special screws, which are orthogonal and perpendicular to each other and are called three principal screws. The three principal screws are unique. Any screw in a three-screw system is a linear combination of the three principal screws. In addition, two pitches of the three principal screws are extremum and the pitches of all other screws lie between the maximum and minimum pitches. The principal screw is important in screw analysis. Tsai and Lee [4] and Zhang and Xu [5] proposed methods to solve the principal screw using three given screws. Huang and Wang [6] proposed a method based on quadric degenerating theory to solve the principal screws of a three-screw system; the application of this theory is favorable for mechanism analysis.

2.3.1 Principal Screws

The pitches of the three principal screws of a three-screw system are denoted as h_α , h_β , and h_γ . Without losing generality, we assume $h_\alpha \geq h_\beta \geq h_\gamma$. The axes of the three principal screws are vectors α , β , and γ , which are mutually orthogonal. As previously mentioned, when the axes of the three principal screws α , β , and γ are selected as coordinate axes X , Y , and Z , the coordinate frame is called the principal coordinate system. Generally, all the axes of the three-screw system with the same pitch lie on a hyperboloid of one sheet. In 1900, Ball [1] provided the equation for the hyperboloid of one sheet in the principal coordinate system as follows

$$(h_\alpha - h)x^2 + (h_\beta - h)y^2 + (h_\gamma - h)z^2 + (h_\alpha - h)(h_\beta - h)(h_\gamma - h) = 0 \quad (2.24)$$

From the analysis above, we know that

1. When four screws with the same pitch are linearly dependent, the four screws lie on the same hyperboloid of one sheet;
2. The screws obtained by the linear combination of three linearly independent screws lie on the hyperboloid formed by the three screws;
3. When one of the four screws with the same pitch does not lie on the hyperboloid determined by the other three, the four screws are linearly independent.

In the principal coordinate system, the Plücker coordinates of the three principal screws can be expressed as follows

$$\begin{aligned} \$\alpha &= (1 \quad 0 \quad 0; \quad h_\alpha \quad 0 \quad 0) \\ \$\beta &= (0 \quad 1 \quad 0; \quad 0 \quad h_\beta \quad 0) \\ \$\gamma &= (0 \quad 0 \quad 1; \quad 0 \quad 0 \quad h_\gamma) \end{aligned} \quad (2.25)$$

The distribution of screws in a three-screw system in 3-D space has the following characteristics [2]:

1. When $h = h_\alpha$, the hyperboloid degenerates as a straight line, i.e., the screw expression is $(\alpha; \quad h_\alpha\alpha)$, and its pitch is h_α and axis vector is α .
2. When $h_\alpha > h > h_\beta$, each h between h_α and h_β corresponds to ∞ screws and these ∞ screws with the same pitch form a hyperboloid. Since there are screws with infinite different pitches between h_α and h_β , infinite hyperboloids are also formed. Infinite hyperboloids have the same center axis α .
3. When $h = h_\beta$, the hyperboloid degenerates as a straight line, i.e., the screw expression is $(\beta; \quad h_\beta\beta)$, and its pitch is h_β and axis is vector β .
4. When $h_\beta > h > h_\gamma$, each h inside h_β and h_γ corresponds to ∞ screws also and these ∞ screws with the same pitch form a hyperboloid. Because there are screws with infinite different pitches between h_β and h_γ , there are infinite hyperboloids with the same centre axis γ .
5. When $h = h_\gamma$, the hyperboloid degenerates as a straight line, i.e., the screw expression is $(\gamma; \quad h_\beta\gamma)$.

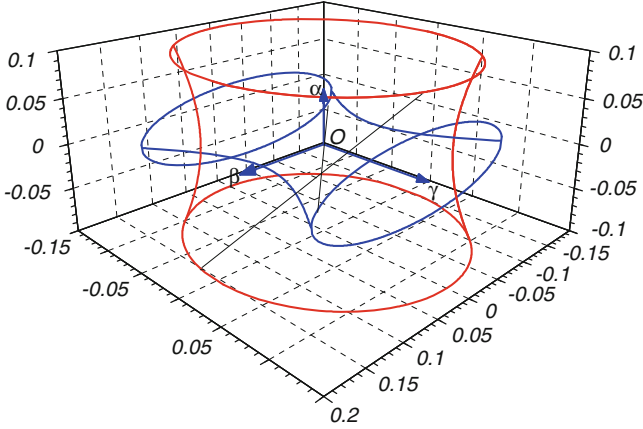


Fig. 2.5 General three-screw system

2.3.2 Special Three-Screw Systems

Hunt [2] provided ten kinds of special three-screw systems according to their different pitches. In the present study, several kinds of special three-screw systems are introduced.

General three-screw system When the pitches of the three principal screws satisfy $h_\alpha > h_\beta > h_\gamma$, they make up a general three-screw system and the axes of all the screws in this system lie on infinite hyperboloids, Fig. 2.5.

Only three special three-screw systems are introduced as follows.

1. First special three-screw system

For the first special three-screw system, the pitches of the three principal screws satisfy $h_\alpha \neq h_\beta = h_\gamma$ or $h_\alpha = h_\beta \neq h_\gamma$. In the first situation (i.e., $h_\alpha \neq h_\beta = h_\gamma$), the three principal screws are expressed as follows

$$\begin{aligned} \mathcal{S}_\alpha &= (1 \quad 0 \quad 0; \quad h_\alpha \quad 0 \quad 0) \\ \mathcal{S}_\beta &= (0 \quad 1 \quad 0; \quad 0 \quad h \quad 0) \\ \mathcal{S}_\gamma &= (0 \quad 0 \quad 1; \quad 0 \quad 0 \quad h) \end{aligned} \quad (2.26)$$

The linear combination of the three principal screws yields

$$\mathcal{S}_\Sigma = \mathcal{S}_\alpha + \lambda_1 \mathcal{S}_\beta + \lambda_2 \mathcal{S}_\gamma = \{1 \quad \lambda_1 \quad \lambda_2; \quad h_\alpha \quad \lambda_1 h \quad \lambda_2 h\} \quad (2.27)$$

In addition, the pitch of the resulted screw is expressed as

$$h_\Sigma = \frac{h_\alpha + \lambda_1^2 h + \lambda_2^2 h}{(1 + \lambda_1 + \lambda_2)^2}$$

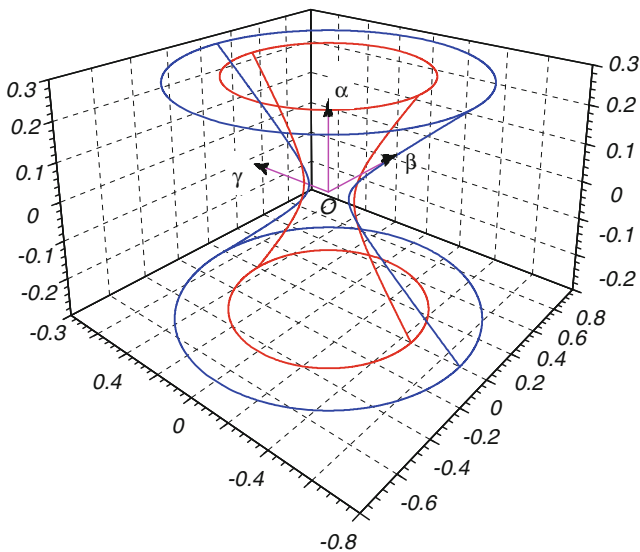


Fig. 2.6 The first special three-screw system

All the axes of this three-screw system form infinite hyperboloids with the same center axes, Fig. 2.6.

2. Second special three-screw system

In the second special three-screw system, the pitches satisfy $h_\alpha = h_\beta = h_\gamma = h$ and the three principal screws are

$$\begin{aligned} \mathcal{S}_\alpha &= (1 \ 0 \ 0; \ h \ 0 \ 0) \\ \mathcal{S}_\beta &= (0 \ 1 \ 0; \ 0 \ h \ 0) \\ \mathcal{S}_\gamma &= (0 \ 0 \ 1; \ 0 \ 0 \ h) \end{aligned} \quad (2.28)$$

The screw obtained by the linear combination of the three principal screws is

$$\mathcal{S}_\Sigma = \mathcal{S}_\alpha + \lambda_1 \mathcal{S}_\beta + \lambda_2 \mathcal{S}_\gamma = \{1 \ \lambda_1 \ \lambda_2; \ h \ h\lambda_1 \ h\lambda_2\} \quad (2.29)$$

Screw \mathcal{S}_Σ can be expressed as $\mathcal{S}_\Sigma = (\mathcal{S}; \ h\mathcal{S})$, and its axis equation is $\mathbf{r} \times \mathcal{S} = 0$, indicating that the pitches of all the screws are h and their axes pass the origin, as shown in Fig. 2.7.

3. Seventh special three-screw system

In this system, the pitches of the three principle screws satisfy $h_\alpha = \infty; h_\beta$ and h_γ are finite; $\mathcal{S}_\gamma \perp \mathcal{S}_\beta$; and $0 < \zeta < 90^\circ$. The three principal screws are expressed as follows

$$\begin{aligned} \mathcal{S}_\alpha &= (0 \ 0 \ 0; \ 0 \ 0 \ 1) \\ \mathcal{S}_\beta &= (\cos \zeta \ 0 \ \sin \zeta; \ h_\beta \cos \zeta \ 0 \ h_\beta \sin \zeta) \\ \mathcal{S}_\gamma &= (0 \ 1 \ 0; \ 0 \ h_\gamma \ 0) \end{aligned} \quad (2.30)$$

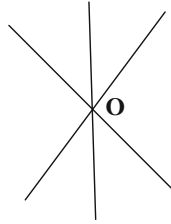


Fig. 2.7 Second special three-screw system

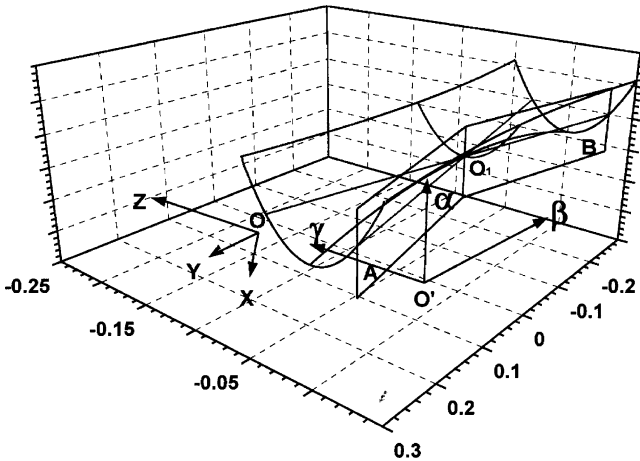


Fig. 2.8 Seventh special three-screw system

The linear combination of the three screws is

$$\mathcal{S}_\Sigma = \mathcal{S}_\alpha + \lambda_1 \mathcal{S}_\beta + \lambda_2 \mathcal{S}_\gamma = (\lambda_1 \cos \zeta \quad \lambda_2 \quad \lambda_1 \sin \zeta; \quad h_\beta \lambda_1 \cos \zeta \quad \lambda_2 h_\gamma h_\beta \lambda_1 \sin \zeta) \tag{2.31}$$

Since the direction of the common perpendicular of the two principal screws \mathcal{S}_β and \mathcal{S}_γ is

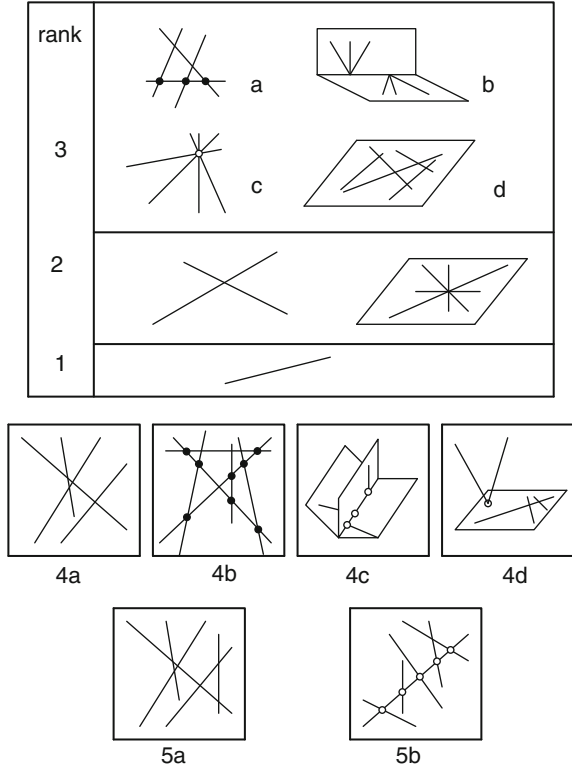
$$\mathbf{S}_\beta \times \mathbf{S}_\gamma = (-\sin \zeta \quad 0 \quad \cos \zeta) \tag{2.32}$$

and the direction of screw \mathcal{S}_Σ is $\mathbf{S}_\Sigma(\lambda_1 \cos \zeta \quad \lambda_2 \quad \lambda_1 \sin \zeta)$. Considering vectors \mathbf{S}_Σ and $\mathbf{S}_\beta \times \mathbf{S}_\gamma$ are orthogonal, all the screws of the seventh special three-screw system are parallel to a plane determined by two axes β and γ . Geometrically, three skew lines parallel to a plane determine a hyperbolic paraboloid, as shown in Fig. 2.8.

2.4 Grassmann Line Geometry

A straight line in space can be expressed by two vectors \mathbf{S} and \mathbf{S}_0 in screw theory. Their dual combination is called a line vector. The geometrical arrangement of joint axes in a mechanism influences the mobility of the mechanism, and each joint axis

Fig. 2.9 Grassmann line geometry



can be associated with a line vector. Hence, the calculation of the ranks of screws under different geometrical conditions is a useful approach for mobility analysis. Varieties of lines have been studied by H. Grassmann (1809–1877). The geometrical characteristics of each variety were determined. In 1989, the Grassmann line geometry was introduced into mechanism analysis by Merlet [7]. The method can be used to evaluate the rank or linear dependency of line vectors. The Grassmann line geometry is briefly introduced here.

A line vectors in 3-D space is ranked 1. The line vectors associated with either a pair of skew lines in 3-D space or a flat pencil of lines are ranked 2. The line vectors that are ranked 3 have four types of lines, Fig. 2.9

1. a regulus (3a);
2. the union of two flat pencils having a common line, but lying in distinct planes and with distinct centers (3b);
3. all lines through a point (3c); and
4. all lines in a plane (3d).

When the line vectors are ranked 4, they are called linear congruences and can be classified into four types, Fig. 2.9:

1. a linear spread generated by four skew lines (4a);

2. all the lines concurrent with two skew lines (4b);
3. a one-parameter family of flat pencils having one line in common and forming a variety (4c); and
4. all the lines in a plane or passing through one point in that plane (4d).

The line vectors ranked 5 are also called linear congruences and can be classified into two types, Fig. 2.9:

1. non-singular (or general): generated by five independent skew lines (5a); and
2. singular (or special): all the lines meeting a given line (5b).

2.5 Screw Dependency in Different Geometrical Spaces

In mechanism analysis, a problem often encountered is the evaluation of the dependency of some screws, including line vectors and couples in different geometrical spaces. This section discusses this issue.

2.5.1 Basic Concepts

Definition 2.1. Screw dependency: When n screws

$$\mathcal{S}_i = (\mathbf{S}_i; \mathbf{S}_i^o) \quad i = 1, 2, \dots, n$$

are linearly dependent, a set of non-zero numbers $\omega_i, i = 1, 2, \dots, n$, can be found to derive the following summation and hold

$$\sum_n \omega_i \mathcal{S}_i = 0 \quad (2.33)$$

When n screws satisfy Eq. (2.33), these screws are linearly dependent on the basis of the principle of screw sum, we have

$$\sum_n \omega_i \mathbf{S}_i = 0 \quad \text{and} \quad \sum_n \omega_i \mathbf{S}_i^o = 0 \quad (2.34)$$

Theorem 2.1. *Screw dependency is coordinate free.*

Proof: In coordinate system O , there are n screws $\mathcal{S}_i^O = (\mathbf{S}_i; \mathbf{S}_i^o), i = 1, 2, \dots, n$, which are linearly dependent. When the coordinate system moves from O to A , one of the above-mentioned screws becomes $\mathcal{S}_i^A = (\mathbf{S}_i; \mathbf{S}_i^A)$, where

$$\mathbf{S}_i^A = \mathbf{S}_i^o + \overline{AO} \times \mathbf{S} \quad (2.35)$$

The linear combination of screws in coordinate A is given by

$$\begin{aligned} \sum_n \omega_i \mathcal{S}_i^A &= \sum_n \omega_i \mathbf{S}_i + \in \sum_n \omega_i \mathbf{S}_i^A \\ &= \sum_n \omega_i t \mathbf{S}_i + \in \left[\sum_n \omega_i \mathbf{S}_i^o + \overline{A\mathbf{O}} \times \sum_n \omega_i \mathbf{S}_i \right] \end{aligned} \quad (2.36)$$

Substituting Eq. (2.34) into Eq. (2.36) yields

$$\sum_n \omega_i \mathcal{S}_i^A = 0 \quad (2.37)$$

Equation (2.37) indicates that the linear dependency of screws is coordinate free.

Using this theorem as basis, choosing a proper coordinate system is important in making the Plücker coordinate of a screw as simple as possible and facilitating the analysis of screw dependency. When an appropriate coordinate system is selected, the Plücker coordinates of a screw will have many zero elements, as shown in Fig. 1.5. The Plücker coordinates with many zero elements easily determine the dependency or reciprocity of a screw system.

When the Plücker coordinates of a screw are written as $(L, M, N; P, Q, R)$, the dependency of n screws can be determined by analyzing the rank of the Jacobian matrix below.

$$\mathbf{J} = \begin{bmatrix} L_1 & M_1 & N_1 & P_1 & Q_1 & R_1 \\ L_2 & M_2 & N_2 & P_2 & Q_2 & R_2 \\ \vdots & \vdots & \vdots & \vdots & \vdots & \vdots \\ L_n & M_n & N_n & P_n & Q_n & R_n \end{bmatrix} \quad (2.38)$$

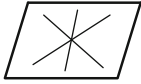
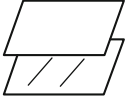
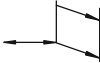
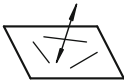
Because the Plücker coordinates of a screw have six components, the maximum number of linearly independent screws in 3-D space is six. A line vector also has six components, and the maximum number of linearly independent line vectors in 3-D space is also six.

2.5.2 Different Geometrical Spaces

The following section discusses the number of linearly independent line vectors and screws in different geometrical spaces, Table 2.1.

1. **Coaxial screws** Any two coaxial line vectors are always linearly dependent. The maximum number of linearly independent coaxial screws with different pitches ($\infty \neq h_i \neq 0$, $i = 1, 2$) is two.

Table 2.1 Screw dependency in different geometrical spaces

No.	Geometrical condition	Figure	Line vectors $h = 0$	Couples $h = \infty$
1.	Coaxial		1	1
2.	Coplanar and parallel		2	1
3.	Coplanar and concurrent		2	2
4.	Parallel in space		3	1
5.	Coplanar		3	2
6.	Concurrent in space		3	3
7.	Hyperboloid of one sheet		3	-
8.	(a) Normally intersecting at a common line		4	-
	(b) Have a common line		5	-
	(c) Have 2 common lines		4	-
	(d) Have 3 common lines		3	-
9.	Parallel a plane and no common normal		5	-
10.	Stewart platform rotates 90°		5	-
11.	3-D space		6	3
12.	Two parallel lines and a normal couple		2	-
13.	Three lines in a plane and a normal couple		3	-
14.	Three parallel lines and a normal couple		3	-

2. **Coplanar and parallel** When n screws with different pitches are coplanar and parallel, a coordinate frame O - XYZ can be established so that all the screws are on XY plane and parallel to X -axis. Thus, the screws have the form

$$S_i = (1 \ 0 \ 0; \ p_i \ 0 \ r_i), \quad i = 1, 2, \dots, n \tag{2.39}$$

where the fifth element is zero because the screw axis intersects at the Y -axis. The fourth element is non-zero because its pitch is non-zero, $h \neq 0$. Since p and r can be any real number, the maximum number of linearly independent screws is three. However, the maximum number of linearly independent line vectors is two because the pitch of a line vector is zero, $p = 0$.

3. **Coplanar and concurrent** When n screws with different pitches are coplanar and intersect at a common point, a coordinate frame O - XYZ can be established so that all the screws are in the XY plane and the origin is the intersecting point. Thus, all the screws have the following form

$$\mathcal{S} = (l_i \quad m_i \quad 0; \quad h_i l_i \quad h_i m_i \quad 0), \quad i = 1, 2, \dots, n \quad (2.40)$$

There are two zero elements; thus, the maximum number of linearly independent screws with different pitches is four. Conversely, the maximum number of linearly independent screws with identical pitch is only two. For line vectors being coplanar and concurrent under the above-mentioned coordinate system, all three rear elements in the Plücker coordinates are zero. Therefore, the maximum number of linearly independent line vectors is two.

4. **Parallel in space** When all n screws are parallel, (e.g., to the X -axis in space), all the second and third elements in the Plücker coordinates of the n screws are zero:

$$\mathcal{S} = (1 \quad 0 \quad 0; \quad h_i \quad q_i \quad r_i), \quad i = 1, 2, \dots, n \quad (2.41)$$

In the expression there are two elements are zero, it is ranked 4. For line vectors, the fourth element in the Plücker coordinates is also zero. Thus, the line vector is ranked 3. The presence of three common constraints for all the planar mechanisms is attributed to the aforementioned factors.

5. **Coplanar screws** When n screws with different pitches lie on the same plane (e.g., on the XY plane) and their third element of the Plücker coordinates is zero, \mathcal{J} is ranked 5. For the same coordinate system, the maximum number of linearly independent line vectors is three.
6. **Concurrent in space** The maximum number of linearly independent screws is six when all the screws are concurrent in space. Any screw with arbitrary pitch in space can be obtained by the linear combination of six linearly independent screws. When the concurrent point is selected as the origin, all the line vectors assume the following form

$$\mathcal{S}_i = (l_i \quad m_i \quad n_i; \quad 0 \quad 0 \quad 0) \quad (2.42)$$

The maximum number of linearly independent line vectors in 3-D space is three. When there are two sets of concurrent line vectors in 3-D space, the system is ranked 5 because two concurrent points can be connected by a line. Hence, n lines simultaneously meet a line.

7. **Line vectors lying on a hyperboloid** As analyzed in Sect. 2.3, the maximum number of linearly independent line vectors lying on the hyperboloid of one sheet is three.
8. **All the lines intersecting at a common line** Linear dependency is evaluated when all the screw axes intersect at one line. When two line vectors intersect, they are definitely reciprocal. The following conclusions can be derived on the basis of the theorem 2.3:

- (a) If all the lines are perpendicular to and intersect at a line (e.g., the Z-axis), their Plücker coordinates are as follows

$$\mathcal{S}_i = (l_i \quad m_i \quad 0; \quad p_i \quad q_i \quad 0), \quad i = 1, 2, \dots, n \quad (2.43)$$

where the third and sixth components are zero. The maximum number of linearly independent screws is four.

- (b) When all the line vectors simultaneously intersect at a line, the maximum number of linearly independent screws is five.
- (c) When all the line vectors simultaneously intersect at two lines, the maximum number of linearly independent screws is four.
- (d) When all the line vectors simultaneously intersect at three lines, the maximum number of linearly independent screws is three.
9. **All lines parallel to a plane and without a common normal** When all the screw axes are located on different parallel planes and have no common normal, one of the planes can be selected as the XY plane and the normal of those planes can be chosen as the Z-axis. The third elements of the Plücker coordinate of all screws are zero. The maximum number of linearly independent screws is five.
10. **3/6 or 6/6-Stewart mechanisms² rotate 90° about Z-axis** In this case, the mechanism is singular and six lines associated with six legs are linearly dependent. The six lines are ranked 5 [8].
11. **Couples only** For couples, the situation is simpler. Three independent couples are in 3-D space and two couples on the plane. There is only one independent couple when couples have an identical direction.
12. **Two parallel line vectors and a normal couple** There are three screws \mathcal{S}_1 , \mathcal{S}_2 , and \mathcal{S}_3 . The first two are line vectors and the third is a couple, which is normal to the plane determined by the first two axes, Fig. 2.10. The coordinate system is shown in the Fig. 2.10. The three screws can be expressed as

$$\begin{aligned} \mathcal{S}_1 &= (0 \quad 1 \quad 0; \quad 0 \quad 0 \quad 0) \\ \mathcal{S}_2 &= (0 \quad 1 \quad 0; \quad p \quad 0 \quad 0) \\ \mathcal{S}_3 &= (0 \quad 0 \quad 0; \quad 1 \quad 0 \quad 0) \end{aligned} \quad (2.44)$$

² 3/6-Stewart mechanism means its upper platform is a triangle and its lower one is a hexagon; similar for “6/6-”, the upper platform is also a hexagon.

Fig. 2.10 Two parallel line vectors and a normal couple

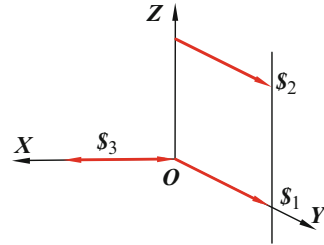
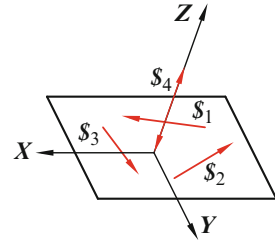


Fig. 2.11 Three coplanar line vectors and a normal couple



The screw system shows that they are linearly dependent and only two of them are linearly independent.

13. **Three coplanar line vectors and a normal couple** There are four screws $\$1$, $\$2$, $\$3$, and $\$4$. The first three line vectors are coplanar, whereas the fourth is a couple normal to the plane determined by the first three lines, Fig. 2.11. The four screws are expressed as follows

$$\begin{aligned}
 \$1 &= (l_1 \quad m_1 \quad 0; \quad 0 \quad 0 \quad r_1) \\
 \$2 &= (l_2 \quad m_2 \quad 0; \quad p \quad 0 \quad r_2) \\
 \$3 &= (l_3 \quad m_3 \quad 0; \quad 0 \quad 0 \quad r_3) \\
 \$4 &= (0 \quad 0 \quad 0; \quad 0 \quad 0 \quad 1)
 \end{aligned}
 \tag{2.45}$$

The four screws are linearly dependent and are ranked 3.

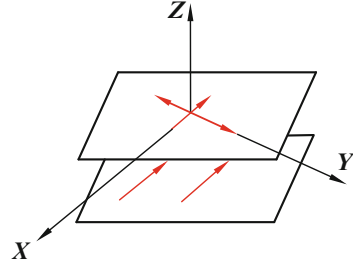
14. **Three parallel line vectors and a normal couple** There are four screws $\$1$, $\$2$, $\$3$, and $\$4$. The first three are parallel line vectors in space, whereas the fourth is a couple normal to the first three lines, Fig. 2.12. The screws are expressed as follows

$$\begin{aligned}
 \$1 &= (1 \quad 0 \quad 0; \quad 0 \quad 0 \quad 0) \\
 \$2 &= (1 \quad 0 \quad 0; \quad 0 \quad q_2 \quad r_2) \\
 \$3 &= (1 \quad 0 \quad 0; \quad 0 \quad q_3 \quad r_3) \\
 \$4 &= (0 \quad 0 \quad 0; \quad 0 \quad 1 \quad 0)
 \end{aligned}
 \tag{2.46}$$

The line vectors are linearly dependent and are ranked 3.

On the basis of the analysis above, we can determine the dependency of line vectors and couples for different geometrical spaces, Table 2.1.

Fig. 2.12 Three parallel line vectors and a normal couple



2.6 Reciprocal Screws

2.6.1 Concept of a Reciprocal Screw

Given a rigid body constrained by a revolute pair, the motion of the rigid body can be described by a screw

$$\omega\mathcal{S}_1 = \omega(\mathcal{S}_1; \mathcal{S}_{01}) = (\omega; v_0) \quad (2.47)$$

where ω is the angular velocity and v_0 denotes the velocity of a point coincident with the origin. Let us assume that the rigid body is subjected to a force screw

$$f\mathcal{S}_2 = f(\mathcal{S}_2; \mathcal{S}_{02}) = (f; C_0) \quad (2.48)$$

where f is the force and C_0 represents the moment to the origin.

The instantaneous work of force $f(\mathcal{S}_2; \mathcal{S}_{02})$ acting on the rigid body is equal to the sum of the work done by force f and couple C_0

$$P = f \cdot v_0 + \omega \cdot C_0 \quad (2.49)$$

On the other hand, from the reciprocal product of force and couple in Eq. (1.45), the following equation is derived:

$$\omega\mathcal{S}_1 \circ f\mathcal{S}_2 = f \cdot v_0 + \omega \cdot C_0 \quad (2.50)$$

By comparing Eqs. (2.49) and (2.50), the physical meaning of the reciprocal product of two screws is known as the instantaneous work of the force to the motion of the body. This physical meaning is important and useful in practice.

When the reciprocal product of the two screws is zero, we have

$$\omega\mathcal{S}_1 \circ f\mathcal{S}_2 = 0 \quad (2.51)$$

Equation (2.51) indicates that the force has imposed no work on the motion of the rigid body. Hence, regardless of how large the amplitude of the force is, no work is imposed on the body and the motion of the body cannot be modified by the force.

Table 2.2 Reciprocity conditions of two screws

 No. Reciprocity conditions of two screws

1. The necessary and sufficient condition for the reciprocity of two line vectors is they should be coplanar
 2. Two couples are always reciprocal
 3. Line vector and couple are reciprocal only when they are perpendicular
-

Definition 2.2. Reciprocal screw When the reciprocal product of two screws $\$1$ and $\$2$ is zero

$$\$1 \circ \$2 = 0 \quad (2.52)$$

the two screws are mutually reciprocal. $\$2$ is the reciprocal screw of $\$1$ and $\$1$ is the reciprocal screw of $\$2$. Generally, the reciprocal screw is denoted as $\r .

When two screws are reciprocal, one of them denotes the motion of a rigid body and the other denotes the constraint of the mechanical system acting on the rigid body. When one screw represents the constraint force, its reciprocal screw is the motion permitted by the mechanical system. From another point of view, if the reciprocal product of two screws is non-zero, non-zero work is indicated. Thus, the screw denoting the force is active and imposing work on the rigid motion.

Therefore, the reciprocal screw is an important and useful concept and tool for analyzing a mechanical system. Furthermore, when a screw system reflects the various motions of a body, its reciprocal screw system denotes the constraint screw system corresponding to limited motions and vice versa.

The expression of the reciprocal product of two screws being zero is in the form

$$\$1 \circ \$2 = 0 \quad (2.53)$$

The reciprocal product can also be expressed as

$$l_1 p_2 + m_1 q_2 + n_1 r_2 + p_1 l_2 + q_1 m_2 + r_1 n_2 = 0. \quad (2.54)$$

When the pitches of two screws are non-zero, the reciprocal product can be expressed as [1]

$$(h_1 + h_2) \cos \alpha_{12} - a_{12} \sin \alpha_{12} = 0 \quad (2.55)$$

where h_1 and h_2 are the pitches of the two screws, a_{12} is the perpendicular distance between the two screws, and α_{12} denotes the twist angle between the two screws. From Eq. (2.55), the following theorem is formulated:

Theorem 2.2. *The reciprocity of two screws is coordinate free.*

According to Eq. (2.55), two line vectors ($h_1 = h_2 = 0$) are reciprocal when they are coplanar. Two screws with any pitch values are reciprocal if they are perpendicular because $\alpha_{12} = 90^\circ$ and $\cos \alpha_{12} = 0$. Table 2.2 enumerates the conditions of two reciprocal screws.

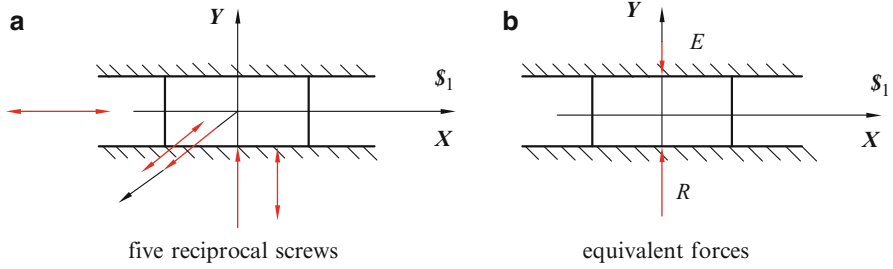


Fig. 2.13 Reciprocal screws acting on a slider (a) Five reciprocal screws (b) Equivalent forces

2.6.2 Dualism in the Physical Meaning of Reciprocal Screws

In terms of physical meaning, reciprocal screws have dual physical connotations. First, reciprocal screws can be interpreted as constrained displacements or the mobility of a rigid body.

Example 2.2. Figure 2.13a illustrates a slider inside a slideway. The motion of the slider can be expressed as a screw

$$\mathcal{S}_1 = (0 \ 0 \ 0; \ 1 \ 0 \ 0) \quad (2.56)$$

The screw has five reciprocal screws

$$\begin{aligned} \mathcal{S}_1^r &= (0 \ 1 \ 0; \ 0 \ 0 \ 0) \\ \mathcal{S}_2^r &= (0 \ 0 \ 1; \ 0 \ 0 \ 0) \\ \mathcal{S}_3^r &= (0 \ 0 \ 0; \ 1 \ 0 \ 0) \\ \mathcal{S}_4^r &= (0 \ 0 \ 0; \ 0 \ 1 \ 0) \\ \mathcal{S}_5^r &= (0 \ 0 \ 0; \ 0 \ 0 \ 1) \end{aligned} \quad (2.57)$$

The five reciprocal screws have various physical meanings. First, the five reciprocal screws indicate that the mechanical system exerts five constraints or limiting conditions to the slider. The first two constraint forces limit two translations along Y - and Z -axes of the rigid body. The last three reciprocal screws with infinite pitches limit three rotations about X -, Y - and Z -axes, where the red arrow indicates the reciprocal force acting on the slider and the bi-directional arrow denotes the constraint couple, Fig. 2.13. Thus, the five reciprocal screws represent the limited motions of the rigid body. In addition, the screws cannot be linearly combined because each reciprocal screw has its own special meaning and is not a real force.

Second, each reciprocal screw can express a constraint force if its pitch is zero or a constraint couple if its pitch is infinite. The five reciprocal screws indicate that three constraint couples and two constraint forces act on the slider. In practice, however, real constraint forces acting on the slider depend completely on the force equilibrium

Table 2.3 Symbols for kinematic screws and constraint screws

Arrows	Moving screw	Constraint force	Constraint couple	Rotation axis	Translation direction	Screw motion
Expression	Black arrow	Red arrow	Red bi-directional arrow	Red hollow arrow	Red hollow bi-directional arrow	Red double arrow
Symbol						

of the slider. All simultaneous external forces should be considered. For instance, if there is an external force E acting on the slider, Fig. 2.13b, only one reaction force R exists, which is only one of the five reciprocal screws. If no external force acts on the slider and the deadweight is disregarded, no real reactions occur despite the presence of the five reciprocal screws. Therefore, the reciprocal screw may be used to express the reactions applied to the rigid body, and the real forces depend completely on the force equilibrium of that body. Reciprocal forces can therefore be combined and decomposed.

For the convenient analysis of screws and their reciprocal screws, the symbols in Table 2.3 are used.

2.7 Reciprocal Screw System

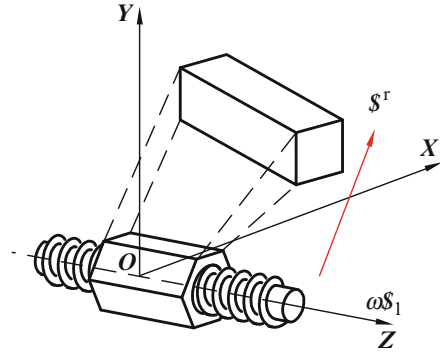
A screw pair \mathcal{S}_1 connects a rigid body to the frame, and the rigid body has one degree of freedom, Fig. 2.14. As the rigid body is constrained, it can only twist about \mathcal{S}_1 . If the angular velocity is ω_1 , the moving screw is expressed as $\omega\mathcal{S}_1$. Another force screw $f\mathcal{S}^r$ acts on the body with Plücker coordinates of $(L^r, M^r, N^r, P^r, Q^r, R^r)$. If the force screw is also the reciprocal screw of moving screw $\omega\mathcal{S}_1$, the following expression is obtained:

$$L_r P^r + M_1 Q^r + N_1 R^r + P_1 L^r + Q_1 M^r + R_1 N^r = 0 \tag{2.58}$$

When moving screw $\omega\mathcal{S}_1$ is known, the reciprocal force screw can be solved by this equation.

There are six elements in the Plücker coordinate; thus, there are ∞^5 reciprocal screws to a moving screw in 3-D space. However, this study is focuses only on linearly independent solutions. When some unit screw \mathcal{S}^r is one of the solutions, all screws $\lambda\mathcal{S}^r$ become solutions, where λ can be of any value. Because they are linearly dependent, there are ∞^4 unit reciprocal screws.

Fig. 2.14 Reciprocal screw



From linear algebra theory, a set of homogeneous equations has n unknowns and the rank of the coefficient matrix is r . When $r=n$, the equation has a unique zero solution. When $r < n$, the equation has infinite solutions. In the infinite solutions, the maximum linearly dependent number is $n-r$. The $n-r$ linearly independent screws form the basic solution system. Hence, the summation of the ranks of a screw system and its reciprocal screw system is six.

Theorem 2.3. The summation of the ranks of the screw system and its reciprocal screw system is six.

Consider a linear equation for a single kinematic screw ωS_1 as shown in Eq. (2.58). The linear equation is ranked 1 and the number of unknowns is six. Thus, the basic solution system of the equation should contain five screws, indicating that five screws are reciprocal to screw ωS_1 .

Example 2.3. Rotational body

In Fig. 2.15, a rigid body 2 is connected to a rigid body 1 by a revolute pair S_1 . The S can be expressed as

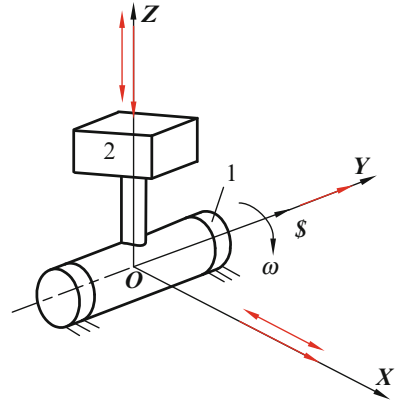
$$S = (0 \quad 1 \quad 0; \quad 0 \quad 0 \quad 0). \tag{2.59}$$

Using Eq. (2.58), five linearly independent reciprocal screws can be found:

$$\begin{aligned} S_1^r &= (1 \quad 0 \quad 0; \quad 0 \quad 0 \quad 0) \\ S_2^r &= (0 \quad 1 \quad 0; \quad 0 \quad 0 \quad 0) \\ S_3^r &= (0 \quad 0 \quad 1; \quad 0 \quad 0 \quad 0) \\ S_4^r &= (0 \quad 0 \quad 0; \quad 1 \quad 0 \quad 0) \\ S_5^r &= (0 \quad 0 \quad 0; \quad 0 \quad 0 \quad 1) \end{aligned} \tag{2.60}$$

The five reciprocal screws are linearly independent and any other reciprocal screw is the linear combination of the five screws. The first three screws S_1^r , S_2^r , and S_3^r are constraint forces with zero pitch along the X-, Y-, and Z-axes, respectively. They denote that the mechanical system constrains the translation of the rigid body along X-, Y-, and Z-axes. The rigid body loses three translational freedoms. The last two

Fig. 2.15 Rotational body



reciprocal screws $\$4$ and $\$5^r$ with infinite pitch constrain two rotational motions of the rigid body about X - and Z -axes, and the body loses two rotational freedoms. The five screws indicate that the rigid body is allowed to rotate only about Y -axis and has only one freedom.

2.8 Reciprocal Screw and Constrained Motion

For a motion screw system, a reciprocal screw system exist and constrains the motions of the body while the body retains some remaining and permitting freedoms. This section discusses the relationship between the reciprocal screw and permitting freedoms.

Example 2.4. A ball rolls on a plane

When a ball rolls on a plane, the plane exerts a zero-pitch constraint force $\$1^r$ to the ball, Fig. 2.16

$$\$1^r = (0 \ 0 \ 1; \ 0 \ 0 \ 0) \tag{2.61}$$

The ball clearly loses a translational mobility along the Z -axis because after translation along this axis, the kinematic pair is broken and prohibited.

The ball still has two translational and three rotational freedoms (i.e., translations along X - and Y -axes and rotations about X -, Y -, and Z -axes). Translation along any direction in the plane is permitted. For example, a permitted motion screw exists in the form

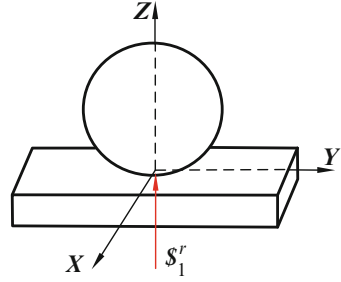
$$\$1^m = (0 \ 0 \ 0; \ d_1 \ e_1 \ 0) \tag{2.62}$$

because it satisfies the condition

$$\$1^m \circ \$1^r = 0, \tag{2.63}$$

where the elements d_2 and e_1 can be of any value.

Fig. 2.16 A ball rolls on a plane



Although the ball has three rotational freedoms, the rotational axis cannot be arbitrarily selected and should strictly satisfy the relationship $\mathcal{S}_2^m \circ \mathcal{S}_1^r = 0$.

$$\mathcal{S}_2^r = (a_2 \quad b_2 \quad c_2; \quad d_2 \quad e_2 \quad 0) \tag{2.64}$$

where the five parameters a_2, b_2, c_2, d_2 , and e_2 can be arbitrarily selected. However, they need to satisfy the line vector condition. The elements a_2, b_2 , and c_2 , cannot be zero simultaneously, and d_2 and e_2 should satisfy the zero-pitch condition. That is,

$$a_2 + b_2 + c_2 \neq 0; \quad a_2d_2 + b_2d_2 = 0 \tag{2.65}$$

From the geometrical point of view, the possible line vectors denoting the permitted rotational axes should intersect at reciprocal screw \mathcal{S}_1^r . Otherwise, no line vectors function as the rotational axes.

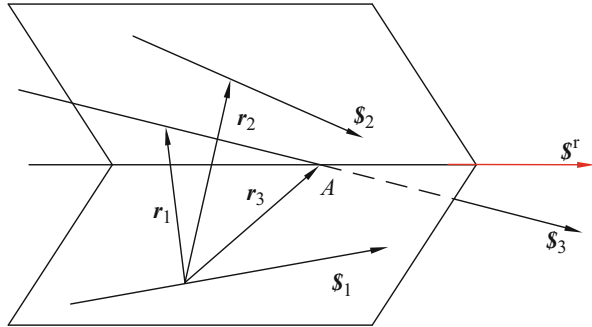
If two reciprocal forces with zero pitch act on a rigid body, all the axes of the rotational screws of the rigid body should simultaneously intersect at the two reciprocal screws. Similarly, if three reciprocal screws act on a body, the permitted rotational axes have to simultaneously cross the three reciprocal screw axes. Can a line be found intersecting at three lines? This is the general case for a rigid body subjected to three constraint forces. This case is discussed further.

2.8.1 Three Skew Lines in Space

Consider a rigid body subjected to three reciprocal screw forces $\mathcal{S}_1^r, \mathcal{S}_2^r$ and \mathcal{S}_3^r . That is, the rigid body is subjected to three physical constraints from the mechanical system and loses three freedoms. The three constraints are distributed differently in 3-D space; thus, they have different effects on the rigid body. If the three constraint forces are linearly independent, the three translational freedoms are constrained and the rigid body has only three rotational freedoms.

As previously mentioned, the constraint force not only limits translational freedom but also influences rotational freedom given that the rotational axis has to pass the axis of the constraint force. Hence, the rotational axes have to be coplanar with each

Fig. 2.17 Screw reciprocal three screws



constraint force. When three constraint forces act on the rigid body, the only possible rotational axes are the lines simultaneously intersecting at the three forces.

Infinite lines are to be able to intersect at the three forces in space. Two methods can be used to solve this problem.

When three line vectors are expressed as $(S_1; S_{01}), (S_2; S_{02})$, and $(S_3; S_{03})$, the line intersecting at the three line vectors is $(S; S_0)$ and satisfies

$$S \circ S_i^r = 0 \quad i = 1, 2, 3 \tag{2.66}$$

The unknown screw can be simultaneous solved by three equations and there are infinite solutions.

From a geometrical perspective, Fig. 2.17, a line intersecting at three skew lines is easily found.

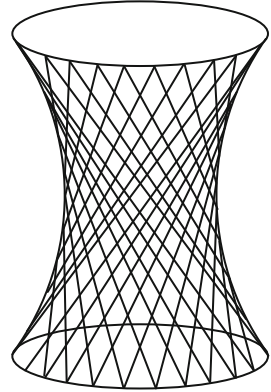
Consider three skew lines in space, Fig. 2.17. The origin is selected on the first line $S_1(S_1; 0)$ and a point A is selected from the third line. Point A and two lines $S_1(S_1; S_{01})$ and $S_2(S_2; S_{02})$ form two planes. Evidently, the intersecting line of the two planes has to meet the third line; that is, the intersecting line passes three lines S_1^r, S_2^r and S_3^r . The intersecting line is only the reciprocal screw of the three screws. Point A is arbitrarily selected in $S_1(S_1; 0)$ and different selected points correspond to different reciprocal screw. Thus, infinite reciprocal screws are obtained. Generally, the three reciprocal screw axes are skewed in space. Hence, the three translational freedoms are constrained and the body has only three rotational freedoms. However, any rotational axis has to meet the three lines.

All the lines that can intersect at three given lines S_1^r, S_2^r and S_3^r form a hyperboloid of one sheet, Fig. 2.18, where two reguluses cover the entire surface of the hyperboloid of one sheet, and the two reguluses are mutually reciprocal. One line in a regulus has to intersect at all the lines in the other regulus, and vice versa.

2.8.2 Three Lines Parallel to a Plane Without a Common Normal

When three lines lie on three parallel planes, they constrain two translations along two directions in the parallel plane. Meanwhile, the linear combination of

Fig. 2.18 Regulus in a hyperboloid



three constraint forces forms a unique constraint couple [9, 10], and constrains a rotational freedom. In this case, the rigid body has three freedoms including a translation along the normal of the planes and two rotational freedoms, whose rotational axes have to intersect at all the three force axes.

2.8.3 Three Non-concurrent Coplanar Lines

Three non-concurrent coplanar lines limit two translational freedoms that are parallel to the plane, and a rotational freedom along the normal of the plane. They permit the body to translate along the normal of the plane and rotate about any axis in the plane.

2.8.4 Three Coplanar and Concurrent Line Vectors

The three line vectors are linearly dependent and belong to rank 2. Thus, two translational freedoms with directional lines on the plane are constrained and the rigid body has four degrees of freedom, including the translation along the normal of the plane and three rotational freedoms whose axes pass the intersecting point of the three forces.

2.8.5 Three Line Vectors Concurrent in Space

The body loses three translational freedoms and gains three rotational freedoms. However, any axis has to pass the intersecting point of the three forces.

2.8.6 Three Line Vectors Parallel in Space

The body loses a translational freedom and two rotational freedoms. Translation can occur along two directions normal to the forces and rotate about the axes parallel to the constraint forces.

References

1. Ball R (1900) A treatise on the theory of screws. Cambridge University Press, Cambridge
2. Hunt KH (1978) Kinematic geometry of mechanisms. Oxford University Press, Oxford
3. Phillips J (1984) Freedom in machinery. Cambridge University Press, Sydney
4. Tsai MJ, Lee HW (1993) On the spatial bases of two- and three-screw systems. *ASME J Mech Des* 115:540–546
5. Zhang WX, Xu ZC (1998) Algebraic construction of the three-system of screw. *Mech Mach Theory* 33(7):925–930
6. Huang Z, Wang J (2001) Identification of principal screws of 3-DOF parallel manipulators by quadric degeneration. *Mech Mach Theory* 36(8):893–911
7. Merlet J-P (1989) Singular configurations of parallel manipulator and Grassmann geometry. *Int J Rob Res* 8(5):45–56
8. Huang Z, Qu YY (1987) The analysis of the special configuration of the spatial parallel manipulators. In: The 5th national mechanism conference, Lu Shan, China, pp 1–7
9. Huang Z, Kong LF, Fang YF (1997) Mechanism theory of parallel robotic manipulator and control. China Mechanical Press, Beijing (in Chinese)
10. Huang Z, Zhao YS, Zhao TS (2006) Advanced spatial mechanism. Higher Education Press, Beijing (In Chinese)

Chapter 3

Mobility Analysis Part-1

One of the most basic topics in the field of mechanism is to obtain the number of degrees of freedom (DOF), namely, the mobility of a mechanism. The most well-known formula for mobility analysis is the Grübler–Kutzbach criterion (G-K criterion). This criterion is based on simple arithmetic and can be successfully used in analyzing almost all planar and some spatial mechanisms. Hence, it became very popular and is currently used by a great number of engineers. However, the G-K criterion fails to analyze many over-constrained mechanisms. Recently, lower-mobility parallel manipulators with various merits have attracted many researchers. Given that most of these mechanisms are over-constrained, the G-K criterion fails to analyze them. Hence, mobility analysis becomes a critical issue. Looking for a unified mobility formula has been one of the hot points in mechanical engineering for about 150 years, and is an open issue up to the present. In the current and subsequent Chapters, a mobility principle based on the screw theory and modified G-K formulas is introduced. Many classical and modern PMs are analyzed by the mobility principle. All the works indicate that the mobility principle is really unified.

3.1 The Concept and Definition of Mobility

Degree of freedom, also known as mobility, is defined by the IFToMM (International Federation for the Promotion of Mechanism and Machine Science) in *Terminology for the Theory of Machines and Mechanisms* in 1991 (MMT 1991, 26(5): 450) and in 2003 (MMT 1991, 26(5): 450) as¹:

Degree of freedom [mobility] of a kinematic chain or a mechanism: Number of independent coordinates needed to define the configuration of a kinematic chain or mechanism.

¹ The first edition of the IFToMM standard terminology was published in MMT, 18(6) in 1983.

Mechanical engineering developed rapidly over the past half century after World War II. The mechanism evolved from planar to spatial, single-degree to multi-freedom, single-loop to multi-loop, serial-robot to parallel-robot, lower speed to high speed, and rigid to flexible. New challenges and opportunities require the mechanism theory to keep pace with the times. For instance, a great number of multi-DOF over-constrained new mechanisms have appeared. To use these mechanisms, engineers must first know their mobility, including the number of degrees of freedom and properties such as rotation, translation, or a combination of both. However, the traditional definition of mobility given by IFToMM only involves the number of DOF, which is inadequate in practice. In view of this, we believe that the definition of mobility should be revised into a more comprehensive and integrated concept.

Definition 3.1. Degree of Freedom or Mobility: The stably independent motion capability of a mechanism or kinematic chain is defined as its degree of freedom or mobility. This capacity includes the following three aspects:

1. In magnitude, this capacity represents the number of independent coordinates needed to define the configuration of a kinematic chain or mechanism;
2. In property, this capacity represents the mobility to be rotational or translational; to be full and continuous airspace or to be discrete; with determined or undetermined rotational axes; (the last one will be explained later); and
3. The mobility in space-time is instantaneous or full-cycle.

The “stably” in the definition means that the magnitude and property all have a stably finite motion area and that the area is not infinite or discrete. In this case, the mobility is full-cycle. The mobility, which only exists on an infinitesimal area, is not the mobility of mechanism that we recognize.

In this chapter, the second and third items are proposed for spatial multi-mobility mechanisms and parallel mechanisms. Different mobility mechanisms have different applications. For example, some printer localizers need to use a planar two-dimension translation mechanism only; the space localizer needs a three-dimension translation mechanism; a Robot SCARA needs three-D translation and one-D rotation space mechanism; a weld robot needs three-translational and two-rotational kinematic capacities, etc.

The parallel mechanisms can be classified by its mobility property. For example, the two-DOF PMs can be classified into three categories: RR, TT, and RT, where R denotes rotational freedom and T denotes translational freedom. This means that the output link of the two-DOF PM may have two rotational freedoms, two translational freedoms or one rotational, and one translational freedom, respectively.

For spatial mechanisms, there are 12 kinds of freedom by mobility property, as shown in Table 3.1.

In practice, the mobility property can be divided into a more detailed manner. For instance, based on the axis direction of rotation about and translation along when a mechanism has two freedoms including one rotation and one translation, the mobility can be divided into two different cases: the two axes are coincident or perpendicular. But the text does not discuss these further.

Table 3.1 Classification of mobility

No.	Number of mobility	Mobility property
1	2	RR, TT, RT
2	3	RRR, TTT, RRT, TTR
3	4	RRRT, TTTR, RRRT
4	5	RRRTT, TTTRR

The mobility property includes the screw motion, but it is not considered here
 R denotes rotational mobility, T denotes translational mobility

3.2 Mobility Open Issue

3.2.1 Grübler-Kutzbach Criterion

Obtaining the number of degrees of freedom (DOF), also known as mobility for a mechanism, is one of the most basic topics in the field of mechanism.

To analyze the mobility of mechanisms, the Grübler–Kutzbach Criterion (G–K formula), which was proposed initially by Grübler and developed by Kutzbach, is used. This criterion, which is based on a simple arithmetic, is successful in analyzing almost all of the planar mechanisms and some spatial mechanisms. Hence, the criterion has become very popular, and a great number of engineers use it in practice. For planar mechanisms, the G–K formula is in the form of

$$M = 3(n - 1) - 2p_L - P_H$$

or

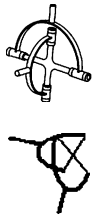
$$M = 3(n - g - 1) + \sum f_i \quad (3.1)$$

For spatial mechanisms, it is

$$M = 6(n - g - 1) + \sum f_i \quad (3.2)$$

However, the G–K Criterion failed to analyze a number of over-constrained mechanisms. For example, in 1978, Suh and Radcliffe wrote in their book [1], “*In certain cases the answers obtained using the G–K Criterion can be misleading.*” The authors particularly illustrated this assertion using the Bennett mechanism, as well as the Goldberg, Bricard, Sarrus, and Franke mechanisms. Thus, these mechanisms were called “Maverick mechanisms” or “Paradoxical mechanisms.” In 1999, Tsai emphasized, “It should be noted that there are mechanisms that do not obey the Grübler criterion. Those mechanisms that require special link lengths to achieve mobility are called over-constrained mechanisms.” In 2000, Merlet [2] contended, “The use of this strictly combinational formula can sometimes lead to mistakes because it does not take the geometric relations between the joints into consideration.”

Table 3.2 Kinematic pairs and their screw expressions

Kinematic Pair	Sign	Mobility	Screw
Revolute (R)		1	$\$R_1 = (1 \ 0 \ 0; \ 0 \ 0 \ 0) \quad h = 0$
Prism (P)		1	$\$P_1 = (0 \ 0 \ 0; \ 1 \ 0 \ 0) \quad h = \infty$
Screw (H)		1	$\$H_1 = (1 \ 0 \ 0; \ h_1 \ 0 \ 0) \quad h = \text{constant}$
Cylinder (C)		2	$\$C_1 = (1 \ 0 \ 0; \ 0 \ 0 \ 0) \quad h = 0$ $\$C_2 = (0 \ 0 \ 0; \ 1 \ 0 \ 0) \quad h = \infty$
Universal (U)		2	$\$U_1 = (1 \ 0 \ 0; \ 0 \ 0 \ 0) \quad h = 0$ $\$U_2 = (0 \ 1 \ 0; \ 0 \ 0 \ 0) \quad h = 0$
Flat (E)		3	$\$E_1 = (0 \ 0 \ 0; \ 1 \ 0 \ 0) \quad h = \infty$ $\$E_2 = (0 \ 0 \ 0; \ 0 \ 1 \ 0) \quad h = \infty$ $\$E_3 = (0 \ 0 \ 1; \ 0 \ 0 \ 0) \quad h = 0$

Sphere (S)		3	$\$S_1 = (1 \ 0 \ 0; \ 0 \ 0 \ 0) \ h=0$ $\$S_2 = (0 \ 1 \ 0; \ 0 \ 0 \ 0) \ h=0$ $\$S_3 = (0 \ 0 \ 1; \ 0 \ 0 \ 0) \ h=0$
Hole-cylinder (K)		3	$\$S_1 = (S_1; 0) = (1 \ 0 \ 0; \ 0 \ 0 \ 0) \ h=0$ $\$S_2 = (S_2; 0) = (0 \ 1 \ 0; \ 0 \ 0 \ 0) \ h=0$ $\$S_3 = (0; S_3) = (0 \ 0 \ 0; \ 0 \ 0 \ 1) \ h=\infty$
Sphere-hole (Q)		4	$\$S_1 = (S_1; 0) = (1 \ 0 \ 0; \ 0 \ 0 \ 0) \ h=0$ $\$S_2 = (S_2; 0) = (0 \ 1 \ 0; \ 0 \ 0 \ 0) \ h=0$ $\$S_3 = (S_3; 0) = (0 \ 0 \ 1; \ 0 \ 0 \ 0) \ h=0$ $\$S_4 = (0; S_4) = (0 \ 0 \ 0; \ 0 \ 0 \ 1) \ h=\infty$

The most famous counter-examples are Cardan's joint, and Bennett and Goldberg's mechanisms. In 2004, Waldron analyzed mobility and pointed out that [3] "there is no way to derive information about the linkage without performing a complete position analysis."

Much important progress concerning mobility analysis has been made by many researchers, including Chebychev (1854) [4], Grübler (1883) [5], and Hochman [6] in the nineteenth century. In the twentieth century, among the researchers who attained such progress were Grübler [7]; Kutzbach (1929) [8]; Dobrovolski [9]; Artobolevski [10]; Hunt and Phillips (1965) [11]; Hunt [12]; Hervé [13]; Waldron (1966) [14]; Bagci (1971) [15]; Freudenstein and Alizade (1975) [16]; Hunt (1978) [17]; Hervé (1978) [18]; Baker (1980) [19]; Davies (1983) [20]; Zhang (1984) [21]; Angeles and Gosselin (1988) [22]; Alizade (1988) [23]; Huang (1991, 1997) [24, 25]; Tsai (1999) [26]; and McCarthy (2000) [27].

Recently, the parallel manipulators, especially the lower-mobility parallel mechanisms, gain a lot of merits and have attracted many researchers. Hunt [12] proposed a 3-DOF 3-RPS manipulator. Gosselin and Angeles [28] studied the 3-DOF spherical parallel manipulator. Pierrot et al. (1999) [29] studied H4 mechanism, Wenger and Chablat (2000) [30] proposed Orthoglide-type mechanisms. Kim and Tsai [31] proposed a 3-DOF translational cartesian parallel manipulator. Hervé and Sparacino [32] proposed a 3-DOF 3-RRC translational manipulator. Clavel invented the famous Delta robot [33]. Kong and Gosselin [34] analyzed the mobility by screw theory. In 2000, Zhao and Huang [35] proposed the first symmetrical 4-DOF 4-URU manipulator. In 2001, Huang and Li [36] invented two symmetrical 5-DOF parallel manipulators. Carricato and Parenti-Castelli [37] also proposed a new mechanism. Since most of these mechanisms are over-constrained, the G-K criterion still fails to analyze them. To determine the mobility of these mechanisms, many researchers adopted different methods, aside from a unified formula. Sometimes a prototype mechanism should be built to check whether the design is right or not, which is time-consuming and costly. Therefore, it would be of great significance to establish a valid and unified mobility criterion for all mechanisms.

3.2.2 Mobility Open Issue

In 2005, reference [38] systematically enumerated a great number of so-called puzzle and paradoxical mechanisms, which were divided into classical mechanisms and modern parallel mechanisms, as shown below.

Classical mechanisms: Altman [39], Baker [40, 41], Bennett [42], Bricard [43], Delassus [44–46], Eckhardt [47], Goldberg [48], Hervé [49, 50], Mabie [51], Myard [52], Myszka [53], Norton [54], Phillips [55, 56], Roberval [57], Sarrus [58], Waldron [59]

Modern parallel mechanisms: Carricato, CPM [60], Delta [61], H4, Kong and Gosselin [62], Orthoglide [63], Star [64], Gogu [65], etc.

These mechanisms are all over-constraint and hence cannot be solved by a unified formula, including the G-K formula. Thus, many formulas have been proposed but none of these are recognized to be universal by this community and the engineering community. This is the most significant problem our community faces until now, in the beginning of the twenty-first century. Therefore,

1. It is very important to find a general and universal mobility formula that can suit any mechanism, including planar and spatial, serial and parallel, single-loop and multi-loop, normal and over-constraint, etc., or at least suit all the classical and modern parallel mechanisms enumerated above [38].
2. The mobility analysis should also be able to estimate the mobility properties.
3. In the meantime, it is considered that the mobility analysis is a very practical technique in engineering, and that it is the basic and the first step operation in every mechanical design that all engineers face frequently. Thus, the mobility principle should be simple and easy to understand for engineers.

From the analysis above, this event can be called a “*mobility open issue*” (MOI).

Recently, many researchers made great efforts and have been continuously proposing a number of novel mobility methods. For example, Rico et al. (2003) [66] discussed this topic using group theory and Lie algebra. Kong and Gosselin [67] presented a mobility method. Zhao (2004) [68] discussed mobility also using the screw theory. Alizade and Bayram (2004) [69] proposed a new method. Gogu [70] suggested using the method of linear transformations. Shukla and Whitney [71] also proposed a new method for mobility analysis; Wampler and Larson (2007) [72] proposed a method. In 2007 Rico et al. [73] as well as Müller (2009) [74], Yang (2008) [75], and Zhang (2010) [76] discussed mobility. Almost all of these authors claimed that their formulas are universal.

The real validity and significance of any mobility formula can only be recognized after the formula is applied successfully to all MOI’s paradoxical mechanism as a unified formula and generates correct results. The paradoxical mechanisms include the modern parallel manipulators and the classical mechanisms, including the three mechanisms pointed out by Merlet [3] in 2000. Merlet wrote, “The most famous counter-examples are Cardan’s joint, and Bennett and Goldberg’s mechanisms.”

More mechanisms could be explained or forecasted using a mobility criterion, which proves to be reasonable under the current cognitive level. Nevertheless, to our knowledge, no other methods have been used to approach this aim up to now.

3.3 Mobility Principle Based on Reciprocal Screw

3.3.1 Mechanism Can Be Expressed as a Screw System

Spatial mechanism consists of links and kinematic pairs. All kinematic pairs can be expressed as different screws, as follows: the revolute pair can be denoted by a screw with zero-pitch, $h = 0$, also known as a line vector; the prismatic pair is a

screw with infinite-pitch, $h = \infty$, also known as a couple; the screw pair has a non-zero finite pitch; the cylindrical pair is equal to the combination of a revolute pair and a translational pair; and the spherical pair is the combination of three rotation pairs. Therefore, a kinematic chain and mechanism can be expressed as a screw system, and their kinematics can be analyzed using screw theory. All kinematic pairs are expressed in the following table 3.2.

3.3.2 Development of Our Unified Mobility Principle

In 1991, using screw theory, Huang [24] first defined the common constraint of a mechanism as a screw reciprocal to the screw system spanned by unit screws associated with all kinematic pairs in the mechanism. Then, he defined the “order” of a mechanism as the number of independent screws reciprocal to the common constraint screw. These definitions are conveniently applicable to single-loop mechanism and closed-loop mechanism. In fact, in Huang’s book [24], the mobility of a four-bar linkage and the freedoms of output links of some mechanisms were discussed. The mobility of many single-loop spatial mechanisms can be directly solved using these two concepts. The main feature of Huang’s definition is the application of reciprocal screw, which is also the principal difference with other methods based on screw theory. Then, in 1996 [79, 80], the mobility of some parallel mechanisms was discussed using reciprocal screw theory, wherein Hunt’s 3-RPS parallel mechanism was also used as an example to show this method.

In 1997, Huang et al. [25] further redefined the concept of “redundant constraint,” which appeared frequently in parallel mechanisms. The above investigation then led to “the mobility principle based on constraint screws,” wherein the mobility of an over-constrained 3-RRRH parallel mechanism was obtained correctly. Subsequently, a “*Modified Grübler–Kutzbach criterion*” (Modified G–K criterion), Equation (26) in ref. [25], was given as

$$M = \sum_{i=1}^g f_i - dl + I \quad (3.3)$$

where d is the order of the mechanism, and $d = 6 - \lambda$ where λ is the common constraint of that mechanism, and I is the virtual constraint after deducting the common constraint.

In 2003, the Modified Grübler–Kutzbach criterion, Eq. (3.5), ([81] Eq. (4)), was proposed by Huang and Li. This can be derived directly from Eq. (3.3) and is identical to Eq. (3.3). The aim of transferring Eq. (3.3) to Eq. (3.5) is that people are more familiar with the latter form.

In 2006, Dai, Huang, and Lipkin [80] further demonstrated theoretically the mobility method based on screw theory. In [79, 81–85], many modern parallel mechanisms in MOI are analyzed, including DELTA, CPM, H4, 3-CRR, Orthoglide,

Star, Carricato, and Cardan. In [86], for the first time, a breakthrough to obtain the mobility of the most difficult Bennett mechanism by our mobility formula using reciprocal screw was achieved. Regretfully, in that article [86], the full-cycle mobility was not demonstrated. Therefore, a complement article [87], published in 2006, demonstrated the reason for the full-cycle mobility of Bennett mechanism, although only one sentence was added. In the same year, based on the analysis of Bennett, another difficult mechanism, Goldberg, was discussed in [88].

Until 2009, almost all of the MOI's classical mechanisms were solved; in 2011, a book entitled *About the mobility of mechanisms* was published. This book summarizes our mobility principle and the procedures to solve all of the MOI's classical mechanisms as well as modern parallel mechanisms [89].

As mentioned above, we have dealt with this 150-year MOI for about 20 years since 1991. The basic principle of mobility analysis based on reciprocal screw theory was proposed at 1997. Throughout history, some methods are based on screw theory; however, our method is based on reciprocal screw, and some technical operations are used to facilitate our method.

In this chapter, the Modified G-K Criterion is regarded as a methodology instead of only a single formula. It consists of the Modified G-K formula and some other key techniques, including the identification of redundant-constraint, the choice of reference frame, the judgment of the instantaneous or full-cycle mobility, and the disposal of the closed-loop chain in limb for a complex mechanism, etc.

It should be noted that many methods for mobility analysis are based on a simple idea, i.e., the mobility of a mechanism equals the total number of degrees-of-freedom of links minus the sum of constraints produced by all kinematic pairs, and then plus the number of redundant constraints. Therefore, these formulas have no essential differences although they appear in different forms, and most of them can even be transformed easily from one to another. However, the big and essential difference among them is the process of identifying the redundant constraints.

3.3.3 The Modified G-K Formulas

1. Considering a lot of scholars and engineers are familiar with the G-K criterion, in the beginning of the new century, for the convenience of readers, the Modified G-K formula was rewritten in this form

$$M = 6(n - g - 1) + \sum_{i=1}^g f_i + \mu \quad (3.4)$$

where M is the mobility of a mechanism, n is the number of links including frame, g is the number of kinematic pairs, f_i is the freedom of the i th kinematic pair, and μ is the total number of the over-constraints of the mechanism.

2. Another form of the Modified G-K formula, considering the common constraint, is

$$M = d(n - g - 1) + \sum_{i=1}^g f_i + v \quad (3.5)$$

where d is the order of a mechanism and related to common constraint, and $d = 6 - \lambda$, where λ is the number of common constraint, and v is the parallel constraint, which is also called virtual constraint, for a single-loop mechanism $v = 0$. The result of Eq. (3.5) is the mobility of the output platform of the parallel mechanism. In the meantime, we can transform Eq. (3.5) into

$$\begin{aligned} M &= d(n - g - 1) + \sum_{i=1}^g f_i + v \\ &= (6 - \lambda)(n - g - 1) + \sum f_i + v \\ &= 6(n - g - 1) + \sum f + \mu \end{aligned}$$

where $\mu = v + \lambda l$. After substituting the Euler formula, $l = g - n + 1$, Eq. (3.5) is identical to Eq. (3.4). Both formulas consider common constraint.

Comparing Eqs. (3.4) and (3.5), it can be seen that they are based on two different ideas. For classical and parallel mechanisms, Eq. (3.5) is recommended. It has not only pointed out the order of the analyzed mechanism but it is also convenient for applications on planar and spherical mechanisms with $d = 3$. When the mechanisms are more complicated, Eq. (3.4) is more suitable, as shown in Sects. 4.4 and 4.5.

Readers may find that many different mobility formulas have similar forms and that these can be transformed between each other. Certainly, the key questions are as follows: What principle and technique is the method dependent on? How can over-constraint be dealt with using these different methods? The difference is prodigious and even makes the result incorrectness.

3. As we know, different links have different freedoms in a mechanism. In mechanism analysis, we often need to find the freedom of some pointed links in a mechanism, and there are two methods to deal with this.

We can assume the pointed link as the output link of some parallel mechanism with some limbs. The mobility of the imaginary parallel mechanism is just the freedom of this pointed link. The first method directly uses Eq. (3.5) to calculate the mobility of the imaginary parallel mechanism.

The other method adopts the formula as follows

$$M_G = 6 - \sigma \quad (3.6)$$

where M_G is the freedom of the rigid body, and σ is the number of independent reciprocal screws acting on the rigid body.

There needs to consider another case, i.e. relative freedom issue. The relative freedom in a mechanism is the mobility of a pointed body respective to another moving body in the mechanism. For this case, the second one can be dealt with as an imaginary frame. The freedom can be obtained by analyzing the freedom of the first one relative the imaginary frame.

4. The nominal mobility

When there is local mobility in a mechanism, its real mobility or the mobility people know is different from that of the results from Eqs. (3.4) and (3.5). For instance, if we apply Eq. (3.5) to the 6-SPS Stewart platform, the result is 12. However, people have known that its mobility is only six. The reason is that in each SPS limb, the S-S chain can independently rotate about its axis. This motion does not affect the output motion of its platform, and is called local freedom, passive freedom, or idle freedom. The output of six freedoms is the “nominal mobility” of the Stewart platform. Thus, the nominal mobility of a mechanism is given by

$$M_N = d(n - g - 1) + \sum_{i=1}^g f_i + v - \zeta \quad (3.7)$$

where M_N is the nominal mobility, and ζ is the number of local freedoms in the mechanism.

As pointed out earlier, the local mobility does not affect the output mobility of the mechanism. The local mobility can be determined by checking the linear dependency of a screw system. In practice, the dependency of a screw system can be obtained frequently using the geometrical method, as shown in Table 2.1. It should be noted that the common key step of the above-mentioned four Modified G-K formulas is the constraint analysis using reciprocal screw.

3.4 Constraint Analysis Based on Reciprocal Screw

For mobility analysis, two important factors need to be determined, namely, common constraint and parallel constraint. Essentially, the core of problem of mobility analysis is how to determine the redundant constraints or over-constraints, including the common constraint λ and the parallel constraint v .

3.4.1 The Common Constraint

When all kinematic pairs are associated with screws, all the screws form a screw system called kinematic screw system, $\hat{\mathcal{S}}^m$. When all the kinematic pairs in a limb of a parallel mechanism are associated with screws, all the screws form a screw system called limb screw system, $\hat{\mathcal{S}}_i^b$. A new definition for common constraints is then given.

Definition 3.2. *Common Constraint:* If there exists a reciprocal screw \mathcal{S}^r that is reciprocal to all the screws in \mathcal{S}^m , the screw \mathcal{S}^r is defined as a common constraint of the mechanism.

All linearly independent reciprocal screws of the screw system $\hat{\mathcal{S}}^m$ determine the number of the common constraints, which explains why $d = 6 - \lambda$. All the common constraint screws form a common constraint screw system, \mathcal{S}^c , and the rank of a common constraint screw system is the number of common constraints. This can be expressed in the following form:

$$\lambda = \text{Rank}(\hat{\mathcal{S}}^c) = \text{Rank}\left(\{\mathcal{S}^r | \mathcal{S}^r \circ \mathcal{S}^m = 0, \quad \forall \mathcal{S}^m \in \hat{\mathcal{S}}^m\}\right) \quad (3.8)$$

For a serial kinematic chain where the freedom of the end-effector is δ ($\delta < 6$), it indicates that all links in the serial chain are subjected to $6 - \delta$ constraints, and that it has $6 - \delta$ common constraints.

For a parallel mechanism, the situation is more complex. The common constraints can be obtained directly using Eq. (3.8). However, it may be more convenient when the following theorem is followed.

Theorem 3.1. *For a parallel mechanism, a common constraint exists if and only if*

1. Every limb constraint system can provide an identical constraint screw acting on the moving platform.
2. If these identical screws are constraint forces, they must be coaxial; if these identical screws are couples, they must be parallel.

Clearly the common constraint satisfying Theorem 3.1 is consequentially satisfying Eq. (3.8). Using Theorem 3.1, one can find the common constraint for a parallel mechanism. Essentially, Theorem 3.1 is an interpretation of geometrical condition for a common constraint.

3.4.2 Parallel Constraint

Aside from common constraints, there are still redundant constraints that exist when some limbs connect to the upper and lower platforms simultaneously. That is the reason why it is called parallel constraint. It also needs to consider the parallel constraint when analyzing parallel mechanisms.

Let q_i be the number of constraint screws of the i th limb constraint system and p as the limb number of a parallel mechanism. The platform constraint system consists of $\sum_1^p q_i$ screws. After the screws forming the common constraints are removed from the platform constraint system, the remaining screws lead to a new screw system spanned by $\sum_1^p q_i - \lambda \cdot p$ constraint screws. Let k be the dimension of the new screw system. The number of parallel constraints is given by

$$v = \sum_1^p q_i - \lambda \cdot p - k \quad (3.9)$$

3.4.3 Over-Constraint

The over-constraint or redundant constraint is the core issue for mobility analysis, which leads to the following questions: why and where does the over-constraint appear? References [14, 21] introduced that when the end-link of a serial chain was connected with the fixed frame to form a closed loop, the over-constraint appeared. The end-link may completely and rigidly be connected with the frame, or be connected with the frame by another kinematic pair.

When the end-link of a serial chain is connected with the frame, it is said to be rigidly closed. Note that the numbers of kinematic pairs before and after connections are constant. If the serial chain has δ , ($\delta < 6$) mobility and it is rigidly closed, the end-link is completely fixed and the freedoms of end-link are constrained. In this case, $6 - \delta$ constraints are repeated in the new closed mechanism. For instance, when an arbitrary spatial five-pair serial chain is rigidly closed to form a closed-loop linkage the number of over-constraint is one. Hence, the over-constraint of a closed-loop mechanism is given by

$$\mu = 6 - \delta \quad (3.10)$$

When the end-link of a serial chain is connected with the frame by a kinematic pair, it is said to be moving closed. In this case, the number of kinematic pairs of the closed-loop is one more than that before it is closed. Assume that the screw system of the serial chain is $\hat{\mathcal{S}}^{\delta m}$ and the additional kinematic pair is \mathcal{S}^R . If there exists $\mathcal{S}^R \in \hat{\mathcal{S}}^{\delta m}$, the number of over-constraint is also $6 - \delta$, as shown in Eq. (3.10). Otherwise, when $\mathcal{S}^R \notin \hat{\mathcal{S}}^{\delta m}$, the number of common constraint of the single-loop chain is less than one compared to the serial chain. We will then have

$$\mu = 5 - \delta \quad (3.11)$$

This is called the closing-constraint method. Theoretically, this principle of determining over-constraint is reasonable and has been proven in practice. However, it is not applicable to some mechanisms, such as the Bennett and Goldberg mechanisms, etc.

3.4.4 The Generalized Kinematic Pair

In practice, there are a great number of mechanisms with a sub-closed-loop η inside another closed-loop ε , as shown in Fig. 3.1a, making the mechanism more complex. To simplify the mobility analysis, this sub-loop of the mechanism can be dealt with as a generalized kinematic pair with mobility m , and the sub-loop chain can be replaced by a serial chain with the same number and characters of mobility of the

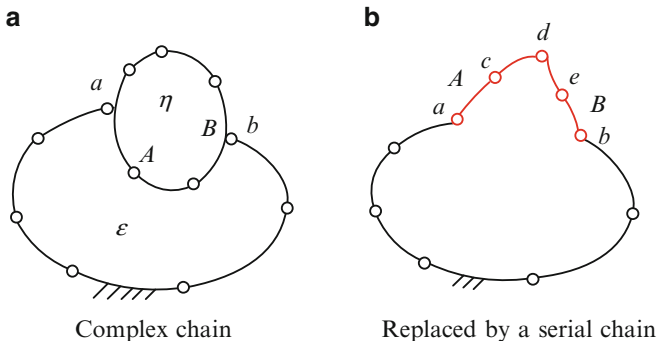


Fig. 3.1 Generalized kinematic pair (a) complex chain (b) replaced by a serial chain

sub-loop η . The complex mechanism then becomes a single loop chain, as shown in Fig. 3.1b, and the mobility analysis can proceed.

3.5 Mobility Property Analyses

As mentioned before, in practice, it is not enough to only calculate the number of mobility, because we also need to know the mobility characteristics. For example, it should be known if the mechanism can realize the translation along a given direction, if it can rotate about a determined axis, whether the rotation is with or without parasitic motion, and whether the mobility is instantaneous or full-cycle. All of these issues should be addressed.

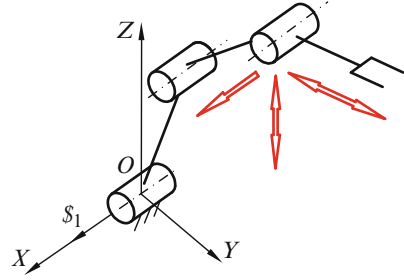
3.5.1 Translation and Rotation

Theoretically, the maximum number of linearly independent screws in 3-D space is six, and they form a six-system. Any six-system screw can be expressed as a linear combination of the following six unit screws:

$$\begin{aligned}
 \mathcal{S}_1 &= (1 \ 0 \ 0; \ 0 \ 0 \ 0) \\
 \mathcal{S}_2 &= (0 \ 1 \ 0; \ 0 \ 0 \ 0) \\
 \mathcal{S}_3 &= (0 \ 0 \ 1; \ 0 \ 0 \ 0) \\
 \mathcal{S}_4 &= (0 \ 0 \ 0; \ 1 \ 0 \ 0) \\
 \mathcal{S}_5 &= (0 \ 0 \ 0; \ 0 \ 1 \ 0) \\
 \mathcal{S}_6 &= (0 \ 0 \ 0; \ 0 \ 0 \ 1)
 \end{aligned}
 \tag{3.12}$$

The six-system screws can be expressed as three screws with zero-pitch and three screws with infinite-pitch. This means that three of them are line vectors and the other three are couples. Thus, the physical meaning is evident. When it denotes

Fig. 3.2 A 3-DOF serial robot



a moving screw, the first three in Eq. (3.12) express rotational motions and the other three correspond to translational motions. On the other hand, when the screws denote forces, the first three express constraint forces and the other three are constraint couples. When they denote freedom, the first three denote rotation freedoms and the other three denote translational freedoms. The screw abounding in expressions and all those important concepts of screws are easily transferred with each other. This plays many important roles and has so many applications in spatial mechanisms.

Example 3.1. A 3-DOF planar robot

A 3-DOF planar robot with three revolute pairs is shown in Fig. 3.2. To analyze its mobility, we need to set the screw system of the three revolute pairs in these forms:

$$\begin{aligned}
 \$_1 &= (1 \ 0 \ 0; \ 0 \ 0 \ 0) \\
 \$_2 &= (1 \ 0 \ 0; \ 0 \ e_2 \ f_2) \\
 \$_3 &= (1 \ 0 \ 0; \ 0 \ e_2 \ f_3)
 \end{aligned}
 \tag{3.13}$$

Their reciprocal screws are

$$\begin{aligned}
 \$_1^r &= \$_1^c = (1 \ 0 \ 0; \ 0 \ 0 \ 0) \\
 \$_2^r &= \$_2^c = (0 \ 0 \ 0; \ 0 \ 1 \ 0) \\
 \$_3^r &= \$_3^c = (0 \ 0 \ 0; \ 0 \ 0 \ 1)
 \end{aligned}
 \tag{3.14}$$

which are constraint screws, including a constraint force and two constraint couples. Based on the reciprocal screw system, the motion of the end-effector of the robot can be obtained by further analyzing the constraints. However, we can directly take the second-time reciprocal screw of Eq. (3.14) to obtain the motion-screw system of the end-link. Solving the screws reciprocal to Eq. (3.14) yields

$$\begin{aligned}
 \$_1^{rr} &= \$_1^{mm} = (1 \ 0 \ 0; \ 0 \ 0 \ 0) \\
 \$_2^{rr} &= \$_2^{mm} = (0 \ 0 \ 0; \ 0 \ 1 \ 0) \\
 \$_3^{rr} &= \$_3^{mm} = (0 \ 0 \ 0; \ 0 \ 0 \ 1)
 \end{aligned}
 \tag{3.15}$$

From Eq. (3.15), it is clear that the first motion-screw indicates a rotational freedom about the axes parallel to the X axis, and the last two indicate two translational freedoms along the Y and Z axes, respectively. Figure 3.2 shows the three

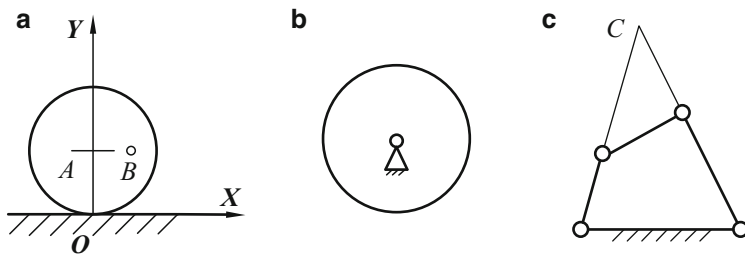


Fig. 3.3 Incomplete rotational freedom (a) wheel (b) roller (c) four-bar linkage

possible motions, where the red hollow arrow denotes the rotational motion and the bi-directional hollow arrow indicates the translational motion. It should be noted that the three revolute pairs correspond to three screws with zero-pitch. However, in the second-time reciprocal screw, the three pitches are not the same and are differentiated as zero-pitch and non-zero pitch, which indicates the mobility properties to be rotational or translational or others. Therefore, solving the second-time reciprocal screw is a very good method for obtaining the motion property of a rigid body.

3.5.2 Rotational Axis

One important question is that when a rigid body has rotational freedom and even 3D rotational freedom, could it consequentially rotate about any axis? The answer is not always. One must consider if the rigid body is subjected to some constraint forces. If so, the rotational axes should intersect all the axes of the constraint forces [77]. In other words, when a rigid body is subjected to a constraint force, it still has rotational freedom about some direction, but the rotational freedom is incomplete. It cannot rotate about some axis being skewed to the direction of the constraint force, and it can only rotate about the axes intersecting the axis of constraint force.

For instance, a roller rolls on a plane, as shown in Fig. 3.3a. It is acted upon by a reactional force from the base. The roller still has five freedoms, including three rotational freedoms. However, its rotational axis cannot pass point B and parallel to Z -axis. If so, the kinematic pair will separate and be broken. Thus, many points in the roller cannot be chosen as the rotating center. All the points in the center line can be the rotating center, and all the rotational freedoms are instantaneous except point A , about which the rigid body can continuously rotate. Rotation about point O is a roll without any slide. The second example, as shown in Fig. 3.3b, is a wheel fixed in a point. It is clear that the rotational axis must pass the center. Thus, the rotational freedom is incomplete. The third example, as shown in Fig. 3.3c, is a four-bar linkage. The link CD has one freedom, but it can only rotate about point E at this moment.

The three examples are very simple and clear. However, for multi-mobility mechanisms, such as the parallel mechanisms, the problem becomes complex and requires careful analysis.

3.5.3 *Instantaneous Mobility and Full-Cycle Mobility*

The IFToMM mobility definition did not clearly consider the mobility characteristics whether it is instantaneous or full-cycle. However, the mobility of a mechanism should be full-cycle and unchangeable in different configurations. Otherwise, the mechanism cannot work normally. For modern multi-freedom mechanisms, distinguishing the two mobility concepts, instantaneous and full-cycle, is necessary.

Definition 3.3. Full-cycle Mobility: The mobility, including the number and property, is not dependent on configuration.

Our three modified G-K criteria, as shown in Eqs. (3.4), (3.5), and (3.6), are based on the screw theory, and the results are dependent on the configuration or the geometrical condition of that configuration. In other words, the obtained mobility is instantaneous, not full-cycle. From this viewpoint, the checkout of the full-cycle for each mobility analysis is necessary and indispensable. Otherwise, it does not accord with the IFToMM definition. Nevertheless, the checkout of the full-cycle mobility using the screw theory is not difficult. All of these can be found in the examples below.

In this study, we found that the instantaneous characteristics of screw theory are very useful for mechanism analysis because it can deeply recognize the mechanism. It can help us to not only find the instantaneous mechanism, but also find the singularity of mechanisms as well as their motion screw at singularity. It can also be applied to mechanisms with changeable mobility and changeable topology.

3.5.4 *Full-Field Mobility*

A 2UPU-UU mechanism, as shown in Fig. 3.4, has three limbs where the first two are UPU chains and the third one is a UU chain. The first kinematic pair of each limb is fixed on the base platform and lies flatly on it. The first pairs of the first two limbs are parallel with each other and are normal to A_1A_2 , and the first pair of the third limb is parallel to A_1A_2 . The axes of the second rotational pair of the three limbs are aligned with the corresponding link A_iB_i and the last pair of each limb is fixed on the moving platform. The last pair axes of the first two limbs are collinear, and the pair of the third limb is parallel to B_1B_2 .

In the initial configuration, as shown in Fig. 3.4a, from Table 2.2, the first two limbs with five rotational pairs both exert two parallel constraint forces, $\$1^r$ and $\$2^r$, to the moving platform. The constraint forces pass the centers of the two cross-heads and are parallel to the base, respectively. The third limb has four rotational pairs and it

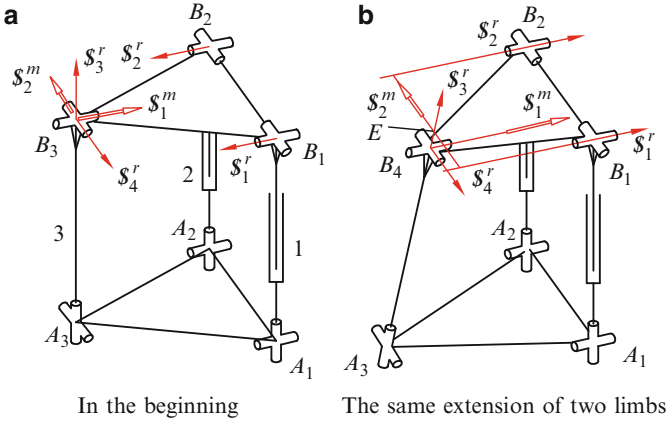


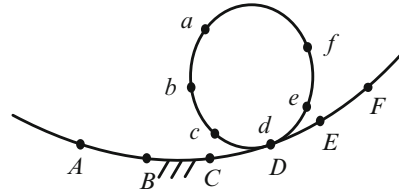
Fig. 3.4 Non-full-field mobility (a) in the beginning (b) the same extension of two limbs

also exerts two constraint forces, S_3^r and S_4^r , to the platform. One is along the link itself and the other one is parallel to the axis of the first pair counted from the base and passes the center of the upper cross-head. In the original configuration, the platform is constrained by four linearly independent constraint forces and loses four freedoms. Thus, it only has two freedoms. The two freedoms are rotational, and all rotational axes of the two freedoms lie on the plane of the platform and passing point B_3 , as shown in Fig. 3.4a.

To analyze the mobility characteristics, some different configurations should be taken into consideration, such as the configuration shown in Fig. 3.4b where the first two limbs are extended. Based on the structure, quadrilateral $A_1A_2B_2B_1$ remains perpendicular to the base, and the upper two cross-heads are parallel to the base. In the meantime, the third limb is no longer normal to the base. The four constraint forces are shown in Fig. 3.4b. The first two reciprocal forces produced by the first two legs are still parallel to each other and parallel to the base. One of the two forces of the third limb is still along the link and the other one is parallel to the axis of the first pair of the limb and passes the upper cross-head. The upper platform acted four independent constraints also has two degrees of freedom.

All the possible moving screws of the platform in this configuration must intersect the four forces simultaneously, as mentioned above. However, there are only two straight lines satisfying the condition, which are S_1^m and S_2^m in Fig. 3.4b. One of them, S_1^m , passes the upper cross-head and is parallel to S_1^r . The other one, S_2^m , is parallel to the first pair of the third limb and passes the intersection point E of S_3^r and the plane formed by S_1^r and S_2^r . In this case, only two line vectors are able to satisfy the reciprocal condition. There are no other line vectors that can satisfy the condition except these two lines. Although the mechanism in this configuration has two degrees of freedom, the two freedoms only correspond to two revolute axis lines. The two lines do not intersect and they are isolated and discrete. Generally, a mechanism like this is useless, and we call this mobility a non-full-field mobility. When designing mechanisms, this case should be avoided.

Fig. 3.5 Parasitic motion



3.5.5 Parasitic Motion

A strange phenomenon often appears in some parallel mechanisms. For instance, the well-known 3-RPS mechanism has three freedoms with one translation along the z -axis and two rotations about the x and y axes in the upper plane. However, people found out that when its platform rotates about the x -axis, its center point also has an unwanted displacement along the x direction, which was called parasitic motion.

In reality, this phenomenon is not strange in kinematics. The simplest example is a roller rolling on the ground, as shown in Fig. 3.5. Is it translational? No. Is it rotational? Not yet. It is not similar to normal rotation. It rolls forward along a surface by revolving on an instant axis or by repeatedly turning over. This motion should belong to the category of rotation, a special rotation. Theoretically, this special rotation is that a moving axodes rolls along a fixed axodes without sliding. Every point in the rolling body forms a different locus. From this point of view, the so-called “parasitic motion” of platform of 3-RPS is not an independent motion but this motion mentioned above.

3.5.6 Self-motion

Several links in a mechanism may continuously move while all inputs are locked, and this phenomenon is called self-motion and can be explained easily by the screw theory. When all inputs are locked, the constraint-screw system becomes linearly dependent and self-motion occurs. There are some freedoms that are not constrained, and their linear dependency is unchangeable for continuous configurations, wherein the self-motion becomes full-cycle. This issue will be discussed further in another chapter.

References

1. Suh CH, Radcliffe CW (1978) Kinematics and mechanisms design. Wiley, New York, pp 103–110
2. Merlet JP (2000) Parallel robots. Kluwer Academic, Dordrecht, pp 10–11
3. Waldron KJ, Kinzel GL (2004) Kinematics dynamics and design of machine. Wiley, New York, pp 25–29

4. Chebychev P A(1854) Théorie des mécanismes connus sous le nom de parallélogrammes, 1ère partie, Mémoires présentés a' l'Académie impériale des sciences de Saint-Pétersbourg par divers savants
5. Grübler M (1883) Allgemeine eigenschaften der zwangläufigen ebenen kinematische kette: I. Civilingenieur 29:167–200
6. Hochman KI (1890) Kinematics of machinery. Odesa (in Russian)
7. Grübler M (1916) Das Kriterium der Zwänglaufigkeit der Schraubenketten. Festschrift, O. Muhr. Zum 80. Gubertstag, Berlin
8. Kutzbach K (1929) Mechanische Leitungsverzweigung, ihre Gesetze und Anwendungen. Maschinenbau Der Betrieb 8(21):710–716
9. Dobrovolskii VV (1939) Main principles of rational classification, AS USSR, pp 5–48
10. Artobolevskii II (1939) Structural analysis experience of mechanisms, structure and classification of mechanisms, AS USSR, pp 49–66
11. Hunt KH, Phillips JR(1965) Zur Kinematic mechanischer Verbindung für räumliche Bewegung, Maschinenbau Getriebe 14:657–664
12. Hunt KH (1983) Structural kinematics of in-parallel actuated robot arm. J Mech Trans Autom Des 105:705–712
13. Hervé JM (1978) Analyse structurelle des mécanismes par groupe des déplacements. Mech Mach Theory 13:437–450
14. Waldron KJ (1966) The constraint analysis of mechanisms. J Mech 1:101–114
15. Bagci C (1971) Degrees of freedom of motion in mechanisms. ASME J Eng Ind 93B:140–148
16. Freudenstein F, Alizade R(1975) On the degree-of-freedom of mechanisms with variable general constraint. In: Fourth world congress on the theory of machines and mechanisms, Newcastle upon Tyne, pp 51–56
17. Hunt KH (1978) Kinematic geometry of mechanisms. Oxford University Press, Oxford, pp 375–382
18. Hervé JM (1978) Analyse structurelle des mécanismes par groupe des déplacements. Mech Mach Theory 13:437–450
19. Baker JE (1980) On relative freedom between links in kinematic chains with cross-jointing. Mech Mach Theory 15:397–413
20. Davies TH (1983) Mechanical networks—I: passivity and redundancy. Mech Mach Theory 18:95–101
21. Zhang QX (1984) Spatial mechanism. Part 1. Mechanical Press, Beijing, pp 49–59
22. Angeles J, Gosselin C (1988) Détermination du degré de liberté des chaînes cinématiques. Trans CSME 12(4):219–226
23. Alizade RI (1988) On degree of freedom of kinematic chain. Azerbaijan Polytechnic Institute of Automation Design of Mechanisms, Manipulators and Robots, Baku, pp 3–14
24. Huang Z (1991) Spatial mechanisms. Mechanical Press, Beijing, pp 133–138 (in Chinese)
25. Huang Z, Kong LF, Fang YF (1997) Mechanism theory of parallel robotic manipulator and control. China Mechanical Press, Beijing (in Chinese)
26. Tsai LW (1999) Robot analysis: the mechanics of serial and parallel manipulators. Wiley, New York, pp 9–16
27. McCarthy JM (2000) Geometric design of linkages. Springer, New York, pp 3–8
28. Gosselin CM, Angeles J (1989) The optimum kinematic design of a spherical three-DOF parallel manipulator. ASME J Mech Trans Autom Des 111:202–207
29. Pierrot F, Company O (1999) H4: a new family of 4-DOF parallel robot. In: Proceedings of IEEE/ASME international conference on advanced intelligent mechatronics, Atlanta, pp 508–513
30. Wenger P, Chablat D (2005) Design strategies for the geometric synthesis of orthoglide-type mechanisms. Mech Mach Theory 40(8):907–930
31. Kim HS, Tsai LW (2002) Design optimization of a cartesian parallel manipulator. ASME DETC2002/MECH-34301
32. Hervé JM, Sparacino F (1991) Structural synthesis of parallel robots generating spatial translation. In: Proceedings of 5th IEEE international conference on advanced robotics, Pisa, Italy, pp 808–813

33. Clavel R (1988) Delta, a fast robot with parallel geometry. In: Proceedings of the international symposium on industrial robot, Switzerland, pp 91–100
34. Kong XW, Gosselin CM (2005) Mobility analysis of parallel mechanisms based on screw theory and the concept of equivalent serial kinematic chain, ASME paper No. DETC-85337
35. Zhao TS, Huang Z (2000) A novel 4-dof parallel mechanism and its position analysis. *Mech Sci Technol* 19(6):927–929 (in Chinese)
36. Huang Z, Li QC (2001) Two novel 5-DOF parallel mechanisms. *J Yanshan Univ* 25(4):283–286
37. Carricato M, Parenti-Castelli V (2002) Singularity-free fully isotropic translational parallel mechanism. *Int J Robot Res* 21(2):161–174
38. Gogu G (2005) Mobility of mechanisms: a critical review. *Mech Mach Theory* 40(9):1068–1097
39. Altman FG (1952) Sonderformen Raumlieher Koppelgetriebe und Grenzen Ihrer Verwendbarkeit, *Konstruktion. Werkstoffe Versuchswesen* 4:97–106
40. Baker JE (1978) Overconstrained 5-bars with parallel adjacent joint axes. *Mech Mach Theory* 13:213–218
41. Baker JE, Duclong T, Khoo PSH (1982) On attempting to reduce undesirable characteristics of the Schatz mechanism. *ASME J Mech Des* 104:192–205
42. Bennett GT (1903) A new mechanism. *Engineering* 76:777–778
43. Bricard R (1927) *Lec, ons De Cinématique*, vol 2. Gauthier-Villars, Paris, pp 7–12
44. Delassus E (1900) Sur les systèmes articulés gauches. Première partie, *Ann Sci Ecole Norm Supérieure*, Paris, 3_Séries 17: 455–499
45. Delassus E (1900) Sur les systé'mes articulés gauches Deuxième partie, Sur les systèmes articulés gauches. Deuxième partie 19:119–152
46. Delassus E (1922) Les chaînes articulés fermées et déformables à quatre membres. *Bull Sci Math Paris* 46:283–304
47. Eckhardt HD (1998) *Kinematic design of machines and mechanisms*. McGraw-Hill, New York, pp 20–37
48. Goldberg M (1943) New 5-bar and 6-bar linkages in three dimensions. *ASME J Mech* 65:649–661
49. Hervé JM (1978) Analyse structurelle des mécanismes par groupe des déplacements. *Mech Mach Theory* 13:437–450
50. Hervé JM (1978) Principes fondamentaux d'une théorie des mécanismes. *Rev Roum Sci Tech—Méc Appl* 23(5):693–709
51. Mabie HH, Reinholtz CF (1987) *Mechanisms and dynamics of machinery*. Wiley, New York, pp 13–15
52. Myard FE (1931) Contribution à la géométrie des systèmes articulés. *France Bull Soc Math* 59:183–210
53. Myszka DH (2001) *Machines and mechanisms: applied kinematic analysis*. Prentice Hall, Upper Saddle River, pp 21–26
54. Norton RL (1999) *Design of machinery: an introduction to the synthesis and analysis of mechanisms and machines*. McGraw-Hill, Boston, pp 37–38
55. Phillips J (1984) *Freedom in machinery introducing screw theory*, vol I. Cambridge University Press, Cambridge, p 5
56. Phillips J (1990) *Freedom in machinery screw theory exemplified*, vol II. Cambridge University Press, Cambridge, pp 147–166
57. De Roberval P (1670) Nouvelle manière de balance, *Mémoires de mathématiques et de physique. Tirez des registres del_Académie Royale des Sciences depuis 1666 jusqu'à 1699*, Tome X, Institut de France, Académie des sciences, pp 494–496
58. Sarrus PF (1853) Note sur la transformation des mouvements rectilignes alternatifs en mouvements circulaires et réciproquement. *Académie des Sciences, CR Hebd Sci Paris* 36: 1036–1038
59. Waldron KJ (1979) Overconstrained linkages. *Environ Plan B* 6:393–402
60. Kim HS, Tsai LW (2002) Evaluation of a Cartesian parallel manipulator. In: Lenarcic J, Thomas F (eds) *Advances in robot kinematics*. Kluwer Academic, Dordrecht, pp 21–28

61. Clavel R (1988) Delta, a fast robot with parallel geometry. In: 18th international symposium on industrial robots, Lausanne
62. Kong X, Gosselin CM (2002) Type synthesis of linear translational parallel manipulators. In: Lenarcic J, Thomas F (eds) *Advances in robot kinematics*. Kluwer Academic, Dordrecht, pp 453–462
63. Wenger P, Chablat D (2000) Kinematic analysis of a new parallel machine tool: the orthoglide. In: Lenarcic J, Stanisic ML (eds) *Advances in robot kinematics*. Kluwer Academic, Dordrecht, pp 305–314
64. Hervé JM, Sparacino F (1992) STAR, a new concept in robotics. In: 3rd international workshop on advances in robot kinematics, Ferrara, pp 176–183
65. Gogu G (2003) Structural synthesis of parallel robotic manipulators with decoupled motions. Report ROBEA MAX—CNRS
66. Rico JM, Gallardo J, Ravani B (2003) Lie algebra and the mobility of kinematic chains. *J Robot Syst* 20(8):477–499
67. Kong XW, Gosselin CM (2005) Mobility analysis of parallel mechanisms based on screw theory and the concept of equivalent serial kinematic chain. ASME paper No. DETC-85337
68. Zhao JS, Zhou K, Feng ZJ (2004) A theory of degrees of freedom for mechanisms. *Mech Mach Theory* 39(6):621–643
69. Alizade R, Bayram C (2004) Structural synthesis of parallel manipulators. *J Mech Mach Theory* 39:857–870
70. Gogu Gogu G (2005) Mobility and spatiality of parallel robots revisited via theory of linear transformations. *Eur J Mech A/Solids* 24:690–711
71. Shukla G, Whitney DE (2005) The path method for analyzing mobility and constraint of mechanisms and assemblies. *Trans IEEE Autom Sci Eng* 2(2):184–192
72. Wampler CB, Larson T (2007) A new mobility formula for spatial mechanisms. ASME DETC2007-35574
73. Rico JM (2007) Mobility and redundant-constraint in kinematic chains and assemblies. ASME DETC2007-34937
74. Müller A (2009) Generic mobility of rigid body mechanisms. *Mech Mach Theory* 44:1240–1255
75. Yang TL, Sun DJ (2008) A general formula of degree of freedom for parallel mechanisms. ASME DETC2008-49077
76. Zhang Y, Mu D (2010) New concept and new theory of mobility calculation for multi-loop mechanisms. *Sci China Ser E* 53(6):1598–1604
77. Huang Z, Tao WS, Fang YF (1996) Study on the kinematic characteristics of 3-DOF in-parallel actuated platform mechanisms. *Mech Mach Theory* 31(8):999–1007
78. Huang Z, Fang Y (1996) Kinematic characteristics analysis of 3-DOF in-parallel actuated pyramid mechanisms. *Mech Mach Theory* 31(8):1009–1018
79. Huang Z, Li Q (2003) Type synthesis of symmetrical lower-mobility parallel mechanisms using constraint-synthesis method. *Int J Robot Res* 22(1):59–79
80. Dai JS, Huang Z, Lipkin H (2006) Mobility of overconstrained parallel mechanisms. *Trans ASME J Mech Des* 128(1):220–229
81. Huang Z, Li QC (2002) General methodology for type synthesis of lower-mobility symmetrical parallel manipulators and several novel manipulators. *Int J Robot Res* 21(2):131–145
82. Huang Z, Li QC (2002) Type synthesis principle of minor-mobility parallel manipulators. *Sci China Ser E* 45(3):241–248
83. Li QC, Huang Z (2003) A family of symmetrical lower-mobility parallel mechanisms with spherical and parallel subchains. *J Robot Syst* 20(6):297–305
84. Huang Z (2004) The kinematics and type synthesis of lower-mobility parallel manipulators. In: *Proceedings of the 11th world congress in mechanism and machine science*, Tianjin, China, pp 65–76
85. Li QC, Huang Z (2004) Mobility analysis of a novel 3-5r parallel mechanism family. ASME J Mech Des 126(1):79–82

86. Huang Z, Xia P (2004) Mobility analysis of the Bennett mechanism. *J Yanshan Univ* 8 (3):189–192
87. And HZ, Xia P (2006) Mobility analysis of some “paradoxical mechanisms” including Bennett. *J Yanshan Univ* 30(1):1–9
88. Liu JF, Zhu SJ, Zeng DX, Huang Z (2006) Mobility analysis of several mechanisms including two novel parallel mechanisms and some “paradoxical linkages”. *J Yanshan Univ* 30 (6):487–494
89. Huang Z, Liu JF, Li YW (2011) *On mobility of mechanisms*. Science Press, Beijing

Chapter 4

Mobility Analysis Part-2

In this chapter we will introduce the mobility analysis by using our mobility principle based on reciprocal screw theory. First, we discuss some simple mechanisms, and then focus on the mobility-open-issue mechanisms including the classical mechanisms and modern parallel mechanisms with interesting characteristics. Besides, more complex mechanisms, such as the Multi-loop-coupling mechanisms, are also discussed.

4.1 Mobility Analysis of Simple Mechanisms

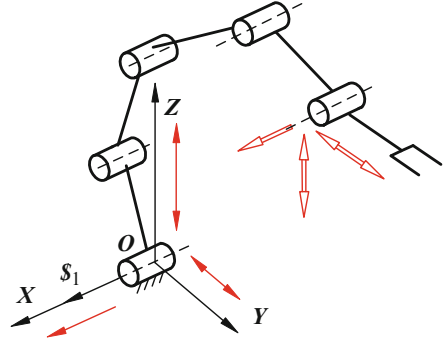
4.1.1 Open Chain Linkage

The open-chain linkage is a serial kinematic chain, when $n + 1$ links are connect by n kinematic pairs. Their first link is fixed as a frame and the last link is the hand of a robot manipulator. Figure 4.1 shows a robot with 6 links and 5 kinematic pairs. All its axes are parallel to each other and it is a planar robot.

For analyzing the mobility of the planar serial chain using the Modified G-K formula by screw theory, we need firstly to set the screw Plücker coordinates of the mechanism. The coordinate system is shown in the figure, and then we have

$$\begin{aligned} \$_1 &= (1 \ 0 \ 0; \ 0 \ 0 \ 0) \\ \$_2 &= (1 \ 0 \ 0; \ 0 \ e_2 \ f_2) \\ \$_3 &= (1 \ 0 \ 0; \ 0 \ e_3 \ f_3) \\ \$_4 &= (1 \ 0 \ 0; \ 0 \ e_4 \ f_4) \\ \$_5 &= (1 \ 0 \ 0; \ 0 \ e_5 \ f_5) \end{aligned} \tag{4.1}$$

Fig. 4.1 A serial robot



where e_i and f_i depend on the structure parameters and moving parameters of the mechanism. To solve those elements are quite complex and never necessary, since the mobility analysis is often in the beginning for a new mechanical design, and many different mechanism schemes are continuously proposed for comparing and selecting. In this moment their parameters are not determined yet. For this difficulty, in practice, there need not solve out any above-mentioned parameters and the reciprocal screw can be completely correctly obtained without those parameters. That is because based on the Plücker coordinate expression of screws shown in Chap. 1, there are many zero-elements and the reciprocal screws can be written directly. For this example, consider the fact that the 2nd, 3rd, and 4th elements in the above five screws are all zeros, the reciprocal screws are in the form

$$\begin{aligned} \mathcal{S}_1^r &= (0 \ 0 \ 0; \ 0 \ 1 \ 0) \\ \mathcal{S}_2^r &= (0 \ 0 \ 0; \ 0 \ 0 \ 1) \\ \mathcal{S}_3^r &= (1 \ 0 \ 0; \ 0 \ 0 \ 0) \end{aligned} \quad (4.2)$$

The correction can be easily testified by Eq. (2.52), $\mathcal{S}_i \circ \mathcal{S}_j = 0$. The three screws satisfy the screw reciprocal condition. In Eq. (4.2), there are many zero-elements and they give clear physical meaning. \mathcal{S}_1^r and \mathcal{S}_2^r are constraint couples with ∞ -itches about Y and Z axes, and \mathcal{S}_3^r is a constraint force along X-axis direction. They constrain the end-link rotation about Y and Z axes and translation along X axis, and the end link has only three freedoms. The three reciprocal screws also correspond to three common constraints, $\lambda = 3$ then $d = 6 - \lambda = 3$, since it is not a parallel mechanism, $v = 0$. The mobility of the mechanism is obtained by using the modified G-K formula (3.5) as follows

$$M = d(n - g - 1) + \sum_{i=1}^g f_i + v = 3(6 - 5 - 1) + 5 + 0 = 5 \quad (4.3)$$

Readers may ask there are five screws in Eq. (4.1) why Eq. (4.2) contains three reciprocal screws? That is because the five screws in Eq. (4.1) are linearly dependent and only three of them are independent, as shown in Table 2.1. In other words,

the mobility of the serial chain with five parallel rotation pairs is 5, but the freedom of the end-link is only 3. The other two are local freedoms inside the kinematic chain and do not affect the mobility of the end-link.

From above analysis, we know that ***the mobility of serial chain is equal to the number of the kinematic pairs of the serial chain.***

Other three screws reciprocal to the three reciprocal screws in Eq. (4.2), are obtained

$$\begin{aligned} \$_1^{rr} &= \$_1^m = (1 \ 0 \ 0; \ 0 \ 0 \ 0) \\ \$_2^{rr} &= \$_2^m = (0 \ 0 \ 0; \ 0 \ 1 \ 0) \\ \$_3^{rr} &= \$_3^m = (0 \ 0 \ 0; \ 0 \ 0 \ 1) \end{aligned} \quad (4.4)$$

The screw which is obtained by taking reciprocal procedure once more for a screw $\r is called second-time reciprocal screw and denoted as $\rr . ***The second-time reciprocal screw indicates the motion of the link.*** These three second-time reciprocal screws in Eq. (4.4) just denote the motions of the end-link including the rotation about X axis and two translations along Y and Z axes, respectively. It is found that all the pitches of screws in Eq. (4.1) are zeros as they are rotational pairs. However, after taking reciprocal procedure two times the pitches become as zero or infinite and they denote rotation or translation. ***So, to calculate the second-time reciprocal for a motion screw of a link is a shortcut for obtaining its mobility property.***

Since all the axis directions of the kinematic pairs of the serial robot in any configuration are parallel to X axis and unchangeable, as shown in Fig. 4.1, and the screw expressions are also unchangeable and the common constraints unchangeable as well, the mobility of the mechanism is unchangeable. Then the mobility is full-cycle.

The common constraint of the planar robot is three and $\lambda = 3$, then $d = 6 - \lambda = 3$, that is because all its axes are parallel. ***Actually, all axes of planar mechanisms are parallel and their screw expressions also have three zero-elements no matter what kinematic pairs, rotational or prismatic. They all has three common constraints, $\lambda = 3$ and $d = 3$.*** That is why when calculate the mobility of planar mechanisms the readers are told to substitute 3 into G-K Criterion. The same reason $d = 3$ is for spherical mechanisms. This is why all textbooks tell students to take 3 for planar and spherical mechanisms [1].

4.1.2 Roberval Mechanism

Figure 4.2 shows the Roberval mechanism [2]. It is a planar five-bar linkage. In practice, it is often illustrated in many textbooks as a typical over-constraint mechanism, such as introduced by Nordon [3] and Mabie and Reinholtz[4]. However, the Roberval mechanism is much different with those shown in

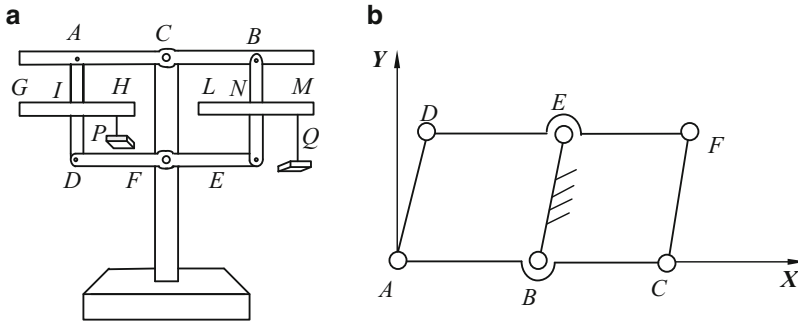


Fig. 4.2 Roberval mechanism (a) Roberval mechanism (b) sketch

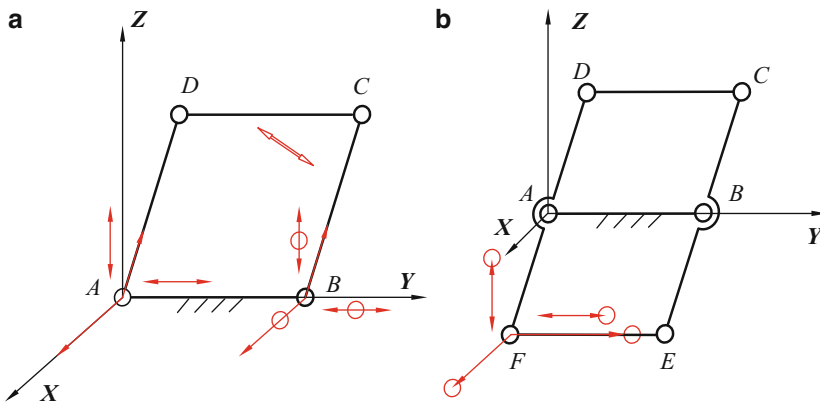


Fig. 4.3 Roberval analysis (a) parallelogram (b) double parallelogram

textbooks, as it has different frame selected. The mobility analysis of Roberval mechanism is more difficult than Norton’s one. The sketch of the Roberval mechanism is shown in Fig. 4.2b. The mechanism may be considered as a typical parallel mechanism. Firstly a parallelogram linkage is taken to analyze.

(1) A parallelogram linkage

Figure 4.3a shows a parallelogram linkage, and the coordinate system is given in the figure. It is also a parallel mechanism with two limbs. The screw system of limb AD is as follows

$$\begin{aligned}
 \mathcal{S}_A &= (1 \ 0 \ 0; \ 0 \ 0 \ 0) \\
 \mathcal{S}_D &= (1 \ 0 \ 0; \ 0 \ e \ -f)
 \end{aligned}
 \tag{4.5}$$

For the two screws their reciprocal screws are in the form

$$\begin{aligned}
 \mathcal{S}_1^r &= (1 \ 0 \ 0; \ 0 \ 0 \ 0) \\
 \mathcal{S}_2^r &= (0 \ f \ e; \ 0 \ 0 \ 0) \\
 \mathcal{S}_3^r &= (0 \ 0 \ 0; \ 0 \ 1 \ 0) \\
 \mathcal{S}_4^r &= (0 \ 0 \ 0; \ 0 \ 0 \ 1)
 \end{aligned} \tag{4.6}$$

The first two reciprocal screws denote two constraint forces along X and AD directions, respectively. The other two are constraint couples about Y and Z axes, respectively. Note that, although the two forces both pass the origin, as shown in the figure, in practice, they act on the moving link CD anyway.

Consider the two limbs are the same and their reciprocal screw systems are also the same. In this case, the end-link CD is subjected to eight constraints including four constraint forces and four couples, as shown in Fig. 4.3a. Analyzing the dependency, four constraint couples coming from the two limbs are either parallel to each other or collinear. They are linearly dependent, and only two of them are independent, which are parallel to Y or Z axes, respectively. For those two parallel forces and a couple normal to the two forces they are also linearly dependent, as shown in Table 2.1. Then, two of the three are independent. The dependent forces are drawn with a small red circle in Fig. 4.3. For the eight reciprocal screws three constraints are dependent in total and five are independent, which constrain five freedoms of link CD . That is three rotational freedoms and two translational motion along X and AD directions. Therefore, link CD has only one freedom and can only translate along a line normal to AD , red bi-directional arrow, and link AD can only rotate about point A .

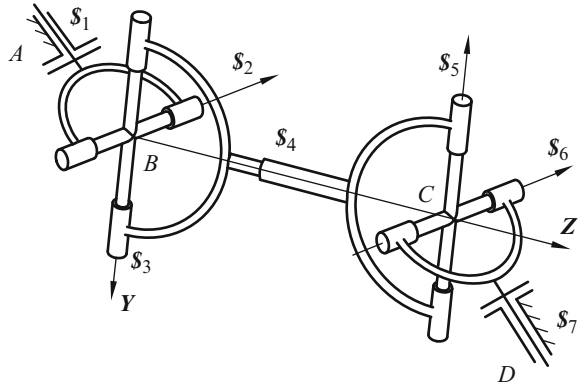
(2) Roberval Mechanism

To obtain this Roberval mechanism, we add a link FE parallel to AB to the parallelogram, as shown in Fig. 4.3b. What constraint is applied to the parallelogram by adding link EF ? The coordinate system can be set the same as before, and the constraints acting to link BC by link EF are similar to Eq. (4.6), i.e. two constraint forces and two constraint couples. The two forces are parallel to X and Y axes, and two couples are about Y and Z axes, respectively.

Comparing with the constraints of the previous parallelogram, the actions of two couples are repetitive being virtual constraints; the force parallel to X direction is also not independent or virtual; and that constraint force along EF limits the displacement unchangeable between points E and F and it is also a virtual one as it is well-known that the distance between the two corresponding points of a parallelogram is unchangeable. Therefore, the four constraints arising by adding the link EF all are virtual and the link BC does not subject any new constraint and keeps its motion unchangeable. The whole mechanism has $3 + 4 = 7$ virtual constraints. We have

$$M = d(n - g - 1) + \sum f_i + \mu = 6(5 - 6 - 1) + 6 + (3 + 4) = 1 \tag{4.7}$$

Fig. 4.4 RUPUR serial chain



As considering the screw system is unchangeable for any new configuration, common constraints are the same and the resulted mobility is also the same. Mobility is full-cycle.

4.1.3 RUPUR Mechanism

As Merlet pointed out that the Cardan joint is one of the difficult test problems [5]. Figure 4.4 shows the mechanism with double Cardan joints and a slide pair in the middle. This mechanism is often applied as a transmission axis in a car. Besides it has a revolute mobility which allows a relative displacement between the two middle axes connecting the rear wheel and the engine.

For mobility analysis the coordinate system B - XYZ is shown in the Fig. 4.4. The seven kinematic pairs are denoted as seven screws

$$\begin{aligned}
 \mathcal{S}_1 &= (a_1 \ b_1 \ c_1; \ 0 \ 0 \ 0) \\
 \mathcal{S}_2 &= (c_1 \ 0 \ -a_1; \ 0 \ 0 \ 0) \\
 \mathcal{S}_3 &= (0 \ 1 \ 0; \ 0 \ 0 \ 0) \\
 \mathcal{S}_4 &= (0 \ 0 \ 0; \ 0 \ 0 \ 1) \\
 \mathcal{S}_5 &= (0 \ 1 \ 0; \ d_4 \ 0 \ 0) \\
 \mathcal{S}_6 &= (a_5 \ 0 \ c_5; \ 0 \ e_5 \ 0) \\
 \mathcal{S}_7 &= (c_5 \ b_6 \ -a_5; \ d_6 \ e_6 \ 0)
 \end{aligned} \tag{4.8}$$

The rank of the seven screws is 6 and the mobility of the mechanism is

$$M = d(n - g - 1) + \sum_{i=1}^g f_i + v = 6(7 - 7 - 1) + 7 + 0 = 1 \tag{4.9}$$

When another rotational pair is added to the right end of the kinematic chain and normal to that end axis of \mathcal{S}_6 , as shown in Fig. 4.4, the end can both rotate and translate up and down. In this case, the mechanism has eight pairs in total. They can be expressed as a screw system in the form

$$\begin{aligned}
 \mathcal{S}_1 &= (a_1 \ b_1 \ c_1; \ 0 \ 0 \ 0) \\
 \mathcal{S}_2 &= (c_1 \ 0 \ -a_1; \ 0 \ 0 \ 0) \\
 \mathcal{S}_3 &= (0 \ 1 \ 0; \ 0 \ 0 \ 0) \\
 \mathcal{S}_4 &= (0 \ 0 \ 0; \ 0 \ 0 \ 1) \\
 \mathcal{S}_5 &= (0 \ 1 \ 0; \ d_4 \ 0 \ 0) \\
 \mathcal{S}_6 &= (a_5 \ 0 \ c_5; \ 0 \ e_5 \ 0) \\
 \mathcal{S}_7 &= (c_5 \ b_6 \ -a_5; \ d_6 \ e_6 \ 0) \\
 \mathcal{S}_8 &= (0 \ 0 \ 0; \ 1 \ 1 \ c_5 + b_6/a_5)
 \end{aligned} \tag{4.10}$$

Since the rank of the screw system is still six, by the Modified G-K formula we have

$$M = d(n - g - 1) + \sum_{i=1}^g f_i + v = 6(8 - 8 - 1) + 8 + 0 = 2 \tag{4.11}$$

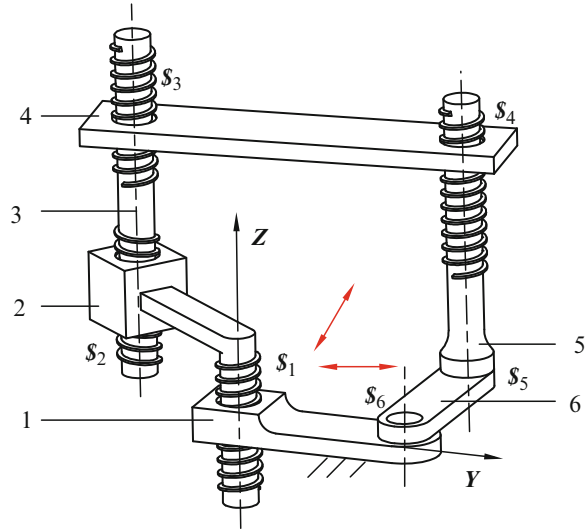
It indicates the mechanism has two DOF. One aspect it still can transfer the rotation from one end to another, and the two end axes can move relatively up and down. This mechanism is often applied for power transmission for a car.

4.1.4 *Hervé Six-Bar Mechanism*

Figure 4.5 shows a 2R4H mechanism proposed by Hervé [6]. It has six kinematic pairs, including two rotational pairs and four screw pairs with different pitches. All the axes are parallel. The screw system of the mechanism is in the form

$$\begin{aligned}
 \mathcal{S}_1 &= (0 \ 0 \ 1; \ 0 \ 0 \ h_1) \\
 \mathcal{S}_2 &= (0 \ 0 \ 1; \ d_2 \ e_2 \ h_2) \\
 \mathcal{S}_3 &= (0 \ 0 \ 1; \ d_2 \ e_2 \ h_3) \\
 \mathcal{S}_4 &= (0 \ 0 \ 1; \ d_4 \ e_4 \ h_4) \\
 \mathcal{S}_5 &= (0 \ 0 \ 1; \ d_4 \ e_4 \ 0) \\
 \mathcal{S}_6 &= (0 \ 0 \ 1; \ d_6 \ 0 \ 0)
 \end{aligned} \tag{4.12}$$

Fig. 4.5 Hervé six-bar linkage



Their reciprocal screws are in the form

$$\begin{aligned} \mathcal{S}_1^r &= (0 \ 0 \ 0; \ 1 \ 0 \ 0) \\ \mathcal{S}_2^r &= (0 \ 0 \ 0; \ 0 \ 1 \ 0) \end{aligned} \tag{4.13}$$

They are two constraint couples. The mobility of this mechanism is obtained by using the modified G-K formula as follows

$$M = d(n - g - 1) + \sum_{i=1}^g f_i + v = 4(6 - 6 - 1) + 6 = 2 \tag{4.14}$$

That means the mobility is two. For any different configuration, above analysis is unchangeable and the freedom is full-cycle.

When all the pitches of the four screws become zero, $h_1 = h_2 = h_3 = h_4 = 0$, the sixth component of each screw is also zero. Then, the number of the common constraint is more than one. Then we have

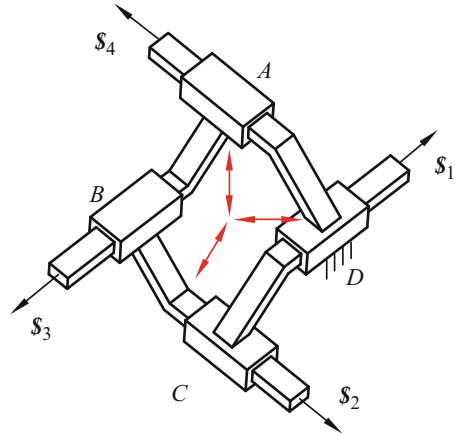
$$M = d(n - g - 1) + \sum_{i=1}^g f_i + v = 3(6 - 6 - 1) + 6 = 3 \tag{4.15}$$

In this case, the mobility is 3 and also it is full-cycle.

4.1.5 Spatial 4P Mechanism

The spatial 4P mechanism was proposed by Delassus in 1900 [7], as shown in Fig. 4.6.

Fig. 4.6 Spatial 4P linkage



Its four directions of slider are in four different directions in space and can be expressed as

$$S_i = (0 \ 0 \ 0; \ a_i \ b_i \ c_i) \quad i = 1, 2, 3, 4 \quad (4.16)$$

They are four couples in space, and they have only three reciprocal screws

$$\begin{aligned} S_1^r &= (0 \ 0 \ 0; \ 1 \ 0 \ 0) \\ S_2^r &= (0 \ 0 \ 0; \ 0 \ 1 \ 0) \\ S_3^r &= (0 \ 0 \ 0; \ 0 \ 0 \ 1) \end{aligned} \quad (4.17)$$

That means the mechanism has three common constraints, $\lambda = 3, \nu = 0$. Then its mobility is

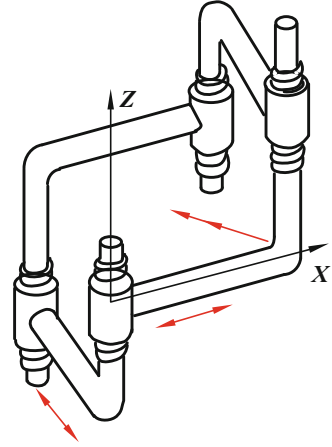
$$M = d(n - g - 1) + \sum_{i=1}^g f_i + \nu = 3(4 - 4 - 1) + 4 + 0 = 1 \quad (4.18)$$

Evidently, its mobility is fully-cycle.

4.1.6 Delassus H-H-H-H Mechanism

The Delassus H-H-H-H mechanism has five different types [7], here only one of them is discussed here, Fig. 4.7. Its four axes are parallel and four pitches keep $h_1 + h_3 = h_2 + h_4$. Assume that the lengths of the two sides are a and b , respectively. The angle between the two sides is α . Then we have

Fig. 4.7 Delassus $H-H-H-H$ -linkage



$$\begin{aligned}
 \mathcal{S}_A &= (0 \ 0 \ 1; \ 0 \ 0 \ h_1) \\
 \mathcal{S}_B &= (0 \ 0 \ 1; \ 0 \ -a \ h_2) \\
 \mathcal{S}_C &= (0 \ 0 \ 1; \ b \sin \alpha \ -a - b \cos \alpha \ h_3) \\
 \mathcal{S}_D &= (0 \ 0 \ 1; \ b \sin \alpha \ -b \cos \alpha \ h_4)
 \end{aligned} \tag{4.19}$$

It has three reciprocal screws as follows

$$\begin{aligned}
 \mathcal{S}_1^r &= (0 \ 0 \ 0; \ 1 \ 0 \ 0) \\
 \mathcal{S}_2^r &= (0 \ 0 \ 0; \ 0 \ 1 \ 0) \\
 \mathcal{S}_3^r &= \left[\frac{h_2 - h_1}{ab \sin \alpha} (a + b \cos \alpha) + \frac{h_1 - h_3}{b \sin \alpha} \frac{h_2 - h_1}{a} \ 1; \ 0 \ 0 - h_1 \right]
 \end{aligned} \tag{4.20}$$

They are two constraint couples about X and Y directions and a kinematic screw with finite pitch, which is expressed in Fig. 4.7 as the double arrow. Then $\lambda = 3$, $d = 3$, $v = 0$, we have

$$M = d(n - g - 1) + \sum_{i=1}^g f_i + v = 3(4 - 4 - 1) + 4 = 1 \tag{4.21}$$

The mobility is full-cycle.

4.1.7 Hervé's CCC Mechanism

Figure 4.8 illustrates the CCC mechanism proposed by Hervé in 1978 [8]. It is a single-loop mechanism consisting of three cylindrical pairs. Corresponding to the coordinate system the six screws are as follows

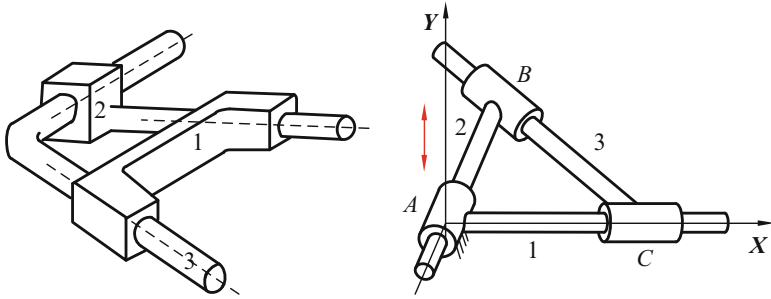


Fig. 4.8 Hervé CCC mechanism

$$\begin{aligned}
 \mathcal{S}_1 &= (a_1 \ b_1 \ 0; \ 0 \ 0 \ 0) \\
 \mathcal{S}_2 &= (0 \ 0 \ 0; \ a_1 \ b_1 \ 0) \\
 \mathcal{S}_3 &= (a_3 \ b_3 \ 0; \ 0 \ 0 \ f_3) \\
 \mathcal{S}_4 &= (0 \ 0 \ 0; \ a_3 \ b_3 \ 0) \\
 \mathcal{S}_5 &= (1 \ 0 \ 0; \ 0 \ 0 \ 0) \\
 \mathcal{S}_6 &= (0 \ 0 \ 0; \ 1 \ 0 \ 0)
 \end{aligned} \tag{4.22}$$

Since the third components in the six screws all are zero and their reciprocal screw is

$$\mathcal{S}^r = (0 \ 0 \ 0; \ 0 \ 0 \ 1) \tag{4.23}$$

It is a constraint couple and limits the rotation about Z axis. From the geometrical point of view, as shown in Table 2.1, since all the six screws are coplanar, only five of them are independent. Then there is a common constraint and we have $\lambda = 1$, $d = 5$, $v = 0$. Based on the modified mobility formula the mobility is

$$M = d(n - g - 1) + \sum_{i=1}^g f_i + v = 5(3 - 3 - 1) + 6 + 0 = 1 \tag{4.24}$$

Under any different configurations, the geometry keeps invariable and the mobility is full-cycle.

4.2 Mobility Analysis of Classical Mechanisms

4.2.1 Bennett Mechanism

The Bennett mechanism [9] is the unique spatial mechanism with the highest order in single-loop linkages, as shown in Fig. 4.9. Its mobility analysis is widely

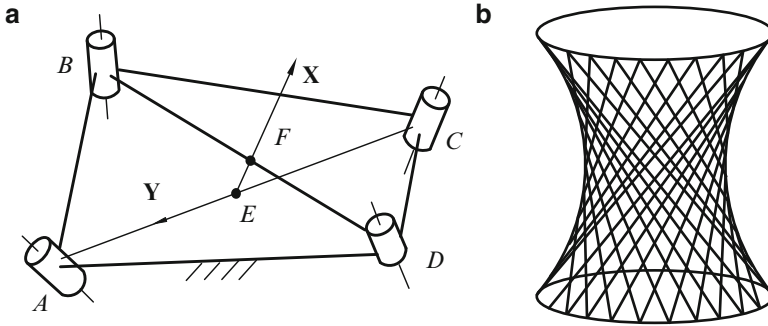


Fig. 4.9 The Bennett mechanism (a) the Bennett (b) the hyperboloid

known as the most difficult and has never been succeeded by using any *unified mobility formula* before.

A Bennett mechanism is a spatial four-bar linkage with four revolute axes with different directions in 3-D space. Each hinge axis is perpendicular to its two adjacent sides. For the mechanism, $AB = CD$ and $BC = AD$. α and β denote two relative twist angles. The Bennett linkage has a pair of links of length a , and twist angle α , and another pair of links of length d and twist angle δ . It keeps the following conditions

$$AB = CD \text{ and } BC = AD \quad (4.25)$$

$$\frac{a}{\sin \alpha} = \frac{d}{\sin \delta}$$

The Bennett mechanism is like a spatial tetrahedron. Its four joint points are four vertices of the tetrahedron. Let diagonals $AC = 2l$ and $BD = 2m$. The angle between AC and BD is β . The midpoints of AC and BD are E and F , respectively. $EF = n$. It can be found that $\triangle ABD \cong \triangle BCD$, then $\angle ABD = \angle BDC$ and $\triangle ABF \cong \triangle CDF$, thus $AF = CF$. With the same reason, $BE = DE$. Then both $\triangle AFC$ and $\triangle BED$ are of isosceles triangle, and EF is normal to both AC and BD . The coordinate system is shown in the Figure. E is the origin point; X -axis is along the common normal EF , Y -axis along EA ; Z -axis is in accordance with the right-hand rule.

The coordinates of the four vertices are then:

$$A(0 \quad l \quad 0), \quad B(n, \quad m \cos \beta, \quad -m \sin \beta),$$

$$C(0 \quad -l \quad 0), \quad D(n, \quad -m \cos \beta, \quad m \sin \beta)$$

The directions of the four revolute pairs are as follows

$$S_A = \mathbf{BA} \times \mathbf{AD}, \quad S_B = \mathbf{CB} \times \mathbf{BA}, \quad S_C = \mathbf{DC} \times \mathbf{CB}, \quad S_D = \mathbf{AD} \times \mathbf{DC} \quad (4.26)$$

Then we have

$$\begin{aligned}
 \mathbf{S}_A &= (l \sin \beta, n \sin \beta, n \cos \beta) \\
 \mathbf{S}_B &= (m \sin \beta, 0, n) \\
 \mathbf{S}_C &= (-l \sin \beta, n \sin \beta, n \cos \beta) \\
 \mathbf{S}_D &= (-m \sin \beta, 0, n)
 \end{aligned} \tag{4.27}$$

When the four axes of revolute pairs are expressed as screws, $(\mathbf{S}; \mathbf{S}_0)$ where \mathbf{S} denotes direction of the joint axis and, $\mathbf{S}_0 = \mathbf{r} \times \mathbf{S}$. The four screws are as follows

$$\begin{aligned}
 \mathcal{S}_A &= (l \sin \beta, n \sin \beta, n \cos \beta; \ln \cos \beta, 0, -l^2 \sin \beta) \\
 \mathcal{S}_B &= (m \sin \beta, 0, n; mn \cos \beta; -m^2 \sin^2 \beta - n^2, -m^2 \sin \beta \cos \beta) \\
 \mathcal{S}_C &= (-l \sin \beta, n \sin \beta, n \cos \beta; -ln \cos \beta, 0, -l^2 \sin \beta) \\
 \mathcal{S}_D &= (-m \sin \beta, 0, n; -mn \cos \beta; -m^2 \sin^2 \beta - n^2, -m^2 \sin \beta \cos \beta)
 \end{aligned} \tag{4.28}$$

From Eq. (4.28), the following quite important expression could be rapidly directed out

$$m \cdot (\mathcal{S}_A - \mathcal{S}_B) = l \cdot (\mathcal{S}_B - \mathcal{S}_D) \tag{4.29}$$

It means that the four screws are linearly dependent, and their rank is only three. It is because that any three skew straight lines in space are definitely linearly independent, as shown in Table 2.1, and lie on a hyperboloid of one sheet. Then the four skew hinge axes being linearly dependent simultaneously lie on the same hyperboloid, Fig. 4.9b. Their reciprocal screw system also contains three screws with zero-pitches lying on the same hyperboloid but in the other regulus. For a hyperboloid of one sheet there are two sets of straight lines corresponding two reguli. The Bennett mechanism has three common constraints, $\lambda = 3$. For the single-loop mechanism, $v = 0$ and $\zeta = 0$. Using the Modified G-K Criterion, Eq. (3.5), we have

$$M = d(n - g - 1) + \sum_{i=1}^g f_i + v = 3(4 - 4 - 1) + 4 + 0 = 1 \tag{4.30}$$

Therefore, Bennett mechanism has one DOF, and its four axes all lie on a hyperboloid. Note that, in the same regulus of a hyperboloid, any four lines being able to be taken as the axes for four revolute pairs compose a four-bar linkage with one DOF, since the four line vectors are linearly dependent. And there are infinite four-bar linkages with one DOF in the same regulus. Using constraint screws, we will prove that the Bennett mechanism is a unique full-cycle four-bar linkage among all other infinite four-bar linkages without the geometrical conditions like

the Bennett mechanism. The four axes of any other linkage no longer lie on a hyperboloid after any possible small motion of that linkage, therefore their motilities all are instantaneous.

Evidently, it is a difficult issue to prove the mobility of Bennett mechanism being full-cycle by a same unified mobility principle, i.e. to prove that the four axes of the Bennett mechanism still lying on a hyperboloid after any finite motion used be difficult by a unified mobility formula.

Based on our mobility principle, from Eq. (4.28), we find that when the mechanism moves, parameters, l , m , n and β are variables, and their values are dependent on the different configurations of the mechanism. However, for any chosen configuration Eq. (4.29) always holds and unchangeable, which means the four screws are certainly linearly dependent, and the mobility of the Bennett mechanism always keeps invariable. Whereas for the skew four-bar linkage without the geometrical condition like Bennett mechanism, it has no such relations described by Eq. (4.25) and (4.28), then the mobility of the four-bar linkage is not full-cycle.

Clearly the mobility analysis and full-cycle analysis of Bennett mechanism using the Modified G-K Criterion is also quite simple. ***In our limited knowledge, we do not find the mobility and its full-cycle analysis of Bennett mechanism has also been succeeded by any other unified formula till now.***

4.2.2 Five-Bar Goldberg Linkage

The Goldberg five-bar mechanism [10], $ABCGH$, is a special spatial five-bar linkage shown in Fig. 4.10a, whose mobility analysis is also one of the well-known difficult issues. The Goldberg five-bar mechanism consists of two Bennett mechanisms, $ABCD$ and $EFGH$, as shown in Fig. 4.10b, which have a link in common. One Bennett linkage has a pair of links of length a , and twist angle α , and another pair of links of length b and twist angle β . The other Bennett linkage has a pair of links of length a , and twist angle α , and another pair of links of length c and twist angle γ . The two Bennett linkages satisfy the condition [10].

$$\frac{\sin \alpha}{a} = \frac{\sin \beta}{b} = \frac{\sin \gamma}{c} \quad (4.31)$$

and when the two Bennett mechanisms are combined, the following relations are remained

$$\mathcal{S}_C = \mathcal{S}_F, \mathcal{S}_D = \mathcal{S}_E \quad (4.32)$$

Since the four screws of Bennett mechanism $ABCD$ are linearly dependent, which is proven in Eq. (4.29), the four line vectors lie on one hyperboloid. Considering that both the linearly dependency and reciprocity of screws are not

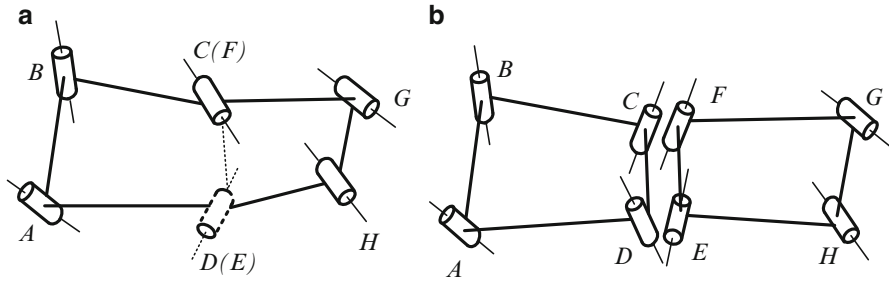


Fig. 4.10 Five-bar Goldberg (a) five-bar Goldberg (b) two Bennett linkages

origin dependent, the coordinate system for the two Bennetts can be built, and two linear equations are as follows

$$a\$A + b\$B + c\$C + d\$D = 0 \tag{4.33}$$

$$e\$E + f\$F + g\$G + h\$H = 0 \tag{4.34}$$

where a, b, c, d, e, f, g and h are coefficients.

Multiplying Eq. (4.33) by e and Eq. (4.34) by d , subtracting the two new equations, we get

$$ae\$A + be\$B + ce\$C + de\$D - ed\$E - fd\$F - gd\$G - hd\$H = 0 \tag{4.35}$$

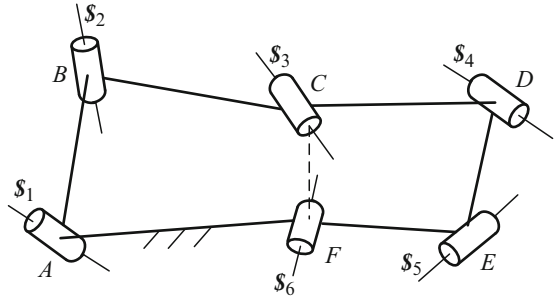
Substituting Eq. (4.32) into the above equation yields

$$ae\$A + be\$B + (ce - fd)\$F - gd\$G - hd\$H = 0 \tag{4.36}$$

Equation (4.36) indicates that the five screws, $\$A, \$B, \$F, \$G, \$H$, are linearly dependent, and their rank is less than five. Since the four screws, $\$A, \$B, \$C, \D , belonging to the first Bennett mechanism all lie on the first hyperboloid, points A and D locate on the hyperboloid as well. Since point H locates on the extending line of AD , the axis passing point H no longer lies on that hyperboloid $ABCD$, and in other words, it is outside the hyperboloid. That means the four line vectors, $\$A, \$B, \$C, \H , are linearly independent and the rank of the five screws, $\$A, \$B, \$F, \$G, \$H$, is four.

This conclusion can also be obtained from another point of view. Considering $\$C = \F , it means their two axes are coincident. We may imagine that angle $\angle BCG$ in Fig. 4.10a depends on a relative rotation of link CD about the axis of $\$C$ from direction CD to CG . That means screw $\$G$ cannot lie on the same hyperboloid formed by the four screws $\$A, \$B, \$C, \D . Therefore the four screws $\$A, \$B, \$F, \G are also linearly independent. From the above analysis, the five screws,

Fig. 4.11 6R Goldberg



$\$A, \$B, \$C, \$G, \$H,$ have two reciprocal screws, $\lambda = 2$ and $\nu = 0$. Substituting them into Eq. (3.5) yields

$$M = d(n - g - 1) + \sum_{i=1}^g f_i + \nu = 4(5 - 5 - 1) + 5 + 0 = 1 \quad (4.37)$$

Hence, the mobility of the five-bar Goldberg mechanism is one. For any possible motion of the mechanism the previous analysis is also correct, and there also exists $\lambda = 2$ and $\nu = 0$, then Eq. (4.36) keeps correct and the mobility is not instantaneous.

4.2.3 Six-Bar Goldberg Linkage

The Goldberg six-bar mechanism [10] is also composed of two Bennett mechanisms, $ABCF$ and $CDEF$, as shown in Fig. 4.11. The screw equations of the two Bennett mechanisms can be expressed as

$$k_{11}\$1 + k_{12}\$2 + k_{13}\$3 + k_{16}\$6 = 0 \quad (4.38)$$

$$k_{23}\$3 + k_{24}\$4 + k_{25}\$5 + k_{26}\$6 = 0 \quad (4.39)$$

Let “(4.38) + (4.39)” the screw equation for linkage $ABCDEF$ can be obtained as follows

$$t_1\$1 + t_2\$2 + t_3\$3 + t_4\$4 + t_5\$5 + t_6\$6 = 0 \quad (4.40)$$

where

$$\begin{aligned} t_1 &= k_{11}, & t_2 &= k_{12}, & t_3 &= k_{13} + k_{23}, \\ t_4 &= k_{24}, & t_5 &= k_{25}, & t_6 &= k_{16} + k_{26} \end{aligned} \quad (4.41)$$

Table 4.1 Six sub-screw systems

Item	Screw system
SS ₁	$\$1, \$2, \$3, \$4, \$5$
SS ₂	$\$1, \$2, \$3, \$4, \$6$
SS ₃	$\$1, \$2, \$3, \$5, \$6$
SS ₄	$\$1, \$2, \$4, \$5, \$6$
SS ₅	$\$1, \$3, \$4, \$5, \$6$
SS ₆	$\$2, \$3, \$4, \$5, \$6$

From Eq (4.40), the screw system of linkage *ABCDEF* is linearly dependent and then $d < 6$. In addition, the four screws, $\$1, \$2, \$3$ and $\$4$ is linearly independent, then $d \geq 4$. Therefore, the order of the mechanism d is in the range [4, 6), that means the possible value is $d = 4$ or $d = 5$.

If $d = 4$, any five screws for *ABCDEF* are linearly dependent. The six screws ($\$1, \$2, \$3, \$4, \$5, \6), include six sub-system with five screws, Table 4.1

Now let's to estimate the dependency of the sub-system:

1. Let $k_{26} \times (4.38) - k_{16} \times (4.39)$ to exclude $\$6$, and find the sub-system SS₁. Clearly, it is linearly dependent.
2. AS SS₂ and SS₃ both contain four screws $\$1, \$2, \$3, \6 , which belong to the 1st Bennett and are linearly dependent. Thus, the SS₂ and SS₃ are linearly dependent;
3. By $k_{23} \times (4.38) - k_{13} \times (4.39)$ to exclude $\$3$, the SS₄ is linearly dependent;
4. As SS₅ and SS₆ both contain four screws $\$3, \$4, \$5, \6 , which belong to the 2nd Bennett and are linearly dependent. Thus, the SS₅ and SS₆ are linearly dependent;

Based on above analysis, the order of the mechanism is $d = 4$. No matter what configuration, mechanisms, *ABCF* and *CDEF* both are Bennett form and the order of the six-bar linkage always keeps the unique value, $d = 4$. From the Modified G-K formula, Eq. (3.5), we have

$$M = d(n - g - 1) + \sum_{i=1}^g f_i + v = 4(6 - 6 - 1) + 6 + 0 = 2 \tag{4.42}$$

The mobility of the 2-bar Goldberg is 2 and full-cycle.

4.2.4 Myard Linkage with Symmetrical Plane

Figure 4.12 shows the *ABCDE* Myard linkage with a symmetrical plane, and it is a five-bar linkage [11]. It consists of two Bennetts, *ABCF* and *AEDF* and by concealing a couple of superposition kinematic pairs in point *F*. In the mean time the angles between $\$2$ and $\$3$ as will as $\$4$ and $\$5$ both are $\pi/2$ [12].

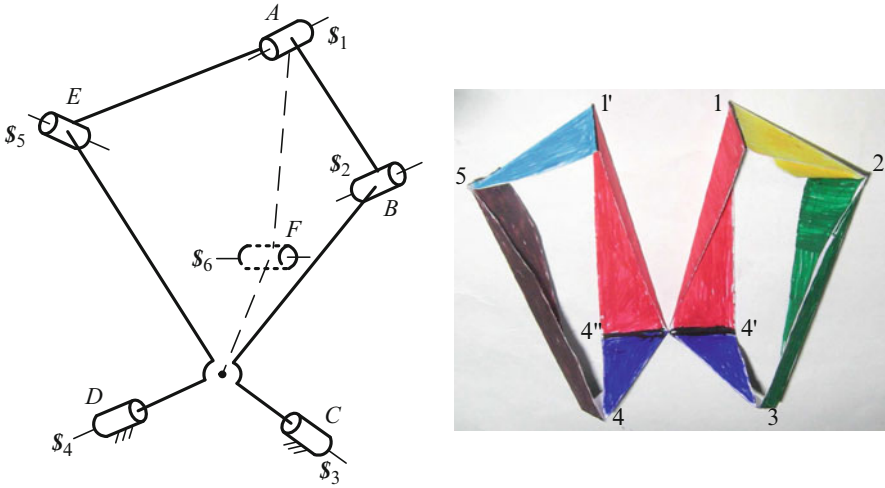


Fig. 4.12 5R Myard

Since $ABCF$ and $AEDF$ both are Bennetts, in respective limb systems we have

$$a_1\$1 + a_2\$2 + a_3\$3 + a_6\$6 = 0 \tag{4.43}$$

$$a_1\$1 + a_5\$5 + a_4\$4 + a_6\$6 = 0 \tag{4.44}$$

It is easily to eliminate $\$6$ from the two equations, and yield

$$a_1\$1 + a_2\$2 + a_3\$3 + a_4\$4 + a_5\$5 = 0 \tag{4.45}$$

That means the order of the mechanism is less 5, $d < 5$. Considering $\$1, \$2, \$3$ and $\$4$ being linearly independent as they are not in an identical Bennett, $d \geq 4$. So that, for this mechanism it should be $d = 4$. From the Modified G-K formula, we have

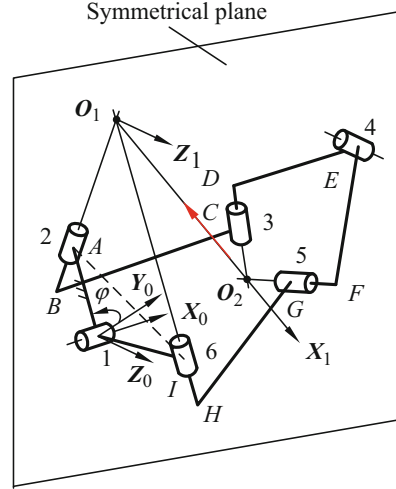
$$M = d(n - g - 1) + \sum_{i=1}^g f_i + v = 4(5 - 5 - 1) + 5 + 0 = 1 \tag{4.46}$$

And evidently, the mechanism is full-cycle.

4.2.5 Bricard with Symmetrical Plane

The Bricard mechanism to be analyzed here is the general form of Bricard shown in Fig. 4.13 [13]. Baker also provides the following D-H geometrical parameters for the mechanism in [13].

Fig. 4.13 Bricard with symmetrical plane



$$\begin{aligned}
 a_{12} &= a_{61}, & a_{23} &= a_{56}, & a_{34} &= a_{45} \\
 \alpha_{12} + \alpha_{61} &= \pi, & \alpha_{23} + \alpha_{56} &= \pi, & \alpha_{34} + \alpha_{45} &= \pi \\
 R_1 &= R_4 = 0, & R_2 &= R_6, & R_3 &= R_5 \\
 \theta_2 + \theta_6 &= 2\pi, & \theta_3 + \theta_5 &= 2\pi
 \end{aligned}
 \tag{4.47}$$

Based on the geometrical conditions, it is not difficult to prove that the linkage can always keep having a symmetrical plane. Coordinate system $O_0\text{-}X_0Y_0Z_0$ is established as shown in the Figure. X_0 -axis is along the axis of joint 1 and Y_0 -axis passing through points O and J . Here, J is the midpoint of the line AI .

Using those relations in Eq. (4.47) and after some coordinates transform, we can get all the coordinates of the points including from A to I in the reference frame $O_0\text{-}X_0Y_0Z_0$. The results are not given here for limited space. Then, the following relations can be obtained

$$\begin{aligned}
 X_A &= X_I & X_B &= X_H & X_C &= X_G & X_D &= X_F \\
 Y_A &= Y_I & Y_B &= Y_H & Y_C &= Y_G & Y_D &= Y_F \\
 Z_A &= -Z_I & Z_B &= -Z_H & Z_C &= -Z_G & Z_D &= -Z_F & Z_A &= 0
 \end{aligned}
 \tag{4.48}$$

Furthermore, we have

$$\begin{aligned}
 S_1 &= \mathbf{OA} \times \mathbf{OI} = (-2Y_A Z_A \quad 2X_A Z_A \quad 0) \\
 S_4 &= \mathbf{ED} \times \mathbf{EF} = (-2(Y_D - Y_E)Z_D \quad 2(X_D - X_E)Z_D \quad 0)
 \end{aligned}
 \tag{4.49}$$

Using Eqs. (4.48) and (4.49), we know that the axes of joints 1 and 4 both lie on the plane $X_0O_0Y_0$. From above analysis, we can conclude that the linkage is symmetrical about plane $X_0O_0Y_0$.

Angle φ between Y -axis and O_0A is a variable, but the Eqs. (4.48) and (4.49) are independent of the angle φ . So we can further consider there always has a plane about which the linkage is symmetrical no matter what the configuration of this mechanism is. This symmetrical plane is composed of the axis of joint 1 and the line passing through the points O and J .

Since the whole linkage is symmetrical about a plane, the intersection points O_1 and O_2 both lie on the symmetrical plane. Here, O_1 is the intersection point of axes 2 and 6, and O_2 is the intersection point of axes 3 and 5. Then a new coordinate system $O_1-X_1Y_1Z_1$ is established in Fig. 4.13, where O_1Z_1 is perpendicular to the symmetrical plane and O_1X_1 passes through the point O_2 . Plane $X_1O_1Y_1$ is just the symmetrical plane of the mechanism.

So the six screws of this linkage can be expressed as follows

$$\begin{aligned}
 \mathcal{S}_1 &= (a_1 \quad b_1 \quad 0; \quad 0 \quad 0 \quad f_1) \\
 \mathcal{S}_2 &= (a_2 \quad b_2 \quad c_2; \quad 0 \quad 0 \quad 0) \\
 \mathcal{S}_3 &= (a_3 \quad b_3 \quad c_3; \quad 0 \quad e_3 \quad f_3) \\
 \mathcal{S}_4 &= (a_4 \quad b_4 \quad 0; \quad 0 \quad 0 \quad f_4) \\
 \mathcal{S}_5 &= (a_3 \quad b_3 \quad -c_3; \quad 0 \quad e_3 \quad -f_3) \\
 \mathcal{S}_6 &= (a_2 \quad b_2 \quad -c_2; \quad 0 \quad 0 \quad 0)
 \end{aligned} \tag{4.50}$$

where the elements, a_i , b_i , c_i , e_i , and f_i , are variables and depended on the poses of the screw axes, but their values do not affect to get the reciprocal screws yet. In addition, the 1st and the 4th axes lie on plane $X_1O_1Y_1$, and the 2nd and 6th axes pass through the origin point, and the 3rd and 5th axes intersect X -axis. Clearly the fourth elements in all screw expressions are zero. Based on the simplified method mentioned in Table 2.2, their reciprocal screw is

$$\mathcal{S}_1^r = (1 \quad 0 \quad 0; \quad 0 \quad 0 \quad 0) \tag{4.51}$$

Consequently, we have $\lambda = 1$, $d = 5$, and $v = 0$. Based on the ‘‘Modified Grübler-Kutzbach Criterion’’, Eq. (3.5), the mobility of the linkage is

$$M = d(n - g - 1) + \sum_{i=1}^g f_i + v = 5(6 - 6 - 1) + 6 + 0 = 1 \tag{4.52}$$

After any possible movement of this linkage, there always exists a plane about which the linkage is symmetrical and the kinematic and reciprocal screw systems can always be expressed as the Eqs. (4.50) and (4.51). The mechanism always has one common constraint and the order is five, so the mobility is not instantaneous.

From another point of view, from Table 2.2, it is easy to find that there is a line which intersect the six screws, $\mathcal{S}_1, \mathcal{S}_2, \mathcal{S}_3 \dots \mathcal{S}_6$, simultaneously. That line is just the X_1 axis and the constraint reciprocal force is aligned on the line, as shown in Fig. 4.13.

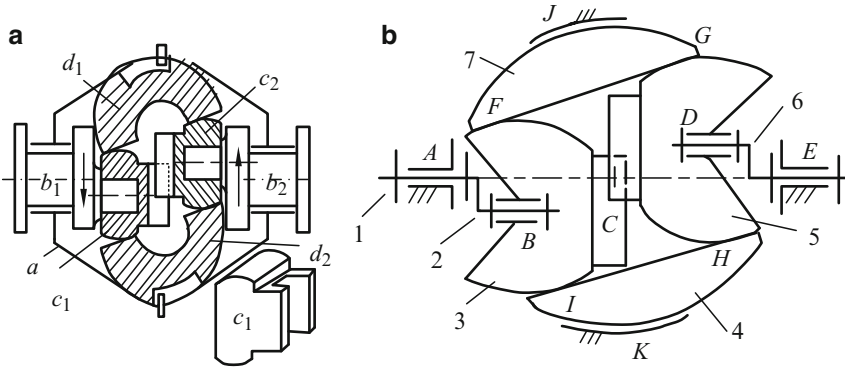


Fig. 4.14 Altmann Abb. 34 mechanism (a) Altmann Abb. 34 (b) sketch of the mechanism

4.2.6 Altmann Abb.34 Mechanism

Figure 4.14 shows the Altmann Abb.34 mechanism [14]. It can be considered as his most complex mechanisms. The mechanism structure is symmetrical, as shown in Fig. 4.14a, and its input and output axes are aligned. Crank 1 connects a cylinder 3 with a slideway. The left and right cylinders 3 and 5 are connected by a slide pair C as well as connected to upper and lower two half-moon cylinders, 4 and 7 by four “cylinder-plane pair”, shown in four points, F, G, H and I. The upper and lower half-moon cylinders can revolute about a common center point locating on the center line AE. The half-moon cylinders cannot translate along the line normal to the paper as a pin fixed on the frame, as shown in Fig. 4.14a.

(1) ABCDE closed-loop sub-chain

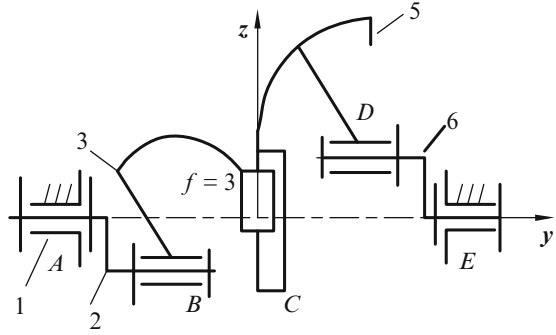
Firstly, the links 1, 2, 3, 5, 6 constitute a single-loop subchain, as shown in Fig. 4.15, and in coordinate system C-xyz, y axis is along line AE, z axis is along the center line of the mechanism. The screw system is in the form

$$\begin{aligned}
 \mathcal{S}_1 &= (0 \ 1 \ 0; \ 0 \ 0 \ 0) \\
 \mathcal{S}_2 &= (0 \ 1 \ 0; \ d_2 \ 0 \ f_2) \\
 \mathcal{S}_3 &= (0 \ 0 \ 0; \ 0 \ 0 \ 1) \\
 \mathcal{S}_4 &= (0 \ 1 \ 0; \ d_4 \ 0 \ f_4) \\
 \mathcal{S}_5 &= (0 \ 1 \ 0; \ 0 \ 0 \ 0)
 \end{aligned}
 \tag{4.53}$$

As all the 1st, 3rd and 5th components in screws are zero, it indicates the rank of the screw system is 3 and it has three common constraints, $d=3$, i.e. it has three over-constraints, $\mu=3$. Using the modified G-K formula Eq. (3.5), the mobility is as follows

$$M = d(n - g - 1) + \sum f_i + v = 3(5 - 5 - 1) + 5 + 0 = 2
 \tag{4.54}$$

Fig. 4.15 *ABCDE* sub-linkage



The mobility of the mechanism is 2. This result can also be obtained by using Eq. (3.4)

$$M = 6(n - g - 1) + \sum f_i + \mu = 6(5 - 5 - 1) + 5 + 3 = 2 \quad (4.55)$$

(2) The motion of cylinder 3

The different link in the mechanism with 2-DOF has different freedom, however. Here it is necessary to analyze the freedom of link 3. In order to do this, kinematic chain in Fig. 4.15 can be regarded as a parallel mechanism with two limbs and link 3 is its out-put link. The left limb has two revolute pair RR

$$\begin{aligned} \mathcal{S}_{11} &= (0 \ 1 \ 0; \ 0 \ 0 \ 0) \\ \mathcal{S}_{12} &= (0 \ 1 \ 0; \ d_2 \ 0 \ f_2) \end{aligned} \quad (4.56)$$

Their reciprocal screws are

$$\begin{aligned} \mathcal{S}_{11}^r &= (0 \ 0 \ 0; \ 1 \ 0 \ 0) \\ \mathcal{S}_{12}^r &= (0 \ 0 \ 0; \ 0 \ 0 \ 1) \\ \mathcal{S}_{13}^r &= (0 \ 1 \ 0; \ 0 \ 0 \ 0) \\ \mathcal{S}_{14}^r &= (f_2 \ 0 \ -d_2; \ 0 \ 0 \ 1) \end{aligned} \quad (4.57)$$

The screw system for right chain including corresponding to two revolute and one prismatic pairs is

$$\begin{aligned} \mathcal{S}_{21} &= (0 \ 1 \ 0; \ 0 \ 0 \ 0) \\ \mathcal{S}_{22} &= (0 \ 1 \ 0; \ d_3 \ 0 \ f_3) \\ \mathcal{S}_{23} &= (0 \ 0 \ 0; \ 0 \ 0 \ 1) \end{aligned} \quad (4.58)$$

Their reciprocal screws are

$$\begin{aligned}\$_{21}^r &= (0 \ 0 \ 0; \ 1 \ 0 \ 0) \\ \$_{22}^r &= (0 \ 0 \ 0; \ 0 \ 0 \ 1) \\ \$_{23}^r &= (0 \ 1 \ 0; \ 0 \ 0 \ 0)\end{aligned}\tag{4.59}$$

Comparing Eq. (4.57) with (4.59), the independent reciprocal screws among the seven screws is 4, $\sigma = 4$, then from Eq. (3.6) the freedom of the cylinder 3 is

$$M_G = 6 - \sigma = 6 - 4 = 2\tag{4.60}$$

Similarly cylinder 5 also has two freedoms. They can rotate about y axis and translate along two different directions parallel plane XY.

(3) The whole mechanism

For the whole mechanism, it is comprised of above-mentioned closed-loop subchain and two half-moon cylinders. Let us analyze what constraints will appear when two half-moon cylinders are inserted into those two small opening.

Considering the cylinder-plane pair (C-P pair) in point F, the C-P pair has four freedoms including two rotational and two translational ones. They can be expressed as four screws

$$\begin{aligned}\$_{11} &= (1 \ 0 \ 0; \ 0 \ e_1 \ f_1) \\ \$_{12} &= (0 \ 0 \ 1; \ d_2 \ 0 \ 0) \\ \$_{13} &= (0 \ 0 \ 0; \ 1 \ 0 \ 0) \\ \$_{14} &= (0 \ 0 \ 0; \ 0 \ 1 \ 0)\end{aligned}\tag{4.61}$$

Their two reciprocal screws are as follows

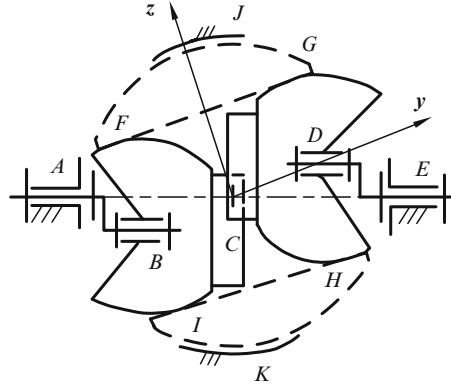
$$\begin{aligned}\$_{11}^r &= (0 \ 0 \ 0; \ 0 \ 1 \ 0) \\ \$_{12}^r &= (0 \ 0 \ 1; \ -f_1 \ 0 \ 0)\end{aligned}\tag{4.62}$$

One of them is a constraint couple limiting the link 3 rotations about y axis, and the other one is a constraint force limiting the separation of two parts of the pair along its normal.

For the whole mechanism, the four C-P pairs of the upper and lower two half-moon cylinders exert eight constraints to the mechanism, four of them are constraint couples and the other four are constraint forces. It is clear, as shown in Fig. 4.16, that the half-moon cylinders limits rotation motion of the link 3 about y axis.

As the cylinder 3 cannot rotate about any axis parallel to line FG , and also clearly, as the left and right cylinders, 3 and 5, connected by a slide pair C, the cylinder 5 also cannot revolute about any axis parallel to line FG similarly. From this analysis *three of the four couples are virtual constraint*. On the other hand, in idealization manufacture with enough precision, in order to keep 4 points, F , G , H and I , not separate, only 2 of the 4 constraint conditions are necessary. That means

Fig. 4.16 Two half-moon cylinders



when left cylinder 3 can contact with the upper and lower two half-moon cylinders simultaneously at points *F* and *I*, and the right cylinder 5 can also touch the same two half-moon cylinders at points *G* and *H*. There appear *two more virtual constraints*. In a word, two half-moon cylinders bring five virtual constraints. For the whole mechanism, there are 7 links, 11 kinematic pairs, where 4 of them are 4-DOF pairs. Besides, there are eight virtual constraints in total. Then from the Modified G-K formula (3.4), we have

$$M = d(n - g - 1) + \sum f_i + \mu = 6(7 - 11 - 1) + (7 \times 1 + 4 \times 4) + 8 = 1 \tag{4.63}$$

From above analysis, when left crank rotates, two links, 3 and 5, with slider do not rotate and can only translate forward and backward, as well as the right crank rotates in opposite direction.

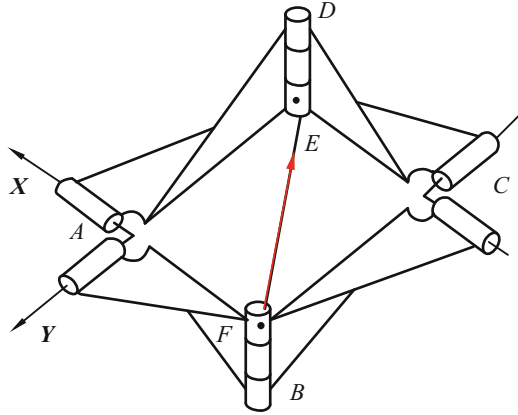
When the crank rotates the configuration changes, above analysis is unchangeable and the mobility is full-cycle.

4.2.7 Altmann Six-Bar Linkage

Figure 4.17 shows an Altmann six-bar single-loop RURU linkage [15]. Its D-H parameters are as follows

$$\begin{aligned} a_{12} = a_{45} = 0, \quad a_{23} = a_{56} = b, \quad a_{34} = a_{61} = a \\ \alpha_{12} = \alpha_{23} = \alpha_{45} = \alpha_{61} = \frac{\pi}{2}, \quad \alpha_{34} = \alpha_{56} = \frac{3\pi}{2} \\ S_i = 0 \quad (i = 1, 2, \dots, 6) \\ \theta_1 = \theta_4, \quad \theta_2 = \theta_5, \quad \theta_3 + \theta_6 = 2\pi \end{aligned} \tag{4.64}$$

Fig. 4.17 Altmann line
symmetrical mechanism



From which we can set the screw system as

$$\begin{aligned}
 \mathcal{S}_1 &= (1, 0, 0; 0, 0, 0) \\
 \mathcal{S}_2 &= (0, 1, 0; 0, 0, 0) \\
 \mathcal{S}_3 &= (-c\theta_2, 0, s\theta_2; 0, -b, 0) \\
 \mathcal{S}_4 &= (-s\theta_2s\theta_3, c\theta_3, \frac{c\theta_2s\theta_2(a+bc\theta_3)}{a}; -c\theta_2(a+bc\theta_3), 0, s\theta_2(a+bc\theta_3)) \quad (4.65) \\
 \mathcal{S}_5 &= (c\theta_2, s\theta_1s\theta_3, \frac{c\theta_1s\theta_2(ac\theta_3+b)}{b}; 0, -c\theta_1(ac\theta_3+b), s\theta_1(ac\theta_3+b)) \\
 \mathcal{S}_6 &= (0, -c\theta_1, s\theta_1; -a, 0, 0)
 \end{aligned}$$

Its reciprocal screw is

$$\mathcal{S}^r = (bs\theta_1 \quad as\theta_2 \quad 0; 0 \quad 0 \quad ab) \quad (4.66)$$

Then $\lambda = 1$, $d = 5$, and we have

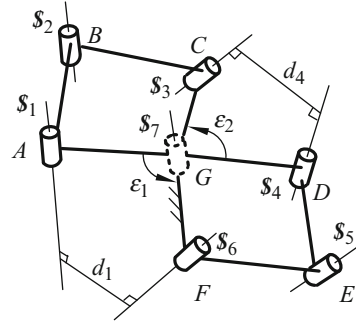
$$M = d(n - g - 1) + \sum f_i + v = 5(6 - 6 - 1) + 6 + 0 = 1 \quad (4.67)$$

From the geometrical point of view, it is easier to determine. From Fig. 4.17 four screws of those six screws lie on the same XY plane. The line connects two point E and F, which locate on the 3rd and 6th screws, respectively. This line can intersect those six screws and is collinear with their reciprocal screw. There is a reciprocal screw, as shown in Table 2.2, and the $\lambda = 1$, $d = 5$, the result is the same.

4.2.8 Waldron Six-Bar Linkage

In 1999 Waldron proposed a quite special six-bar mechanism consisting also of two Bennett linkages [16], ABCG and GDEF, Fig. 4.18.

Fig. 4.18 Waldron six-bar linkage



In order to analyze its mobility, it can set the screw equation for each Bennett linkage and then eliminate $\$7$, we have

$$q_1\$1 + q_2\$2 + q_3\$3 + q_4\$4 + q_5\$5 + q_6\$6 = 0 \tag{4.68}$$

where q_i ($i = 1, 2, \dots, 6$) are the coefficients of the equation. Evidently, the six screws are linearly dependent and the mobility of the mechanism is not zero.

Since the four screws, $\$1, \$2, \$3$ and $\$4$ are not in a same Bennett and also not lie on the identical hyperboloid, then they are linearly independent. So the possible rank of the six screws is 4 or 5. Let us firstly suppose the rank of those six screws be 4. If so, any five screws of those six screws are certainly linearly dependent. Considering any screw in the four screw, $\$4, \$5, \$6$ and $\$7$, can be expressed by the linear combination of the four screws, $\$1, \$2, \$3$ and $\$4$; and also considering that the four screws, $\$4, \$5, \$6$ and $\$7$ belong to a same Bennett and they lie the same hyperboloid. They are linearly dependent

$$a_4\$4 + a_5\$5 + a_6\$6 + a_7\$7 = 0 \tag{4.69}$$

When screws, $\$5, \6 and $\$7$ all are substituted by $\$1, \$2, \$3$ and $\$4$, then Eq. (4.69) becomes a homogeneous linear equation consisting of four screws, $\$1, \$2, \$3$ and $\$4$. This result is contradiction with above-mentioned supposition. Then the only possible value of the rank of the mechanism is 5. Then, $d = 5$ and

$$M = d(n - g - 1) + \sum_{i=1}^g f_i + v = 5(6 - 6 - 1) + 6 + 0 = 1 \tag{4.70}$$

The mobility of the mechanism is full-cycle, clearly.

4.3 Mobility Analysis of Modern Parallel Mechanisms

4.3.1 4-DOF 4-URU Mechanism

The mechanism proposed in 2000 [17], as shown in Fig. 4.19, is the first 4-DOF structure symmetrical parallel mechanism in the world with identical four limbs. Each limb consists of two U pairs and one R pair, where U denotes a universal joint and is equivalent to two revolute pairs. Therefore, each limb contains equivalent five single-DOF revolute pairs. Note that, the three axes, the 2nd, 3rd and the 4th, in each limb are parallel. For every limb the axes of the first pair fixed on the base and the 5th axis fixed on the platform are normal to the base and the moving platform, respectively. Thus, the four axes fixed on the base and four axes fixed on the platform are parallel. In addition, the direction of the second pair in each limb is parallel to the base. And the second pairs of the four limbs are in two different directions at least.

Let us consider the 1st limb. The local coordinate system is shown in Fig. 4.19. Its Z_I -axis is along the 1st revolute pair upward and Y_I -axis along the 2nd pair parallel to the base. The origin point of the limb system locates the center of the crosshead. Then the five screws with above mentioned geometrical conditions are given by

$$\begin{aligned}
 \mathcal{S}_1^1 &= (0 \ 0 \ 1; \ 0 \ 0 \ 0) \\
 \mathcal{S}_2^1 &= (0 \ 1 \ 0; \ 0 \ 0 \ 0) \\
 \mathcal{S}_3^1 &= (0 \ 1 \ 0; \ d_3 \ 0 \ f_3) \\
 \mathcal{S}_4^1 &= (0 \ 1 \ 0; \ d_4 \ 0 \ f_4) \\
 \mathcal{S}_5^1 &= (0 \ 0 \ 1; \ 0 \ e_5 \ 0)
 \end{aligned} \tag{4.71}$$

where d_i , e_i and f_i depend on the mechanism configuration and kinematic parameters. Values of these elements are not important since they do not affect to obtain reciprocal screws. Clearly the first element in every screw expression is zero. Based on the simplified geometrical method, Table 2.2, their reciprocal screw is

$$\mathcal{S}^r = (0 \ 0 \ 0; \ 1 \ 0 \ 0) \tag{4.72}$$

It is a constraint couple acting on the moving platform with its direction being along the local X_1 -axis, in other words, parallel to the base. For other three limbs they are identical with the 1st one and from the “*logical ratiocination*”, they each also has a constraint couple.

For the whole mechanism, the four identical limbs impose four constraint couples upon the platform in total; they are all parallel to the base but in two different directions at least. Among the four constraint couples only two of them are independent, from Table 2.1. It has no any common constraint, $\lambda = 0$ and $d = 6$,

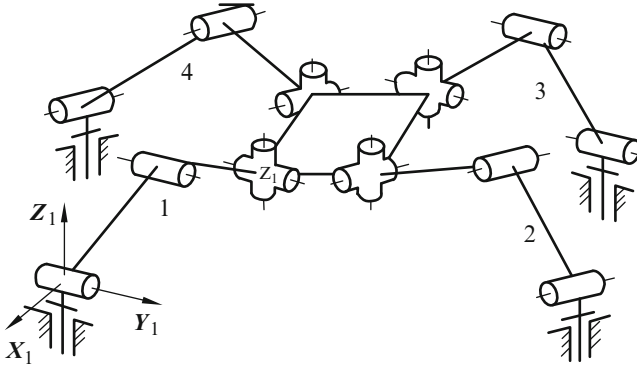


Fig.4.19 The 4-DOF 4-URU mechanism

and $v = 2$. There is no any passive freedom. Then using Eq. (3.5), we can obtain the mobility of the 4-UPU parallel mechanism as follows

$$M = d(n - g - 1) + \sum_{i=1}^g f_i + v = 6(10 - 12 - 1) + 20 + 2 = 4 \quad (4.73)$$

There exist two independent constraint couples, and the mechanism loses two rotational freedoms and has three translational and one rotational degree of freedom. This mechanism is like the famous SCARA robot with the same mobility, Schönflies motions.

After any possible platform motion, including the translation and rotation, the screw systems, in Eqs. (4.71) and (4.72), are invariable. Therefore, the mobility is full-cycle.

Based on the analysis of this parallel mechanism here we want make an explanation on this method to show how easy and why easy the mobility method are.

From the example it is clear **that for this limb coordinate system to set those screw expressions with many zero-elements is possible and easy to find their reciprocal screws**. Whereas, if we choose any global coordinate system for all limbs, it would be very difficult and even impossible to establish Plücker coordinates of screws with different directions and positions in 3D space, and then impossible to quickly get the reciprocal screws as well as mechanism mobility. That is not only because we even do not know any dimension of the mechanism at the mobility analysis phase, but also in this case the elements in screw expressions would not be zero any more. In this case, to obtain the reciprocal screw is almost impossible and so for the mobility. In addition, after obtaining Eq. (4.72), we use the words “*parallel to the base*” to depict the direction of the constraint screw apart from the local system (such as parallel X_1 -axis, etc.), then we may easily discuss the constraints for other limbs. This is the “**logical ratiocination**”. A great number of mechanisms are in the similar case, and it has to choose appropriate local system and logical ratiocination. This is the shortcut for mobility analysis.

Moreover, it is also easy to find the mobility’s change using the method, say, to find the singularity. For example, if the three successive revolute pairs, the 2nd, 3rd and the 4th in a limb were coplanar, the three screws would be consequentially linearly dependent from Table 2.1, and the number of their reciprocal screws would change, and then mobility changes also. The mechanism would be singular.

On the mobility analysis of parallel mechanisms, the basic idea is that analyzing the constraint of each limb firstly, and then considering all the constraints acting on platform to get the mechanism mobility by using ‘limb coordinate system’ and ‘logical ratiocination’. Take the Stewart platform as a example, as each limb is a 6-DOF kinematic chain and no any constraint acting on the platform, the manipulator mobility is six undoubtedly.

4.3.2 3-CRR Mechanism

Figure 4.20 shows the 3-CRR mechanism with three translational freedoms proposed by Kong and Gosselin [18] in 2002. The similar 3-D translational mechanism CPM was proposed by Kim and Tsai in 2002 [19]. Actually, the same mechanism had been proposed in 2001 [20]. The 3-CRR mechanism has three identical limbs. Each limb consists of three parallel kinematic pairs including one cylinder pair and two revolute pairs. The coordinate system is selected as shown in Fig. 4.20. The 1st limb is taken to analyze. Then the screw system of the limb is

$$\begin{aligned}
 \mathcal{S}_1 &= (0 \ 0 \ 0; \ 1 \ 0 \ 0) \\
 \mathcal{S}_2 &= (1 \ 0 \ 0; \ 0 \ 0 \ 0) \\
 \mathcal{S}_3 &= (1 \ 0 \ 0; \ 0 \ e_3 \ f_3) \\
 \mathcal{S}_4 &= (1 \ 0 \ 0; \ 0 \ e_4 \ f_4)
 \end{aligned}
 \tag{4.74}$$

Evidently, its reciprocal screw system is

$$\begin{aligned}
 \mathcal{S}_1^r &= (0 \ 0 \ 0; \ 0 \ 1 \ 0) \\
 \mathcal{S}_2^r &= (0 \ 0 \ 0; \ 0 \ 0 \ 1)
 \end{aligned}
 \tag{4.75}$$

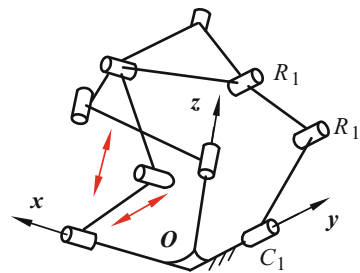


Fig. 4.20 Sketch of 3-CRR mechanism

They are two constraint couples parallel with y - and z -axes, respectively. In other words, they are normal to the 1st revolute pair of that limb.

Similarly, two constraint couples for the 2nd or 3rd limbs can directly be obtained only by simple logical ratiocination: because the structures of the 2nd or 3rd limbs are identical with the 1st limb, the corresponding two constraint couples of the 2nd or 3rd limb are also normal to their 1st revolute axis, respectively. Therefore, for the whole mechanism there are six constraint couples normal to three different axes acting on the moving platform. Based on the Table 2.1, there are three redundant constraints and no any common constraint, that is $\nu = 3$ and $\lambda = 0$. From the Modified Grübler-Kutzbach Criterion, the mobility is

$$M = d(n - g - 1) + \sum_{i=1}^g f_i + \nu = 6(11 - 12 - 1) + 12 + 3 = 3 \quad (4.76)$$

After any finite translation of the mechanism, Eqs. (4.74), (4.75) and (4.76) are invariable and the mobility is also not instantaneous.

4.3.3 Zlatanov and Gosselin's Mechanism

In 2001 Zlatanov and Gosselin proposed a 4-DOF parallel mechanism [21], as shown in Fig. 4.21. It consists of three (RRR)RR kinematic chains. The axes of the first three intersect at a common centre point and the last two are parallel to each other and parallel to the upper platform. Three limbs of the mechanism are fixed to the basic plane symmetrically and three centre points are coincident.

To analyze the mechanism one of the limb is taken to show the coordinate system, as shown in Fig. 4.21b. The limb screw system is as follows

$$\begin{aligned} \mathcal{S}_1 &= (1 \ 0 \ 0; \ 0 \ 0 \ 0) \\ \mathcal{S}_2 &= (a_2 \ b_2 \ c_2; \ 0 \ 0 \ 0) \\ \mathcal{S}_3 &= (a_3 \ b_3 \ c_3; \ 0 \ 0 \ 0) \\ \mathcal{S}_4 &= (a_4 \ b_4 \ 0; \ d_4 \ e_4 \ f_4) \\ \mathcal{S}_5 &= (a_4 \ b_4 \ 0; \ d_5 \ e_5 \ f_5) \end{aligned} \quad (4.77)$$

Let us take one point (x_4, y_4, z_4) in axis 4 and a point (x_5, y_5, z_5) in axis 5, we have

$$\begin{aligned} d_4 &= -b_4 z_4, & e_4 &= a_4 z_4 \\ d_5 &= -b_4 z_5, & e_5 &= a_4 z_5 \end{aligned}$$

To solve the reciprocal screw the following equations are used

$$\mathcal{S}^r \circ \mathcal{S}_i = 0 \quad i = 1, 2, 3, \dots, 5$$

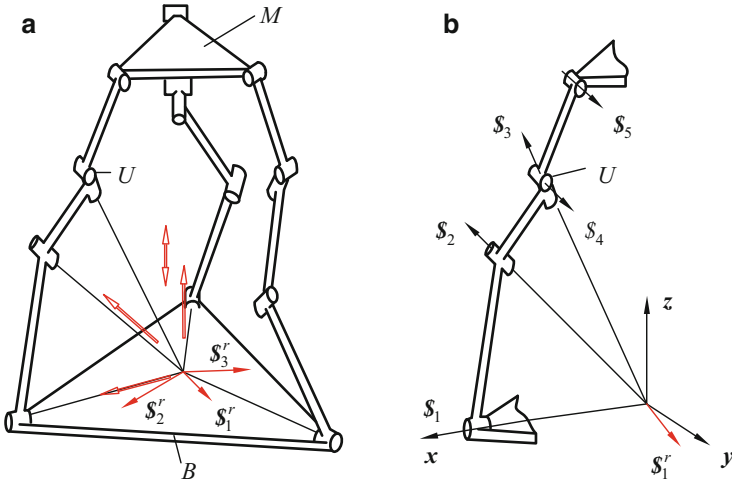


Fig. 4.21 Zlatanov and Gosselin mechanism (a) 3-(RRR)RR mechanism (b) a limb

For the five screw equations a reciprocal screw is obtained as

$$\mathcal{S}^r = (a_4 \quad b_4 \quad 0; \quad 0 \quad 0 \quad 0) \tag{4.78}$$

It is a constraint force passing through the origin point and parallel to the 5th screw axis and also parallel to the moving platform. Three limbs have three constraint forces all parallel to moving platform. Therefore they are coplanar and intersect at a common point and linearly dependent as well, Table 2.1. $\lambda = 0$, $d = 6$, $v = 1$. So that

$$M = d(n - g - 1) + \sum_{i=1}^g f_i + v = 6(14 - 15 - 1) + 15 + 1 = 4 \tag{4.79}$$

Since there two independent constraint forces exist and two translational motions are limited. The mechanism has 4 DOF including three rotational and one translational freedoms.

4.3.4 Carricato’s Mechanism

Figure 4.22 shows the Carricato’s mechanism [22]. It has four limbs and three of them are identical 4-DOF PRPR kinematic chain and the other one is a 7-DOF

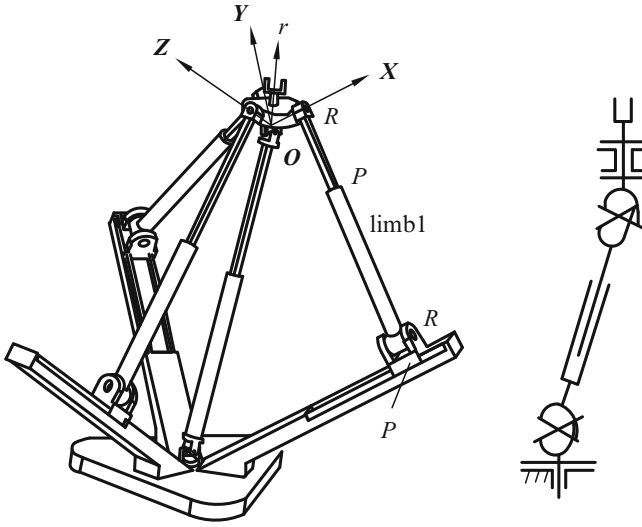


Fig. 4.22 Carricato mechanism

RUPUR chain located in the middle of both the lower and upper platforms. The upper end of the 4th limb is attached on the moving platform and follows the motion of moving platform. The three slide-ways in the base platform and three revolute axes in the moving platform of three PRPR chains are perpendicular to each other, respectively. The middle chain RUPUR connects with the fixed and the moving platforms by two revolute pairs, as shown in Fig. 4.22b, and something like that in Sect. 4.1.3 Fig. 4.4. The robot hand is just the end-link of the RUPUR chain and can rotate about the axis of the last rotational pair R of RUPUR chain, which is connected to the moving platform. Set the coordinate system $o-xyz$, as shown in Fig. 4.22, where x, y and z axes are parallel to the three slider-ways, respectively.

Firstly, let's analyze the 1st PRPR limb. The axis of the last pair of the limb is aligning with the x axis. The four screws are expressed as follows

$$\begin{aligned}
 \mathcal{S}_1^1 &= (0 \ 0 \ 0; \ 1 \ 0 \ 0) \\
 \mathcal{S}_2^1 &= (1 \ 0 \ 0; \ 0 \ e_2 \ f_2) \\
 \mathcal{S}_3^1 &= (0 \ 0 \ 0; \ 0 \ e_3 \ f_3) \\
 \mathcal{S}_4^1 &= (1 \ 0 \ 0; \ 0 \ 0 \ 0)
 \end{aligned}
 \tag{4.80}$$

Their reciprocal screw system is

$$\begin{aligned}
 \mathcal{S}_{11}^r &= (0 \ 0 \ 0; \ 0 \ 1 \ 0) \\
 \mathcal{S}_{12}^r &= (0 \ 0 \ 0; \ 0 \ 0 \ 1)
 \end{aligned}
 \tag{4.81}$$

They have two constraint couples both normal to the axis of the rotational pair of the limb.

The other two identical limbs have similar results. For the 4th chain, it has seven screws, which are linearly dependent and six of them are independent, and it does not impose any constraint to the platform.

That means the four limbs act six constraint couples to the upper platform in total, only three of them are independent and the platform is subjected three constraint couples and loses three rotational freedoms. That means the platform has three translational freedoms. For the whole mechanism $v = 3$ and the mobility of the mechanism is

$$M_p = d(n - g - 1) + \sum_{i=1}^g f_i + v = 6(15 - 17 - 1) + 19 + 3 = 4 \quad (4.82)$$

For Carricato's mechanism, the mobility is the sum of that of the parallel mechanism and the serial one, i.e. the mobility is four.

Note that, for this mechanism no matter what displacement occurs, the screw systems are unchangeable and the mobility is full-cycle.

For more clear here an explanation is given. As the seven screws of the 7-freedom RUPUR branch are linearly dependent, their rank is 6. The end-link of this branch is moveably attached on the moving platform and follows any motion of the platform. Meanwhile, as its seven screws are linearly dependent, there appears a "local freedom", which does not affect to the motion of the platform on the one hand, but that local freedom is used for the rotation of the robot effector on the other hand.

4.3.5 Delta Mechanism

The mobility analysis of the Delta robot [23], Fig. 4.23, is also not difficult by using the method. Here the constraint screw principle and generalized pair are used in analysis. The mechanism has a four-spherical-joint closed-loop chain in each limb. The closed-loop can be considered as a generalized kinematic pair and replaced by an equivalent serial chain with the same mobility for mobility analysis.

In Fig. 4.24a, A , B , C and D are four spherical pairs. There are two cases for the closed-loop: AD and BC are parallel, $AD//BC$; and AD and BC are not parallel.

(1) 4S loop coplanar

When AD and BC are parallel, the 4S loop is coplanar. To analyze the mobility of the output link CD , it can be considered as a parallel mechanism with two limbs and each limb is a SS kinematic chain. For its 1st limb, the SS chain has six equivalent single-DOF kinematic pairs which can be written as follows

Fig. 4.23 Sketch of Delta robot

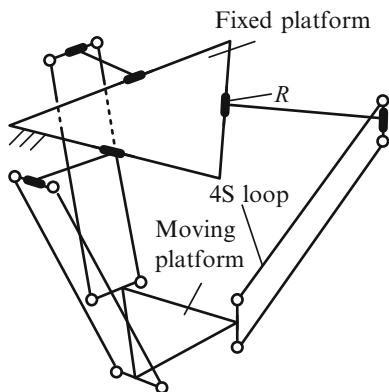
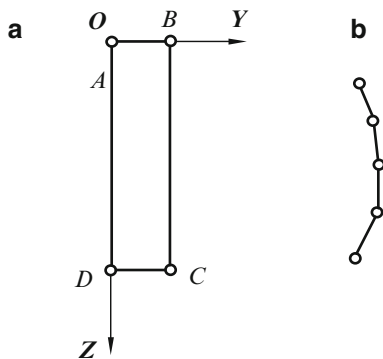


Fig. 4.24 The 4S loop and equivalent serial chain (a) the 4S closed-loop (b) the serial chain



$$\begin{aligned}
 \mathcal{S}_{11} &= (1 \ 0 \ 0; \ 0 \ 0 \ 0) \\
 \mathcal{S}_{12} &= (0 \ 1 \ 0; \ 0 \ 0 \ 0) \\
 \mathcal{S}_{13} &= (0 \ 0 \ 1; \ 0 \ 0 \ 0) \\
 \mathcal{S}_{14} &= (1 \ 0 \ 0; \ 0 \ e_4 \ 0) \\
 \mathcal{S}_{15} &= (0 \ 1 \ 0; \ d_5 \ 0 \ 0) \\
 \mathcal{S}_{16} &= (0 \ 0 \ 1; \ 0 \ 0 \ 0)
 \end{aligned} \tag{4.83}$$

Evidently, they are linearly dependent and there is a reciprocal screw

$$\mathcal{S}'_1 = (0 \ 0 \ 1; \ 0 \ 0 \ 0) \tag{4.84}$$

It is a constraint force along the direction of link AD .

For the 2nd limb, similarly, there is a constraint force along BC

$$\mathcal{S}'_2 = (0 \ 0 \ 1; \ d_2 \ 0 \ 0) \tag{4.85}$$

For the whole 4S planar single-loop chain each imposes a constraint force along the link to the CD . The end-link CD of the closed loop is constrained by two forces along AD and BC , respectively, and then the link CD loses two freedoms, including a translational freedom along direction AD and a rotational freedom about the normal of plane $ABCD$. The mobility, Eq. (3.7), of the link CD is

$$M_N = d(n - g - 1) + \sum_{i=1}^g f_i + v - \zeta = 6(4 - 4 - 1) + 12 + 0 - 2 = 4 \quad (4.86)$$

Therefore the mobility of link CD of the 4S loop is four. In order to determine the characteristics of the mobility it can take the second-time reciprocal screw of Eqs. (4.84) and (4.85) as follows

$$\begin{aligned} \mathcal{S}_1^m &= (0 \ 1 \ 0; \ 0 \ 0 \ 0) \\ \mathcal{S}_2^m &= (0 \ 0 \ 1; \ 0 \ 0 \ 0) \\ \mathcal{S}_3^m &= (0 \ 0 \ 0; \ 1 \ 0 \ 0) \\ \mathcal{S}_4^m &= (0 \ 0 \ 0; \ 0 \ 1 \ 0) \end{aligned} \quad (4.87)$$

Then the generalized pair has four freedoms, which can be expressed as those four kinematic screws. The link CD can rotate about Y - and Z -axes and translate along X - and Y -axes, respectively. By the way, if the 4S loop is not a rectangle but a parallelogram the result is the same.

Each limb of Delta consists of a 4S closed-loop and a revolute pair connected to the upper platform, the frame. Then the equivalent limb of the Delta has five kinematic pairs including three revolute pairs and two prismatic pairs, RRRPP. In this Delta limb, the Y -axis of the limb coordinate system is still along the axis of AB of the 4S loop, and X -axis along the normal of the 4S loop. Therefore, the equivalent limb of Delta consists of five serial kinematic pairs, and the limb screws are as follows

$$\begin{aligned} \mathcal{S}_0^m &= (0 \ 1 \ 0; \ d \ 0 \ f) \\ \mathcal{S}_1^m &= (0 \ 1 \ 0; \ 0 \ 0 \ 0) \\ \mathcal{S}_2^m &= (0 \ 0 \ 1; \ 0 \ 0 \ 0) \\ \mathcal{S}_3^m &= (0 \ 0 \ 0; \ 1 \ 0 \ 0) \\ \mathcal{S}_4^m &= (0 \ 0 \ 0; \ 0 \ 1 \ 0) \end{aligned} \quad (4.88)$$

The reciprocal screw is

$$\mathcal{S}_i^r = (0 \ 0 \ 0; \ 1 \ 0 \ 0) \quad (4.89)$$

That indicates each limb acts a constraint couple about X -axis to the moving platform, i.e. normal to the plane of 4S plane.

Considering the whole mechanism three identical limbs will exert three constraint couples in total on the moving platform *about three different inclined lines*. They are linearly independent and constrain three rotational motions. Therefore, the mechanism has three translational freedoms. In the meantime there is no any common constraint and redundant constraint, $\lambda = \nu = 0$. For the mechanism with three generalized pairs using the Modified G -K Criterion, we have

$$M = d(n - g - 1) + \sum_{i=1}^g f_i + \nu = 6(14 - 15 - 1) + 15 + 0 = 3 \quad (4.90)$$

The result also shows that the mechanism has three freedoms.

The reader may ask since the mobility of Delta before using the Modified G-K criterion has been derived as above-mentioned by reciprocal screw analysis, and the analysis using the Modified G-K Criterion seems not necessary. For the Delta parallel mechanisms the result may be obtained not directly using the modified G-K criterion, however the two methods can be proved mutually. In addition, the Modified G-K Criterion is often indispensable to mobility analysis of many single-loop mechanisms. That is to say, the Modified G-K Criterion is universally applicable to all mechanisms.

The above analysis is based on generalized pairs and the equivalent mechanism. However, we can analyze the mobility directly by using Eq. (3.5), as all the virtual constraints have been obtained from above-analysis procedure. The whole mechanism has 11 links and 15 kinematic pairs. From above analysis we also know that not only there is no any virtual constraint inside the 4S loop, but also no virtual constraint for three limbs connecting two upper and lower platforms. Then applying Eq. (3.5), yields

$$M = d(n - g - 1) + \sum_{i=1}^g f_i + \nu = 6(11 - 15 - 1) + 39 + 0 = 9$$

Considering that there are six local freedoms for six SS chains corresponding to three 4S loops, the mobility of the Delta is also 3. The two results are identical. This analysis also proves the Delta mechanism is not an over-constrained one.

(2) 4S Loop non-coplanar

For the second case, when the closed loop cannot keep a parallelogram, which means links AD and BC are not parallel any more, as shown in Fig. 4.25a. The two reciprocal screws are as follows

$$\begin{aligned} \mathcal{S}_1^r &= (0 \quad 0 \quad 1; \quad 0 \quad 0 \quad 0) \\ \mathcal{S}_2^r &= (a \quad b \quad c; \quad c \quad 0 \quad -a) \end{aligned} \quad (4.91)$$

In this case, the output link CD of the closed loop will be subjected to two constraint forces as follows

$$\begin{aligned}\mathcal{S}_1^r &= (0 \ 0 \ 1; \ 0 \ 0 \ 0) \\ \mathcal{S}_2^r &= (a \ b \ c; \ c \ 0 \ -a)\end{aligned}\quad (4.92)$$

Those two forces limit two translation freedoms and allow four freedoms as follows

$$\begin{aligned}\mathcal{S}_1^m &= (0 \ 1 \ 0; \ 0 \ 0 \ 0) \\ \mathcal{S}_2^m &= (0 \ 0 \ 1; \ 1 \ 0 \ 0) \\ \mathcal{S}_3^m &= (a \ b \ c; \ 0 \ 0 \ 0) \\ \mathcal{S}_4^m &= (0 \ 0 \ 0; \ -b \ a \ 0)\end{aligned}\quad (4.93)$$

The 1st one is rotation freedom about Y -axis. The 2nd one is also a rotation freedom about Z -axis. The 3rd one is also a rotation freedom about a direction $(a \ b \ c)$, and the 4th one is a translational freedom along direction $(-b \ a \ 0)$. Then, the 4S loop is still a 4-DOF one but 3R1T.

Also considering that there is another revolute pair fixed on the fixed platform, the limb screw system containing five screws is as follows

$$\begin{aligned}\mathcal{S}_0^m &= (0 \ 1 \ 0; \ d \ 0 \ f) \\ \mathcal{S}_1^m &= (0 \ 1 \ 0; \ 0 \ 0 \ 0) \\ \mathcal{S}_2^m &= (0 \ 0 \ 1; \ 1 \ 0 \ 0) \\ \mathcal{S}_3^m &= (a \ b \ c; \ 0 \ 0 \ 0) \\ \mathcal{S}_4^m &= (0 \ 0 \ 0; \ -b \ a \ 0)\end{aligned}\quad (4.94)$$

The reciprocal screw can be obtained by solving the following equations

$$\mathcal{S}^r \circ \mathcal{S}_i = 0 \quad i = 1, 2, \dots, 5$$

The reciprocal screw is

$$\mathcal{S}^r (af \quad bf \quad -ad; \ cf \quad 0 \quad -af) \quad (4.95)$$

From the result it is known that the pitch of the screw is non-zero limited value, as $\mathcal{S}^r \cdot \mathcal{S}_0^r \neq 0$. That means that the pitch of the reciprocal screw is neither zero nor infinite.

This can also be explained by using geometrical method. As shown in Fig. 4.25b, above five moving screws are denoted by five red hollow arrows. The rotation pair \mathcal{S}_0^m fixed on frame is parallel to Y -axis. \mathcal{S}_1^m is along Y -axis, and \mathcal{S}_2^m passes point 4 and parallel to Z -axis, and \mathcal{S}_3^m passes origin and parallel link 3–4, and finally, \mathcal{S}_4^m normal to \mathcal{S}_1^r and \mathcal{S}_2^r . Plane P is determined by Z -axis and \mathcal{S}_3^m and parallel to \mathcal{S}_2^m . All lines in plane P intersect \mathcal{S}_4^m orthogonally.

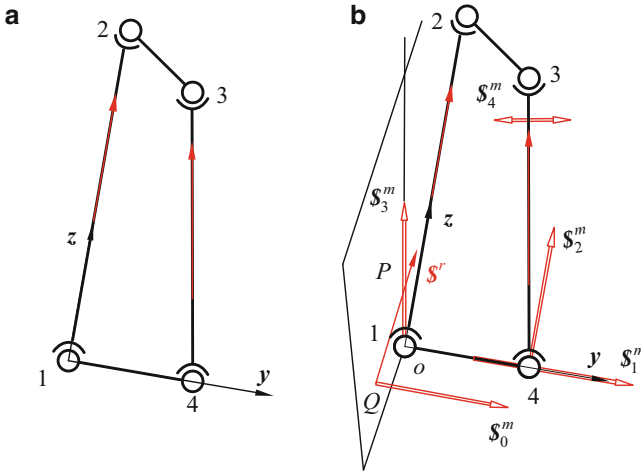


Fig. 4.25 4S closed loop (a) two constraint forces (b) reciprocal screws

If a line can intersect all constraint forces and normal to constraint couple, it can be a constraint force screw with pitch zero, Table 2.2. This is impossible, if draw a line passes point Q and parallel to S_2^m , the line is impossible to pass point O any more and meet S_1^m . That indicates there the constraint force does not exist. Does there a constraint couple exist? It is also impossible to find a vector normal to all different-direction four screws with zero-pitch, Fig. 4.25b. From the above analysis, the possible pitch of constraint screw is non-zero limited value.

Suppose that one of the limbs of the Delta mechanism is in the 2nd cases. The limb exerts a constraint screw with pitch non-zero limited value to the moving platform. In this case, the mechanism is not a 3D translational mechanism. From the analysis we know that, for a Delta mechanism it has to keep every closed-loop being a planar parallelogram after being assembled.

4.3.6 H4 Manipulator

H4 is a complex parallel manipulator proposed by Pierrot and Company [24], as shown in Fig. 4.26. The mechanism consists of four limbs. All four limbs connect the fixed frame and centre moving “H”, which is a three-bar movable platform. From another point of view, link EF can also be selected as the centre moving platform of H4 mechanism and then the mechanism has only two limbs. In this case, each limb of the mechanism is a double-layer closed loop: the inner-loop being a 4S parallelogram, as shown in Fig. 4.27a, and the outer-loop is $GHBAlJ$, as shown in Fig. 4.27b. We take the second view for mobility analysis.

Fig. 4.26 Sketch of H4 manipulator

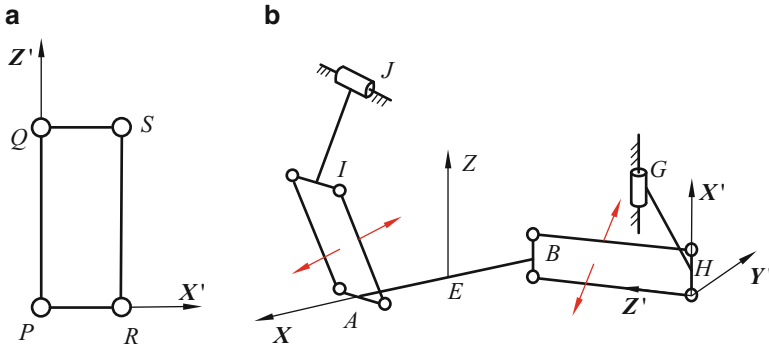
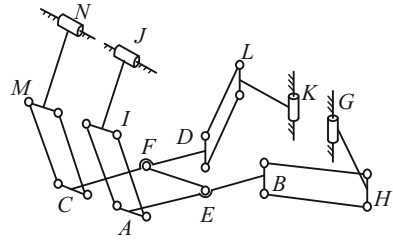


Fig. 4.27 The two loops of the mechanism (a) PQRS subchain (b) the outer loop

(1) The inner-loop parallelogram

The inner-loop *PQRS*, Fig. 4.27a, corresponding parallelogram *BH*, Fig. 4.26b, consists of four spherical pairs and can be treated as a generalized kinematic pair similar to that for Delta mechanism. There are two cases for the closed-loop of the parallelogram also.

1. *PQ* is parallel to *RS*;
2. *PQ* is not parallel to *RS*;

Similar to Delta mechanism, for the first case, *PQ*//*RS*, the generalized pair, parallelogram *PQRS*, can be replaced by a four-pair kinematic chain containing two revolute pairs and two prismatic pairs, *RRPP*. For the system *P-X'Y'Z'* the four-pair chain is as follows

$$\begin{aligned}
 \mathcal{S}_1 &= (1 \ 0 \ 0; \ 0 \ 0 \ 0) \\
 \mathcal{S}_2 &= (0 \ 0 \ 1; \ 0 \ 0 \ 0) \\
 \mathcal{S}_3 &= (0 \ 0 \ 0; \ 1 \ 0 \ 0) \\
 \mathcal{S}_4 &= (0 \ 0 \ 0; \ 0 \ 1 \ 0)
 \end{aligned}
 \tag{4.96}$$

(2) The outer-loop

The outer-loop, $GHBAIJ$, Fig. 4.27b, can be treated as another generalized kinematic pair with the output link AB . It has two identical limbs and each limb consists of five kinematic pairs: besides the 4-DOF equivalent $RRPP$ serial chain, as shown in Eq. (4.96), the fifth rotational pair is at point G or J , respectively. The screw of kinematic pair G which is parallel to X' -axis and fixed on the base with respect to system $P-X'Y'Z'$ (Y' -axis is normal to parallelogram) is as follows

$$\mathcal{S}_5 = (1 \ 0 \ 0; \ 0 \ e_5 \ f_5) \quad (4.97)$$

For the equivalent limb with five screws, Eqs. (4.96) and (4.97), a reciprocal screw is obtained as follows

$$\mathcal{S}^r = (0 \ 0 \ 0; \ 0 \ 1 \ 0) \quad (4.98)$$

It is a constraint couple about the direction *normal to the parallelogram* $PQRS$, and constrains a rotation freedom of link AB about that normal.

For the whole out-loop $GHBAIJ$, its two limbs exert two constraint couples on link AB , which are screws with infinity-pitch and their axes are *perpendicular to two parallelograms*, respectively. The coordinate system $E-XYZ$ is shown in Fig. 4.27b, then the first constraint screw lies in plane $E-XY$, and the other in plane $E-XZ$. The two constraint couples can be rewritten as

$$\begin{aligned} \mathcal{S}_1^r &= (0 \ 0 \ 0; \ d_1 \ e_1 \ 0) \\ \mathcal{S}_2^r &= (0 \ 0 \ 0; \ d_2 \ 0 \ f_2) \end{aligned} \quad (4.99)$$

Then the generalized pair corresponding to the outer loop, $GHBAIJ$, has four relative degrees of freedom and can be replaced by a 4-DOF serial chain with four screws, which are reciprocal to \mathcal{S}_1^r and \mathcal{S}_2^r in Eq. (4.99), simultaneously. The four freedoms include one rotational and three translational freedoms. The rotation axis is perpendicular to both \mathcal{S}_1^r and \mathcal{S}_2^r . The four-screw equivalent serial chain of the outer-loop is

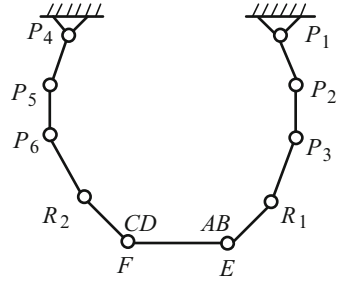
$$\begin{aligned} \mathcal{S}_1 &= (0 \ 0 \ 0; \ 1 \ 0 \ 0) \\ \mathcal{S}_2 &= (0 \ 0 \ 0; \ 0 \ 1 \ 0) \\ \mathcal{S}_3 &= (0 \ 0 \ 0; \ 0 \ 0 \ 1) \\ \mathcal{S}_4 &= (e_1 f_2 \quad -d_1 f_2 \quad -e_1 d_2; \ 0 \ 0 \ 0) \end{aligned} \quad (4.100)$$

Note that, for the outer-loop sub-chain the four passive freedoms, appearing in S-S chain, are already ignored here.

(3) The whole H4 mechanism

When analyzing mobility of the whole H4 mechanism, the two outer-loop closed-chains, $GHBAIJ$ and $KLDFCMN$, of the original H4 mechanism can be replaced

Fig. 4.28 The equivalent mechanism



by two equivalent serial kinematic chains, $P_1P_2P_3R_1R_E$ and $P_4P_5P_6R_2R_F$, Fig. 4.28. The mobility of the whole H4 is equivalent to a single-loop mechanism with two limbs. Let us firstly consider the serial chain, $P_1P_2P_3R_1R_E$. For the same coordinate system $E-XYZ$, there are five kinematic pairs. Besides the four in Eq. (4.100) the other one is a revolute pair at point E , Fig. 4.26b, along Z -axis and passes the origin point E of the coordinate system $E-XYZ$, then it is

$$\mathcal{S}_5 = (0 \quad 0 \quad 1; \quad 0 \quad 0 \quad 0) \tag{4.101}$$

The reciprocal screw of the five screws including Eqs. (4.100) and (4.101) is

$$\mathcal{S}_1^r = (0 \quad 0 \quad 0; \quad d_1 \quad e_1 \quad 0) \tag{4.102}$$

The screw with ∞ -pitch is a constraint couple lying in plane $E-XY$. In other words, the first limb exerts a couple *normal to Z -axis upon the output link EF* .

The similar result is obtained for the other outer-loop, $KLDFCMN$. The 2nd limb $P_4P_5P_6R_2R_F$, also exerts a couple upon EF *normal to Z -axis* and with the similar form of Eq. (4.102)

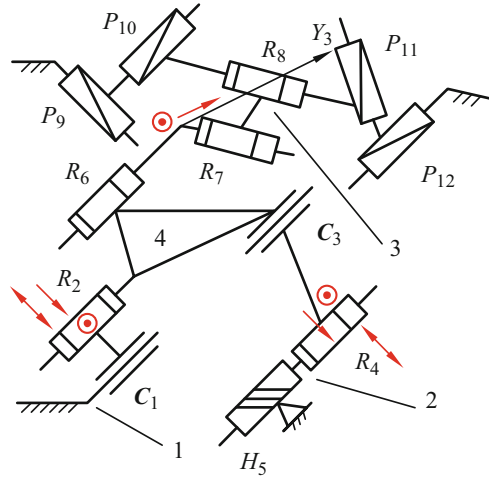
$$\mathcal{S}_2^r = (0 \quad 0 \quad 0; \quad d_2^r \quad e_2^r \quad 0) \tag{4.103}$$

Generally, $d_1 \neq d_2^r$ and $e_1 \neq e_2^r$, then $\mathcal{S}_1^r \neq \mathcal{S}_2^r$. Thus, there are two independent constraint couples acting on EF and *lying in the same plane $E-XY$ with different directions* and constraining two rotational freedoms. They can be considered as equivalent couples along X - and Y -axis, respectively. The mechanism has four degrees of freedom including one rotational and three translational freedoms. The rotational freedom is about Z -axis. Meanwhile, we know that for the equivalent mechanism, $\lambda = \nu = 0$, and using the Modified G-K Criterion, Eq. (3.7), for the equivalent mechanism in Fig. 4.28, the nominal mobility of H4 is

$$M_N = d(n - g - 1) + \sum_{i=1}^g f_i + \nu - \zeta = 6(10 - 10 - 1) + 10 = 4 \tag{4.104}$$

Therefore, the nominal mobility of H4 mechanism is four. In fact, H4 mechanism has eight passive freedoms. Here we take $\zeta = 0$ because these passive

Fig. 4.29 Yang linkage



freedoms have been ignored in the middle analysis procedure. In addition, after any possible finite displacement of the mechanism, the mobility evidently keeps invariable. From above analysis it also indicates that the mechanism is not an over-constraint one.

4.3.7 Yang’s Mechanism

Figure 4.29 shows a mechanism with 10 links and 12 kinematic pairs proposed by Yang in 2005 [25]. The mechanism keeps some special geometrical characteristics, as $C_1//C_3//R_2//R_4//R_6, R_7//R_8$. In the mean time, the six axes: C_1, C_3, R_2, R_4, R_7 and R_8 , are not coplanar.

In order to analyze the mobility of the mechanism, it can be considered as a parallel mechanism with three limbs. Its 4th link is a centre moving platform. Its 1st limb includes two kinematic pairs: cylindrical pair C_1 and rotational pair R_2 . The 2nd limb contents helical pair H_5 parallel to C_1 , rotational pair R_4 and cylinder pair C_3 . The 3rd limb consists of a special 4-slider loop, P_9, P_{10}, P_{11} and P_{12} as well as two rotational pairs, R_6 and R_7 .

For the 1st limb, let the x_1 -axis of the coordinate system be along the common perpendicular line of C_1 and R_2 , and y_1 along R_2 . Then the screw system of the 1st limb is as follows

$$\begin{aligned}
 \$_{11} &= (0 \quad 1 \quad 0; \quad 0 \quad 0 \quad f_{11}) \\
 \$_{12} &= (0 \quad 0 \quad 0; \quad 0 \quad 1 \quad 0) \\
 \$_2 &= (0 \quad 1 \quad 0; \quad 0 \quad 0 \quad 0)
 \end{aligned} \tag{4.105}$$

Their reciprocal screws are

$$\begin{aligned}\$_{11}^r &= (0 \ 0 \ 0; \ 1 \ 0 \ 0) \\ \$_{12}^r &= (0 \ 0 \ 0; \ 0 \ 0 \ 1) \\ \$_{13}^r &= (1 \ 0 \ 0; \ 0 \ 0 \ 0)\end{aligned}\tag{4.106}$$

The three reciprocal screws are expressed as red arrow and red bi-directional arrow in Fig. 4.29, respectively. They are two constraint couples and one constraint force.

For the 2nd limb, let x_2 axis along the common perpendicular line of axes C_3 and R_4 , and y_2 along R_4 axis. Then four single-DOF kinematic pairs of the 2nd limb are expressed as

$$\begin{aligned}\$_5 &= (0 \ 1 \ 0; \ 0 \ h \ 0) \\ \$_4 &= (0 \ 1 \ 0; \ 0 \ 0 \ 0) \\ \$_{31} &= (0 \ 1 \ 0; \ 0 \ 0 \ f_{31}) \\ \$_{32} &= (0 \ 0 \ 0; \ 0 \ 1 \ 0)\end{aligned}\tag{4.107}$$

As they are linearly dependent, and only three of them are independent. They have three reciprocal screws as

$$\begin{aligned}\$_{21}^r &= (0 \ 0 \ 0; \ 1 \ 0 \ 0) \\ \$_{22}^r &= (0 \ 0 \ 0; \ 0 \ 0 \ 1) \\ \$_{23}^r &= (1 \ 0 \ 0; \ 0 \ 0 \ 0)\end{aligned}\tag{4.108}$$

The three reciprocal screws include two constraint couples and one constraint force also.

For the 3rd limb, firstly consider the four-slider loop in that limb, from Sect. 4.1.5 we know it is a one-DOF closed-loop and can be considered as a generalized prismatic pair here and denoted as P^G . In this case, the 4th limb becomes a kinematic chain contained pairs P^G , R_8 , R_7 and R_6 . Let the intersecting point of the axes R_6 and R_7 be the origin point of the coordinate system, and the plane determined by two axes R_7 and R_8 be the coordinate system xy plane as well as the direction of y -axis be normal to the direction of the slide of the P^G pair (in a plane it always can find a line be normal to a direction in space).¹ Then, screw system of the 3rd limb including a generalized pair is as follows

$$\begin{aligned}\$_P &= (0 \ 0 \ 0; \ d_P \ 0 \ f_P) \\ \$_8 &= (a_7 \ b_7 \ 0; \ 0 \ 0 \ f_8) \\ \$_7 &= (a_7 \ b_7 \ 0; \ 0 \ 0 \ 0) \\ \$_6 &= (a_6 \ b_6 \ c_6; \ 0 \ 0 \ 0)\end{aligned}\tag{4.109}$$

¹ Here it needs not know the actual direction of P^G .

It has two reciprocal screws. One is a line-vector force passing through origin point and aligning with y-axis

$$\mathcal{S}_{31}^r = (0 \quad 1 \quad 0; \quad 0 \quad 0 \quad 0) \quad (4.110)$$

And the other is a constraint couple

$$\mathcal{S}_{32}^r = (0 \quad 0 \quad 0; \quad b_7c_6 \quad -a_7c_6 \quad a_7b_6 - a_6b_7) \quad (4.111)$$

It is about the direction determined by $\mathcal{S}_7 \times \mathcal{S}_6$, i.e. normal to R_6 denoted by a red point in the figure.

When analyzing the centre link 4, Fig. 4.29, the above-mentioned three limbs has eight reciprocal screws in total acting on link 4, where five screws are constraint couples in space and only three of them are independent. There exist two virtue constraints. Those three constraint forces are independent. That means the centre platform 4 has no any freedom. In the mean time, there is no any common constraint, $\lambda = 0$, $d = 6$ and $v = 2$. We have

$$M = d(n - g - 1) + \sum_{i=1}^g f_i + v = 6(8 - 9 - 1) + 11 + 2 = 1 \quad (4.112)$$

The mobility of the system is one. It is not inconsequent with above analysis. The centre platform 4 has no any freedom, but the system has mobility and it exists in limb 2, as there the screw system is linearly dependent.

Considering the full links Eq. (3.4) is used to analyze the mobility. The mechanism has 10 links and 12 kinematic pairs and 5 over-constraints besides the above-mentioned two virtual constraints there include other three coming from 4P closed-loop chain, Sect. 4.1.5. Then

$$M_N = 6(n - g - 1) + \sum_{i=1}^g f_i + \mu - \zeta = 6(10 - 12 - 1) + 14 + 5 - 1 = 0 \quad (4.113)$$

It indicates that the freedom of link 4 is zero. The mobility is full-cycle.

4.4 Mobility Analysis of Hoberman Switch-Pitch Ball

There are some mechanisms which structure is more complex and even with not only multi-loop but coupling also. It can be called as Multi-loop coupling mechanisms. In the following sections two kind of this mechanism are discussed.

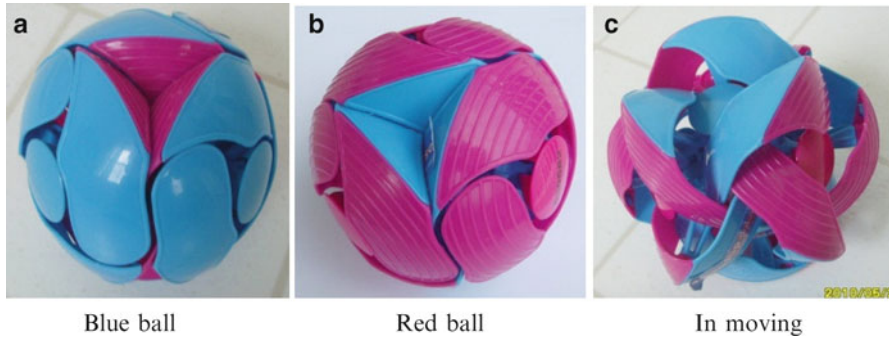


Fig. 4.30 Hoberman switch-pitch ball (a) blue ball (b) red ball (c) in moving

The 2002 winter Olympics in Salt Lake City still dwells in our memories. Especially, a color-changing toy also catches our view. It is called as “Hoberman Switch-pitch ball”, Fig. 4.30 [26]. The colors will be magically flipped as long as it is tossed in air. It can be named as “coupling multi-loop mechanism”. Wei et al. [27] made some kinematic analysis of the Hoberman switch-pitch ball. Here we want to study the mobility of this coupling multi-loop mechanism.

4.4.1 Structure Analysis

As shown in Fig. 4.30, the surface of the Hoberman switch-pitch ball is spliced by 4 round sheets and 12 laminas all with the same color. Each round sheet is surrounded with three laminas. Each lamina belongs to a beanpod-like link with two different color laminas, blue and red, and the two different laminas form an angle of about 60° . Each round sheet has three revolute joints fixed on its reverse distributed in an equilateral triangle. Every connecting rod is Ω -shaped, Fig. 4.31, and its vertex connects the beanpod-like lamina. The Ω -rod connects two round sheets with two joints in its two ends. The ball comprises of eight round sheets, four of them are red and other four are blue, 20 links inside the ball and 24 revolute joints in total.

When the laminas of ball turn over the four identical-color round sheets move outwards and other four inward, the ball then changes color, and the ball surface keeps symmetrical with respect to its center point all long.

It can find that there exists an exceptive configuration when the ball turns its color. At this configuration all the 8 round sheets locate at identical spherical surface with the same distance to the ball center and the 12 connecting rods are all in the directions normal to the corresponding radii of the ball. The whole mechanism forms a convex ball as we have seen in Fig. 4.30c. In addition, all rods and platforms have the same dimension.



Fig. 4.31 Ω -shaped link and laminas

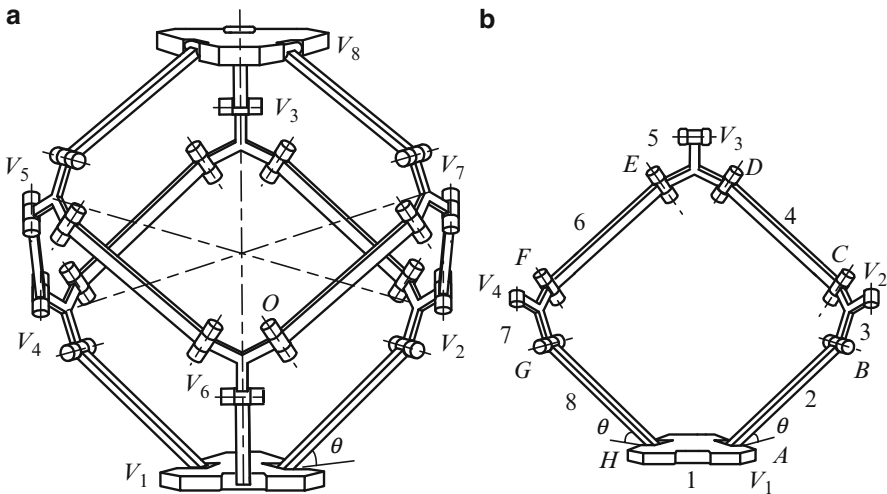


Fig. 4.32 Sketch of the ball mechanism (a) sketch of the ball mechanism (b) spatial single- closed loop

In order to express the Hoberman switch-pitch ball into a normal mechanism, every round sheet can be expressed by a triangle platform V_i on which three joints are located. The Ω -shaped connecting rod can be abstracted to a straight link, which connects two platforms. Therefore, the inner mechanism of the ball is schematically shown as Fig. 4.32a. From the figure, the mechanism has six closed-loops and each spatial closed-loop contains eight revolute pairs and eight links including four platforms, Fig. 4.32b.

In order to analyze the mechanism, the initial configuration of the mechanism is assumed to be symmetric about its centre point O , as shown in Fig. 4.32a.

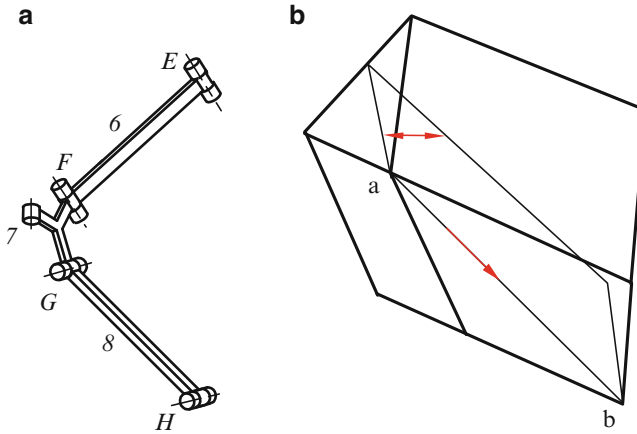


Fig. 4.33 Three-link four-pair chain (a) three-link chain (b) constraint screws

As we have introduced before, when the laminas of ball turn over the ball changes its color, and it can keep symmetrical with respect to its center point all long. For this assumption, we will analyze how the mechanism can keep symmetrical when it continuously moves.

4.4.2 Three-Link Chain

Firstly, a three-rod chain is taken to analyze from the view of the single-closed loop, Fig. 4.33a. In this three-rod serial chain, $EFGH$, the axes of two pairs of joints, E and F , G and H , are parallel, respectively. In the initial configuration, every loop is plane-symmetric, therefore, the four axes intersect at two points a and b , respectively, as shown in Fig. 4.33b. Since the three-rod serial chain has three links and four kinematic pairs, it will bring two constraints to the platform V_3 , Fig. 4.33b, by mobility principle, $M = 3 \times 6 - 4 \times 5 = -2$.

The two constraints will limit two freedoms of that platform, V_3 . The two constraints can be obtained by screw analysis, but for facilitating here the geometrical method is applied also based on screw theory and Table 2.2.

1. There a constraint couple exists, since the four kinematic screws are respectively parallel. By Table 2.2, only when line vector and couple are perpendicular they are reciprocal. The constraint couple should be normal to the platform triangle and also normal to the four revolute pairs, as shown by the bi-directional arrow, Fig. 4.33b. The constraint couple limits the relative rotation between two platforms connected by the three-rod chain.

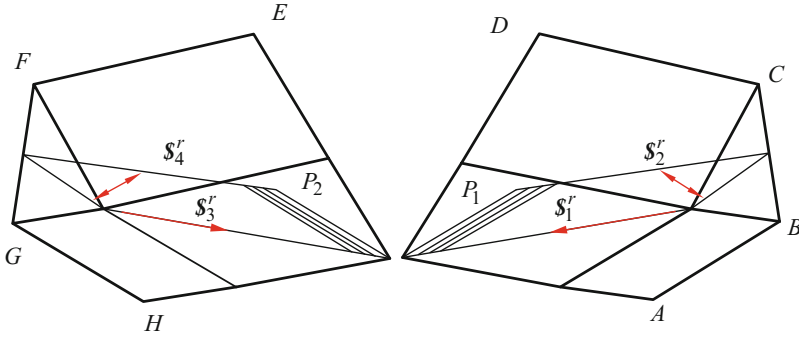


Fig. 4.34 Constraints acting on V_3

2. The other reciprocal screw is analyze as follows
 - (a) When the three-rod chain is symmetrical, from Table 2.2 the reciprocal screw is a constraint force passing points a and b. This is because it can intersect with axes of the four revolute pairs, Fig. 4.33b. The constraint force limits the relative translation between two platforms connected by the three-rod chain.
 - (b) When the three-rod chain is asymmetrical, the reciprocal screw is a screw with ∞ -pitch. But as we have assumed the mechanism is symmetrical the case cannot appears and here we also do not give more explanation.

Based on the symmetric assumption before the three-rod chain acts to the V_3 by two reciprocal screws, one of them is a constraint force and the other is a constraint couple, as shown in Fig. 4.33b. The constraint couple is normal to the triangle platform of the three-rod chain, and the force passes the two intersecting points a and b of the four revolute axes.

4.4.3 Eight-Link Loop

The eight-link loop, Fig. 4.32b, contains four triangle platforms, and four links, eight revolute pairs. The eight-link loop has four pairs of parallel axes for the eight revolute pairs. For analyzing the mobility of the eight-rod loop, it can be considered as a parallel mechanism with two limbs, and V_3 is the moving platform of the parallel mechanism. Its each limb has four revolute pairs and their four axes form two pair of parallel axes, respectively (Fig. 4.34).

Let us firstly consider $ABCD$ limb in Fig. 4.32b. Based on the analysis above corresponding to the four moving screws of $ABCD$ limb connecting platforms V_1 and V_3 , the four axes form two pairs of parallel lines, respectively. The limb acts two constraints to V_3 . One of them, S_1^r , is a constraint force passing through those

two intersecting points formed by corresponding four revolute pairs, and other one, \mathcal{S}_2^r , is a constraint couple normal to the triangle platform, V_2 . Also it is known that the two constraints lie on the plane bisector the dihedral angle. Similarly, limb $EFGH$ also acts similar two constraints to V_3 .

As each limb acts two constraints to V_3 the moving platform V_3 is subjected to four constraints including two forces, \mathcal{S}_1^r and \mathcal{S}_3^r and two couples as well, \mathcal{S}_2^r and \mathcal{S}_2^r . For the four constraints there are two reciprocal screws corresponding its two moving screws. That means the eight-rod loop has two freedoms. When using the Modified G-K formula, Eq. (3.5), to analyze the mobility, there is neither any common constraint nor parallel constraint, $\lambda = 0$, $\nu = 0$. Then we have

$$M = 6(n - g - 1) + \sum_{i=1}^g f_i + \nu = 6(8 - 8 - 1) + 8 + 0 = 2 \quad (4.114)$$

In order to know the mobility property being rotational or translational, using screw theory that reciprocal screw, which can be normal to all constraint couples and intersect all constraint forces, expresses a rotational-motion screw with zero-pitch; and that reciprocal screw, which can be normal to all constraint forces, denotes a translational motion screw with ∞ -pitch. Then, the platform V_3 has two freedoms, one is rotational and the other is translational.

Figure 4.35a illustrates two constraint couples, red bi-directional arrow, which determine a plane and its normal, red hollow arrow, is just the axis direction about which V_3 is able to rotate, \mathcal{S}_2^m , and its axis also passes the intersection point of \mathcal{S}_1^r and \mathcal{S}_3^r , Table 2.2; Fig. 4.35b illustrates two constraint forces, \mathcal{S}_1^r and \mathcal{S}_3^r , and the translational screw, \mathcal{S}_1^m , of platform V_3 is along the normal line of plane determined by \mathcal{S}_1^r and \mathcal{S}_3^r .

Since the mechanism is symmetrical, the four screws, \mathcal{S}_1^r , \mathcal{S}_2^r , \mathcal{S}_3^r , \mathcal{S}_4^r are also symmetrical. Then the two moving screws \mathcal{S}_1^m and \mathcal{S}_2^m should also locate on the symmetrical plane of the eight-rod loop in Fig. 4.35.

Two moving screws, \mathcal{S}_1^m and \mathcal{S}_2^m , indicate V_3 can translate up and down along axis of \mathcal{S}_1^m , as well as rotate about axis of \mathcal{S}_2^m . When V_3 translates downwards V_3 is close to the center of ball, and in other words, V_3 is close to V_1 . Meanwhile, the distance between V_2 and V_4 increases also. However, the figure is still symmetrical.

On the other hand, if V_3 rotates about \mathcal{S}_2^m in any case the eight-bar loop becomes asymmetrical, Fig. 4.36.

4.4.4 Double Loop

When adding a five-bar chain, $IJKLMN$, to that eight-rod loop, a double-loop chain with 13 links and 14 revolute pairs is obtained, Fig. 4.37a. Since the five-bar six-pair chain does not bring into any new constraints to the original linkage, $M = 5$

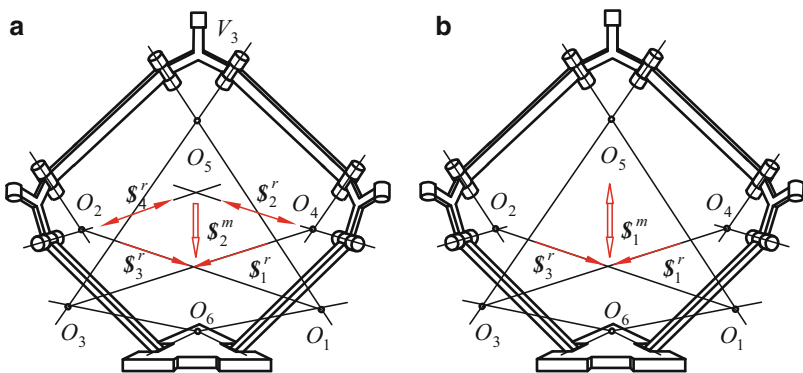


Fig. 4.35 Eight-link loop (a) rotation axis (b) translation direction

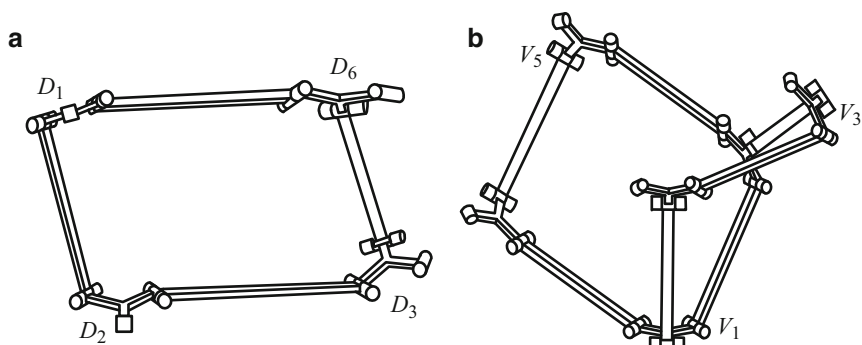


Fig. 4.36 The asymmetrical configuration (a) a single loop (b) the double loop

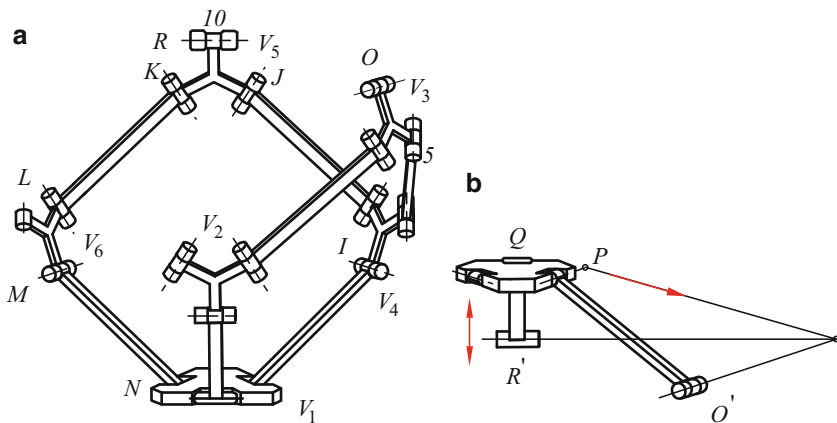


Fig. 4.37 Double-loop 13-link chain (a) double loop (b) $O'PQR'$ open chain

$\times 6 - 6 \times 5 = 0$, the double-loop chain has also two freedoms. From the modified G-K formula, Eq. (3.4), we have

$$M = 6(n - g - 1) + \sum_{i=1}^g f_i + \mu = 6(13 - 14 - 1) + 14 + 0 = 2 \quad (4.115)$$

Evidently, the additional chain, $IJKLMN$, does not bring into any new constraint, then

1. V_3 as well as V_5 have similar motion, when V_3 moves downwards, V_5 also goes down; meanwhile, V_2, V_4 and V_6 move outwards. In this case the mechanism can still keep symmetrical.
2. When V_3 rotates, the motion of V_5 becomes complex and the mechanism is defective, as shown in Fig. 4.36b, and mechanism cannot keep symmetrical any more.

4.4.5 Three-Loop Chain

When adding a three-rod chain $O'PQR'$ to the two points, O and R , of the double-loop chain, Fig. 4.37a, a three-loop chain with 16 bars is obtained, Fig. 4.38b. The $O'PQR'$ chain brings two constraints to the double-loop mechanism and will limit the relative motion between points O and R of the double-loop chain.

1. As shown in Fig. 4.37b, the constraint force will limit the relative translation between platforms V_3 and V_5 along the direction of the constraint force. However, it has known before that points O and R in double-loop are impossible to translate along this direction. Then this constraint is redundant.
2. $O'PQR'$ chain also brings into a constraint couple, and it wants also limit the possible relative rotation between the two platforms V_3 and V_5 . That means the angle between axes O and R in double-loop chain is limited to be unchangeable. In other words, the constraint couple limits the relative rotational motion of the platforms between V_3 and V_5 . Then, this constraint is not redundant and the three-loop chain becomes the one with only one DOF.

Using Modified G-K formula, Eq. (3.4), $\mu = 1$, we have

$$M = 6(n - g - 1) + \sum_{i=1}^g f_i + \mu = 6(16 - 18 - 1) + 18 + 1 = 1 \quad (4.116)$$

The calculation also proves above analysis by using screw analysis.

From the above analysis we know that after adding the three-rod chain $O'PQR'$ to the double-loop chain, a three-loop chain is formed. The platforms V_3 and V_5 in three-loop chain cannot rotate, and the three-loop

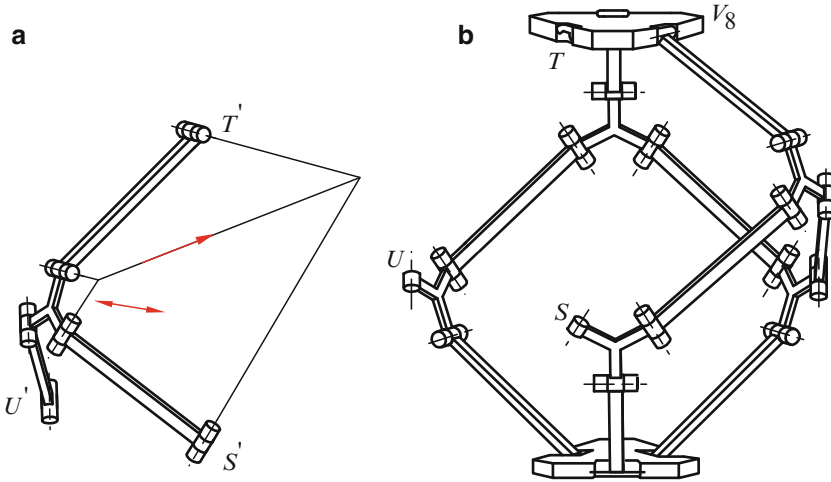


Fig. 4.38 The last combination (a) four-link six-pair chain (b) three-loop chain

chain is impossible to be asymmetry any more. The three-loop chain has to be symmetrical. Now, the assumption for the mechanism should be a symmetrical ball is proved.

4.4.6 The Whole Mechanism

When adding a trifurcate chain, $S'T'U'$, Fig. 4.38a, to the three-loop chain, an integrated Hoberman Switch-Pitch mechanism is obtained, Fig. 4.32. For the trifurcate chain, $S'T'U'$, it has three limbs and as any pair of limbs exerts two constraints to the three-loop chain, the three-loop chain is acted upon by six constraints in total. Meanwhile, for the trifurcate chain, $S'T'U'$ with four bars and six kinematic pairs, it brings the six constraints to the three-loop chain as: $M = 4 \times 6 - 6 \times 5 = -6$. From Fig. 4.38a, between any two limbs there are two constraints limiting two relative motions to the connected two points. Therefore, among the three outside kinematic pairs of the trifurcate chain, $S'T'U'$, there appear six constraints including three couple and three forces.

Firstly, considering the three couples, as we have known before, they all should be normal to the same platform V_7 , and we have know also that the platforms of the three-loop chain has been not to be able to rotate any more. Therefore the three couples all are redundant. On the other hand, those three constraint forces limit the possible displacements between connected two points, respectively; however, it is also proved that it is impossible. So the three constraint forces are also redundant.

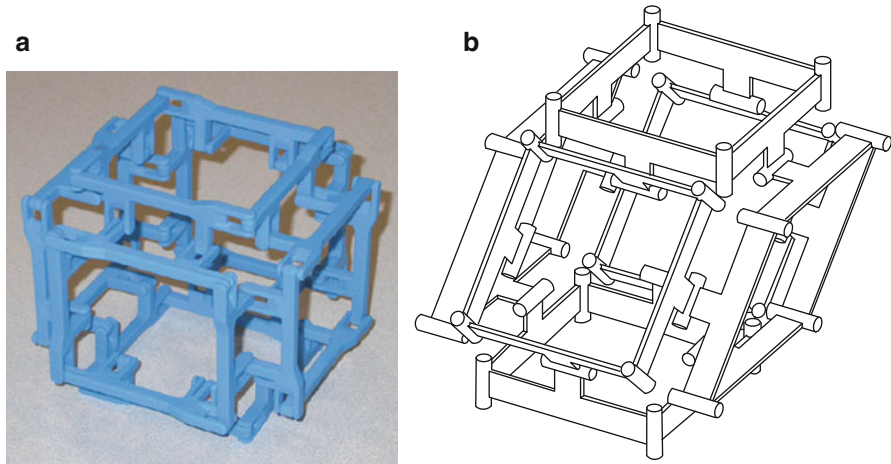


Fig. 4.39 Six-hole cubiform mechanism (a) externality (b) mechanism

Now, for the whole magic ball there are 20 links, 24 rotational pairs, and 7 redundant constraints in total. Considering $\mu = 7$, from the Modified G-K formula (3.4), we have

$$M = 6(n - g - 1) + \sum f + \mu = 6(20 - 24 - 1) + 24 + 7 = 1 \quad (4.117)$$

From the analysis procedure we know that the mobility should be full-cycle, undoubtedly.

4.5 Six-Hole Cubiform Mechanism

Figure 4.39 illustrates another Multi-loop coupling mechanism proposed by Laliberté and Gosselin [28], who called it as Polyhedra with Articulated Faces. It is completely comprised of identical ternary links. Its mechanism sketch is shown in Fig. 4.39b. Here it is called as six-hole cubiform mechanism and its mobility is discussed here.

Each plane of the hexahedron is an equilateral four-bar linkage and each equilateral four-bar linkage connects four equilateral four-bar linkages by four rotational pairs. All links has the same precise parameters. The mechanism has 24 links and 36 kinematic pairs in total. The hexahedron has eight vertices and each vertex of the hexahedron is composed of three intersecting axes of three rotational pairs.

In order to analyze the mobility of the mechanism, let us firstly consider the equilateral four-bar linkage. For a four-bar linkage, it has one-DOF and three virtual

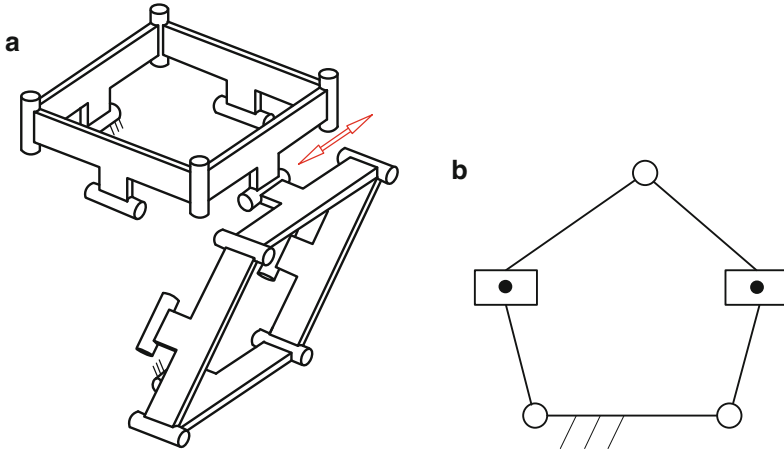


Fig. 4.40 The double-hole linkage (a) the double-hole linkage (b) the single-loop chain

constraints. The connecting link of the four-bar loop has a translational freedom and the direction of the translational freedom is normal to the link connecting to the based. Next, the double-hole linkage is considered.

4.5.1 Double-Hole Linkage

The double-hole linkage is consists of two equilateral four-bar linkages connected by a revolute pair and they are connected to frame by other two revolute pairs, as shown in Fig. 4.40a.

The double-hole linkage contains two four-bar chains. When mobility analysis the two four-bar closed-loop chains can be replaced by two generalized translational pairs. The double-hole linkage is a RPRPR single-loop chain as shown in Fig. 4.40b. Its screw system is

$$\begin{aligned}
 \mathcal{S}_1 &= (1 \ 0 \ 0; \ 0 \ 0 \ f_1) \\
 \mathcal{S}_2 &= (0 \ 0 \ 0; \ 1 \ 0 \ 0) \\
 \mathcal{S}_3 &= (1 \ 0 \ 0; \ 0 \ e_3 \ f_1) \\
 \mathcal{S}_4 &= (0 \ 0 \ 0; \ 1 \ 0 \ 0) \\
 \mathcal{S}_5 &= (1 \ 0 \ 0; \ 0 \ 0 \ f_5)
 \end{aligned} \tag{4.118}$$

They are linearly dependent and two reciprocal screws are as follows

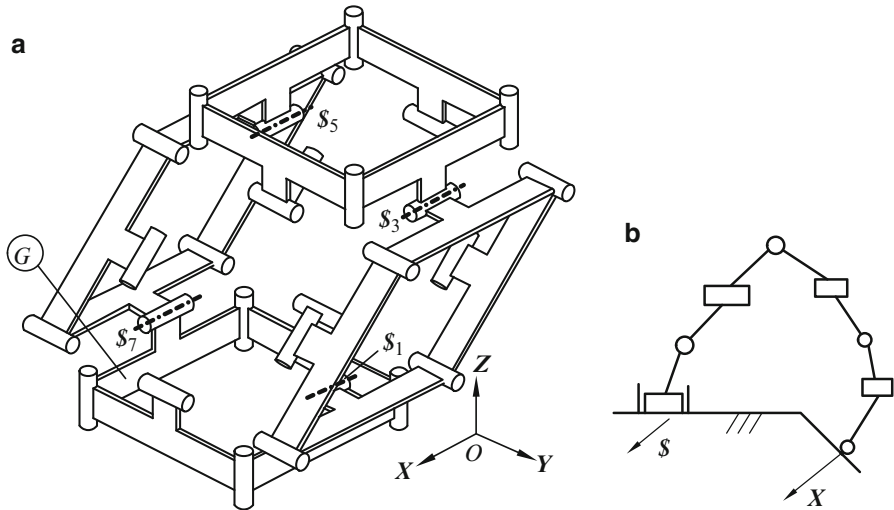


Fig. 4.41 Four-hole linkage (a) mechanism (b) equivalent mechanism

$$\begin{aligned} \mathcal{S}_1^r &= (0 \ 0 \ 0; \ 0 \ 1 \ 0) \\ \mathcal{S}_2^r &= (0 \ 0 \ 0; \ 0 \ 0 \ 1) \end{aligned}$$

They are two common constraints, and $d = 4$, we have

$$M = d(n - g - 1) + \sum_{i=1}^g f_i + v = 4(5 - 5 - 1) + 5 + 0 = 1 \quad (4.119)$$

If consider the full-link analysis there are eight over-constraints: three for each four-bar closed-loop and two for RPRPR loop. The mobility is

$$M = d(n - g - 1) + \sum_{i=1}^g f_i + v = 6(9 - 11 - 1) + 11 + (2 \times 3 + 2) = 1 \quad (4.120)$$

4.5.2 Four-Hole Linkage

When four four-bar loops are connected by four revolute pairs, a four-hole linkage is formed, Fig. 4.41a. The four-hole linkage forms a spatial hexahedron; its four planes are four four-bar linkages. Each of them can move relatively and is

equivalent a translational pair. When link G is selected as the frame of the linkage, and the four-bar loop in the base is also moveable.

(1) The Mobility analysis of the four-hole linkage

The whole four-hole linkage can be expressed as PRPRPRPR in anti-clockwise direction. It is equivalent a single-loop eight-bar chain, Fig. 4.41b. The origin locates on the axis of the 1st pair $\$1$. When the linkage is in cubiform the eight kinematic pairs can be expressed as eight screws as follows

$$\begin{aligned}
 \$1 &= (1 \ 0 \ 0; \ 0 \ 0 \ 0) \\
 \$2 &= (0 \ 0 \ 0; \ 1 \ 0 \ 0) \\
 \$3 &= (1 \ 0 \ 0; \ 0 \ e_3 \ 0) \\
 \$4 &= (0 \ 0 \ 0; \ 1 \ 0 \ 0) \\
 \$5 &= (1 \ 0 \ 0; \ 0 \ e_3 \ f_5) \\
 \$6 &= (0 \ 0 \ 0; \ 1 \ 0 \ 0) \\
 \$7 &= (1 \ 0 \ 0; \ 0 \ 0 \ f_5) \\
 \$8 &= (0 \ 0 \ 0; \ 1 \ 0 \ 0)
 \end{aligned} \tag{4.121}$$

Evidently, they are linearly dependent, only four of them are independent

$$\begin{aligned}
 \$1 &= (1 \ 0 \ 0; \ 0 \ 0 \ 0) \\
 \$2 &= (0 \ 0 \ 0; \ 1 \ 0 \ 0) \\
 \$3 &= (1 \ 0 \ 0; \ 0 \ e_3 \ 0) \\
 \$5 &= (1 \ 0 \ 0; \ 0 \ e_3 \ f_5)
 \end{aligned} \tag{4.122}$$

and they have two reciprocal screws,

$$\begin{aligned}
 \$1^r &= (0 \ 0 \ 0; \ 0 \ 0 \ 1) \\
 \$2^r &= (0 \ 0 \ 0; \ 0 \ 1 \ 0)
 \end{aligned} \tag{4.123}$$

The two reciprocal screws are just two common constraints or over-constraints. They indicate that there is no any link being able to rotate about Y- and Z-axes. To calculate the mobility using Eq. (3.5) we have

$$M = 4(n - g - 1) + \sum_{i=1}^g f_i + v = 4(8 - 8 - 1) + 8 + 0 = 4 \tag{4.124}$$

That indicates the mobility of the linkage is 4. As we know that generally, the mobility of a general spatial eight-bar linkage is 2 only. That is because the linear dependency of the screw system formed by the four generalized translational pairs and four revolute pairs.

Totally, there are 16 links and 20 kinematic pairs as well as 14 over-constraints (each four-bar linkage has three over-constraints and those two over-constraints corresponding to Eq. (4.123)). Based on Eq. (3.4) we have

$$M = 6(n - g - 1) + \sum_{i=1}^g f_i + \mu = 6(16 - 20 - 1) + 20 + (4 \times 3 + 2) = 4 \quad (4.125)$$

The two methods got the same result, and they are proved each other.

(2) The Relative Freedom Between Links Q and P

Two links Q and P are selected in the four-hole linkage, as shown in Fig. 4.42a, and to analyze the relative freedom between the two links. So the rear two links of the two four-bar loops located on the upper and the lower of the four-hole linkage are takeoff, Fig. 4.42b.

1) In the beginning all 4-bar loops are square

For Fig. 4.42b, considering the mechanism is a parallel mechanism with two branches, both is RRPRR chains. The limb coordinate system is illustrated in that figure, and its three coordinate axes are along three revolute-pair axes, respectively. The screw system of the left branch is given by

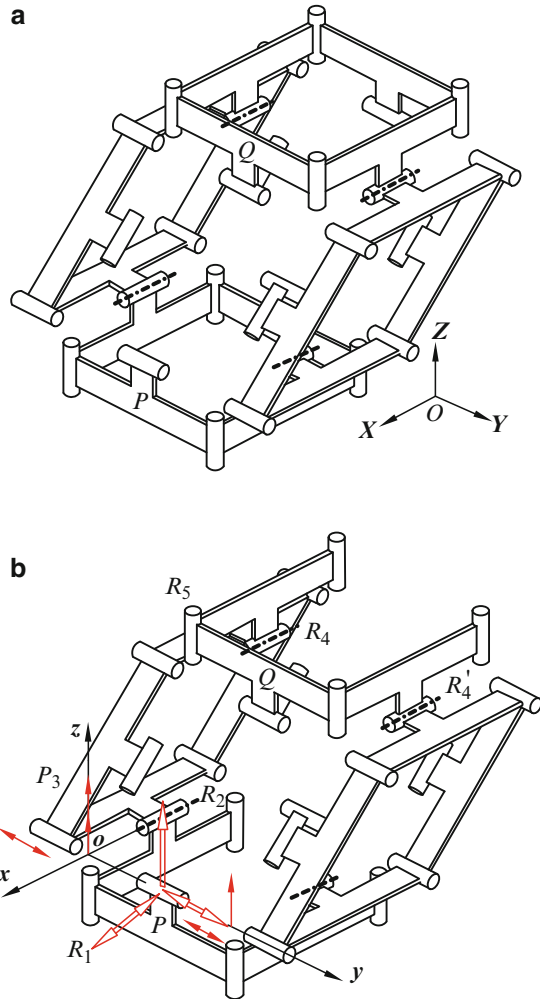
$$\begin{aligned} \$_1 &= (0 \ 0 \ 1; \ 0 \ 0 \ 0) \\ \$_2 &= (1 \ 0 \ 0; \ 0 \ 0 \ 0) \\ \$_3 &= (0 \ 0 \ 0; \ 1 \ 0 \ 0) \\ \$_4 &= (1 \ 0 \ 0; \ 0 \ e \ 0) \\ \$_5 &= (0 \ 0 \ 1; \ 0 \ 0 \ 0) \end{aligned} \quad (4.126)$$

They are linearly dependent and their two reciprocal screws are

$$\begin{aligned} \$_1^r &= (0 \ 0 \ 0; \ 0 \ 1 \ 0) \\ \$_2^r &= (0 \ 0 \ 1; \ 0 \ 0 \ 0) \end{aligned} \quad (4.127)$$

The two reciprocal screws acting on the platform Q are one constraint force along z-axis and a constraint couple about y-axis, respectively, and illustrated by red arrows (one is the constraint force and the other red bi-directional arrow the constraint couple). Similarly, the right branch with the same kinematic pairs should have the same reciprocal screws. Comparing the two branches, firstly, since the directions of the two constraint couples are the same, they are linearly dependent, and there exist a common constraint. That means the link Q is subjected to three independent constraints including the constraint couple about y-axis and two constraint forces along left and right two links, respectively. Considering also two parallel forces to be equivalent a force and a couple normal to the plane determined by the two parallel forces, the link Q is subjected to three constraints including two constraint couples about x- and y-axes, as well as a constraint force along z-axis, we have

Fig. 4.42 Relative freedom between links Q and P (a) two links Q and P in four-hole linkage (b) without rear links



$$\begin{aligned}
 \mathcal{S}_1^r &= (0 \ 0 \ 0; \ 1 \ 0 \ 0) \\
 \mathcal{S}_2^r &= (0 \ 0 \ 0; \ 0 \ 1 \ 0) \\
 \mathcal{S}_3^r &= (0 \ 0 \ 1; \ 0 \ 0 \ 0)
 \end{aligned} \tag{4.128}$$

In order to get the motion of link Q , it may take the second-time reciprocal screw as follows

$$\begin{aligned}
 \mathcal{S}_1^m &= (0 \ 0 \ 1; \ 0 \ 0 \ 0) \\
 \mathcal{S}_2^m &= (0 \ 0 \ 0; \ 1 \ 0 \ 0) \\
 \mathcal{S}_1^m &= (0 \ 0 \ 0; \ 0 \ 1 \ 0)
 \end{aligned} \tag{4.129}$$

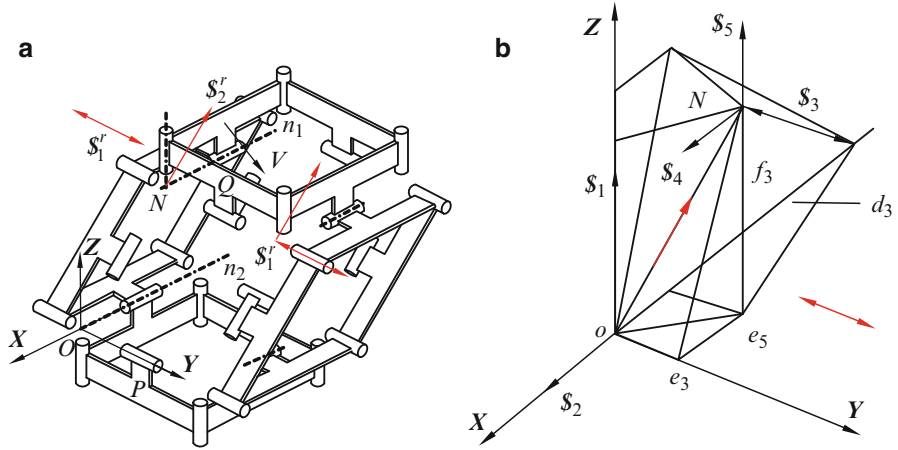


Fig. 4.43 Constraint analysis of link Q (a) link Q acted upon by constraints (b) screw analysis

That means the link Q relative to link P has three freedoms including two relative translations along x - and y -axes, respectively, and one rotation about z -axis, as shown by the hollow arrows in Fig. 4.42b.

Note that, the above analysis is for the mechanism shown in Fig. 4.42b. Considering the two kinematic pairs, R_4 and R_4' both axes keeps to be parallel always, whether link U exist or not the relative motion between Q and P is the same, therefore the above result is correct for the four-hole linkage, Fig. 4.42a.

2) In the beginning all 4-bar loops are rhombic

Let us discuss the relative motion between links Q and P under the four-hole linkage, which is after some rotations and four closed-loops all are rhombic, as shown in Fig. 4.43a. Also let us analyze the left branch firstly. Supposing the vector ON be expressed as $(-e_5, e_3, f_3)$, the translational direction of the generalized pair $\$3$ is normal to ON , i.e. the vector V as shown in Fig. 4.43b, and its direction number is $(-d_3, -e_3, -f_3)$. The branch screw system consists of five screws. Since $\$3$ is normal to ON , the following identical equation holds

$$e_5 d_3 - e_3 e_3 - f_3 f_3 \equiv 0 \tag{4.130}$$

And the screw system is

$$\begin{aligned} \$1 &= (0 \ 0 \ 1; \ 0 \ 0 \ 0) \\ \$2 &= (1 \ 0 \ 0; \ 0 \ 0 \ 0) \\ \$3 &= (0 \ 0 \ 0; \ -d_3 \ -e_3 \ -f_3) \\ \$4 &= (1 \ 0 \ 0; \ 0 \ f_3 \ -e_3) \\ \$5 &= (0 \ 0 \ 1; \ e_3 \ e_5 \ 0) \end{aligned} \tag{4.131}$$

For the five screws there exist two reciprocal screws

$$\begin{aligned}\mathcal{S}_1^r &= (0 \ 0 \ 0; \ 0 \ 1 \ 0) \\ \mathcal{S}_2^r &= (-e_5 \ e_3 \ f_3; \ 0 \ 0 \ 0)\end{aligned}\quad (4.132)$$

The 1st one is a constraint couple about Y -axis and the 2nd one is a constraint force along vector ON and normal to V direction.

Similarly, the right branch with the same kinematic pairs should have the same reciprocal screws. Comparing the two branches, there is an over-constraint couple. Then the link Q is subjected to three independent constraints, including two parallel forces along ON and a couple about Y -axis. Also consider two parallel forces can be replaced by a force and a couple, then the three relative motions between links Q and P include two translational motions normal to ON and a revolute about the axis parallel ON .

4.5.3 Five-Hole Linkage

In this step a new four-bar loop, Fig. 4.44a, is added to the four-hole linkage to form a new five-hole linkage, Fig. 4.44b. There are two steps for connecting the four-bar loop to the four-hole chain. Firstly, connect two points, q and p , in four-bar loop to two points Q and P in four-hole chain. The attached kinematic chain is a RPR open chain. And then connect the two lateral kinematic pairs.

(1) The first step

The kinematic chain is an equivalent serial chain RPR with generalized kinematic pair P . Now let us analyze the influence adding the serial chain RPR to the four-hole loop. The RPR chain is a new limb for mechanism shown in Fig. 4.44a. It is a kinematic chain with three screws as

$$\begin{array}{cc} \text{in the beginning} & \text{after rotation} \\ \mathcal{S}_1 = (0 \ 1 \ 0; \ 0 \ 0 \ 0) & \mathcal{S}_1 = (0 \ 1 \ 0; \ 0 \ 0 \ 0) \\ \mathcal{S}_2 = (0 \ 0 \ 0; \ 0 \ 1 \ 0), & \mathcal{S}_2 = (0 \ 0 \ 0; \ 0 \ e_2 \ -f_2) \\ \mathcal{S}_3 = (0 \ 1 \ 0; \ d_3 \ 0 \ 0) & \mathcal{S}_3 = (0 \ 1 \ 0; \ d'_3 \ 0 \ 0)\end{array}\quad (4.133)$$

The corresponding reciprocal screws

$$\begin{aligned}\mathcal{S}_1^r &= (0 \ 0 \ 0; \ 1 \ 0 \ 0) & \mathcal{S}_1^r &= (0 \ 0 \ 0; \ 1 \ 0 \ 0) \\ \mathcal{S}_2^r &= (0 \ 0 \ 0; \ 0 \ 0 \ 1), & \mathcal{S}_2^r &= (0 \ 0 \ 0; \ 0 \ 0 \ 1) \\ \mathcal{S}_3^r &= (0 \ 0 \ 1; \ 0 \ 0 \ 0) & \mathcal{S}_3^r &= (0 \ f_2 \ e_2; \ 0 \ 0 \ 0)\end{aligned}\quad (4.134)$$

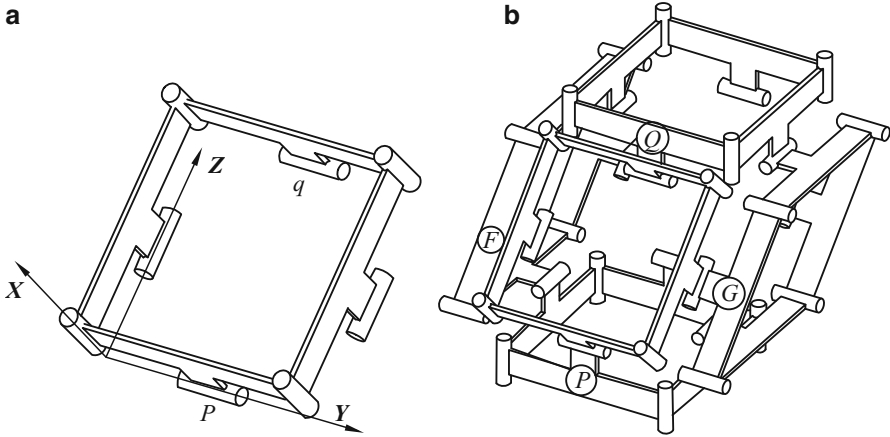


Fig. 4.44 The fifth hole attached to the four-hole chain (a) four-bar chain (b) five-hole linkage

It brings three reciprocal screws to link Q including constraint two revolute about X - and Z -axes and one translation along Z -direction. AS we have analyzed before, in the beginning the mechanism is a cubiform and the link Q is limited not revolute about X and Z -axes and translation along Z -axis. Compared with Eq. (4.134), the constraints \mathcal{S}_1^r and \mathcal{S}_3^r are two over-constraints and constraint \mathcal{S}_2^t is a real one. Then, link Q will lose one mobility and the relative mobility between links Q and P is two only.

(2) The second step

The five-hole chain is formed by connecting two lateral kinematic pairs. Considering all the mechanism parameters are austere consistent, the connection of two lateral kinematic pairs does not bring into any real constraint. That means those $2 \times 5 = 10$ constraints are virtual.

(3) The whole five-hole loop

Applying Eq. (3.4), the total number of link is $n = 20$, the number of kinematic pairs is, $g = 28$, the total number of virtual constraints is

$$\mu = 3 \times 5 + 2 + 2 \times 5 = 29$$

The first item is considering four-bar loop, each has three virtual constraints and there are five four-bar loops; the 2nd and the 3rd items correspond to those appearing in steps 1 and 2, respectively. For the five-hole loop, the mobility is

$$\begin{aligned}
 M &= 6(n - g - 1) + \sum_{i=1}^g f_i + \mu = 6(20 - 28 - 1) + 28 + \mu \\
 &= -54 + 28 + 29 = 3
 \end{aligned}
 \tag{4.135}$$

4.5.4 The Whole Six-Hole Mechanism

One more four-bar loop is connected to that five-hole loop form the final six-hole mechanism. There are also two steps to form the whole six-hole mechanism. Similarly, when a RPR chain including the generalized kinematic pair is attached to the five-hole loop, it brings into three constraints, which limit two revolutions about X and Z -axes and one translation along Z -axis. At this moment, the three constraints all are virtual. And then consider the connection of two lateral kinematic pairs, which bring into 10 constraints and the 10 constraints all are virtual. That means when attaching the last four-bar loop it brings into 13 virtual constraints to the mechanism.

For the whole six-hole mechanism the total number of its virtual constraints are as follows

$$\mu = 6 \times 3 + (2 + 12) + (3 + 10) = 45$$

Based on Eq. (3.4), we have

$$\begin{aligned} M &= 6(n - g - 1) + \sum_{i=1}^g f_i + \mu = 6(24 - 36 - 1) + 36 + 33 \\ &= -78 + 36 + 45 = 3 \end{aligned} \quad (4.136)$$

The result is identical with the move simulation and is full-cycle.

References

1. Suh CH, Radcliffe CW (1978) Kinematics and mechanisms design. Wiley, New York
2. De Roberval P (1670) Nouvelle manière de balance, Mémoires de mathématiques et de physique. Tirez des registres de l'Académie Royale des Sciences depuis 1666 jusqu'à 1699, Tome X, Institut de France, Académie des sciences, pp 494–496
3. Norton RL (1999) Design of machinery: an introduction to the synthesis and analysis of mechanisms and machines. McGraw-Hill, Boston
4. Mabie HH, Reinholtz CF (1987) Mechanisms and dynamics of machinery. Wiley, New York
5. Merlet JP (2000) Parallel robots. Kluwer, Dordrecht
6. Hervé JM (1978) Principes fondamentaux d'une théorie des mécanismes. Rev Roum Sci Tech — Méc Appl 23(5):693–709
7. Delassus E (1900) Sur les systèmes articulés gauches, Première partie. Ann Sci Ecole Norm. Supérieure, Paris, 3_Séries 17:455–499
8. Hervé JM (1978) Analyse structurelle des mécanismes par groupe des déplacements. Mech Mach Theory 13:437–450
9. Bennett GT (1903) A new mechanism. Engineering 76:777–778
10. Goldberg M (1943) New 5-bar and 6-bar linkages in three dimensions. ASME J Mech 65:649–661

11. Myard FE (1931) Contribution à la géométrie des systèmes articulés. France Bull Soc Math 59:183–210
12. Chen Y (2003) Design of structural mechanisms. Doctor Dissertation, University of Oxford
13. Bricard R (1927) Leçons De Cinématique, vol 2. Gauthier-Villars, Paris, pp 7–12
14. Altmann FG (1952) Sonderformen Raumliefer Koppelgetriebe und Grenzen Ihrer Verwendbarkeit. Konstruktion. Werkstoffe Versuchswesen 4:97–106
15. Altmann FG (1954) His communication to a paper by Paul Grodzinski and Ewen M'Ewen, link mechanisms in modern kinematics. Proc I Mech E Lond 168(37):877–896
16. Waldron KJ, Kinzel GL (1999) Kinematics, dynamics, and design of machinery. Wiley, New York
17. Zhao TS HZ (2001) The kinematic analysis of a 3-D translational parallel mechanism. Chinese Mech Eng 12(6):613–616
18. Kong X, Gosselin CM (2002) Type synthesis of linear translational parallel manipulators. In: Advances in robot kinematics. Kluwer, Dordrecht
19. Kim HS, Tsai LW (2002) Design optimization of a Cartesian parallel manipulator. ASME DETC2002/MECH-34301
20. Huang Z, Li Q (2001) A kind of symmetrical parallel mechanism with five degrees-of-freedom and decoupled kinematics, China Patent No. ZL011222274.3
21. Zlatanov D, Gosselin CM (2001) A new parallel architecture with four degrees of freedom. In: Proceedings of the 2nd workshop on computational kinematics, 19–22 May, Seoul, Korea
22. Carricato M, Parenti-Castelli V (2002) Singularity-free fully isotropic translational parallel mechanism. Int J Rob Res 21(2):161–174
23. Clavel R., Delta, a fast robot with parallel geometry, in: 18th international symposium on industrial Robots, Lausanne, 1988.
24. Pierrot F, Company O (1999) H4: a new family of 4-DOF parallel robot. In: Proceedings of IEEE/ASME international conference on advanced intelligent mechatronics, Atlanta, pp 508–513
25. Yang TL (2004) The topological constructure of robot. Mechanical Press, Beijing
26. Hoberman C (2002) Folding covering panels for expanding structures, US Patent App. 10/303, 550, Publ No. 2003/0097801 A1, Filing date: 25 Nov 2002
27. Wei G, Ding X, Dai JS (2009) Geometric and kinematic analysis of the Hoberman switch-pitch ball and its variant. ASME paper, DETC2009-87329
28. Laliberté T, Gosselin CM. (2007) Polyhedra with articulated faces. In: 12th IFToMM world congress, Besanc, 18–21 June 2007

Chapter 5

Kinematic Influence Coefficient and Kinematics Analysis

The concept of kinematic influence coefficient (KIC) of mechanism was proposed by Tesar et al. [1–4]. Benedict and Tesar [1, 2] proposed a completely general model formulation using first- and second-order KIC. This theory has been extensively applied to both open-loop and closed-loop planar mechanisms [3]. Thomas and Tesar [4] further developed this theory into a spatial serial manipulator. Huang [5, 6] has further developed to modern parallel mechanisms.

The KIC principle is important in the analysis of machinery, as it deeply reflects the kinematic essence of mechanisms. Many kinematic issues of mechanisms can be expressed quite clearly and concisely using the KIC principle, such as velocity analysis, acceleration analysis, error analysis, force analysis, and so on. In addition, some deep analyses of mechanisms can be dealt with from the KIC of mechanisms, such as special configuration, the map between driving space and workspace, dexterity, isotropy, manipulability, and so on. The calculation of KIC itself is quite simple and requires no derivation. The merits of KIC method include the following:

- The first- and second-order KICs can be conveniently standardized during set up and are not dependent on moving parameters. They can be set up before kinematic analysis.
- All direct and reverse issues of velocity and acceleration expressions are explicit using KIC.
- The map between any two links in a complicated parallel mechanism can be simple and explicitly expressed.
- Transforming from KIC to other mathematic methods is easy.
- The more complicated the mechanism, the clearer its merit.

KIC is a powerful tool for analyzing complicated mechanisms. In this chapter, the concept of KIC is introduced. Then, first- and second-order KICs are derived, followed by a discussion of the velocity and acceleration analyses. At the last part, the lower-mobility parallel mechanisms are analyzed.

5.1 Concept of KIC

First, let us discuss a planar 3-degree of freedom (DOF) mechanism, Fig. 5.1, to illustrate the KIC concepts. When three input parameters, ϕ_1 , ϕ_2 , and ϕ_3 are given for the 3-DOF linkage, all the link motions of the mechanism are determined.

For the more common situation, where an N -DOF mechanism is present, we may give the common expressions for the i^{th} link as follows:

$$\begin{aligned}\Phi_i &= f_1(\varphi_1 \varphi_2 \cdots \varphi_N) \\ X_i &= f_2(\varphi_1 \varphi_2 \cdots \varphi_N) \quad i = 1, 2, \dots, m \\ Y_i &= f_3(\varphi_1 \varphi_2 \cdots \varphi_N)\end{aligned}\quad (5.1)$$

where Φ_i , X_i , Y_i are the three configuration parameters for link i , and $\varphi_1, \varphi_2, \dots, \varphi_N$ are N input variables. Considering $\varphi_1, \varphi_2, \dots, \varphi_N$ as time variables, we have

$$\begin{aligned}\dot{\Phi}_i &= \sum_{n=1}^N \frac{\partial f_1}{\partial \varphi_n} \dot{\varphi}_n \\ \dot{X}_i &= \sum_{n=1}^N \frac{\partial f_2}{\partial \varphi_n} \dot{\varphi}_n \\ \dot{Y}_i &= \sum_{n=1}^N \frac{\partial f_3}{\partial \varphi_n} \dot{\varphi}_n\end{aligned}\quad (5.2)$$

Let $U_i: \{\Phi_i, X_i, Y_i\}^T$ represent the generalized coordinate of that mechanism. Then, Eqs. (5.1) and (5.2) can be rewritten as follows:

$$U = f(\phi_1 \phi_2 \cdots \phi_N) \quad (5.3)$$

$$\dot{U} = \sum_{n=1}^N \frac{\partial U}{\partial \varphi_n} \dot{\varphi}_n \quad (5.4)$$

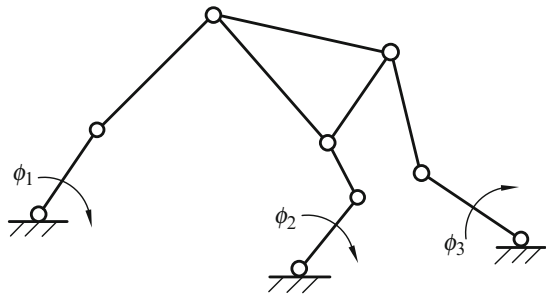


Fig. 5.1 A 3-DOF planar linkage

These partial derivatives are defined as first-order KIC and can be expressed in matrix form as

$$\dot{U} = [G]\dot{\varphi} \quad (5.5)$$

where

$$[G] = \begin{bmatrix} \frac{\partial U}{\partial \varphi_1} & \frac{\partial U}{\partial \varphi_2} & \dots & \frac{\partial U}{\partial \varphi_N} \end{bmatrix}_{1 \times N} = \begin{bmatrix} \frac{\partial f_1}{\partial \varphi_1} & \frac{\partial f_1}{\partial \varphi_2} & \dots & \frac{\partial f_1}{\partial \varphi_N} \\ \frac{\partial f_2}{\partial \varphi_1} & \frac{\partial f_2}{\partial \varphi_2} & \dots & \frac{\partial f_2}{\partial \varphi_N} \\ \frac{\partial f_3}{\partial \varphi_1} & \frac{\partial f_3}{\partial \varphi_2} & \dots & \frac{\partial f_3}{\partial \varphi_N} \end{bmatrix} \in R^{3 \times N}$$

$$\dot{\varphi} = \{\dot{\varphi}_1 \dot{\varphi}_2 \dots \dot{\varphi}_N\}_{N \times 1}^T$$

The first-order KIC is just the Jacobian matrix.

Correspondingly, the acceleration of some links in the mechanism can be obtained by derivation of Eq. (5.4)

$$\ddot{U} = \sum_{p=1}^N \sum_{q=1}^N \frac{\partial^2 U}{\partial \phi_p \partial \phi_q} \dot{\phi}_p \dot{\phi}_q + \sum_{n=1}^N \frac{\partial U}{\partial \phi} \ddot{\phi}_n \quad (5.6)$$

where $\partial^2 U / (\partial \phi_p \partial \phi_q)$

is defined as the second-order KIC. Thus, we have

$$\ddot{U} = \{\ddot{U}_1, \ddot{U}_2, \ddot{U}_3\}^T = \{\ddot{\Phi}_i, \ddot{X}_i, \ddot{Y}_i\}^T.$$

Equation (5.6) can be rewritten in the form

$$\ddot{U} = \dot{\varphi}^T [H]\dot{\varphi} + [G]\ddot{\varphi} \quad \ddot{\varphi} = \{\ddot{\varphi}_1 \ddot{\varphi}_2 \dots \ddot{\varphi}_N\}_{N \times 1}^T \quad (5.7)$$

$$[H] = \begin{bmatrix} \frac{\partial^2 U}{\partial \varphi_1 \partial \varphi_1} & \frac{\partial^2 U}{\partial \varphi_1 \partial \varphi_2} & \dots & \frac{\partial^2 U}{\partial \varphi_1 \partial \varphi_N} \\ \frac{\partial^2 U}{\partial \varphi_2 \partial \varphi_1} & \frac{\partial^2 U}{\partial \varphi_2 \partial \varphi_2} & \dots & \frac{\partial^2 U}{\partial \varphi_2 \partial \varphi_N} \\ \vdots & \vdots & \ddots & \vdots \\ \frac{\partial^2 U}{\partial \varphi_N \partial \varphi_1} & \frac{\partial^2 U}{\partial \varphi_N \partial \varphi_2} & \dots & \frac{\partial^2 U}{\partial \varphi_N \partial \varphi_N} \end{bmatrix} \in R^{3 \times N \times N} \quad (5.8)$$

$$\begin{aligned}
 \mathbf{H}^3 = & \begin{bmatrix} \frac{\partial^2 U_3}{\partial \phi_1 \partial \phi_1} & \frac{\partial^2 U_3}{\partial \phi_1 \partial \phi_2} & \dots & \frac{\partial^2 U_3}{\partial \phi_1 \partial \phi_N} \\ \frac{\partial^2 U_3}{\partial \phi_2 \partial \phi_1} & \dots & \dots & \dots \\ \vdots & \vdots & \vdots & \vdots \\ \frac{\partial^2 U_3}{\partial \phi_N \partial \phi_1} & \dots & \dots & \dots \end{bmatrix} \\
 \mathbf{H}^2 = & \begin{bmatrix} \frac{\partial^2 U_2}{\partial \phi_1 \partial \phi_1} & \frac{\partial^2 U_2}{\partial \phi_1 \partial \phi_2} & \dots & \frac{\partial^2 U_2}{\partial \phi_1 \partial \phi_N} \\ \frac{\partial^2 U_2}{\partial \phi_2 \partial \phi_1} & \dots & \dots & \dots \\ \vdots & \vdots & \vdots & \vdots \\ \frac{\partial^2 U_2}{\partial \phi_N \partial \phi_1} & \dots & \dots & \dots \end{bmatrix} \\
 \mathbf{H}^1 = & \begin{bmatrix} \frac{\partial^2 U_1}{\partial \phi_1 \partial \phi_1} & \frac{\partial^2 U_1}{\partial \phi_1 \partial \phi_2} & \dots & \frac{\partial^2 U_1}{\partial \phi_1 \partial \phi_N} \\ \frac{\partial^2 U_1}{\partial \phi_2 \partial \phi_1} & \frac{\partial^2 U_1}{\partial \phi_2 \partial \phi_2} & \dots & \frac{\partial^2 U_1}{\partial \phi_2 \partial \phi_N} \\ \vdots & \vdots & \vdots & \vdots \\ \frac{\partial^2 U_1}{\partial \phi_N \partial \phi_1} & \frac{\partial^2 U_1}{\partial \phi_N \partial \phi_2} & \dots & \frac{\partial^2 U_1}{\partial \phi_N \partial \phi_N} \end{bmatrix}_{N \times N}
 \end{aligned}$$

Fig. 5.2 The second-order KIC matrix

The second-order KIC matrix is also called Hessian matrix. Each element is a vector with three components as follows

$$\ddot{U}_k = \dot{\phi}^T [\mathbf{H}^k] \dot{\phi} + [\mathbf{G}]_{k;} \ddot{\phi} \quad k = 1, 2, 3 \tag{5.9}$$

The second-order KIC matrix can be considered a 3-D cubic matrix, as shown in Fig. 5.2. Each level is a scalar matrix. Equation (5.7) can also be rewritten as

$$\ddot{U}_k = \dot{\varphi}^T [\mathbf{H}^k] \dot{\varphi} + [\mathbf{G}]_{k;} \ddot{\varphi} \quad k = 1, 2, 3$$

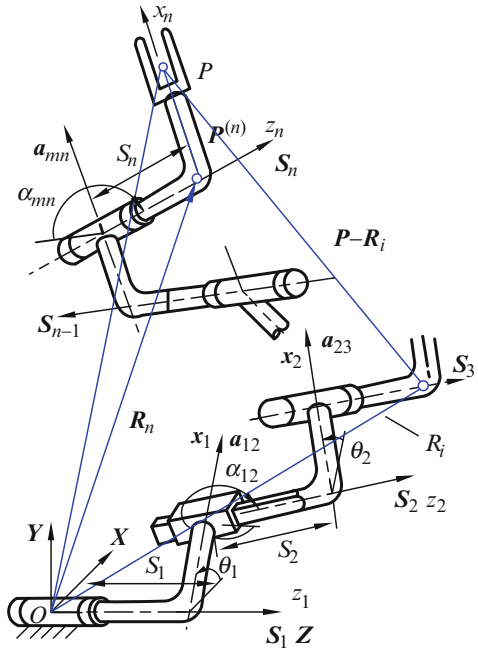
5.2 KIC and Kinematic Analysis of Serial Chains

The analysis of a serial chain [4] is the basic requirement for parallel mechanism. Figure 5.3 shows a typical serial chain consisting of $n + 1$ links, as well as n kinematic pairs.

5.2.1 Position Analysis

Figure 5.3 illustrates the respective kinematic pairs $S_1S_1, S_2S_2, \dots, S_nS_n$, and the corresponding common perpendicular vectors $a_{12}a_{12}, a_{23}a_{23}, \dots, a_{ij}a_{ij}$. The corresponding offset is S_i , the rotation angle is θ_i , and the twist angle is α_{ij} . The global coordinate system is $O-XYZ$ and the local system is $O_i-X_iY_iZ_i$.

Fig. 5.3 A spatial serial chain



The axis Z_i is along S_i , X_i along the common normal a_{ij} . T_i indicates the transformation matrix of the system i with respect to the global system.

Vector $\mathbf{a}_{ij}^{(i)} = \{X_{ij}^{(i)} \ Y_{ij}^{(i)} \ Z_{ij}^{(i)}\}^T$ indicates vector \mathbf{a}_{ij} with respect to O_i - X_i Y_i Z_i . Thus,

$$\mathbf{a}_{ij} = T_i \mathbf{a}_{ij}^{(i)}. \tag{5.10}$$

The transformation matrix is

$$T_i = [\mathbf{a}_{ij} \ S_i \times \mathbf{a}_{ij} \ S_i] = \begin{bmatrix} X_{ij} & |Y_i \ Z_{ij}| & X_i \\ Y_{ij} & |Z_i \ X_{ij}| & Y_i \\ Z_{ij} & |X_i \ Y_{ij}| & Z_i \end{bmatrix} \tag{5.11}$$

where $|Y_j \ Z_{jk}|$ indicates

$$|Y_i \ Z_{ij}| = \begin{vmatrix} Y_i & Z_i \\ Y_{ij} & Z_{ij} \end{vmatrix} = Y_{ij}Z_{ij} - Z_iY_{ij}.$$

When all the structures and moving parameters $S_i S_i$, $a_{ij} \mathbf{a}_{ij}$, θ_i , α_{ij} , $i = 1, 2, \dots, n$ are given, the position vector of point P on the robot hand is as follows:

$$\mathbf{P} = \mathbf{R}_n + T_n \mathbf{P}^{(n)} \tag{5.12}$$

where \mathbf{R}_n is the distance between two origins of O - XYZ and O_n - $X_nY_nZ_n$, which can be expressed in the form

$$\mathbf{R}_n = S_1\mathbf{S}_1 + a_{12}\mathbf{a}_{12} + S_2\mathbf{S}_2 + \cdots + S_n\mathbf{S}_n \quad (5.13)$$

where

$$\mathbf{S}_1 = \{0 \ 0 \ 1\}^T \quad \mathbf{a}_{23} = \{\cos \theta_1 \ \sin \theta_1 \ 0\}^T$$

$$\mathbf{T}_1 = [\mathbf{a}_{12} \ \mathbf{S}_1 \times \mathbf{a}_{12} \ \mathbf{S}_1]$$

$$\mathbf{S}_2 = \begin{Bmatrix} X_2 \\ Y_2 \\ Z_2 \end{Bmatrix} = \mathbf{T}_1 \begin{Bmatrix} 0 \\ -\sin \alpha_{12} \\ \cos \alpha_{12} \end{Bmatrix}; \mathbf{a}_{12} = \begin{Bmatrix} X_{23} \\ Y_{23} \\ Z_{23} \end{Bmatrix} = \mathbf{T}_1 \begin{Bmatrix} \cos \theta_2 \\ \cos \alpha_{12} \cdot \sin \theta_2 \\ \sin \alpha_{12} \cdot \sin \theta_2 \end{Bmatrix}$$

The general equation can be given as follows

$$\mathbf{S}_i = \begin{Bmatrix} X_i \\ Y_i \\ Z_i \end{Bmatrix} = \mathbf{T}_{i-1} \begin{Bmatrix} 0 \\ -\sin \alpha_{(i-1)i} \\ \cos \alpha_{(i-1)i} \end{Bmatrix} \quad (5.14)$$

$$\mathbf{a}_{ij} = \begin{Bmatrix} X_{ij} \\ Y_{ij} \\ Z_{ij} \end{Bmatrix} = \mathbf{T}_{i-1} \begin{Bmatrix} \cos \theta_i \\ \cos \alpha_{(i-1)i} \sin \theta_i \\ \sin \alpha_{(i-1)i} \sin \theta_i \end{Bmatrix}_{i=2,3,\dots} \quad (5.15)$$

When the parameters \mathbf{S}_i and \mathbf{a}_{ij} are given, \mathbf{T}_i can be obtained by Eq. (5.11), and the position and orientation of every link in space can be determined.

5.2.2 First-Order KIC

The angular velocity of the end-link, robot hand, can be obtained by the summation of the angular velocities of serial links

$${}^n \boldsymbol{\omega}_h = {}^n \boldsymbol{\omega}_1 + {}^n \boldsymbol{\omega}_2 + \cdots + \boldsymbol{\omega}_n$$

where $\boldsymbol{\omega}_h$ indicates the absolute angular velocity of the end-link a_{mn} or some pointed other link, such as $m.\omega_i$ is the relative angular velocity of the i^{th} link about axis \mathbf{S}_i . Then, it can be expressed as $\boldsymbol{\omega}_i = \dot{\theta}_i \mathbf{S}_i$. Thus, we have

$$\boldsymbol{\omega}_h = \sum_{i=1}^n \dot{\theta}_i \mathbf{S}_i. \quad (5.16)$$

The equation can be rewritten in matrix form as follows:

$$\boldsymbol{\omega}_h = [\mathbf{G}_\varphi^h] \dot{\boldsymbol{\phi}} \quad (5.17)$$

where the KIC matrix of end-link a_{mn} is in the form

$$[\mathbf{G}_\varphi^h] = \begin{bmatrix} \frac{\partial \boldsymbol{\omega}_h}{\partial \dot{\varphi}_1} & \frac{\partial \boldsymbol{\omega}_h}{\partial \dot{\varphi}_2} & \cdots & \frac{\partial \boldsymbol{\omega}_h}{\partial \dot{\varphi}_n} \end{bmatrix} \quad (5.18)$$

where $\dot{\varphi}_i$ is the i^{th} component of generalized velocity vector $\dot{\boldsymbol{\phi}}$. The i^{th} column vector of $[\mathbf{G}]$ is expressed as $[\mathbf{G}]_{:i}$.

$$[\mathbf{G}_\varphi^h]_{:i} = \frac{\partial \boldsymbol{\omega}_h}{\partial \dot{\varphi}_i} = \begin{bmatrix} \frac{\partial \boldsymbol{\omega}_h^x}{\partial \dot{\varphi}_i} & \frac{\partial \boldsymbol{\omega}_h^y}{\partial \dot{\varphi}_i} & \frac{\partial \boldsymbol{\omega}_h^z}{\partial \dot{\varphi}_i} \end{bmatrix}^T \quad (5.19)$$

Where ‘ i ’ indicates the i^{th} column of matrix $[\mathbf{G}]$. KIC can be obtained by taking the partial derivative of Eq. (5.16) with respect to $\dot{\varphi}$ [4]

$$[\mathbf{G}_\varphi^h]_{:i} = \begin{cases} \mathbf{S}_i & i < n, \quad i \text{ is revolute pairs} \\ 0 & \text{for other cases} \end{cases} \quad (5.20)$$

where n is the end-effector of the serial chain or some interested link in the chain. Point P in Fig. 5.3, is on the robot hand n and its vector is as follows

$$\mathbf{P} = \mathbf{S}_1 \mathbf{S}_1 + \sum_{i=2}^n (a_{(i-1)i} \mathbf{a}_{(i-1)i} + S_i \mathbf{S}_i) + T_n \mathbf{P}^{(n)} \quad (5.21)$$

Taking the time derivative to obtain the velocity of point P yields

$$\mathbf{v}_P = \dot{\mathbf{S}}_1 \mathbf{S}_1 + \sum_{i=2}^n (a_{(i-1)i} \dot{\mathbf{a}}_{(i-1)i} + \cdots + \dot{\mathbf{S}}_i \mathbf{S}_i + S_i \dot{\mathbf{S}}_i) + \frac{d}{dt} (T_n \mathbf{P}^{(n)})$$

This expression can be rewritten in the form

$$\mathbf{v}_P = \sum_{i=1}^n \left\{ \dot{\mathbf{S}}_i \mathbf{S}_i + \dot{\theta}_i \mathbf{S}_i \times \left[\sum_{r=i+1}^n (a_{(r-1)r} \mathbf{a}_{(r-1)r} + S_r \mathbf{S}_r) + T_n \mathbf{P}^{(n)} \right] \right\} \quad (5.22)$$

From Fig. 5.3, the item after sign ‘ \times ’ indicates a vector from the i^{th} origin \mathbf{R}_i to point P , that is

$$\sum_{r=i+1}^n (a_{(r-1)r} \mathbf{a}_{(r-1)r} + S_r \mathbf{S}_r) + (T_n \mathbf{P}^{(n)}) = \mathbf{P} - \mathbf{R}_i.$$

Then, Eq. (5.22) is rewritten as follows

$$\mathbf{v}_P = \sum_{i=1}^n \left[\dot{S}_i \mathbf{S}_i + \dot{\theta}_i \mathbf{S}_i \times (\mathbf{P} - \mathbf{R}_i) \right] \quad (5.23)$$

Considering that any joint has only one freedom, one of the two items enclosed in the brackets should vanish for a single pair. Then, Eq. (5.23) can be rewritten in the form

$$\mathbf{v}_P = \left[\mathbf{G}_\varphi^P \right] \dot{\boldsymbol{\phi}} \quad (5.24)$$

The i^{th} component of the $\left[\mathbf{G}_\varphi^P \right]$ is

$$\left[\mathbf{G}_\varphi^P \right]_{:i} = \frac{\partial \mathbf{v}_P}{\partial \dot{\boldsymbol{\phi}}_i}$$

From Eq. (5.23), the first KIC can be expressed as

$$\left[\mathbf{G}_\varphi^P \right]_{:i} = \begin{cases} \mathbf{S}_i \times (\mathbf{P} - \mathbf{R}_i), & i \leq n, \text{ } i - \text{revolute pair} \\ \mathbf{S}_i & i \leq n, \text{ } i - \text{prismatic pair} \\ 0 & i > n \end{cases} \quad (5.25)$$

where for $\mathbf{S}_i \times (\mathbf{P} - \mathbf{R}_i)$, we have

$$\|\mathbf{S}_i \times (\mathbf{P} - \mathbf{R}_i)\| = |\mathbf{P} - \mathbf{R}_i| \cdot \sin(\mathbf{S}_i \wedge (\mathbf{P} - \mathbf{R}_i))$$

which is the distance from point \mathbf{P} to axis \mathbf{S}_i . Equations (5.20) and (5.25) express the first-order KIC of the open serial chain. When the position and orientation of the serial chain are given, all the KICs can be easily obtained.

5.2.3 Second-Order KIC

To determine the second-order KIC of the serial chain [3], we may take the time derivative for Eq. (5.17)

$$\varepsilon_{jk} = \frac{d}{dt} \left(\left[\mathbf{G}_\phi^{jk_1} \right] \right) \phi + \left[\mathbf{G}_\phi^{jk_1} \right] \dot{\phi}. \quad (5.26)$$

For the first item in Eq. (5.26), we have

$$\frac{d}{dt} \left(\left[\mathbf{G}_\varphi^h \right]_{:i} \right) = \begin{cases} \dot{\mathbf{S}}_i, & i \leq n, \text{ } i - \text{revolute pair} \\ 0 & \text{other cases} \end{cases} \quad (5.27)$$

The definition of the element of the second-order KIC matrix is as follows

$$\left[\mathbf{H}_\varphi^h \right]_{ij} = \frac{\partial}{\partial \dot{\varphi}_i} \left\{ \frac{d}{dt} \left(\left[\mathbf{G}_\varphi^h \right]_{:j} \right) \right\}$$

which can be rewritten as

$$\left[\mathbf{H}_\varphi^h \right]_{ij} = \frac{\partial}{\partial \varphi_i} \left(\left[\mathbf{G}_\varphi^h \right]_{:j} \right) \quad (5.28)$$

where ‘ $i:j$ ’ indicates an element in i^{th} row and j^{th} column of matrix $[\mathbf{H}]$ and ‘ $:j$ ’ means the j^{th} column of the matrix. The derivative in Eq. (5.27) can be written in the form

$$\frac{d}{dt} \left(\left[\mathbf{G}_\varphi^h \right]_{:i} \right) = \dot{\varphi}^T \left[\mathbf{H}_\varphi^h \right]_{:i}$$

Then, the angular acceleration of link n is

$$\boldsymbol{\varepsilon}_h = \dot{\varphi}^T \left[\mathbf{H}_\varphi^h \right] \dot{\varphi} + \left[\mathbf{G}_\varphi^h \right] \ddot{\varphi} \quad (5.29)$$

where $\left[\mathbf{H}_\varphi^h \right]$ is a $3 \times N \times N$ matrix whose element has three components. Equation (5.29) contains three scalar equations. For instance, its first scalar equation is

$$\boldsymbol{\varepsilon}_h^x = \dot{\varphi}^T \left[\mathbf{H}_\varphi^h \right]^x \dot{\varphi} + \left[\mathbf{G}_\varphi^h \right]^x \ddot{\varphi} \quad (5.30)$$

From Eqs. (5.27) and (5.28), the second-order KIC is in the form

$$\left[\mathbf{H}_\varphi^h \right]_{ij} = \begin{cases} \mathbf{S}_i \times \mathbf{S}_j, & i < j \\ 0, & \text{\textit{i, j are revolute pair}} \\ & \text{\textit{for other cases}} \end{cases} \quad (5.31)$$

Equation (5.29) indicates the angular acceleration $\boldsymbol{\varepsilon}_h$ of link n on the robot hand. Similarly, the linear acceleration \mathbf{a}_P of point P in link n is as follows

$$\mathbf{a}_P = \dot{\varphi}^T \left[\mathbf{H}_\varphi^P \right] \dot{\varphi} + \left[\mathbf{G}_\varphi^P \right] \ddot{\varphi}. \quad (5.32)$$

This variable is obtained by the time derivative for Eq. (5.24). The definition of translational second-order KIC is given by

$$\left[\mathbf{H}_\varphi^P \right]_{ij} = \frac{\partial}{\partial \dot{\varphi}_i} \left\{ \frac{d}{dt} \left(\left[\mathbf{G}_\varphi^P \right]_{:j} \right) \right\}$$

Table 5.1 Kinematic influence coefficients

expression	Kinematic pair		KIC	
	i	j		
Revolute first-order KIC				
$\left[G_{\varphi}^h \right]_j$	–	R	$J \leq n$	S_j
	–	R	$J > n$	0
	–	P	any j	0
Translation first-order KIC				
$\left[G_{\varphi}^p \right]_j$	–	R	$J \leq n$	$S_j \times (P - R_j)$
	–	P	$J \leq n$	S_j
	–	–	$J > n$	0
Revolute second-order KIC				
$\left[H_{\varphi}^h \right]_{ij}$	R	R	$i < j \leq n$	$S_i \times S_j$
	R	R	$i \geq j$ or $j > n$	0
	P	P	any i, j	0
	R	P	any i, j	0
Translation second-order KIC				
$\left[H_{\varphi}^p \right]_{ij}$	R	R	$j \leq j \leq n$	$S_i \times [S_j \times (P - R_j)]$
	R	R	$j < i \leq n$	$S_j \times [S_i \times (P - R_i)]$
	P	R	$i < j \leq n$	0
	P	R	$j < i \leq n$	$S_j \times S_i$
	R	P	$i < j \leq n$	$S_i \times S_j$
	R	P	$j < i \leq n$	0
	–	–	$(i \text{ or } j) > n$	0
	P	P	any i, j	0

or

$$\left[H_{\varphi}^p \right]_{ij} = \frac{\partial}{\partial \varphi_i} \left(\left[G_{\varphi}^p \right]_j \right) \quad (5.33)$$

The values of the second-order KIC can be obtained by taking the time derivative for Eq. (5.25). The values are expressed in Table 5.1. The table indicates that the translational second-order KICs are symmetrical, that is,

$$\left[H_{\varphi}^p \right]_{ij} = \left[H_{\varphi}^p \right]_{ji}$$

5.3 Kinematic Analysis of Parallel Mechanism

In reference [7], Hunt pointed out the possible merits of parallel mechanisms and showed a model of a robot with six parallel inputs. In the present research, the common six-DOF manipulator will be considered. We will investigate how to set the kinematic modeling of this complex parallel mechanism.

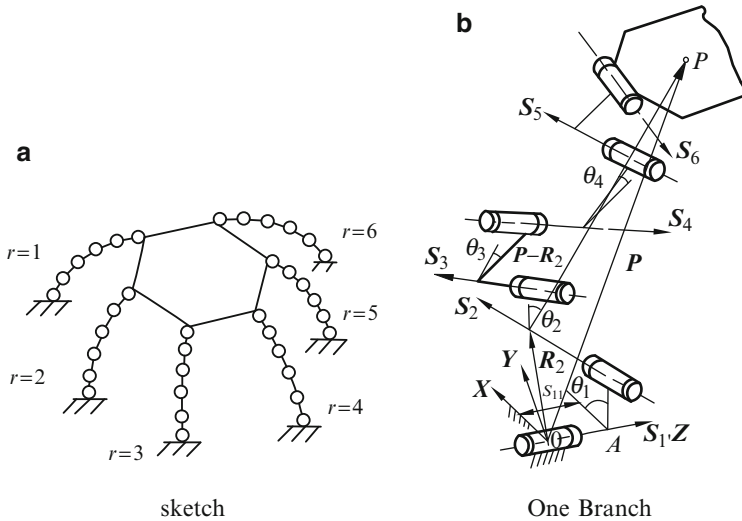


Fig. 5.4 A 6-6R Multi-Loop Mechanism (a) sketch (b) one branch

A multi-loop parallel mechanism is constructed by connecting the central platform to ground by N branches. Every branch may have several basic joints, either revolute or prismatic. If some kinematic pair is neither revolute nor prismatic, then it should be decomposed into a combination of revolute and prismatic pairs. The multi-loop robot is composed of N branches. When $N = 1$, the mechanism becomes an open-loop manipulator. When $N = 2$, the mechanism is a single-loop chain. When $N > 2$ the mechanism is a multi-loop device. When $N > 6$, at least $N-6$ branches are passive, which means no actuator is found in the $N-6$ branches. The platform has six DOF, so at least six inputs are necessary. Theoretically, any six single-DOF kinematic pair from this mechanism may be freely selected as inputs to make its motion well-controlled.

The 6-6R mechanism, Fig. 5.4a, is a typical 6-DOF parallel manipulator^[8] consisting of six limbs. Each limb has six single-DOF revolute pairs. Its kinematic analysis is an important theoretical foundation suitable for all parallel mechanisms, including 6-DOF and lower-DOF parallel mechanisms. In the following two sections, we focus on the kinematic analysis of the 6-6R parallel mechanism.

In 1985, Huang made an important contribution by first setting both the velocity and acceleration analyses of the complicated 6-6R parallel mechanism using KIC method, setting its dynamic modal, and analyzing a numerical example [5, 6]. In this section, we introduce the KIC principle.

5.3.1 First-Order KIC and Mechanism Velocity Analysis

Let us first discuss the velocity analysis and derive the first-order-KIC.

5.3.1.1 Velocity of Point P in the Platform

Initially, let us consider one of the limbs which is a serial chain, Fig. 5.4b [6]. The absolute angular velocity of the platform can be expressed as

$$\boldsymbol{\omega}_h = [\mathbf{G}_\varphi^h] \dot{\boldsymbol{\varphi}} \quad (5.34)$$

where $\boldsymbol{\omega}_h = \{\omega_{hx}, \omega_{hy}, \omega_{hz}\}^T$; $\dot{\boldsymbol{\varphi}} = \{\dot{\varphi}_1, \dot{\varphi}_2, \dots, \dot{\varphi}_6\}^T$; and $\dot{\varphi}_i$, the i^{th} component of the generalized velocity vector, is either θ_i or \mathbf{S}_i depending on whether joint i is a revolute or prismatic joint. $[\mathbf{G}_\varphi^h]$ is a 3×6 first-order KIC matrix defined as

$$[\mathbf{G}_\varphi^h] = \begin{pmatrix} \frac{\partial \omega_h}{\partial \dot{\varphi}_1} & \frac{\partial \omega_h}{\partial \dot{\varphi}_2} & \dots & \frac{\partial \omega_h}{\partial \dot{\varphi}_6} \end{pmatrix} \quad (5.35)$$

For the serial open chain, the first-order KICs can be evaluated as

$$[\mathbf{G}_\varphi^h] = \begin{cases} \mathbf{S}_i, & \text{for revolute pair} \\ 0, & \text{for prismatic pair} \end{cases} \quad (5.36)$$

If the joints are all revolute pairs as shown in Fig. 5.4b,

$$[\mathbf{G}_\varphi^h] = (\mathbf{S}_1 \quad \mathbf{S}_2 \quad \dots \quad \mathbf{S}_6) \quad (5.37)$$

In Eqs. (5.36) and (5.37), \mathbf{S}_i is the unit vector of the i^{th} revolute pair.

The linear velocity of an interested point on the central platform, say point P , is given by

$$\mathbf{V}_P = [\mathbf{G}_\varphi^P] \dot{\boldsymbol{\varphi}} \quad (5.38)$$

where

$$\mathbf{V}_P = (\mathbf{v}_{Px} \quad \mathbf{v}_{Py} \quad \mathbf{v}_{Pz})^T \quad (5.39)$$

$[\mathbf{G}_\varphi^P]$ is a 3×6 matrix corresponding to the first-order KIC of point P

$$[\mathbf{G}_\varphi^P] = (\partial \mathbf{V}_P / \partial \dot{\varphi}_1 \quad \partial \mathbf{V}_P / \partial \dot{\varphi}_2 \quad \dots \quad \partial \mathbf{V}_P / \partial \dot{\varphi}_6) \quad (5.40)$$

For the serial open chain, the column i of this matrix can be expressed as

$$\left[\mathbf{G}_\varphi^p \right]_{:i} = \begin{cases} \mathbf{S}_i \times (\mathbf{P} - \mathbf{R}_i) & i \leq n \quad i - \text{revolute pair} \\ \mathbf{S}_i & i \leq n \quad i - \text{translation pair} \\ 0 & i > n \end{cases} \quad (5.41)$$

where n is the end-link of the serial chain or some interested link in the chain.

Both the angular velocity $\boldsymbol{\omega}_h$ and the linear velocity \mathbf{V}_p of the platform are 3D vectors, which can be combined to form a vector of length six. Thus, from Eqs. (5.34) and (5.38), we obtain the following compact equation

$$\mathbf{V}_H = \left[\mathbf{G}_\varphi^H \right] \dot{\boldsymbol{\varphi}} \quad (5.42)$$

where \mathbf{V}_H is a six-component vector and $\left[\mathbf{G}_\varphi^H \right]$ is a 6×6 scalar matrix

$$\mathbf{V}_H = \begin{Bmatrix} \boldsymbol{\omega}_h \\ \cdots \\ \mathbf{V}_p \end{Bmatrix} = (\boldsymbol{\omega}_{hx} \ \boldsymbol{\omega}_{hy} \ \boldsymbol{\omega}_{hz} \ V_{Px} \ V_{Py} \ V_{Pz})^T \quad (5.43)$$

$$\left[\mathbf{G}_\varphi^H \right] = \begin{bmatrix} \left[\mathbf{G}_\varphi^h \right] \\ \cdots \\ \left[\mathbf{G}_\varphi^p \right] \end{bmatrix} \in \mathbf{R}^{6 \times 6} \quad (5.44)$$

The inverse of (5.42) is

$$\dot{\boldsymbol{\varphi}} = \left[\mathbf{G}_\varphi^H \right]^{-1} \mathbf{V}_H \quad (5.45)$$

where $\left[\mathbf{G}_\varphi^H \right]$ is nonsingular.

For the 6-6R parallel manipulator, the platform has six degrees of freedom. To establish the motion relationship between the platform and the six inputs, we write all the matrix Eq. (5.45) of these six branches when the motion of the platform is given as follows

$$\dot{\boldsymbol{\varphi}}^{(r)} = \left[\mathbf{G}_\varphi^H \right]^{-1(r)} \mathbf{V}_H \quad r = 1, 2 \cdots 6 \quad (5.46)$$

where the superscript r indicates the r th branch. Hence, there are six matrix equations for the six branches. Therefore, Eq. (5.46) expresses 36 linear equations. All the 36 scalar generalized velocities including the six inputs can be evaluated when the motion of the platform is given. Thus, no matter where the

input actuators are, we can always find the six vector equations corresponding to the input, $\dot{\varphi}$

$$\begin{aligned}\dot{\varphi}_\alpha^{(a)} &= \left[\mathbf{G}_\varphi^H \right]_{\alpha:}^{-1(a)} \mathbf{V}_H \\ \dot{\varphi}_\beta^{(b)} &= \left[\mathbf{G}_\varphi^H \right]_{\beta:}^{-1(b)} \mathbf{V}_H \\ &\vdots \\ \dot{\varphi}_\zeta^{(f)} &= \left[\mathbf{G}_\varphi^H \right]_{\zeta:}^{-1(f)} \mathbf{V}_H\end{aligned}\quad (5.47)$$

where $\dot{\varphi}^{(a)}$ is the input angular velocity, the superscript $a b \dots$, indicates the number of the branch, and the subscript α, β, \dots , indicates the number of the kinematic pair whose motion is known in the branch. $\left(\left[\mathbf{G}_\varphi^H \right]^{-1} \right)_{\alpha:}$ is the α^{th} row of the matrix $\left(\left[\mathbf{G}_\varphi^H \right]^{-1} \right)$. If the subscript is located after the semicolon ': α ', it refers to the α th column of that matrix. The six linear equations in Eq. (5.47) can also be combined as a matrix equation

$$\dot{\mathbf{q}} = [\mathbf{G}_H^q] \mathbf{V}_H \quad (5.48)$$

where $\dot{\mathbf{q}}$ is the input angular velocity and the independent generalized input

$$\dot{\mathbf{q}} = \{ \dot{\varphi}_\alpha \quad \dot{\varphi}_\beta \quad \dots \quad \dot{\varphi}_\zeta \}^T \quad (5.49)$$

and

$$[\mathbf{G}_H^q] = \begin{bmatrix} \left[\mathbf{G}_\varphi^H \right]_{\alpha:}^{-1(a)} \\ \left[\mathbf{G}_\varphi^H \right]_{\beta:}^{-1(b)} \\ \vdots \\ \left[\mathbf{G}_\varphi^H \right]_{\zeta:}^{-1(f)} \end{bmatrix} \in R^{6 \times 6} \quad (5.50)$$

Matrix (5.50) is also a 6×6 scalar matrix. From Eq. (5.48), we can get

$$\mathbf{V}_H = \left[\mathbf{G}_q^H \right] \dot{\mathbf{q}} \quad (5.51)$$

when

$$\left[\mathbf{G}_q^H \right] = \left[\mathbf{G}_H^q \right]^{-1} \quad (5.52)$$

$[\mathbf{G}_H^q]$ is nonsingular and is also a 6×6 scalar matrix.

5.3.1.2 Velocity of Point Q in Link k of Limb r

Now let us discuss the velocity of the point in limb-link of the 6-6R mechanism. In general, this is a very difficult problem using a common method. However, using the KIC method, the problem is easily solved.

After we substitute Eq. (5.51) into (5.46), we get

$$\dot{\varphi}^{(r)} = \left[\mathbf{g}_q^\varphi \right]^{(r)} \dot{\mathbf{q}} \quad (5.53)$$

where $\left[\mathbf{g}_q^\varphi \right]$ is a 6×6 matrix.

$$\left[\mathbf{g}_q^\varphi \right]^{(r)} = \left[\mathbf{G}_\varphi^H \right]^{-1(r)} \left[\mathbf{G}_q^H \right], \quad r = 1, 2, \dots, 6 \quad (5.54)$$

and

$$\left[\mathbf{g}_q^\varphi \right]_{ij}^{(r)} = \left[\mathbf{G}_\varphi^H \right]_{i:}^{-1(r)} \left[\mathbf{G}_q^H \right]_{:j}$$

The absolute angular velocity $\boldsymbol{\omega}_k^{(r)}$ of link k in branch r is in the form

$$\boldsymbol{\omega}_k^{(r)} = \boldsymbol{\omega}_1^{(r)} + \boldsymbol{\omega}_2^{(r)} + \dots + \boldsymbol{\omega}_{jk}^{(r)} \quad (5.55)$$

where $\boldsymbol{\omega}_k$ is the absolute angular velocity of the k^{th} link and $\boldsymbol{\omega}_{jk}$ is the relative angular velocity of the k^{th} link to the j^{th} link.

$$\boldsymbol{\omega}_k = \sum_{i=1}^k \dot{\theta}_i \mathbf{S}_i \quad (5.56)$$

$$\boldsymbol{\omega}_k^{(r)} = \left[\mathbf{G}_{\varphi_{1k}}^k \right]^{(r)} \dot{\varphi}_{1k}^{(r)}, \quad r = 1, 2 \dots 6; \quad k = 1, 2 \dots < 6 \quad (5.57)$$

where

$$\boldsymbol{\varphi}_{1k}^{(r)} = (\dot{\varphi}_1 \quad \dot{\varphi}_2 \quad \dots \quad \dot{\varphi}_k)^{T(r)}$$

$$\left[\mathbf{G}_{\varphi_{1k}}^k \right] = [\mathbf{S}_1 \quad \mathbf{S}_2 \quad \dots \quad \mathbf{S}_k]_{3 \times k}$$

We are also interested in the linear velocities of point Q in the link k of branch r . Similar to Eqs. (5.21), (5.22), (5.23), and (5.24), we have

$$\mathbf{v}_{kQ}^{(r)} = \left[\mathbf{G}_{\varphi_{1k}}^{kQ} \right]^{(r)} \dot{\varphi}_{1k}^{(r)} \quad r = 1, 2 \dots 6; \quad k = 1, 2 \dots < 6 \quad (5.58)$$

where the $3 \times k$ first-order coefficient matrix $\left[\mathbf{G}_{\varphi_{1k}}^K \right]$ can also be evaluated by Table 5.1 [6].

Similarly, combining Eqs. (5.57) and (5.58), the compact form is expressed by

$$\mathbf{V}_K^{(r)} = \left[\mathbf{G}_{\varphi_{1k}}^K \right]^{(r)} \dot{\varphi}_{1k}^{(r)} \quad (5.59)$$

We are looking for $\left[\mathbf{G}_q^K \right]$ which is the partial derivative of \mathbf{V}_k with respect to the generalized velocities

$$\frac{\partial \mathbf{V}_K}{\partial \dot{\mathbf{q}}} = \frac{\partial \mathbf{V}_K^{(r)}}{\partial \dot{\varphi}_{1k}} \cdot \frac{\partial \dot{\varphi}_{1k}^{(r)}}{\partial \dot{\mathbf{q}}} \quad (5.60)$$

Substituting Eq. (5.54) into Eq. (5.60) in matrix form yields

$$\left[\mathbf{G}_q^K \right]^{(r)} = \left[\mathbf{G}_{\varphi_{1k}}^K \right]_{6 \times k}^{(r)} \left[\mathbf{g}_q^{\varphi_{1k}} \right]_{k \times 6}^{(r)} = \left[\mathbf{G}_{\varphi_{1k}}^K \right]_{6 \times k}^{(r)} \left(\left[\mathbf{G}_{\varphi}^H \right]_{1k:}^{-1(r)} \right) \left[\mathbf{G}_q^H \right] \quad (5.61)$$

$$r = 1, 2, \dots, 6; \quad k = 1, 2, 3, 4, 5$$

where $\left[\mathbf{g}_q^{\varphi_{1k}} \right]$ and $\left[\mathbf{G}_{1k:}^H \right]$ are $k \times 6$ matrices.

Therefore, the absolute velocity of link k in branches r can be evaluated as

$$\mathbf{V}_k^{(r)} = \left[\mathbf{G}_q^k \right]^{(r)} \dot{\mathbf{q}} \quad k = 2, 3, 4, 5; \quad r = 1, 2 \dots 6 \quad (5.62)$$

Using this method, the velocities of the platform and the links in the branches can be determined.

5.3.2 Second-Order KIC and Mechanism Accelerations

5.3.2.1 Acceleration of Platform

The inertial loads of the mechanism depend on the accelerations, so the latter is the next point of interest. First, let us investigate the central platform. We take one branch from this multi-loop mechanism as we did before. The angular acceleration of the platform ε_h can be written as follows

$$\varepsilon_h = \dot{\varphi}^T \left[\mathbf{H}_{\varphi}^h \right] \dot{\varphi} + \left[\mathbf{G}_{\varphi}^h \right] \ddot{\varphi} \quad (5.63)$$

where

$$\boldsymbol{\varepsilon}_h = \{\boldsymbol{\varepsilon}_{hx} \quad \boldsymbol{\varepsilon}_{hy} \quad \boldsymbol{\varepsilon}_{hz}\}^T \quad (5.64)$$

$$\ddot{\boldsymbol{\varphi}} = \{\ddot{\varphi}_1 \quad \ddot{\varphi}_2 \quad \cdots \quad \ddot{\varphi}_6\}^T \quad (5.65)$$

$[\mathbf{H}_\varphi^h]$ is the second-order KIC matrix defined as

$$[\mathbf{H}_\varphi^h] = \begin{bmatrix} \frac{\partial^2 \boldsymbol{\omega}_h}{\partial \dot{\varphi}_1 \partial \varphi_1} & \frac{\partial^2 \boldsymbol{\omega}_h}{\partial \dot{\varphi}_1 \partial \varphi_2} & \cdots & \frac{\partial^2 \boldsymbol{\omega}_h}{\partial \dot{\varphi}_1 \partial \varphi_6} \\ \frac{\partial^2 \boldsymbol{\omega}_h}{\partial \dot{\varphi}_2 \partial \varphi_1} & \frac{\partial^2 \boldsymbol{\omega}_h}{\partial \dot{\varphi}_2 \partial \varphi_2} & \cdots & \frac{\partial^2 \boldsymbol{\omega}_h}{\partial \dot{\varphi}_2 \partial \varphi_6} \\ \vdots & \vdots & \vdots & \vdots \\ \frac{\partial^2 \boldsymbol{\omega}_h}{\partial \dot{\varphi}_6 \partial \varphi_1} & \frac{\partial^2 \boldsymbol{\omega}_h}{\partial \dot{\varphi}_6 \partial \varphi_2} & \cdots & \frac{\partial^2 \boldsymbol{\omega}_h}{\partial \dot{\varphi}_6 \partial \varphi_6} \end{bmatrix} \in R^{3 \times 6 \times 6} \quad (5.66)$$

This is a 6×6 matrix whose components are vectors of length three.

Similarly, the linear acceleration of a point P in the platform can be written as

$$\mathbf{a}_P = \dot{\boldsymbol{\varphi}}^T [\mathbf{H}_\varphi^P] \dot{\boldsymbol{\varphi}} + [\mathbf{G}_\varphi^P] \ddot{\boldsymbol{\varphi}} \quad (5.67)$$

The elements of matrix $[\mathbf{H}_\varphi^P]$ are also vectors of length three. For the serial open chain, the second-order coefficients are given by Table 5.1 in a particularly simple form.

Combining the two 3D matrix equations (5.63) and (5.67), we obtain a more compact equation result

$$A_H = \dot{\boldsymbol{\varphi}}^T [\mathbf{H}_\varphi^H] \dot{\boldsymbol{\varphi}} + [\mathbf{G}_\varphi^H] \ddot{\boldsymbol{\varphi}} \quad (5.68)$$

where

$$A_H = \left\{ \begin{array}{c} \boldsymbol{\varepsilon}_h \\ \cdots \\ \mathbf{a}_p \end{array} \right\}$$

$[\mathbf{H}_\varphi^H]$ is a 6×6 vector matrix, i.e., $[\mathbf{H}_\varphi^H] \in R^{6 \times 6 \times 6}$. Its element in row m and column n , $[\mathbf{H}_\varphi^H]_{m:n}$, is a combination of two vector components, $[\mathbf{H}_\varphi^H]_{m:n}$ and $[\mathbf{H}_\varphi^P]_{m:n}$, and forms a six-element vector as follows

$$[\mathbf{H}]_{m:n} = \left\{ \begin{array}{c} [\mathbf{H}^h]_{m:n} \\ \cdots \\ [\mathbf{H}^P]_{m:n} \end{array} \right\}_{1 \times 6}$$

Its element can be obtained using Table 5.1. From Eq. (5.68), when A_H is given, we can obtain

$$\ddot{\phi} = \left[G_{\phi}^H \right]^{-1} \left\{ A_H - \dot{\phi}^T \left[H_{\phi}^H \right] \dot{\phi} \right\} \quad (5.69)$$

or in the form

$$\ddot{\phi}^{(r)} = \left[G_{\phi}^H \right]^{-1(r)} \left\{ A_H - \dot{\phi}^{T(r)} \left[H_{\phi}^H \right]^{(r)} \dot{\phi}^{(r)} \right\} \quad r = 1, 2 \dots 6 \quad (5.70)$$

Where $\left[G_{\phi}^H \right]$ is nonsingular. The matrix $\left[H_{\phi}^H \right]$ is regarded as a 36×6 scalar matrix. However, to be precise, it is a 6×6 matrix whose elements are vectors of length six. The matrix equations (5.68) and (6.69) are the two basic formulae from which we can calculate A_H when $\dot{\phi}$ is given, and compute $\dot{\phi}$ when A_H is specified.

Equation (5.69) also indicates six linear equations. Similarly in velocity analysis, we may obtain the following set of equations:

$$\begin{aligned} \ddot{\phi}_{\alpha}^{(a)} &= \left[G_{\phi}^H \right]_{\alpha:}^{-1(a)} \left\{ A_H - \dot{\phi}^T \left[H_{\phi}^H \right] \dot{\phi} \right\}^{(a)} \\ \ddot{\phi}_{\beta}^{(b)} &= \left[G_{\phi}^H \right]_{\beta:}^{-1(b)} \left\{ A_H - \dot{\phi}^T \left[H_{\phi}^H \right] \dot{\phi} \right\}^{(b)} \\ &\vdots \\ \ddot{\phi}_{\zeta}^{(f)} &= \left[G_{\phi}^H \right]_{\zeta:}^{-1(f)} \left\{ A_H - \dot{\phi}^T \left[H_{\phi}^H \right] \dot{\phi} \right\}^{(f)} \end{aligned} \quad (5.71)$$

where $\dot{\phi}_{\beta}^{(b)}$ is the given acceleration of β^{th} joint in the b^{th} branch. Without loss of generality, we can assume the six basic links connected to the ground of the six limbs as the six input links, i.e., $\alpha = \beta = \dots = \zeta = 1$, $(a \ b \ \dots \ f) = (1 \ 2 \ \dots \ 6)$. The six input angular velocities are constant. Equation (5.71) can be put together in matrix form as

$$\ddot{\mathbf{q}} = \left[G_H^q \right] A_H - \left\{ \begin{array}{l} \dot{\mathbf{q}}^T \left[L_1 \right]^{(1)} \dot{\mathbf{q}} \\ \dot{\mathbf{q}}^T \left[L_1 \right]^{(2)} \dot{\mathbf{q}} \\ \vdots \\ \dot{\mathbf{q}}^T \left[L_1 \right]^{(6)} \dot{\mathbf{q}} \end{array} \right\} \quad (5.72)$$

$$\ddot{\mathbf{q}} = \{ \ddot{q}_1 \ \ddot{q}_2 \ \dots \ \ddot{q} \}^T = \{ \ddot{\phi}_{\alpha}^{(a)} \ \ddot{\phi}_{\beta}^{(b)} \ \dots \ \ddot{\phi}_f^{(\zeta)} \}^T$$

$$\ddot{\mathbf{q}} = \left[G_H^q \right] A_H - \left\{ \begin{array}{l} \dot{\mathbf{q}}^T \left[L_1 \right]^{(1)} \dot{\mathbf{q}} \\ \dot{\mathbf{q}}^T \left[L_1 \right]^{(2)} \dot{\mathbf{q}} \\ \vdots \\ \dot{\mathbf{q}}^T \left[L_1 \right]^{(6)} \dot{\mathbf{q}} \end{array} \right\}$$

indicate the input accelerations. The 6×6 scalar matrix $[\mathbf{L}]$ is

$$[\mathbf{L}_1]^{(r)} = [\mathbf{g}_q^\varphi]^{T(r)} \left[\left[[\mathbf{G}_\varphi^H]^{-1} \right] * [\mathbf{H}_\varphi^H] \right]^{(r)} [\mathbf{g}_q^\varphi]^{(r)} \quad r = 1, 2, \dots, 6 \quad (5.73)$$

where the notation $[(\mathbf{A}) * (\mathbf{B}_{mn})]$ is defined to be multiplying the matrix A by the “*” product of every vector element of matrix B, and all the new elements compose a new 6×6 matrix. This definition of “*” product can also be expressed as follows:

$$[\mathbf{A}] * [\mathbf{B}] = \begin{bmatrix} [\mathbf{A}]b_{11} & [\mathbf{A}]b_{12} & \cdots & [\mathbf{A}]b_{1N} \\ [\mathbf{A}]b_{21} & [\mathbf{A}]b_{22} & \cdots & [\mathbf{A}]b_{2N} \\ \vdots & \vdots & \vdots & \vdots \\ [\mathbf{A}]b_{N1} & [\mathbf{A}]b_{N2} & \cdots & [\mathbf{A}]b_{NN} \end{bmatrix} \quad (5.74)$$

Therefore, Eq. (5.72) can be further simplified as

$$\ddot{\mathbf{q}} = [\mathbf{G}_H^q] \mathbf{A}_H - \dot{\mathbf{q}}^T [\mathbf{H}_H^q] \dot{\mathbf{q}} \quad (5.75)$$

where $[\mathbf{H}_H^q]$ is a scalar $6 \times 6 \times 6$ matrix, and its component is

$$(\mathbf{H}_H^q)_{mn} = \left\{ \mathbf{L}_{mn}^{(1)} \quad \mathbf{L}_{mn}^{(2)} \quad \cdots \quad \mathbf{L}_{mn}^{(6)} \right\}^T \quad (5.76)$$

Then, the 6-D acceleration of the center platform can be expressed by six inputs in the form

$$\mathbf{A}_H = \dot{\mathbf{q}}^T [\mathbf{H}_q^H] \dot{\mathbf{q}} + [\mathbf{G}_q^H] \ddot{\mathbf{q}} \quad (5.77)$$

where $[\mathbf{H}_q^H] = [\mathbf{G}_q^H] * [\mathbf{H}_H^q]$.

5.3.2.2 Acceleration of Link k in Limb r

To analyze the acceleration of the arbitrary link in the arbitrary limb, substituting Eq. (5.70) yields

$$\ddot{\boldsymbol{\varphi}}^{(r)} = [\mathbf{G}_\varphi^H]^{-1(r)} \left[[\mathbf{G}_q^H] (\ddot{\mathbf{q}} + \dot{\mathbf{q}}^T [\mathbf{H}_H^q] \dot{\mathbf{q}}) - \dot{\boldsymbol{\varphi}}^T [\mathbf{H}_\varphi^H] \dot{\boldsymbol{\varphi}} \right]^{(r)} \quad (5.78)$$

Taking the time derivative for Eq. (5.53) yields

$$\ddot{\boldsymbol{\varphi}}^{(r)} = \dot{\mathbf{q}}^T [\mathbf{h}_a^\varphi]^{(r)} \dot{\mathbf{q}} + [\mathbf{g}_q^\varphi]^{(r)} \ddot{\mathbf{q}} \quad (5.79)$$

where

$$\mathbf{h}_{ij}^{\phi} = \left\{ \begin{array}{ccc} \frac{\partial^2 \phi_1}{\partial q_i \partial q_j} & \frac{\partial^2 \phi_2}{\partial q_i \partial q_j} & \dots & \frac{\partial^2 \phi_6}{\partial q_i \partial q_j} \end{array} \right\}^T$$

From Eqs. (5.78) and (5.79) as well as Eqs. (5.53) and (5.54), we have

$$\left[\mathbf{h}_q^{\varphi} \right]^{(r)} = \left[\left[\mathbf{g}_q^{\varphi} \right]^{(r)} * \left[\mathbf{H}_H^q \right] \right] - \left[\mathbf{g}_q^{\varphi} \right]^{T(r)} \left[\left[\mathbf{G}_{\varphi}^H \right]^{-1} * \left[\mathbf{H}_{\varphi}^H \right] \right]^{(r)} \left[\mathbf{g}_q^{\varphi} \right]^{(r)} \quad (5.80)$$

That is

$$\left[\mathbf{h}_q^{\varphi} \right]^{(r)} = \left[\left[\mathbf{g}_q^{\varphi} \right]^{(r)} * \left[\mathbf{H}_{\varphi}^H \right] \right] - \left[\mathbf{L} \right]^{(r)}$$

where $\left[\mathbf{L} \right]^{(r)} = \left[\mathbf{g}_q^{\varphi} \right]^{T(r)} \left[\left[\mathbf{G}_{\varphi}^H \right]^{-1} * \left[\mathbf{H}_{\varphi}^H \right] \right]^{(r)} \left[\mathbf{g}_q^{\varphi} \right]^{(r)}$ is a 6×6 matrix and its element is a 6-D vector.

The 6-D angular acceleration of link k in limb r can be expressed as follows:

$$\mathbf{A}_K^{(r)} = \left\{ \varepsilon_{Kx} \quad \varepsilon_{Ky} \quad \varepsilon_{Kz} \quad a_{Kpx} \quad a_{Kpy} \quad a_{Kpz} \right\}^{T(r)}$$

The acceleration can be obtained by taking the time derivative of Eq. (5.59) or (5.62) as follows:

$$\mathbf{A}_K^{(r)} = \left(\dot{\boldsymbol{\varphi}}^T \left[\mathbf{H}_{\varphi}^K \right]^{(r)} \dot{\boldsymbol{\varphi}} \right) + \left[\mathbf{G}_{\varphi}^K \right]^{(r)} \ddot{\boldsymbol{\varphi}}, \quad r = 1, 2, \dots, 6 \quad (5.81)$$

Substituting Eq. (5.79) into (5.81) yields

$$\mathbf{A}_K^{(r)} = \left(\dot{\boldsymbol{\varphi}}^T \left[\mathbf{H}_{\varphi}^K \right]^{(r)} \dot{\boldsymbol{\varphi}} \right) + \ddot{\mathbf{q}}^T \left[\left[\mathbf{G}_{\varphi}^K \right] * \left[\mathbf{h}_q^{\varphi} \right] \right]^{(r)} \dot{\mathbf{q}} + \left(\left[\mathbf{G}_{\varphi}^K \right] \left[\mathbf{g}_q^{\varphi} \right] \right)^{(r)} \ddot{\mathbf{q}}$$

Considering Eqs. (5.53) and (5.61), we have

$$\left[\mathbf{H}_q^K \right]^{(r)} = \left(\left[\mathbf{g}_q^{\varphi} \right]_{1k}^T \left[\mathbf{H}_{\varphi}^K \right] \left[\mathbf{g}_q^{\varphi} \right]_{1k} + \left[\left[\mathbf{G}_{\varphi 1k}^K \right] * \left[\mathbf{h}_q^{\varphi 1k} \right] \right] \right)^{(r)} \quad (5.82)$$

and

$$\left[\mathbf{G}_q^K \right]^{(r)} = \left(\left[\mathbf{G}_{\varphi}^K \right] \left[\mathbf{g}_q^{\varphi} \right] \right)^{(r)} \quad (5.83)$$

Finally, we obtain the final formula as follows:

$$\mathbf{A}_K^{(r)} = \dot{\mathbf{q}}^T \left[\mathbf{H}_q^K \right]^{(r)} \ddot{\mathbf{q}} + \left[\mathbf{G}_q^K \right]^{(r)} \ddot{\mathbf{q}} \quad (5.84)$$

We derived the first and second-order KIC for the central platform and the link in the six-DOF 6-6R multiloop parallel manipulator in a quite relatively simple form.

All the velocities and accelerations of the manipulator can be solved when the input $\dot{\mathbf{q}}$ and $\ddot{\mathbf{q}}$ are known. The inverse problem is also specified. The KIC \mathbf{G} and \mathbf{H} -function depend on only the geometry, so they can be obtained before the kinematic analysis.

5.4 Virtual Mechanism Principle of Lower-Mobility Parallel Mechanisms

For lower-mobility PM, the first-order KIC matrix (Jacobian matrix) is not square and has no inverse. Schilling [9] used the generalized inverse to solve the problem. Gregorio [10] analyzed a 3-RPS wrist by vector method.

In 1985, Yan and Huang proposed the virtual-mechanism principle (VMP) for the kinematic analysis of the lower-mobility PM [11] by adding some virtual pairs to the mechanism. Then, the reversible square matrix for the lower-mobility PM can be built. The virtual mechanism is the kinematic equivalent of the original real mechanism, so both the forward and inverse kinematic analyses for the virtual mechanisms are available. Like the KIC principle for 6-DOF PM, the VMP can also provide a uniform way to analyze the lower-mobility PM, regardless if the PM is symmetrical or not and how many mobility it has. Thus, the process is time-saving. The more complex the mechanism, the more effective the method.

5.4.1 Virtual Mechanism Principle

For lower-mobility PM, building square first-order KIC matrices is impossible and inverse kinematic analysis is difficult. To solve this problem, we proposed the VMP to build new reversible square KIC matrices so the velocity and acceleration analyses can go through. In the current study, the spatial 3-DOF 3-RPS PM is taken as an example, Fig. 5.5a, to explain how to build the virtual mechanism for lower-mobility PM.

To solve this problem, the virtual mechanism principle requires two conditions:

1. Transferring the lower-mobility mechanism to a 6-DOF. To achieve this aim, some single-DOF kinematic pairs should be added to each limb until the number of the kinematic pairs is six. The added kinematic pair is called as ‘virtual kinematic pair’ and the corresponding mechanism is the ‘virtual mechanism’. The virtual

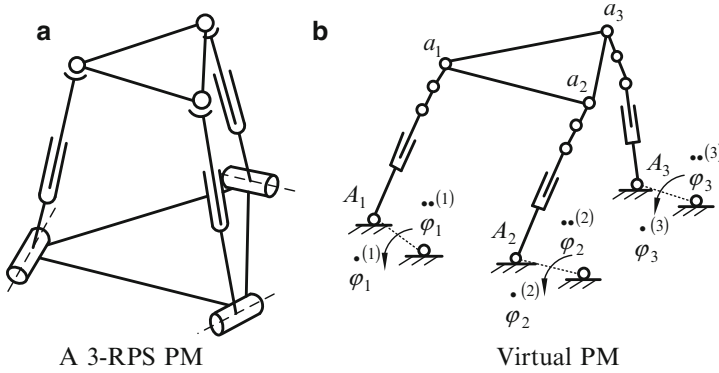


Fig. 5.5 Virtual mechanism principle (a) a 3-RPS PM (b) virtual PM

kinematic pair can be in any orientation and located in any position relative to the limb. The only condition to be satisfied is that the corresponding six screws in each limb are linearly independent.

2. To guarantee equivalent kinematics between the virtual mechanism and the real one, all virtual kinematic pairs added to the mechanism should be selected as ‘inputs’ and all the rates of both the relative velocities and accelerations of the virtual pairs have to be set zeros.

Under the two conditions, the lower-mobility mechanism is transferred to a 6-DOF one on the one hand, and the same motion of the mechanism, which should not be variable on the other hand.

The correctness of the virtual mechanism method is indubitable because when all the virtual inputs including velocities and accelerations all are given as zeros, none of the virtual links is moveable, the additional input links of the virtual mechanism all are fixed, and the virtual mechanism is just the real mechanism itself [1]. Many of our previous studies on lower-mobility PMs were based on VMP [12–18].

For the 3-RPS mechanism, one virtual revolute pair should be added to each limb, as shown in Fig. 5.5b. For the first revolute pair in the *i*th limb, the corresponding amplitude of velocity and acceleration are $\dot{\phi}_1^{(i)}$ and $\ddot{\phi}_1^{(i)}$, respectively. Then, the original 3-DOF 3-RPS real mechanism is transferred into a virtual 6-DOF 3-RRPS chain. The sufficient and necessary conditions for the kinematic analyses of both mechanisms being equal are as follows:

$$\begin{aligned}
 \dot{\phi}_1^{(1)} &= \dot{\phi}_1^{(2)} = \dot{\phi}_1^{(3)} = 0 \\
 \ddot{\phi}_1^{(1)} &= \ddot{\phi}_1^{(2)} = \ddot{\phi}_1^{(3)} = 0
 \end{aligned}
 \tag{5.85}$$

The virtual angular velocities and accelerations in a limb can be written as follows:

$$\begin{aligned} [\dot{\phi}_1 \quad \dot{\phi}_2 \quad \cdots \quad \dot{\phi}_6]^{\text{T}(i)} &= [0 \quad \dot{\phi}_2 \quad \dot{S}_i \quad \dot{\phi}_4 \quad \cdots \quad \dot{\phi}_6]^{\text{T}(i)} & i = 1, 2, 3 \\ [\ddot{\phi}_1 \quad \ddot{\phi}_2 \quad \cdots \quad \ddot{\phi}_6]^{\text{T}(i)} &= [0 \quad \ddot{\phi}_2 \quad \ddot{S}_i \quad \ddot{\phi}_4 \quad \cdots \quad \ddot{\phi}_6]^{\text{T}(i)} & i = 1, 2, 3 \end{aligned} \quad (5.86)$$

where corresponding the 1st items, zeros, in both equations above are the virtual input and the 3rd items are actuated.

Every limb of the virtual mechanism has six single-DOF pairs, so building a square virtual KIC matrix for each limb is possible. Therefore, both the forward and inverse kinematic analyses of the virtual PM can be carried through using the KIC method.

5.4.2 Kinematic Analysis Based on Virtual Mechanism Principle

After the virtual PM is built, all formulas given in Sects. 5.2, 5.3, and 5.4 can be directly applied for the virtual mechanism [19].

The speed rates of the virtual joints given to be zeros can be considered as the ‘inputs’. The rates, including the virtual inputs of the six kinematic joints in limb i , can be rewritten as

$$\dot{\phi}^{(i)} = \left(\dot{\phi}_1, \cdots, \dot{\phi}_n, 0, \cdots, 0 \right)^T \in R^{6 \times 1} \quad (5.87)$$

where n denotes the number of single-DOF real pairs in each limb of the original real PM and the velocity rate of the virtual joint denotes 0. Then, the generalized input velocity rates of the whole virtual PM are expressed as a six-element vector

$$\dot{q} = \left(\dot{q}_1, \cdots, \dot{q}_k, 0, \cdots, 0 \right)^T \in R^{6 \times 1} \quad (5.88)$$

where k denotes the number of freedoms of the lower-mobility PM, i.e., the number of the real inputs.

Similarly, the input acceleration rates, including the virtual inputs of the i^{th} limb, can be rewritten as

$$\ddot{\phi}^{(i)} = \left(\ddot{\phi}_1, \cdots, \ddot{\phi}_n, 0, \cdots, 0 \right)^T \in R^{6 \times 1} \quad (5.89)$$

where the acceleration rate of the virtual joint denotes 0. The generalized input acceleration rates of the whole virtual PM are

$$\ddot{q} = \left(\ddot{q}_1, \cdots, \ddot{q}_k, 0, \cdots, 0 \right)^T \in R^{6 \times 1} \quad (5.90)$$

The forward and inverse solutions for the velocity of limb i of the virtual mechanism are

$$\mathbf{V}_H = \left[\mathbf{G}_\varphi^H \right]^{(i)} \dot{\boldsymbol{\phi}}^{(i)} \quad (5.91)$$

$$\dot{\boldsymbol{\phi}}^{(i)} = \left[\mathbf{G}_\varphi^H \right]^{(i)} \mathbf{V}_H \quad (5.92)$$

where $\mathbf{V}_H \in R^{6 \times 1}$ denotes the velocity of the end-effector. $\left[\mathbf{G}_\varphi^H \right]^{(i)} \in R^{6 \times 6}$ denotes the virtual first-order KIC matrix of limb i , $\left[\mathbf{G}_H^\varphi \right] = \left[\mathbf{G}_\varphi^H \right]^{-1}$.

The forward and inverse solutions for the velocity of virtual PM with respect to the generalized coordinates are

$$\mathbf{V}_H = \left[\mathbf{G}_q^H \right] \dot{\mathbf{q}} \quad (5.93)$$

$$\dot{\mathbf{q}} = \left[\mathbf{G}_q^H \right] \mathbf{V}_H \quad (5.94)$$

where $\left[\mathbf{G}_q^H \right] \in R^{6 \times 6}$ denotes the virtual first-order synthesis KIC matrix of the virtual PM with respect to the generalized coordinates $\left[\mathbf{G}_q^H \right] = \left[\mathbf{G}_q^H \right]^{-1}$.

The forward and inverse solutions for the acceleration of the i th limb are

$$\mathbf{A}_H = \left[\mathbf{G}_\varphi^H \right]^{(i)} \ddot{\boldsymbol{\phi}}^{(i)} + \dot{\boldsymbol{\phi}}^{(i)T} \left[\mathbf{H}_\varphi^H \right]^{(i)} \dot{\boldsymbol{\phi}}^{(i)} \quad (5.95)$$

$$\ddot{\boldsymbol{\phi}}^{(i)} = \left[\mathbf{G}_H^\phi \right]^{(i)} \mathbf{A}_H - \dot{\boldsymbol{\phi}}^{(i)T} \left[\mathbf{H}_H^\phi \right]^{(i)} \dot{\boldsymbol{\phi}}^{(i)} \quad (5.96)$$

where $\mathbf{A}_H \in R^{6 \times 1}$ denotes the acceleration of the end-effector. $\left[\mathbf{H}_\varphi^H \right]^{(i)} \in R^{6 \times 6 \times 6}$ denotes the virtual second-order KIC matrix of limb i . $\left[\mathbf{H}_H^\varphi \right] \in R^{6 \times 6 \times 6}$ is similar to $\left[\mathbf{H}_H^\varphi \right]$.

The forward and inverse solutions for the acceleration of virtual PM are

$$\mathbf{A}_H = \left[\mathbf{G}_q^H \right] \ddot{\mathbf{q}} + \dot{\mathbf{q}}^T \left[\mathbf{H}_q^H \right] \dot{\mathbf{q}} \quad (5.97)$$

$$\ddot{\mathbf{q}} = \left[\mathbf{G}_q^H \right] \mathbf{A}_H - \dot{\mathbf{q}}^T \left[\mathbf{H}_q^H \right] \dot{\mathbf{q}} \quad (5.98)$$

where $\left[\mathbf{H}_q^H \right]^{(i)} \in R^{6 \times 6 \times 6}$ denotes the virtual second-order synthesis KIC matrix of PM. $\left[\mathbf{H}_H^q \right] \in R^{6 \times 6 \times 6}$ is similar to $\left[\mathbf{H}_H^q \right]$.

If function $y = f(x)$ is correct, then its inverse function $x = f^{-1}(y)$ is also correct as long as the inverse function exists. Therefore, if Eq. (5.91) is correct and matrix

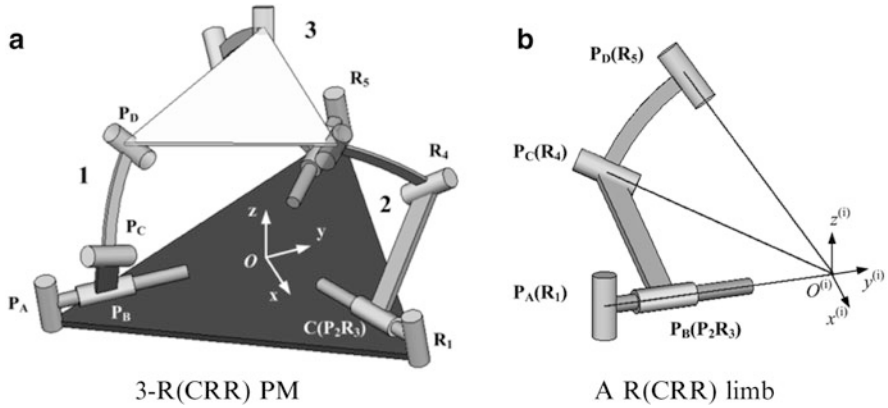


Fig. 5.6 A 3-R(CRR) PM (a) 3-R(CRR) PM (b) a R(CRR) limb

$[G_\varphi^H]$ is reversible, then Eq. (5.92) is undoubtedly correct. This rule also applies in Eqs. (5.93), (5.94), (5.95), (5.96), (5.97), and (5.98).

Example 5.1.

As shown in Fig. 5.6a, the 3-R(CRR) chain is a 5-DOF PM with three revolute and two translate freedoms. The base and moving platforms of the 3-R(CRR) mechanism are connected by three limbs, each with three revolute joints and one cylindrical pair. Both the upper and lower platforms are equilateral triangles. Each R(CRR) limb can be represented by five single-DOF pairs, as shown in Fig. 5.6b. The cylindrical pair can be replaced by one revolute joint and a coaxial prismatic pair. The first joints in the three limbs are perpendicular to the base platform. All other axes of the pairs intersect at one point called rotation center O .

As a lower-mobility PM, the Jacobian and Hessian matrices for the 3-R(CRR) are not square or cubic, which consequently adds obstacles in achieving the reverse kinematic modeling. To obtain the accurate solutions, VMP is adopted in the present example for forward/reverse velocity and acceleration analyses. According to the VMP, every limb of a 6-DOF virtual PM should be built by adding a prismatic pair or a revolute pair to the initial lower-mobility PM until every limb becomes a 6-DOF chain. For the 3-R(CRR), a virtual prismatic pair is added to every limb because every limb has only five single-DOF pairs. All three limbs in the mechanism have one common constrain that limits the translation along the z -axis. The axis directions of all the virtual prismatic pairs are the same and are all along the z -axis. Thus, a virtual 6-DOF 3- P_v R (CRR) PM (P_v denotes the virtual prismatic pair) is built, as shown in Fig. 5.7.

The KIC method (Sect. 5.3) for the 6-DOF PM can be adopted for the kinematic analyses. All the rates of the virtual pairs have to be zero to guarantee that the virtual PM is equivalent to the initial mechanism, 3-R(CRR), on the kinematics.

Let the side length of base platform $R_{bp} = 0.3$ m; the side length of moving platform $R_{mp} = 0.1$ m; both angle α_{23} and α_{34} are 47.2° ; the maximum translational distance for the cylindrical pair $L_{max} = 0.1$ m. At the initial configuration

Fig. 5.7 A virtual limb

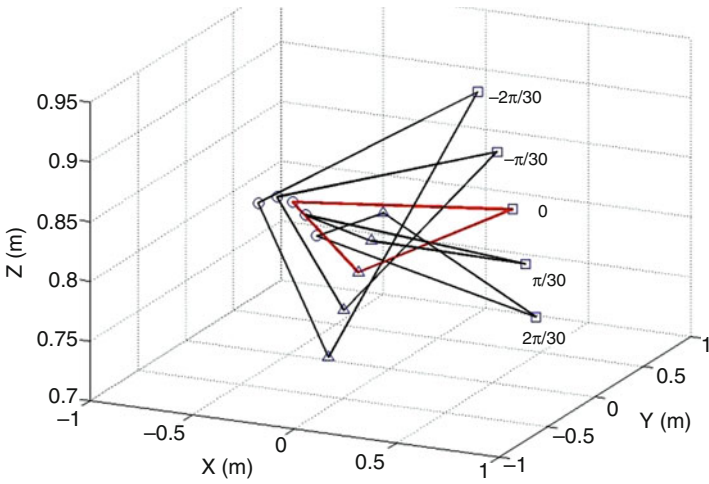
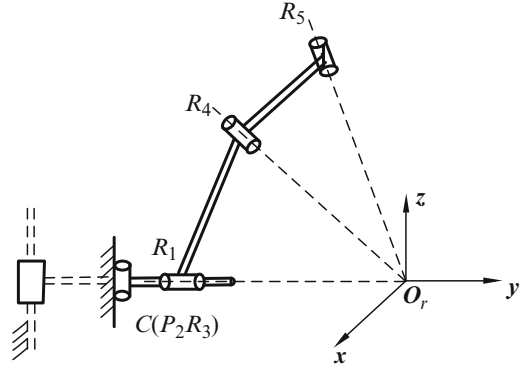


Fig. 5.8 Motion trajectory of the movable platform

(all five beginning real input angles are zero), the rotation center is coincident with the center of the base platform. We let the input angle in the first limb change from -15° to 15° with an angular velocity of 1 rad/s. The other four actuators are locked.

The generalized input velocities and accelerations of the virtual mechanism are assumed to be as follows:

$$\begin{aligned} \dot{q} &= [1 \ 0 \ 0; \ 0 \ 0 \ 0]^T \\ \ddot{q} &= [0 \ 0 \ 0; \ 0 \ 0 \ 0]^T \end{aligned} \tag{5.99}$$

Figure 5.8 shows the locus of the moving platform. The angles in Fig. 5.8 indicate the different input angles. Figures 5.9 and 5.10 show the kinematic curves, including the angular and linear velocities and accelerations, respectively. From Fig. 5.10, both the components of the velocity and acceleration vectors along the z -axis vanish, which also proves that the mechanism is a five-DOF PM.

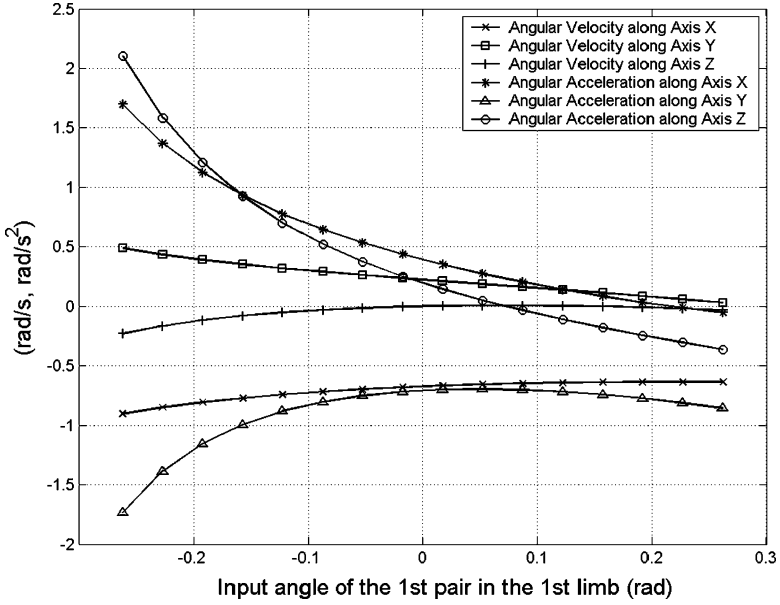


Fig. 5.9 Curves of angular kinematics

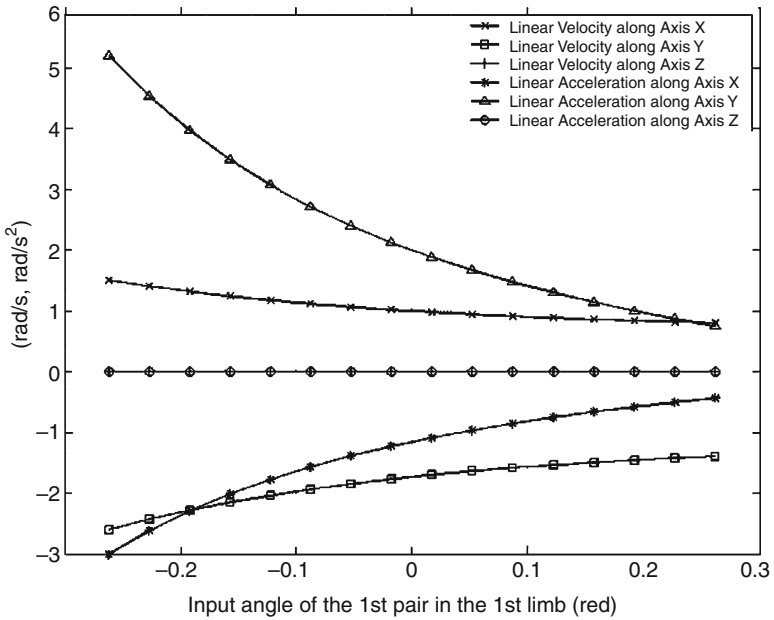


Fig. 5.10 Curves of linear kinematics

References

1. Benedict CE, Tesar D (1978) Model formulation of complex mechanisms with multiple input: Part 1, Geometry. *ASME J Mech Des* 100:747
2. Benedict CE, Tesar D (1978) Model formulation of complex mechanisms with multiple input: Part 2, The dynamic model. *ASME J Mech Des* 100:755
3. Freeman RA, Tesar D (1982) The generalized coordinate selection for the dynamics of complex planar mechanical system. *ASME J Mech Des* 104:206–217
4. Thomas M, Tesar D (1982) Dynamic modeling of serial manipulator arms. *ASME J Dyn Syst Meas Control* 104:218
5. Huang Z (1985) Modeling formulation of 6-DOF multi-loop parallel manipulators, Part-1, Kinematic influence coefficients. In: *Proceedings of the 4th IFToMM international symposium on linkage and computer aided design methods*, vol II-1. Bucharest, Romania, pp 155–162
6. Huang Z (1985) Modeling formulation of 6-DOF multi-loop parallel manipulators, Part-2, Dynamic modeling and example. In: *Proceedings of the 4th IFToMM international symposium on linkage and computer aided design methods*, vol II-1. Bucharest, Romania, pp 163–170
7. Hunt KH (1973) *Kinematic geometry of mechanisms*. Oxford University Press, Oxford
8. Mohamed MG, Sanger J, Duffy J (1983) Instantaneous kinematics of fully-parallel devices. Presented on sixth-IFToMM conference, New Delhi, India
9. Schilling RJ (1990) *Fundamentals of robotics: analysis and control*. Prentice-Hall, Englewood
10. Gregorio RD (2002) The 3-RRS wrist: a new, very simple and not overconstrained spherical parallel manipulator. In: *Proceedings of 2002 ASME design engineering technical conferences*, Montreal, Canada
11. Yan J, Huang Z (1985) Kinematical analysis of multi-loop spatial mechanism. In: *Proceedings of the 4th IFToMM international symposium on linkage and computer aided design methods*, vol II-2, Bucharest, Romania, pp 439–446
12. Huang Z, Wang HB (1992) Dynamic force analysis of n-DOF multi-loop complex spatial mechanisms. *Mech Mach Theory* 27(1):97–105
13. Huang Z, Zhao YS (1994) The accordance and optimization-distribution equations of the over-determinate inputs of walking machines. *Mech Mach Theory* 29(2):327–332
14. Wang HB, Ishimatus T, Schaerer C, Huang Z (1998) Kinematics of a five-degrees-of-freedom prosthetic arm. *Mech Mach Theory* 33(7):895–908
15. Huang Z, Wang J (2001) Identification of principal screws of 3-DOF parallel manipulators by quadric degeneration. *Mech Mach Theory* 36(8):893–911
16. Huang Z, Wang J (2002) Analysis of instantaneous motions of deficient-rank 3-RPS parallel manipulators. *Mech Mach Theory* 37(2):229–240
17. Huang Z, Li SH, Zuo RG (2004) Feasible instantaneous motions and kinematic characteristics of a special 3-DOF 3-UPU parallel manipulator. *Mech Mach Theory* 39(9):957–970
18. Zhu S, Huang Z, Ding H (2007) Forward/reverse velocity and acceleration analysis for a class of lower-mobility parallel mechanisms. *Trans ASME J Mech Des* 129(4):390–396
19. Huang Z, Zhu SJ (2005) Kinematic analyses of 5-DOF 3-RCRR parallel mechanism. *ASME DETC2005-84462*

Chapter 6

Full-Scale Feasible Instantaneous Screw Motion

This chapter presents a study on the full-scale instant twist motions of parallel manipulators. The study aims to understand and correctly apply a mechanism and is based on the principal screws of the screw system. The key problem is to derive three principal screws from a given 3-DOF mechanism, and then set the relation between the pitches of the principal screws and the three linear inputs of the mechanism.

In this chapter, the effective method to identify the principal screws of a third-order screw system of 3-DOF mechanisms is presented. For obtaining the principal screws, we introduce the quadratic curve degenerating theory and quadric degenerating theory. In addition, the virtual-mechanism influence coefficient principle is also used.

In the following sections three mechanisms are discussed using the principle. This Chapter presents an analysis of the full-scale screws, the planar representations of pitches, and the spatial distributions of the axes. Based on this theory a novel and interesting 3-DOF rotational parallel mechanism without intersecting axes is synthesized.

6.1 Introduction

With the development of parallel robots, various lower-mobility parallel mechanisms are proposed. Among these, the 3-DOF parallel mechanisms have gained increasing interest from researchers in recent years.

An often primary and basic step towards understanding a mechanism is to find all the feasible instantaneous motions or twists that can be produced in any specified moment for a mechanism. In other words, there is a need to determine both the range of the twist pitches and the distribution of the twist axes in space for the output link of a manipulator. It is important to correctly use a robot manipulator and plan its trajectory. For a specified moment or in a configuration, the total variable range of the moving-screw pitches and the spatial distribution of the moving-screw axes of the selected link are named as *full-scale feasible instantaneous screws* in the current Chapter.

In robotics application, the end-effector of a six-DOF manipulator has infinite moving possibility and can realize any given twist motion in 3D space. A lower-mobility manipulator also has infinite moving possibility; however, it is clear that some motions are impossible to realize. Finding all the feasible instantaneous motions of a lower-mobility serial robot is easier than that of the 6-DOF one. The possible twists of a lower-mobility serial robot are obtained only by linear combination of its joint screws. Nevertheless, it is extraordinary difficult for lower-mobility parallel mechanism. We use screw theory to solve the problem.

One hundred years ago, Ball published his classical work [1], and Hunt further developed the screw systems [2]. The screw systems were basically distinguished as general and special cases according to the pitches of their principal screws. Gibson and Hunt classified the first-order, second-order and third-order screw systems further by means of projective geometry and gave the planar representation of the general three-system [3]. Any screw motion of a 3-DOF rigid body can be expressed by a linear combination of its three principal screws in the three-system. The axes of all the screws of a screw system in 3D space have regular spatial distribution. For example, all the screws of the second-order screw system lie on a cylindroid. For a third-order screw system or three-system, all screws with the same pitches may lie on a hyperboloid of one sheet. The cylindroid or hyperboloid then depicts the distributions of the positions and orientations of all screw axes of that screw system.

The key to determine both the range of the twist pitches and the distribution of the twist axes in 3D space is to get the principal screws of the screw system. The principal screw is a very important concept in screw theory. Once the principal screws are obtained, it is easy to know all possible motions of the mechanisms at any given instant. There are two and three principal screws in second-order and third-order screw systems, respectively. Of the two, the latter is the more important and complicated one.

The twist screw system of a 3-DOF parallel mechanism belongs to a third-order screw system. To study the mechanism, we should determine its 3 principal screws. Parkin specified the principal screws of the three-system from three given screws by adopting the mutual moment operation [4]. Tsai and Lee studied the principal screws from three known screws using the eigenvector [5]. Zhang and Xu constructed the principal screws from three known screws using the algebraic method [6]. All the above principal screws have been obtained using three known screws. From another point of view, we put forward a directly analytical method for identifying the principal screws of a 3-DOF parallel mechanism in the current work. Fang and Huang first established the important relationship between the principal screws and Jacobian matrix of the mechanism [7]; they then identified the principal screws of the third-order screw system using the quadratic equation degenerating theory. Two equations are then obtained based on the relationship between the pitch/axis and the Jacobian matrix of the mechanism, after which another simpler and more effective principle [8], the quadric degenerating theory, was further proposed for identifying the principal screws.

For applying the principle to lower-mobility parallel mechanisms, corresponding two Jacobian matrices must be established first. This can be realized with the

virtual-mechanism method proposed by Yan and Huang [9] and later developed by Huang and Wang [10].

In this Chapter, three typical examples are discussed: a 3-DOF 3-RPS parallel manipulator [11], a special 3-UPU parallel mechanism [12], and the pyramid 3-RPS mechanism [8]. Based on the analysis, some interesting and exceptional characteristics of these mechanisms are illustrated [13]. All above analysis is important in enriching the mechanism theory and it can benefit future mechanical designs for similar mechanical systems. Based on this theory, a novel 3-DOF rotational parallel mechanism without intersecting axes [14] is analyzed.

6.2 Determination of Principal Screws

In order to determine the full-scale instantaneous screws including the pitches and axes, there is a need to obtain the principal screws first. The principal screw principle can be used to study the feasible instant motion. Its important merit is that it can illustrate a full-scale feasible instantaneous motion of the mechanism at any given configuration.

6.2.1 The Representation of Pitch and Axes

In screw theory [1, 2], a straight line in 3D space can be expressed by two vectors, namely, \mathbf{S} and \mathbf{S}_0 . Their dual combination is called a line vector, $(\mathbf{S}, \mathbf{S}_0)$, $\mathbf{S} \cdot \mathbf{S}_0 = 0$. When $\mathbf{S}_0 = \mathbf{0}$, the line vector, $(\mathbf{S}; 0)$, passes through the origin point. When $\mathbf{S} \cdot \mathbf{S}_0 \neq 0$, it is defined as a screw. The pitch of the screw is given by:

$$h = \mathbf{S} \cdot \mathbf{S}_0 / \mathbf{S} \cdot \mathbf{S}. \quad (6.1)$$

If the pitch of a screw is equal to zero, the screw degenerates into a line vector, which can be used to express a revolute pair in kinematics or a unit force along the line in statics. If the pitch of a screw goes to infinity, $h = \infty$, the screw is expressed as $(\mathbf{0}; \mathbf{S})$ and is called a couple in screw theory. The couple can be used to express a prismatic pair or translation motion in kinematics or a couple in statics.

The twist motion of a robot end-effector can be described by a screw. The linear velocity \mathbf{v}_p of a selected reference point P on the end-effector and the angular velocity $\boldsymbol{\omega}$ of the end-effector are given according to the task requirements. Therefore, the moving screw of the end-effector can be expressed by the given \mathbf{v}_p and $\boldsymbol{\omega}$ as follows:

$$\mathcal{S}_i = (\boldsymbol{\omega}; \mathbf{v}^o) = (\boldsymbol{\omega}; \mathbf{v}_p + \mathbf{r}_p \times \boldsymbol{\omega}),$$

where \mathbf{v}^o is the velocity of the point coincident with the original point in the body; \mathbf{r}_P is a positional vector indicating the reference point on the end-effector. When the original point of the coordinate system is coincident with point P , the pitch and axis can be respectively determined by the following equations:

$$h = \frac{\boldsymbol{\omega} \cdot \mathbf{v}_P}{\boldsymbol{\omega} \cdot \boldsymbol{\omega}}, \quad (6.2)$$

$$\mathbf{r} \times \boldsymbol{\omega} = \mathbf{v}_P - h\boldsymbol{\omega}. \quad (6.3)$$

If a mechanism has three DOFs, the order of the screw system is three. The motion of the three-order mechanism can be determined by three independent generalized coordinates: $\dot{\mathbf{q}} = \{\dot{q}_1 \quad \dot{q}_2 \quad \dot{q}_3\}^T$. These independent generalized coordinates are often selected as three input-joint rates. The \mathbf{v}_P and $\boldsymbol{\omega}$ of a robot can then be determined by the following three input joint rates:

$$\begin{aligned} \mathbf{v}_P &= [\mathbf{G}]\dot{\mathbf{q}}, & \dot{\mathbf{q}} &= \{\dot{q}_1 \quad \dot{q}_2 \quad \dot{q}_3\}^T, \\ \boldsymbol{\omega} &= [\mathbf{G}']\dot{\mathbf{q}}, \end{aligned} \quad (6.4)$$

where $[\mathbf{G}]$ and $[\mathbf{G}']$ are 3×3 first-order influence coefficient matrices [15, 16]. Substituting Eq. (6.4) into Eqs. (6.2) and (6.3), the screw can also be described as the function of the joint rates [7] (Fang and Huang 1998):

$$h = \frac{\dot{\mathbf{q}}^T [\mathbf{G}']^T [\mathbf{G}] \dot{\mathbf{q}}}{\dot{\mathbf{q}}^T [\mathbf{G}']^T [\mathbf{G}'] \dot{\mathbf{q}}}, \quad (6.5)$$

$$[\mathbf{r}][\mathbf{G}']\dot{\mathbf{q}} = ([\mathbf{G}] - h[\mathbf{G}'])\dot{\mathbf{q}}, \quad (6.6)$$

where $[\mathbf{r}]$ is a skew-symmetrical matrix of vector $\mathbf{r} = (x \quad y \quad z)^T$. Suppose we give the following expressions:

$$u = \dot{q}_1/\dot{q}_3; \quad w = \dot{q}_2/\dot{q}_3, \quad (6.7)$$

and then $\dot{\mathbf{q}} = (u \quad w \quad 1)\dot{q}_3$. In this case, the pitch and the axis equations are given by:

$$h = \frac{\{\mathbf{u} \quad \mathbf{w} \quad 1\}[\mathbf{G}']^T [\mathbf{G}] \{\mathbf{u} \quad \mathbf{w} \quad 1\}^T}{\{\mathbf{u} \quad \mathbf{w} \quad 1\}[\mathbf{G}']^T [\mathbf{G}'] \{\mathbf{u} \quad \mathbf{w} \quad 1\}^T}, \quad (6.8)$$

$$[\mathbf{r}][\mathbf{G}']^T \{\mathbf{u} \quad \mathbf{w} \quad 1\}^T = ([\mathbf{G}] + [\mathbf{r}_P][\mathbf{G}'] - h[\mathbf{G}']) \{\mathbf{u} \quad \mathbf{w} \quad 1\}^T, \quad (6.9)$$

where $[\mathbf{r}_P]$ is also a skew-symmetrical matrix of coordinate of the point P .

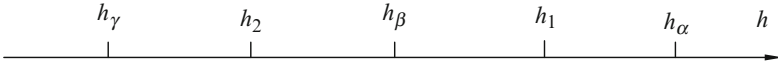


Fig. 6.1 Three principal screws

6.2.2 Principal Screws of a Third-Order Screw System

A third-order screw system has three principal screws. Generally, the three principal screws are mutually perpendicular and intersecting at a common point. Any screw in the system is the linear combination of the three principal screws. In the third-order screw system, two pitches of three principal screws are extremum, and the pitches of all other screws lie between the maximum and minimum pitches.

Therefore, obtaining the three principal screws is the key step in analyzing the full-scale instantaneous motion of any 3-DOF mechanism. Two principles, the quadratic curve degenerating theory and the quadric degenerating theory, are followed.

6.2.2.1 Quadratic Curve Degenerating Theory

Let h_x, h_β , and h_γ be the pitches of the three principal screws, respectively, and suppose $h_\gamma < h < h_x$, Fig. 6.1. Ball [1] illustrates the full-scale plane representation of a third-order system with quadratic curves [1]; it indicates that the points in each quadratic curve has identical pitch. If the pitch of any screw in the system is equal to h_x, h_β or h_γ , the quadratic equation is degenerated. When $h = h_x$ or $h = h_\gamma$, the quadratic equation degenerates into two virtual straight lines intersecting at a real point; when $h = h_\beta$, the quadratic equation degenerates into two real straight lines [3].

Expanding Eq. (6.8), we have:

$$a_{11}u^2 + 2a_{12}uw + a_{22}w^2 + 2a_{13}u + 2a_{23}w + a_{33} = 0, \quad (6.10)$$

where the coefficient a_{ij} , ($i, j = 1 \sim 3$), is a function of pitch h and the elements in matrices $[\mathbf{G}]$ and $[\mathbf{G}']$. From the quadratic equation degenerate principle, the determinant of the coefficient matrix should be zero, that is:

$$D = \begin{vmatrix} a_{11} & a_{12} & a_{13} \\ a_{21} & a_{22} & a_{23} \\ a_{31} & a_{32} & a_{33} \end{vmatrix} = 0, \quad (a_{ij} = a_{ji}). \quad (6.11)$$

Expanding Eq. (6.11), we have:

$$c_1h^3 + c_2h^2 + c_3h + c_4 = 0, \quad (6.12)$$

where c_i , ($i = 1 \sim 4$), is a function of the elements of $[\mathbf{G}]$ and $[\mathbf{G}']$. The three roots of Eq. (6.12) are the pitches, h_x, h_β and h_γ , of the three principal screws.

Substituting the pitch of the principal screw into Eq. (6.10), the above quadratic equation can be degenerated into two straight line equations, and the root, $(u_i \ w_i)$, of the two equations becomes:

$$\begin{aligned} u_i &= \frac{a_{22}a_{13} - a_{12}a_{23}}{a_{12}^2 - a_{11}a_{22}}, \\ w_i &= -\frac{a_{23}}{a_{22}} - \frac{a_{12}}{a_{22}}u_i, \end{aligned} \quad i = 1, 2, 3. \quad (6.13)$$

Each set of $(u_i \ w_i)$ corresponds to three inputs $(u_i \ w_i \ 1)$, and three sets of $(u_i \ w_i)$, $i = \alpha, \beta, \gamma$, correspond to three output twists, i.e., three principal screws with pitches, h_α, h_β and h_γ .

When the pitches of three principal screws are obtained, the axis equations of three principal screws can also be obtained when the three values are substituted into Eq. (6.9).

6.2.2.2 Quadric Degenerating Theory

The quadric degenerating theory is an easier method in calculating the principal screws. Equation (6.6) can be further simplified as:

$$[A] \dot{\mathbf{q}} = 0, \quad (6.14)$$

where

$$[A] = [\mathbf{r}][\mathbf{G}'] - [\mathbf{G}] + h[\mathbf{G}']$$

is a 3×3 matrix. Both $[\mathbf{G}]$ and $[\mathbf{G}']$ are 3×3 first-order kinematic influence coefficient matrices that are functions of the structure parameters of the mechanism. Since not all the components of vector $\dot{\mathbf{q}}$ are zeros in general, the necessary and sufficient condition that ensures the solutions of Eq. (6.14) are non-zero is that the determinant of the matrix $[A]$ must be equal to zero [8], that is:

$$\text{Det}[A] = 0. \quad (6.15)$$

Expanding Eq. (6.15), we obtain the position equation describing all the screw axes as follows:

$$\begin{aligned} c_{11}x^2 + c_{22}y^2 + c_{33}z^2 + 2c_{12}xy + 2c_{23}yz + 2c_{13}xz + 2c_{14}x + 2c_{24}y \\ + 2c_{34}z + c_{44} = 0. \end{aligned} \quad (6.16)$$

In the equation above, the following coefficients:

$$c_{ij}(i = 1, 2, 3, 4, j = 1, 2, 3, 4)$$

are the functions of pitch h as well as coefficients g_{ij}, b_{ij} . The latter are relative with the elements of the matrices $[\mathbf{G}]$ and $[\mathbf{G}']$ given in Appendix A in [8]. Equation (6.16) is a quadratic equation with three variables, namely, x, y and z , and it expresses a quadratic surface in space. The spatial distribution of all the screw axes in 3-D is quite complex, generally, all the screw axes lie on a hyperboloid of one sheet if every coefficient in Eq. (6.16) contains the same pitch h .

1. Pitches of the Three Principal Screws

For a third-order screw system, three principal screws (α, β and γ) exist. Let h_α, h_β , and h_γ be the pitches of three principal screws respectively, and suppose that $h_\alpha > h_\beta > h_\gamma$. We know that, when $h = h_\alpha$ or $h = h_\gamma$, respectively, the quadric surface, Eq. (6.16), degenerates into a straight line where the principal screws α or γ lies. When $h = h_\beta$, the quadric surface degenerates into two intersecting planes, and the intersecting line is just the axis of the principal screw β [2]. According to this nature, we can identify the three principal screws of the three-system.

The quadric has four invariants, I, J, D and Δ , and they are given as follows:

$$I = c_{11} + c_{22} + c_{33},$$

$$\Delta = \begin{vmatrix} c_{11} & c_{12} & c_{13} & c_{14} \\ c_{21} & c_{22} & c_{23} & c_{24} \\ c_{31} & c_{32} & c_{33} & c_{34} \\ c_{41} & c_{42} & c_{43} & c_{44} \end{vmatrix}; \quad D = \begin{vmatrix} c_{11} & c_{12} & c_{13} \\ c_{21} & c_{22} & c_{23} \\ c_{31} & c_{32} & c_{33} \end{vmatrix} \quad (6.17)$$

$$J = c_{11}c_{22} + c_{22}c_{33} + c_{11}c_{33} - c_{12}^2 - c_{23}^2 - c_{13}^2 \quad (c_{ij} = c_{ji}).$$

Expanding D , and assuming that it is equal to zero, $D = 0$, we have the expression:

$$a_1 h^3 + a_2 h^2 + a_3 h + a_4 = 0, \quad (6.18)$$

where the coefficients a_i ($i = 1, \dots, 4$) are also the functions of g_{ij} and b_{ij} and h . Three possible roots can be obtained by solving Eq. (6.18), and these three roots correspond to the pitches of the three principal screws h_α, h_β , and h_γ . When the pitch in the system is equal to one of the three principal screw pitches, the invariant Δ is zero as well. This satisfies the condition that the quadric degenerates into a line or two intersecting planes. Therefore, the key to identify the principal screws in the third-order system is that the quadric, Eq. (6.16), degenerates into a line or a pair of intersecting planes.

2. The axes of the Principal Screws and Principal Coordinate System

The coordinate system consisting of three principal screws is named the principal coordinate system. We know that the most concise equation of a hyperboloid is under its principal coordinate system. Thus, we look for the principal coordinate system of the hyperboloid.

Equation (6.16), which is represented in the base coordinate system, can be transformed into the normal form of the hyperboloid of one sheet in the principal

coordinate system. As soon as the pitches of the three principal screws are obtained, the pitch of any screw in the system falls within the range of $h_\gamma < h < h_\alpha$. The general three-system [2] appears only when three pitches of the three principal screws all are finite and satisfy $h_\gamma \neq h_\beta \neq h_\alpha$. The axes of all the screws with the same pitch ranging from h_γ to h_β or from h_β to h_α form a hyperboloid of one sheet. In this case the invariant D is not equal to zero, and the quadrics are the concentric hyperboloids. By solving Eq. (6.19):

$$\begin{cases} c_{11}x + c_{12}y + c_{13}z + c_{14} = 0 \\ c_{21}x + c_{22}y + c_{23}z + c_{24} = 0, \\ c_{31}x + c_{32}y + c_{33}z + c_{34} = 0 \end{cases} \quad (6.19)$$

the root of Eq. (6.19) is just the center point $o' (x_0 \ y_0 \ z_0)$ of the hyperboloid. It is clear that the point o' is also the origin of the principal coordinate system. The coordinate translation is given by:

$$\begin{cases} x = x' + x_0 \\ y = y' + y_0. \\ z = z' + z_0 \end{cases} \quad (6.20)$$

The eigenequation of the quadric is:

$$k^3 - Ik^2 + Jk - D = 0. \quad (6.21)$$

Its three real roots (k_1, k_2 , and k_3) are the three eigenvalues, and not all the roots are zeros. In general, $k_1 \neq k_2 \neq k_3$. The corresponding three unit eigenvectors, $(\lambda_1 \ \mu_1 \ v_1)$, $(\lambda_2 \ \mu_2 \ v_2)$ and $(\lambda_3 \ \mu_3 \ v_3)$, are perpendicular to each other, and correspond to three principal screws, α β and γ , respectively, thus forming the coordinate system $(o'-x'y'z')$. The principal coordinate system $(o'-\alpha\beta\lambda)$ can then be constructed by the following coordinate rotation:

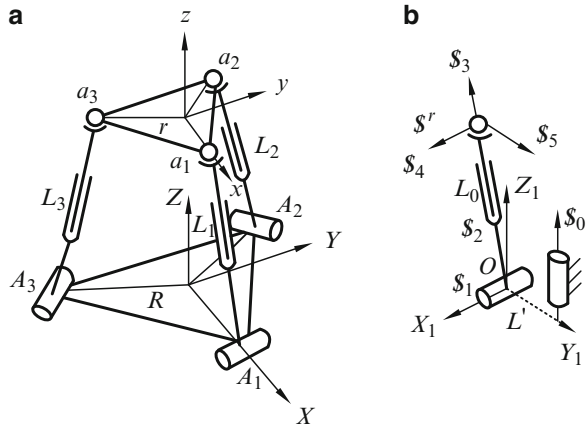
$$\begin{cases} x = \lambda_1x' + \lambda_2y' + \lambda_3z' \\ y = \mu_1x' + \mu_2y' + \mu_3z', \\ z = v_1x' + v_2y' + v_3z' \end{cases} \quad (6.22)$$

After the coordinate transformation, the normal form of the hyperboloid becomes:

$$k_1x^2 + k_2y^2 + k_3z^2 + \frac{\Delta}{D} = 0. \quad (6.23)$$

Hunt [2] stated that when h lay within the range $h_\beta < h < h_\alpha$, the central symmetrical axis of the hyperboloid is α , and the semi-major axis of its central elliptical section in the $\beta\gamma$ -plane always lies along β . For $h_\gamma < h < h_\beta$, the central symmetrical axis of the hyperboloid is γ , and the semi-major axis of its central elliptical section in the $\beta\gamma$ -plane is also along β . Therefore, we can determine easily the three axes of the principal coordinate system [2].

Fig. 6.2 3-DOF 3-RPS parallel mechanism
 (a) Mechanism sketch
 (b) Virtual branch



6.3 Full-Scale Feasible Instantaneous Screws of the 3-RPS Mechanism

Now let us discuss the full-scale feasible instantaneous screws of the 3-RPS mechanism [11] shown in Fig. 6.2. In order to determine the full-scale feasible instantaneous screws of the 3-RPS mechanism, there is a need to determine three principal screws by applying Eqs. (6.8) and (6.9); this depends on the elements of the matrices $[G]$ and $[G']$. The latter are explained in Sect. 5.4. To determine the $[G]$ and $[G']$, the virtual mechanism and the virtual Jacobian of the 3-RPS must first be established.

6.3.1 Virtual Mechanism and Jacobian Matrix

To determine the pitches and axes according to Eqs. (6.8) and (6.9), the key problem is to determine 3×3 Jacobian matrices $[G]$ and $[G']$. However, it is difficult for a 3-DOF parallel mechanism to determine $[G]$ and $[G']$. In the current work, the virtual-mechanism principle (as shown in Sect. 5.4 and in [10, 16]) will be used. However, the virtual-mechanism principle with unified formulas is a general method, which can be applied to analyze any lower-mobility mechanism. This example is also taken to introduce the process of setting the matrices $[G]$ and $[G']$.

Figure 6.2a shows a 3-DOF 3-RPS mechanism [17] consisting of an upper platform, a base platform, and three kinematic branches; each of its three branches is comprised of a revolute joint R , a prismatic pair P , and a spherical pair S , which is a RPS serial chain. The axes of the revolute joints in the base are tangential to the circumference of the lower triangle. The mechanism has three linear inputs $(\dot{L}_1, \dot{L}_2, \dot{L}_3)$.

Each kinematic branch of the 3-RPS mechanism can be represented by five single-DOF kinematic pairs. In order to obtain the Jacobian matrix, we should first transform this 3-DOF mechanism into a virtual 6-DOF one. A virtual link and a virtual revolute pair, $\$0$, with single-DOF are then added to each branch of the mechanism.

Each branch becomes a virtual 6-DOF serial chain. In order to keep a kinematic equivalent effect, we allow the amplitude ω_0 of the virtual screw \mathcal{S}_0 of each branch to remain at zero, moreover, each screw system formed by virtual, and the other five screws of the primary branch must be linearly independent.

Considering the virtual pair \mathcal{S}_0 , the Plücker coordinates of all six screws shown in Fig. 6.2b, with respect to local $o-X_1Y_1Z_1$ coordinate system are given as follows:

$$\begin{aligned}
 \mathcal{S}_1 &= (1 \quad 0 \quad 0; \quad 0 \quad 0 \quad 0) \\
 \mathcal{S}_2 &= (0 \quad 0 \quad 0; \quad 0 \quad \psi \quad \varsigma) \\
 \mathcal{S}_3 &= (0 \quad \psi \quad \varsigma; \quad 0 \quad 0 \quad 0) \\
 \mathcal{S}_4 &= (1 \quad 0 \quad 0; \quad 0 \quad L_0\varsigma \quad -L_0\psi), \\
 \mathcal{S}_5 &= (0 \quad \varsigma \quad -\psi; \quad -L_0 \quad 0 \quad 0) \\
 \mathcal{S}_6 &= (0 \quad 0 \quad 1; \quad L' \quad 0 \quad 0)
 \end{aligned} \tag{6.24}$$

where elements ψ and ζ are the cosines of the screw axes \mathcal{S}_2 and \mathcal{S}_3 . The screw matrix of each branch with respect to the local coordinate system is:

$$[\mathbf{G}\mathbf{g}] = [\mathcal{S}_0, \mathcal{S}_1, \mathcal{S}_2, \mathcal{S}_3, \mathcal{S}_4, \mathcal{S}_5].$$

After coordinate transformation, we have:

$$[\mathbf{G}_i^0] = [\mathbf{A}_i^0][\mathbf{G}\mathbf{g}].$$

For each serial branch, the motion of the end-effector of the 3-RPS mechanism can be represented by the following expression:

$$\mathbf{V}_H = [\mathbf{G}_i^0] \dot{\boldsymbol{\phi}}^{(i)} \quad i = 1, 2, 3, \tag{6.25}$$

where $\mathbf{V}_H = \{\omega \mathbf{v}_P\}^T$ is a six-dimension vector, $\boldsymbol{\omega}$ is the angular velocity of the moving platform, \mathbf{v}_P is the linear velocity of the reference point \mathbf{P} in the moving platform; and

$$\dot{\boldsymbol{\phi}}^{(i)} = \begin{pmatrix} \dot{\phi}_0^{(i)} & \dot{\phi}_1^{(i)} & \dot{\phi}_2^{(i)} & \dot{\phi}_3^{(i)} & \dot{\phi}_4^{(i)} & \dot{\phi}_5^{(i)} \end{pmatrix}$$

is a vector of joint rates. If $[\mathbf{G}_i^0]$ is non-singular, then:

$$\dot{\boldsymbol{\phi}}^{(i)} = [\mathbf{G}_0^i] \mathbf{V}_H \quad i = 1, 2, 3, \tag{6.26}$$

where $[\mathbf{G}_0^i] = [\mathbf{G}_i^0]^{-1}$.

The input rates $(\dot{L}_1, \dot{L}_2, \dot{L}_3)$ of the mechanism are known, and the rate of each virtual link is zero, which is also known. Then for each branch we have:

$$\begin{aligned}
 \dot{\boldsymbol{\phi}}^{(i)} &= (\dot{\phi}_0 \quad \dot{\phi}_1 \quad \dot{\phi}_2 \quad \dot{\phi}_3 \quad \dot{\phi}_4 \quad \dot{\phi}_5)^{(i)} = (0 \quad \dot{\phi}_1 \quad \dot{L}_1 \quad \dot{\phi}_3 \quad \dot{\phi}_4 \quad \dot{\phi}_5)^{(i)} \\
 &i = 1, 2, 3.
 \end{aligned}$$

Taking the first and third rows from the matrix $[\mathbf{G}_0^i]$ in Eq. (6.26) of each branch, there are now six linear equations. A new matrix equation can then be established as follows:

$$\dot{\mathbf{q}} = [\mathbf{G}_H^q] \mathbf{V}_H \quad \dot{\mathbf{q}} = \{\dot{L}_1 \quad \dot{L}_2 \quad \dot{L}_3 \quad 0 \quad 0 \quad 0\}, \quad (6.27)$$

where

$$[\mathbf{G}_H^q] = \left[[\mathbf{G}_0^1]_{3:} \quad [\mathbf{G}_0^2]_{3:} \quad [\mathbf{G}_0^3]_{3:} \quad [\mathbf{G}_0^1]_{1:} \quad [\mathbf{G}_0^2]_{1:} \quad [\mathbf{G}_0^3]_{1:} \right]^T \in \mathbf{R}^{6 \times 6},$$

in which $[\mathbf{G}_0^i]_{i:}$ represents the i th row of matrix $[\mathbf{G}_0^i]$. If the matrix $[\mathbf{G}_H^q]$ is non-singular, then from Eq. (6.27), we have:

$$\mathbf{V}_H = [\mathbf{G}_q^H] \dot{\mathbf{q}}, \quad (6.28)$$

where $[\mathbf{G}_q^H] = [\mathbf{G}_H^q]^{-1}$.

Since the 3-RPS mechanism has three freedoms, it only needs three inputs. The matrix $[\mathbf{G}_L^H]$, formed by taking the first three columns of the matrix $[\mathbf{G}_q^H]$, is a 6×3 Jacobian matrix. Therefore, the corresponding relation between the inputs and the outputs is:

$$\mathbf{V}_H = [\mathbf{G}_L^H] \dot{\mathbf{L}}. \quad (6.29)$$

As $\mathbf{V}_H = \{\omega \quad \mathbf{v}_p\}^T$, Eq. (6.29) can be separated into two equations, namely:

$$\mathbf{v}_p = [\mathbf{G}] \dot{\mathbf{L}}, \quad (6.30)$$

$$\omega = [\mathbf{G}'] \dot{\mathbf{L}}, \quad (6.31)$$

where $[\mathbf{G}']$ represents the first three rows of $[\mathbf{G}_L^H]$, and $[\mathbf{G}]$ represents the last three rows of $[\mathbf{G}_L^H]$. Then, we obtain the 3×3 matrices $[\mathbf{G}]$ and $[\mathbf{G}']$. From the analysis process, we know that the matrices $[\mathbf{G}]$ and $[\mathbf{G}']$ are not dependent on the chosen virtual pairs.

6.3.2 Upper Platform Is Parallel to the Base

Here, we continue to study the 3-RPS mechanism shown in Fig. 6.2, in order to get the full-scale feasible instantaneous motion. The parameters of the mechanism are as follows: $R = 0.05$ m, $r = 0.05$ m, $L_0 = 0.2$ m, and $L' = 0.04$ m. The following

configurations are also discussed in this section. Substituting the given geometrical parameters and expanding Eq. (6.8), we have Eq. (6.10):

$$a_{11}u^2 + 2a_{12}uw + a_{22}w^2 + 2a_{13}u + 2a_{23}w + a_{33} = 0, \quad (6.32)$$

where the coefficient a_{ij} is a function of the geometrical parameters of the mechanism as well as the pitch of twist screw of the moving platform. Equation (6.32) is a quadratic equation with two variables, u and w , and degenerates if Eq. (6.11) is satisfied. Expanding Eq. (6.11), we have Eq. (6.12), which is given by:

$$ah^3 + bh^2 + ch + d = 0. \quad (6.33)$$

The three roots of Eq. (6.33) are just the respective pitches of the three principal screws. Substituting each root h into Eq. (6.32), the quadratic equation degenerates into two linear equations expressing two straight lines, respectively. The intersecting point (u, w) of the two lines can be obtained, after which the axis of the principal screw can also be obtained by substituting point (u, w) into Eq. (6.9).

When the moving platform is parallel to the fixed one, it follows that $a = b = c = d = 0$, i.e., all the coefficients of Eq. (6.33) are zeros. The three roots, h , can be any constant. For some reasons presented below, however, the three roots denoting three principal screw pitches of Eq. (6.33) should be:

$$(\infty \ 0 \ 0). \quad (6.34)$$

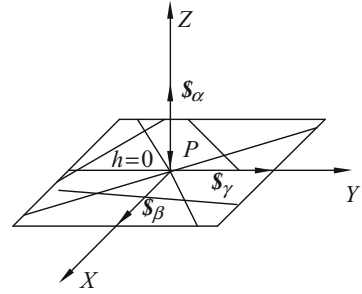
When $h \rightarrow \infty$, we have $u = 1$ and $w = 1$, and the inputs are $\dot{\mathbf{L}} = \{u \ w \ 1\} = \{1 \ 1 \ 1\}$. The output motion is a pure translation given by: $\$_{Z1} = \{0 \ 0 \ 0; \ 0 \ 0 \ 1\}$. When the pitch of the principal screw is zero, $h = 0$, $u = 0/0$, and $w = 0/0$. Mathematically, u and w can both be any value except one. All other roots of Eq. (6.33) are not considered because they are algebraically redundant. Then, the corresponding three principal screws can be written as:

$$\begin{aligned} \$_{z1} &= (0 \ 0 \ 0; \ 0 \ 0 \ 1) \\ \$_{z2} &= (0 \ 1 \ 0; \ -P_x \ 0 \ 0). \\ \$_{z3} &= (1 \ 0 \ 0; \ 0 \ P_z \ 0) \end{aligned} \quad (6.35)$$

Any output motion may be considered as a linear combination of the three principal screws. The full-scale distribution result (Fig. 6.3) of all screws obtained by linear combinations of the three principal screws can also be verified using another method presented in [18]. This is also identical to the actual mechanism model in our laboratory. The three principal screws belong to a fourth special three-system reported by Hunt [2].

When the upper platform is parallel to the fixed platform, all possible output twists of the upper platform, except the translation along the Z direction, are considered rotations corresponding to screws with zero pitch. Their axes all lie in the moving platform and in all the directions. Figure 6.3 shows the full-scale possible twist

Fig. 6.3 Screw distribution in initial configuration



screws with zero pitch. Therefore, from this figure, we did not attempt to make the moving platform rotate about any axis that is not on the plane shown in Fig. 6.3. This is impossible.

6.3.3 The Upper Platform Rotates by an Angle α About Line $\alpha_2\alpha_3$

When the upper platform continually rotates about line a_2a_3 by an angle α , this means that the mechanism is in the configuration that the lengths of the two input links are the same. Note that for this kind of mechanism, the platform cannot continually rotate about the axes lying in the plane shown in Fig. 6.3, except some three axes including a_2a_3 . In other words, it is very often impossible that the platform can continually rotate around an axis lying in the plane, as shown in Fig. 6.3 [19].

The coordinates of point a_1 on the upper platform and point A_1 on the base have the following values:

$$a_1 = \{r(3 \cos \alpha - 1)/2 \quad 0 \quad L_0 + 3r \sin \alpha/2\}, \quad A_1 = \{R \quad 0 \quad 0\}. \quad (6.36)$$

In this configuration, the screw system, including the virtual pair of the first limb corresponding to $[G_1^0]$ with respect to the fixed coordinate system, is given by the following:

$$\begin{aligned} \mathcal{S}_1 &= \{\mathcal{S}_1; \mathcal{S}_{01}\} = \{\mathcal{S}_1; \mathbf{A}_1 \times \mathcal{S}_1\} \\ \mathcal{S}_2 &= \{\mathcal{S}_2; \mathcal{S}_{02}\} = \{\mathbf{0}; \mathbf{L}_1\}/\|\mathbf{L}_1\| \\ \mathcal{S}_3 &= \{\mathcal{S}_3; \mathcal{S}_{03}\} = \{\mathbf{L}_1; \mathbf{a}_1 \times \mathbf{L}_1\}/\|\mathbf{L}_1\| \\ \mathcal{S}_4 &= \{\mathcal{S}_4; \mathcal{S}_{04}\} = \{\mathcal{S}_1; \mathbf{a}_1 \times \mathcal{S}_1\} \\ \mathcal{S}_5 &= \{\mathcal{S}_5; \mathcal{S}_{05}\} = \{\mathbf{L}_1 \times \mathcal{S}_4; \mathbf{a}_1 \times \mathbf{L}_1 \times \mathcal{S}_4\}/\|\mathbf{L}_1 \times \mathcal{S}_4\| \\ \mathcal{S}_0 &= \{0 \quad 0 \quad 1; \quad 0 \quad -L' \quad 0\} \end{aligned} \quad (6.37)$$

where

$$\mathcal{S}_1 = \mathcal{S}_4 = \{0 \quad -1 \quad 0\}, \quad \mathbf{L}_1 = \mathbf{a}_1 - \mathbf{A}_1. \quad (6.38)$$

The twist screw systems of the other two chains corresponding to $[\mathbf{G}_2^0]$ and $[\mathbf{G}_3^0]$ are the same as the case, in which the upper platform is parallel to the base. Establishing matrices $[\mathbf{G}]$ and $[\mathbf{G}']$, we can solve principal screws using the previous method.

Suppose $\alpha = 30^\circ$, the pitches of three principal screws can be obtained by solving Eq. (6.33). They are given as follows:

$$h_\alpha = 5.13 \times 10^5; \quad h_\beta = 0; \quad h_\gamma = -5.13 \times 10^5. \quad (6.39)$$

When $I_2 = 0$, where I_2 is the two-order determinant of coefficients of the quadratic equation, its two roots are $h_1 = -0.0057$ and $h_2 = 0.0165$. There are six types of the quadratic curve for the same configuration of the mechanism, as shown in Table 6.1. The pitch h varies between h_α and h_γ . Each point in Fig. 6.4 denotes a pitch h of a twist screw of the moving platform, with respect to the three inputs $(u, w, 1)$. We can obtain the output pitch of the instantaneous twist when three inputs are given. Figure 6.4 also shows the relation between inputs and the six types of quadratic curves with different pitches in this configuration of the mechanism.

The twist screws with the same pitch, h , form a quadratic curve. The pure rotations with zero pitch are illustrated as a pair of intersecting real straight lines in the figure. The two straight lines can also be obtained and proven using another method proposed in [18]. The three principal screws are given as follows:

$$\begin{aligned} \mathcal{S}_m^1 &= \{0 \quad -1 \quad 0; \quad 0.2 \quad 0 \quad 0.1\}, \\ \mathcal{S}_m^2 &= \{0.966 \quad 0 \quad 0.259; \quad 0 \quad 0.22 \quad 3.96 \times 10^6\}, \\ \mathcal{S}_m^3 &= \{-0.966 \quad 0 \quad -0.259; \quad 0 \quad -0.22 \quad 3.96 \times 10^6\}. \end{aligned} \quad (6.40)$$

The screw \mathcal{S}^m with infinite pitch can be obtained by a linear combination of \mathcal{S}_m^2 and \mathcal{S}_m^3 given as:

$$\mathcal{S}^m = \{0 \quad 0 \quad 0 \quad ; \quad 0 \quad 0 \quad 1\}. \quad (6.41)$$

It expresses a pure translation along the Z-direction. Meanwhile, \mathcal{S}_m^1 with zero pitch is a pure rotation around the axis parallel to the Y-axis, whereas \mathcal{S}_m^2 is a twist screw with $h \neq 0$ and deviates from the normal direction of \mathcal{S}^m . The three screws, \mathcal{S}^m , \mathcal{S}_m^1 and \mathcal{S}_m^2 , represented by:

$$\begin{aligned} \mathcal{S}^m &= \{0 \quad 0 \quad 0 \quad ; \quad 0 \quad 0 \quad 1\}, \\ \mathcal{S}_m^1 &= \{0 \quad -1 \quad 0 \quad ; \quad 0.2 \quad 0 \quad 0.1\}, \\ \mathcal{S}_m^2 &= \{0.966 \quad 0 \quad 0.259 \quad ; \quad 0 \quad 0.22 \quad 3.96 \times 10^6\}, \end{aligned} \quad (6.42)$$

form a set of new principal screws, which corresponds to the seventh special three-system screws presented by Hunt [2] as well as Tsai and Lee [5].

Table 6.1 Six types of quadratic curves

The range of the value of h		
In 30° configuration	In general configuration	Type of conics
$0.0165256 < h < 5.13 \times 10^5$ or $-5.13 \times 10^5 < h < -0.0057003$	$0.0131215 < h < 4.28 \times 10^5$ or $-4.28 \times 10^5 < h < -0.0160208$	Real ellipse
$h > 5.13 \times 10^5$ or $h < -5.13 \times 10^5$	$h > 4.28 \times 10^5$ or $h < -4.28 \times 10^5$	Imaginary ellipse
$h_x = 5.13 \times 10^5$ or $h_y = -5.13 \times 10^5$ $-0.0057003 < h < 0.0165256$	$h_x = 4.28 \times 10^5$ or $h_y = -4.28 \times 10^5$ $-0.0160208 < h < 0.0131215$	Dot ellipse
$h_\beta = 0$	$h_\beta = 0.0079$	Hyperbola
		A pair of intersecting real lines
$h = 0.0165256$ or $h = -0.0057003$	$h = 0.0131215$ or $h = -0.0160208$	Parabola

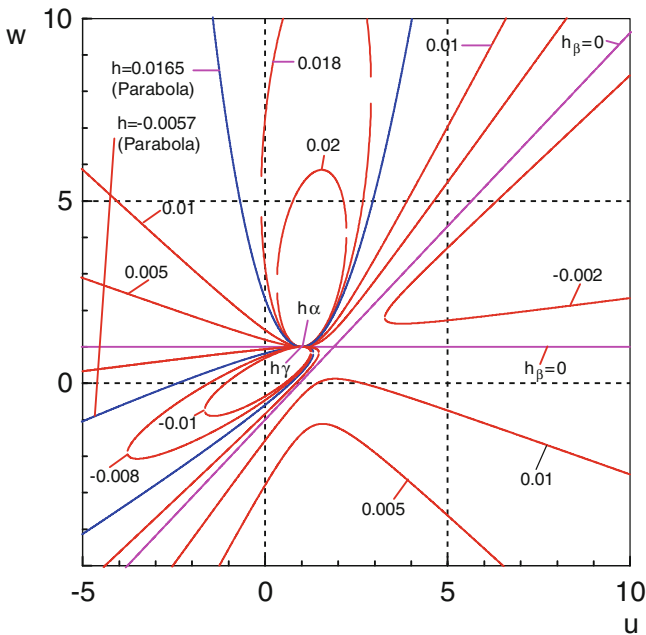


Fig. 6.4 Upper platform rotating at 30° around a_2a_3

6.3.4 General Configuration of the 3-RPS Mechanism

In a general configuration, the lengths of three legs of the parallel manipulator are different. The coordinates of the points a_1 , a_2 and a_3 , with respect to the coordinate system P - xyz are as follows:

$$\begin{aligned}
 \mathbf{a}_1 &= \{r \quad 0 \quad 0\}^T \\
 \mathbf{a}_2 &= \{-r/2 \quad \sqrt{3}r/2 \quad 0\}^T, \\
 \mathbf{a}_3 &= \{-r/2 \quad -\sqrt{3}r/2 \quad 0\}^T
 \end{aligned}
 \tag{6.43}$$

Since the transformation matrix from the system P -xyz to the fixed system O -XYZ is $[T]$, the coordinates of the points with respect to the fixed coordinate system O -XYZ are:

$$\{\mathbf{P}_i \ 1\}^T = [T]\{\mathbf{a}_i \ 1\}^T \quad i = 1, 2, 3. \quad (6.44)$$

The unit vectors \mathbf{u}_1 , \mathbf{u}_2 and \mathbf{u}_3 , representing revolute axes with respect to the fixed system are:

$$\begin{aligned} \mathbf{u}_1 &= \{0 \ 1 \ 0\}^T \\ \mathbf{u}_2 &= \{-\sqrt{3}/2 \ -1/2 \ 0\}^T \\ \mathbf{u}_3 &= \{\sqrt{3}/2 \ -1/2 \ 0\}^T. \end{aligned} \quad (6.45)$$

The screw systems of the three serial chains in the fixed system can be expressed as follows:

$$\begin{aligned} \mathcal{S}_1^i &= \{\mathcal{S}_1; \ \mathcal{S}_{01}\} = \{\mathbf{u}_1; \ \mathbf{A}_i \times \mathbf{u}_i\} \\ \mathcal{S}_2^i &= \{\mathcal{S}_2; \ \mathcal{S}_{02}\} = \{0; \ \mathbf{L}_i\}/\|\mathbf{L}_i\| \\ \mathcal{S}_3^i &= \{\mathcal{S}_3; \ \mathcal{S}_{03}\} = \{\mathbf{L}_i; \ \mathbf{P}_i \times \mathbf{L}_i\}/\|\mathbf{L}_i\| \quad i = 1, 2, 3. \\ \mathcal{S}_4^i &= \{\mathcal{S}_4; \ \mathcal{S}_{04}\} = \{\mathbf{u}_i; \ \mathbf{P}_i \times \mathbf{u}_i\} \\ \mathcal{S}_5^i &= \{\mathcal{S}_5; \ \mathcal{S}_{05}\} = \{\mathbf{L}_i \times \mathbf{u}_i; \ \mathbf{P}_i \times \mathbf{L}_i \times \mathbf{u}_i\}/\|\mathbf{L}_i \times \mathbf{u}_i\| \end{aligned} \quad (6.46)$$

Three virtual revolute pairs added to three branches are supposed to be all in the Z -direction, passing through points k_1 , k_2 and k_3 , respectively, and are on the lines from original point O to the points A_1 , A_2 and A_3 , respectively. All lengths are L' , and then the coordinates of the points k_1 , k_2 and k_3 are expressed as three vectors given by:

$$\begin{aligned} \mathbf{k}_1 &= \{L' \ 0 \ 0\} \\ \mathbf{k}_2 &= \{-L'/2 \ \sqrt{3}L'/2 \ 0\} \\ \mathbf{k}_3 &= \{-L'/2 \ -\sqrt{3}L'/2 \ 0\}. \end{aligned} \quad (6.47)$$

The three corresponding virtual twist screws are:

$$\mathcal{S}_0^i = \{\mathcal{S}_0; \ \mathbf{k}_i \times \mathcal{S}_0\} \quad i = 1, 2, 3, \quad (6.48)$$

where $\mathcal{S}_0 = \{0 \ 0 \ 1\}$.

The matrices $[\mathbf{G}_i^0]$, corresponding to screw systems of the three branches with respect to the fixed coordinate system, are given as:

$$[\mathbf{G}_i^0] = \{\mathcal{S}_0^i \ \mathcal{S}_1^i \ \mathcal{S}_2^i \ \mathcal{S}_3^i \ \mathcal{S}_4^i \ \mathcal{S}_5^i\} \quad i = 1, 2, 3. \quad (6.49)$$

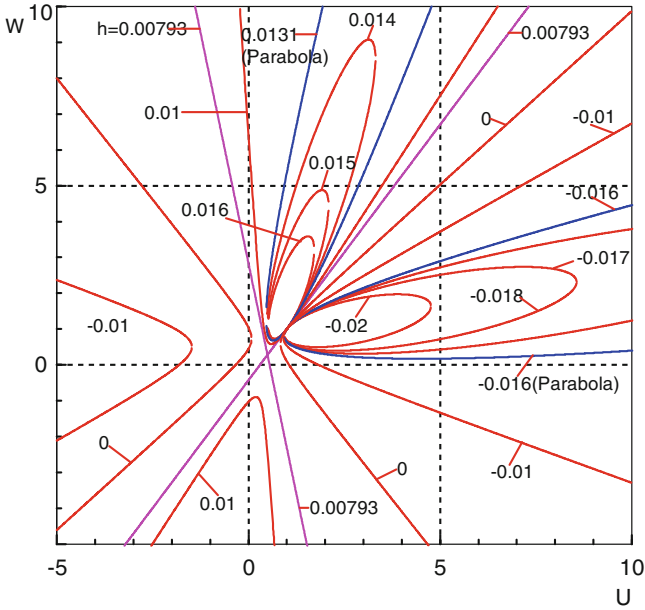


Fig. 6.5 Twist screws in a general configuration

When the coordinates of the center point of the upper platform with respect to the fixed system are given as

$$X = 0.002 \text{ m}, \quad Y = 0.001 \text{ m}, \quad Z = 0.22 \text{ m},$$

then the pitches of the three principal screws can be obtained as:

$$h_x = 4.28 \times 10^5; \quad h_y = 0.0079; \quad h_z = -4.28 \times 10^5, \quad (6.50)$$

respectively. Meanwhile, when $I_2 = 0$, two possible roots of the pitch are $h_1 = -0.016$ and $h_2 = 0.013$. There are also six types of conics in this configuration as shown in Table 6.1. Figure 6.5 illustrates a planar representation of pitches of all possible twist screws in this case.

The coordinates (u, w) of the principal screw with h_x are $(1.0004133965, 1.000387461)$. The (u, w) corresponding to h_z are $(1.0004134267, 1.000387451)$, and both are too close to be distinguished by the naked eye in the figure. The three principal screws can be obtained as follows:

$$\begin{aligned} \mathcal{S}_m^1 &= \{-0.97 \quad 0.23 \quad 0 \quad ; \quad -0.06 \quad -0.22 \quad 0.06\}, \\ \mathcal{S}_m^2 &= \{0.22 \quad 0.95 \quad 0.21 \quad ; \quad -0.204 \quad 0.395 \quad 4.1 \times 10^6\} \\ \mathcal{S}_m^3 &= \{-0.22 \quad -0.95 \quad -0.21 \quad ; \quad 0.204 \quad -0.395 \quad 4.1 \times 10^6\} \end{aligned} \quad (6.51)$$

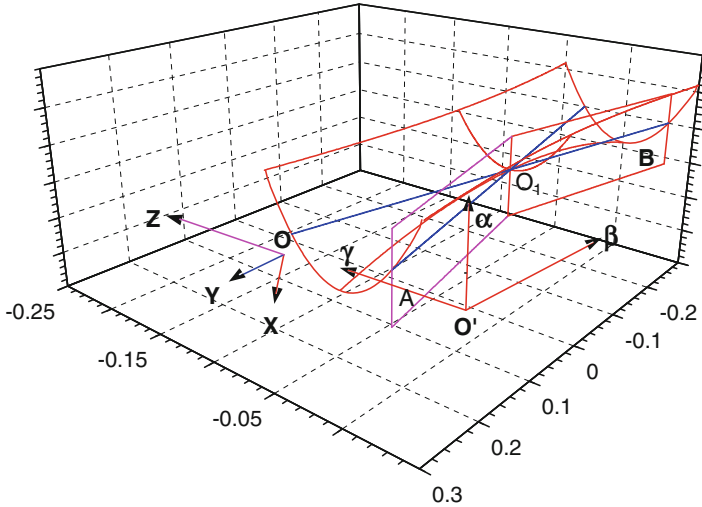


Fig. 6.6 Spatial distribution of the screws in a general configuration

The screw $\mathcal{S}^m = \{0 \ 0 \ 0 \ ; \ 0 \ 0 \ 1\}$ with infinite pitch, $h^m = \infty$, can be obtained by the linear combination of \mathcal{S}_m^2 and \mathcal{S}_m^3 . \mathcal{S}^m expresses a pure translation along the Z direction. \mathcal{S}_m^1 with $h_m^1 = 0$ is perpendicular to Z-axis, and \mathcal{S}_m^2 with $h_m^2 \neq 0$ deviates from the normal direction of \mathcal{S}^m . Therefore, the three principal screws \mathcal{S}^m , \mathcal{S}_m^1 and \mathcal{S}_m^2 , also form the seventh special three-system. Therefore, the formation of all linear combinations of \mathcal{S}^m , \mathcal{S}_m^1 , and \mathcal{S}_m^2 in 3D space is a hyperbolic paraboloid, as shown in Fig. 6.6.

6.4 Full-Scale Feasible Instantaneous Screw of a 3-UPU Mechanism

In this section, we discuss an interesting 3-DOF special 3-UPU mechanism [8, 13]. It has some special inconceivable characteristics and is different from the general 3-D translational 3-UPU parallel mechanism proposed by Tsai in 1996 [20].

The 3-UPU mechanism, as shown in Fig. 6.7a, consists of a fixed pyramid $A_1A_2A_3$, a moving pyramid $B_1B_2B_3$, and three UPU kinematic chains. In this configuration, the mechanism is cubic, and the UPU chain consists of three kinematic pairs, two universal pairs, and a prismatic pair in their middle. The middle two revolute pairs, \mathcal{S}_2 and \mathcal{S}_4 , adjacent to the prismatic pair in every branch, Fig. 6.7b, are mutually perpendicular and are both perpendicular to the prismatic pair. The base coordinate system is O -XYZ. The first pair of UPU chains aligns with the X-, Y- and Z-axes, respectively. The centerlines of the three prismatic pairs in the initial position are mutually perpendicular. The length of each side of the cubic mechanism is m , and its mobility is very special. Thus, we analyze mobility first.

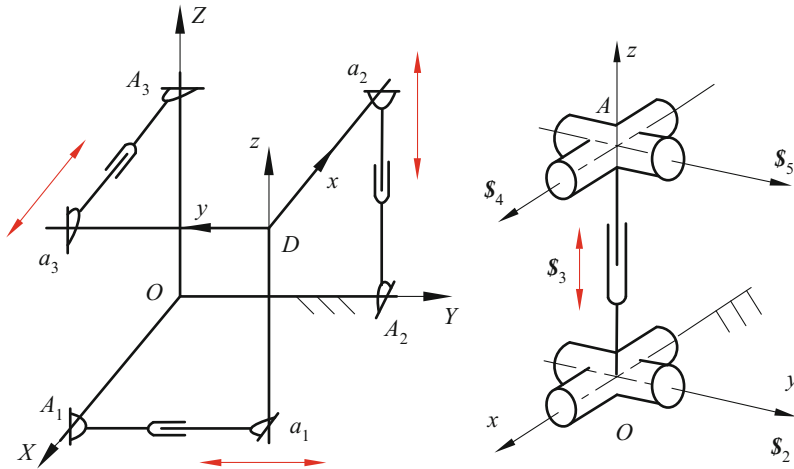


Fig. 6.7 3-UPU pyramid mechanism (a) Mechanism (b) A branch

6.4.1 Mobility Analysis

6.4.1.1 Analysis of Limb

The coordinate system is shown in Fig. 6.7b. Its limb is a UPU chain corresponding to five single-freedom pairs. Four cases of the limbs are analyzed here.

1. **The first case.** The two planes of the upper and lower U-pairs are parallel, and the link OA is normal to the U-pair planes, Fig. 6.7b.

In this case the reciprocal screw of the five screws of the limb is a constraint couple along the direction of the prismatic pair, Table 2.2, and is given by:

$$\mathcal{S}^r = (0 \ 0 \ 0; \ 0 \ 0 \ 1). \tag{6.52}$$

2. **The second case.** The link OA lies in the xz plane, and \mathcal{S}_5 is still parallel with \mathcal{S}_2 as shown in Fig. 6.8a

The five kinematic pairs of the limb may be expressed as five screws, yielding the following:

$$\begin{aligned} \mathcal{S}_1 &= (1 \ 0 \ 0; \ 0 \ 0 \ 0) \\ \mathcal{S}_2 &= (0 \ 1 \ 0; \ 0 \ 0 \ 0) \\ \mathcal{S}_3 &= (0 \ 0 \ 0; \ \alpha \ 0 \ \beta) \\ \mathcal{S}_4 &= (\beta \ 0 \ -\alpha; \ 0 \ 1 \ 0) \\ \mathcal{S}_5 &= (0 \ 1 \ 0; \ -\beta \ 0 \ \alpha). \end{aligned} \tag{6.53}$$

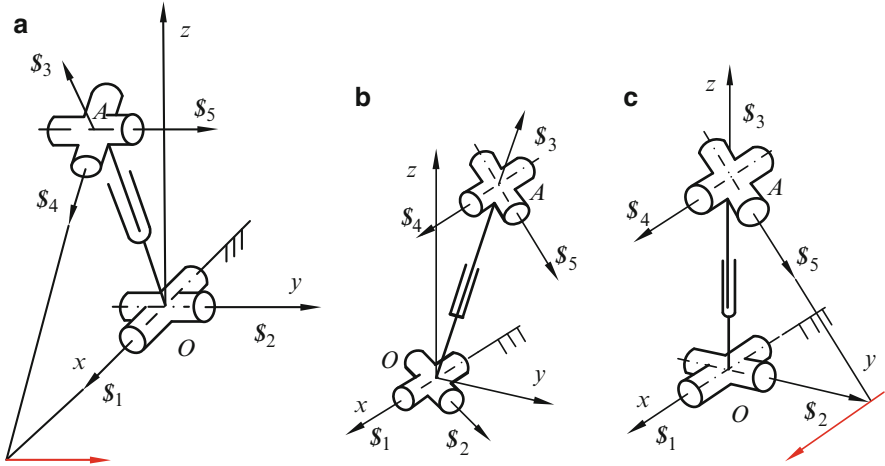


Fig. 6.8 The branch (a) The second case (b) The third case A (c) The third case B

To solve the reciprocal screw of the five screws, as shown in Eq. (6.53), assuming the reciprocal screw is as follows:

$$\mathcal{S}^r = (a \ b \ c; \ d \ e \ f), \tag{6.54}$$

then the reciprocal screw should satisfy the condition as follows:

$$\mathcal{S}_i \circ \mathcal{S}^r = 0, \quad i = 1, 2, \dots, 4.$$

The reciprocal screw of the limb System can thus be obtained as:

$$\mathcal{S}^r = \left(0 \ 1 \ 0; \ 0 \ 0 \ \frac{1}{\alpha} \right). \tag{6.55}$$

It is a reciprocal force parallel y-axis.

The result can also be explained by geometrical principle. Based on Table 2.2, if a screw is reciprocal to those five screws, $\mathcal{S}_1, \mathcal{S}_2, \dots, \mathcal{S}_5$, then it should be coplanar with screws $\mathcal{S}_1, \mathcal{S}_2, \mathcal{S}_4$, and \mathcal{S}_5 and normal to \mathcal{S}_3 . The unique possibility is the screw, which passes the intersecting point of \mathcal{S}_1 and \mathcal{S}_4 and is parallel to \mathcal{S}_2 . The two results are the same.

3. **The third case.** The link OA is in the yz plane and \mathcal{S}_4 is parallel to \mathcal{S}_1 as shown in Fig. 6.8b. For this case, the coordinate system can also be selected as Fig. 6.8c;

we also allow the x and y axes to align with $\$1$ and $\$2$, respectively. Then the five screws are as follows:

$$\begin{aligned}\$1 &= (1 \ 0 \ 0; \ 0 \ 0 \ 0) \\ \$2 &= (0 \ 1 \ 0; \ 0 \ 0 \ 0) \\ \$3 &= (0 \ 0 \ 0; \ 0 \ 0 \ 1) \\ \$4 &= (1 \ 0 \ 0; \ 0 \ 1 \ 0) \\ \$5 &= (0 \ b_5 \ c_5; \ d_5 \ 0 \ 0).\end{aligned}\tag{6.56}$$

Their reciprocal screw is represented by:

$$\$^r = (1 \ 0 \ 0; \ 0 \ 0 \ f).$$

It is a constraint force parallel to $\$1$, which also passes the intersecting point formed by $\$5$ and $\$2$.

4. *All other cases*

For example, in Fig. 6.8a, if $\$5$ and $\$2$ are not parallel but are intersecting, in this case, it is impossible to find a screw with zero-pitch reciprocal to those five screws, $\$1, \$2, \dots, \$5$, i.e., that screw is neither coplanar with screws $\$1, \$2, \$4$, and $\$5$ nor normal to $\$3$ simultaneously. In addition, it is impossible to find a couple to reciprocate all five screws. For this situation, the possible reciprocal screw is a reaction wrench with the pitch, $0 \neq h \neq \infty$.

6.4.1.2 Whole Mechanism

After we analyze the limb screw system, we will consider the whole mechanism.

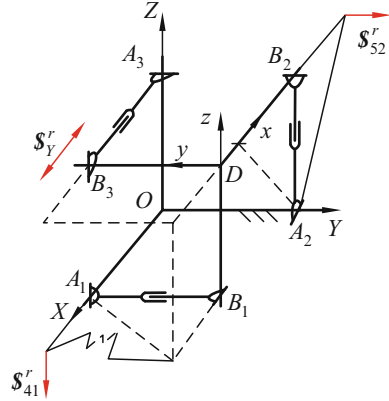
1. *In the initial configuration*

The mechanism is a cubiform with equal lengths of three limbs as shown in Fig. 6.7a. In this case, the three limbs all belong to the first case, and each acts a constraint couple upon the end-pyramid. The pyramid is subjected to three reciprocal screws with infinite pitches. Figure 6.7a shows the coordinate system $O\text{-}XYZ$. The three reciprocal screws are:

$$\begin{aligned}\$1^r &= (0 \ 0 \ 0; \ 0 \ 1 \ 0) \\ \$2^r &= (0 \ 0 \ 0; \ 1 \ 0 \ 0) \\ \$3^r &= (0 \ 0 \ 0; \ 0 \ 0 \ -1).\end{aligned}\tag{6.57}$$

The three constraint couples limit three rotations, and the end-pyramid of the mechanism has only three translational freedoms. However, although the mechanism has three translation freedoms, any linear combination of the three allowing freedoms denotes a new translation direction, which does not align with any coordinate axis, and the freedom is instantaneous. Based on the analysis stated above, except the first case, all other cases denote the reciprocal screw to be not a couple but a force, and the constrained motion is considered as translation. Then,

Fig. 6.9 End-pyramid translates along the X -axis



the pyramid is not a 3D translational mechanism any more. In other words, the mechanism is a 3D translation mechanism, although it cannot translate along the direction of the linear combination of the X , Y and Z -axes.

2. The end-pyramid translates along the X -axis for a distance

Here, another configuration of the mechanism is discussed, as shown in Fig. 6.9. In this case, the moving pyramid only translates along the X -axis. The configurations of the three limbs are different. Limb A_3B_3 only extends along its axis and belongs to the 1st case of limb displacements. The reciprocal screw of this limb is a constraint couple, as indicated in Eq. (6.52). Limb A_1B_1 is in the 2nd case and it rotates an angle of ϕ . It $\$5$ intersects with $\$2$, and there is a constraint force, Eq. (6.55). For limb A_2B_2 , it also rotates an angle of ζ , which belongs to the 3rd case, and $\$4$ is parallel $\$1$. Its reciprocal screw is also a constraint force.

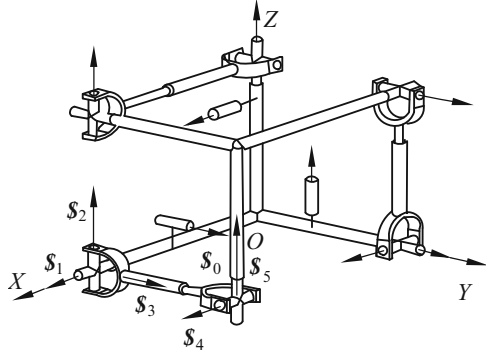
The three reciprocal screws act on the moving pyramid, which are expressed using three red arrows, Fig. 6.9. Since the three reciprocal screws include one couple and two forces, the moving pyramid loses one rotation and two translation freedoms. It has three freedoms including one translation along the X -axis and two rotation freedoms about the lines parallel to the Y - and Z -axes, respectively.

From this analysis, we know that the mechanism is quite strange. It has 3D translation freedoms and can translate, respectively, along the X , Y , Z -axes. However, it cannot translate along any direction of the linear combination of the X , Y , and Z -axes.

6.4.2 First-Order Influence Matrices and Kinematic Analysis

In order to analyze the full-scale feasible motion, there is a need to establish the first-order influence matrices. For this special 3-UPU mechanism, each branch of the mechanism has equivalent five single-DOF kinematic pairs. According to the virtual-mechanism method mentioned in Sect. 5.4, a virtual link and an imaginary virtual pair

Fig. 6.10 Initial position of virtual mechanism



denoted by a screw with zero pitch, $\$_{0,i}$, are added to each branch, as shown in Fig. 6.10. Then, each branch has six single-DOF kinematic pairs. Note that it is necessary to let the angular velocity amplitude of $\$_{0}$ for each branch always be zero.

For each 6-DOF serial branch, the motion of the end-effector of the 3-UPU mechanism can be represented as:

$$V_H = [G_i^0] \dot{\phi}^i \quad (i = 1, 2, 3). \tag{6.58}$$

Based on Eq. (6.58) and Sect. 6.2, the key matrix equations $[G']$ and $[G]$ can be obtained as follows:

$$V_H = [G_L^H] \dot{q} \tag{6.59}$$

$$V_p = [G] \dot{q} \quad \omega = [G'] \dot{q}, \tag{6.60}$$

where $[G']$ represents the first three rows of $[G_L^H]$, and $[G]$ represents the last three rows of $[G_L^H]$. They are both 3×3 matrices.

6.4.3 Initial Configuration

Figure 6.10 shows the initial configuration of the mechanism, $m = 1.0$ m, $l = 0.3$ m, and $d_1 = d_2 = d_3$, where d_i is the distance between the virtual pair to the 1st pair of the limb. For each branch of the mechanism, ϕ_0^i , ($\phi_0^i = 0$) and \dot{q}_i , ($i = 1, 2, 4$) are denoted as their inputs.

We assume that the three lengths from the origin O to the centers of the three virtual pairs are all $l = m - d_i$, which lie on the X, Y and Z -axes, respectively.

The first-order influence coefficient matrices of the three branches are given, respectively, as:

$$[G_i^0] = (\$_{0,i} \quad \$_{1,i} \quad \$_{3,i} \quad \$_{i,4} \quad \$_{5,i}), \quad (i = 1, 2, 3).$$

According to Eqs. (6.30) and (6.31), we obtain the two matrices as follows:

$$[\mathbf{G}'] = \begin{bmatrix} 0 & 0 & 0 \\ 0 & 0 & 0 \\ 0 & 0 & 0 \end{bmatrix}, \quad [\mathbf{G}] = \begin{bmatrix} 0 & 0 & 1 \\ 1 & 0 & 0 \\ 0 & 1 & 0 \end{bmatrix}. \quad (6.61)$$

From Eq. (6.61), we obtain the coefficients of Eq. (6.12) as:

$$c_1 = c_2 = c_3 = c_4 = 0. \quad (6.62)$$

The result is very special and implies that the roots of Eq. (6.12) can be any value. For this special situation to determine the three values, we should consider the three other conditions. From Sect. 6.2.2 as well as from Huang [12] and [21], the three roots should all be infinite. This means that the three roots, h_α , h_β and h_γ , are all ∞ as stated in:

$$h_\alpha = h_\beta = h_\gamma = \infty.$$

The three principal screws belong to the sixth special third-order system presented by Hunt [2]. The three mutually perpendicular screws correspond with three independent translational motions, indicating that an instant translational motion exists along any direction in space, through the linear combination of the three screws.

However, we have found before that only three feasible translational motions can continue along the three coordinate axes, respectively. The feasible translational motions along all other directions in 3D space are only instantaneous. Therefore, the mechanism is not the same as the general 3D translational parallel mechanism proposed by Tsai and Stamper [20].

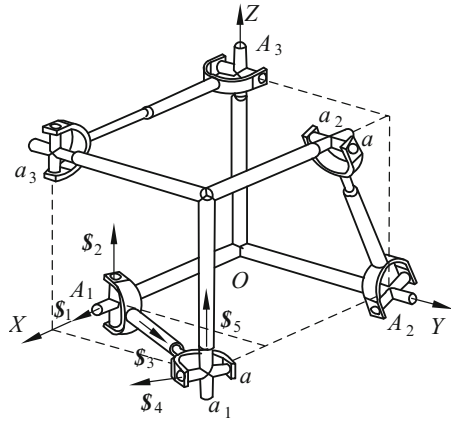
6.4.4 The Second Configuration

The mechanism parameters are assumed as follows: $m = 1.0$ m and $l = 0.3$ m. In addition, $a = 0.2$ m is the displacement of the moving pyramid along the X -axis, as shown in Fig. 6.11 [12, 13]. In this case, we have:

$$[\mathbf{G}'] = \begin{bmatrix} 0 & 0 & 0 \\ 0.00567188 & 0.170156 & -0.0344828 \\ 0.170156 & 0.0567188 & 1.03448 \end{bmatrix},$$

$$[\mathbf{G}] = \begin{bmatrix} -0.0567188 & -0.170156 & 1.03448 \\ 0.850782 & 0.0283594 & -0.172414 \\ 0.0351657 & 1.05497 & -0.213793 \end{bmatrix}. \quad (6.63)$$

Fig. 6.11 The second position of virtual mechanism



Substituting $[G]$ and $[G']$ into Eq. (6.8) and according to Eq. (6.10), we have:

$$D = \begin{vmatrix} a_{11} & a_{12} & a_{13} \\ a_{21} & a_{22} & a_{23} \\ a_{31} & a_{32} & a_{33} \end{vmatrix} = 0. \tag{6.64}$$

Expanding and solving the equation, we obtain the following:

$$\begin{aligned} h_x &= 5.5 \\ h_\beta &= -5.6 \\ h_y &= -2.16318 \times 10^{17}, \end{aligned} \tag{6.65}$$

where one is infinite and the other two are finite values with opposite signs. Therefore, any screw in the screw system is the linear combination of the three principal screws, and its pitch is inside the scope, $-5.6 \leq h \leq 5.6$. The three principal kinematic screws are given, respectively, by

$$\begin{aligned} \mathcal{S}_\alpha &= (0 \quad 1.0 \quad 1.0; 88.4053 \quad 5.0 \quad 6.2)/\sqrt{2} \\ \mathcal{S}_\beta &= (0 \quad -1.0 \quad 1.0; 71.7085 \quad 5.0 \quad -6.2)/\sqrt{2} \\ \mathcal{S}_\gamma &= (0 \quad 0 \quad 0; 1 \quad 0 \quad 0), \end{aligned} \tag{6.66}$$

and the vector equations of three axes are also given, respectively, by:

$$\begin{aligned} \mathbf{r} \times \mathcal{S}_\alpha &= (88.4053 \quad 5 \quad 6.2)^T/\sqrt{2} \\ \mathbf{r} \times \mathcal{S}_\beta &= (71.7085 \quad 5 \quad 6.2)^T/\sqrt{2} \\ \mathbf{r} \times \mathcal{S}_\gamma &= (0 \quad 0 \quad 0)^T, \end{aligned} \tag{6.67}$$

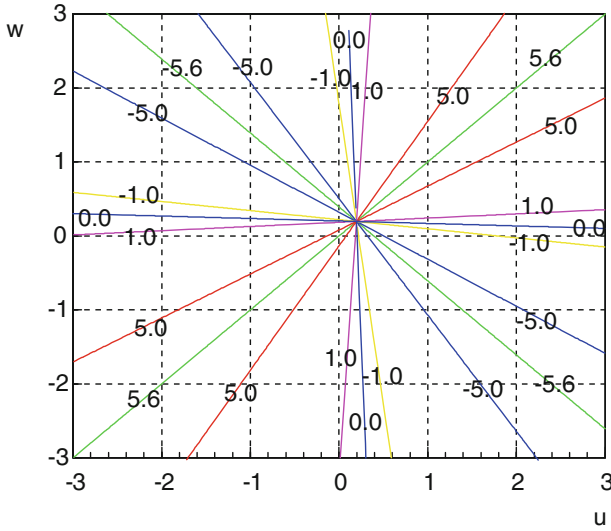


Fig. 6.12 Pitch distribution for the second configuration

where S_α , S_β , and S_γ are the three direction vectors of the three principal screws, respectively. This system belongs to a third special three-system screw.

When different h values are substituted into Eq. (6.10), we may obtain different quadratic equations. Giving one set of input ($u \ w \ 1$), the corresponding pitch of the output motion is shown in Fig. 6.12, which also illustrates the full-scale feasible instantaneous motion at that moment.

We know that each pitch of the screw determines a quadratic Eq. (6.10). Here, all quadratic equations degenerate into a pair of intersecting straight lines, when h lies within the range $-5.6 < h < 5.6$. This is because that two invariants of all the quadratic equations, Eq. (6.10), satisfy $D = 0$ and $\delta < 0$. Similarly, when $h = 5.6$ and $h = -5.6$ both quadratic equations collapse into two pairs of superposed straight lines, and are given, respectively, as follows:

$$\begin{aligned}
 &u = w \\
 &0.173127u + 0.173127w = 0.0679061. \tag{6.68}
 \end{aligned}$$

In addition, as shown in Fig. 6.12, the quadratic equation collapses into a point, which is just the intersecting point of all the straight lines, when:

$$h = h_\gamma = -2.16381 \times 10^{17} = -\infty$$

Figure 6.12 illustrates the finite-and-infinite pitch graph of the third special three-system screw, including the finite pitches in the scope from -5.6 to 5.6 and an infinite pitch. Each point in the figure indicates the relation between the

input $(u \ w \ 1)$ and the output pitch, h . It is necessary to point out that, for a 6-DOF mechanism, infinite pitches of the infinite feasible instant motions are distributed in an infinite scope $(-\infty \ \infty)$, but for this special 3-UPU mechanism its infinite possibility is only in a limited scope $(-5.6, 5.6)$ plus a point with an infinite pitch value.

From Fig. 6.12, we can find that all the straight lines pass through a common point, which is a very special point. The pitch values of all the straight lines are finite, but at the special point, the pitch suddenly becomes infinite.

6.5 Full-Scale Feasible Instantaneous Screw of a 3-RPS Pyramid Mechanism

In this section, we study the 3-RPS pyramid mechanism in detail. The fixed element, $A_1A_2A_3$, and the moving one $a_1a_2a_3$ are both pyramids as shown in Fig. 6.13a. Each of its three branches is formed by a revolute joint R, a prismatic pair P, and a spherical pair S, which is an RPS kinematic chain. The 1st pair of each limb aligns with the X , Y and Z -axes, respectively. Three prismatic pairs are selected as inputs. The base coordinate system is O - XYZ . The branch screw system is shown in Fig. 6.13b.

6.5.1 First-Order Influence Coefficient Matrix

In order to obtain the Jacobian matrices $[G]$ and $[G]'$, we use the virtual mechanism method. There are five unit-DOF kinematic pairs in each branch of the 3-RPS mechanism. A virtual link and a virtual pair denoted by a screw with zero pitch, $\$0$, are added to each of the branches. Then, each branch of this mechanism has six single-DOF pairs. In order to maintain equivalent kinematic effects between the virtual mechanism and the previous one, we allow the velocity amplitude of the virtual unit screw $\$0$ of each branch to be zero and $\$0$ be linearly independent with the other five real screws of the primary branch. Then, the virtual mechanism is a 6-DOF mechanism.

We assume that the length of any side of the cubic mechanism is m . Then, the coordinates of the fixed points A_1, A_2, A_3 in the base coordinate system O - XYZ are given by:

$$\begin{aligned} A_1 &= \{m \ 0 \ 0\}^T \\ A_2 &= \{0 \ m \ 0\}^T \\ A_3 &= \{0 \ 0 \ m\}^T. \end{aligned} \tag{6.69}$$

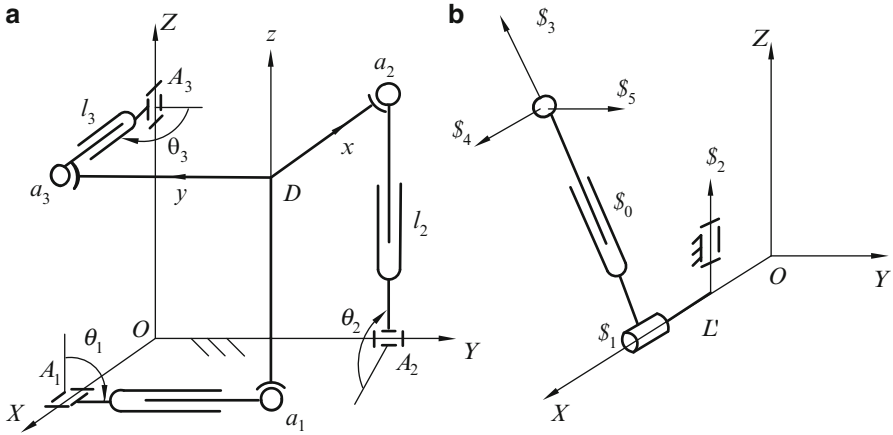


Fig. 6.13 3-DOF 3-RPS pyramid mechanism (a) Mechanism sketch (b) Virtual branch

In the general case, the coordinates of the moving points, a_1 , a_2 , a_3 , in the base coordinate system O - XYZ are given by:

$$\begin{aligned}
 \mathbf{a}_1 &= \{m \quad l_1 \sin \theta_1 \quad l_1 \cos \theta_1\}^T \\
 \mathbf{a}_2 &= \{l_2 \cos \theta_2 \quad m \quad l_2 \sin \theta_2\}^T \\
 \mathbf{a}_3 &= \{l_3 \sin \theta_3 \quad l_3 \cos \theta_3 \quad m\}^T,
 \end{aligned} \tag{6.70}$$

where l_i and θ_i ($i = 1, 2, 3$) are input and output kinematic parameter, as shown in Fig. 6.13a.

Considering the constraints of the structure of the mechanism, a_1 , a_2 , and a_3 have to satisfy the following three equations:

$$\left. \begin{aligned}
 |a_1 a_2| &= \sqrt{(l_2 \cos \theta_2 - m)^2 + (m - l_1 \sin \theta_1)^2 + (l_2 \sin \theta_2 - l_1 \cos \theta_1)^2} = \sqrt{2}m \\
 |a_2 a_3| &= \sqrt{(l_3 \sin \theta_3 - l_2 \cos \theta_2)^2 + (l_3 \cos \theta_3 - m)^2 + (m - l_2 \sin \theta_2)^2} = \sqrt{2}m \\
 |a_1 a_3| &= \sqrt{(l_3 \sin \theta_3 - m)^2 + (l_3 \cos \theta_3 - l_1 \sin \theta_1)^2 + (m - l_1 \cos \theta_1)^2} = \sqrt{2}m
 \end{aligned} \right\}. \tag{6.71}$$

When the lengths l_1 , l_2 , and l_3 of the three input links are given, the three angles θ_i may be obtained by solving Eq. (6.71). The position and orientation of the moving pyramid of this mechanism can then be determined. This is the direct kinematics of such mechanism.

The vectors of the three links are given by:

$$\mathbf{L}_i = \mathbf{a}_i - \mathbf{A}_i \quad i = 1, 2, 3. \tag{6.72}$$

The directional vectors of the axes of the three rotational pairs in the base coordinate system are:

$$\begin{aligned} \mathbf{u}_1 &= \{1 \ 0 \ 0\} \\ \mathbf{u}_2 &= \{0 \ 1 \ 0\} \\ \mathbf{u}_3 &= \{0 \ 0 \ 1\}. \end{aligned} \quad (6.73)$$

The Plücker coordinates of the three original branches in the base coordinate system are given as follows:

$$\begin{aligned} \mathcal{S}_1^i &= \{\mathcal{S}_1; \ \mathcal{S}_{01}\} = \{u_i; \ A_i \times u_i\} \\ \mathcal{S}_2^i &= \{\mathcal{S}_2; \ \mathcal{S}_{02}\} = \{0; \ L_i\} / \|L_i\| \\ \mathcal{S}_3^i &= \{\mathcal{S}_3; \ \mathcal{S}_{03}\} = \{L_i; \ a_i \times L_i\} / \|L_i\| \\ \mathcal{S}_4^i &= \{\mathcal{S}_4; \ \mathcal{S}_{04}\} = \{u_i; \ a_i \times u_i\} \\ \mathcal{S}_5^i &= \{\mathcal{S}_5; \ \mathcal{S}_{05}\} = \{L_i \times u_i; \ a_i \times L_i \times u_i\} / \|L_i \times u_i\| \end{aligned} \quad i = 1, 2, 3. \quad (6.74)$$

The Plücker coordinates of the virtual screws \mathcal{S}_0 of the three branches in base system are respectively given as:

$$\begin{aligned} \mathcal{S}_0^1 &= (0 \ 0 \ 1 \ ; \ 0 \ -L' \ 0) \\ \mathcal{S}_0^2 &= (1 \ 0 \ 0 \ ; \ 0 \ 0 \ -L') \\ \mathcal{S}_0^3 &= (0 \ 1 \ 0 \ ; \ -L' \ 0 \ 0). \end{aligned} \quad (6.75)$$

The three lengths from the origin O to the centers of the three virtual pairs are all equal to L' , which lie along the X , Y and Z -axes, respectively. The screw systems of the three branches of the virtual mechanism in the base coordinate system are:

$$[\mathbf{G}_i^0] = [\mathcal{S}_0^i \ \mathcal{S}_1^i \ \mathcal{S}_2^i \ \mathcal{S}_3^i \ \mathcal{S}_4^i \ \mathcal{S}_5^i] \quad i = 1, 2, 3, \quad (6.76)$$

where $[\mathbf{G}_i^0]$ is just the first-order influence matrix

6.5.2 Principal Screws and Full-Scale Feasible Motions

Three configurations of this mechanism will be analyzed as follows:

6.5.2.1 Original Configuration

In this configuration, the parameters of the 3-RPS pyramid mechanism are taken as follows: $m = 0.2 \text{ m}$; $l_1 = l_2 = l_3 = 0.2 \text{ m}$; and $\theta_1 = \theta_2 = \theta_3 = 90^\circ$.

Using the previous method, we obtain the Jacobian matrices $[G]$ and $[G']$, respectively, as follows:

$$[G] = \begin{bmatrix} 0.5 & -0.5 & 0.5 \\ 0.5 & 0.5 & -0.5 \\ -0.5 & 0.5 & 0.5 \end{bmatrix}, \quad [G'] = \begin{bmatrix} 2.5 & 2.5 & -2.5 \\ -2.5 & 2.5 & 2.5 \\ 2.5 & -2.5 & 2.5 \end{bmatrix}. \quad (6.77)$$

Substituting the elements of matrices $[G]$ and $[G']$ into Eq. (6.18), we can obtain the pitches of the three principal screws from the condition $D = 0$. They are as follows:

$$\begin{aligned} h_x &= 0.2, \\ h_\beta &= h_\gamma = -0.1. \end{aligned}$$

The twist screw system under this configuration belongs to the first special three-system presented by Hunt. Ball [1] described a planar representation of the three-system. Using the theory shown in [8], we also obtain the same pitches of the principal screws. Substituting the elements of matrices $[G]$ and $[G']$ into the conic equation in [8], the coefficients of the conic are now as follows:

$$\begin{aligned} a_{11} &= a_{22} = a_{33} = 1.25 + 18.75h, \\ a_{12} &= a_{23} = a_{13} = 0.5(-2.5 - 12.5h). \end{aligned} \quad (6.78)$$

When $I_2 = 0$ ($I_2 = a_{11}a_{22} - a_{12}^2$), two possible roots of h are $h_1 = -0.1$ and $h_2 = 0$. However, only h_2 satisfies the condition of the parabola. There are six conic types for the original configuration of the mechanism as shown in Table 6.2. Figure 6.14 illustrates a planar representation of all possible twist screws in this case. It denotes the relations between the pitches of the output twist screws and the three linear inputs. Let $u = \dot{L}_1/\dot{L}_3$ and $w = \dot{L}_2/\dot{L}_3$. When $h_x = 0.2$, the corresponding inputs are $\dot{L} = (1 \ 1 \ 1)$, which is a point in Fig. 6.14. When $h_\beta = h_\gamma = -0.1$, the conic degenerates into a pair of superposition lines, whose equation is $y = -x - 1$.

Table 6.2 Original configuration

The range of the values of h	The types of conic
$0 < h < 0.2$	(1) Real ellipse
$h > 0.2$ or $h < -0.1$	(2) Imaginary ellipse (motions of the nonexistence)
$h_x = 0.2$	(3) Dot ellipse (a pair of imaginary intersecting lines)
$-0.1 < h < 0$	(4) Hyperbola
$h = 0$	(5) Parabola
$h_\beta = h_\gamma = -0.1$	(6) A pair of superposition lines

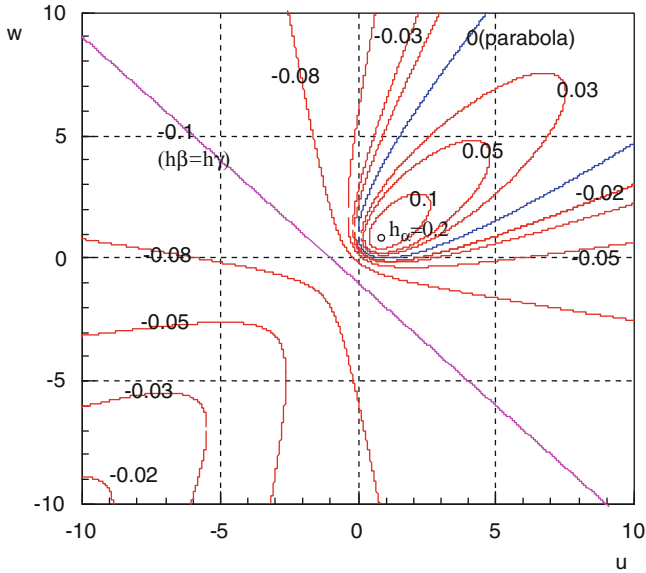


Fig. 6.14 Possible pitches for original configuration

Substituting the elements of matrices $[G]$ and $[G']$ into the quadric equation (6.15) or (6.16), the coefficients of the quadric are given by:

$$\begin{aligned}
 c_{11} &= c_{22} = c_{33} = 62.5h, \\
 c_{12} &= c_{23} = c_{13} = -6.25, \\
 c_{12} &= c_{23} = c_{13} = 0.5(2.5 - 12.5h), \\
 c_{44} &= -0.5 + 62.5h^3.
 \end{aligned}
 \tag{6.79}$$

The invariants of the quadric are as follows:

$$\begin{aligned}
 I &= 187.5h, \\
 J &= -117.187 + 11,718.8h^2, \\
 D &= 24,414(h + 0.1)^2(h - 0.2), \\
 \Delta &= 1.53 \times 10^7(h + 0.1)^2(h - 0.2)^2(h^2 + 0.2h + 0.01).
 \end{aligned}
 \tag{6.80}$$

According to the abovementioned theory, we can easily identify the three principal axes, α , β , and γ . The coordinates of the origin in the principal system can be obtained by solving Eq. (6.18), specifically $\mathbf{o}' = (0.1 \ 0.1 \ 0.1)$. The eigenvector $(-0.57725, -0.57735, \text{ or } -0.57735)$ corresponding to the eigenvalue k_1 is taken as the z' -axis in the system $(\mathbf{o}'-x'y'z')$. It implies that the angles between the z' -axis and the $X, Y,$ and Z -axes in the base system are all 54.7 . In fact, the points \mathbf{o}' and z' -axis

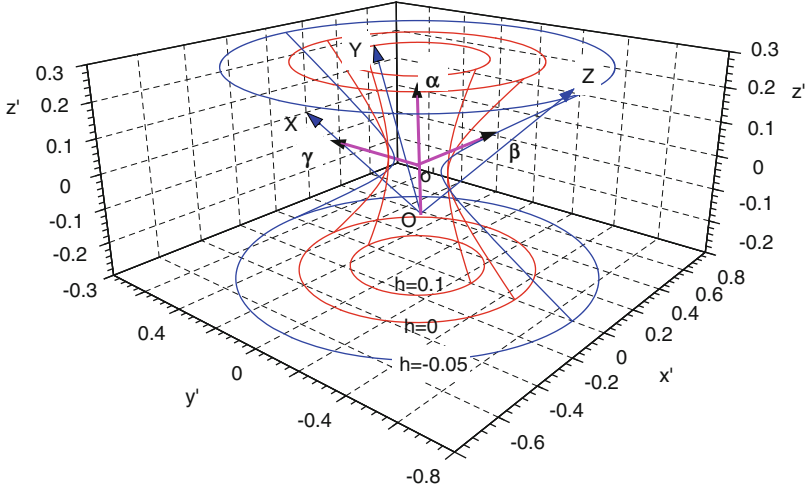


Fig. 6.15 Axis distribution for the original configuration

are the center and nodal axis of the hyperboloid, respectively. Since $k_2 = k_3$, we can arbitrarily select the x' -axis and y' -axis that are perpendicular to the z' -axis in a plane. For convenience, the x' -axis and y' -axis are taken as follows:

$$\begin{aligned} x' &= (0 \quad -0.707107 \quad 0.707107), \\ y' &= (0.816497 \quad -0.408248 \quad 0.408248). \end{aligned} \quad (6.81)$$

When $h = -0.05$, $h = 0$ and $h = 0.1$, the normal equations of the hyperboloid in the system $o'-x'y'z'$ are given by:

$$\begin{aligned} \frac{x^2}{0.0125} + \frac{y^2}{0.0125} - \frac{z^2}{0.0125} &= 1 \quad (h = -0.05), \\ \frac{x^2}{0.02} + \frac{y^2}{0.02} - \frac{z^2}{0.01} &= 1 \quad (h = 0), \\ \frac{x^2}{0.02} + \frac{y^2}{0.02} - \frac{z^2}{0.04} &= 1 \quad (h = 0.1). \end{aligned} \quad (6.82)$$

In Fig. 6.15, there are three hyperboloids that give out the three different distributions of all the screws with the above three pitches in space, respectively. They are all revolving hyperboloids with the same center and nodal axes. The system $O-XYZ$ is the base system, and the system $o'-x'y'z'$ is the principal system. When h takes any value within the range of $h_y < h < h_x$, all corresponding hyperboloids still have the same center and nodal axes. When the pitch of the screw vanishes, $h = 0$, the output motion of the end-effector becomes a pure rotation. Infinite pure rotations can be realized by the end-effector of the manipulator. These rotational axes lie on the same hyperboloid of one sheet with $h = 0$, as shown in Fig. 6.15.

6.5.2.2 Three Input Links Have the Same Length

In this second configuration, we take the parameters of the 3-RPS pyramid mechanism as follows: $m = 0.2$ m; $l_1 = l_2 = l_3 = 0.2795$ m; and $\theta_1 = \theta_2 = \theta_3 = 80^\circ$. Similarly, we obtain the Jacobian matrices $[G]$ and $[G']$ as follows:

$$[G] = \begin{bmatrix} 0.355 & -0.703 & 0.881 \\ 0.881 & 0.355 & -0.703 \\ -0.703 & 0.881 & 0.355 \end{bmatrix}, \quad [G'] = \begin{bmatrix} 3.368 & 0.946 & -1.960 \\ -1.960 & 3.368 & 0.946 \\ 0.946 & -1.960 & 3.368 \end{bmatrix}. \quad (6.83)$$

In this configuration, the corresponding coefficients of the conic are:

$$\begin{aligned} a_{11} = a_{22} = a_{33} &= 1.19469 + 16.0974h, \\ a_{12} = a_{23} = a_{13} &= 0.5(-2.45063 - 10.5395h). \end{aligned} \quad (6.84)$$

By means of the quadric degenerating theory, the pitches of the three principal screws are:

$$\begin{aligned} h_x &= 0.226708, \\ h_\beta = h_\gamma &= -0.113354. \end{aligned}$$

The twist screw system in this configuration also belongs to the first special screw system. When $l_2 = 0$, two possible roots of h are $h_1 = -0.1133$ and $h_2 = 0.0028$. However, only h_2 satisfies the condition of the parabola. There are also six conic types at this case, as shown in Table 6.3. Figure 6.16 illustrates all possible twist screws by a planar representation. When $h_x = 0.2267$, the corresponding inputs are $\vec{L} = (1 \ 1 \ 1)$, which is a point in Fig. 6.16. When $h_\beta = h_\gamma = -0.1133$, the conic degenerates into a pair of superposition lines, whose equation is also $y = -x - 1$.

In this configuration, the coefficients of the quadric are:

$$\begin{aligned} c_{11} = c_{22} = c_{33} &= 50.25h, \\ c_{12} = c_{23} = c_{13} &= -5.70, \\ c_{14} = c_{24} = c_{34} &= 0.5(3.688 - 16.269h), \\ c_{44} &= -1.042 + 2.0137h + 50.25h^3. \end{aligned} \quad (6.85)$$

The invariants of the quadric are as follows:

$$\begin{aligned} I &= 150.75h, \\ J &= -97.133 + 7,574.99h^2, \\ D &= 126,880(h + 0.1133)^2(h - 0.2267), \\ \Delta &= 6.38 \times 10^6(h + 0.1133)^2(h - 0.2267)^2(h^2 + 0.2267h + 0.0128). \end{aligned} \quad (6.86)$$

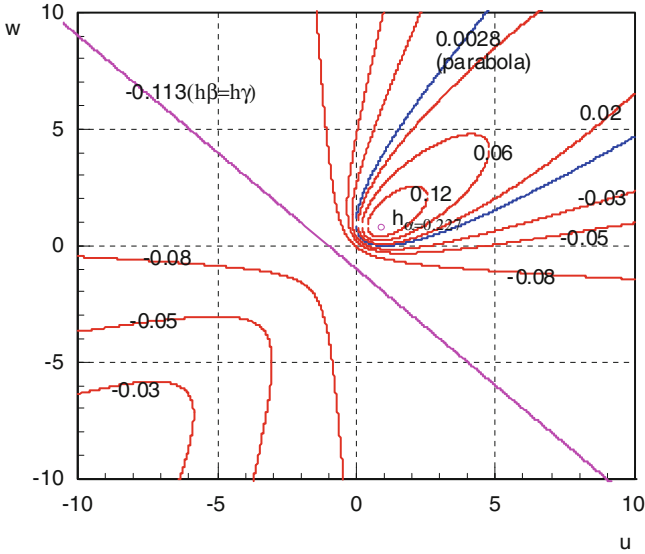


Fig. 6.16 Pitch distribution for the second configuration

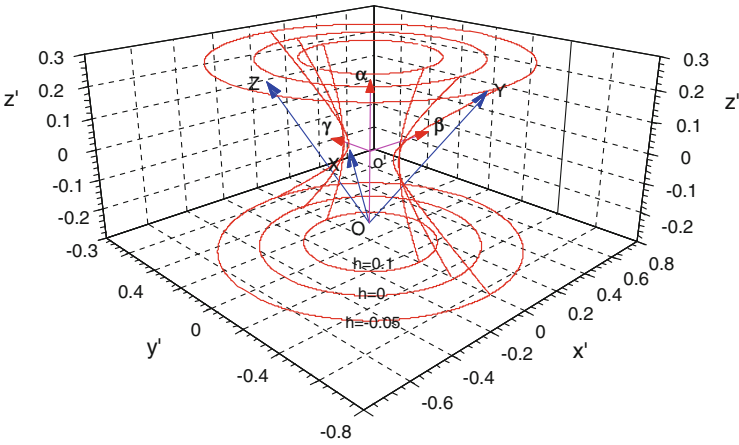


Fig. 6.17 Axis distribution for the second configuration

Then three axes of α , β and γ may be obtained. The coordinates of the center point o' of the hyperboloid are $(0.162 \ 0.162 \ 0.162)$ by solving Eq. (6.16). The Fig. 6.17 is similar to Fig. 6.15. The characteristic equation of the matrix $[D]$ has the same roots. The direction $(-0.57725, -0.57735, -0.57735)$ is taken as the z' -axis. The x' -axis and y' -axis are as follows:

$$\begin{aligned}
 x' &= (-0.630531 \ 0.764513 \ -0.133982), \\
 y' &= (-0.510824 \ -0.296216 \ 0.807041)
 \end{aligned}$$

Table 6.3 Three lengthened input links have the same length

The range of the values of h	The types of conic
$0.0028 < h < 0.2267$	1. Real ellipse
$h > 0.2267$ or $h < -0.1133$	2. Imaginary ellipse (motions of the nonexistence)
$h_x = 0.2267$	3. Dot ellipse (a pair of imaginary intersecting lines)
$-0.1133 < h < 0.0028$	4. Hyperbola
$h = 0.0028$	5. Parabola
$h_\beta = h_\gamma = -0.1133$	6. A pair of superposition lines

When $h = -0.05$, $h = 0$ and $h = 0.1$, the normal equations of the hyperboloid can be obtained as follows:

$$\begin{aligned}
 \frac{x^2}{0.0175} + \frac{y^2}{0.0175} - \frac{z^2}{0.004} &= 1 & (h = -0.05) \\
 \frac{x^2}{0.0257} + \frac{y^2}{0.0257} - \frac{z^2}{0.0129} &= 1 & (h = 0) \\
 \frac{x^2}{0.027} + \frac{y^2}{0.027} - \frac{z^2}{0.0455} &= 1 & (h = 0.1)
 \end{aligned} \tag{6.87}$$

Figure 6.17 shows the three principal screws and the spatial distributions of the axes of all possible screws. They are all hyperboloids of revolution with the same nodal z' -axes, and the difference between the two configurations is that the center points of the two sets of hyperboloids are different (Table 6.3).

6.5.2.3 Common Configuration

When the parameters of this mechanism are taken as $m = 0.2$ m; $l_1 = 0.195$ m, $l_2 = 0.164$ m, $l_3 = 0.117$ m; and $\theta_1 = 80^\circ$, $\theta_2 = 110^\circ$, $\theta_3 = 100^\circ$, this mechanism is under a common configuration. The matrices $[G]$ and $[G']$ are then given by:

$$[G] = \begin{bmatrix} 0.63 & -0.48 & 0.20 \\ 0.42 & 0.44 & -0.28 \\ -0.32 & 0.32 & 0.44 \end{bmatrix}, \quad [G'] = \begin{bmatrix} 1.74 & 3.62 & -2.50 \\ -3.07 & 2.13 & 4.27 \\ 2.72 & -2.10 & 1.79 \end{bmatrix}. \tag{6.88}$$

In this configuration, the coefficients of the conic are:

$$\begin{aligned}
 a_{11} &= 1.062 + 19.825h & a_{12} &= 0.5(-2.522 - 11.89h) \\
 a_{22} &= 1.461 + 22.086h & a_{23} &= 0.5(-2.823 - 7.364h) \\
 a_{33} &= 0.922 + 27.695h & a_{13} &= 0.5(-2.082 - 25.238h),
 \end{aligned} \tag{6.89}$$

Table 6.4 General configuration

The range of the values of h	The types of conic
$0.00100035 < h < 0.169387$ or $-0.111568 < h < -0.0939974$	(1) Real ellipse
$h > 0.169387$ or $h < -0.111568$	(2) Imaginary ellipse
$h_x = 0.169387$ or $h_y = -0.111568$	(3) Dot ellipse (a pair of imaginary intersecting lines)
$-0.0939974 < h < -0.057819$ or $-0.057819 < h < -0.00100035$	(4) Hyperbola
$h = 0.00100035$ or $h = -0.0939974$	(5) Parabola
$h_\beta = -0.057819$	(6) A pair of superposition lines

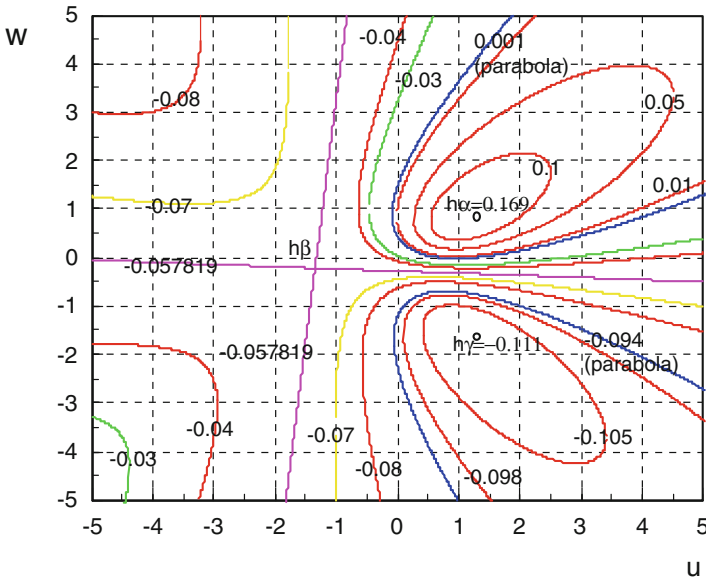


Fig. 6.18 Screw representations for the general configuration

The pitches of the three principal screws are:

$$\begin{aligned}
 h_x &= 0.169387 \\
 h_\beta &= -0.057819 \\
 h_\gamma &= -0.111568.
 \end{aligned}
 \tag{6.90}$$

They all are finite and different from each other. The twist system of this configuration forms a general three-system. When $I_2 = 0$, two possible roots, $h_1 = -0.0939974$ and $h_2 = 0.00100035$, corresponding to two parabolas are obtained. There are also six conic types in this case, as shown in Table 6.4. Figure 6.18 illustrates a planar representation of all possible twist screws. When $h_x = 0.169387$,

the corresponding inputs are $\dot{\mathbf{L}} = (1.08482 \ 0.907773 \ 1)$, which is a point shown in Fig. 6.18. When $h_\gamma = -0.111568$, the corresponding point is $\dot{\mathbf{L}} = (-1.35046 \ -0.215642 \ 1)$ in Fig. 6.18. When $h_\beta = -0.057819$, the conic degenerates into a pair of intersecting real lines whose equations are $w = 10.0108u + 13.3036$ and $w = -0.045641u - 0.277278$, respectively. The inputs corresponding to the intersecting point of the two lines are $\dot{\mathbf{L}} = (1.2135 \ -1.72073 \ 1)$.

In this configuration, the coefficients of the quadric are given by:

$$\begin{aligned}
 c_{11} &= c_{22} = c_{33} = 82.5173h \\
 c_{12} &= -4.9505, c_{23} = -7.06637, c_{13} = -8.7751 \\
 c_{14} &= 0.5(2.49987 - 4.88798h) \\
 c_{24} &= 0.5(1.62049 - 14.1963h) \\
 c_{34} &= 0.5(1.7355 - 15.4988h) \\
 c_{44} &= -0.278376 - 0.424558h + 85.5173h^3.
 \end{aligned} \tag{6.91}$$

The invariants of the quadric are as follows:

$$\begin{aligned}
 I &= 247.55h, \\
 J &= -151.44 + 20427.3h^2 \\
 D &= 561869(h + 0.111468)(h + 0.057819)(h - 0.169387) \\
 \Delta &= 4.64 \times 10^7 (h + 0.111568)^2 (h + 0.057819)^2 (h - 0.169387)^2
 \end{aligned} \tag{6.92}$$

The coordinates of the center point of the hyperboloid are $\mathbf{o}' = (0.0296 \ 0.086 \ 0.0939)$. Since the three eigenvalues of the matrix $[\mathbf{D}]$ are all different, the eigenvectors corresponding to the eigenvalues may be taken as the three axes in system $(o'-x'y'z')$. They are as follows:

$$\begin{aligned}
 x' &= (0.571619 \ -0.807634 \ 0.144837) \\
 y' &= (0.581944 \ 0.274608 \ -0.765462) \\
 z' &= (0.57844 \ 0.52184 \ 0.626969)
 \end{aligned}$$

When $h = -0.08$ and $h = 0.08$, the normal equations of the hyperboloid in system $o'-x'y'z'$ are:

$$\begin{aligned}
 \frac{x^2}{0.01712} + \frac{y^2}{0.0123} - \frac{z^2}{0.0264} &= 1 \quad (h = 0.08) \\
 \frac{x^2}{0.00787} + \frac{z^2}{0.0007} - \frac{y^2}{0.00553} &= 1 \quad (h = -0.08).
 \end{aligned} \tag{6.93}$$

Figure 6.19 expresses the three principal screws and the formations of all possible twist screws with the above two pitches for this configuration in 3D space. The two hyperboloids have different nodal axes. For h is within $h_\beta < h < h_\alpha$,

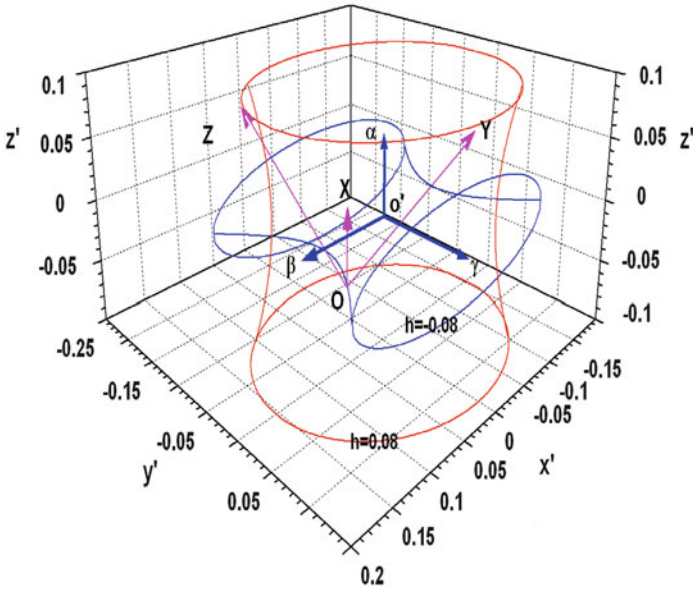


Fig. 6.19 Axis distribution for the general configuration

the corresponding hyperboloids of one sheet have the same shape as that of the one with $h = 0.08$. The direction of the nodal axes is along the z' -axis, namely, the α -axis. For $h_\gamma < h < h_\beta$, the shape of the hyperboloid is the same as that of the one with $h = -0.08$. The direction of the nodal axes is along the y' -axis, namely, the γ -axis. Compared with the first two configurations, the hyperboloids in this case are not revolving but the most general hyperboloids.

6.6 A 3-DOF Rotational Parallel Manipulator Without Intersecting Axes

In this section, we discuss an interesting new issue. This will use the above theory, although it is only presented as an idea for further study.

Parallel manipulators with less than 6 DOF attract much attention due to their fewer active legs, large workspace, simple structure, ease of control, and simpler kinematic solutions. 3-DOF spherical parallel manipulators (SPMs) are a class of parallel manipulators with reduced DOF. The 3-RRR parallel manipulator proposed by Cox [22] in 1981 is one of the most famous SPMs. This manipulator consists of a base, a moving platform and three branches. It is difficult to obtain higher precision in manufacturing the parallel manipulators comprising a 3-RRR chain with multiple revolute joint axes intersecting at one point. This is a new important issue. It is difficult to make parallel manipulators (PMs) with multiple revolute joint axes intersecting at one point. These types containing similar issues besides 3-RRR SPMs include many different 4-DOF 3R1T and 2R2T as well as 5-DOF 3R2T PMs, to name a few. This problem makes it hard to achieve the expected mobility.

Including the abovementioned issue for the lower-mobility parallel mechanisms, this has resulted four issues in mechanical-structure design and manufacture problems that have gradually gained attention in recent years. These include the following:

- (i) **Coupled motions:** Most PMs suffer from the problems of coupled motions, which bring us some difficulties with regards to motion planning and controlling in applications.
- (ii) **Over-constrained:** The over-constrained manipulators have the drawback of jamming or undergoing high internal loads when geometric errors occur [23].
- (iii) **Parasitic motions:** The parasitic motions means the motions in the unspecified motion [24]. The parasitic motions lead to complex kinematics, require real-time compensation, and increase the difficulties of calibrating.
- (iv) **Intersecting axes:** This kind of problem exist in some types of PMs, including the 3-DOF spherical parallel manipulators (SPMs), the 4-DOF 3R1T and 2R2T PMs, and the 5-DOF 3R2T PMs, to name a few. The restricted geometrical conditions in these PMs are usually difficult to fulfill.

The first three problems have already been studied by many researchers. Some decoupled PMs have been invented to solve the problem of coupled motions [25–27]. Many non-over-constrained PMs have also been designed [23, 28]. Some optimization methods have been introduced to avoid or minimize the parasitic motions [24], and some mechanism without parasitic motion was proposed [29]. However, few works have studied the problem of intersecting axes [14].

In 1996, a 3-DOF 3-RPS cubic PM was proposed by Huang [21]. Recently, we noticed that this PM has 3 revolute freedoms but does not have intersecting axes.

Could this mechanism be applied to the requirement of 3D revolute motion? If so, the next question that should be answered is how big is its orientation capability? Can the capability satisfy a general requirement for a 3D revolute mechanism? It is the key issue that must be discussed for the mechanism to be a 3D rotational one. In order to study the orientation capability, there is a need to analyze the full-scale feasible instant screws of a mechanism to obtain its work extension. Therefore, we discuss this issue in this Chapter.

6.6.1 An Open Problem of the PMs with Intersecting Axes

There is a need to further analyze this issue. We should consider the effect of the PMs having intersecting rotational axes. Here, we take the 3-RRR spherical parallel mechanism (SPM) as an example to show this issue [14].

The 3-RRR SPM, as shown in Fig. 6.20a, was first proposed by Cox in 1981[22]. Its mobility is 3; however, the number is only a theoretical result [32]. Due to the unavoidable errors that may occur during the manufacturing process, it would be impossible to realize all the joint axes intersecting at one point. It is very likely that these axes would intersect at different points. One possible example is shown in Fig. 6.20b.

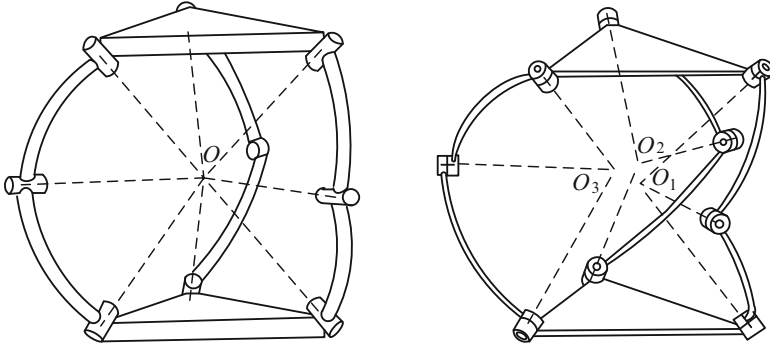


Fig. 6.20 3-RRR SPM with manufacturing errors

The example can be described as follows. First, the axes of the three revolute joints in the i -th branch intersect at a point O_i , but the three intersecting points O_1, O_2, O_3 of the three limbs do not coincide with each other. For each limb, the common point is selected as the origin point of the limb coordinate system and the three screws can be expressed as follows:

$$\begin{aligned} \mathcal{S}_{i1} &= (a_{i1} \quad b_{i1} \quad c_{i1}; \quad 0 \quad 0 \quad 0) \\ \mathcal{S}_{i2} &= (a_{i2} \quad b_{i2} \quad c_{i2}; \quad 0 \quad 0 \quad 0) \\ \mathcal{S}_{i3} &= (a_{i3} \quad b_{i3} \quad c_{i3}; \quad 0 \quad 0 \quad 0). \end{aligned} \quad (6.94)$$

where a_{ij}, b_{ij} , and c_{ij} stands for the direction cosines of axis of the j -th revolute joint in the i -th branch; and $i, j = 1, 2, 3$.

This is a three-screw system, and there are three reciprocal screws \mathcal{S}^r given by:

$$\begin{aligned} \mathcal{S}_{i1}^r &= (1 \quad 0 \quad 0; \quad 0 \quad 0 \quad 0) \\ \mathcal{S}_{i2}^r &= (0 \quad 1 \quad 0; \quad 0 \quad 0 \quad 0) \\ \mathcal{S}_{i3}^r &= (0 \quad 0 \quad 1; \quad 0 \quad 0 \quad 0). \end{aligned} \quad (6.95)$$

The three reciprocal screws with zero-pitch pass the intersecting point. Under this case, among all nine constraints, there are six constraint forces being linearly independent, as shown in Table 2.1. Thus, three redundant constraint forces exist, i.e., $\nu = 3$. Then, using the modified G-K criterion, Eq. (3.5), we have:

$$M = 6(n - g - 1) + \sum_{i=1}^g f_i + \nu = 6(8 - 9 - 1) + 9 + 3 = 0, \quad (6.96)$$

which indicates that the mobility of the mechanism vanishes. In other words, when the abovementioned errors occur, axes cannot intersect at a single point, and the manipulator cannot move at all. This example discussed above is one of the possible cases during the manufacturing process. In practice, among the nine axes, the pose of each

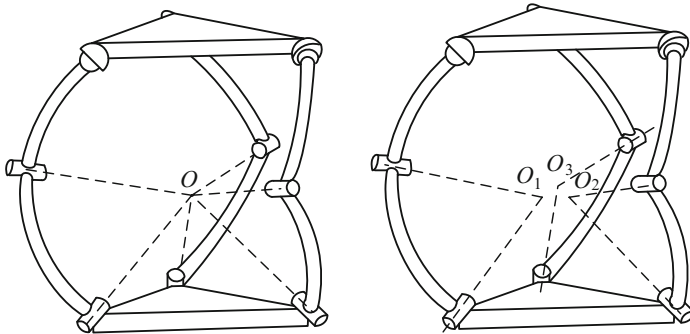


Fig. 6.21 The 3-RRS SPM

axis is variable and even no lines intersect, this is the worst situation. In other words, if all these axes are not converging to a point, the 3-RRR SPM cannot move at all. This is why many mechanisms of this type cannot work well as expected when they have been manufactured. Somebody may point out that many practical 3-RRR SPMs can realize 3D rotation. Actually, it is impossible unless there are enough clearances in kinematic pairs, and this can greatly reduce mechanism accuracy.

The 3-RRR SPM is an over-constrained PM. However, there are also many non-over-constrained SPMs [28], such as 3-RRS. Does it also have this problem? The next section briefly analyzes the problem.

For a non-over-constrained SPM, e.g., a 3-RRS SPM [28], the third kinematic pair in each limb is replaced by a spherical pair. Compared with the 3-RRR SPM, the number of all constraint forces exerted on the 3-RRS platform is reduced to three, but nine have no over-constraints. However, it still requires six intersecting axes, as shown in Fig. 6.21a. The platform maintains three rotational freedoms and can rotate about any line passing through the intersecting point of the three constraint forces. However, when the three constraint forces do not intersect at a point under the influence of manufacturing errors, as shown in Fig. 6.21b, the mobility of the non-over-constrained SPM cannot rotate about a fixed point, which means it is not an SPM anymore.

This similar problem of the 3-DOF SPMs also occurs on other kinds of 3-5 DOF PMs with intersecting axes.

Can we find or synthesize a kind of lower mobility PMs, as shown above (iv), without intersecting joint axes and can realize the same motion? This is an open problem that can be fully understood with further research.

6.6.2 A 3-D Revolute Mechanism Without Intersecting Axes

Here, a 3-RPS cubic PM [21] without intersecting axes is introduced. This can also achieve 3D rotational motions.

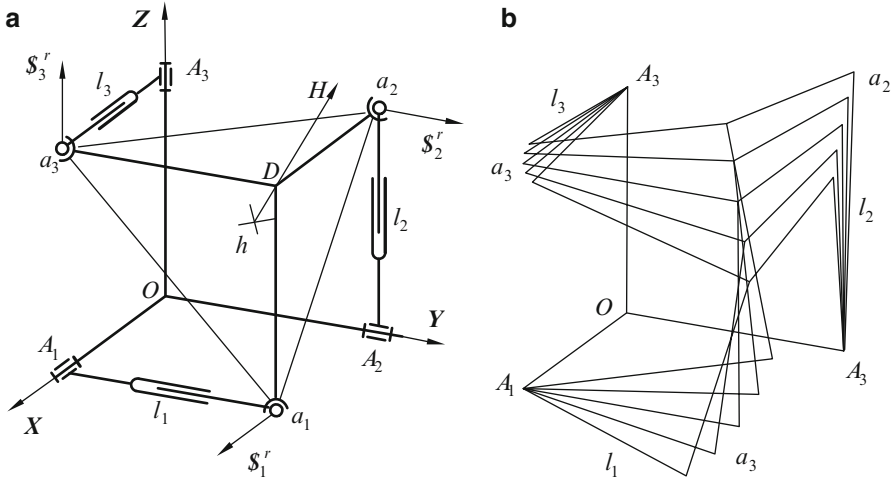


Fig. 6.22 3-RPS cubic parallel manipulator (a) 3-RPS pyramid mechanism (b) PM at different configurations

As shown in Fig. 6.22a, the 3-RPS cubic PM consists of a pyramid base, a pyramid platform and three branches; it also has a cubic origin configuration. In addition, each branch is formed by a revolute joint R, an actuated prismatic joint P, and a spherical joint S.

6.6.2.1 Mobility Analysis of the 3-RPS Cubic PM

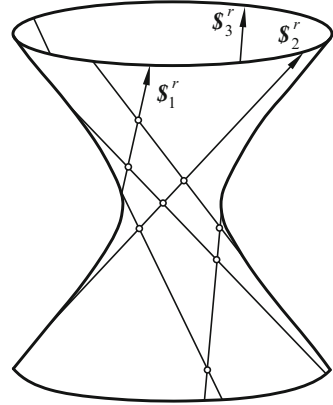
For the whole manipulator, the constraint screw system consists of three constraint forces ($\mathcal{S}_1^r, \mathcal{S}_2^r$ and \mathcal{S}_3^r) that do not intersect with each other. As shown in Fig. 6.23, at the initial configuration, the constraint screws can be written in the coordinate system O - XYZ as:

$$\begin{aligned} \mathcal{S}_1^r &= (1 \quad 0 \quad 0; \quad 0 \quad 0 \quad -1) \\ \mathcal{S}_2^r &= (0 \quad 1 \quad 0; \quad -1 \quad 0 \quad 0) \\ \mathcal{S}_3^r &= (0 \quad 0 \quad 1; \quad 0 \quad -1 \quad 0), \end{aligned} \tag{6.97}$$

The three constraint forces, as shown in Fig. 6.23, lying on a hyperboloid of one sheet are linearly independent. Their reciprocal screws are the rotational axes. Using the modified G-K criterion, Eq. (3.4), we can obtain the mobility of the 3-RPS cubic PM as:

$$\begin{aligned} M &= 6(n - g - 1) + \sum_{i=1}^g f_i + v \\ &= 6(8 - 9 - 1) + 15 + 0 = 3 \end{aligned} \tag{6.98}$$

Fig. 6.23 Three constraint forces lying on a hyperboloid of one sheet



When the configuration of the platform changes, the constraint screw system still contains three linearly independent constraint forces, as shown in Fig. 6.23; thus, the mobility is not instantaneous.

6.6.2.2 The Property of Mobility and Full-Scale Feasible Moving Screws

Since the platform is constrained by three constraint forces, its three translational freedoms are constrained; thus, this manipulator only has three rotational freedoms. However, the rotation axes must intersect with three constraint forces simultaneously. Those rotation-axis lines do not pass a common point, and this manipulator is not a SPM.

The 3-DOF 3-RRR SPM has a sufficient orientation workspace, as shown in Fig. 6.24. If we transfer all the possible revolute screw axes of that mechanism to a common point O , they can also form a coniform, as shown in Fig. 6.24a.

As shown in Fig. 6.23, three constraint forces lie on a hyperboloid of one sheet, and all of these are in the same regulus. All the lines forming the other reguli also lie on the same hyperboloid, which intersect with all the three constraint forces, thereby satisfying the requirements to be rotational axes. This means that the possible revolute axes with different directions are infinite; moreover, they all lie on the same hyperboloid, but on different reguli. Furthermore, from the analysis in Sect. 6.5, each configuration of the 3-RPS pyramid mechanism has full-scale feasible screws, as exemplified by the following two figures shown. Figure 6.25 denotes all the possible infinite pitches. When different three inputs are given, they fulfill the entire u - w coordinate plane, as shown in Fig. 6.25a. This means that every point in the coordinate plane indicates a screw with corresponding h . The h is between two extrema, namely, h_x and h_y . The pitches of points in each curve in the u - w coordinate plane are identical h . Different curves have different pitches, and all the curves are quadratic curves. Each quadratic curve corresponds to a hyperboloid of one sheet, and there are infinite quadratic curves providing full coverage of the space shown in Fig. 6.24. All the screw axes, no matter how big each pitch itself is, congregate in Fig. 6.25b.

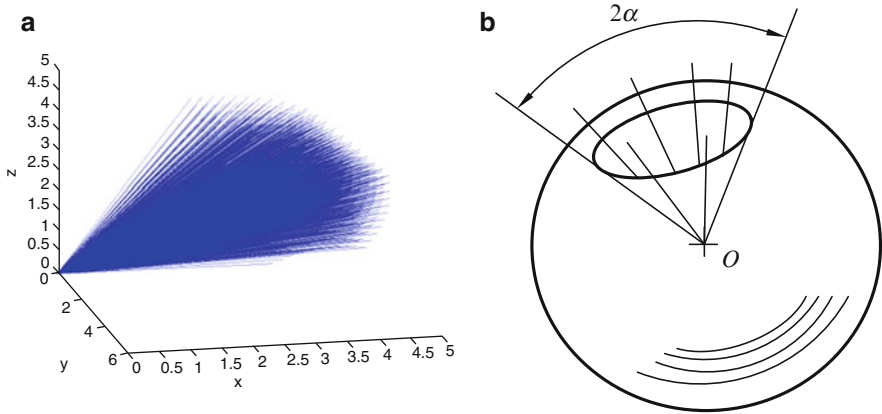


Fig. 6.24 Orientation workspace for the mechanism (a) Axes distribution passing a point (b) Orientation space

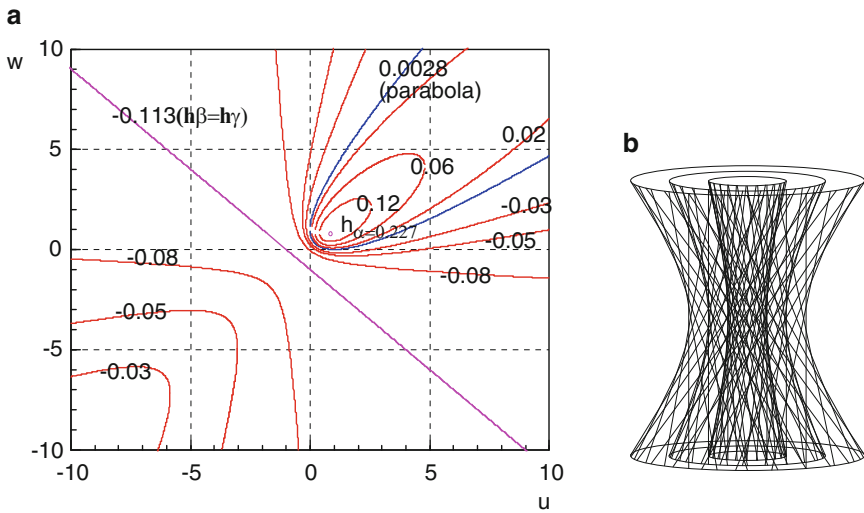
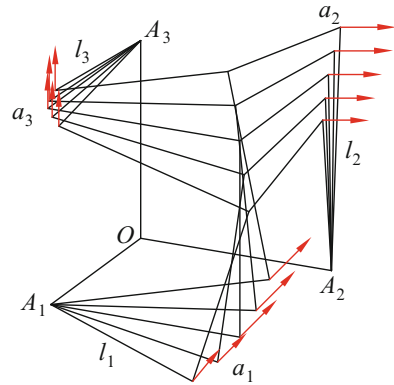


Fig. 6.25 A continuously changeable space (a) Continuously changeable pitches (b) Continuously changeable axes

Figure 6.25 illustrates full-scale feasible screw axes for the configuration of this mechanism. It certainly can overflow with a part of space. There are now two more questions that must be addressed:

1. For different configurations, is the occupying area in space variable?
2. How big is the maximum occupying spatial area? Can it satisfy the work requirement?

Fig. 6.26 Different hyperboloids



When the configuration of this manipulator continuously changes (Fig. 6.26), the positions of the three constraint forces change and they are also linearly independent and do not intersect on a common point. Thus, when the manipulator is at different configurations, the different hyperboloids also exist and the reguli for the rotational axes also exist and overflow with a part of space similar to that shown in Fig. 6.24. It is clear that the directions of the rotational axes are continuously changeable.

This 3-RPS cubic PM has three rotational freedoms, and the three constraint forces are designed not to intersect at a point. When the manufacturing errors exist, it only changes the position or direction of the constraint forces, but the property of three constraint screw system is still the same. Thus, the manufacturing error has no influence on the motion property of this manipulator. From the above analysis, we know that it is possible to synthesize a 3D rotation mechanism without intersecting axes. Following the 3D rotation motion of this mechanism, the parasitic motions also exist, which is a disadvantage. Unfortunately, the parasitic motion is unavoidable, but it can be accurately calculated and completely compensated.

6.6.3 The Orientation Workspace

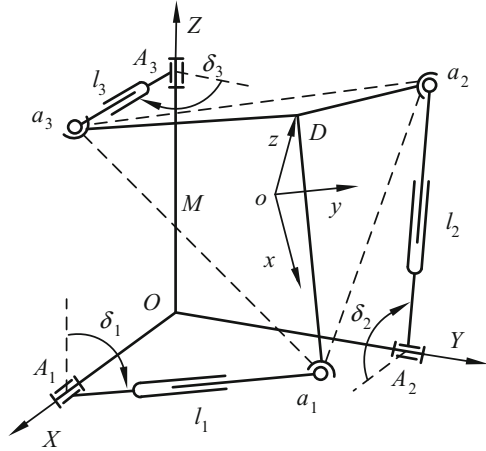
To judge its work power, we determine the angular range or angular workspace of this mechanism. For its application, it should have sufficient workspace.

6.6.3.1 Position Analysis of the 3-RPS Cubic PM

For a manipulator with three rotational freedoms, the orientation workspace is very important. In order to obtain the orientation workspace, the position analysis of this PM is introduced first.

The coordinate systems of the 3-RPS cubic PM are shown in Fig. 6.27. The length of the base side OA_i and the platform side a_iD of the cubic PM are M . We let

Fig. 6.27 The coordinate systems of the 3-RPS cubic PM



$\{\mathbf{B}\}$ be the global coordinate systems O - XYZ fixed on the base on O , and the three coordinate axes of $\{\mathbf{B}\}$ are coaxial with the three revolute joint axes of this manipulator. Let $\{\mathbf{m}\}$ be the coordinate system o - xyz fixed on the platform on o , which is located on the center of the equilateral triangle (a_1, a_2, a_3) . The z -axis of $\{\mathbf{m}\}$ is perpendicular to the plane defined by a_1, a_2 and a_3 , and the y -axis is parallel with a_3, a_2 (Fig. 6.27).

(1) Direct Position Analysis

The direct position analysis has been solved in [8]. When the lengths l_i of the three input links are given, the three angles δ_i can be obtained. Then, we can also obtain the coordinates of the three moving points a_i and the orientation of the platform.

(2) Inverse Position Analysis and Parasitic Motions

The orientation of the platform with respect to the base frame $\{\mathbf{B}\}$ is given by the orientation matrix \mathbf{R} , given by:

$$\mathbf{R} = \begin{bmatrix} r_{11} & r_{12} & r_{13} \\ r_{21} & r_{22} & r_{23} \\ r_{31} & r_{32} & r_{33} \end{bmatrix}. \quad (6.99)$$

The coordinates of the fixed point A_i in $\{\mathbf{B}\}$ are:

$$\mathbf{A}_1 = \begin{bmatrix} M \\ 0 \\ 0 \end{bmatrix}, \quad \mathbf{A}_2 = \begin{bmatrix} 0 \\ M \\ 0 \end{bmatrix}, \quad \mathbf{A}_3 = \begin{bmatrix} 0 \\ 0 \\ M \end{bmatrix}. \quad (6.100)$$

The coordinates of the points a_i in $\{\mathbf{m}\}$ are:

$$\mathbf{a}'_1 = \begin{bmatrix} \sqrt{6}M/3 \\ 0 \\ 0 \end{bmatrix}, \quad \mathbf{a}'_2 = \begin{bmatrix} -\sqrt{6}M/6 \\ \sqrt{2}M/2 \\ 0 \end{bmatrix}, \quad \mathbf{a}'_3 = \begin{bmatrix} -\sqrt{6}M/6 \\ -\sqrt{2}M/2 \\ 0 \end{bmatrix}. \quad (6.101)$$

The origin of $\{\mathbf{m}\}$ corresponding to $\{\mathbf{B}\}$ are:

$$\mathbf{o} = \begin{bmatrix} \mathbf{o}_x \\ \mathbf{o}_y \\ \mathbf{o}_z \end{bmatrix}. \quad (6.102)$$

The coordinate transformation formula between $\{\mathbf{B}\}$ and $\{\mathbf{m}\}$ is given by:

$$\mathbf{a}_i = \mathbf{o} + \mathbf{R}\mathbf{a}'_i. \quad (6.103)$$

Substituting Eqs. (6.99), (6.100), (6.101) and (6.102) into Eq. (6.103), we get:

$$\begin{aligned} \mathbf{a}_1 &= \begin{bmatrix} \mathbf{o}_x + \frac{\sqrt{6}}{3}\mathbf{M}r_{11} \\ \mathbf{o}_y + \frac{\sqrt{6}}{3}\mathbf{M}r_{21} \\ \mathbf{o}_z + \frac{\sqrt{6}}{3}\mathbf{M}r_{31} \end{bmatrix}, \quad \mathbf{a}_2 = \begin{bmatrix} \mathbf{o}_x - \frac{\sqrt{6}}{6}\mathbf{M}r_{11} + \frac{\sqrt{2}}{2}\mathbf{M}r_{12} \\ \mathbf{o}_y - \frac{\sqrt{6}}{6}\mathbf{M}r_{21} + \frac{\sqrt{2}}{2}\mathbf{M}r_{22} \\ \mathbf{o}_z - \frac{\sqrt{6}}{6}\mathbf{M}r_{31} + \frac{\sqrt{2}}{2}\mathbf{M}r_{32} \end{bmatrix}, \quad \mathbf{a}_3 \\ &= \begin{bmatrix} \mathbf{o}_x - \frac{\sqrt{6}}{6}\mathbf{M}r_{11} - \frac{\sqrt{2}}{2}\mathbf{M}r_{12} \\ \mathbf{o}_y - \frac{\sqrt{6}}{6}\mathbf{M}r_{21} - \frac{\sqrt{2}}{2}\mathbf{M}r_{22} \\ \mathbf{o}_z - \frac{\sqrt{6}}{6}\mathbf{M}r_{31} - \frac{\sqrt{2}}{2}\mathbf{M}r_{32} \end{bmatrix}. \end{aligned} \quad (6.104)$$

Given that A_i are all revolute pairs, the link $A_i a_i$ can only rotate about OA_i , which makes the x -coordinate of the point a_1 always equal to M , the y -coordinate of the point a_2 always equal to M , and the z -coordinate of the point a_3 always equal to M as follows:

$$\begin{cases} a_{1x} = M \\ a_{2y} = M \\ a_{3z} = M \end{cases} \quad (6.105)$$

Substituting Eq. (6.104) into Eq. (6.105), we obtain the coordinate of \mathbf{o} as:

$$\mathbf{o} = \begin{bmatrix} \mathbf{o}_x \\ \mathbf{o}_y \\ \mathbf{o}_z \end{bmatrix} = \mathbf{M} \begin{bmatrix} 1 - \frac{\sqrt{6}}{3}r_{11} \\ 1 + \frac{\sqrt{6}}{6}r_{21} - \frac{\sqrt{2}}{2}r_{22} \\ 1 + \frac{\sqrt{6}}{6}r_{31} + \frac{\sqrt{2}}{2}r_{32} \end{bmatrix}. \quad (6.106)$$

Equation (6.106) indicates that the coordinate of point o can vary depending on the orientation of the platform. Thus, this 3-RPS cubic PM has parasitic motions that are three translational motions along the three axes of $\{\mathbf{B}\}$. Although the platform has no translational freedoms, since the three rotational axes do not intersect at a point, the center of the platform can move a little while the rotations occur.

According to the definition of the link length, we have:

$$l_i = |A_i a_i|. \quad (6.107)$$

Substituting Eqs. (6.100) and (6.104) into Eq. (6.107), we obtain the values of the actuated joints as:

$$\begin{bmatrix} l_1 \\ l_2 \\ l_3 \end{bmatrix} = M \begin{bmatrix} \sqrt{\left(1 + \frac{\sqrt{6}}{2} r_{21} - \frac{\sqrt{2}}{2} r_{22}\right)^2 + \left(1 + \frac{\sqrt{6}}{2} r_{31} + \frac{\sqrt{2}}{2} r_{32}\right)^2} \\ \sqrt{\left(1 - \frac{\sqrt{6}}{2} r_{11} + \frac{\sqrt{2}}{2} r_{12}\right)^2 + \left(1 + \sqrt{2} r_{32}\right)^2} \\ \sqrt{\left(1 - \frac{\sqrt{6}}{2} r_{11} - \frac{\sqrt{2}}{2} r_{12}\right)^2 + \left(1 - \sqrt{2} r_{32}\right)^2} \end{bmatrix}. \quad (6.108)$$

The results of the position analysis show that when the orientation of the platform is given, we can obtain the value of actuated joints l_i . As the orientation matrix can be given freely, this manipulator can achieve any orientation continuously, and the same is true for the SPMs mentioned above. Moreover, as shown in Eq. (6.106), the expression of the coordinate of point o in $\{\mathbf{B}\}$, which indicates the parasitic motions of this manipulator, is so simple that the parasitic motions of the platform can be easily calculated when its orientations are given.

6.6.3.2 The Orientation Workspace

As mentioned above, the 3-RPS cubic PM can realize 3D rotation; however we do not know how big its orientation capability is. Can it satisfy a general requirement? In this section, we study the orientation workspace of 3-RPS cubic PM, which is defined as all reachable orientations of the platform in 3D space [30, 31].

(1) The Modified Euler Angles

To express the orientation, we use the modified Euler angles (φ, θ, ψ) proposed by Bonev and Ryu [30], which are slightly different from the traditional Euler angles and have some advantages [31].

By the definition of the modified Euler angles, as shown in Fig. 6.28, the coordinate system of the platform changes from its initial orientation o -xyz to the final orientation o -x'''y'''z''' by four steps. The platform (1) first rotates about its z -axis by an angle φ , (2) its y' -axis by an angle θ , (3) its z'' -axis by an angle $-\varphi$, and (4) finally its z''' -axis by an angle ψ . Defined in this way, ψ is the roll angle, θ is

Fig. 6.28 The modified Euler angles

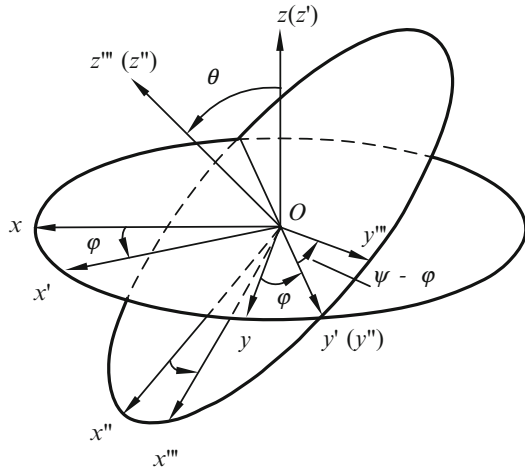
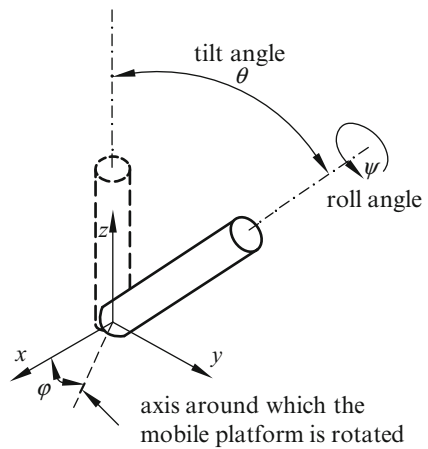


Fig. 6.29 The modified Euler angles [30]



the tilt (pitch) angle, and φ is the angle (yaw), indicating the axis around which the platform is rotated (tilted) (Fig. 6.29). The rotation matrix R_m in this case is given by:

$$\begin{aligned}
 R_m &= R_z(\phi)R_y(\theta)R_z(-\phi)R_z(\psi) \\
 &= \begin{bmatrix} c\phi c\theta c(\psi - \phi) - s\phi s(\psi - \phi) & -c\phi c\theta s(\psi - \phi) - s\phi c(\psi - \phi) & c\phi s\theta \\ s\phi c\theta c(\psi - \phi) + c\phi c(\psi - \phi) & -s\phi c\theta s(\psi - \phi) + c\phi c(\psi - \phi) & s\phi s\theta \\ -s\phi c(\psi - \phi) & s\phi s(\psi - \phi) & c\theta \end{bmatrix}, \tag{6.109}
 \end{aligned}$$

where s_*, c_* means $\sin(*)$, $\cos(*)$.

(2) The Calculation of the Orientation Matrix

For the 3-RPS cubic PM shown in Fig. 6.22a, at the initial position, which means the three modified Euler angles (φ, θ, ψ) are all equal to zero, the length of the three actuated joints are equal to M . This manipulator is a real cube at this position. Based on the definition of the platform frame $\{\mathbf{m}\}$, it is clear that the three axes of the frame $\{\mathbf{m}\}$ are not parallel with those of the base frame $\{\mathbf{B}\}$, indicating that the manipulator has an initial orientation, denoted by \mathbf{R}_0 as:

$$\mathbf{R}_0 = \begin{bmatrix} 0.408 & -0.707 & 0.577 \\ 0.408 & 0.707 & 0.577 \\ 0.816 & 0 & 0.577 \end{bmatrix}. \quad (6.110)$$

The rotation matrix \mathbf{R}_m is not the orientation matrix \mathbf{R} defined in Eq. (6.99). Actually, \mathbf{R}_m denotes the rotation of the platform with respect to its initial orientation \mathbf{R}_0 . Thus, the orientation matrix \mathbf{R} which denotes the orientation of platform with respect to the base frame is given as:

$$\mathbf{R} = \mathbf{R}_0 \mathbf{R}_m. \quad (6.111)$$

(3) The Mechanical Constraints

There are three main mechanical constraints that limit the workspace of the 3-RPS cubic PM: (1) the actuators' stroke, (2) the range of the spherical joints, and (3) the link interference:

$$\begin{aligned} l_{\min} &\leq l_i \leq l_{\max}, \\ \beta_i &\leq \beta_{\max}, \\ D &\leq D_{ij}, \end{aligned} \quad (6.112)$$

where l_{\min} and l_{\max} are the minimum and maximum lengths of actuated joints, respectively; β_i is the angle between the vector along the i -th link and the axis of the symmetry of the spherical joint, which is connected with the i -th link; β_{\max} is the maximum angle of the spherical joint; D_{ij} is the distance between the i -th link and the j -th link ($i \neq j$); and D is the diameter of each link.

(4) The Calculation and Representation of the Orientation Workspace

When three angles (φ, θ, ψ) are given, we can obtain the rotation matrix \mathbf{R}_m , and the orientation matrix \mathbf{R} . Then using the method shown in Sect. 6.3.3 to solve the inverse kinematics and applying the constraint check defined by Eq. (6.112), we can know whether or not these given angles are in the orientation workspace.

Thus, the orientation workspace of the 3-RPS cubic PM can be represented by the range of the three modified Euler angles (φ, θ, ψ) . Here, we choose to represent the orientation workspace in a cylindrical coordinate system, as shown in Fig. 6.30, where φ , θ and ψ are the angular coordinate, radial coordinate and the height coordinate, respectively [30].

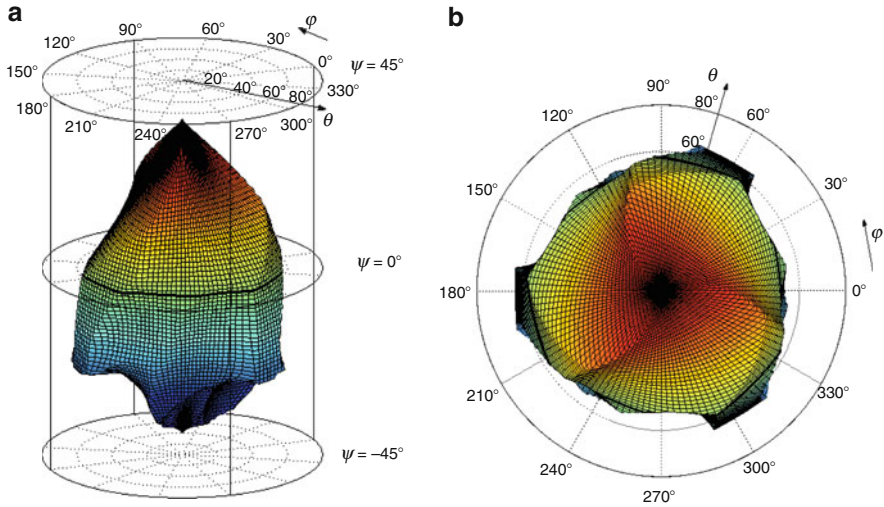


Fig. 6.30 The orientation workspace of the 3-RPS cubic PM (a) Isometric view (b) Top view

6.6.4 Examples

Figure 6.30 shows the orientation workspace of the 3-RPS cubic PM with the parameters given as $M = 100$, $l_{min} = 30$, $l_{max} = 175$, $\beta_{max} = 45^\circ$, and $D = 10$

From Fig. 6.30, we can derive the following:

1. The tilt angle θ of the 3-RPS cubic PM can be at least $\pm 51.6^\circ$ when the roll angle ψ is equal to 0° .
2. The maximum range of ψ can be $(-40^\circ, 36^\circ)$ which can be obtained while the tilt angle θ is equal to 0° .

Two numerical examples are studied here to show the orientation capability of the 3-RPS cubic PM.

Case 1. Let the three modified Euler angles (φ, θ, ψ) be equal to $(20^\circ, 50^\circ$ and 0° , respectively), where this PM is near its maximum tilt angle. The 3-RPS cubic PM at this configuration is shown in Fig. 6.31.

Case 2. Let the three modified Euler angles (φ, θ, ψ) be equal to $(0^\circ, 0^\circ$ and -35° , respectively), where this PM is near its maximum roll angle. The 3-RPS cubic PM at this configuration is shown in Fig. 6.32.

Fig. 6.31 Numerical example with $(\varphi, \theta, \psi) = (20^\circ, 50^\circ, 0^\circ)$

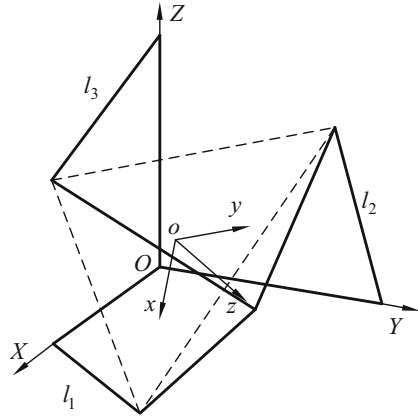
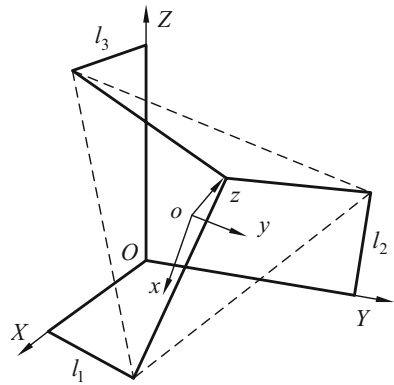


Fig. 6.32 Numerical example with $(\varphi, \theta, \psi) = (0^\circ, 0^\circ, -35^\circ)$



6.6.5 Discussions About the Differences Between the SPMs and the 3-RPS Cubic PM

From the analysis and the results obtained in the above sections, we can see that some differences between these two kinds (3-RRR and 3-RPS) of 3D rotational manipulators exist.

1. The Influences of Manufacturing Errors

The influences of the manufacturing errors on these manipulators are different. For the SPMs, when errors exist, their motion properties change, and the SPMs are not SPMs any more. It is a kind of theoretical error that cannot be compensated. For the 3-RPS cubic PM, the manufacturing errors have little impact on the motion property of the 3-RPS cubic PM, although the positions of the three rotational axes only slightly change when the errors occur.

Intersecting axes also exist and even perpendicular axes in the 3-RPS cubic PM with three fixed revolute joint axes all pass through the origin point O and are perpendicular to each other. However, it should be pointed out that these are not necessary conditions. From the mobility analysis, we can know that if the manufacturing errors occur and the three fixed revolute joints do not pass through the origin point O or are not perpendicular to each other anymore, there are still three constraint forces exerted on the platform; moreover, the property of the three constraint forces and the motions of the platform are the same with the theoretical result.

2. The Parasitic Motions

For the 3-RPS cubic manipulator, while the rotations happen, the platform also has some translational motions that are shown by the coordinate of the platform origin o , with respect to the base frame $\{B\}$. However, the translation motions of the 3-RPS cubic manipulator can be accurately calculated using Eq. (6.106), while the orientations of the platform are given. This means that the motions can be completely compensated and not affect the rotations.

References

1. Ball RS (1900) The theory of screws. Cambridge University Press, England
2. Hunt KH (1978) Kinematic geometry of mechanisms. Oxford University Press, England
3. Gibson CG, Hunt KH (1990) Geometry of screw systems-1 screws genesis and geometry. Mech Mach Theory 25(1):1–10
4. Parkin JA (1990) Co-ordinate transformations of screws with application to screw systems and finite twists. Mech Mach Theory 25(6):689–699
5. Tsai MJ, Lee HW (1993) On the special bases of two-and-three screw systems. Trans ASME J Mech Design 115:540–546
6. Zhang WX, Xu ZC (1998) Algebraic construction of the three-system of screws. Mech Mach Theory 33(7):925–930
7. Fang YF, Huang Z (1998) Analytical identification of the principal screw of the third order screw system. Mech Mach Theory 33(7):987–992
8. Huang Z, Wang J (2001) Identification of principal screws of 3-DOF parallel manipulators by quadric degeneration. Mech Mach Theory 36(8):893–911
9. Yan J, Huang Z (1985) Kinematic analysis of multi-loop spatial mechanism. In: Proceedings of the 4th IFToMM international symposium on linkage and computer aided design method, vol 2-2, Bucharest, pp 439–446
10. Huang Z, Wang HB (1992) Dynamic force analysis of n-DOF multi-loop complex spatial mechanism. Mech Mach Theory 27(1):97–105
11. Huang Z, Wang J (2002) Analysis of instantaneous motions of deficient-rank 3-RPS parallel manipulators. Mech Mach Theory 37(2):229–240
12. Huang Z, Li SH, Zuo RG (2004) Feasible instantaneous motions and kinematic characteristics of a special 3-DOF 3-UPU parallel manipulator. Mech Mach Theory 39(9):957–970
13. Huang Z, Wang J, Li SH (2008) Principal screws and full-scale feasible instantaneous motions of some 3-DOF parallel manipulators. In Lazinica A (eds) Parallel manipulators, new developments. I-Tech Education and Publishing, Vienna. <http://www.proof.i-techonline.com/pama/pmnd.htm>
14. Huang Z, Chen ZM, Liu JF et al (2011) A 3DOF rotational parallel manipulator without intersecting axes. J Mech Robot 3(2):021014-1–7

15. Thomas M, Tesar D (1983) Dynamic modeling of serial manipulator arms. *J Dyn Sys Meas Cont* 104(9):218–227
16. Huang Z (1985) Modeling formulation of 6-DOF multi-loop parallel manipulators, Part-1: Kinematic influence coefficients. In: Proceedings of the 4th IFToMM international symposium on linkage and computer aided design methods, vol II-1, Bucharest, Romania, pp 155–162
17. Hunt KH (1983) Structural kinematics of in-parallel-actuated robot arms. *Trans ASME J Mech Trans Auto Des* 105(4):705–712
18. Huang Z, Tao WS, Fang YF (1996) Study on the kinematic characteristics of 3-DOF parallel actuated platform mechanisms. *Mech Mach Theory* 31(8):999–1007
19. Zhao TS, Zhao YS, Huang Z (1999) Physical and mathematical conditions of existence of axes about which platform of deficient-rank parallel robots can rotate continuously. *Robot* 21(5):347–351 (in Chinese)
20. Tsai LW, Stamper R (1996) A parallel manipulator with only translational degrees of freedom. ASME 96-DETC-MECH-112, Irvine, USA
21. Huang Z, Fang YF (1996) Kinematic characteristics analysis of 3-DOF in-parallel actuated pyramid mechanisms. *Mech Mach Theory* 31(8):1009–1018
22. Cox D (1981) The dynamic modeling and command signal formulation for parallel multi-parameter robotic devices. Ph.D. thesis, University of Florida
23. Di Gregorio R (2001) A new parallel wrist employing just revolute pairs: the 3-RUU wrist. *Robotica* 19(3):305–309
24. Carretero JA, Podhorodeski RP, Nahon MA et al (2000) Kinematic analysis and optimization of a new three degree-of-freedom spatial parallel manipulator. *ASME J Mech Des* 122(1):17–24
25. Kong X, Gosselin CM (2002) Type synthesis of linear translational parallel manipulators. In: Lenarčič J, Thomas F (eds) *Advances in robot kinematics – theory and applications*. Kluwer Academic Publishers, Boston
26. Altuzarra O, Loizaga M, Petuya V (2007) Partially decoupled parallel manipulators based on multiple platforms. In: Proceedings of the IFToMM world congress, France
27. Zeng D, Huang Z, Lu W (2007) A family of Novel 2 DOF rotational decoupled parallel mechanisms. In: Proceedings of 2007 international conference on mechatronics and automation, Haerbin, China
28. Di Gregorio R (2002) The 3-RRS wrist: a new, very simple and not overconstrained spherical parallel manipulator. ASME Design Engineering Technical Conferences, Montreal, MECH-34344
29. Li QC, Herve JM (2010) 2R1T parallel mechanisms without parasitic motion. *J IEEE Trans Robot* 26(3)
30. Bonev IA, Ryu J (2001) A new approach to orientation workspace analysis of 6-DOF parallel manipulators. *Mech Mach Theory* 36(1):15–28
31. Bonev IA, Zlatanov D, Gosselin CM (2002) Advantages of the modified Euler angles in the design and control of PKMs. Parallel kinematic machines international conference, Chemnitz, Germany, 23–25 Apr, pp 171–188
32. Gosselin CM, Angeles J (1989) The optimum kinematic design of a spherical three-degree-of-freedom parallel manipulator. *ASME J Mech Trans Auto Design* 111(2):202–207

Chapter 7

Special Configuration of Mechanisms

This chapter resumptively introduces our studies on the singularity of parallel mechanisms for the Stewart manipulator and the 3-RPS mechanism. It analyzes the singular kinematic principle and the singularity classification based on the kinematic status of the machinery and the linear-complex and focuses on discussing the structure and property of the singularity loci of 3/6- and 6/6-Stewart platform for special and general orientations. The singularity of the 3-RPS mechanism is also discussed in the latter parts. Many interesting properties, such as the remarkable intersection of all six segments of the six legs of the 6/6-Stewart platform with one common line, are discovered.

7.1 Introduction

One of the important problems in robot kinematics is the special configuration or singularity.¹ The end effector of the parallel manipulators in such configurations keeps at least one remnant freedom while all actuators are locked. This phenomenon temporarily destabilizes the end effector. Meanwhile, the articular forces may go to infinity and cause mechanical damage.

The determination of the special configurations of the six-degrees of freedom (DOF) Stewart parallel manipulators is a very important problem and one of the main concerns in the analysis and design of manipulators. The singularity analysis of parallel manipulators has attracted considerable attention in the past two decades. Hunt (1983) first discovered a special configuration for this manipulator [1] that occurs

¹We prefer to adopt the term “special configuration” instead of “singularity” because the latter originates from mathematics, whereas the former originates from mechanical engineering and its meaning in physics is clear and can easily be understood by mechanical students and engineers. However, the term “singularity” is also used in the paper a number of times to simplify the expression.

when the moving triangle platform is coplanar, with two legs meeting at a vertex of its triangle and all six segments associated with the six prismatic actuators intersect a common line. Fichter (1986) discovered a singularity of the Stewart parallel manipulator [2] that occurs when the moving platform rotates by $\varphi = \pi/2$ around the Z – axis regardless of the position of the moving platform. This mechanism has a triangular mobile platform and a hexagonal base platform and may be called a 3/6-Stewart platform (3/6-SP). Huang and Qu (1987) also studied the singularity of the parallel manipulator [3] occurring when $\varphi = \pi/2$ and whose moving and basic platforms are both semiregular hexagons (6/6-SP). Merlet studied the singularity of the six-DOF 3/6-SP more systematically based on the Grassman line geometry [4]. He discovered that many new singularities, including 3c, 4b, 4d, 5a, and 5b.3c, occurs when four lines of the six legs intersect at a common point: 4b occurs when five lines are concurrent with two skew lines; 4d occurs when all five lines are in one plane or pass through one common point in that plane; 5a is in a general complex; and 5b occurs when the six segments cross the same line. Singularity analyses for platform devices based on line geometry have been presented by Collins and Long [5]. Hao and McCarthy considered line-based singularities in a spatial platform manipulator [6]. Gosselin and Angeles (1990) pointed that singularities of closed-loop mechanisms can be classified into three different groups based on Jacobian matrices [7]. This classification was further discussed by Zlatanov et al. [8]. Zlatanov et al. further discussed constraint singularities [9]. Ma and Angeles (1991) studied the architecture singularities of parallel manipulators [10]. Kong discussed the architecture singularities of 6-SPS parallel manipulators [11]. McAree and Daniel discussed the singularity and motion property of a 3/3-parallel manipulator [12]. Karger and Husty [13] and Karger [14] described the singular positions and self-motions of a special class of planar parallel manipulators, wherein the platform is similar to the base. This platform has no self-motions unless it is architecturally singular. Kong and Gosselin [15] also studied self-motion. Chan and Ebert-Uphoff [16] studied the nature of the kinematic deficiency in a singular configuration by calculating the nullspace of the Jacobian matrix. Di Gregorio studied the SX-YS-ZS structures and singularities [17].

Many studies focused only on isolated singular points in space. However, in the practical configuration space of parallel manipulators, the singularity configuration should be a continuous singularity curve or even be a high-dimension surface. One of the main concerns is to further determine the singularity loci and their graphical representations, structure, and property, which is of great significance in a context of analysis and design because it allows one to obtain a complete picture of the location of the singular configurations in space. For a given practical application, determining whether the singularities can be avoided is therefore easy. Sefrioui and Gosselin studied the singularity loci of planar and spherical parallel mechanisms [18, 19]. Wang and Gosselin used a numerical method to study the singularity loci of spatial four- and five-DOF parallel manipulators [20, 21]. Collins and McCarthy [22, 23] studied the singularity loci of the planar 3-RPR parallel manipulator and the 2-2-2 and 3-2-1 platforms and obtained cubic singularity surfaces. However, for the six-DOF Stewart platform, the singularity expression is generally quite complicated and difficult to analyze. Recently, Wang presented a method [24] to analyze the singularity of a special form of the Stewart platform and derived the corresponding

analytical singularity conditions. Di Gregorio also discussed the singularity loci of 3/6 and 6/6 fully parallel manipulators [25, 26]. In particular, Mayer St-Onge and Gosselin (2000) analyzed the Jacobian matrix of general Stewart manipulators using two new different approaches [27]. They derived a simpler explicit expression from the Jacobian matrix and pointed out that the singularity locus of the general Stewart manipulator should be a polynomial expression of degree three. They also provided graphical representations of the singularity loci.

For practical applications, we want to obtain a simpler algebraic expression, as well as accurate graphical representations, for the singularity loci to determine whether they consist of some typical geometric figures. However, the application of this process to the Stewart manipulator is very difficult. Huang et al. (1999, 2003, 2005) [28–30] studied the singularity kinematics principle of parallel manipulators and proved a new, sufficient and necessary kinematics condition to determine the singularity. They first discovered the characteristics of a singularity locus of the 3/6-Stewart platform using this method. The singularity locus of the 3/6-Stewart platform is resolvable and consists of two typical geometric graphs, namely, a plane and a hyperbolic paraboloid, with the special orientation $\phi = \pm 30^\circ, \pm 90^\circ, \pm 150^\circ$. However, the singularity locus expression of degree three is irresolvable, and the locus graph in infinite parallel principal sections for the general orientations $\phi \neq \pm 30^\circ, \pm 90^\circ, \pm 150^\circ$ includes a parabola, four pairs of intersecting straight lines, and infinite hyperbolas.

For the singularity loci of the 6/6-SP, which is a more general structure and widely used form in practice, the graphical representations of the singularity loci for the different orientations are varied and complex. Huang and Cao (2005) [30] analyzed the singularity loci both in three-dimensional (3D) space and in the principal section on which the moving platform lies. The singularity locus equation for this class of Stewart manipulators in 3D space is also irresolvable, and the curves in the infinite parallel principal sections of the singularity loci also contain one parabola, four pairs of intersecting straight lines, and infinite hyperbolas. We also observed a special configuration involving six lines associated with the six extensible links of the 6/6-Stewart manipulator intersecting the same common line, and the remnant instantaneous motion of the manipulator is a pure rotation.

All the aforementioned analyses are only on positional singularities when the orientation of the moving platform is specified and invariable. Therefore, the orientation-singularity space when the position of the moving platform is specified and invariable needs to be determined. Some researchers, such as Pernkopf and Husty [31] and Cao et al. [32], began to study the issue. However, a more intensive study is needed for this topic.

7.2 Classification of the Special Configuration

To understand an object, it must be viewed from different perspectives. Several different classification methods were proposed for the special configuration (SC). However, the effects of the SC phenomenon on the kinematic status of machineries should first be considered [33] and is the concern of all mechanical engineers.

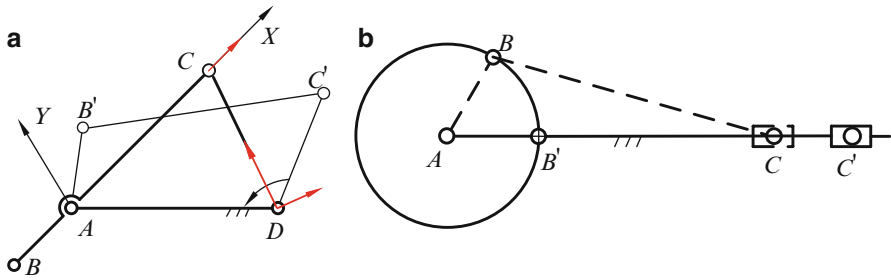


Fig. 7.1 Dead-point singularity (a) four-bar linkage (b) crank-slider linkage

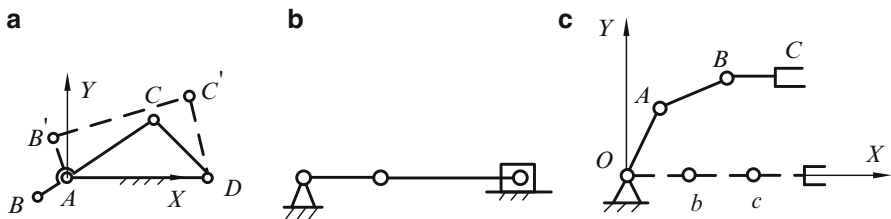


Fig. 7.2 Extreme-displacement singularity (a) four-bar linkage (b) crank-slider linkage (c) serial robot

7.2.1 Singular Kinematics Classification

Case 1 Dead-point singularity

A machinery is in the dead-point singularity when the driver link is in a terminal position and the device can no longer be moved, as shown in Fig. 7.1.

Figure 7.1a shows a four-bar linkage with an input link CD . When the connecting link BC and crank AB are aligned, the mechanism is in SC. Figure 7.1b illustrates a crank-slide linkage with a slider input; when the crank and the connecting link are aligned, the mechanism is in a dead-point SC.

Case 2 Extreme-displacement singularity

A machinery is in the extreme-displacement singularity when the output link is in a terminal position. In this configuration, the output link can only be in a countermove. Figure 7.2 shows three mechanisms in this SC.

Case 3 Constraint-dependency singularity

A mechanism is in a constraint-dependent singularity when it is in a configuration in which all inputs are locked, resulting in an unstable mechanism.

Figure 7.3 shows the Stewart platform as an example. The mechanism is in a constraint-dependent singularity when the upper platform rotates about the Z -axis until a 90° angle is reached because the six screws associated with the six extendable links are linearly dependent.

Fig. 7.3 Stewart platform

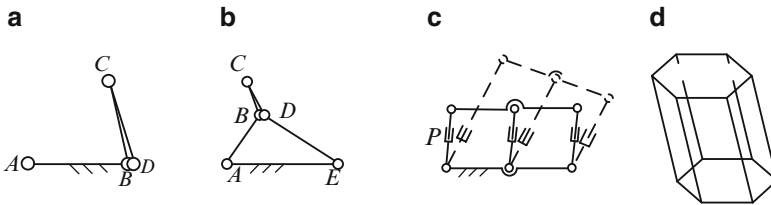
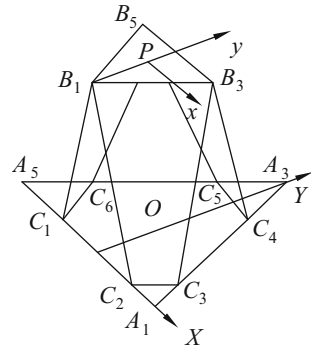
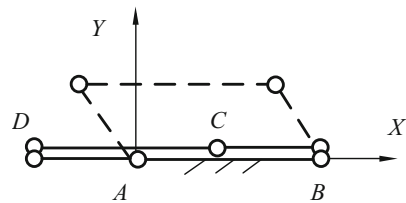


Fig. 7.4 Full-cycle geometric singularity (a) four-bar linkage (b) five-bar linkage (c) eight-bar linkage (d) Stewart platform

Fig. 7.5 Parallelogram linkage



Case 4 Full-cycle geometry singularity

Under some geometric conditions and configurations, all inputs are locked so that the linkage can continuously rotate (Fig. 7.4).

Figure 7.4d illustrates one of the Stewart platforms with two identical regular hexagons connected by six identical legs. The mechanism has three DOFs when the lengths of the six legs are kept equal and constant [34].

Case 5 Instantaneous mobility increase

The mobility of the linkage can instantaneously increase under certain geometries and configurations. Figure 7.5 illustrates a parallelogram linkage. The linkage attains this SC when the four links are aligned, instantaneously doubling the mobility.

Case 6 Mobility transfers to a local

The total number of mobility for this SC is unchangeable and one of the mobilities transfers to a local one. Figure 7.6b shows a diagram of this SC, wherein two connecting links, *CD* and *DE*, are aligned.

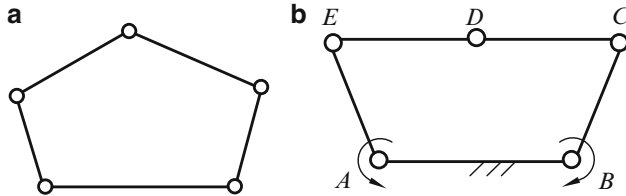


Fig. 7.6 Five-bar linkage (a) five-bar linkage (b) EDC are aligned

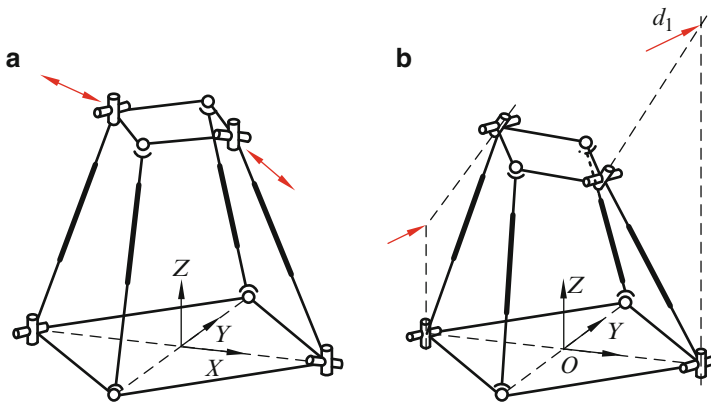


Fig. 7.7 2-UPU/2-SPS mechanisms (a) both platforms are parallel (b) the platforms are not parallel

A local freedom exists inside the two links (CD and DE) because the three points are collinear and the corresponding three screws are linearly dependent.

Case 7 Variety-mobility-property singularity

The mobility property includes rotational and translational freedoms. Therefore, if the rotational freedom in some configuration suddenly becomes a translational one, the linkage also becomes singular and is called a variety mobility property singularity. For example, Fig. 7.7 shows a 2-UPU/2-SPS mechanism. It has two 7-DOF SPS limbs that do not provide any constraint to the platform, and two UPU limbs. The 1st and 5th revolute pairs of each UPU limb are normal to the upper and lower two platforms, respectively. Each UPU limb acts a constraint to the platform. Two different configurations are shown in the figure. For the 1st configuration, the upper and lower platforms are parallel, and two constraint couples acting on the moving platform and the mechanism loses two rotational freedoms. For the other configuration two platform are not parallel, the platform is subjected to two constraint forces. Both linkages have four mobilities, but the first one is a 3T1R mechanism, where T denotes the translational freedom and R is the rotational freedom. The second one is a

3R1T mechanism. Once the platform begins rotating from the 1st toward the 2nd configuration, the freedom property changes and the mechanism becomes singular.

The detailed analysis of this mechanism is found in a previous report [35].

7.2.2 Classification of the Singularity via a Linear Complex

A general algebraic equation for a linear complex [36, 37] is

$$a_1P + a_2Q + a_3R + a_4L + a_5M + a_6N = 0 \quad (7.1)$$

where the six coefficients denote a twist screw

$$\mathcal{S}^m = (a_1 \ a_2 \ a_3; \ a_4 \ a_5 \ a_6) \quad (7.2)$$

Its pitch is

$$h^m = \frac{a_1a_4 + a_2a_5 + a_3a_6}{a_1^2 + a_2^2 + a_3^2} \quad (7.3)$$

Its reciprocal screw satisfying Eq. (7.1) is

$$\mathcal{S} = (L \ M \ N; \ P \ Q \ R) \quad (7.4)$$

When,

$$LP + MQ + NR = 0 \quad (7.5)$$

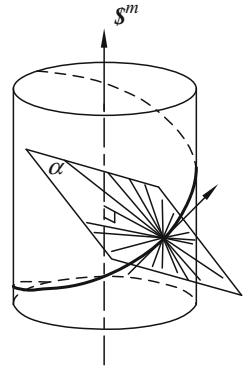
where \mathcal{S} denotes a line vector, i.e., a screw with zero pitch. The infinite line vectors satisfying Eq. (7.1) compose a line complex.

In a linear complex[37], the lines that pass through any pole must all lie in the same polar plane, and lines that lie in any polar plane must all pass the same point. Figure 7.8 shows the pole and polar plane of a linear complex, with a pencil of lines in the α plane. All lines that pass through the pole are normal to the helix.

The linear complex can be divided into three parts according to its pitch h^m , as follows:

- Case 1.** When h^m is finite and nonzero, the linear complex is general;
- Case 2.** When $h^m = 0$, the first special linear complex is formed, in which all coaxial helices collapse into homocentric circles with a common axis \mathcal{S}^m and all lines of the complex intersect \mathcal{S}^m or are parallel to it; and
- Case 3.** When $h^m = \infty$, the second special linear complex is formed, in which all lines of the complex comprise planar fields of lines in all planes normal to the direction \mathcal{S}^m , and \mathcal{S}^m is a free vector no longer occupying a specific line.

Fig. 7.8 Linear complex



The last two forms are associated with pure rotation and pure translation, respectively; for the former, the platform appears in a twist motion.

All singularities belong to the linear-complex type. Therefore, the singularity can be classified into three kinds depending on the different instant output motions, as follows:

- (a) General linear-complex singularity. The possible motion of the moving platform is a twist, with h^m being finite and nonzero, i.e., $0 < h^m < \infty$;
- (b) First special linear-complex singularity. The possible motion of the moving platform is a pure rotation, with $h^m = 0$; and
- (c) Second special linear-complex singularity. The possible motion of the moving platform is a pure translation, with $h^m = \infty$.

7.3 Singular Kinematic Principle

The following theorems introduce the principle of a novel method analyzing the singularities of parallel manipulators [28, 29, 38, 39]:

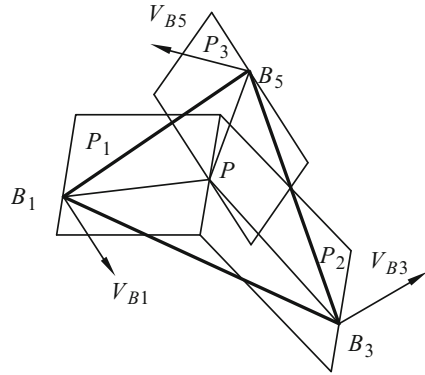
Theorem 7.1. A necessary and sufficient condition for the three possible velocity directions of three non-collinear points in a rigid body to express that the body has a possible twist motion is that the point of intersection of three normal planes of the three velocities lies in the plane determined by the three points.

To prove the sufficient condition of the theorem, the velocity relationship of the three points in a moving body must first be discussed.

(1) Sufficient condition of the theorem.

When three possible velocity directions of three points in a rigid body are known, then the three normal planes of the three velocities can be determined. If the intersecting point of the three planes lies in the plane determined by the three points, the three velocities can determine a twist; in other words, the body is movable [28].

Fig. 7.9 Velocity relationship of the three points



Proof: If three velocity directions of three points $B_1, B_3,$ and B_5 in a rigid body are given, and the point of intersection P of three normal planes $P_1, P_2,$ and P_3 is in plane $B_1B_3B_5$ (Fig. 7.9), then the three velocities $\mathbf{V}_{B_1}, \mathbf{V}_{B_3},$ and \mathbf{V}_{B_5} can always be resolved into two sets, as follows: $\mathbf{V}_{B_1}^T, \mathbf{V}_{B_3}^T,$ and $\mathbf{V}_{B_5}^T$ parallel to plane $B_1B_3B_5;$ and $\mathbf{V}_{B_1}^n, \mathbf{V}_{B_3}^n,$ and $\mathbf{V}_{B_5}^n$ perpendicular to the plane. The three tangent components are still normal to the corresponding lines $PB_1, PB_3,$ and $PB_5,$ and they can form a pure rotation about point P with zero pitch. The three vertical ones can form another pure rotation about an axis, which is an intersecting line of two planes: one is determined by the three tip points of three vertical velocity vectors, and the other is plane $B_1B_3B_5.$ The possible motion of the body is the sum of the two rotational motions. Generally, the motion is a twist with a finite and nonzero pitch, but it may also be a pure rotation if one of the two rotations vanishes or the two rotary axes intersect [28]. When the intersecting point of three normal planes does not lie in plane $B_1B_3B_5,$ the analysis above does not apply.

Now let us prove the necessary condition of the theorem.

(2) Necessary condition of the theorem

The three velocities of three points in a moving body have three corresponding normal planes. In general, the three planes intersect at a common point, and the intersecting point necessarily lies in the plane determined by the three points [29].

Proof: When the plane $B_1B_3B_5$ is in a twist motion (Fig. 7.9), the loci of points $B_1, B_3,$ and B_5 are all helical. Three planes, $P_1, P_2,$ and $P_3,$ are normal to three velocities $\mathbf{V}_{B_1}, \mathbf{V}_{B_3},$ and \mathbf{V}_{B_5} at the corresponding points $B_1, B_3,$ and $B_5,$ respectively. Generally, the three planes have a common point $P,$ and $\mathbf{V}_{B_1} \perp PB_1, \mathbf{V}_{B_3} \perp PB_3,$ and $\mathbf{V}_{B_5} \perp PB_5$

The moving locus of any point in a twist-motion body is a screw thread or helix. A plane perpendicular to the helix at any selected point is a polar plane, and the intersecting point is the pole of the polar plane. Furthermore, the pole is the only point in the plane whose velocity is normal to the polar plane. All lines crossing the pole in the polar plane belong to a linear complex. In particular, Hunt in [37] (p. 270) pointed out that any normal to a helix at an arbitrary point is normal to all the helices it meets at the point of intersection.

Based on the statement above, we know that plane P_1 is a polar plane with a pole $B_1,$ and line PB_1 is normal to the helix passing through $B_1.$ Therefore, PB_1 is also a

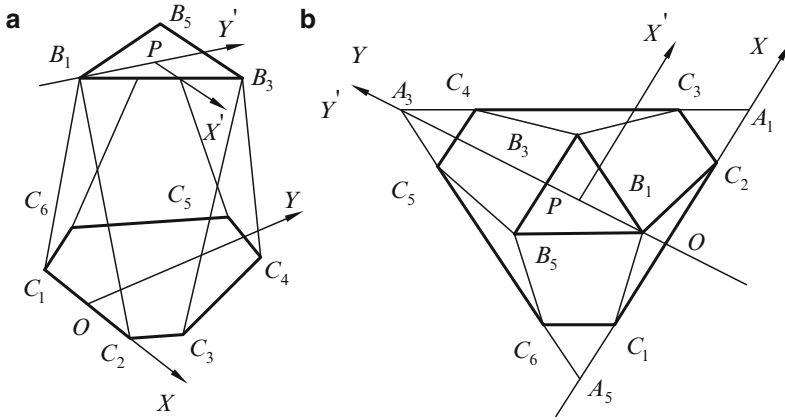


Fig. 7.10 A 3/6-Stewart parallel manipulator (a) a 3/6-Stewart manipulator (b) top view

normal of the helix crossing point P ; that is, PB_1 is normal to V_P . In the same way, lines PB_3 and PB_5 are also normal to V_P . Moreover, lines PB_1 , PB_3 , and PB_5 all intersect at the same point P , so that they lie in the same plane determined by the three points B_1 , B_3 , and B_5 . Thus, point P lies in the plane $B_1B_3B_5$.

Deduction 7.1. Plane $B_1B_3B_5$ is a polar plane of the helix crossing point P , and point P is its pole; moreover, P is the only point whose velocity is normal to the polar plane $B_1B_3B_5$ (Fig. 7.9).

The 3/6-SP is a typical manipulator that has been extensively studied by many researchers. Its schematic representation is shown in Fig. 7.10. 3/6-SP consists of an equilateral-triangle mobile platform $B_1B_3B_5$ and a semiregular hexagon platform $C_1 \dots C_6$, and they are connected via six extensible prismatic actuators.

When all the legs of 3/6-SP are locked, the three normal planes of three possible velocities V_{B_1} , V_{B_3} , and V_{B_5} are $B_1C_1C_2$, $B_3C_3C_4$, and $B_5C_5C_6$, respectively (Fig. 7.10). According to Theorem 7.1, the following deduction can be made to determine the singularity of 3/6-SP. First, let us define a “Star-frame $C-B_1B_3B_5$ ” in the moving platform. It is constructed by three rays passing the three points B_1 , B_2 , and B_3 of the triangle $B_1B_3B_5$, which are correspondingly coplanar with the three sides of the base, i.e., CB_1 intersects A_1A_5 , CB_3 intersects A_1A_3 , and CB_5 intersects A_3A_5 . When the three rays are coplanar and intersect at a common point C , the configuration is called a star frame.

Deduction 7.2. If three rays CB_1 , CB_3 , and CB_5 of star frame $C-B_1B_3B_5$ are coplanar with three sides C_1C_2 , C_3C_4 , and C_5C_6 of the base of the 3/6-SP, respectively, the mechanism is singular.

Planes $B_1A_1A_5$, $B_3A_1A_3$, and $B_5A_3A_5$ are clearly just the three normal planes of the corresponding velocities. Based on Theorem 7.1, Theorem 7.2 and the two deductions can be deduced, and an important theorem is derived.

Theorem 7.2. A necessary and sufficient condition of the singularity of a mechanism is that the four planes intersect at a common point. These four planes include

three normal planes of three velocities of three non-collinear points in the end effector, and the plane is determined by these three points themselves.

Deduction 7.3. If three velocities of three points in a body are parallel to the same plane and the three normal planes at the corresponding points intersect at the same line, the three velocities can determine a pure rotation with zero pitch, and the rotary axis is the line of intersection of the three normal planes.

Deduction 7.4. If three velocity directions of three points in a body are parallel, then the three normal planes of the three velocities are also parallel. Generally, these three velocities can determine a pure translation with an infinite pitch.

Theorem 7.1 can be conveniently used to determine the singularity and is very important. It indicates that all singularities should satisfy the Theorem because it is a necessary and sufficient condition of singularity; no other singular configurations exist except the ones determined by the Theorem. The singularity principle can also directly apply to many mechanisms with a triangle-moving platform, such as the SX-YS-ZS structures [39].

7.4 Singularity Loci of 3/6-Stewart for Special Orientations

The kinematics method can determine the singularity of the manipulator. If the six extensible legs of the SP are locked and the mechanism has an instantaneous freedom, the manipulator is singular. In this section, the kinematics properties of typical singularity structures, including the singularities 3c, 4b, 4d, 5b (Merlet 1989) [4] and others, are discussed.

To investigate the singularity of the Stewart mechanism, we may lock all six inputs and then identify whether the mechanism has mobility. When all inputs are locked, some mobilities still exist, and the mechanism is singular.

7.4.1 Typical Singularity Structures of 3/6-SP

Eight kinds of typical singularity structures are available for 3/6-SP. Fichter's singularity [2] occurs when the upper platform rotates by $\pi/2$ about the Z-axis, and the mechanism holds one remnant twist with a finite pitch. Aside from Fichter's singularity, the other seven kinds of typical singularities will be discussed in this section.

Case 1. Two disconnecting legs are collinear with two sides of the mobile platform

Figure 7.11a shows that legs 4 and 6 are collinear with sides B_1B_3 and B_3B_5 , respectively. Four lines, namely, 1, 2, 4, and 6, intersect at a common point B_1 (Merlet 3c [4]). While all the extensible legs are locked, \mathbf{V}_{B_3} and \mathbf{V}_{B_5} are perpendicular to planes $B_3C_3C_4$ and $B_5C_5C_6$, respectively; so that $\mathbf{V}_{B_3} \perp B_1B_3$ and $\mathbf{V}_{B_5} \perp B_1B_5$. Thus, $\mathbf{V}_{B_1} \perp B_1B_3$ and $\mathbf{V}_{B_1} \perp B_1B_5$, namely, $\mathbf{V}_{B_1} \perp B_1B_3B_5$. Point B_1 is then the pole of the polar plane $B_1B_3B_5$. Meanwhile, $\mathbf{V}_{B_1} \perp B_1C_1C_2$. Given that

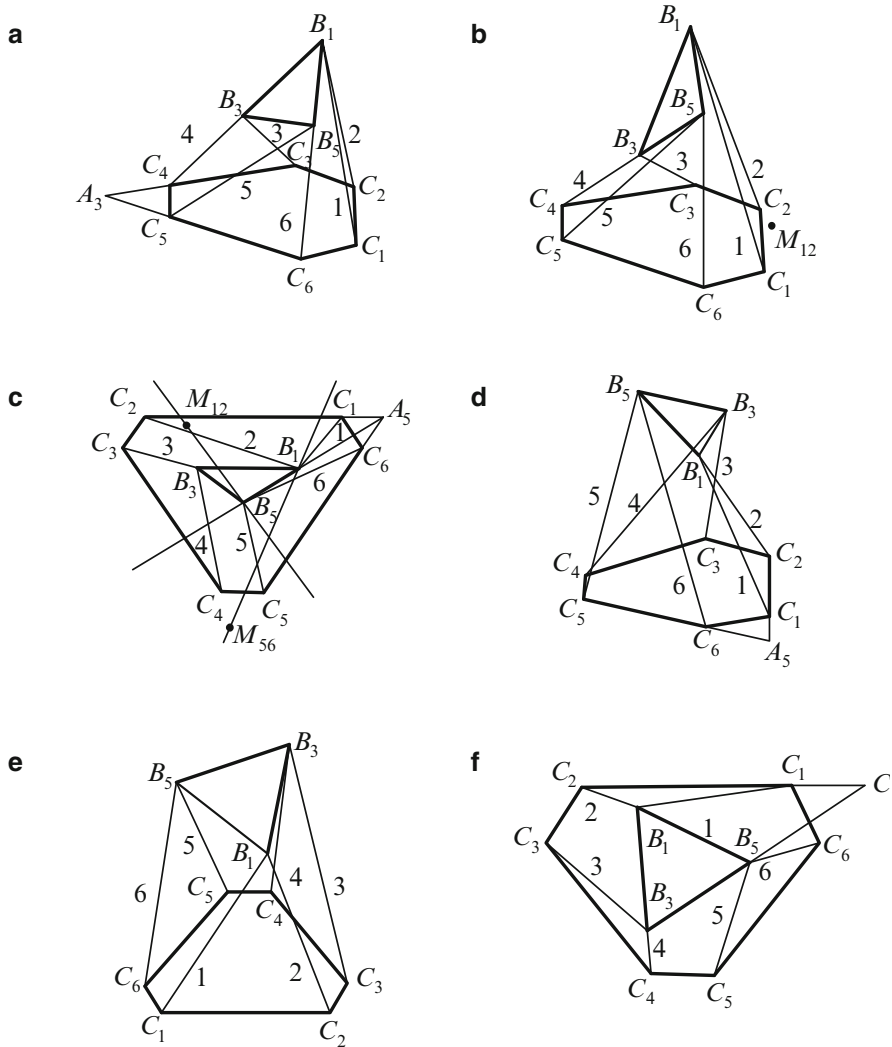


Fig. 7.11 Configuration graphs of several linear-complex singularities (a) a singular configuration of type 3c (b) a singular configuration of type 4d (c) a singular configuration of type 4b (d) a singular configuration of type 5b (e) Hunt's singularity (f) a singular configuration of type 3d

the two planes $B_1B_3B_5$ and $B_1C_1C_2$ are not coplanar, $\mathbf{V}_{B_1} = 0$. \mathbf{V}_{B_1} , \mathbf{V}_{B_3} , and \mathbf{V}_{B_5} form two pure rotations (see the proof of Theorem 7.1). The two rotary axes intersect at point B_1 , so that the sum of the two rotations is also a pure rotation with zero pitch. This configuration is the first special-linear-complex singularity, and the six lines (1, 2, ..., 6) intersect line B_1A_3 , which is the intersecting line of two planes determined by point B_1 and line 3, as well as B_1 and line 5.

Case 2. Three Legs Intersect at a Vertex Lying on another Normal Plane

Figure 7.11b shows three legs, namely, 4, 5, and 6, intersecting at a vertex B_5 , which lies on another normal plane $B_1C_1C_2$. This is the case for the Merlet configuration 4d [4], and can also be described as all lines in a plane or passing through a point in that plane (Table 2.1).

For the same reason stated in the previous section, $\mathbf{V}_{B_1} \perp B_1B_5$ and $\mathbf{V}_{B_3} \perp B_3B_5$. Therefore, $\mathbf{V}_{B_5} \perp B_1B_3B_5$. However, it should also be normal to plane $B_5C_5C_6$; thus, $\mathbf{V}_{B_5} = 0$. The motion of the mobile is also a pure rotation with zero pitch. Line 3 is elongated and intersects plane $B_1C_1C_2$ at point M_{12} , and line B_5M_{12} intersects all six lines (1, 2, ..., 6), indicating that this is the first special-linear-complex singularity.

Case 3. Two Vertices Both Lie on Two Normal Planes

Figure 7.11c shows a top view of the mechanism in a Merlet 4b case, which can also be described as five lines concurrent with two skew lines. Two vertices, B_1 and B_5 , both lie on two normal planes, $B_1C_1C_2$ and $B_5C_5C_6$.

In this case, three points, namely, A_5 , B_1 , and B_5 , belong to the same line that is the intersecting line of planes $B_1C_1C_2$ and $B_5C_5C_6$. Thus, $\mathbf{V}_{B_1} \perp B_5A_5$ and $\mathbf{V}_{B_5} \perp B_5A_5$. However, \mathbf{V}_{B_1} and \mathbf{V}_{B_5} are not parallel to each other, and B_5A_5 is their common normal in plane $B_1B_3B_5$.

The normal plane of the nonzero \mathbf{V}_{B_3} intersects line B_5A_5 at a certain point, and Theorem 7.1 is satisfied. In general, the three velocities can determine a twist with finite and nonzero pitches, so all six lines belong to a general linear complex. However, the motion of the mobile may also be a pure rotation when the rotary axes of the two pure rotations formed by the three velocities intersect.

Case 4. One Vertex of the Mobile Lying on the Other Two Normal Planes

Figure 7.11d shows that vertex B_5 lies on both normal planes $B_1C_1C_2$ and $B_3C_3C_4$. This configuration is the Merlet singularity 5b. Thus, point B_5 lies in the intersecting line of planes $B_1C_1C_2$ and $B_3C_3C_4$. Given that \mathbf{V}_{B_1} and \mathbf{V}_{B_3} are orthogonal to planes $B_1C_1C_2$ and $B_3C_3C_4$, respectively, $\mathbf{V}_{B_1} \perp B_1B_5$ and $\mathbf{V}_{B_3} \perp B_3B_5$. Thus, $\mathbf{V}_{B_5} \perp B_1B_5$ and $\mathbf{V}_{B_5} \perp B_3B_5$; that is, $\mathbf{V}_{B_5} \perp B_1B_3B_5$. Meanwhile, $\mathbf{V}_{B_5} \perp B_5C_5C_6$, so $\mathbf{V}_{B_5} = 0$. Therefore, \mathbf{V}_{B_1} , \mathbf{V}_{B_3} , and \mathbf{V}_{B_5} can determine a pure rotation with zero pitch. The six lines intersect the same line B_5A_1 .

Case 5. Mobile is Coplanar with Two Connecting Legs

Figure 7.11e illustrates Hunt's singular configuration, in which line B_3B_5 lies in plane $B_1C_1C_2$. \mathbf{V}_{B_1} is normal to plane $B_1B_3B_5$, so $\mathbf{V}_{B_3} \perp B_1B_3$ and $\mathbf{V}_{B_5} \perp B_1B_5$. On the other hand, $\mathbf{V}_{B_3} \perp B_3C_3C_4$ and $\mathbf{V}_{B_5} \perp B_5C_5C_6$. Given that line B_1B_3 does not lie in plane $B_3C_3C_4$, and line B_1B_5 does not belong to plane $B_5C_5C_6$, both \mathbf{V}_{B_3} and \mathbf{V}_{B_5} are zero. Thus, \mathbf{V}_{B_1} , \mathbf{V}_{B_3} , and \mathbf{V}_{B_5} can determine a pure rotation, and B_3B_5 is the rotary axis. Clearly, Hunt's singular configuration also belongs to the first special-linear-complex singularity.

Case 6. Two Vertices Lie on the Basic Plane

Figure 7.11f shows that B_3 and B_5 lie on the base plane, and four lines (3, 4, 5, and 6) are coplanar.

Thus, all six lines (1, 2, ..., 6) cross the same line C_1C_2 , and this case belongs to that of 3d, where \mathbf{V}_{B_3} and \mathbf{V}_{B_5} are parallel to each other and are both normal to the

basic plane. Line B_3B_5 is their common normal. The normal plane of \mathbf{V}_{B_1} intersects B_3B_5 at point C , which is the intersecting point of lines C_1C_2 and B_3B_5 . \mathbf{V}_C is normal to plane $B_1B_3B_5$, so point C is the pole of the pole plane $B_1B_3B_5$. The tip points of all the velocities of the points along a line in a rigid body are in a straight line. Thus, \mathbf{V}_C is also normal to the basic plane and should only be zero. Based on the velocity analysis indicated in the proof of Theorem 7.1, \mathbf{V}_{B_1} , \mathbf{V}_{B_3} , and \mathbf{V}_{B_5} can form two pure rotations, and the two rotary axes pass through point C . This case is the first special-linear-complex singularity.

Case 7. Three Vertices Lie on the Basic Plane

When three points, namely, B_1 , B_3 , and B_5 all lie in the basic plane, the two platforms are coplanar, and all six lines are in a plane. Thus, \mathbf{V}_{B_1} , \mathbf{V}_{B_3} , and \mathbf{V}_{B_5} are parallel to one another and perpendicular to the basic plane so that their three normal planes are coplanar. Considering that the six lines are in a plane, only three independent line vectors are present for the six coplanar lines. In this case, three velocities, namely, \mathbf{V}_{B_1} , \mathbf{V}_{B_3} , and \mathbf{V}_{B_5} , can form three different independent motions. This case is the fourth special three-system [37], and the three reciprocal principal screws on the base with respect to the fixed frame are as follows:

$$\begin{aligned} \mathcal{S}_\alpha &= (0 \ 0 \ 0; \ 0 \ 0 \ 1) \\ \mathcal{S}_\beta &= (1 \ 0 \ 0; \ 0 \ 0 \ 0) \\ \mathcal{S}_\gamma &= (0 \ 1 \ 0; \ 0 \ 0 \ 0) \end{aligned} \quad (7.6)$$

The pitches of the three principal screws are in the form,

$$\begin{aligned} h_\alpha &= \infty \\ h_\beta &= h_\gamma = 0 \end{aligned} \quad (7.7)$$

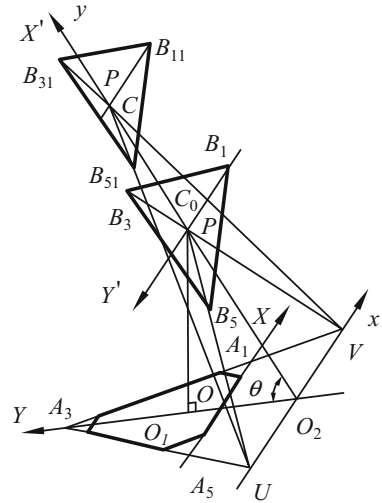
The mobile can rotate about any axis in the basic plane; this case is the first special-linear-complex singularity. The mobile can also translate along a direction orthogonal to the basic plane, which is the second special-linear-complex singularity.

Considering the eight aforementioned cases, when six lines lie in a plane, the end effector of the mechanism holds three remnant DOFs while all the legs are locked. Generally, only one DOF is obtained in the previous seven cases. In particular, if line 3 can intersect with the two skew lines $M_{12}B_5$ and $M_{56}B_1$ simultaneously [4], such as in Case 3, two DOFs may also be obtained.

7.4.2 Hyperbolic Singularity Equation Derived in an Oblique Plane

Our task is to find the entire singularity loci of SP and identify their structure and property, which is an important and difficult issue. In this section, three Euler

Fig. 7.12 θ Oblique plane for the orientation $(90^\circ \theta 0)$



angles, namely, ϕ , θ , and ψ , are used to represent the orientation of the mobile in terms of a rotation ϕ , about the Z -axis, followed by a rotation θ about the new Y' -axis, and finally a rotation ψ about the new Z'' -axis.

To find the entire singularity loci and solve the problem, the singularity equation in a special plane is first investigated (Huang et al. [29]). The problem is divided into two parts, as follows:

- (a) When the first Euler angle ϕ is equal to one of the three values, namely, $\pm 30^\circ$, $\pm 90^\circ$, and $\pm 150^\circ$, the case is a special orientation one and thus is easier to analyze; and
- (b) When ϕ is any value except $\pm 30^\circ$, $\pm 90^\circ$, and $\pm 150^\circ$, the case is a general case.

We now solve the equation for the singularity curve of the 3/6-SP in a certain plane while the orientation of the mobile is provisionally set to $\phi = \pm 90^\circ$, $\psi = 0$, and θ is any finite nonzero value. The parameters of the parallel manipulator are as follows: the circumcircle radius of the basic hexagon platform is R_a , and that of the triangle mobile is R_b ; and β_0 denotes the central angle of the circumcircle of the basic hexagon corresponding to side C_1C_2 . Point P is the geometric center of the mobile (Fig. 7.10). The stationary frame O - XYZ is fixed to the base, and the moving frame P - $X'Y'Z'$ is attached to the mobile.

Figure 7.12 shows the position after the mobile rotates $(90^\circ \theta 0)$. The oblique plane in which the moving platform lies intersects the basic plane at line UV , which is parallel to axis X . For the orientation, B_1P (Y') is parallel to A_5A_1 (X). Initially, provided that point P is located at a special point C_0 in the perpendicular bisector of UV , and the distance from O_2 to point C_0 is equal to that between point O_2 and A_3 , then we deduce that C_0B_3 and A_3A_1 intersect at point V , and C_0B_5 and A_3A_5 intersect at U . Therefore, the mechanism is singular, according to Deduction 7.2. The included angle between the oblique plane and the basic one is θ . To conveniently express the

oblique plane below, the plane is called the θ plane. Suppose that the mobile translates to the position $B_{11}B_{31}B_{51}$ in the θ plane and line $B_{11}P$ intersects line O_2C_0 at C . If line $B_{31}C$ intersects A_1A_3 at point V , and line CB_{51} intersects A_3A_5 at point U , the mechanism is also singular (Deduction 7.2), and the center of the star frame always lies in line O_2C_0 for the orientation. In general, the singularity is a general linear-complex singularity. Based on this analysis, the singularities of 3/6-SP when the mobile translates arbitrarily in the θ plane are determined. The coordinates of points C_0 and O_2 with respect to the fixed frame are $(0, Y_0, Z_0)$ and $(0, u, 0)$, respectively. The frame O_2 -xyz is attached to the θ plane. The angle θ (Fig. 7.12) about the Y' axis is notably negative.

The coordinates of points P, C, B_{31} , and V with respect to O_2 -xyz are

$$\begin{aligned} P &: (x, y, 0) \\ C &: (0, y, 0) \\ B_{31} &: \left(x - \frac{R_b}{2}, y + \frac{\sqrt{3}}{2}R_b, 0 \right) \\ V &: \left(-\frac{\sqrt{3}}{3} \frac{Z_0}{\sin \theta}, 0, 0 \right) \end{aligned} \quad (7.8)$$

Considering that $O_2C_0 = O_2A_3$, we can obtain

$$O_2O_1 - OO_1 + OA_3 = O_2C_0 \quad (7.9)$$

that is,

$$3R_a \cos(\beta_0/2) - Z_0 \frac{\cos \theta}{\sin \theta} - Y_0 = -\frac{Z_0}{\sin \theta} \quad (7.10)$$

In the right-angled triangle $\Delta O_1O_2C_0$, we obtain

$$Y_0 - u = -Z_0 \frac{\cos \theta}{\sin \theta} \quad (7.11)$$

Solving Eqs. (7.10) and (7.11) for Y_0 and Z_0 , we obtain

$$\begin{aligned} Y_0 &= u(1 - \cos \theta) + 3R_a \cos(\beta_0/2) \cos \theta \\ Z_0 &= u \sin \theta - 3R_a \cos(\beta_0/2) \sin \theta \end{aligned} \quad (7.12)$$

Provided that the coordinates of an arbitrary point in line $B_{31}V$ are $(x_x, y_y, 0)$, its equation is written as follows:

$$\frac{y_y - y - \frac{\sqrt{3}}{2}R_b}{-y - \frac{\sqrt{3}}{2}R_b} = \frac{x_x - x + \frac{R_b}{2}}{-\frac{\sqrt{3}}{3} \frac{Z_0}{\sin \theta} - x + \frac{R_b}{2}} \quad (7.13)$$

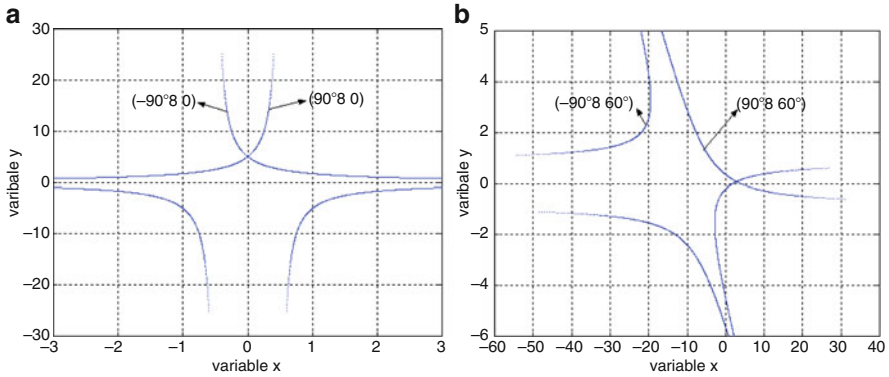


Fig. 7.13 Singularity curve in the θ plane (a) For orientation $(\pm 90^\circ \ \theta \ 0)$ (b) For orientation $(\pm 90^\circ \ \theta \ 60^\circ)$

Given that point C lies in line $B_{31}V$, the coordinates of point C ($x_x = 0$ and $y_y = y$) are substituted into Eq. (7.13) and simplified, yielding

$$xy - \frac{R_b}{2}y - \frac{Z_0R_b}{2 \sin \theta} = 0 \tag{7.14}$$

Substituting Eq. (7.12) into Eq. (7.14) and eliminating Z_0 yields

$$xy - \frac{R_b}{2}y + \frac{(3R_a \cos(\beta_0/2) - u)R_b}{2} = 0 \tag{7.15}$$

Equation (7.15) denotes a hyperbola and is independent of the Euler angle θ . The coordinates of its center are $(R_b/2, 0)$, and its vertical and horizontal asymptotes are $x = R_b/2$ and $y = 0$, respectively.

The conclusion obtained is an important one, given that the singularity equation for SP in 3D space is a polynomial expression of degree three. However, Eq. (7.15) is only a quadratic equation in the special θ plane and only contains the variables x and y ; thus, it denotes the position of point P when the mechanism is singular. The equation is called the equation of the singularity curve in the θ plane.

When the orientation of the mobile is given by the three Euler angles $(90^\circ \ \theta \ 0)$, the singularity equation can also be obtained in the θ plane with respect to the frame $O_2 - xyz$, similar to that in Fig. 7.12.

$$xy + \frac{R_b}{2}y - \frac{(3R_a \cos(\beta_0/2) - u)R_b}{2} = 0 \tag{7.16}$$

When the mechanism parameters are set to $R_a = \sqrt{2}$, $R_b = 1$, $\beta_0 = 90^\circ$, and $u = -2$, the hyperbolas denoted by Eqs. (7.15) and (7.16) are illustrated in Fig. 7.13a. Given that the result comes from the aforementioned Theorem and

satisfies the necessary and sufficient condition for singularity, no other singularity exists except the points on the hyperbolas in the θ plane.

7.4.3 Singularity Equation Derived in 3D Space

Equations (7.15) and (7.16) are deduced via the geometric method in an oblique plane. Using Theorem 7.1, the distribution properties of the singularities of 3/6-SP in 3D space can be analyzed.

The coordinates of the point $B_i (i = 1, 2, 3)$ of the mobile are denoted as $B'_i (B'_{ix}, B'_{iy}, B'_{iz})$ in the moving frame and as (B_{ix}, B_{iy}, B_{iz}) in the fixed frame; the coordinates of point $C_i (i = 1, 2, \dots, 6)$ are denoted as (C_{ix}, C_{iy}, C_{iz}) in the fixed frame (Fig. 7.10).

$$\begin{aligned} B'_1 &: (0, -R_b, 0)^T \\ B'_3 &: (R_b \cos 30^\circ, R_b \sin 30^\circ, 0) \\ B'_5 &: (-R_b \cos 30^\circ, R_b \sin 30^\circ, 0) \\ C_1 &: (-R_a \sin(\beta_0/2), 0, 0)^T \\ C_2 &: (R_a \sin(\beta_0/2), 0, 0) \end{aligned} \quad (7.17)$$

$$\begin{aligned} C_3 &: (R_a \cos(30^\circ - \beta_0/2), \sqrt{3}R_a \cos(30^\circ + \beta_0/2), 0)^T \\ C_4 &: (R_a \cos(30^\circ + \beta_0/2), \sqrt{3}R_a \cos(30^\circ - \beta_0/2), 0)^T \\ C_5 &: (-R_a \cos(30^\circ + \beta_0/2), \sqrt{3}R_a \cos(30^\circ - \beta_0/2), 0)^T \\ C_6 &: (-R_a \cos(30^\circ + \beta_0/2), \sqrt{3}R_a \cos(30^\circ + \beta_0/2), 0)^T \end{aligned} \quad (7.18)$$

The transformation matrix $[T]$ of the moving frame with respect to the fixed matrix can be written using the Euler angles ϕ , θ , and ψ , as follows:

$$[T] = \begin{bmatrix} \cos \varphi \cos \theta \cos \psi - \sin \varphi \sin \psi & -\cos \varphi \cos \theta \sin \psi - \sin \varphi \cos \psi & \cos \varphi \sin \theta & X \\ \sin \varphi \cos \theta \cos \psi + \cos \varphi \sin \psi & -\sin \varphi \cos \theta \sin \psi + \cos \varphi \cos \psi & \sin \varphi \sin \theta & Y \\ -\sin \theta \cos \psi & \sin \theta \sin \psi & \cos \theta & Z \\ \mathbf{0} & \mathbf{0} & \mathbf{0} & \mathbf{1} \end{bmatrix} \quad (7.19)$$

Where (X, Y, Z) are the coordinates of point P with respect to the fixed frame. The coordinates of point B_i in the mobile with respect to the fixed frame are

$$\begin{Bmatrix} B_{ix} \\ B_{iy} \\ B_{iz} \\ 1 \end{Bmatrix} = [T] \begin{Bmatrix} B'_{ix} \\ B'_{iy} \\ B'_{iz} \\ 1 \end{Bmatrix}, \quad i = 1, 2, 3 \quad (7.20)$$

7.4.3.1 Singularity Equation for the Orientation (90° θ 0)

When the three Euler angles are 90°, θ , and 0, the transformation matrix $[\mathbf{T}]$ is expressed as

$$[\mathbf{T}] = \begin{bmatrix} 0 & -1 & 0 & X \\ \cos \theta & 0 & \sin \theta & Y \\ -\sin \theta & 0 & \cos \theta & Z \\ 0 & 0 & 0 & 1 \end{bmatrix} \quad (7.21)$$

The coordinates of the three points B_i ($i = 1, 3, 5, \dots$) in the mobile with respect to the fixed frame can be obtained using Eq. (7.20). Thus, the three equations for the three normal planes $B_1C_1C_2$, $B_3C_3C_4$, and $B_5C_5C_6$ and the one that the mobile belongs to can be written using the coordinates of the three corresponding points. The equation for plane $B_1C_1C_2$ is as follows:

$$\begin{vmatrix} x - B_{1x} & y - B_{1y} & z - B_{1z} \\ C_{1x} - B_{1x} & C_{1y} - B_{1y} & C_{1z} - B_{1z} \\ C_{2x} - B_{1x} & C_{2y} - B_{1y} & C_{2z} - B_{1z} \end{vmatrix} = 0 \quad (7.22)$$

where x , y , and z are the coordinates of a moving point in plane $B_1C_1C_2$ with respect to the fixed frame. Substituting the coordinates of points B_1 , C_1 , and C_2 into the Eq. (7.22) gives

$$Zy - Yz = 0 \quad (7.23)$$

Similarly, the equation for plane $B_3C_3C_4$ can be obtained as follows:

$$\begin{aligned} & \left(-3R_b \sin \theta + 2\sqrt{3Z}\right)x + \left(2Z - \sqrt{3}R_b \sin \theta\right)y \\ & + \left(-2Y + 6R_a \cos(\beta_0/2) - \sqrt{3}R_b \cos \theta + \sqrt{3}R_b - 2\sqrt{3}X\right)z \\ & - 6ZR_a \cos(\beta_0/2) + 3\sqrt{3}R_a R_b \sin \theta \cos(\beta_0/2) = 0 \end{aligned} \quad (7.24)$$

and that of plane $B_5C_5C_6$ is

$$\begin{aligned} & \left(-3R_b \sin \theta + 2\sqrt{3Z}\right)x + \left(2Z + \sqrt{3}R_b \sin \theta\right)y + (-2Y \\ & + 6R_a \cos(\beta_0/2) + \sqrt{3}R_b \cos \theta - \sqrt{3}R_b + 2\sqrt{3}X)z \\ & - 6ZR_a \cos(\beta_0/2) + 3\sqrt{3}R_a R_b \sin \theta \cos(\beta_0/2) = 0 \end{aligned} \quad (7.25)$$

The equation for plane $B_1B_3B_5$ is

$$(\sin \theta)y + (\cos \theta)z - (\sin \theta)Y - (\cos \theta)Z = 0 \quad (7.26)$$

Note that the equations for these planes are under the same condition that point P (X, Y, Z) is point, and the orientation denoted by the three Euler angles ($90^\circ \theta 0$).

Solving Eqs. (7.23), (7.24), and (7.25) for $x, y,$ and $z,$ substituting them into Eq. (7.26), and eliminating $x, y,$ and z gives

$$\begin{aligned} &[(\sin \theta)Y + (\cos \theta)Z][2XZ + R_b(\sin \theta)Y + R_b(\cos \theta)Z \\ &\quad - R_b Z - 3R_b R_a \sin \theta \cos(\beta_0/2)] = 0 \end{aligned} \quad (7.27)$$

According to Theorem 7.1, Eq. (7.27) denotes the singularity locus of point P for the orientation ($90^\circ \theta 0$). Obviously, the singularity includes a plane and a conicoid. The plane equation is

$$(\sin \theta)Y + (\cos \theta)Z = 0 \quad (7.28)$$

Equation (7.28) denotes that the singularity locus of point P is a plane containing line C_1C_2 , namely, the X -axis. As the plane and plane $B_1B_3B_5$ denoted by Eq. (7.26) have the same normal vector, and when plane $B_1B_3B_5$ translates and coincides with the plane expressed by Eq. (7.28), the configuration is singular. The case belongs to Hunt's singularity and is the first special-linear-complex singularity explained in Case 5. Equation (7.28) shows that the mechanism is singular regardless of the location of point P in the plane.

The conicoid equation is as follows:

$$\begin{aligned} &2XZ + R_b(\sin \theta)Y + R_b((\cos \theta) - 1)Z \\ &\quad - 3R_b R_a \sin \theta \cos(\beta_0/2) = 0 \end{aligned} \quad (7.29)$$

When θ is constant, Eq. (7.29) denotes a hyperbolic paraboloid, which will be discussed later.

When the orientation is determined by the three Euler angles ($-90^\circ \theta 0$), the singularity locus is similar to the one previously described. The first equation is then

$$(\sin \theta)Y - (\cos \theta)Z = 0 \quad (7.30)$$

Equation (7.30) also denotes a plane crossing line C_1C_2 . The second equation is as follows:

$$\begin{aligned} &2XZ + R_b(\sin \theta)Y - R_b((\cos \theta) - 1)Z \\ &\quad - 3R_b R_a \sin \theta \cos(\beta_0/2) = 0 \end{aligned} \quad (7.31)$$

Equation (7.31) also represents a hyperbolic paraboloid.

7.4.3.2 Singularity Equation for the Orientation ($\pm 90^\circ \theta 0$)

Derivation of the Equation

For the orientation ($90^\circ \theta 0$), the transformation matrix $[\mathbf{T}]$ is

$$[\mathbf{T}] = \begin{bmatrix} -c & -d & 0 & X \\ bd & -bc & a & Y \\ -ad & ac & b & Z \\ 0 & 0 & 0 & 1 \end{bmatrix} \quad (7.32)$$

where

$$a = \sin \theta; \quad b = \cos \theta; \quad c = \sin \psi; \quad d = \cos \psi \quad (7.33)$$

The equations for the three normal planes can be obtained using the previously described method.

$$(acR_b - Z)y + (bcR_b + Y)z = 0 \quad (7.34)$$

$$\begin{aligned} & \sqrt{3} \left(\sqrt{3}adR_b - acR_b - 2Z \right) x + \left(\sqrt{3}adR_b - 2Z - acR_b \right) y \\ & + \left(2Y + 2\sqrt{3}X + \sqrt{3}bdR_b - 3cR_b - \sqrt{3}dR_b - bcR_b \right. \\ & - 6R_a \cos(\beta_0/2) \left. \right) z + 3R_a \cos(\beta_0/2) (2Z + acR_b \\ & - \sqrt{3}adR_b) = 0 \end{aligned} \quad (7.35)$$

$$\begin{aligned} & \sqrt{3} \left(acR_b + 2Z + \sqrt{3}adR_b \right) x - \left(2Z + \sqrt{3}adR_b + acR_b \right) y + (2Y \\ & - bcR_b - 6R_a \cos(\beta_0/2) - \sqrt{3}bdR_b - 3cR_b + \sqrt{3}dR_b - 2\sqrt{3}X) z \\ & + 3R_a \cos(\beta_0/2) \left(2Z + acR_b + \sqrt{3}adR_b \right) = 0 \end{aligned} \quad (7.36)$$

The equation for plane $B_1B_3B_5$ is

$$ay + bz - aY - bZ = 0 \quad (7.37)$$

Solving Eqs. (7.34), (7.35), and (7.36) for x , y , and z , respectively, and then substituting them into Eq. (7.37), the singularity equation is obtained as

$$\begin{aligned} & (aY + bZ) [2c(b+1)Z^2 - 2adXZ + 2acYZ + 2R_b a^2 c d X \\ & - R_b a^2 (d^2 - c^2) Y + (a(d^2 - c^2)(1-b)R_b \\ & - 6acR_a \cos(\beta_0/2)) Z + 3a^2 (d^2 - c^2) R_b R_a \cos(\beta_0/2) \\ & - R_b^2 a^2 c] = 0 \end{aligned} \quad (7.38)$$

Substituting Eq. (7.33) into Eq. (7.38), we obtain

$$\begin{aligned} &[(\sin \theta)Y + (\cos \theta)Z](eZ^2 - fXZ + gYZ + hX \\ &\quad - iY + jZ + k) = 0 \end{aligned} \quad (7.39)$$

where

$$\begin{aligned} e &= 2 \sin \psi (1 + \cos \theta) \\ f &= 2 \sin \theta \cos \psi \\ g &= 2 \sin \theta \sin \psi \\ h &= R_b \sin^2 \theta \sin(2\psi) \\ i &= R_b \sin^2 \theta \cos(2\psi) \\ j &= \sin \theta (R_b \cos(2\psi)(1 - \cos \theta) - 6R_a \sin \psi \cos(\beta_0/2)) \\ k &= 3R_b R_a \sin^2 \theta \cos(2\psi) \cos(\beta_0/2) - R_b^2 \sin^2 \theta \sin \psi \end{aligned} \quad (7.40)$$

Equation (7.39) shows that the singular loci include a plane and a conicoid, and the plane equation is the same as Eq. (7.28). It also shows that in this case, all six lines cross a common line. This case belongs to the first special-linear-complex singularity. The quadratic equation is as follows:

$$eZ^2 - fXZ + gYZ + hX - iY + jZ + k = 0 \quad (7.41)$$

Equation (7.41) is a singularity equation with respect to the fixed frame $O - XYZ$. When the mobile shown in Fig. 7.12 again rotates at an angle ψ about the Z'' -axis, its orientation is $(90^\circ \theta \psi)$. The plane in which the mobile lies is still the θ plane. After the coordinate transformation, the equation for the singularity curve in the θ plane with respect to the frame $O_2 - xyz$ is

$$\begin{cases} 2(\sin \psi)y^2 + 2(\cos \psi)xy + R_b \sin(2\psi)x + (-2u \sin \psi + \\ 6R_a \sin \psi \cos(\beta_0/2) - R_b \cos(2\psi))y - R_b^2 \sin \psi + \\ R_b \cos(2\psi)(3R_a \cos(\beta_0/2) - u) = 0 \\ z = 0 \end{cases} \quad (7.42)$$

which is also a hyperbola. In addition, Eq. (7.42) is independent of the Euler angle θ .

The singularity equation for the orientation $(-90^\circ \theta \psi)$ of the mobile can also be obtained. It consists of a simple equation and a quadratic equation. The simple equation is the same as Eq. (7.30), whereas the quadratic equation is

$$eZ^2 + fXZ - gYZ - hX + iY + j_1Z - k_1 = 0 \quad (7.43)$$

where

$$\begin{aligned} j_1 &= \sin \theta (R_b \cos(2\psi)(1 - \cos \theta) + 6R_a \sin \psi \cos(\beta_0/2)) \\ k_1 &= 3R_b R_a \sin^2 \theta \cos(2\psi) \cos(\beta_0/2) + R_b^2 \sin^2 \theta \sin \psi \end{aligned} \quad (7.44)$$

When the frame $O_2 - xyz$ (Fig. 7.12) is defined in the θ plane, the equation for the singularity curve can also be obtained as follows:

$$\begin{cases} 2(\sin \psi)y^2 + 2(\cos \psi)xy - R_b \sin(2\psi)x + (-2u \sin \psi + \\ 6R_a \sin \psi \cos(\beta_0/2) + R_b \cos(2\psi))y - R_b^2 \sin \psi + \\ R_b \cos(2\psi)(u - 3R_a \cos(\beta_0/2)) = 0 \\ z = 0 \end{cases} \quad (7.45)$$

The hyperbolas denoted by Eqs. (7.42) and (7.45) when $R_x = \sqrt{2}$, $R_b = 1$, $\beta_0 = 90^\circ$, $u = -2$, and $\psi = 60^\circ$ are shown in Fig. 7.13b.

Analysis of the Singularity Property

The four invariants Δ , D , I , and J of Eq. (7.41) are

$$\Delta = \begin{vmatrix} 0 & 0 & -\frac{f}{2} & \frac{h}{2} \\ 0 & 0 & \frac{g}{2} & -\frac{i}{2} \\ -\frac{f}{2} & \frac{g}{2} & e & \frac{j}{2} \\ \frac{h}{2} & -\frac{i}{2} & \frac{j}{2} & k \end{vmatrix} = \frac{R_b^2 \sin^6 \theta \cos^2 3\psi}{4} \geq 0 \quad (7.46)$$

$$D = \begin{vmatrix} 0 & 0 & -\frac{f}{2} \\ 0 & 0 & \frac{g}{2} \\ -\frac{f}{2} & \frac{g}{2} & e \end{vmatrix} = 0 \quad (7.47)$$

$$\begin{aligned} I &= 2 \sin \psi (1 + \cos \theta) \\ J &= -\sin^2 \theta \end{aligned} \quad (7.48)$$

The following cases are discussed according to its invariants, in which D is always zero regardless of θ and ψ .

1. If $\theta \neq 0$, $\psi \neq \pm 30^\circ$, $\pm 90^\circ$, or $\pm 150^\circ$, then $D = 0$, $\Delta > 0$, the singular locus denoted by Eq. (7.41) is a hyperbolic paraboloid, and, in the same way, the one by

Eq. (7.29) is also a hyperbolic paraboloid, with $\psi = 0$. Generally, the six lines (1, 2, ..., 6) belong to a general linear complex when point P is located at the surface.

2. If $\theta = 0$, Eq. (7.39) can be written as

$$4(\sin \psi)Z^3 = 0 \quad (7.49)$$

- (a) When $\psi = 0$ and $Z \neq 0$, namely, the orientation is $(90^\circ \theta 0)$, Eq. (7.49) is an identical equation and the mechanism is singular regardless of the position of point P in 3D space. This is the Fichter's singular configuration, and all six lines belong to a general linear complex.
 - (b) When $Z = 0$, the moving platform and the base are coplanar. The mechanism is also singular regardless of the Euler angle ψ . This case is similar to Sect. 7.4.1, Case 7. The mechanism holds three remnant freedoms when all legs are locked. In this case, the first and second special-linear-complex singularities exist.
3. If $\theta \neq 0$, $\psi = \pm 30^\circ$, $\pm 90^\circ$, or $\pm 150^\circ$, then $D = 0$, $\Delta = 0$, and $J \neq 0$, and the conicoid degenerates into a pair of intersecting planes. For instance, when $\psi = 30^\circ$, the two equations are as follows

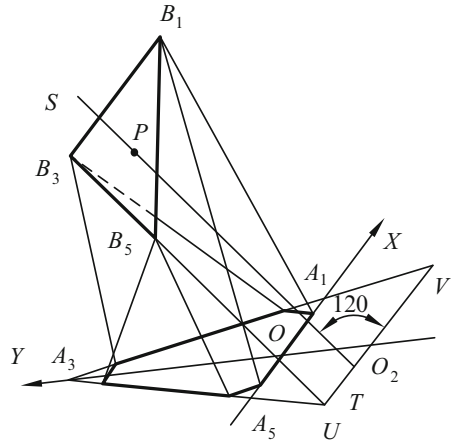
$$2Z - R_b \sin \theta = 0 \quad (7.50)$$

$$\begin{aligned} \sqrt{3}(\sin \theta)X - (\sin \theta)Y - (1 + \cos \theta)Z - R_b \sin \theta \\ + 3R_a \sin \theta \cos(\beta_0/2) = 0 \end{aligned} \quad (7.51)$$

- (a) Equation (7.50) denotes a plane, which is parallel to the basic plane $X-O-Y$. When point P lies in the plane, the mechanism is singular for the orientation $(90^\circ \theta 30)$ because points B_1 and B_3 lie in the basic plane. This situation is similar to that in Case 6. All six lines cross the same line (C_5C_6).
- (b) Equation (7.51) also denotes a plane. Given that $\psi = 30^\circ$, line B_1B_3 is always parallel to line A_1A_5 . The intersecting line ST of the plane is denoted in Eq. (7.51), and the θ plane is parallel to line B_3B_5 . Moreover, line B_3B_5 always intersects point U when point P translates along the intersecting line (Fig. 7.14). Considering that B_1B_3 is parallel to line A_1A_5 , and B_3B_5 intersects point U , B_3 is the common point of plane $B_1C_1C_2$ and $B_5C_5C_6$. Thus, B_3A_5 is the line of intersection of the two planes. Therefore, all six lines cross line B_3A_5 , and the singularity belongs to the first special-linear-complex singularity. B_3A_5 is the rotary axis of the pure rotation. In this case, two sides, namely, B_1B_3 and B_3B_5 , of the mobile are coplanar with the two corresponding sides (A_1A_5 and A_3A_5) of the base, and point B_3 is just the center point of the defined star frame. This situation is similar to that in Case 4.

When $\psi = -30^\circ$, $\pm 90^\circ$, or $\pm 150^\circ$, the conicoid also degenerates into two planes, and the singularity cases are similar to those previously mentioned.

Fig. 7.14 Singular case denoted by Eq. (7.51)



Analysis of Other Singularities

The singularities discussed above are all for the orientation $(\pm 90^\circ \theta \psi)$ of the mobile. In these cases, the intersecting lines between the oblique moving plane and the basic one are parallel to line C_1C_2 or A_1A_5 , which is one of the three sides of the triangle $A_1A_3A_5$ (Fig. 7.10). Similar singularities with a plane equation and a quadratic one can also occur when the orientations are as follows:

1. The Euler angles are

$$(-150^\circ \theta \psi) \quad \text{or} \quad (30^\circ \theta \psi)$$

All intersecting lines between the oblique mobile and the base are parallel to line C_3C_4 or A_1A_3 .

2. The Euler angles are

$$(150^\circ \theta \psi) \quad \text{or} \quad (-30^\circ \theta \psi)$$

All intersecting lines between the oblique mobile and the base are parallel to line C_5C_6 or A_3A_5 .

For the two cases, the singularity equation can also resolve into two parts: one is a plane equation containing the corresponding side C_iC_j , and the other is also a hyperbolic paraboloid equation. When $\psi = \pm 130^\circ, \pm 90^\circ, \text{ or } \pm 150^\circ$, the hyperbolic paraboloid also degenerates into two planes.

When the Euler angle ϕ is any value except $\pm 30^\circ, \pm 90^\circ, \text{ and } \pm 150^\circ$, the intersecting lines between the two planes above are not parallel to any one of the three sides of the basic triangle $A_1A_3A_5$. These cases are more general, and their singularity properties will not be discussed here. However, when the orientation is

$$(\phi \theta \pm 30^\circ), \quad (\phi \theta \pm 90^\circ), \quad (\phi \theta \pm 150^\circ)$$

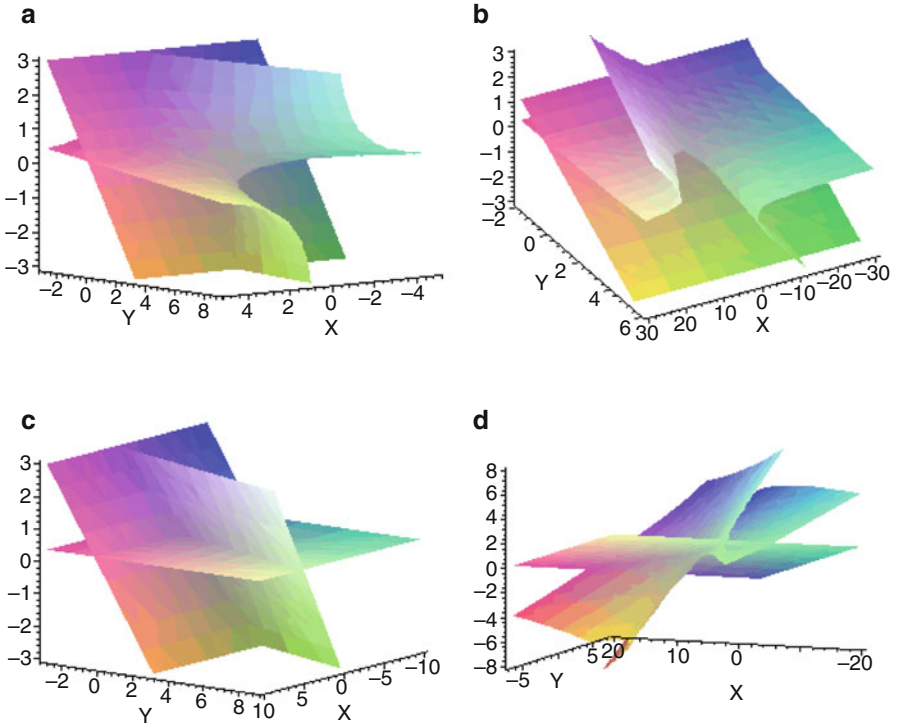


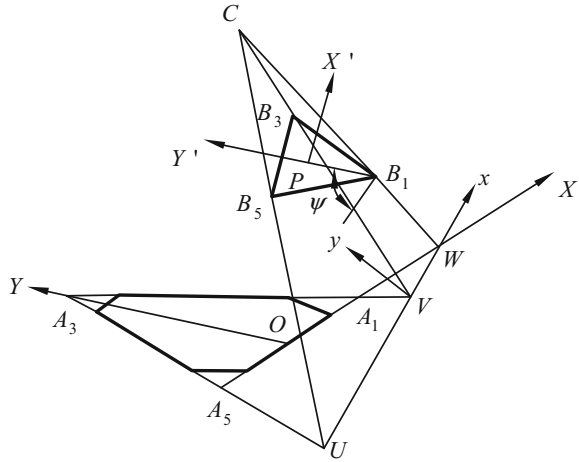
Fig. 7.15 Singularity loci for the 3/6-Stewart parallel manipulator (a) (90°45°0°) orientation (b) (90°30°60°) orientation (c) (90°45°30°) orientation (d) (45°25°30°) orientation

in which ϕ and θ can be arbitrary values, the singularity locus also consists of two parts, namely, a plane and a hyperbolic paraboloid. When point P translates in the plane, two of three points $B_1, B_3,$ and B_5 lie in the basic plane. These cases are similar to that in Case 6. Obviously, when $\phi = \pm 30^\circ, \pm 90^\circ,$ or $\pm 150^\circ,$ the hyperbolic paraboloid can also resolve into two planes.

7.4.4 Singularity Distribution in 3D Space

According to the aforementioned analysis, the distribution characteristics of the singularity loci of the 3/6-Stewart manipulator can be easily obtained, and their singularity surface for different orientations of the mobile in frame $O\text{-}XYZ$ can be drawn in 3D space (Fig. 7.10). In this section, the parameters of the mechanism are set to $R_a = \sqrt{2}, R_b = 1,$ and $\beta_0 = 90^\circ;$ the surfaces are shown in Fig. 7.15.

Fig. 7.16 General case



One may ask, if the singularity loci are so huge and completed, how can the manipulator work? In practice, the workspace of the manipulator is smaller relative to the singularity loci shown in the figures. A manipulator with its workspace located over the singularity loci can easily be designed, and the singularity is avoided.

7.5 Structure and Property of the Singularity Loci of 3/6-Stewart for General Orientations ($\phi \neq \pm 30^\circ, \pm 90^\circ, \pm 150^\circ$)

When ϕ takes any value except $\pm 30^\circ, \pm 90^\circ$ and $\pm 150^\circ$, the case is that of a general orientation of the 3/6-SP mobile, and the analysis of the singularity loci is more difficult. In this case, UV is not parallel to any side of the triangle $A_1A_3A_5$, as shown in.

7.5.1 Singularity Equation Based on Theorem 7.2 for General Orientations

For the most general orientations of the mobile ($\phi \neq \pm 30^\circ, \pm 90^\circ, \pm 150^\circ$), the singularity equation can be directly obtained using Theorem 7.2. The equation for the normal plane $B_1C_1C_2$ is as follows:

$$\begin{vmatrix} x' - B_{1x} & y' - B_{1y} & z' - B_{1z} \\ C_{1x} - B_{1x} & C_{1y} - B_{1y} & C_{1z} - B_{1z} \\ C_{2x} - B_{1x} & C_{2y} - B_{1y} & C_{2z} - B_{1z} \end{vmatrix} = 0 \tag{7.52}$$

where (x', y', z') denotes the coordinates of the moving point on plane $B_1C_1C_2$ in the fixed frame. Thus,

$$Fy' + Gz' = 0 \quad (7.53)$$

where

$$F = R_b \sin \theta \sin \psi - Z \quad (7.54)$$

$$G = -R_b \cos \phi \cos \psi + R_b \sin \phi \cos \theta \sin \psi + Y \quad (7.55)$$

Similarly, the equations for the three planes $B_3C_3C_4$, $B_5C_5C_6$, and $B_1B_3B_5$ can also be obtained. According to Theorem 7.2, to solve the linear equation system of the four planes for the intersecting point C , the singularity locus equation for the general orientations is as follows:

$$\begin{aligned} f_1Z^3 + f_2XZ^2 + f_3YZ^2 + f_4X^2Z + f_5Y^2Z + f_6XYZ + f_7Z^2 + f_8X^2 \\ + f_9Y^2 + f_{10}XY + f_{11}XZ + f_{12}YZ + f_{13}Z + f_{14}X + f_{15}Y + f_{16} = 0 \end{aligned} \quad (7.56)$$

where (X, Y, Z) are the coordinates of center point P . Equation (7.56) is a polynomial expression of degree three. The equation is still very complicated and difficult to further analyze, but it is very simple in the subsequent special cases.

When $\phi \neq \pm 30^\circ, \pm 90^\circ, \pm 150^\circ$, and ψ are $\pm 30^\circ, \pm 90^\circ$, or $\pm 150^\circ$, Eq. (7.56) degenerates into a plane and a hyperbolic paraboloid. For example, when $\psi = 90^\circ$, the singularity equation is

$$\begin{aligned} (2Z + R_b \sin \theta)(a_{11}X^2 + a_{22}Y^2 + a_{33}Z^2 + 2a_{23}YZ + 2a_{31}ZX + 2a_{12}XY \\ + 2a_{14}X + 2a_{24}Y + 2a_{34}Z + a_{44}) = 0 \end{aligned} \quad (7.57)$$

Equation (7.57) indicates a plane and a hyperbolic paraboloid. The first factor forms a plane equation

$$2Z + R_b \sin \theta = 0 \quad (7.58)$$

which is parallel to the basic plane. When point P lies in the plane, the mechanism is singular for the orientation $(\phi \quad \theta \quad 90^\circ)$ because points B_3 and B_5 lie in the basic plane. This condition is similar to that in Case 6. All six lines cross the same line C_1C_2 .

To verify its correctness via another method, point $P(X, Y, Z) = (0, 0, -3/8)$ is taken from the plane equation $2Z + R_b \sin \theta = 0$ when $R_a = 2$, $R_b = 1.5$,

$\beta_0 = \pi/2$, $\phi = \pi/3$, $\theta = \pi/6$, $\psi = \pi/4$, and $(\phi \ \theta \ \psi) = (60^\circ \ 30^\circ \ 90^\circ)$; the corresponding Jacobian matrix of the parallel mechanism is as follows:

$$\mathbf{J} = \begin{pmatrix} 0.8489 & -0.3230 & -0.9914 & -0.5489 & 0.2025 & 0.7246 \\ 0.3343 & 0.5986 & -0.1310 & -0.8359 & -0.9793 & -1.6892 \\ -0.4094 & -0.7331 & 0 & 0 & 0 & 0 \\ 0 & 0 & 0 & 0 & 0 & 0 \\ -0.5790 & 1.0367 & 0 & 0 & 0 & 0 \\ 0.4727 & 0.8465 & 0.6358 & 1.4038 & -0.1707 & 0.6818 \end{pmatrix}$$

$$\det(\mathbf{J}) = 7.0616 \times 10^{-17} = 0$$

(7.59)

The mechanism is also singular. Further analysis shows that in this case, two vertices B_3 and B_5 lie on the base plane. This is a case of four lines lying in a plane, which is of the type 3d [4] and belongs to the first special-linear-complex singularity. Its instantaneous motion is a pure rotation.

7.5.2 Singularity Analysis Using Singularity-Equivalent-Mechanism

The singularity locus expression, Eq. 7.56, for the general orientations has been derived using Theorem 7.2. However, it is still quite complicated, and whether it consists of some typical geometric figures remains to be determined. Meanwhile, the properties of the singularity loci are still unknown. To answer this question, a ‘‘Singularity-Equivalent Mechanism,’’ which is a planar mechanism based on Deduction 7.2, is proposed. Thus, the difficult singularity analysis of the SP can be transformed into a positional analysis of a simpler planar mechanism.

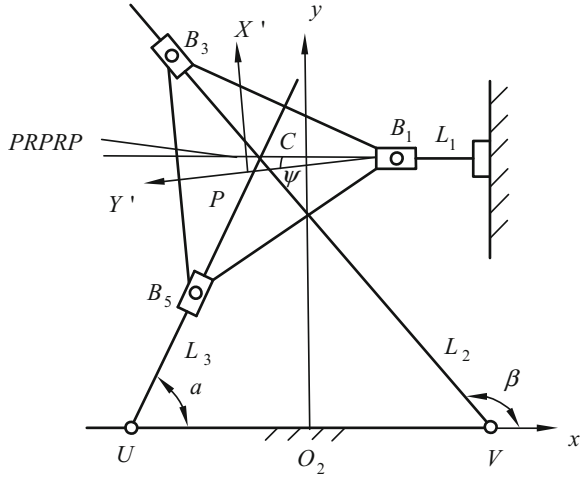
7.5.2.1 Parallel Case

Singularity-Equivalent-Mechanism

In the parallel case, the three Euler angles of the mobile platform are $(90^\circ, \theta, \psi)$, whereas θ and ψ can be any nonzero value. The mobile plane of the mechanism lies on the θ plane (Fig. 7.12). The corresponding imaginary planar singularity-equivalent-mechanism is shown in Fig. 7.17.

When R denotes a revolute pair and P is a prismatic pair, triangle $B_1B_3B_5$ is connected to the ground by three kinematic chains, namely, RPP , RPR , and RPR . The latter two pass through points U and V , respectively, whereas the first slides along the vertical direction and maintains $B_1C//UV$. Three slotted links, L_1 , L_2 ,

Fig. 7.17 Singularity-equivalent-mechanism for $(90^\circ \theta \psi)$



and L_3 , intersect at a common point C . To maintain the intersection of the three links at a common point and satisfy Deduction 7.2, a concurrent kinematic chain, $PRPRP$, is used. It consists of five kinematic pairs, wherein two R pairs connect three sliders. The three sliders and three slotted links form three P pairs. The $PRPRP$ chain coincides with a single point C from the top view. Based on the Modified G-K Criterion, the mobility of the mechanism is two.

The planar mechanism can clearly guarantee that the three lines passing through the three vertices intersect at a common point, and these three lines can always intersect the corresponding sides of the basic triangle. From Deduction 7.2, every position of the planar mechanism corresponds to an SC of the original SP. Thus, it is called a “singularity-equivalent-mechanism,” and the position solution of the planar mechanism expresses the singularity of the original mechanism.

Forward Position Analysis of the Singularity Equivalent-Mechanism

The frames are set similar to those in Figs. 7.12 and 7.17. The coordinates of point P in frame O_2-xy are (x, y) . ψ denotes the orientation of the triangle $B_1B_3B_5$ in the θ plane. To obtain the locus equation for point P , the three equations of the three lines passing through the three vertices are first set, and the coordinates of points B_1, B_3 , and B_5 are substituted into the equations to obtain (x, y) and ψ .

Considering that the mobility of this mechanism is two, two inputs, α and β , are necessary. The three equations for the three lines CU, CV , and CB_1 in the reference frame O_2-xy are

$$Y = (\tan \alpha)(X + a/2) \tag{7.60}$$

$$Y = (\tan \beta)(X - a/2) \tag{7.61}$$

and

$$Y = -\frac{a \tan \alpha \tan \beta}{\tan \alpha - \tan \beta}, \quad (7.62)$$

respectively. Solving Eqs. (7.60), (7.61), and (7.62) yields

$$x = \frac{R_b \cos \psi J_1 - (\sqrt{3}R_b \sin \psi + a)J_3}{2(\tan \alpha - \tan \beta)} \quad (7.63)$$

$$y = \frac{R_b \sin \psi J_2 - \sqrt{3}R_b J_3 \cos \psi - 2a \tan \alpha \tan \beta}{2(\tan \alpha - \tan \beta)} \quad (7.64)$$

and

$$\tan \psi = \frac{(\tan \beta + \tan \alpha)}{\sqrt{3} \tan \alpha - \sqrt{3} \tan \beta - 2 \tan \alpha \tan \beta} \quad (7.65)$$

Where $J_1 = \tan \alpha - \tan \beta - 2\sqrt{3}$, $J_2 = \tan \alpha - \tan \beta - 2\sqrt{3}\tan \alpha \tan \beta$, $J_3 = \tan \alpha + \tan \beta$, and Eqs. (7.63), (7.64), and (7.65) denote the direct kinematics of the mechanism.

Once the concept of the singularity-equivalent-mechanism with two DOFs is proposed, and considering Eqs. (7.63), (7.64), and (7.65), the following conclusions can be made:

- The singularity can occur at any point all over the θ plane because the planar mechanism has two DOFs and point P can reach everywhere in the entire plane. However, ψ may be different for a different position of point P;
- When ψ is also specified and invariable, an infinite number of singularity points forming a singularity curve exists; and
- When line UV is coincident with A_5A_1 , any values of (x,y) and ψ can satisfy Deduction 7.2. This singularity is called Hunt's singularity [37].

Singularity Equation in the θ Plane

Once the orientation (90° , θ , ψ) of the mobile platform is specified (Fig. 7.17), the Euler angle ψ is an invariant. Thus, it only needs to choose one input in this case. From Eq. (7.65), one obtains

$$\tan \beta = \frac{\tan \alpha (\sqrt{3} \tan \psi - 1)}{\sqrt{3} \tan \psi + 2 \tan \alpha \tan \psi + 1} \quad (7.66)$$

Thus, the singularity equation in the θ plane for the orientation $(90^\circ, \theta, \psi)$ can be obtained from Eqs. (7.63), (7.64), and (7.66) by eliminating parameters α and β , as follows:

$$2(\sin \psi)y^2 + 2(\cos \psi)xy + R_b \sin(2\psi)x + \left(\sqrt{3}a \sin \psi - R_b \cos(2\psi)\right)y - R_b^2 \sin \psi + \sqrt{3}aR_b \cos(2\psi)/2 = 0 \quad (7.67)$$

Where $a = 2(3R_a \cos(\beta_0/2) - u)/\sqrt{3}$. Equation (7.67) denotes a hyperbola. In particular, when $\psi = \pm 90^\circ$, Eq. (7.67) degenerates into a pair of intersecting straight lines. Two of the four equations are

$$y - R_b/2 = 0 \quad y + R_b/2 = 0 \quad (7.68)$$

In both cases, two points, namely, B_3 and B_5 , lie in line UV so that the four lines are coplanar with the base plane, which is the singularity in Case 6. A similar situation is when $\psi = 30^\circ$, $\psi = -150^\circ$, $\psi = -30^\circ$, and $\psi = 150^\circ$.

7.5.3 General Case

When $\phi \neq (\pm 30^\circ, \pm 90^\circ, \pm 150^\circ)$, the intersecting line UVW between the θ plane and the base plane is not parallel to any side of triangle $A_1A_3A_5$. This case is the most general and also the most difficult.

7.5.3.1 Singularity-Equivalent-Mechanism

Figure 7.18 shows the singularity-equivalent-mechanism. The triangle $B_1B_3B_5$ is connected to the ground passing through three points W , V , and U by three RPR kinematic chains. The three points, namely, U , V , and W (Fig. 7.18), are three intersecting points between the θ plane and sides A_3A_5 , A_1A_3 , and A_1A_5 , respectively. Three slotted links, L_1 , L_2 , and L_3 , intersect at a common point C . To retain the intersection of the three links at a common point, a concurrent kinematic chain, $PRPRP$, is also used. Therefore, all configurations of the equivalent mechanism satisfying Deduction 7.2 are SCs of the Stewart manipulator, and the direct kinematics of the equivalent mechanism can be analyzed to find the singularity loci. Similarly, the mobility of the equivalent mechanism is two, and two inputs are needed to analyze its position.

7.5.3.2 Forward Position Analysis of the Singularity-Equivalent-Mechanism

The frames are set as shown in Fig. 7.18. Similar to Sect. 7.5.2.1.2, three equations of three straight lines passing through three vertices can be set, and the coordinates

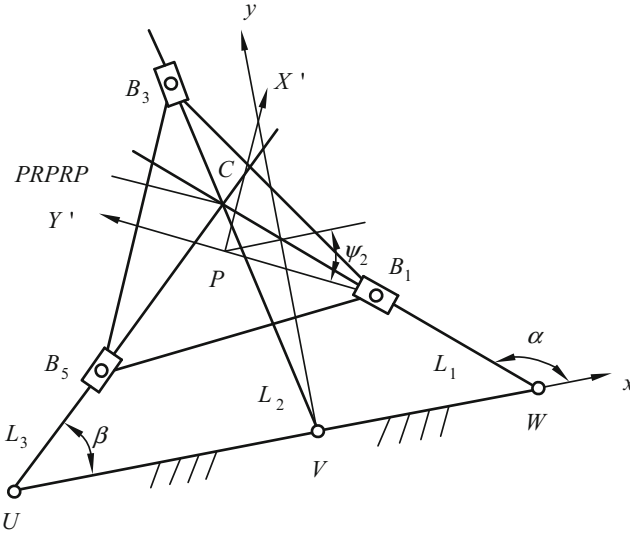


Fig. 7.18 Singularity-equivalent-mechanism for a general case

of points B_1 , B_3 , and B_5 are substituted into the equations to obtain the solutions (x, y) and ψ , as follows:

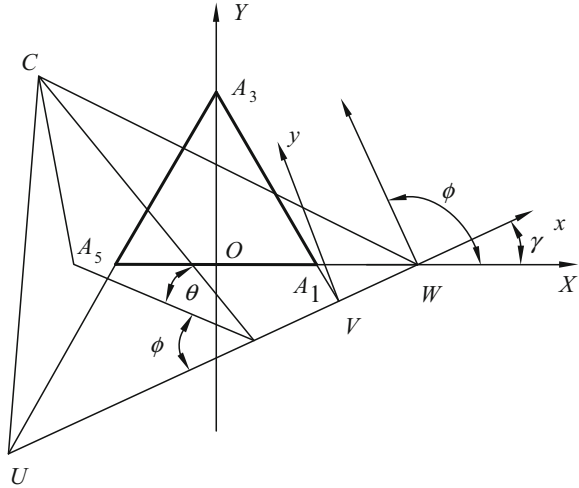
$$x = - \left(3R_b \sin \psi - 2R_b \tan \alpha \cos \psi + 2w \tan \alpha + \sqrt{3}R_b \cos \psi - R_b \tan \beta \cos \psi + \sqrt{3}R_b \tan \beta \sin \psi - 2u \tan \beta \right) / (2 \tan \beta - 2 \tan \alpha) \tag{7.69}$$

$$y = \left(-R_b \tan \alpha \sin \psi - \sqrt{3}R_b \tan \alpha \cos \psi + 3R_b \tan \alpha \tan \beta \cos \psi + 2u \tan \alpha \tan \beta - \sqrt{3}R_b \tan \alpha \tan \beta \sin \psi - 2R_b \tan \beta \sin \psi - 2w \tan \alpha \tan \beta \right) / (2 \tan \beta - 2 \tan \alpha) \tag{7.70}$$

$$\tan \psi = \frac{2\sqrt{3} w \tan \alpha - 3u \tan \alpha \tan \beta - \sqrt{3} u \tan \beta}{\tan \beta (-2\sqrt{3} w \tan \alpha + \sqrt{3} u \tan \alpha - 3u)} \tag{7.71}$$

Where u is the distance from point U to V , and w the distance from V to W . Substituting Eq. (7.71) into Eqs. (7.70) and (7.69) and eliminating ψ , the relationship between (x, y) and the inputs α, β can be obtained. This process is the direct kinematics of the equivalent mechanism.

Fig. 7.19 Intersecting line UW of two planes



7.5.3.3 Singularity Equation in the θ Plane

Under a general case, the Euler angle ϕ can be any value except $\pm 30^\circ$, $\pm 90^\circ$, and $\pm 150^\circ$. From Eq. (7.71),

$$\tan \beta = \frac{2\sqrt{3} w \tan \alpha}{-2\sqrt{3} w \tan \alpha \tan \psi + \sqrt{3} u \tan \alpha \tan \psi - 3u \tan \psi + 3 u \tan \alpha + \sqrt{3} u} \tag{7.72}$$

For some specified ψ , the same three particular situations, namely, B_1 and B_5 , B_1 and B_3 , or B_3 and B_5 , lie in the line UV . The singularity loci are three pairs of intersecting straight lines.

To use the aforementioned formulas, u and w in Eq. (7.72) should be calculated in advance. They depend on their relative positions in UV , as shown in Fig. 7.19.

The distance w between V and W is

$$|w| = |WV| = \left| \frac{3R_a \cos(\beta_0/2) - \sqrt{3}x_V}{\cos \phi} \right| \tag{7.73}$$

The distance u between U and V is

$$|u| = |UV| = \left| \frac{2\sqrt{3}x_V}{(\sqrt{3} + \cot \phi) \sin \phi} \right| \tag{7.74}$$

The sign of w is positive when point W is on the right side of V , and it is negative when W is on the left side of V . The same is true for u .

For a given x_v , the singularity equation in the θ plane can be obtained by eliminating the parameter α , as follows:

$$bxy + cy^2 + dx + ey + f = 0 \quad (7.75)$$

where the coefficients are functions of the architecture parameters (R_a, R_b, β_0) and the orientations (ϕ, θ, ψ). Equation 7.5 is a quadratic equation.

The two invariants D, δ of Eq. (7.75) are

$$D = \begin{vmatrix} 0 & b/2 & d/2 \\ b/2 & c & e/2 \\ d/2 & e/2 & f \end{vmatrix} = -\frac{1}{4}(b^2f + d^2c - bde) \quad (7.76)$$

and

$$\delta = \begin{vmatrix} 0 & b/2 \\ b/2 & c \end{vmatrix} = -\frac{1}{4}b^2 < 0 \quad (7.77)$$

Generally, $D \neq 0$ and $\delta < 0$ for a general value of x_v , so that Eq. (7.75) indicates a set of hyperbolas.

7.5.4 Five Special Cases of the Singularity Equation

The singularity equation can be one of five special cases. For the given parameters (R_a, R_b, β_0) and (ϕ, θ, ψ), D is a quartic equation, whereas δ is a quadratic equation with respect to the single variable x_v . Generally, x_v has four real roots when $D = 0$ and $\delta \neq 0$, and Eq. (7.75) degenerates into four pairs of intersecting straight lines. For the same reason, one real root of multiplicity 2 exists when $\delta = 0$ and $D \neq 0$, and Eq. (7.75) degenerates into a parabola.

Case 1. The line UV passes through point A_1 (Fig. 7.20). In this case, $x_v = \sqrt{3}R_a \cos(\beta_0/2)$, and the two points W and V coincide with point A_1 . The singularity equation denoted by Eq. (7.75) degenerates into a pair of intersecting straight lines, as follows:

$$[y - R_b \sin(\psi + 60^\circ)] \left[\left(-\sqrt{3} \sin(\psi) + \cos(\psi) \right) x + \left(\sqrt{3} \cos(\psi) + \sin(\psi) \right) y + R_b \right] = 0 \quad (7.78)$$

One of the intersecting lines is

$$y - R_b \sin(\psi + 60^\circ) = 0 \quad (7.79)$$

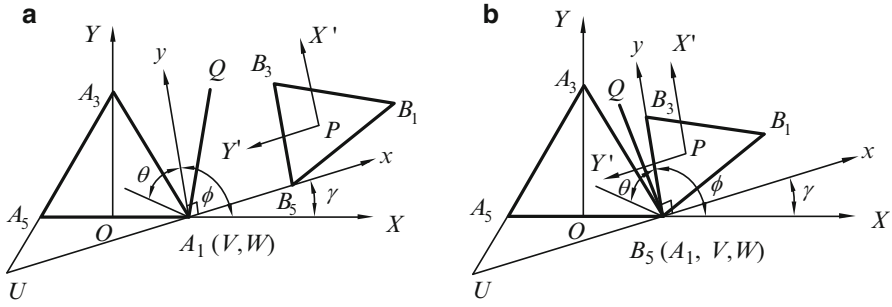


Fig. 7.20 UV passes through point A_1 (a) B_5 does not coincide with A_1 (b) B_5 coincides with A_1

Its correctness can also be proven via an alternative method based on Theorem 7.2. Equation (7.79) indicates a straight line parallel to the x -axis of frame V - xy . Meanwhile, $B_{5y} = 0$, and thus, B_5 is located on the base plane. The normal plane $B_5A_3A_5$ coincides with the base plane. Therefore, the intersecting line between two normal planes, $B_5A_3A_5$ and $B_1A_1A_5$, is A_1A_5 ; the intersecting line between normal planes $B_5A_3A_5$ and $B_3A_1A_3$ is A_1A_3 ; and the intersecting line between normal planes $B_1A_1A_5$ and $B_3A_1A_3$ is A_1Q . Thus, A_1 is the intersecting point of three normal planes ($B_5A_3A_5$, $B_1A_1A_5$, and $B_3A_1A_3$). Considering that A_1 lies in line UV , which also lies in the mobile $B_1B_3B_5$, point A_1 also lies in the mobile $B_1B_3B_5$. According to Theorem 7.2, the mechanism is singular.

For Fig. 7.20a, when $\psi = 0$ and the coordinates of point P are $x \neq R_b/2$, $y = \sqrt{3}R_b/2$, B_5 does not coincide with A_1 but belongs to the general-linear-complex singularity. The instantaneous motion is a twist with pitch $h^m \neq 0$.

For Fig. 7.20b, when $\psi = 0$ and the coordinates of point P are $x = R_b/2$, $y = \sqrt{3}R_b/2$, point B_5 coincides with point A_1 . A_1Q passing through B_5 is the intersecting line between $B_1A_1A_5$ and $B_3A_1A_3$, which is the case when all six lines associated with the six extensible links of the manipulator intersect one common line A_1Q . The singularity belongs to the first special-linear-complex singularity, and the instantaneous motion is a pure rotation.

Now, let us find the instantaneous motion screw. When the mechanism is singular at the following two configurations, $\dim(J) = 5$, a remnant freedom, which is a twist with pitch h^m , exists for each case, which can be obtained using the following expression proposed by Sugimoto and Duffy [40]:

$$\mathcal{S}^m = \begin{vmatrix} \in i & \in j & \in k & i & j & k \\ L_1 & M_1 & N_1 & P_1 & Q_1 & R_1 \\ L_2 & M_2 & N_2 & P_2 & Q_2 & R_2 \\ L_3 & M_3 & N_3 & P_3 & Q_3 & R_3 \\ L_4 & M_4 & N_4 & P_4 & Q_4 & R_4 \\ L_5 & M_5 & N_5 & P_5 & Q_5 & R_5 \end{vmatrix} \quad (7.80)$$

where

$$\begin{aligned}\mathbf{i} &= (1 \ 0 \ 0; \ 0 \ 0 \ 0) \\ \mathbf{j} &= (0 \ 1 \ 0; \ 0 \ 0 \ 0) \\ \mathbf{k} &= (0 \ 0 \ 1; \ 0 \ 0 \ 0) \\ \in \mathbf{i} &= (0 \ 0 \ 0; \ 1 \ 0 \ 0) \\ \in \mathbf{j} &= (0 \ 0 \ 0; \ 0 \ 1 \ 0) \\ \in \mathbf{k} &= (0 \ 0 \ 0; \ 0 \ 0 \ 1)\end{aligned}$$

\mathcal{S}^m indicates a moving screw that is reciprocal to \mathcal{S}_i , ($i = 1, 2, \dots, 6$), and \mathcal{S}_i denotes a unit screw of the extensible leg of the SP. \mathcal{S}^m can also be expressed as a dual vector as follows:

$$\mathcal{S}^m = \mathbf{S}^m + \in \mathbf{S}_o^m = L^m \mathbf{i} + M^m \mathbf{j} + N^m \mathbf{k} + \in (P^m \mathbf{i} + Q^m \mathbf{j} + R^m \mathbf{k}) \quad (7.81)$$

where \in is the dual symbol. The pitch h^m of the moving reciprocal screw \mathcal{S}^m is

$$h^m = (L^m P^m + M^m Q^m + N^m R^m) / (L^{m^2} + M^{m^2} + N^{m^2}) \quad (7.82)$$

When $(\phi, \theta, \psi) = (60^\circ, 30^\circ, 0^\circ)$, two points, namely,

$$P_1(x_1, y_1) = (R_b/2, \sqrt{3}R_b/2)$$

$$P_2(x_2, y_2) = (0, \sqrt{3}R_b/2)$$

are selected from the straight line in Eq. (7.79). From Eq. (7.80), the corresponding twists and its pitches are as follows:

$$\mathcal{S}_1^m = (0.8762, -0.1090, 0.4695, 0, -1.1501, -0.2669).$$

$$h_1^m = -3.27998 \times 10^{-16} = 0 \quad (7.83)$$

$$\mathcal{S}_2^m = (0.8762, -0.1090, 0.4695, 0.1761, -0.8451, -0.8768)$$

$$h_2^m = -0.165 \neq 0$$

The mechanism is singular in the two positions. The singularities of the points in line PB_1 , Eq. (7.79), are general-linear-complex singularities and the instantaneous motion is a twist with $h^m \neq 0$ when B_5 does not coincide with A_1 . The singularity of the point is the first special-linear-complex singularity, and the instantaneous motion is a pure rotation with pitch $h^m = 0$ when B_5 coincides with A_1 .

Another straight line equation is

$$\left(-\sqrt{3}\sin(\psi) + \cos(\psi)\right)x + \left(\sqrt{3}\cos(\psi) + \sin(\psi)\right)y + R_b = 0 \quad (7.84)$$

Similarly, when $(\phi, \theta, \psi) = (60^\circ, 30^\circ, 0^\circ)$, three points, namely,

$$P_3(x_3, y_3) = (-R_b, 0),$$

$$P_4(x_4, y_4) = \left(0, -\sqrt{3}R_b/3\right)$$

$$P_5(x_5, y_5) = \left(R_b/2, -\sqrt{3}R_b/2\right)$$

are selected from the straight line, Eq. (7.84). The mechanism is singular in the three positions, and the corresponding twists and their pitches are calculated as follows:

$$\begin{aligned} \mathcal{S}_3^m &= (-0.7944, -0.4333, -0.4257; 0, 1.3708, -0.7093) \\ h_3^m &= -0.7093 \neq 0 \\ \mathcal{S}_4^m &= (-0.8002, -0.4194, -0.4288; 0.4185, 1.0414, -0.1054) \\ h_4^m &= -0.7265 \neq 0 \\ \mathcal{S}_5^m &= (0.8015, 0.4160, 0.4295; -0.6315, -1.4168, 0.8497) \\ h_5^m &= -0.7306 \neq 0 \end{aligned} \quad (7.85)$$

Thus, the singularities of the points lying in Eq. (7.84) are all general-linear-complex singularities, and their instantaneous motion is a twist with $h^m \neq 0$.

Case 2. UV passes through point A_3 . In this case, $x_v = 0$, two points, U and V , coincide with point A_3 . Equation (7.75) also degenerates into a pair of intersecting straight lines, as follows:

$$[(y + R_b \sin(\psi))[x \cos(\psi) + y \sin(\psi) - R_b/2] = 0 \quad (7.86)$$

The first part of Eq. (7.86) indicates a straight line parallel to the x -axis. Similarly, when B_1 coincides with point A_3 , the singularity of this point is the first special-linear-complex singularity and the instantaneous motion is a pure rotation. When B_1 does not coincide with A_3 , the singularities of points lying in this straight line are the general-linear-complex singularity, and its instantaneous motion is a twist with $h^m \neq 0$.

The second part of Eq. (7.86) denotes another straight line. The singularities of the points lying in this straight line are all general-linear-complex singularities.

Case 3. UV passes point A_5 . In this case,

$$x_v = \sqrt{3}R_a \cos(\beta_0/2) \left(\sqrt{3} + \cot \phi \right) / \left(\sqrt{3} - \cot \phi \right)$$

and the two points U and W coincide with point A_5 . Equation (7.75) degenerates into a pair of intersecting straight lines.

$$\begin{aligned} & [y - R_b \sin(\psi - 60^\circ)] \left[(\sqrt{3} \sin(\psi) + \cos(\psi))x + (-\sqrt{3} \cos(\psi) + \sin(\psi))y \right. \\ & \left. + R_b - 2\sqrt{3} \cos(\beta_0/2) \sin(\psi + 60^\circ) / \sin(\phi - 60^\circ) \right] = 0 \end{aligned} \quad (7.87)$$

The first factor indicates a straight line parallel to the x -axis. Similarly, when B_3 coincides with A_5 , the singularity of this point is a first special-linear-complex singularity. When B_3 does not coincide with A_5 , the singularities of the points lying in this straight line are general-linear-complex singularities.

Similarly, the second factor of Eq. (7.87) denotes another straight line. The singularities of the points lying in this straight line are all general-linear-complex singularities.

Case 4. When

$$x_v = \frac{(-1 + 2 \cos(2\phi))(R_b \cos \phi - 2R_a \cos(\beta_0/2) \cos \psi)}{(2(\sqrt{3} \sin \phi - \cos \phi) \sin(\phi + \psi))} \quad (7.88)$$

Equation (7.75) degenerates into a pair of intersecting straight lines, as follows:

$$\begin{aligned} & (R_a \cos((\beta_0 - 6\psi)/2) - R_b \cos(\phi - 2\psi) + R_a \cos((\beta_0 + 6\psi)/2) \\ & - 2y \sin(\phi + \psi))(ax + by + c) = 0 \end{aligned} \quad (7.89)$$

For the first straight line when $\beta_0 = 90^\circ$, $(\phi, \theta, \psi) = (60^\circ, 30^\circ, 0)$, and the coordinates of point P_6 are $x = R_b/2, y = (2\sqrt{2}R_a - R_b)/2\sqrt{3}$, point B_5 lies in the intersecting line of two normal planes $B_1A_1A_5$ and $B_3A_1A_3$. Therefore, the six lines associated with the six extensible links of the 3/6-SP intersect a common line B_5A_1 . This singularity is a first special-linear-complex. The instantaneous motion is a pure rotation about line B_5A_1 . The singularities of the points lying in the first line, except for the aforementioned point and the points lying in the second line, all belong to a general-linear-complex singularity.

Case 5. When

$$x_v = R_a \cos(\beta_0/2) \cos \psi \left(\cos \phi + \sqrt{3} \sin \phi \right) / \sin(\phi + \psi),$$

$$\delta = 0 \quad \text{and} \quad D \neq 0,$$

Equation (7.75) degenerates into a parabola, as follows:

$$cy^2 + dx + ey + f = 0 \quad (7.90)$$

When $R_a = 2, R_b = 3/2, \beta_0 = \pi/2$ and the three Euler angles are $(\phi, \theta, \psi) = (60^\circ, 30^\circ, 0)$, three special points,

$$P_7(x_7, y_7) = (-4.9068, 0.3339),$$

$$P_8(x_8, y_8) = (-4.3284, 1.6329),$$

$$P_9(x_9, y_9) = (0.75, 2.932),$$

lie in the parabola. In the three cases, B_3 lies in the intersecting line of two normal planes $B_1A_1A_5$ and $B_5A_3A_5$; B_1 lies in the intersecting line of two normal planes $B_3A_1A_3$ and $B_5A_3A_5$; and B_5 lies in the intersecting line of two normal planes $B_1A_1A_5$ and $B_3A_1A_3$. For the first case, the six lines associated with the six extensible links intersect a common line B_3A_5 . For the second case, the six lines intersect B_1A_3 , and for the final case, the six lines intersect B_5A_1 . Therefore, the singularities of the three points P_7, P_8 , and P_9 are first special-linear-complex singularities, and the singularities of the points lying in the parabola, except for the aforementioned three points, all belong to a general-linear-complex singularity.

Based on this analysis, the singularity expression in the θ plane is not cubic, but rather always quadratic, indicating that the θ plane is a very special cross-section of the singularity surface; thus, the special θ plane can be called the principal section.

Generally speaking, the singularity loci of the 3/6-SP for most general orientations are different from those for some special orientations. The singularity loci in infinite parallel principal sections are all quadratic equations. The structure of the singularity loci in the principal sections of the cubic singularity surface includes a parabola, four pairs of intersecting straight lines, and an infinite number of hyperbolas. The singularity loci in 3D space are illustrated in Fig. 7.21.

In addition, the mechanism is singular at the orientation (ϕ, θ, ψ) , and thus, any orientation with a different variable θ is also singular [29].

7.6 Structure and Property of the Singularity Loci of the 6/6-Stewart

Base on the aforementioned analysis of the 3/6-SP, in this section we focus on the most difficult issue, which is the singularity locus analysis of the 6/6-SP, including the singularity equation and the structure of the singularity surface [30]. 6/6-SP is typical manipulator; its schematic representation is shown in Fig. 7.22. It consists of two semiregular hexagons: a mobile platform $B_1B_3 \dots B_6$ and a base platform $C_1 \dots C_6$, which are connected via six extensible prismatic actuators.

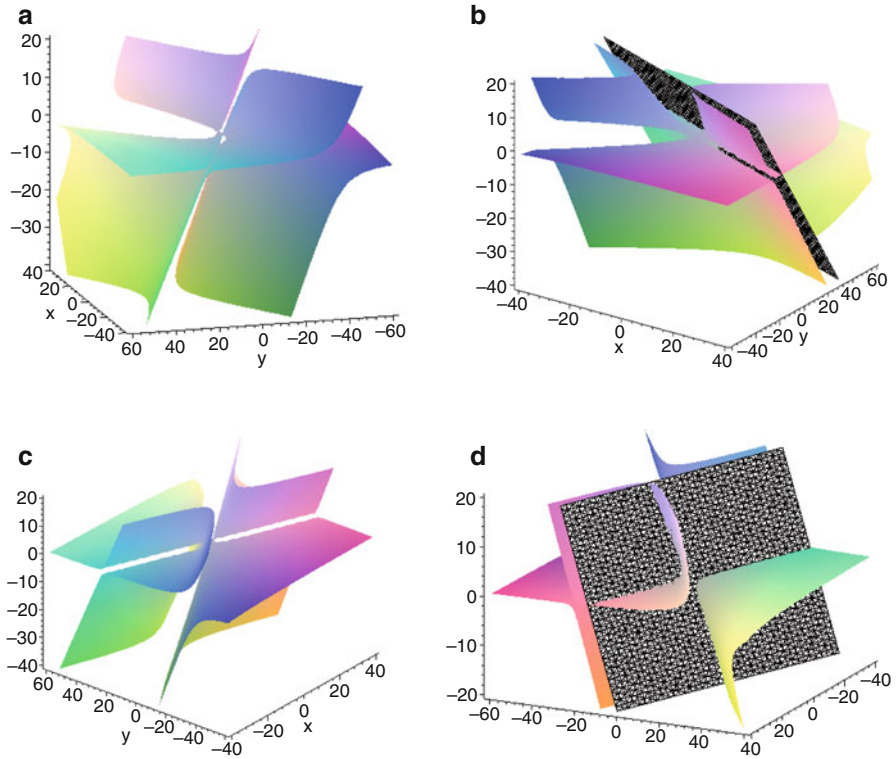


Fig. 7.21 Singularity loci for the general orientations (a) for orientation $(60^\circ, 45^\circ, 45^\circ)$ (b) a principal section $x_v = -4$ (c) for orientation $(60^\circ, 60^\circ, 45^\circ)$ (d) principal section $x_v = -4$

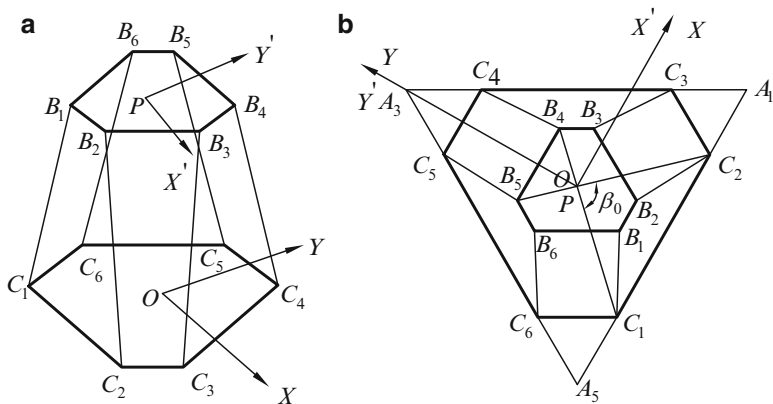


Fig. 7.22 Schematic diagram of a class of Stewart manipulators (a) a 6/6-Stewart manipulators (b) top view

7.6.1 Jacobian Matrix

The Jacobian matrix of this class of 6/6-Stewart manipulators can be constructed according to the theory of static equilibrium (Huang and Qu 1987) [34]. The external force acting on the platform is equilibrated by six reactional forces when the inputs are being clocked. The force equilibrium equation can be set as follows:

$$f_{1i}\$1_i + f_{2i}\$2_i + f_{3i}\$3_i + f_{4i}\$4_i + f_{5i}\$5_i + f_{6i}\$6_i = F\$P$$

where the subscript i ($i = 1, 2, \dots, 6$) indicates the i th limb connected by two vertices B_i, C_i of the moving and base platforms of the manipulator. The equation can be rewritten as a matrix form, as follows:

$$[G]f = F\$P$$

where

$$[G]^T = [\$1 \quad \$2 \quad \dots \quad \$6] = \begin{pmatrix} s_1 & s_2 & s_3 & s_4 & s_5 & s_6 \\ s_{o1} & s_{o2} & s_{o3} & s_{o4} & s_{o5} & s_{o6} \end{pmatrix} \quad (7.91)$$

and we have

$$[G]^T = \begin{pmatrix} \frac{(B_1-C_1)}{|B_1-C_1|} & \frac{(B_2-C_2)}{|B_2-C_2|} & \frac{(B_3-C_3)}{|B_3-C_3|} & \frac{(B_4-C_4)}{|B_4-C_4|} & \frac{(B_5-C_5)}{|B_5-C_5|} & \frac{(B_6-C_6)}{|B_6-C_6|} \\ \frac{(C_1 \times B_1)}{|B_1-C_1|} & \frac{(C_2 \times B_2)}{|B_2-C_2|} & \frac{(C_3 \times B_3)}{|B_3-C_3|} & \frac{(C_4 \times B_4)}{|B_4-C_4|} & \frac{(C_5 \times B_5)}{|B_5-C_5|} & \frac{(C_6 \times B_6)}{|B_6-C_6|} \end{pmatrix} \quad (7.92)$$

where vectors B_i, C_i ($i = 1, 2, \dots, 6$) denote the vertex vectors of the moving and base platforms with respect to the fixed frame, respectively (Fig. 7.22). $\$i$ ($i = 1, 2, \dots, 6$) is a line vector of the corresponding extensible link, and its Plücker coordinates are as follows

$$\$i = (\$i, \$o_i) = (L_i, M_i, N_i; P_i, Q_i, R_i) \quad (7.93)$$

where S_i is a unit vector specifying the direction of line vector $\$i$, and S_{o_i} is a vector indicating the position of the line vector together with S_i .

When the parallel manipulator is singular, a remnant DOF, which is an instantaneous screw motion with pitch h^m , exists. This DOF can be obtained using Eq. (7.80).

7.6.2 Singularity Analysis in 3D Space

A moving reference frame, $P-X'Y'Z'$, and a fixed one, $O-XYZ$, are attached to the moving platform and the base platform of the manipulator, respectively (Fig. 7.22), where the origins P and O are the corresponding geometric center of the moving

and base platforms. The position of the moving platform is given by the position of point P with respect to the fixed frame, designated by (X, Y, Z) , and the orientation of the moving platform is represented by the standard Z - Y - Z Euler angles (ϕ, θ, ψ) . Furthermore, the geometric parameters of the manipulator can be described as follows: the circumcircle radius of the base hexagon is R_a , and that of the mobile hexagon is R_b . β_0 denotes the central angle of the circumcircles of the hexagons corresponding to sides C_1C_2 and B_1B_6 (Fig. 7.22). The coordinates of the six vertices, B_i ($i = 1, 2, \dots, 6$), of the moving platform are denoted by B^i with respect to the moving frame, and B_i with respect to the fixed frame. Similarly, C_i and A_j represent the coordinates of the vertices, C_i ($i = 1, 2, \dots, 6$) and A_j ($j = 1, 3, 5$), of the base platform with respect to the fixed frame.

Gosselin and Angeles [7] pointed out that the singularities of parallel manipulators can be classified into three different types, namely, the inverse kinematic, direct kinematic, and architecture singularities. In this paper, only the direct kinematic singularity of this class of 6/6-Stewart manipulators, which occurs when the determinant of the Jacobian matrix of the manipulator is equal to zero, i.e., $\det(J) = \det(J^T) = 0$, is discussed. By expanding and factorizing the determinant of the Jacobian matrix, the singularity locus equation for the manipulator can be written as

$$\begin{aligned} & f_1Z^3 + f_2XZ^2 + f_3YZ^2 + f_4X^2Z + f_5Y^2Z \\ & + f_6XYZ + f_7Z^2 + f_8X^2 + f_9Y^2 + f_{10}XY \\ & + f_{11}XZ + f_{12}YZ + f_{13}Z + f_{14}X + f_{15}Y + f_{16} = 0 \end{aligned} \quad (7.94)$$

Equation (7.94) represents the constant-orientation singularity locus of this class of Stewart manipulators in the Cartesian space for a constant orientation (ϕ, θ, ψ) . It is a polynomial expression of degree three in the moving platform position parameters XYZ . The coefficients of Eq. (7.94), f_i ($i = 1, 2, \dots, 15, 16$), are all functions of the geometric parameters, R_a, R_b, β_0 , and the orientation parameters, (ϕ, θ, ψ) , of the manipulator. Graphical representations of the constant-orientation singularity locus of the manipulator for different orientations are given to illustrate the result (Fig. 7.23). The geometric parameters used are given as $R_a = 2, R_b = 3/2$, and $\beta_0 = \pi/2$.

From Fig. 7.23, the singularity loci for the different orientations are complex and varied. Among them, the most complicated graph of the singularity loci is similar to a trifoliate surface whose two branches are shaped like a horn with one hole (Fig. 7.23c, d).

7.6.3 Singularity Analysis in Parallel Principal-Sections

7.6.3.1 Singularity Locus Equation in the θ Plane

Huang et al. (2003) [29] pointed out that the cross-sections of the cubic singularity locus equation for the 3/6-SP in parallel θ -planes are all quadratic expressions that

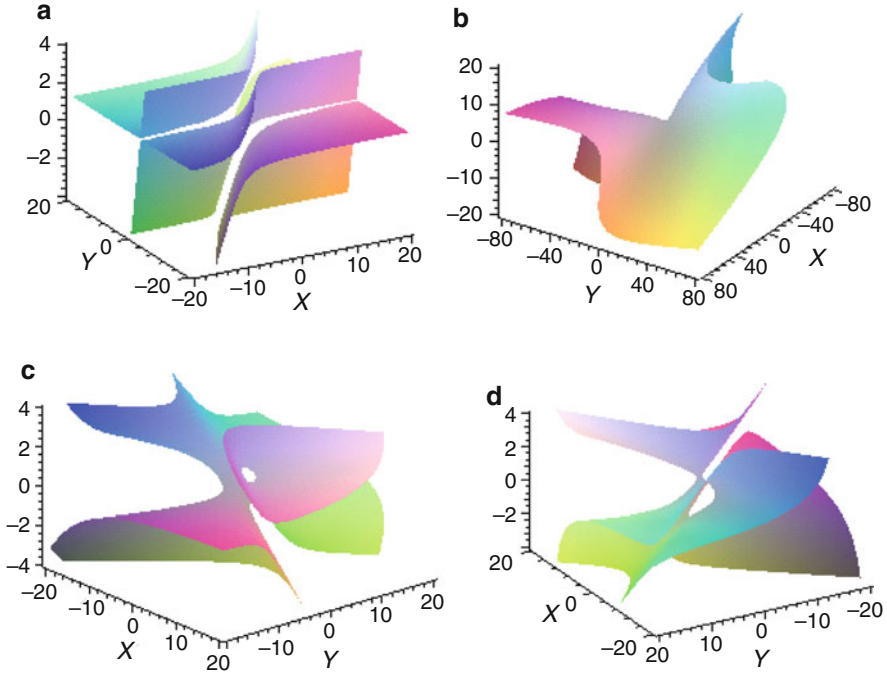


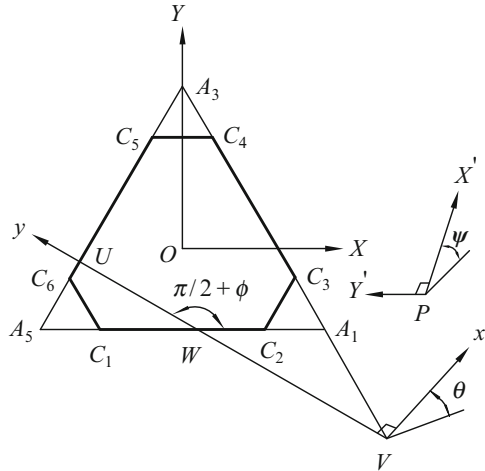
Fig. 7.23 Singularity loci for the different orientations (a) for orientation $(90^\circ, 60^\circ, 30^\circ)$ (b) for orientation $(-90^\circ, 30^\circ, 60^\circ)$ (c) for orientation $(60^\circ, 30^\circ, 45^\circ)$ (d) for orientation $(45^\circ, 30^\circ, 45^\circ)$

include a parabola, four pairs of intersecting lines, and infinite hyperbolas (Sect. 7.4). This conclusion is of great importance for the property identification of the singularity loci of the 3/6-SP. Similarly, to identify the characteristics of the singularity loci of this class of 6/6-SP, the singularity loci of the manipulator in parallel θ planes will also be discussed in this section. Figure 7.24 shows the position of the manipulator for orientation (ϕ, θ, ψ) . The oblique plane is a θ plane on which the moving platform lies.

When $\theta \neq 0$, the moving platform is not parallel to the base platform. The θ plane intersects the base plane at line UWV, where points U,W,V are points of intersection between the θ plane and three sides A_3A_5 , A_1A_5 , and A_3A_1 of the base hexagon (Fig. 7.24). Another moving reference frame V-xy is set in the θ plane, and the coordinates of point P in this moving frame V-xy are denoted by (x, y) .

The equations of the three lines, A_1A_3 , A_3A_5 , and A_1A_5 , in the fixed frame O-XYZ can be easily written. Given the space limitations, these equations are not presented. Point V, i.e., the origin of the moving frame V-xy, lies on line A_1A_3 , and the coordinates of point V with respect to the fixed frame O-XYZ are assumed as $V:(X_V, Y_V, 0)$, where X_V is a variable indicating the position of the θ plane,

Fig. 7.24 Position of the manipulator for the orientation (ϕ, θ, ψ)



i.e., the position of the moving platform for any given geometric and orientation parameters, and Y_V can be established using the following expression:

$$Y_V = 2R_a \cos(\beta_0/2) - \sqrt{3}X_V \tag{7.95}$$

Thus, the equation for line UV can be written as follows:

$$Y_{UV} - 2R_a \cos(\beta_0/2) + \sqrt{3}X_V = -\cot(\phi)(X_{UV} - X_V), \tag{7.96}$$

and the coordinates of points U and W can be easily obtained. The coordinates of point P, designated by (X, Y, Z) with respect to the fixed frame and (x, y) in the moving frame V-xy, satisfy the following expression:

$$\begin{aligned} X &= \cos \phi \cos \theta x - \sin \phi y + X_V \\ Y &= \sin \phi \cos \theta x + \cos \phi y + Y_V \\ Z &= -\sin \theta x \end{aligned} \tag{7.97}$$

Substituting Eq. (7.97) into Eq. (7.94) and after some rearrangements and factorizations, the singularity locus equation for the manipulator in the θ plane can be written as follows:

$$\sin^3 \theta (ax^2 + 2bxy + cy^2 + 2dx + 2ey + f) = 0 \tag{7.98}$$

Given that $\theta \neq 0$, the singularity locus equation for the manipulator with respect to the θ plane becomes

$$ax^2 + 2bxy + cy^2 + 2dx + 2ey + f = 0 \tag{7.99}$$

The coefficient c is always equal to zero, so that Eq. (7.99) is a quadratic polynomial expression with respect to x and y , and the maximum degree of variable x is 2 and y is 1. Coefficients a, b, d, e, f in Eq. (7.99) are all functions of the geometric parameters R_a, R_b, β_0 , the Euler angles (ϕ, ψ) , and X_V . These parameters are all independent of the Euler angle θ . Generally, the intersecting curve between a cubic surface and a plane is also a cubic expression that may also contain a closed-loop curve. For example, when $R_a = 2, R_b = 3/2, \beta_0 = \pi/2, \beta_0 = \pi/2$, and $(\phi, \theta, \psi) = (\pi/3, \pi/6, \pi/4)$, the intersecting curves between the corresponding singularity locus surface and the two planes $Z = -Y/3$ and $Z = -4(X - 14)/45$ are presented as follows:

$$\begin{aligned} &14.0103Y^3 - 1.45655XY^2 - 259.685Y^2 - 44.5538X^2Y \\ &\quad - 148.185XY + 14.1449Y - 136.939X^2 - 213.732X \\ &\quad - 1, 161.68 = 0 \end{aligned} \tag{7.100}$$

$$\begin{aligned} &69,452.4XY^2 - 972,334Y^2 - 50,134.4X^2Y - 28,860.7XY \\ &\quad - 440,308Y - 31,121X^3 - 96,393.6X^2 + 467,953X + \\ &\quad 974,793 = 0 \end{aligned}$$

The intersecting curves between the singularity locus surface of the manipulator and the two aforementioned planes are clearly cubic expressions that contain a closed-loop curve (Fig. 7.25). However, Eq. (7.99) is always a quadratic polynomial expression; the same conclusion holds for any manipulator of this class of Stewart manipulators considered in the current study. Therefore, θ plane reflects the characteristics of the singularity loci of this class of Stewart manipulators, and is the reason behind the principal-section.

7.6.3.2 Property Identification of the Singularity Loci in Parallel Principal Sections

The property of the singularity loci of the manipulator in parallel principal sections can be analyzed using the two invariants, D and δ , of Eq. (7.99), as follows:

$$\delta = \begin{vmatrix} a & b \\ b & c \end{vmatrix} = ac - b^2 = -b^2 \tag{7.101}$$

$$D = \begin{vmatrix} a & b & d \\ b & c & e \\ d & e & f \end{vmatrix} = -(ae^2 + fb^2 - 2bde) \tag{7.102}$$

Generally, for any given geometric and orientation parameters, $D \neq 0$ and $\delta < 0$ for general values of X_V , thus, Eq. (7.99) indicates a set of hyperbolas (Fig. 7.26). The geometric and orientation parameters used in these examples are given as $R_a = 2, R_b = 3/2, \beta_0 = \pi/2, (\varphi, \theta, \psi) = (\pi/3, \pi/6, 0)$.

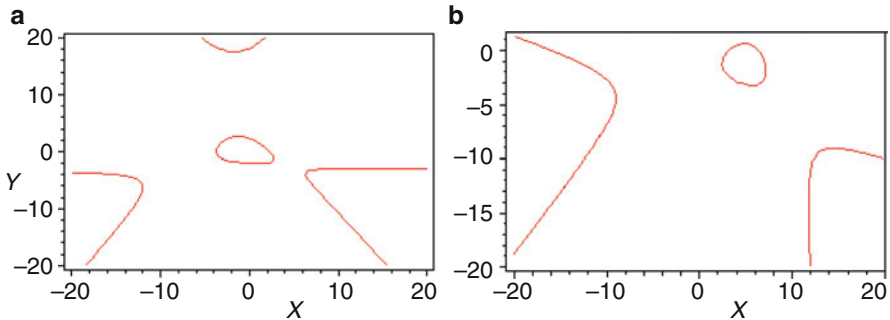


Fig. 7.25 Intersecting curves of a closed-loop with different sections (a) in plane $Z = -Y/3$ (b) in plane $Z = -4(X-14)/45$

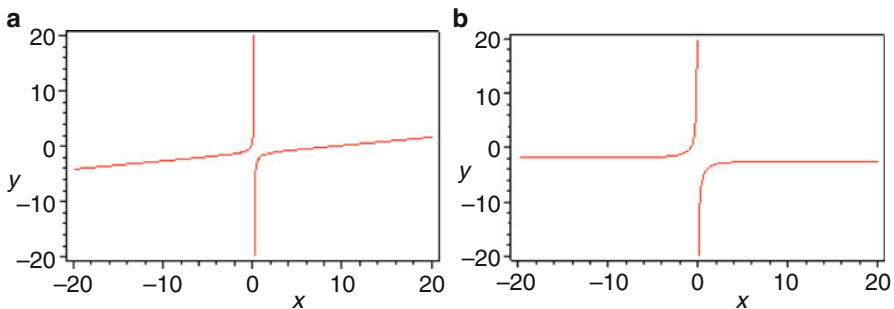


Fig. 7.26 Singularity loci in parallel principal-planes for general values of X_V (a) for orientation $(60^\circ, 30^\circ, 0^\circ)$, $X_V = 0$ (b) for orientation $(60^\circ, 30^\circ, 0^\circ)$, $X_V = -1$

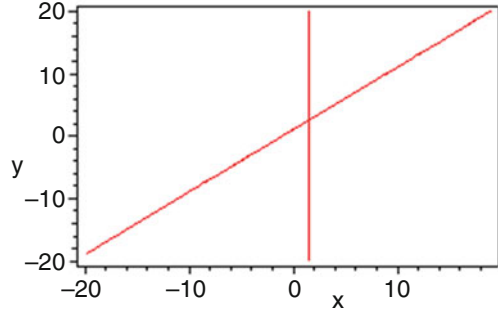
Further research shows that for any given geometric parameters, R_a, R_b, β_0 and orientation parameters (ϕ, θ, ψ) of the manipulator, D is a quartic expression, whereas δ is a quadratic expression with respect to the single variable X_V . Generally, four real roots exist when $D = 0$ and $\delta \neq 0$, and, in each of the four cases, Eq. (7.99) degenerates into two intersecting lines. For the same reason, one real root of multiplicity two exists when $\delta = 0$ and $D \neq 0$; in this case, Eq. (7.99) degenerates into a parabola. To demonstrate the aforementioned theoretical results, a 6/6-SP, whose geometric and orientation parameters are $R_a = 2, R_b = 3/2, \beta_0 = \pi/2$, and $(\phi, \theta, \psi) = (\pi/3, \pi/6, 0)$, will be studied. Note that the subsequent calculations are all based on these parameters.

(1) First Case of Two Intersecting Lines

The intersecting line UV passes through point C_3 , then point V coincides with point C_3 . When $X_{V1} = (\sqrt{6} + \sqrt{2})/2$, Eq. (7.99) degenerates into two intersecting lines (Fig. 7.27).

$$(8x - 3(\sqrt{6} + \sqrt{2}))(x + k_1y + c_1) = 0 \tag{7.103}$$

Fig. 7.27 First case of two intersecting lines



The first part of Eq. (7.103) is

$$8x - 3(\sqrt{6} + \sqrt{2}) = 0 \quad (7.104)$$

which is a line parallel to the y -axis of frame V - xy . Meanwhile, point B_6 can be proven located on the base plane (Fig. 7.28a). The manipulator is always singular regardless of the coordinate y . In particular, when

$$(x, y) = (3(\sqrt{2} + \sqrt{6})/8, 3(\sqrt{2} - \sqrt{6})/8) \quad (7.105)$$

point B_6 coincides with point C_3 (Fig. 7.28b). In this case, the two planes determined by triangles $C_3B_4C_4$ and $C_3B_5C_5$ intersect with one common line C_3Q , which is also the intersecting line of the two planes determined by triangles $C_3B_1C_1$ and $C_3B_2C_2$. C_3Q passes through C_3 and B_6 and thus intersects C_3B_3 and C_6B_6 . Therefore, all segments associated with the six extensible links of the manipulator intersect one common line (C_3Q). This singularity is a first special-linear-complex type. The remnant instantaneous motion is a pure rotation, and C_3Q is the revolute axis of the instantaneous motion, and is also the singularity of 5b [4].

Therefore, the singularities of points lying in the line of Eq. (7.104) are of the general-linear-complex type, when B_6 does not coincide with C_3 . In addition, the singularity of the point is of the first special-linear-complex singularity, when B_6 coincides with C_3 .

The second part of Eq. (7.103) denotes another line. Singularities corresponding to points lying in this line are all of the general-linear-complex type, which is similar to that of 5a [4].

(2) Second Case of Two Intersecting Lines

The intersecting line UV passes through point C_4 , which then coincides with point V . When

$$X_{V2} = (\sqrt{6} - \sqrt{2})/2 \quad (7.106)$$

Equation (7.99) also degenerates into two intersecting lines

$$(8x - 3(\sqrt{6} - \sqrt{2}))(x + k_2y + c_2) = 0 \quad (7.107)$$

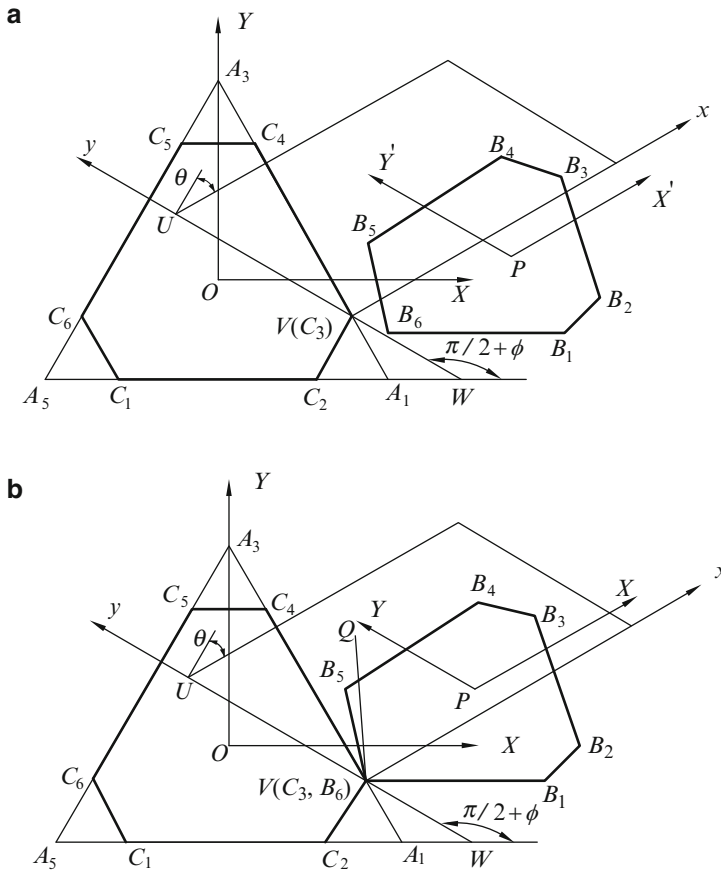


Fig. 7.28 Intersecting line UV passes through point C_3 (a) B_6 does not coincide with C_3 (b) B_6 coincides with C_3

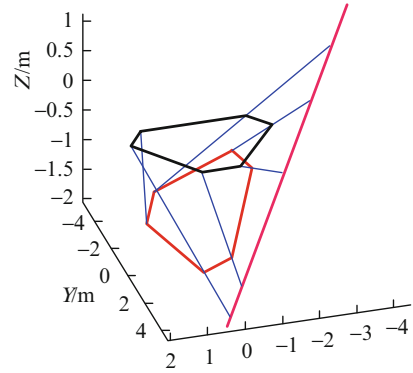
The first part of Eq. (7.107) is

$$8x - 3(\sqrt{6} - \sqrt{2}) = 0 \tag{7.108}$$

which is a line parallel to the y -axis. Meanwhile, point B_1 can be proven located on the base plane. Similarly, when B_1 coincides with C_4 , the singularity of this point is of the first special-linear-complex type. When B_1 does not coincide with C_4 , singularities corresponding to points lying in the line of Eq. (7.108) are of the general-linear-complex type.

The second part of Eq. (7.107) denotes another line. Singularities corresponding to points lying in this line are all of the general-linear-complex type.

Fig. 7.29 A case where all segments intersect one common line



(3) Third Case of Two Intersecting Lines

When $X_{V3} = 3(\sqrt{6} + \sqrt{2})/\sqrt{2}$, $D = 0$ and $\delta \neq 0$, Eq. (7.99) degenerates into two intersecting lines

$$(8x + (9\sqrt{2} + 3\sqrt{6}))(x + k_3y + c_3) = 0 \quad (7.109)$$

The first part of Eq. (7.109) is

$$8x + (9\sqrt{2} + 3\sqrt{6}) = 0 \quad (7.110)$$

which is also a line. The manipulator is always singular regardless of the coordinate y . In particular, a unique point

$$P_1 : (x_1, y_1) = \left(-\left(9\sqrt{2} + 3\sqrt{6}\right)/8, 9.10694 \right),$$

at which that all segments associated with the six extensible links of the manipulator can be proven to intersect one common line, exists (Fig. 7.29); the Plücker coordinates of this point are as follows:

$$(L, M, N; P, Q, R) = (0.48296, 0.83652, -0.25882; 0.50000, -0.86603, -1.86603)$$

Further analysis shows that this line does not pass through any vertex of the moving platform or the base one. It also belongs to the first special-linear-complex singularity.

To verify this remarkable phenomenon, the coordinates of the 12 vertices of the moving and base platforms are presented in Appendix A. Moreover, the Plücker coordinates of the six line vectors, the instantaneously moving reciprocal screw, and the corresponding reciprocal products are also presented.

The second part of Eq. (7.109) denotes another line. Singularities corresponding to points lying on this line are all of the general-linear-complex type.

(4) Fourth Case of Two Intersecting Lines

When $X_{V4} = (11\sqrt{6} - 3\sqrt{2})/12$, $D = 0$, and $\delta \neq 0$, Eq. (7.99) degenerates into two intersecting lines

$$(24x - (15\sqrt{2} + 5\sqrt{6}))(x + k_4y + c_4) = 0 \quad (7.111)$$

The first part of Eq. (7.111) is

$$24x - (15\sqrt{2} + 5\sqrt{6}) = 0 \quad (7.112)$$

which is a line parallel to the y -axis of frame V - xy . In particular, three special points, at which all segments associated with the six extensible links of the manipulator intersect one common line, exist, as follows:

1. When $P_2 : (x_2, y_2) = ((15\sqrt{2} + 5\sqrt{6})/24, -0.40288)$, the two plane triangles $C_3B_4C_4$ and $C_3B_5C_5$ intersect with one common line C_3B_6 , which simultaneously intersect the two plane triangles $C_3B_1C_1$ and $C_3B_2C_2$ because C_3B_6 intersects with C_3B_3 and C_6B_6 . Therefore, all segments associated with the six extensible links of the manipulator intersect one common line (C_3B_6). This singularity belongs to the first special-linear-complex type. In this case, the corresponding determinate of the Jacobian matrix and the instantaneously moving reciprocal screw and its pitch are presented as follows:

$$\begin{aligned} \text{Det}(J_2) &= 9.73 \times 10^{-18} \\ \mathcal{S}_2^m &= (-0.8286, 0.3410, 0.4440; -0.2299, -0.8578, 0.2299) \\ h_2^m &= -1.5025 \times 10^{-16} \end{aligned} \quad (7.113)$$

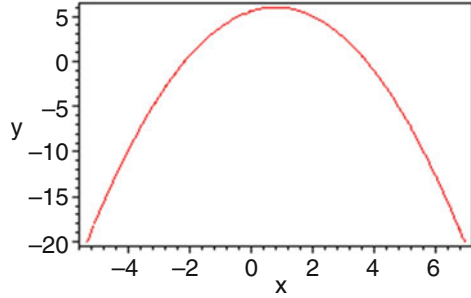
2. When $P_3 : (x_3, y_3) = ((15\sqrt{2} + 5\sqrt{6})/24, 2.45485)$, all segments associated with the six extensible links of the manipulator can be proven to intersect one common line C_4B_1 . This singularity also belongs to the first special-linear-complex type. In this case, we have

$$\begin{aligned} \text{Det}(J_3) &= -4.8638 \times 10^{-18} \\ \mathcal{S}_3^m &= (0.6066, -0.7255, -0.3251; -0.6280, 0.1638, -1.54749) \\ h_3^m &= 1.4603 \times 10^{-14} \end{aligned} \quad (7.114)$$

3. When $P_4 : (x_4, y_4) = ((15\sqrt{2} + 5\sqrt{6})/24, 2.34546)$, all segments associated with the six extensible links can be proven to intersect one common line whose Plücker coordinates are

$$\begin{aligned} (L, M, N; P, Q, R) &= (0.48296, 0.83652, -0.25882; \\ &0.50000, -0.86603, -1.86603) \end{aligned}$$

Fig. 7.30 One case of a parabola



This singularity also belongs to the first special-linear-complex type. In this case, we have

$$\begin{aligned}
 \text{Det}(J_4) &= 1.2129 \times 10^{-17} \\
 \mathcal{S}_4^m &= (0.48296, 0.83652, -0.25882; 0.50000, -0.86603, -1.86603) \\
 h_4^m &= -2.7440 \times 10^{-14}
 \end{aligned}
 \tag{7.115}$$

Generally, singularities corresponding to points lying in the line of Eq. (7.112), with the exception of the aforementioned three points (P_2, P_3, P_4), are all of the general-linear-complex type.

The second part of Eq. (7.111) denotes another line. Singularities corresponding to points lying in this line are all of the general-linear-complex type.

(5) One Case of a Parabola

When $X_{V5} = (7\sqrt{6} + 3\sqrt{2})/6$, $\delta = 0$, and $D \neq 0$, Eq. (7.99) degenerates into a parabola, as shown in Fig. 7.30.

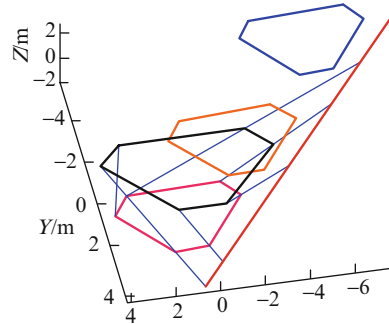
$$\begin{aligned}
 (528\sqrt{6} - 912\sqrt{2})x^2 + (1,423\sqrt{3} - 2,472)x \\
 + (504 - 288\sqrt{3})y + 513\sqrt{6} - 909\sqrt{2} = 0
 \end{aligned}
 \tag{7.116}$$

The manipulator corresponding to the points lying in the parabola is always singular. Similarly, three special points at which all segments associated with the six extensible links of the manipulator intersect one common line exist.

1. When $P_5 : (x_5, y_5) = (3.67960, 0.20950)$, all segments associated with the six extensible links of the manipulator can be proven to intersect one common line, C_3B_6 . This singularity belongs to the first special-linear-complex type.
2. When $P_6 : (x_6, y_6) = (2.61894, 3.67960)$, all segments associated with the six extensible links intersect one common line C_4B_1 . This singularity belongs to the first special-linear-complex type.
3. When $P_7 : (x_7, y_7) = (-0.27884, 5.24324)$, all segments associated with the six extensible links intersect one common line whose Plücker coordinates are

$$(L, M, N; P, Q, R) = (0.48296, 0.83652, -0.25882; 0.50000, -0.86603, -1.86603)$$

Fig. 7.31 Three cases wherein all segments intersect one common line



This singularity also belongs to the first special-linear-complex type.

Generally, the singularities of points lying in the parabola of Eq. (7.116), with the exception of the aforementioned three points (P_5, P_6, P_7), are all of the general-linear-complex type.

For the same orientation $(\phi, \theta, \psi) = (\pi/3, \pi/6, 0)$ of the manipulator, the manipulator has three positions, P_1 in Sect. 7.6.3.2.3, P_4 in Sect. 7.6.3.2.4, and P_7 in Sect. 7.6.3.2.5, at which all segments associated with the six extensible links of the manipulator simultaneously intersect the same line (Fig. 7.31). Similarly, two sets of positions, P_2 and P_3 in Sect. 7.6.3.2.4, P_5 and P_6 in Sect. 7.6.3.2.5, exist at which all segments associated with the six extensible links of the manipulator intersect one common line, namely, C_3B_6 and C_4B_1 , respectively.

Based on the aforementioned analyses, the singularity loci of this class of 6/6-Stewart manipulators in parallel principal sections are always quadratic expressions that generally include infinite hyperbolas. However, for four parallel locations of the principal-section, the quadratic expression degenerates into two intersecting lines, and in one location the quadratic expression is a parabola when $\theta \neq 0$.

7.6.3.3 Singularity Analysis When $\theta = 0$

When $\theta = 0$, the moving platform is parallel to the base one. Meanwhile, Eq. (7.94) can be reduced as follows:

$$Z^3 \cos(\varphi + \psi) = 0 \tag{7.117}$$

When $Z = 0$, the moving and base platforms are coincident. In this SC, the manipulator has three DOFs: two rotational freedoms and one translational freedom.

When $(\varphi + \psi) = \pm\pi/2$, the 6/6-Stewart manipulator is the singularity proposed by Huang and Qu in 1987 [34].

As previously discussed, the singularity loci of this class of 6/6-Stewart manipulators in parallel principal sections include infinite hyperbolas, four cases of two intersecting lines, and one case of a parabola when $\theta \neq 0$.

From analytic geometry, quadric surfaces have five different types with hyperbolic sections: the hyperbolic cylinder, hyperbolic paraboloid, hyperboloid of one

sheet, hyperboloid of two sheets, and a conic surface. However, none of these sections can simultaneously contain infinite hyperbolas, one case of a parabola, and four cases of two intersecting lines. Therefore, the singularity locus equation of this class of 6/6-Stewart manipulators considered in 3D space is a special irresolvable polynomial expression of degree three, whose cross-sections in parallel principal sections contain one case of a parabola, four cases of two intersecting lines, and infinite hyperbolas.

Therefore, the property of the singularity loci of this class of Gough–Stewart manipulators for all different orientations can be finally concluded as follows:

1. The singularity locus equation is a special irresolvable polynomial expression of degree three, whose cross-sections in parallel principal sections contain one case of a parabola, four cases of two intersecting lines, and infinite hyperbolas.
2. The graphical representations of the singularity locus of this class of 6/6-Gough–Stewart manipulators are quite complex and varied for different orientations. The most complex representation of the singularity loci is similar to a trifoliate surface with two holes.
3. We find that, for this class of 6/6-Gough–Stewart manipulators, some special singularity cases occur, wherein six lines associated with the six extensible links of the manipulator can intersect one common line, and the unwanted motion of the manipulator is a pure rotational motion. Even for the same orientation of the manipulator, two or more positions of the manipulator exist at which the six lines all simultaneously intersect one common line.
4. When $\theta = 0$ and $Z = 0$, the manipulator has three unwanted DOFs, namely, two rotational freedoms and one translational freedom.

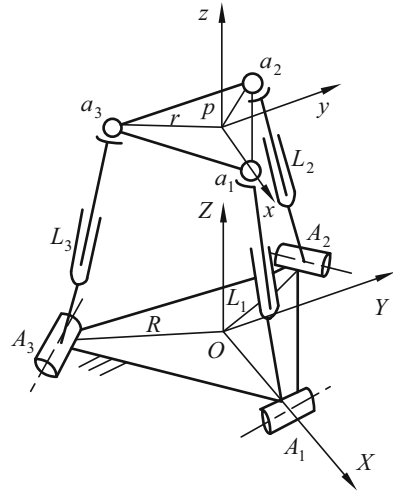
7.7 Singularity of a 3-RPS Manipulator

The 3-RPS mechanism is a very typical one proposed by Hunt [1] in 1983 and was the focus of interest of many researchers. This Section presents a singularity analysis of the 3-RPS parallel manipulator based on the singularity kinematics principle. The general singular equation and the entire singularity distribution in 3D space is discussed, and the singularity characteristics are analyzed. To verify its correctness, the line geometry singular discriminant and the constraint screw theory are also used. Meanwhile, a number of interesting singularities and important structural properties of the manipulator are represented [42].

7.7.1 3-RPS Mechanism

To determine the singularity of the 3-RPS mechanism, we may lock all the three input pairs, and then identify whether the mechanism has mobility. When all inputs

Fig. 7.32 3-RPS mechanism



are locked, several constraint forces are applied to the moving platform by the three branches. These force screws constitute a constraint screw system, which is the screw system reciprocal to the moving screw system of the moving platform. A rank of the constraint screw system less than 6 indicates that instantaneous freedoms exist. The mechanism is singular. Therefore, the Jacobian matrix consisting of the constraint screw system can be used to identify the singularity of the 3-RPS mechanism.

The 3-RPS parallel manipulator (Fig. 7.32) consists of a triangular upper platform and a base platform connected by three RPS chains. It has one translational and two rotational freedoms.

7.7.1.1 Constraint Equation of the 3-RPS Parallel Manipulator

Figure 7.32 shows that the fixed system O - XYZ is attached to the base and P - xyz is attached to the mobile. The length of the branch is L_i ($i = 1, 2, 3$). The circumcircle radius of the basic platform is R and that of the mobile is r . The transformation matrix from P - xyz to O - XYZ can be expressed as follows:

$$T = \begin{bmatrix} x_i & y_i & z_i & X_P \\ x_j & y_j & z_j & Y_P \\ x_k & y_k & z_k & Z_P \\ 0 & 0 & 0 & 1 \end{bmatrix} \tag{7.118}$$

where $x_m, y_m,$ and z_m ($m = i, j, k$) express the direction cosines. $(X_P Y_P Z_P)$ are the coordinates of point P .

Only three parameters are independent and controllable in the three-DOF mechanism. The kinematic loci of the centers a_1 , a_2 , and a_3 have to lie in three vertical planes, as follows:

$$Y = 0 \quad Y = -\sqrt{3}X \quad Y = \sqrt{3}X$$

Thus, the three constraint equations can be derived [41] as follows:

$$x_j - y_i = 0 \quad Y_P = -rx_j \quad X_P = r(x_i - y_j)/2 \quad (7.119)$$

7.7.1.2 Position and Orientation Analysis

Assume the Z-Y-X Euler angles to be (α, β, γ) ; then

$$T = \begin{bmatrix} c \alpha c \beta & c \alpha s \beta s \gamma - s \alpha c \gamma & c \alpha s \beta c \gamma + s \alpha s \gamma & X_P \\ s \alpha c \beta & s \alpha s \beta s \gamma + c \alpha c \gamma & s \alpha s \beta c \gamma - c \alpha s \gamma & Y_P \\ -s \beta & c \beta s \gamma & c \beta c \gamma & Z_P \\ 0 & 0 & 0 & 1 \end{bmatrix} \quad (7.120)$$

where six parameters $(X_P Y_P Z_P \alpha \beta \gamma)$ are included, and $c = \cos$, and $s = \sin$. From Eqs. (7.119) and (7.120), we can obtain the following equations

$$\begin{aligned} X_P &= r(\cos \alpha \cos \beta - \sin \alpha \sin \beta \sin \gamma - \cos \alpha \cos \gamma)/2 \\ Y_P &= -r \sin \alpha \cos \beta \\ \alpha &= \text{arctg}[\sin \beta \sin \gamma / (\cos \beta + \cos \gamma)] \end{aligned} \quad (7.121)$$

From the constraint conditions, the three parameters may be freely chosen for the 3-RPS mechanism; however,

1. Z_P is the only completely independent variable, and its choice is independent of the other five pose parameters $(X_P Y_P \alpha \beta \gamma)$, and vice versa. Z_P has to be one of the three independent parameters;
2. The other two variables are freely chosen from the remaining five $(X_P Y_P \alpha \beta \gamma)$;
3. Although the mechanism has three freedoms, the three Euler angles cannot freely choose simultaneously; and
4. Any given coordinates $(X_P Y_P)$, have a pair of Z-Y-X Euler parameters, $(\beta \gamma)$ and $(-\beta -\gamma)$. For any given Euler angle α , the other two Euler parameters, β and γ , can be obtained as follows:

$$\begin{aligned} \alpha &= f_1(-\beta - \gamma) = f_1(\beta \ \gamma) \\ X_P &= f_2(-\beta - \gamma) = f_2(\beta \ \gamma) \\ Y_P &= f_3(-\beta - \gamma) = f_3(\beta \ \gamma) \end{aligned} \quad (7.122)$$

That is, for each point in the workspace of the mechanism, a pair of conjugate Euler angles with identical α and opposite-sign β and γ exists. In other words, each point with the same $(X_P Y_P)$ has two orientations.

7.7.2 Singularity and Its Spatial Distribution

7.7.2.1 Singularity Equation

The six parameters of the manipulator include three independence output parameters. In this section, Z_P , β , and γ are chosen as the independent variables. The singularity equation for the 3-RPS mechanism can be derived using Theorem 7.2.

The three constraint planes of points a , b , and c are $Y = 0$, $Y = -\sqrt{3}X$, and $Y = \sqrt{3}X$, respectively. Three velocity vectors, namely, v_a , v_b , and v_c , lie in the three planes, respectively. Considering that v_a is normal to aA , v_b to bB , and v_c to cC , the corresponding direction cosines of the three velocities are expressed as $(l_i m_i n_i)$ ($i = a, b, c$), respectively. The three normal planes of the three velocities are as follows:

$$\begin{aligned}
 l_a(X - r \cos \alpha \cos \beta - X_P) + n_a(Z + r \sin \beta - Z_P) &= 0 \\
 l_b[X + r \cos \alpha \cos \beta/2 - \sqrt{3}r(\cos \alpha \sin \beta \sin \gamma - \sin \alpha \cos \gamma)/2 - X_P] \\
 + m_b[Y + r \sin \alpha \cos \beta/2 - \sqrt{3}r(\sin \alpha \sin \beta \sin \gamma + \cos \alpha \cos \gamma)/2 - Y_P] \\
 + n_b[Z + r \sin \beta/2 - \sqrt{3}r \sin \gamma \cos \beta/2 - Z_P] &= 0 \\
 l_c[X + r \cos \alpha \cos \beta/2 + \sqrt{3}r(\cos \alpha \sin \beta \sin \gamma - \sin \alpha \cos \gamma)/2 - X_P] \\
 + m_c[Y + r \sin \alpha \cos \beta/2 + \sqrt{3}r(\sin \alpha \sin \beta \sin \gamma + \cos \alpha \cos \gamma)/2 - Y_P] \\
 + n_c[Z + r \sin \beta/2 + \sqrt{3}r \sin \gamma \cos \beta/2 - Z_P] &= 0 \tag{7.123}
 \end{aligned}$$

The plane equation of the moving platform abc is

$$\begin{vmatrix} X - X_a & Y - Y_a & Z - Z_a \\ X_b - X_a & Y_b - Y_a & Z_b - Z_a \\ X_c - X_a & Y_c - Y_a & Z_c - Z_a \end{vmatrix} = 0 \tag{7.124}$$

Based on Theorem 7.2, substituting Eq. (7.121) into Eq. (7.123) and solving for X , Y , and Z , then substituting them into Eq. (7.124), the general singularity-loci equation of the 3-RPS manipulator can be obtained as follows [42]:

$$P_3 Z_P^3 + P_2 Z_P^2 + P_1 Z_P + P_0 = 0 \tag{7.125}$$

where P_i ($i = 0, 1, 2, 3$) are the coefficients and functions of the Euler angles. After the three Euler angles are determined, all four coefficients of the equation of degree

three are constant. For the equation of the third degree, three roots for Z_P corresponding to three singularity locations exist. That is, each orientation has as much as three singularity positions.

7.7.2.2 Two Special Cases

When $\alpha = 0$, either $\beta = 0, 180^\circ$, or $\gamma = 0, 180^\circ$ can be obtained using Eq. (7.121). Considering the workspace for the general mechanical structure, the only possible values are $\beta = 0$ and $\gamma = 0$.

1. $\alpha = 0, \beta = 0$, and γ is an arbitrary value

The singularity Eq. (7.125) becomes

$$Z_P[4Z_P^2(\cos^2\gamma + \cos \gamma) + r^2\sin^2\gamma\cos^2\gamma - 8R^2\sin^2\gamma - 3r^2\sin^2\gamma \cos \gamma + 4rR\sin^2\gamma \cos \gamma] = 0 \quad (7.126)$$

The equation has three roots, which can be expressed as

$$\begin{aligned} Z_P &= 0 \\ Z_P &= \pm \sqrt{\frac{w+u}{4(\cos \gamma + \cos^2\gamma)}} \end{aligned} \quad (7.127)$$

where $u = -(4rR - 3r^2)\sin^2\gamma \cos \gamma$, and $w = 8R^2\sin^2\gamma - r^2\sin^2\gamma\cos^2\gamma$.

Equation (7.126) shows that for any orientation $(0 \ 0 \ \pm\gamma)$, three singularity Z_P values, which correspond to positive, zero, and negative, can be obtained, respectively. Regardless of the γ value, $Z_P = 0$ is always singular.

When $\gamma = 0$, i.e., the Euler angles are $(0 \ 0 \ 0)$, the 3-RPS mechanism is singular only at $Z_P = 0$, at which the upper and the lower platforms are parallel. The three roots of Eq. (7.126) coincide at $Z_P = 0$.

The singularity curves when the mechanism parameters are $r = 0.5, R = 1.0, \alpha = 0, \beta = 0$, and $\gamma = 0 \sim \pi/2$ are shown in Fig. 7.33. The three singular curves clearly lie in the same vertical cylindrical surface. That is, the three singularity points in a vertical line have the same X and Y coordinates. When $\gamma = 0$, the three curves intersect at a common point. The medium curve lies in a horizontal plane $Z_P = 0$.

2. $\alpha = 0, \gamma = 0$, and β is an arbitrary value

The singular Eq. (7.125) becomes

$$\begin{aligned} &(2Z_P + r \sin \beta)(2 \cos \beta Z_P - 2R \sin \beta \\ &+ r \sin \beta \cos \beta - r \sin \beta)[2(1 + \cos \beta)Z_P \\ &+ 4R \sin \beta - 3r \sin \beta + r \sin \beta \cos \beta] = 0 \end{aligned} \quad (7.128)$$

Fig. 7.33 Singularity loci at $(0 \ 0 \ \gamma)$

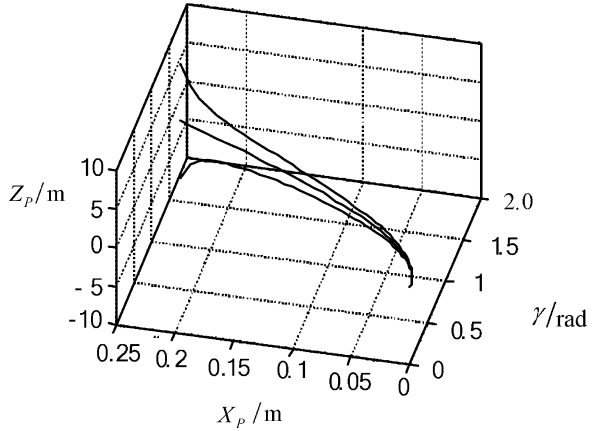
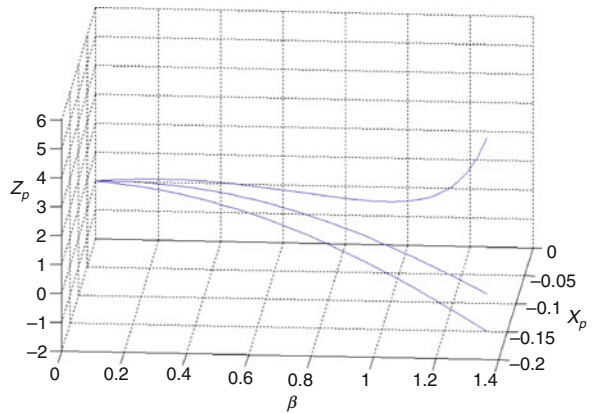


Fig. 7.34 Singularity loci at $(0 \ \beta \ 0)$



Solving Eq. (7.128), the three roots can be obtained as

$$\begin{aligned}
 Z_{P1} &= -r \sin \beta / 2 \\
 Z_{P2} &= -(4R - 3r + r \cos \beta) \sin \beta / (2(1 + \cos \beta)) \\
 Z_{P3} &= (2R + r - r \cos \beta) \operatorname{tg} \beta / 2
 \end{aligned}
 \tag{7.129}$$

This condition also shows that three Z_P can be obtained for the same β when $\alpha = 0$ and $\gamma = 0$. Otherwise, a singular point Z_P only corresponds to a value of β . When $\beta = 0$, the mechanism is singular only at $Z_P = 0$.

When the parameters of the mechanism are $r = 0.5$, $R = 1.0$, $\alpha = 0$, and $\gamma = 0$, the singularity loci include three branches, as shown in Fig. 7.34. The three singular curves also lie in the same vertical cylindrical surface.

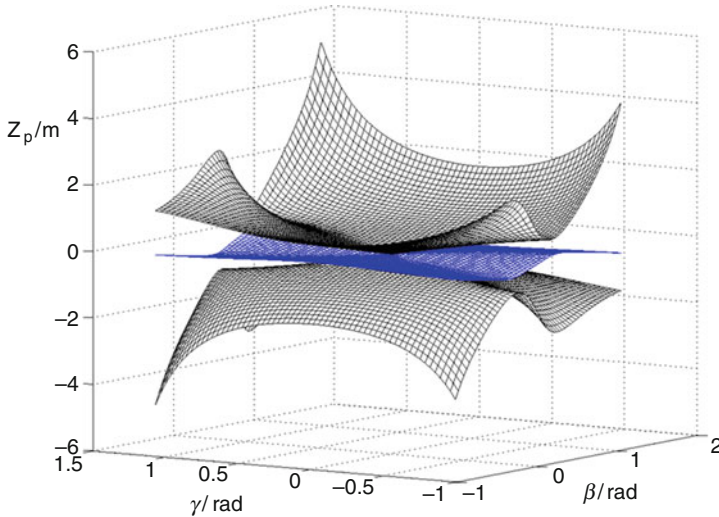


Fig. 7.35 Singularity distribution at $r = 0.5$, $R = 1.0$

7.7.2.3 Singularity Distribution in 3D Space

Singular Surface

To determine the distribution characteristics of the singularity loci of the 3-RPS parallel manipulator in space, their singularity surface can be constructed in 3D space. The parameters of the mechanism are $r = 0.5$ and $R = 1.0$. The singularity surface in the $Z_p-\beta-\gamma$ space can be obtained from Eqs. (7.125) and (7.121), as shown in Fig.7.35. Similarly, the singularity surface in the $X_p-Y_p-Z_p$ space from Eqs. (7.125), (7.121) and is shown in Fig.7.36.

Many singularity points in Fig. 7.36 have been verified using the Jacobian matrix formed by the six constraint screws; some of these singularity points are shown below.

In Fig.7.36, the singularity surface has three symmetrical planes: $Y = -\sqrt{3}X$, $Y = \sqrt{3}X$, and $Y = 0$. In space, the three symmetrical planes intersect at a common line and form three equal angles of 120° because of the inherent symmetry of the mechanism itself.

For example, a point P^1 ($X_p^1 = -0.0528$, $Y_p^1 = 0.0915$, $Z_p^1 = 0$) on line OB in Fig. 7.32 is arbitrarily taken. By solving Eqs. (7.121) for $(\alpha \ \beta \ \gamma)$ and substituting them into Eq. (7.125), three singularity points, namely, $Z'_{p1} = 1.1475$, $Z'_{p2} = -1.1475$, and $Z'_{p3} = -0.6522$ can be obtained. The three points are located on the same vertical line with the same $X_p^1 = -0.0528$ and $Y_p^1 = 0.0915$ coordinates. If another point P^2 ($X_p^2 = -0.0528$, $Y_p^2 = -0.0915$, $Z_p^2 = 0$) on line OC , which is just the symmetrical point of point P^1 about the X axis, is taken, three roots, namely, $Z^2_{p1} = 1.1475$, $Z^2_{p2} = -1.1475$, and $Z^2_{p3} = 0.6522$, can be obtained. A comparison of the six Z_p values verifies that the singular surface is symmetrical about the plane $Y = 0$. Similarly, the singular surface can be verified as symmetrical about the planes $Y = -\sqrt{3}X$ and $Y = \sqrt{3}X$.

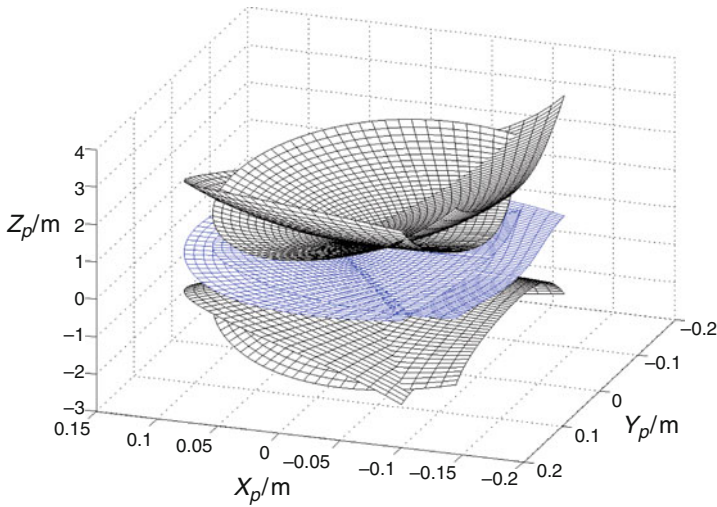


Fig. 7.36 Singularity distribution at $r = 0.5$, $R = 1.0$

Singular Points in a Vertical Line

Figure 7.35 shows that three singular points in any vertical line parallel to Z -axis exist. However, the number of singularity points in the different vertical lines in Fig. 7.36 is different and depends on the coordinates (X_p, Y_p) .

In Fig. 7.36, every vertical line in any nonsymmetrical plane has six singular points because each point in the workspace has a pair of conjugate Euler angles (Sect. 7.7.1.2), and each set of Euler angles has three different singularity positions. Every singular point corresponds only to one orientation. Take a point with $X_p = -0.00003$, $Y_p = -0.0732$ in the base plane, for example, outside the intersecting line between the base and symmetry planes. Solving for the orientations of the upper platform yields

$$\begin{aligned}
 (\alpha^3 \beta^3 \gamma^3) &= (9.7403^\circ \ 30.0115^\circ \ 35.2656^\circ) \\
 (\alpha^4 \beta^4 \gamma^4) &= (9.7403^\circ \ -30.0115^\circ \ -35.2656^\circ)
 \end{aligned}
 \tag{7.130}$$

For $(\alpha^3 \beta^3 \gamma^3)$, the three roots of Z_p are

$$Z_{p1}^3 = 0.6773, \ Z_{p2}^3 = -1.0093, \ Z_{p3}^3 = 0.1160
 \tag{7.131}$$

The other three roots corresponding to $(\alpha^4 \beta^4 \gamma^4)$ are

$$Z_{p1}^4 = -0.6773, \ Z_{p2}^4 = 1.0093, \ Z_{p3}^4 = 0.1160.
 \tag{7.132}$$

Three of these roots are positive and are located over the basic plane.

Note that no singularity point exists when the coordinate Z_P is larger than some value in a vertical line. Considering this and the singularity loci in Fig. 7.36, the singularity can be easily avoided if the useful workspace of this mechanism is placed over the representation in Fig. 7.36.

However, any given set of $(X_P \ Y_P)$ coordinates lying on the symmetry planes $Y = -\sqrt{3}X$, $Y = \sqrt{3}X$ or $Y = 0$ only has three singular points. For example, assume a set of coordinates with $X_P = 0.05$ and $Y_P = 0$, a point at which the coordinates are in the intersecting line between plane $Y = 0$ and the base plane. Solving Eq. (7.121) for the Euler angles, the two roots are

$$\begin{aligned}(\alpha^5 \ \beta^5 \ \gamma^5) &= (0 \ 0 \ 36.8699^\circ) \\(\alpha^6 \ \beta^6 \ \gamma^6) &= (0 \ 0 \ -36.8699^\circ)\end{aligned}\tag{7.133}$$

From Eq. (7.126) the roots corresponding to $(X_P \ Y_P)$ for the two orientations are $Z_{P1} = 0$, $Z_{P2} = 0.6538$, and $Z_{P3} = -0.6538$, which are the same as those previously mentioned.

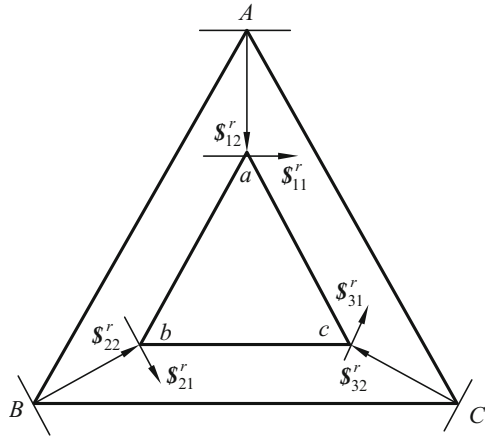
7.7.3 Geometry and Constraint Analysis

This section discusses the geometric conditions for the singular configurations. The 3-RPS mechanism in Fig. 7.32 has three limbs with an RPS chain, with each consisting of five single-DOF kinematic pairs. That is, the limb has five motion screws and one reciprocal-screw constraint force parallel to the first pair passing the center point of the spherical pair. When the singularity is analyzed, the input must be locked and the limb has one more constraint force along the limb-link itself. Each limb then acts in a total of two constraint screw forces to the platform. The singularity of the mechanism has ten cases as follows:

Case 1. All three Euler angles $(\alpha \ \beta \ \gamma)$ are zero, as shown in Fig. 7.37. From Eq. (7.126), the mechanism is singular only at $Z_P = 0$, and the moving platform superposes on the base plane. Two constraint forces are imposed on the platform by each branch while all three inputs are locked. $\$'_{11}$ and $\$'_{12}$ express the two constraint forces, respectively, and their directions are either along the direction of the branch or parallel to the axis of the kinematic pair R in the branch. All forces pass through the center of the spherical pair in each branch.

Thus, the entire mechanism has six coplanar constraint forces $[\$'_{11} \ \$'_{12} \ \$'_{21} \ \$'_{22} \ \$'_{31} \ \$'_{31}]$, that are linearly dependent and whose order is only 3 (Table 2.1). Thus, the mechanism has three instant freedoms while the three inputs are all locked. This singularity is the kind of 3d proposed by Merlet's paper [4]. Given that the instantly

Fig. 7.37 First singular configuration



moving screws and constraint screws are mutually reciprocal, the three moving screws can be solved using Eqs. (2.53) or (2.54), as follows:

$$\begin{aligned}
 \mathcal{S}_{11}^m &= [0 \ 0 \ 0; \ 0 \ 0 \ 1] \\
 \mathcal{S}_{12}^m &= [1 \ 0 \ 0; \ 0 \ a \ b] \\
 \mathcal{S}_{13}^m &= [0 \ 1 \ 0; \ c \ 0 \ d]
 \end{aligned}
 \tag{7.134}$$

Their pitches, obtained by solving Eq. (1.34), are ∞ , 0, and 0, respectively. The possible instant motions are a translational motion along the Z axis and two rotational motions about any axis in the moving plane, respectively. The first singularity belongs to the second special-linear-complex; on the other hand, both latter situations belong to the first special-linear-complex. The three solutions correspond to the intersecting point of the three curves where $\gamma = 0$ (Fig. 7.33).

Case 2. $\alpha = 0, \beta = 0, \gamma \neq 0$, and $Z_P = 0$ (Fig. 7.38). The mechanism is singular at the configuration, and the moving platform *abc* intersects the base platform *ABC* at line *AL*. Line *bc* intersects five forces, namely, $\mathcal{S}_{12}^r, \mathcal{S}_{21}^r, \mathcal{S}_{31}^r, \mathcal{S}_{22}^r$, and \mathcal{S}_{32}^r , simultaneously. Assume that line *MN* is the intersect line between plane *cCNL* determined by axes \mathcal{S}_{31}^r and \mathcal{S}_{32}^r as well as plane *bBLM* determined by \mathcal{S}_{21}^r and \mathcal{S}_{22}^r . Line *MN* passes through point *L* lying on the base. Thus, line *MN* also intersects with the same five forces above. Therefore, the six constraint forces are linearly dependent because the five forces intersect with two lines at the same time. The order of the constraint-force system is 5. This case corresponds to the middle curve in Fig. 7.33, and this singularity belongs to that of 4b [4]. For example, for $\gamma = 30^\circ$, solving Eqs. (2.53) or (2.54) for the moving screw yields

$$\mathcal{S}_{21}^m = [0 \ -0.0205 \ -0.006834; \ 0 \ 0.003759 \ 0.017769]
 \tag{7.135}$$

Its pitch is a finite value (-0.01), and this configuration belongs to the general-linear-complex singularity.

Fig. 7.38 Second singular configuration

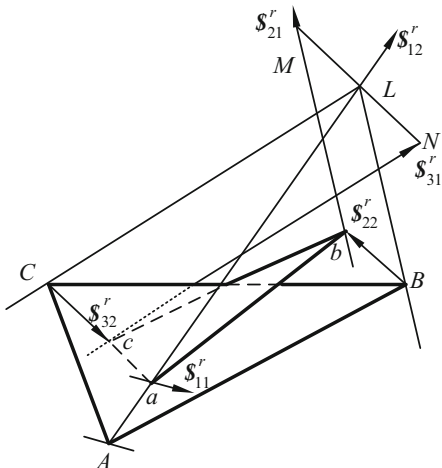
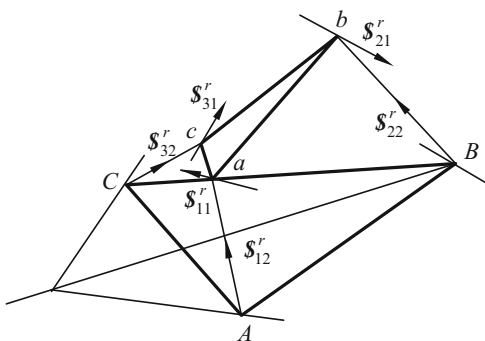


Fig. 7.39 Third singular configuration



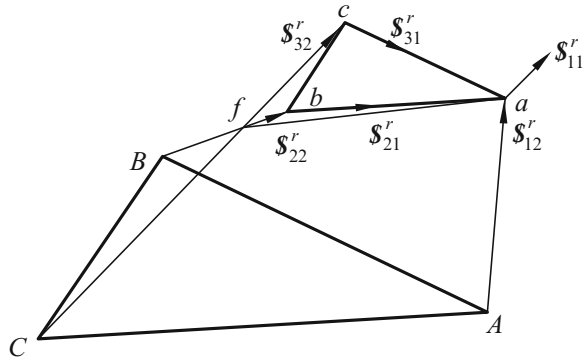
Case 3. $\alpha = 0, \beta = 0, \gamma \neq 0$, and line cC is coplanar with plane abc (Fig. 7.39). Equation (7.127) is used to solve for Z_p . For example, when $\gamma = 36.8699^\circ, Z_p = \pm 0.6538$. By solving Eq. (2.53) or (2.54), we obtain the instant motion screw as follows:

$$S_{31}^m = [0.6562 \quad -0.4516 \quad -0.1505; 0.3937 \quad 0.5118 \quad -0.1807] \quad (7.136)$$

Its pitch is 0.0671. At this point the five screws ($S_{11}^r, S_{21}^r, S_{12}^r, S_{22}^r$, and S_{32}^r) only intersect the line ab , but S_{31}^r , which is parallel to AB , does not intersect the line. This configuration belongs to the general-linear-complex singularity, which correspond to the uppermost and lowest curves in Fig. 7.33 belonging to 5a [4].

Case 4. $\alpha = 0, \beta = 0$, and $\gamma = 180^\circ$ (Fig. 7.40). According to Eq. (7.126), the mechanism is singular for any value of Z_p . When $Z_p = 0$, the singularity is similar to that in Case 1, where the three Euler angles (α, β, γ) are all zero. For example,

Fig. 7.40 Fourth singular configuration



when $Z_p \neq 0, Z_p = 1.0$, and the Jacobian matrix force consists of the six constraint forces as follows:

$$J = \begin{bmatrix} 0 & 0.866 & -0.866 & 0 & 0.75 & 0.75 \\ -1.0 & 0.5 & 0.5 & 0 & -1.299 & 1.299 \\ 0 & 0 & 0 & 1.0 & 1.0 & 1.0 \\ 1.0 & -0.5 & -0.5 & 0 & 0.866 & -0.866 \\ 0 & 0.866 & -0.866 & -1.0 & 0.5 & 0.5 \\ -1.0 & 0.5 & 0.5 & 0 & 0 & 0 \end{bmatrix} \quad (7.137)$$

The determinant of the matrix is -1.2490×10^{-16} and the mechanism is singular. The instantly moving screw is $\$_{41} = [1.6875 \ 0 \ 0.5625; \ 0 \ 1.125 \ 0]$, and its pitch is 0. The motion of the platform is a pure rotation. This singularity belongs to the first special-linear-complex type. Consider that the four screws $\$_{11}^r, \$_{21}^r, \$_{12}^r$, and $\$_{31}^r$ intersect at a common point a , and $\$_{22}^r$ intersects with $\$_{32}^r$ at a point f . The line af intersects with the six force vectors and is the rotational axis. This situation is similar to that of 3c [4].

Case 5. $\alpha = 0, \gamma = 0, \beta \neq 0$, and $Z_p = -r \sin \beta/2$ (Fig. 7.41). This case corresponds to the middle curve in Fig. 7.34. At this configuration, points b and c lie in the base plane ABC , and bc is parallel to BC . The four screws ($\$_{12}^r, \$_{22}^r, \$_{31}^r$, and $\$_{32}^r$) are coplanar. In addition, all six constraint screws intersect a line gk , which passes through point A and is parallel to line BC . Therefore, the motion of the platform at this instant is clearly a pure rotation about gk . This singularity is a first special-linear-complex type, and this situation is similar to that of 3d [4].

Case 6. $\alpha = 0, \gamma = 0, \beta \neq 0$, and $Z_p = -(4R - 3r + r \cos \beta) \sin \beta/2/(1 + \cos \beta)$, as shown in Fig. 7.42. This case corresponds to the lowest curve in Fig. 7.34. For this configuration, $bc//BC$. $\$_{22}^r$ intersects $\$_{32}^r$ at point e , and $\$_{21}^r$ intersects $\$_{31}^r$ at point d . The three points a, e , and d can easily be verified as collinear. When they are collinear, the six line vectors simultaneously intersect a line ad , and the motion of

Fig. 7.41 Fifth singular configuration

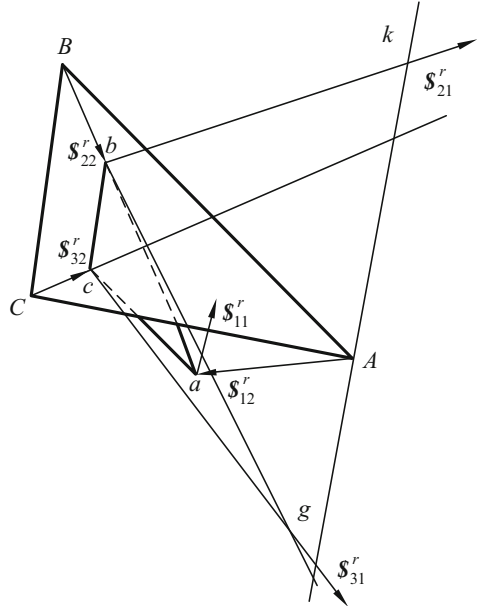
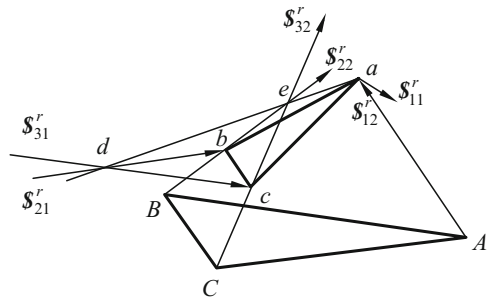


Fig. 7.42 Sixth singular configuration



the mechanism is pure rotation about ad . The singularity belongs to the first special-linear-complex singularity 5b [4].

Case 7. $\alpha = 0, \gamma = 0, \beta \neq 0$, and $Z_P = (2R + r - r \cos \beta)tg\beta/2$ (Fig. 7.43). The mechanism is singular according to Eq. (7.129). This case corresponds to the uppermost curve in Fig. 7.34. At this configuration, line Aa lies in the moving plane and $bc // BC // s_{11}^r$. Thus, the six line vectors intersect a line bc . The motion of the upper platform is pure rotation about bc , and the singularity also belongs to the first special-linear-complex singularity 5b [4].

Case 8. $\alpha = 0, \gamma = 0, \beta = 180^\circ$ (Fig. 7.44). According to Eq. (7.128), the mechanism is singular regardless of the value of Z_P . The singularity when $Z_P = 0$ is

Fig. 7.43 Seventh singular configuration

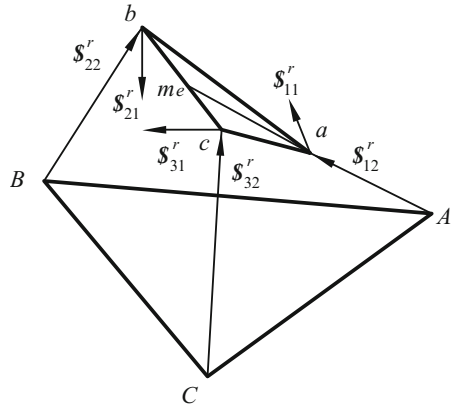
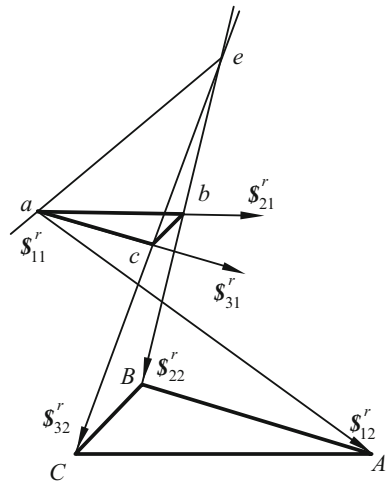


Fig. 7.44 Eighth singular configuration



similar to that in Case 1. When $Z_P \neq 0$, such as $Z_P = 1.1$, the determinant of the Jacobian matrix force is 1.6624×10^{-16} . The moving screw is

$$s_{81}^m = [0.680625 \quad 0 \quad 0.7486875; \quad 0 \quad 1.497375 \quad 0] \tag{7.138}$$

and its pitch is 0. The six line vectors intersect ae . The instant motion of the mechanism is pure rotation about ae , and the singularity belongs to the first special-linear-complex singularity 5b [4].

Case 9. $\alpha = 0$, $\beta = 180^\circ$, and $\gamma = 180^\circ$. According to Eq. (7.125), the mechanism is singular only at $Z_P = 0$. The singularity is the same as when three Euler angles (α , β , γ) are 0 and similar to that 3d [4].

Case 10. For the most general situation, that is, $\beta \neq 0$ and $\gamma \neq 0$. For example, when $\beta = 30.0115^\circ$ and $\gamma = 35.2656^\circ$, we obtain $\alpha = 9.7403^\circ$, $X_P = -3.1932 \times 10^{-5}$,

and $Y_P = -0.0732$ when Eq. (7.121) is solved, and the three Z_P values are $Z_{P1} = 0.6773$, $Z_{P2} = -1.0093$, and $Z_{P3} = 0.1160$. When $Z_{P1} = 0.6773$, the determinant of the Jacobian matrix is -2.6470×10^{-17} . The moving screw is

$$\mathcal{S}_{101}^m = [-0.035 \ 0.093 \ 0.067 \ -0.169 \ -0.044 \ -0.034] \quad (7.139)$$

and its pitch is -0.0227 . This singularity belongs to the general-linear-complex type. When $Z_{P2} = -1.0093$, the pitch is -0.0593 . When $Z_{P3} = 0.1160$, the pitch is 0.4559 . All these situations belong to 5a [4].

Based on the analysis above, the singularity of the 3-RPS parallel manipulator has five situations, namely, 3c, 4b, 3d, 5a, and 5b, as presented in Merlet's paper [4].

Appendix A

To verify the correctness of the remarkable singularity occurring when six segments associated with the six extensible links of the 6/6-Gough-Stewart manipulator intersect one common line, the singularity point P_1 in Sect. 5.3.2.3 is taken as an example. The corresponding data cited from our calculations are given below, including the coordinates of the 12 vertices of the moving platform and the base platform, the Plücker coordinates of the six line vectors, the instantaneously moving reciprocal screw, and the corresponding reciprocal products.

$$C_1 : (-1.41421356237309, \ -1.41421356237309, \ 0)$$

$$C_2 : (1.41421356237309, \ -1.41421356237309, \ 0)$$

$$C_3 : (1.93185165257814, \ -0.51763809020504, \ 0)$$

$$C_4 : (0.51763809020504, \ 1.93185165257814, \ 0)$$

$$C_5 : (-0.51763809020504, \ 1.93185165257814, \ 0)$$

$$C_6 : (-1.93185165257814, \ -0.51763809020504, \ 0)$$

$$B_1 : (-2.09129075934452, \ -5.55407350116214, \ 1.44888873943360)$$

$$B_2 : (-1.75507495728150, \ -4.97173064968147, \ 1.06066017177982)$$

$$B_3 : (-2.88678588817939, \ -3.25767686730291, \ 0.53033008588991)$$

$$B_4 : (-3.63723664069157, \ -3.21263249098023, \ 0.72444436971680)$$

$$B_5 : (-4.55579529423526, \ -4.80362274864996, \ 1.78510454149662)$$

$$B_6 : (-4.14156034378610, \ -5.43100997645331, \ 1.97921882532351)$$

$$\begin{aligned} \$1 &= C_1 B_1 \\ &= (-0.15256, -0.93281, 0.32647; 0.46170, 0.461699, 1.10344) \end{aligned}$$

$$\begin{aligned} \$2 &= C_2 B_2 \\ &= (-0.64930, -0.72883, 0.21730; -0.30731, -0.30730, -1.94896) \end{aligned}$$

$$\begin{aligned} \$3 &= C_3 B_3 \\ &= (-0.86533, -0.49206, 0.09524; -0.04930, -0.18398, -1.39852) \end{aligned}$$

$$\begin{aligned} \$4 &= C_4 B_4 \\ &= (-0.62457, -0.77333, 0.10890; 0.21038, -0.05637, 0.80628) \end{aligned}$$

$$\begin{aligned} \$5 &= C_5 B_5 \\ &= (-0.50141, -0.83633, 0.22165; 0.42820, 0.11474, 1.40157) \end{aligned}$$

$$\begin{aligned} \$6 &= C_6 B_6 \\ &= (-0.38500, -0.85607, 0.34484; 0.17850, 0.66619, 1.45451) \end{aligned}$$

$$\$^m = (0.48296, 0.83652, -0.25882; 0.50000, -0.86603, -1.86603)$$

$$p1 = \$1 \circ \$^m = 0.06939 \times 10^{-16}$$

$$p2 = \$2 \circ \$^m = -0.13878 \times 10^{-16}$$

$$p3 = \$3 \circ \$^m = 1.939478 \times 10^{-16}$$

$$p4 = \$4 \circ \$^m = -0.06939 \times 10^{-16}$$

$$p5 = \$5 \circ \$^m = -0.13878 \times 10^{-16}$$

$$p6 = \$6 \circ \$^m = 0.27756 \times 10^{-16}$$

References

1. Hunt KH (1983) Structural kinematics of in-parallel-actuated robot-arms. ASME J Mech Trans Autom Des 105:705–712
2. Fichter EF (1986) A Stewart platform-based manipulator: general theory and practical construction. Int J Robot Res 5:157–182
3. Huang Z, Qu YY (1987) The analysis of the special configuration of the spatial parallel manipulators. The 5th national mechanism conference, Lu Shan, China, pp 1–7

4. Merlet JP (1989) Singular configurations of parallel manipulators and Grassmann geometry. *Int J Robot Res* 8:45–56
5. Collins CL, Long GL (1995) The singularity analysis of an in-parallel hand controller for force-reflected teleoperation. *IEEE Trans Robot Autom* 11(5):661–669
6. Hao F, McCarthy JM (1998) Conditions for line-based singularities in spatial platform manipulator. *J Robot Syst* 15(1):43–55
7. Gosselin C, Angeles J (1990) Singularity analysis of closed-loop kinematic chains. *IEEE Trans Robot Autom* 6:281–290
8. Zlatanov D, Fenton RG, Benhabib B (1995) A unifying framework for classification and interpretation of mechanism singularities. *ASME J Mech Des* 117:566–572
9. Zlatanov D, Bonev IA, Gosselin CM (2002) Constraint singularities of parallel mechanisms. In: *Proceedings of the 2002 I.E. international conference on robotics and automation, Washington, DC*, pp 496–502
10. Ma O, Angeles J (1991) Architecture singularity of platform manipulators. *IEEE international conference on robotics and automation, Sacramento, USA*, pp 1542–1547
11. Kong XW (1998) Generation of 6-SPS parallel manipulators. In: *Proceedings of the 1998 ASME Design Engineering Technical conference, Atlanta, USA, 98DETC/MECH-5952*
12. McAree PR, Daniel RW (1999) An explanation of never-special assembly changing motions for 3–3 parallel manipulators. *Int J Robot Res* 18(6):556–574
13. Karger A, Husty M (1998) Architecture singular parallel manipulators. In: *Lenarcic J, Husty M (eds) Proceedings of ARK'98, Strobl, Austria*, pp 445–454
14. Karger A (2001) Singularities and self-motions of equiform platforms. *Mech Mach Theory* 36(7):801–805
15. Kong X, Gosselin CM (2002) Generation of architecturally singular 6-SPS parallel manipulators with linearly related planar platforms. *Electr J Comp Kinemat (EJCK)* 1(1), Paper No. 7
16. Chan VK, Ebert-Uphoff I (2000) Investigation of the deficiencies of parallel manipulators in singular configurations through the Jacobian nullspace. In: *Proceedings of IEEE international conference on robotics and automation, Seoul, Korea*
17. Di Gregorio R (2004) Properties of the SX-YS-ZS structures and singularity determination in parallel manipulators which generate those structures. In: *Proceedings of DETC'04: ASME 2004 Design Engineering Technical Conferences and Computers and Information in Engineering Conference, 28 Sept–2 Oct 2004, Salt Lake City, UT, USA*
18. Sefrioui J, Gosselin C (1994) Étude et représentation des lieux de singularité des manipulateurs parallèles sphériques à trois degrés de liberté avec actionneurs prismatiques. *Mech Mach Theory* 29:559–579
19. Sefrioui J, Gosselin C (1995) On the quadratic nature of the singularity curves of planar three-degree-of-freedom parallel manipulators. *Mech Mach Theory* 30:533–551
20. Wang J, Gosselin CM (1996) Kinematic analysis and singularity loci of spatial four-degree-of-freedom parallel manipulators. In: *Proceedings of the 1996 ASME design engineering technical conference and computers in engineering conference, San Diego, CA, USA*
21. Wang J, Gosselin C (1997) Kinematic analysis and singularity representation of spatial five-degree-of-freedom parallel mechanisms. *J Robot Syst* 14:851–869
22. Collins CL, McCarthy JM (1997) The singularity loci of two triangular parallel manipulator. *IEEE ICAR 97', Monterey, CA, 7–9 July*, pp 473–478
23. Collins CL, McCarthy JM (1998) The quartic singularity surfaces of planar platforms in the Clifford algebra of the projective plane. *Mech Mach Theory* 33(7):931–944
24. Wang GZ (1998) Singularity analysis of a class of the 6-6 Stewart platforms. In: *Proceedings of DETC'98 1998 ASME Design Engineering Technical Conference, Atlanta, GA, USA*
25. Di Gregorio R (2001) Analytic formulation of the 6-3 fully-parallel manipulator's singularity determination. *Robotica* 19:663–667
26. Di Gregorio R (2002) Singularity-locus expression of a class of parallel mechanisms. *Robotica* 20:323–328
27. Mayer St-Onge B, Gosselin C (2000) Singularity analysis and representation of the general Gough-Stewart platform. *Int J Robot Res* 19(3):271–288

28. Huang Z, Zhao Y, Wang J et al (1999) Kinematic principle and geometrical condition of general-linear-complex special configuration of parallel manipulators. *Mech Mach Theory* 34:1171–1186
29. Huang Z, Chen LH, Li YW (2003) The singularity principle and property of Stewart manipulator. *J Robot Syst* 20(4):163–176
30. Huang Z, Cao Y (2005) Property identification of the singularity loci of a class of Gough-Stewart manipulators. *Int J Robot Res* 24(8):675–685
31. Pernkopf F, Husty ML (2002) Singularity analysis of spatial Stewart-Gough platforms with planar base and platform. In: *Proceedings of DETC.02 ASME 2002 Design Engineering Technical Conferences and Computer and Information in Engineering Conference*, Montreal, Canada, 29 Sept–2 Oct 2002, DETC2002/MECH-34267
32. Cao Y, Huang Z, Ge QJ (2005) Orientation-singularity and orientation capability analysis of the Stewart-Gough manipulator, ASME 2005 paper DETC2005-84556
33. Huang Z, Zhao YS, Zhao TS (2006) *Advanced spatial mechanism*. Higher Education Press, Beijing (in Chinese)
34. Huang Z, Qu YY (1987) The analysis of the special configuration of the spatial multiple-loop parallel mechanism. The 5th national conference on mechanisms, Lushang, China, pp 1–7
35. Huang Z, Liu JF, Li YW (2011) *On mechanism mobility*. Science Press, Beijing
36. Ball RS (1900) *Theory of screw*. Cambridge University Press, Cambridge
37. Hunt KH (1978) *Kinematic geometry of mechanisms*. Oxford University Press, Oxford
38. Ebert-Uphoff I, Lee JK, Lipkin H (2000) Characteristic tetrahedron of wrench singularities for parallel manipulators with three legs. In: *Proceedings of a symposium commemorating the legacy, works, and life of Sir Robert Stawell Ball upon the 100th anniversary of “A Treatise on the Theory of Screws”* University of Cambridge, Trinity College, Cambridge
39. Kong X, Gosselin CM (2001) Uncertainty singularity analysis of parallel manipulators based on the instability analysis of structures. *Int J Robot Res* 20(11):847–856
40. Sugimoto K, Duffy J (1981) Special configuration of industrial robots. In: *Proceedings of the 11th ISIR*, Tokyo, Japan, pp 309–316
41. Lee KM, Shah DK (1988) Kinematic analysis of a three-degree-of-freedom in-parallel actuated manipulator. *IEEE J Robot Autom* 4(2):354–360
42. Li YW, Huang Z (2006) The singularity analysis of 3-RPS parallel manipulator, ASME paper DETC2006-99028

Chapter 8

Dynamic Problems of Parallel Mechanisms

This chapter introduces our research on some dynamics problems of parallel mechanisms. The first problem is about the over-determinate inputs. This is quite an interesting issue. In practice, there are many machines and animals that work with over-determinate input, i.e., their input-number is much bigger than their mobility number. How to set the inputs to be accordance and optimum distribute and to obtain the expectant motion acceleration is a challenge. For the second part of this chapter, we focus on the dynamic analysis, i.e., the kinetostatic analysis of parallel mechanisms. For a link with two revolute pairs, based on its free-body diagram, its unknown value is 10 for the force analysis, and each link has only six equilibrium equations in the spatial mechanism. As it is, this is insolvable directly. Some time more unknown values may appear; and even up to 130 and it needs to set a 130-order matrix for the 5-5R parallel mechanism. This is extremely difficult. To resolve this issue, we propose a new method based on the screw theory. This method will only require the setting of a six-order matrix each time and the dynamics problem can be readily solved. Moreover, in the following examples we can find the screws, their reciprocal screws, and their corresponding transformations each other, these are very interesting.

8.1 Over-Determine Inputs

Huang and Zhao [1] discussed the accordance and optimum issue of the over-determinate input. As mentioned in Sect. 4.6, in the natural environment, humans and many animals walk on two or more legs. All their joints work together and transfer power. Figure 8.1a shows a six-legged walking machine while Fig. 8.1b shows four robots working together. The input number for both machines is obviously more than that of their mobility. This may be considered as an over-determinate input. If U is the number of inputs and M is the mobility of the machine, when

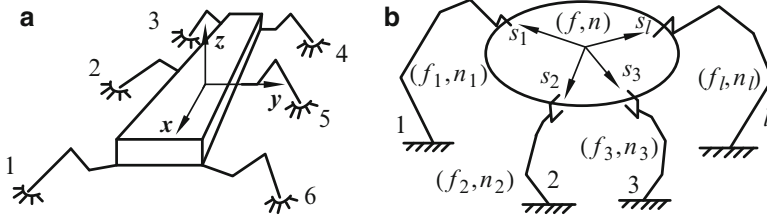


Fig. 8.1 Over-determinate input (a) six-legged walking machine (b) four robots working together

$$U - M > 0 \tag{8.1}$$

It is the over-determinate input or redundant input [2].

8.1.1 Influence Coefficient Matrices and Inertia Forces

The six-legged walking machine, for instance, may move in a triangular-gait, i.e., its main body is supported only by its three legs. The three supporting legs possess nine hinges, while each leg possesses three hinges. All nine hinges can bear the torque and transfer power together. In this case, the number of inputs is greater than that of the 6 of the main-body. This is a typical example of an over-determinate input. Here, the six-legged walking machine (SWM) is taken to show the over-determinate inputs.

Each leg has three hinges and the end point of feet of the SWM that touches the ground can be imagined as a spherical pair, as the friction force between the foot and the ground is large enough. Then, there are six hinges per leg, as shown in Fig. 8.1a.

According to the influence coefficient principle [3] explained in Chap. 5, the relationship between the 6-D velocity $V_B = \{\omega_B, v_P\}^T$ of the main-body and the six joint angular velocities of the limb, $\dot{\varphi}^r = \{\dot{\varphi}_1 \ \dot{\varphi}_2 \ \dots \ \dot{\varphi}_6\}^T$ is expressed as follows

$$\{V_B\} = [G_\varphi^B]^{(r)} \{\dot{\varphi}\}^{(r)}, \quad r = 1, 2, \dots, n \tag{8.2}$$

where the $[G_\varphi^B] \in R^{6 \times 6}$ is the first-order influence coefficient matrix of the main-body of the SWM that depends on the position and orientation of the machine. The superscript r denotes the number of legs and n refers to the number of legs touching the ground at a particular moment. If $[G_\varphi^B]$ is not singular, Eq. (8.2) can be transferred as follows

$$\{\dot{\varphi}\}^{(r)} = [G_\varphi^{B(r)}]^{-1} \{V_B\}, \quad r = 1, 2, \dots, n \tag{8.3}$$

where the first three components of $\{\dot{\varphi}\}$ correspond to the spherical pair. The other three joints can be written as

$$\{\dot{\varphi}^{(r)}\}_{4,5,6} = \left(\left[\mathbf{G}_{\varphi}^B \right]^{-1} \right)_{4,5,6}^{(r)} \{ \mathbf{V}_B \}, \quad r = 1, 2, \dots, n \quad (8.4)$$

where $\{\dot{\varphi}^{(r)}\}_{4,5,6} \in \mathbf{R}^3$ indicates the last three elements in vector $\dot{\varphi}^r$, and $\left[\mathbf{G}_{\varphi}^B \right]_{4,5,6}^{-1} \in \mathbf{R}^{3 \times 6}$ is the sub-matrix of $\left[\mathbf{G}_{\varphi}^B \right]$, i.e., it consists of the 4th, 5th and 6th rows of that matrix in Eq. (8.4). n is the number of supporting legs at that moment. That means Eq. (8.4) contains three linear equations for that leg r .

For the 6-DOF walking machine, all the joint variables form the joint space can be expressed as $\dot{\varphi} = \left(\varphi_{r,j} | r = 1, 2, \dots, n; j = 4, 5, 6; \right)$. When six joint variables are selected from $\dot{\varphi}$ to form the six generalized coordinates, $\mathbf{q} \in \mathbf{R}^6$ ($\hat{\mathbf{q}} \subset \dot{\varphi}$). Corresponding the selected six generalized coordinates, q_i ($i = 1, 2, \dots, 6$), six linear equations are taken from Eq. (8.4) to form a new equation as follows

$$\{\dot{\mathbf{q}}\} = [\mathbf{G}_B^q] \{ \mathbf{V}_B \} \quad (8.5)$$

Where $[\mathbf{G}_B^q] \in \mathbf{R}^{6 \times 6}$ and $\dot{\mathbf{q}} = (\dot{q}_1, \dot{q}_2, \dots, \dot{q}_6)$. When $[\mathbf{G}_B^q]$ is not singular, let $[\mathbf{G}_q^B] = [\mathbf{G}_B^q]^{-1}$, then we have

$$\{ \mathbf{V}_B \} = [\mathbf{G}_q^B] \{\dot{\mathbf{q}}\}, \quad [\mathbf{G}_q^B] \in \mathbf{R}^{6 \times 6} \quad (8.6)$$

From Eqs. (8.3) and (8.6), we obtain

$$\dot{\varphi}_r = \left[\mathbf{G}_q^r \right], \quad r = 1, 2, \dots, n; \quad (8.7)$$

where

$$\left[\mathbf{G}_q^r \right] = \left[\mathbf{G}_B^r \right] \left[\mathbf{G}_q^B \right].$$

Using the symbol ϕ_S to denote the joint variables that do not belong to the generalized coordinates, that is

$$\phi_S = \left\{ \varphi_{r,j} | \varphi_{r,j} \notin \mathbf{q}, r = 1, 2, \dots, n; j = 4, 5, 6; \right\}$$

where j indicates the number of the pair in a limb. Then, we also have

$$\dot{\varphi}_S = \left[\mathbf{G}_q^s \right] \{\dot{\mathbf{q}}\} \quad (8.8)$$

Similarly, the motion relation between the link m th in i th leg and the generalized coordinate q can be written as follows

$$\{\mathbf{V}_m\}^{(r)} = \left[\mathbf{G}_q^m \right]^{(r)} \{\dot{\mathbf{q}}\}, \quad r = 1, 2, \dots, n; \quad m = 1, 2, 3; \quad (8.9)$$

where \mathbf{G}_q^m is the G-matrix of the link m with respect to the six generalized coordinates.

In the meantime, the expressions of the 6-D acceleration of the main-body and the m th link can be written as follows

$$\{\mathbf{A}_B\} = \{\dot{\mathbf{q}}\}^T \left[\mathbf{H}_{qq}^B \right] \{\ddot{\mathbf{q}}\} + \left[\mathbf{J}_q^B \right] \{\ddot{\mathbf{q}}\} \quad (8.10)$$

$$\{\mathbf{A}_m\}^{(r)} = \{\dot{\mathbf{q}}\}^T \left[\mathbf{H}_{qq}^{m(r)} \right] \{\dot{\mathbf{q}}\} + \left[\mathbf{G}_q^{m(r)} \right] \{\ddot{\mathbf{q}}\} \quad (8.11)$$

where $\{\ddot{\mathbf{q}}\} = \{\ddot{q}_1, \ddot{q}_2, \dots, \ddot{q}_6\}^T$, $\left[\mathbf{H}_{qq}^B \right]$ and $\left[\mathbf{H}_{qq}^m \right]$ are the second-order influence coefficient matrices of the main-body and the m th link with respect to the generalized coordinates.

The six-dimension inertia force of the main-body and some links in the walking machine can be calculated from the following expressions [4]

$$\{\mathbf{F}\} = \{\mathbf{M} \mathbf{f}\}^T = -[\mathbf{I}_s] \{\mathbf{A}\} - \left\{ \begin{array}{c} [\boldsymbol{\omega}]^T [\mathbf{I}_c] \{\boldsymbol{\omega}\} \\ \dots \dots \dots \\ \{\boldsymbol{\theta}\} \end{array} \right\} \quad (8.12)$$

The calculations of these matrices are not complicated, and can be readily evaluated in advance.

8.1.2 The Accordant Equation for Over-Determinate Inputs

The main body of the walking machine possesses 6 DOFs. Each leg has three actuators. When n legs contact the ground, the number of actuators is $3 \times n$ for all legs. This requires at least six inputs to control the walking machine. However, it is a better scheme for all the $3 \times n$ actuators to work together in the over-determinate input. Of the $3 \times n$ joint variables, any six variables can be taken as generalized coordinates. All the actuating torques can be expressed with respect to the generalized coordinate q . The expression of equivalent torques is

$$\left\{ \mathbf{T}_q^\varphi \right\}^{(r)} = \left[\mathbf{g}_q^\varphi \right]^{T(r)} \{\mathbf{T}_\varphi\}^{(r)}, \quad r = 1, 2, \dots, n \quad (8.13)$$

where $\{\mathbf{T}_\varphi\}^{(r)}$ with the first three zero-components designates the vector of the six input torques of r th leg. $\{\mathbf{T}_q^\varphi\}$ indicates the six equivalent torques of $\{\mathbf{T}_\varphi\}$ relating to the generalized coordinates. $[\mathbf{g}_q^\varphi]$ is defined as the influence coefficient matrix of the six hinges of the r th branch with respect to the six generalized coordinates.

All applied loads, inertia forces, gravity, and other applied forces acting on the main body form a 6-D resultant force vector, $\{\mathbf{F}_B\}$, that acts on the centroid of the main body. Then, the resultant force is converted into the equivalent torques of the generalized coordinates, $\{\mathbf{T}_q^B\}$. Similarly, the applied forces inertia force, and the gravity of the m th link can also be disposed of as $\{\mathbf{F}_m\}$ and $\{\mathbf{T}_q^m\}$. The expressions of the equivalent torques are

$$\{\mathbf{T}_q^B\} = [\mathbf{G}_q^B]^T \{\mathbf{F}_B\} \quad (8.14)$$

$$\{\mathbf{T}_q^m\}^{(r)} = [\mathbf{G}_q^m]^{T(r)} \{\mathbf{F}_m\}^{(r)} \quad (8.15)$$

According to the virtual displacement principle, the whole force system is in dynamic equilibrium if the inertia forces, gravity, and other applied forces in Eqs. (8.13), (8.14), and (8.15) are treated as the applied load acting on the same linkages. The result of all equivalent torques acting on the generalized coordinates equals zero. This leads to

$$[\mathbf{G}_q^B]^T \{\mathbf{F}_B\} + \sum_{r=1}^n \left\{ [\mathbf{g}_q^\varphi]^{T(r)} \{\mathbf{T}_\varphi\}^{(r)} + \sum_{m=1}^5 [\mathbf{G}_q^m]^{T(r)} \{\mathbf{F}_m\}^{(r)} \right\} = \{\mathbf{0}\} \quad (8.16)$$

This is a *general dynamic equation* that shows the relationship among all applied loads, gravity, inertia forces, and the actuation torque. Only six unknowns of the $3 \times n$ unknowns input torques can be evaluated using this equation. Then, the other $3n-6$ input torques need to be determined before using Eq. (8.16).

The six actuation torques of the generalized coordinates are expressed as a six-D vector $\{\mathbf{T}_Q\}$. The vector $\{\mathbf{T}_S\}$ with the $(3n-6)$ -component denotes the other remaining $(3n-6)$ input torques, $\{\mathbf{T}_S\} = \{\mathbf{T}_{S1}, \mathbf{T}_{S2}, \dots, \mathbf{T}_{Sk}\}^T$, $k = 3n - 6$, T_{Si} is an element in $\{\mathbf{T}_\varphi\}^{(r)}$ in Eq. (8.13). Taking the T_{Si} -related row in $[\mathbf{g}_q^\varphi]^{(r)}$ out of Eq. (8.13) and rearranging these according to a sequence of T_{Si} to form a new matrix $[\mathbf{g}_q^\varphi]_{k \times 6}$, Eq. (8.16) can be rewritten in the following form

$$\{\mathbf{T}_Q\} = [\mathbf{G}_q^B]^T \{\mathbf{F}_B\} - \sum_{r=1}^n \sum_{m=1}^5 [\mathbf{G}_q^m]^{T(r)} \{\mathbf{F}_m\} + [\mathbf{g}_q^\varphi]^T \{\mathbf{T}_S\} \quad (8.17)$$

where $\{F_B\}$ is a 6-D vector referring to the applied loads, weight, and inertia force acting on the main body, and $\{F_m\}$ is the 6-D force acting to each link in the r th branch. These have been determined from the preceding steps. Equation (8.17) denotes the relationship of the six generalized actuation torques and the 3n-6 arbitrarily selected actuation torques.

When the value of the 3n-6 inputs changes, the six generalized-coordinate inputs also change simultaneously based on the general dynamic equation. In other words, when Eq. (8.17) is satisfied, the machine can obtain the expected acceleration calculated in Eq. (8.12). Since $\{T_s\}$ and $\{T_Q\}$ contain all the $3 \times n$ inputs, Eq. (8.17) expresses the relationship accordance of all input torques. It can then be considered an **accordance equation of over-determinate input**.

However, the chosen 3n-6 values may be still inappropriate. Although the expected resulting acceleration may be obtained, the chosen inputs may still be in conflict. The contradictory inputs may counteract each other. Thus, much energy would also be consumed while Eq. (8.17) is satisfied. Therefore, it is necessary to set an optimal-proportion distribution for the 3n-6 inputs.

8.1.3 Optimization of Over-Determinate Input

The energy saving issue is very important especially for walking machines that consumes much energy carried by themselves. As discussed in the previous section, the 3n-6 inputs can be selected arbitrarily. When Eq. (8.17) is satisfied, those inputs are in accordance and the expected acceleration can be obtained. However, the inputs may still be inappropriate. Therefore, it is necessary to set the inputs to avoid contradiction and further to obtain an optimal-proportion distribution. The rational distribution of input torques can realize the minimum consumption of energy.

The objective function of the optimization of energy is

$$F = \sum_{r=1}^n \sum_{i=4}^6 \int_{\varphi_a}^{\varphi_b} \left| T_i^{(r)} d\varphi_i^{(r)} \right| \quad (8.18)$$

The 4th, 5th, and 6th joint of each leg are equipped with actuators, and n refers to the number of legs. Rewriting the objective function into a summation of the square of instantaneous power, we have

$$F = \sum_{h=1}^6 T_{Qh}^2 \dot{\varphi}_{Qh}^2 + \sum_{j=1}^k T_{Sj}^2 \dot{\varphi}_{Sj}^2 \quad (8.19)$$

where the angular velocities $\dot{\varphi}_Q$ and $\dot{\varphi}_S$ refer to T_Q and T_S , respectively. These can be determined from the motion of the main body, however, these are not optimization variables. In Eq. (8.19), because $\{T_Q\}$ has been derived as an explicit function

of $\{T_S\}$, the equation can be simplified by using Eq. (8.17). Thus, only $\{T_S\}$ is the optimization variable. When we differentiate the objective function (8.19) with respect to T_{Sj} , we have

$$\frac{\partial F}{\partial T_{Sj}} = \sum_{h=1}^6 2T_{Qh} \frac{\partial T_{Qh}}{\partial T_{Sj}} \dot{\varphi}_{Qh}^2 + 2T_{Sj} \dot{\varphi}_{Sj}^2, \quad j = 1, 2, \dots, k \quad (8.20)$$

From Eq. (8.17), T_{Qh} is expressed as

$$T_{Qh} = - \left(\sum \sum \left[\mathbf{G}_q^m \right]_{h;}^{T(r)} \{ \mathbf{F}_m \} + \left[\mathbf{G}_q^p \right]_{h;}^T \{ \mathbf{F}_p \} + \left[\mathbf{g}_q^p \right]_{h;} \{ \mathbf{T}_S \} \right), \quad h = 1, 2, \dots, 6 \quad (8.21)$$

Evidently, this partial derivative $\partial T_{Qh} / \partial T_{Sj}$ is remarkably simple and explicit as follows

$$\frac{\partial T_{Qh}}{\partial T_{Sj}} = - \left[\mathbf{g}_q^p \right]_{h;j}^T = - \left[\mathbf{g}_q^p \right]_{j;h} \quad (8.22)$$

The subscript “ $j; h$ ” refers to the element in j th row and h th column of the matrix. Substituting this expression into Eq. (8.20) and rewriting the equation yields

$$\frac{\partial F}{\partial T_{Sj}} = -2 \{ \mathbf{T}_Q \}^T \left[\dot{\boldsymbol{\varphi}}_Q^2 \right] \left(\left[\mathbf{g}_q^p \right]_{j;} \right)^T + 2T_{Sj} \dot{\varphi}_{Sj}^2, \quad j = 1, 2, \dots, k \quad (8.23)$$

The component $\left[\dot{\boldsymbol{\varphi}}_Q^2 \right]$ is defined as

$$\left[\dot{\boldsymbol{\varphi}}_Q^2 \right] = \begin{bmatrix} \dot{\varphi}_{Q1}^2 & & & & & 0 \\ & \dot{\varphi}_{Q2}^2 & & & & \\ & & \ddots & & & \\ & & & \ddots & & \\ & & & & \ddots & \\ 0 & & & & & \dot{\varphi}_{Q6}^2 \end{bmatrix} \quad (8.24)$$

We define a column vector of partial derivative as

$$\left\{ \frac{\partial F}{\partial T_S} \right\} = \left\{ \frac{\partial F}{\partial T_{S1}}, \frac{\partial F}{\partial T_{S2}}, \dots, \frac{\partial F}{\partial T_{Sk}} \right\} \quad (8.25)$$

The expression is

$$\left\{ \frac{\partial F}{\partial T_S} \right\} = 2 \left[\dot{\boldsymbol{\varphi}}_S^2 \right] \{ \mathbf{T}_S \} - 2 \left[\mathbf{g}_q^p \right] \left[\dot{\boldsymbol{\varphi}}_Q^2 \right] \{ \mathbf{T}_Q \} \quad (8.26)$$

In order to derive the optimum results, it is necessary to make the result of Eq. (8.26) zero, so that

$$[\dot{\boldsymbol{\varphi}}_S^2] \{T_S\} - [\mathbf{g}_q^\varphi] [\dot{\boldsymbol{\varphi}}_Q^2] \{T_Q\} = \{\mathbf{0}\} \quad (8.27)$$

where

$$[\dot{\boldsymbol{\varphi}}_S^2] = \begin{bmatrix} \dot{\varphi}_{S1}^2 & & & & 0 \\ & \dot{\varphi}_{S2}^2 & & & \\ & & \ddots & & \\ & & & \ddots & \\ 0 & & & & \dot{\varphi}_{Sk}^2 \end{bmatrix}_{k \times k} \quad (8.28)$$

Substituting Eq. (8.17) into Eq. (8.27) and rearranging it yields

$$\begin{aligned} & \left([\dot{\boldsymbol{\varphi}}_S^2] + [\mathbf{g}_q^\varphi] [\dot{\boldsymbol{\varphi}}_Q^2] [\mathbf{g}_q^\varphi]^T \right) \{T_S\} + [\mathbf{g}_q^\varphi] [\boldsymbol{\varphi}_Q^2] \cdot \\ & \left(\sum_{r=1}^n \sum_{m=1}^5 [\mathbf{G}_q^m]^{T(r)} \{F_m\}^{(r)} + [\mathbf{G}_q^P] \{F_P\} \right) = \{\mathbf{0}\} \end{aligned} \quad (8.29)$$

while the matrix expression $[\dot{\boldsymbol{\varphi}}_S^2] + [\mathbf{g}_q^\varphi] [\dot{\boldsymbol{\varphi}}_Q^2] [\mathbf{g}_q^\varphi]^T$ is nonsingular, rewriting Eq. (8.29), yields

$$\begin{aligned} \{T_S\} = & - \left([\dot{\boldsymbol{\varphi}}_S^2] + [\mathbf{g}_q^\varphi] [\dot{\boldsymbol{\varphi}}_Q^2] [\mathbf{g}_q^\varphi]^T \right)^{-1} [\mathbf{g}_q^\varphi] [\boldsymbol{\varphi}_Q^2] \\ & \cdot \left(\sum_{r=1}^n \sum_{m=1}^5 [\mathbf{G}_q^m]^{T(r)} \{F_m\}^{(r)} + [\mathbf{G}_q^P] \{F_P\} \right) \end{aligned} \quad (8.30)$$

This is the analytical expression of energy optimization. A walking machine will consume smaller energy when the $3 \times n$ input torques are given in terms of Eq. (8.30). The values of the k input torques depend on the applied loads, inertia force, gravity, velocities, and the configuration of the mechanism. In the process of evaluation, the k input torque $\{T_S\}$ is obtained from Eq. (8.30), and the six generalized coordinate-related input torques $\{T_Q\}$ is obtained from Eq. (8.17). All $3 \times n$ input torque values explicitly satisfy the condition of accordance and energy optimization. Equations (8.17) and (8.30) are considered ***the accordant and energy optimum equation of over-determinate input.***

The derivation shows that the condition of minimum energy consumption is not dependent on the selection of the components $\{T_S\}$, while the objective function shown in Eq. (8.19) is established for all $3 \times n$ input torques.

8.1.4 The Weight Distribution of the Input Torques

Equation (8.30) is an expression of energy optimization. If $[\dot{\varphi}_Q^2]$ and $[\dot{\varphi}_S^2]$ are recognized as the weight-factor matrices or weight matrices, and $[A_Q]$ and $[A_S]$ are substituted for $[\dot{\varphi}_Q^2]$ and $[\dot{\varphi}_S^2]$, the general equation of the weighted optimization distribution of the input torques will be

$$\begin{aligned} \{T_S\} = & - \left([A_S] + [g_q^\varphi] [A_Q] [g_q^\varphi]^T \right)^{-1} [g_Q^\varphi] [A_Q] \\ & \cdot \left(\sum_{r=1}^n \sum_{m=1}^5 [G_q^m]^{T(r)} \{F_m\}^{(r)} + [G_q^P] \{F_P\} \right) \end{aligned} \quad (8.31)$$

Therefore,

1. When $[A_Q] = [\varphi_Q^2]$ and $[A_S] = [\varphi_S^2]$, Eq. (8.31) is the same as that of Eq. (8.30), and $\{T_S\}$ is obtained in terms of the minimum consumption of energy.
2. When $[A_Q] = [I]_{6 \times 6}$ and $[A_S] = [I]_{k \times k}$ where $[I]$ is the identity matrix, $\{T_S\}$ is obtained from Eq. (8.31) in terms of the maximum input torque minimization.
3. When $[A_Q]$ and $[A_S]$ are appropriately selected, it can also mean that the farther away from the main body the position of actuator is, the smaller the input torque itself is. That means, the input torque of the shank, the lower part of the leg, is smaller than that of the thigh, the upper part of the leg. The joint torques of the actuator 4th, 5th, and 6th in one leg are in the form

$$T_4 < T_5 < T_6 \quad (8.32)$$

This will make the whole weight of the leg lighter and the consumption of energy smaller.

8.2 Kinetostatic Analysis of 4-UPU Parallel Mechanisms

The kinetostatic analysis for both the active forces and the constraint reactions of the parallel manipulators (PMs) including the lower-mobility PMs is one of the important issues of the design, simulation, and control of the manipulator. This generally needs to solve for the active forces as well as constraint reactions of all kinematic pairs. This serves as a basis for sizing components and bearings of the manipulator and for the selection of the actuators. The results can also be used to control the robot manipulator. The force analysis contains statics and dynamics

analyses. Only the statics analysis is required when the device moves at a lower speed. On the contrary, the dynamics analysis is required when the device moves at a higher speed because the inertia force of each link cannot be neglected.

The statics of the spatial mechanisms can be treated through various methods such as the vector method [5], the dual vector and dual number quaternions [6], and the principle of virtual work [7]. For the dynamics analysis, the principle of d'Alembert is one of the most common methods. Merlet [8] discussed the dynamics of PMs. Zhang and Gosselin [9] discussed a general kinetostatic model for PMs. Lu [10] solved for the active and part of the passive forces of some PMs. Zhou et al. [11] studied the static solving of a 3-DOF 3-RRR parallel mechanism.

Most of aforementioned literature only analyzed the actuator forces of PM, however, these did not discuss the reactions of the kinematic pairs. The latter is quite complicated and there has never been an efficient, alternative method with which to solve it until now.

The parallel mechanisms not only have an over-constrained and statically indeterminate issue, but also involve many kinematic pairs and unknown variables that increase the complexity and difficulty of the reaction analysis. These oblige us to set high-order matrices inevitably. For example, the number of unknown variables of a 5-DOF 5-5R PM is up to 130. The number of its available equilibrium equations is 126. Of course, the static indeterminacy is not a new issue. This may easily be solved by setting some complementary equations. The new issue that is difficult to resolve is the superabundant unknown variables and these unknowns are even coupling. These unknown variables cannot be solved simply and solely, and requires the solving of a high-order matrix.

For the statics analysis of parallel mechanisms, there are two serious problems:

1. the statically indeterminate issue; and
2. the large number of unknowns.

Here, we focus on the second issue.

This chapter introduces a new simple and effective approach in solving the issue based on the reciprocal screw theory. For this method, the main reactions should be solved first, then all other constraint reactions will be easy to obtain. The most important merit of this method is its ability to remarkably reduce the number of unknowns, and keep the number of simultaneous equations under six each time. All the constraint reactions are easily obtained simultaneously by analyzing the equilibrium of each body. We call this process force-decoupling. Another merit of this method is the actual axes of reaction forces and moments can be clearly determined based on the screw theory before the numerical calculation. This is useful for the mechanism analyses and design including the singularity research. First, a 4-DOF 4-UPU parallel mechanism is taken as an example [12] to introduce the approach.

The 4-UPU parallel mechanism, as shown in Fig. 8.2a, consists of the moving platform, the fixed platform, and the four branches with eight universal joints and four prismatic pairs. The centers of the universal joints are at a_i and A_i respectively. Link S and link t are connected through the prismatic pair P . The fixed coordinate system $O-XYZ$, the moving coordinate system $c-xyz$, and the limb coordinate system $A_i-x_iy_iz_i$ are also shown in Fig. 8.2.

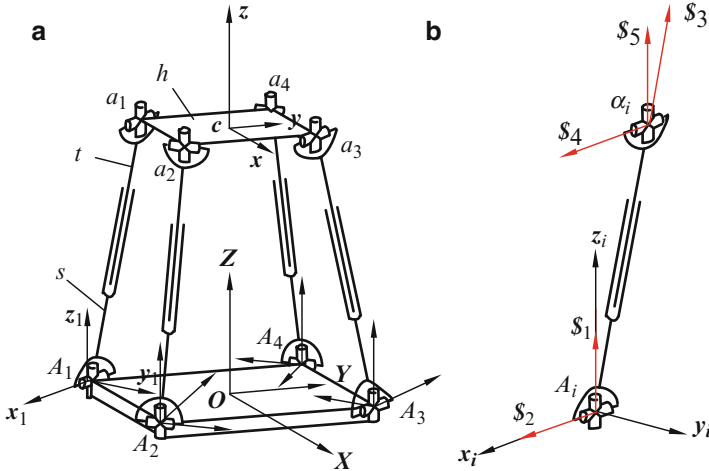


Fig. 8.2 The 4-UPU mechanism (a) the mechanism (b) kinematic screws

One of its limbs, i , is shown in Fig. 8.2b. Its five single-DOF pairs are expressed in the screw Plücker coordinates in $A_i-x_iy_iz_i$ as follows.

$$\begin{aligned}
 \mathcal{S}_{i1} &= (0 \ 0 \ 1; \ 0 \ 0 \ 0) \\
 \mathcal{S}_{i2} &= (1 \ 0 \ 0; \ 0 \ 0 \ 0) \\
 \mathcal{S}_{i3} &= (0 \ 0 \ 0; \ 0 \ c\alpha_i \ s\alpha_i) \\
 \mathcal{S}_{i4} &= (1 \ 0 \ 0; \ 0 \ l_i s\alpha_i \ -l_i c\alpha_i) \\
 \mathcal{S}_{i5} &= (0 \ 0 \ 1; \ l_i c\alpha_i \ 0 \ 0)
 \end{aligned} \tag{8.33}$$

where l_i is the length of the limb and α_i is the angle between the horizontal direction and a limb. The subscript i in \mathcal{S}_{ij} represents the serial number of the limb and j represents the pair in that limb. The five-system screw, Eq. (8.33), has one reciprocal screw.

$$\mathcal{S}_{i1}^r = (0 \ 0 \ 0; \ 0 \ 1 \ 0) \tag{8.34}$$

where \mathcal{S}_{i1}^r is a constraint couple exerted on the platform that is parallel to the base.

Then four identical limbs exert four constraint couples on the same platform. The four couples are all parallel to the same base and in different directions. There is no common constraint between these and the parallel constraint is two. From the Modified G-K Criterion (3.5)

$$M = d(n - g - 1) + \sum_{i=1}^g f_i + v = 6(10 - 12 - 1) + 20 + 2 = 4 \tag{8.35}$$

The platform is simultaneously acted upon by two linearly independent couples that constrain the two rotations of the platform. The mechanism is able to translate along three directions and rotate about Z-axis. After the execution of any possible motion of the platform, including the three translations and a rotation, the screw systems as denoted by Eqs. (8.33) and (8.34) are invariable. Therefore, the mobility is global.

8.2.1 Main-Pair Reaction Forces¹

The position, velocity, acceleration, and inertia force/moment of the mechanism should be determined before initiating force analysis. The analysis process has also been in [13] or many other literatures.

The kinematic pairs connecting the platform and the limbs are named as the main kinematic pairs or main pairs while the reaction of the main pair is referred to as **main-pair reaction** or **main reaction**. The main reactions should be solved first, and then all the other constraint reactions can be easily obtained.

In general, everybody is acted on by gravity, inertial force, and other external forces (moments). All these forces can be vectorially summated as one external force acting on the body. Our method is based on the principle of d'Alembert, the steps of which are as follows:

- (i) Analyze the inertia forces acting on each body, and then add the inertia force, gravity, and other external forces of each body to get the resultant external force of the body;
- (ii) Analyze the active forces and main-pair reactions produced by the force only exerted on the moving platform;
- (iii) Analyze the active forces and main-pair reactions produced by the forces exerted on the links for every limb;
- (iv) Respectively add the active forces and main-pair reactions obtained through the aforementioned steps, (ii) and (iii), by the superposition principle to get the final active forces and main-pair reactions.
- (v) All constraint reactions of the other kinematic pairs can be directly obtained through setting the equilibrium equations of the corresponding bodies one by one.

Since the 4-UPU mechanism has ten bodies, eight U-pairs, four P-pairs, and four unknown inputs, there are two redundant unknowns. This can be considered as a two-order statically indeterminate issue. Generally, this requires the setting of the equilibrium equations and the complementary equations to solve the issue.

Generally, everybody is subjected to the least gravity and inertia force. These forces then need to be considered in the force analysis. Without the loss of generality,

¹ If it does not need to calculate the constraint reactions of kinematic pairs, the active forces can be directly obtained by the principle of virtual work.

to simplify the introduction of the method, we only consider the forces acting on the platform:

$$\mathbf{f}_h = (f_{hx} \ f_{hy} \ f_{hz})^T \quad \text{and} \quad \mathbf{m}_h = (m_{hx} \ m_{hy} \ m_{hz})^T$$

as well as the forces acting on link t of the limb 1:

$$\mathbf{f}_t^l = (f_{tx}^l \ f_{ty}^l \ f_{tz}^l)^T \quad \text{and} \quad \mathbf{m}_t^1 = (m_{tx}^1 \ m_{ty}^1 \ m_{tz}^1)^T$$

where f_i^A represents the total active force of the limb i produced by all the external forces. f_{i1}^A denotes the active force of limb i that only is produced by the forces acting on the platform. f_{i2}^A denotes the active force of limb i that only produced by the forces acting on link t .

Let $F_h \mathcal{S}_h^F$ and $F_t^1 \mathcal{S}_{1t}^F$ denote the corresponding force screws, respectively.

$$F_h \mathcal{S}_h^F = \mathbf{f}_h + \in \mathbf{m}_h \quad (8.36)$$

$$F_t^1 \mathcal{S}_{1t}^F = \mathbf{f}_t^1 + \in \mathbf{r}_{ct}^c \times \mathbf{f}_t^1 + \mathbf{m}_t^1 \quad (8.37)$$

where \mathbf{r}_{ct}^c is the vector from the point c of the platform to the mass center point c_t of link t .

8.2.1.1 Main-Pair Reactions Produced by Force $F_h \mathcal{S}_h^F$

Equation (8.34) has given one of the reactions, a constraint couple, i.e., $m_1^i \mathcal{S}_{i1}^r$. Considering the action of the input force of the limb, there is another main-pair reaction. Its occurrence is equivalent to locking the corresponding prismatic pair P and there are only four screws in the limb screw system.

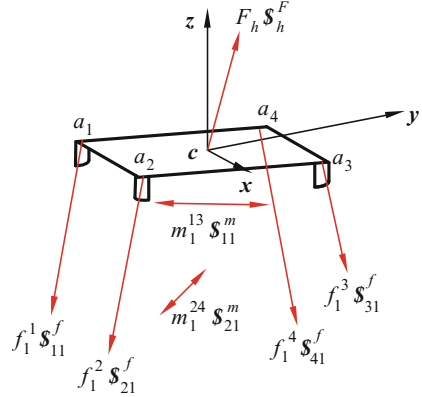
$$\begin{aligned} \mathcal{S}_{i1} &= (0 \ 0 \ 1; \ 0 \ 0 \ 0) \\ \mathcal{S}_{i2} &= (1 \ 0 \ 0; \ 0 \ 0 \ 0) \\ \mathcal{S}_{i4} &= (1 \ 0 \ 0; \ 0 \ l_i s \alpha_i \ -l_i c \alpha_i) \\ \mathcal{S}_{i5} &= (0 \ 0 \ 1; \ l_i c \alpha_i \ 0 \ 0) \end{aligned} \quad (8.38)$$

They have two reciprocal screws

$$\begin{aligned} \mathcal{S}_{i1}^r &= (0 \ 0 \ 0; \ 0 \ 1 \ 0) \\ \mathcal{S}_{i2}^r &= (0 \ c \alpha_i \ s \alpha_i; \ 0 \ 0 \ 0) \end{aligned} \quad (8.39)$$

where \mathcal{S}_{i2}^r is another main-pair constraint force along the axis of the prismatic pair.

Fig. 8.3 Free-body diagram of platform



In this case, each node of the platform has one constraint couple and one constraint force, the directions of which are known while the magnitudes are unknown. Then, the platform is subjected to eight reactions and eight unknowns. However, the maximum linearly independent number of the four coplanar constraint couples is two. Based on this, the issue is solvable because there are only six independent unknowns. The free-body diagram of the moving platform is shown in Fig. 8.3, where the arrows denote the forces and the bi-directional arrow denotes the couple.

f_1^i is the magnitude of the reaction force of the U-pair acting on the platform at a_i and only caused by the applied force $F_h S_h^F$. Couple S_{i1}^m and force S_{i1}^f instead of S_{i1}^r and S_{i2}^r in c -xyz, respectively. S_{11}^m is parallel to S_{31}^m and S_{21}^m is parallel to S_{41}^m . m_1^{13} and m_1^{24} express the resultant couples of m_1^1, m_1^3 and m_1^2, m_1^4 , respectively. m_1^1, m_1^2, m_1^3 and m_1^4 are the four constraint couples of the U-pairs that are exerted on the platform by the four different limbs and caused by the force $F_h S_h^F$.

In the traditional approach, each U pair has four unknown reactions. There are 16 unknowns in the 6 equilibrium equations of the moving platform. As it is, this is insolvable. Therefore, in order to make the equation solvable, we have to consider the equilibrium of all other bodies simultaneously. This may be referred to as force coupling. Clearly, the method described here is able to reduce the number of unknowns and make the solution easy to solve.

The equilibrium equation of the moving platform is

$$-\sum_{i=1}^4 f_1^i S_{i1}^f - m_1^{13} S_{11}^m - m_1^{24} S_{21}^m + F_h S_h^F = 0 \tag{8.40}$$

Equation (8.40) is a screw equation and is equivalent to six linear equations.

We can solve for the six unknowns, including m_1^{13}, m_1^{24} and $f_1^i, i = 1, 2, 3, 4$, from screw Eq. (8.40). However, how to obtain m_1^1, m_1^3 and m_1^2, m_1^4 from m_1^{13}, m_1^{24} will be discussed in next section.

Since $f_1^i S_{i1}^f$ is obtained from Eq. (8.40), the active forces $f_{i1}^A S_{i1}^A$ along the axis of the prismatic pair and produced by the forces acting only on the platform can be solved

from the force equilibrium equations of link t , where the unit vector of active force $\$_{i1}^A$ of limb i acting on link t is parallel to $\$_{i1}^f$ and f_{i1}^A is the magnitude of the active force.

8.2.1.2 Main-Pair Reactions Produced by Limb Applied Force $F_t^1 \$_{1t}^F$

Without the loss of generality, we suppose that there is only an applied force $F_t^1 \$_{1t}^F$ acting on link t of the limb. To calculate the unknown main-pair reaction force caused by $F_t^1 \$_{1t}^F$, the link t is first analyzed.

(1) The equilibrium of link t in limb 1 under limb applied force $F_t^1 \$_{1t}^F$

The free-body diagram of the two-pair link t is shown in Fig. 8.4a. We can analyze the reactions of U and P pairs in link t .

1. Constraint forces in U pair at a_t

The U pair also belongs to the sub-mechanism shown in Fig. 8.4b. In order to determine the reactions of the U pair, we first need to determine the mobility of the right part of the sub-mechanism, which is a 3-UPU mechanism. From the Modified G-K Criterion Eq. (3.5), its mobility is

$$M = 6(8 - 9 - 1) + 15 + 1 = 4 \quad (8.41)$$

Equation (8.41) indicates that the mobility of the sub-mechanism is also four. When its three prismatic pairs are locked, it still has one freedom. Then, for the one-DOF mechanism, there should be five constraints to the platform in total. These are shown in Fig. 8.4b: $f_2^i \$_{i2}^f$, $i = 2, 3, 4$, is the constraint force of the U pair at a_2 , a_3 or a_4 only caused by force $F_t^1 \$_{1t}^F$ along the axis of the prismatic pair of limb i ; $m_2^3 \$_{32}^m$ is the constraint couple of the U pair at a_3 and is only caused by the force $F_t^1 \$_{1t}^F$; $m_2^{24} \$_{22}^m$ is the resultant constraint couple of the U pair at a_2 and a_4 , where $\$_{22}^m$ is parallel to $\$_{42}^m$ and also caused by the force $F_t^1 \$_{1t}^F$. Let m_2^2 and m_2^4 be the magnitudes of the constraint couples of the U pair at a_2 and a_4 , respectively. Then, m_2^{24} is the resultant couple of m_2^2 and m_2^4 . m_2^2 , m_2^3 , and m_2^4 are three couples which are exerted on the platform by the three different limbs 2, 3, 4. f_2^i , $i = 2, 3, 4$ is the magnitude of the constraint force of U-pair at a_i .

For the 3-UPU mechanism, the five constraints acting on the platform can be expressed into screw coordinates in a c -xyz system as follows

$$\begin{aligned} \$_{22}^f &= (s\theta c\alpha \quad -c\theta c\alpha \quad -s\alpha; \quad (c/2)s\alpha \quad (c/2)s\alpha \quad (c/2)c\alpha(s\theta - c\theta)) \\ \$_{32}^f &= (s\theta c\alpha \quad c\theta c\alpha \quad -s\alpha; \quad -(c/2)s\alpha \quad (c/2)s\alpha \quad (c/2)c\alpha(c\theta - s\theta)) \\ \$_{42}^f &= (-s\theta c\alpha \quad c\theta c\alpha \quad -s\alpha; \quad -(c/2)s\alpha \quad -(c/2)s\alpha \quad (c/2)c\alpha(s\theta - c\theta)) \\ \$_{32}^m &= (0 \quad 0 \quad 0; \quad -s\theta \quad -c\theta \quad 0) \\ \$_{22}^m &= (0 \quad 0 \quad 0; \quad s\theta \quad -c\theta \quad 0) \end{aligned} \quad (8.42)$$

where $s\theta$ denotes $\sin\theta$ and $c\alpha$ is $\cos\alpha$.

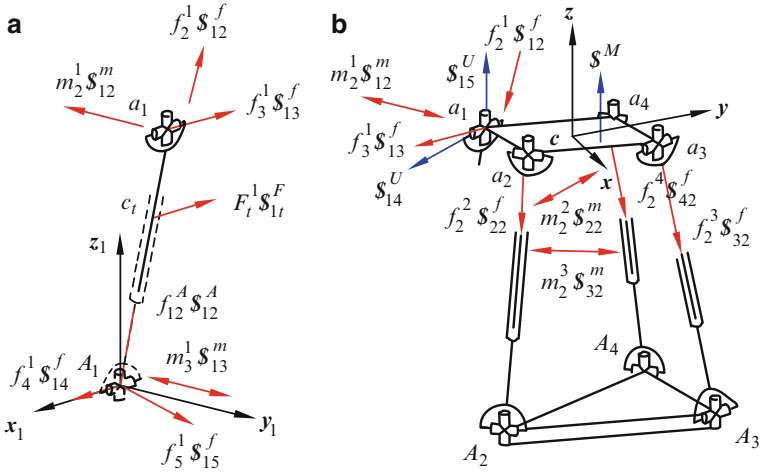


Fig. 8.4 The link in branch 1 and the sub-mechanism (a) free body of link *t* (b) the sub-mechanism

Set screw system

$\hat{\mathcal{S}}^c = \{ \mathcal{S}_{22}^f \quad \mathcal{S}_{32}^f \quad \mathcal{S}_{42}^f \quad \mathcal{S}_{32}^m \quad \mathcal{S}_{22}^m \}^T$ and its two-time reciprocal screw \mathcal{S}^M , denote the motion of the platform in the mechanism shown in Fig. 8.4b. According to the reciprocal product $\mathcal{S} \circ \mathcal{S}^M = 0$ (Chap. 2), we can obtain the two-time reciprocal screw \mathcal{S}^M in *c-xyz*.

$$\mathcal{S}^M = (0 \quad 0 \quad 1; \quad c(s\theta - c\theta)/2s\theta \quad c(s\theta - c\theta)/2c\theta \quad cc\alpha(s\theta - c\theta)/2s\alpha) \tag{8.43}$$

where \mathcal{S}^M denotes a twist motion of the platform, along Z-axis with pitch

$$h = cc\alpha(s\theta - c\theta)/2s\alpha.$$

In *c - xyz*, the kinematic screws of U pair at point *a*₁ can also be expressed in two screw Plücker coordinates as follows

$$\begin{aligned} \mathcal{S}_{14}^U &= (c\theta \quad -s\theta \quad 0; \quad 0 \quad 0 \quad (c/2)(s\theta + c\theta)) \\ \mathcal{S}_{15}^U &= (0 \quad 0 \quad 1; \quad -c/2 \quad c/2 \quad 0) \end{aligned} \tag{8.44}$$

The sub-mechanism has three DOFs, Eqs. (8.43) and (8.44), three blue arrows, as shown in Fig. 8.4b, and is equivalent to a serial chain with three kinematic

pairs connecting the link t of limb 1 and the base. The corresponding Eqs. (8.43) and (8.44) represent the three-system screws.

Its three reciprocal screws, i.e., three constraints are as follows

$$\begin{aligned}\mathcal{S}_{12}^f &= \left(\frac{-(c\theta - s\theta)s\theta c\alpha}{s\alpha(c\theta - 2s\theta)} \quad 0 \quad 1; \quad \frac{-c(s\theta + c\theta)}{2c\theta} \quad 0 \quad \frac{-c(s\theta - c\theta)s\theta c\alpha}{2s\alpha(2s\theta - c\theta)} \right) \\ \mathcal{S}_{13}^f &= \left(\frac{-(s\theta - 2c\theta)s\theta}{c\theta(2s\theta - c\theta)} \quad 1 \quad 0; \quad 0 \quad 0 \quad \frac{-c(s^2\theta - c^2\theta)}{2c\theta(2s\theta - c\theta)} \right) \\ \mathcal{S}_{12}^m &= \left(0 \quad 0 \quad 0; \quad \frac{s\theta}{c\theta} \quad 1 \quad 0 \right)\end{aligned}\quad (8.45)$$

where \mathcal{S}_{13}^f is a pure force, \mathcal{S}_{12}^m is a couple, and \mathcal{S}_{12}^f is a force screw with non-zero pitch, shown as three red arrows in the upper-left portion of Fig. 8.4b. Equation (8.45) is obtained by a three-time reciprocal.

The three constraints of the U-pair can also be rewritten in four elements including three constraint forces along three directions and a dependent constraint couple perpendicular to its axis plane. In c - xyz , the Plücker coordinates of the forces along z_1 -axis, x_1 -axis, y_1 -axis, and the couple around the y_1 -axis are

$$\begin{aligned}& \left(0 \quad 0 \quad 1; \quad -\frac{c}{2} \quad \frac{c}{2} \quad 0 \right) \\ & \left(c\theta \quad -s\theta \quad 0; \quad 0 \quad 0 \quad \frac{c}{2}(s\theta + c\theta) \right) \\ & \left(s\theta \quad c\theta \quad 0; \quad 0 \quad 0 \quad \frac{c(s\theta - c\theta)}{2} \right) \\ & \left(0 \quad 0 \quad 0; \quad s\theta \quad c\theta \quad 0 \right)\end{aligned}\quad (8.46)$$

2. Constraint force in P pair

The kinematic chain consists of the first universal joint and the second prismatic pair, i.e., the UP chain, Fig. 8.4a. The screw system of the UP chain is composed of the first three screws in Eq. (8.33). The three reciprocal screws constrain the link t as follows

$$\begin{aligned}\mathcal{S}_{11}^r &= (0 \quad 0 \quad 0; \quad 0 \quad 1 \quad 0) \\ \mathcal{S}_{13}^r &= (1 \quad 0 \quad 0; \quad 0 \quad 0 \quad 0) \\ \mathcal{S}_{14}^r &= (0 \quad s\alpha_1 \quad -c\alpha_1; \quad 0 \quad 0 \quad 0)\end{aligned}\quad (8.47)$$

In c - xyz , let \mathcal{S}_{13}^m , \mathcal{S}_{14}^f , and \mathcal{S}_{15}^f denote \mathcal{S}_{11}^r , \mathcal{S}_{13}^r , and \mathcal{S}_{14}^r of Eq. (8.47), respectively. Therefore, the P-pair of limb 1 has not five but three reactions including $m_3^1 \mathcal{S}_{13}^m$, $f_4^1 \mathcal{S}_{14}^f$, and $f_5^1 \mathcal{S}_{15}^f$.

Consider the equilibrium of link t in Fig. 8.4a. Since \mathcal{S}_{12}^m is parallel to \mathcal{S}_{13}^m , $m_2^1 \mathcal{S}_{12}^m$ and $m_3^1 \mathcal{S}_{13}^m$ are linearly dependent. $m_{23}^1 \mathcal{S}_{12}^m$ is used to express the resultant couple of $m_2^1 \mathcal{S}_{12}^m$ and $m_3^1 \mathcal{S}_{13}^m$. Six unknowns including the active force $f_{12}^A \mathcal{S}_{12}^A$ can be solved by six equilibrium equations of link t , where screw \mathcal{S}_{12}^A is identical with

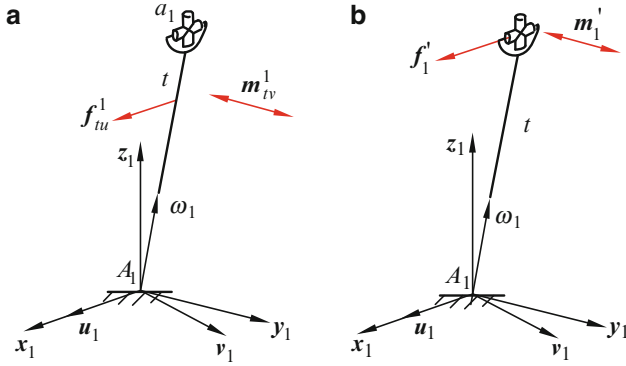


Fig. 8.5 Branch deformed around z_1 -axis (a) external forces on limb (b) reactions on limb

$\$_{11}^A$. The six equilibrium equations of link t with six unknowns are expressed by the following screw equation.

$$\sum_{j=2}^5 f_j^1 \$_{1j}^f + m_{23}^1 \$_{12}^m + f_{12}^A \$_{12}^A + F_t^1 \$_{1t}^F = 0 \tag{8.48}$$

In the above equation, the number of unknowns is not 10 but 6, and the equilibrium equation of link t is solvable. How to get $m_2^1 \$_{12}^m$ and $m_3^1 \$_{13}^m$ from $m_{23}^1 \$_{12}^m$ will be discussed in the next section.

(2) Complementary equation about branch 1 under $F_t^1 \$_{1t}^F$

Another coordinate system is constructed as A_i - u_i - v_i - w_i , as shown in Fig. 8.5. Its w_i -axis is along the axis of the prismatic pair in branch i , u_i -axis is along x_i -axis, and $v_i = w_i \times u_i$.

To determine m_2^1 , an additional equation should be supplemented. Assume that the moving platform has infinite stiffness and all the kinematic pairs are locked. The external force $F_t^1 \$_{1t}^F$ acting on link t allows the branch 1 to have the tendency of deformation curving around v_1 axis in $u_1 - w_1$ plane, as shown in Fig. 8.5a. However, constraint couple m_2^1 will resist the deformation, as Fig. 8.5b shows. Under this condition, the deformation compatibility equations may be constructed. Some forces having little or no relationship with the deformation will not be taken into consideration in the analysis process.

(a) The deformation caused by $F_t^1 \$_{1t}^F$

From [14], the bending Δ_1 at point a_1 caused by the external force $F_t^1 \$_{1t}^F$ can be written as

$$\Delta_1 = \delta_1 + \delta_2 \tag{8.49}$$

where

$$\delta_1 = \frac{f_{iu}^1 \left(l_1 - \frac{1}{2} l_t \right)^2 \left(2l_1 + \frac{1}{2} l_t \right)}{6EI_v}, \quad \delta_2 = \frac{m_{iv}^1 \left(l_1 - \frac{1}{2} l_t \right)}{EI_v} \left(\frac{l_1}{2} + \frac{1}{4} l_t \right).$$

Where EI_v is the bending stiffness of branch 1, f_{iu}^1 is the component of f_i^1 along u_1 -axis, and m_{iv}^1 is the component of m_i^1 around v_1 -axis.

- (b) The deformation caused by constraints exerted by the moving platform
There are three main-pair reactions at a_1 , as shown in Eq. (8.45). Some components including the force f_i^1 along u_1 -axis and the couple m_i^1 around v_1 -axis prevent branch 1 from deforming. The bending Δ_2 at a_1 caused by f_i^1 and m_i^1 can also be written as

$$\Delta_2 = \delta_3 + \delta_4 \quad (8.50)$$

where

$$\delta_3 = f_i^1 l_1^3 / 3EI_v, \quad \delta_4 = m_i^1 l_1^2 / 2EI_v.$$

The deformation compatibility condition is

$$\Delta_1 = -\Delta_2 \quad (8.51)$$

As m_{23}^1, f_2^1 , and f_3^1 have been solved from Eq. (8.48), m_2^1 can be determined from Eq. (8.51). Then $m_3^1 = m_{23}^1 - m_2^1$. Thus, all the reactions of the main pair at a_1 caused by $F_i^1 \mathcal{S}_{1t}^F$ can be solved.

- (c) Complementary equation for the moving platform
Two parallel constraint couples, m_1^1, m_1^3 or $m_j^2, m_j^4, j = 1, 2$, are exerted on the moving platform by two branches that correspond to a diagonal torsion of the moving platform. We know from [15] that if the force and structure are both symmetric, the constraint couple should be divided into two equal parts. We write the complementary equations as follows

$$\begin{aligned} m_1^1 &= m_1^3 = m_1^{13} / 2 \\ m_j^2 &= m_j^4 = m_j^{24} / 2, \quad j = 1, 2 \end{aligned} \quad (8.52)$$

Based on the complementary equations, the unknowns are solvable.

- (d) Equilibrium of the platform under force $F_i^1 \mathcal{S}_{1t}^F$
From Eq. (8.48), we have solved the main-pair reactions at a_1 under limb force. To solve the five main-pair reactions caused by $F_i^1 \mathcal{S}_{1t}^F$ in three other main pairs,

i.e., f_2^i , $i = 2, 3, 4$, m_2^3 , and m_2^{24} , the equilibrium equation of the platform needs to be reconsidered. From Fig. 8.4b, the equation is written as

$$-\left(\sum_{i=1}^4 f_2^i \mathcal{S}_{i2}^f\right) - f_3^1 \mathcal{S}_{13}^f - m_2^1 \mathcal{S}_{12}^m - m_2^3 \mathcal{S}_{32}^m - m_2^{24} \mathcal{S}_{22}^m = 0 \quad (8.53)$$

From Eqs. (8.52) and (8.53), the reactions in other three main pairs caused by $F_i^1 \mathcal{S}_{1i}^F$ are solved. Thus, all the reactions of the main pairs under the applied force $F_i^1 \mathcal{S}_{1i}^F$ have been determined.

Since $f_2^i \mathcal{S}_{i2}^f$, $i = 2, 3, 4$ is obtained from Eq. (8.53), the active forces $f_{i2}^A \mathcal{S}_{i2}^A$, $i = 2, 3, 4$, which are along the axis of the prismatic pair produced by forces only acting on the link t in the branch L_1 , can be solved from the force equilibrium equations of the link t .

(3) Resultant main-pair reactions by principle of superposition

All the reactions of main pairs and the active forces caused by the applied forces $F_h \mathcal{S}_h^F$ and $F_t^1 \mathcal{S}_{1t}^F$ can be ultimately obtained by the principle of superposition of forces. From Eqs. (8.40) and (8.48), the active forces of branch i are

$$f_i^A \mathcal{S}_i^A = f_{i1}^A \mathcal{S}_{i1}^A + f_{i2}^A \mathcal{S}_{i2}^A, \quad i = 1, 2, 3, 4 \quad (8.54)$$

From Eqs. (8.40), (8.48), (8.51), and (8.52) the reactions of the main pair at a_1 include

$$f_1^1 \mathcal{S}_{11}^f + f_2^1 \mathcal{S}_{12}^f + f_3^1 \mathcal{S}_{13}^f + m_{12}^1 \mathcal{S}_{11}^m \quad (8.55)$$

From Eqs. (8.40), (8.52), and (8.53) the reactions of the main pairs at a_i $i = 2, 3, 4$ include

$$f_1^i \mathcal{S}_{i1}^f + f_2^i \mathcal{S}_{i2}^f + m_{12}^i \mathcal{S}_{i1}^m, \quad i = 2, 3, 4 \quad (8.56)$$

where m_{12}^i is the constraint couple of the U pair caused by forces $F_t^1 \mathcal{S}_{1t}^F$ and $F_h \mathcal{S}_h^F$.

8.2.1.3 All the Constraint Reactions of Other Pairs

When the main constraint forces are solved, the constraint reactions of other pairs are easy to obtain by analyzing the equilibrium equation of every body one by one.

8.2.2 Numerical Example

The parameters of the 4-UPU mechanism are as follows: $a = 0.5$ m, $b = 0.3$ m, $c = 0.2$ m, $z_0 = 0.5$ m, $l_t = 0.3$ m, $\mathbf{m}_h = (1 \ 1 \ 0.5)^T$, $\mathbf{m}_t^1 = (1 \ 0.5 \ 1)^T$, $\mathbf{f}_h = (2 \ 1 \ 2)^T$, and $\mathbf{f}_t^1 = (1 \ 2 \ 2)^T$ (N·m and N). The results are listed in Table 8.1.

Table 8.1 The active forces and the main-pair reactions

	f_1^A/N	f_1^i/N	f_2^i/N	f_3^i/N	$m_{12}^i/N\cdot m$
Limb 1	1.698	0.0874	-4.2870	-2.7856	-2.4006
Limb 2	-9.827	2.7094	7.1174	-	-0.1504
Limb 3	-11.825	-12.1487	23.9733	-	7.4448
Limb 4	15.145	11.4495	-26.5945	-	-0.1504

8.3 Kinetostatic Analysis of 4-R(CRR) Parallel Manipulator

A 4-DOF 4-R(CRR) parallel mechanism is analyzed as another example [13]. This manipulator is symmetrical, and the moving platform has two translation and two rotation freedoms.

8.3.1 4-R(CRR) Parallel Manipulator

The 4-R(CRR) parallel mechanism, as shown in Fig. 8.6a, consists of a moving platform, a fixed platform, and four identical branches with four kinematic pairs, R, C, R, and R. The axis of the first pair R in each branch is normal to the base, and the axis of the second pair C is parallel to the base. The axes of the last three pairs intersect at a center point. The four branches have two center points, m and e , respectively.

The moving platform and the base are both square-shaped. The global coordinate system $O-XYZ$, moving system $o-xyz$, limb systems $e-x_iy_iz_i$, and $m-x_iy_iz_i$ are shown in Fig. 8.6a.

To analyze the mobility, the Modified Grübler-Kutzbach Criterion based on screw theory, Eqs. (3.4), (3.5), and (3.6), is used.

The redundant constraints of the whole mechanism can be obtained by screw analysis. For 4-R(CRR), one of its limbs, i , is shown in Fig. 8.6b. Its five single-DOF pairs are expressed into screw Plücker coordinates in $e-x_iy_iz_i$ or $m-x_iy_iz_i$ as follows

$$\begin{aligned}
 \$^i_1 &= (0 \ 0 \ 1; \ 0 \ -x_{Ai} \ 0) \\
 \$^i_2 &= (1 \ 0 \ 0; \ 0 \ 0 \ 0) \\
 \$^i_3 &= (0 \ 0 \ 0; \ 1 \ 0 \ 0) \qquad i = 1, 2, \dots, 4 \qquad (8.57) \\
 \$^i_4 &= (l_{i4} \ m_{i4} \ n_{i4}; \ 0 \ 0 \ 0) \\
 \$^i_5 &= (l_{i5} \ m_{i5} \ n_{i5}; \ 0 \ 0 \ 0)
 \end{aligned}$$

where x_{Ai} relates a geometrical parameter, l_{ij} , m_{ij} , and n_{ij} are direction cosines, and j indicates the serial number of the kinematic pair in limb i . However, the values of x_{Ai} and l_{ij} , m_{ij} , n_{ij} are not important for mobility analysis.

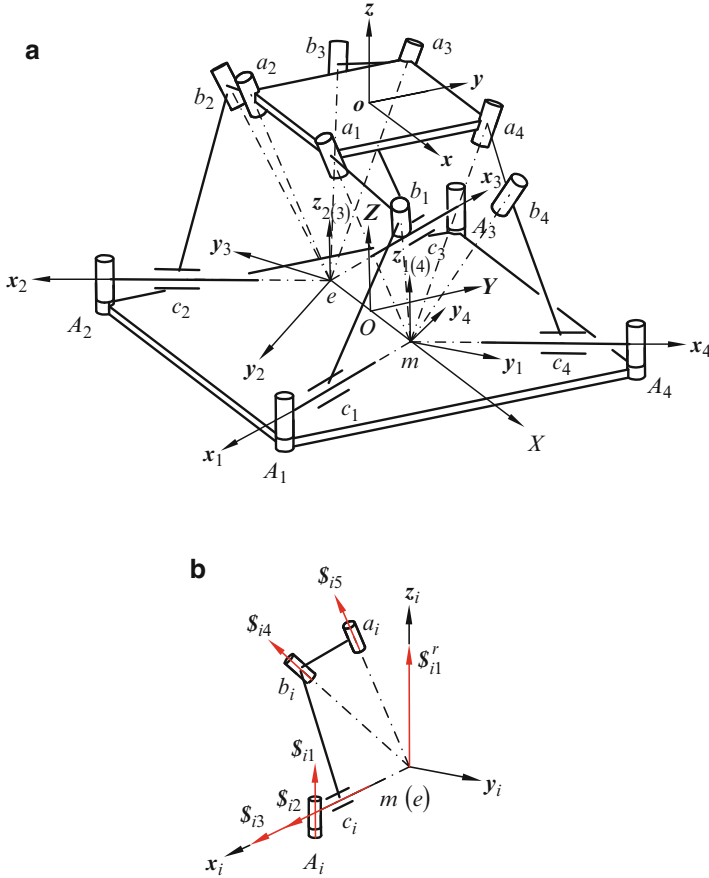


Fig. 8.6 The 4-R(CRR) mechanism (a) the mechanism (b) the limb screw system

The five-screw system, Eq. (8.57), has one reciprocal screw

$$\mathcal{S}_1^{ri} = (0 \ 0 \ 1; \ 0 \ 0 \ 0) \tag{8.58}$$

where \mathcal{S}_1^{ri} is a constraint force applied to the platform by limb i , which is normal to the base and passes its center point, m or e .

Four identical limbs exert a total of four constraint forces on the same platform but passes through two different points, e and m . In the global system O - XYZ , they are

$$\begin{aligned} \mathcal{S}^{r1} &= (0 \ 0 \ 1; \ y_m \ -x_m \ 0) \\ \mathcal{S}^{r2} &= (0 \ 0 \ 1; \ y_e \ -x_e \ 0) \\ \mathcal{S}^{r3} &= (0 \ 0 \ 1; \ y_e \ -x_e \ 0) \\ \mathcal{S}^{r4} &= (0 \ 0 \ 1; \ y_m \ -x_m \ 0) \end{aligned} \tag{8.59}$$

where x_m, y_m and x_e, y_e relate to the geometrical parameters of the mechanism. The four screws comprise a constraint screw system, $\hat{\mathcal{S}}^R$, which is

$$\hat{\mathcal{S}}^R = (\mathcal{S}^{r1}, \mathcal{S}^{r2}, \mathcal{S}^{r3}, \mathcal{S}^{r4})^T \quad (8.60)$$

We find that the rank of system $\hat{\mathcal{S}}^R$ is only two which means that there is no common constraint. The number of the redundant constraints of the whole mechanism is two. From the Modified G-K Criterion, Eq. (3.5), the mobility of the mechanism is

$$M = d(n - g - 1) + \sum_{i=1}^g f_i + v = 6(14 - 16 - 1) + 20 + 2 = 4. \quad (8.61)$$

Therefore, the mechanism has four degrees of freedom.

1. From the analysis, we know that the platform is simultaneously acted upon by two linearly independent parallel constraint forces, which constrain one translational motion along Z-axis and one rotational motion around the normal direction of the plane determined by the two forces. Therefore, the mechanism is able to translate along two directions, X and Y and rotate around two axes, X and Z.
2. After any possible motion including translation or rotation of the platform, the screw systems and Eq. (8.61) are both invariable. Therefore, the mobility is global.

The 4-DOF mechanism needs four inputs. The first revolute pairs of limbs 1, 2, 3, and the single-freedom revolute pair of the cylindrical pair in limb 4 are selected as the four inputs. To prove the correctness of the selection, they need to be locked.

The input selection principle states that after locking all the selected inputs, if the platform is subjected to six linearly independent constraints and has no remnant freedom, the selections are correct.

For limbs 1, 2, and 3, each limb-screw system has only four screws, which are the last four screws in Eq. (8.57). With respect to the limb coordinate system, the four screws are

$$\begin{aligned} \mathcal{S}_2^i &= (1 \ 0 \ 0; \ 0 \ 0 \ 0) \\ \mathcal{S}_3^i &= (0 \ 0 \ 0; \ 1 \ 0 \ 0) \\ \mathcal{S}_4^i &= (l_{i4} \ m_{i4} \ n_{i4}; \ 0 \ 0 \ 0) \\ \mathcal{S}_5^i &= (l_{i5} \ m_{i5} \ n_{i5}; \ 0 \ 0 \ 0) \end{aligned} \quad i = 1, 2, 3 \quad (8.62)$$

The two reciprocal screws of Eq.(8.62) are

$$\begin{aligned} \mathcal{S}_1^{ri} &= (0 \ 0 \ 1; \ 0 \ 0 \ 0) \\ \mathcal{S}_2^{ri} &= (0 \ 1 \ 0; \ 0 \ 0 \ 0) \end{aligned} \quad i = 1, 2, 3 \quad (8.63)$$

For limb 4, when revolute part of the cylindrical pair is locked, the limb screw system becomes

$$\begin{aligned}
 \mathcal{S}_1^4 &= (0 \ 0 \ 1; \ 0 \ -x_{Ai} \ 0) \\
 \mathcal{S}_3^4 &= (0 \ 0 \ 0; \ 1 \ 0 \ 0) \\
 \mathcal{S}_4^4 &= (l_{44} \ m_{44} \ n_{44}; \ 0 \ 0 \ 0) \\
 \mathcal{S}_5^4 &= (l_{45} \ m_{45} \ n_{45}; \ 0 \ 0 \ 0)
 \end{aligned} \tag{8.64}$$

The reciprocal screws of Eq. (8.64) are

$$\begin{aligned}
 \mathcal{S}_1^{r4} &= (0 \ 0 \ 1; \ 0 \ 0 \ 0) \\
 \mathcal{S}_2^{r4} &= \left(0 \ 1 \ 0; \ \frac{x_{Ai}(m_{44}n_{45} - n_{44} - m_{45})}{m_{45}l_{44} - l_{45}m_{44}} \ \frac{-x_{Ai}(n_{45}l_{44} - l_{45}n_{44})}{m_{45}l_{44} - l_{45}m_{44}} \ x_{Ai} \right)
 \end{aligned} \tag{8.65}$$

where the first one is a constraint force and the second one is a constraint wrench with pitch $h \neq 0$. Since Eqs. (8.63) and (8.65) with $\mathcal{S}_1^{r2} = \mathcal{S}_1^{r3}$ and $\mathcal{S}_1^{r1} = \mathcal{S}_1^{r4}$ show the rank of the eight screws as six, the input selection is correct.

8.3.2 Main-Pair Reaction

Since the 4-R(CRR) has 13 movable links, 12 R-pairs, 4 C-pairs, and 4 unknown inputs, the number of unknowns is $12 \times 5 + 4 \times 4 + 4 = 80$, and the number of equations is $13 \times 6 = 78$. Analyzing the reactions applied on moving platform, in generally, each revolute pair brings 5 unknowns, and there are up to 20 unknowns for the free-body diagram of the moving platform. However, there are only six equations for the platform, and the reactions will be insoluble. In this case, it needs to take more links to set a high-order matrix equation.

The new method can reduce the number of unknowns and simplify the solution.

Let $F_h \mathcal{S}_h^f$ and $F_t^1 \mathcal{S}_{1t}^f$ denote the corresponding resultant external force screws with intensities, respectively. The equation is formulated as

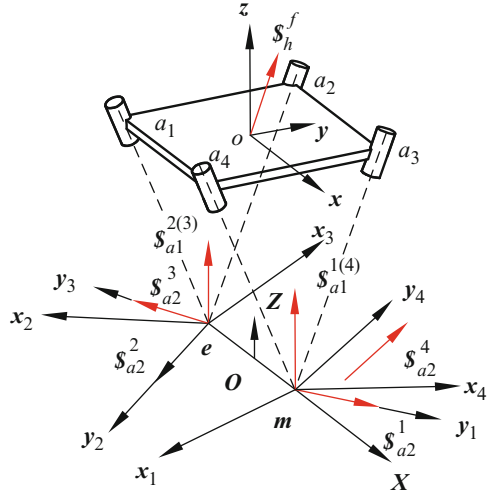
$$\begin{aligned}
 F_h \mathcal{S}_h^f &= \mathbf{f}_h + \in \mathbf{m}_h \\
 F_t^1 \mathcal{S}_{1t}^f &= \mathbf{f}_t^1 + \in \mathbf{r}_{ct}^c \times \mathbf{f}_t^1 + \mathbf{m}_t^1
 \end{aligned} \tag{8.66}$$

where \mathbf{r}_{ct}^c is the radius vector from the origin of the global system to the mass center point of link t ; \in is the Clifford factor.

8.3.2.1 Main-Pair Reactions Produced by Platform Force

Equations (8.63) and (8.65) denote main reactions, and each main pair contains two reactions. \mathcal{S}_{i1}^r and \mathcal{S}_{i2}^r in Eq. (8.63) are unit constraint screws along z_i - and y_i -axes,

Fig. 8.7 Free-body diagram of the platform



respectively. In Eq. (8.65), \mathcal{S}_{41}^r is also a unit screw along z_r -axis, and \mathcal{S}_{42}^r is a screw with $h \neq 0$. All the eight screws are denoted in Fig. 8.7. Their intensities are unknown.

However, the maximum linearly independent number of the eight constraints is six, Table 2.1. From this point of view, there are only six independent unknowns and the issue is solvable.

We use \mathcal{S}_{a1}^i and \mathcal{S}_{a2}^i , $i = 1 \sim 4$, to denote \mathcal{S}_{11}^{ri} and \mathcal{S}_{21}^{ri} , in the global system. The corresponding intensities of the reactions are f_{a1}^i and f_{a2}^i . f_{a1}^{14} and f_{a1}^{23} are the resultant forces of f_{a1}^1, f_{a1}^4 and f_{a1}^2, f_{a1}^3 , respectively. The free-body diagram of the moving platform is shown in Fig. 8.7.

Considering the equilibrium of the platform, we have

$$\sum_{i=1}^4 f_{a2}^i \mathcal{S}_{a2}^i + f_{a1}^{14} \mathcal{S}_{a1}^1 + f_{a1}^{23} \mathcal{S}_{a1}^2 + F_h \mathcal{S}_h^f = 0 \tag{8.67}$$

Equation (8.67) is a screw equation and it is equivalent to six linear equations. The six unknown intensities can be solved.

If we use the traditional approach, each R pair has 5 unknown reactions and there are 20 unknowns corresponding to 6 equilibrium equations of the moving platform and it is insolvable directly. Therefore, for solvability, it has to consider the equilibrium of other bodies, even all other bodies simultaneously. Considering the situation, this may be named as *force coupling*. The new method reduces unknowns and makes the solution decoupled and easy.

From Eq. (8.67), we can solve the six unknowns, including f_{a1}^{14} and f_{a1}^{23} . To get $f_{a1}^1, f_{a1}^4, f_{a1}^2$, and f_{a1}^3 , there is a need to resolve f_{a1}^{14} into limbs 1 and 4, as well as f_{a1}^{23} into limbs 2 and 3. This is “static indeterminacy.” This resolution can be carried out by analyzing the stiffness of two corresponding parts. The two forces are in direct proportion to the stiffness of the two corresponding parts.

However, to simplify the analysis and considering that our core object is not stiffness analysis, we provide a hypothesis where the stiffness proportion of the two parts is η . Therefore, the complementary equations are as follows [14]

$$\begin{aligned} f_{a_1}^1 &= \eta_1 f_{a_1}^4 \\ f_{a_1}^2 &= \eta_2 f_{a_1}^3 \end{aligned} \quad (8.68)$$

8.3.2.2 Main-Pair Reactions Produced by Limb Force²

Suppose link a_1b_1 in limb 1 is subject to a given external force $F_t^1 \mathcal{S}_{1t}^f$, and the force will bring main reactions. Main-pair reactions at a_1 can be obtained by solving the equilibrium equations of link a_1b_1 under the only applied force $F_t^1 \mathcal{S}_{1t}^f$. A free-body diagram of link a_1b_1 is shown in Fig. 8.8a. We should analyze the reactions of R pairs at a_1 and b_1 , respectively.

(1) Reactions of revolute pair of sub-mechanism.

The R pair at a_1 connects link a_1b_1 and a sub-mechanism, 3-R(CRR), as shown in Fig. 8.8b. First, it needs to calculate the mobility of the 3-R(CRR) mechanism. From Eq. (3.5), we have

$$M = 6 \times (11 - 12 - 1) + 15 + 1 = 4$$

It is still a 4-DOF mechanism and there are only three input pairs in the sub-chain. After the three input pairs are locked, it still has one freedom. The platform of the sub-mechanism is then subjected to five constraints. From Eqs. (8.63) and (8.65), the five linearly independent reactions include \mathcal{S}_1^{ri} , $i = 2, 4$, which are upward and pass through the corresponding two centers, \mathcal{S}_2^{ri} , $i = 2, 3$, which are along the corresponding y_i -axes, and \mathcal{S}_2^{r4} , which is a screw with $h \neq 0$ (bi-directional arrow) and parallel to the y -axis.

In the system $m - X_m Y_m Z_m$, Fig. 8.8b, the five constraint screws (shown as red arrows) can be expressed as

$$\begin{aligned} \mathcal{S}_1^{r2} &= (0 \quad 0 \quad 1; \quad 0 \quad l_a \quad 0) \\ \mathcal{S}_2^{r2} &= (l_{22}^{mr} \quad m_{22}^{mr} \quad 0; \quad 0 \quad 0 \quad 0 - l_a m_{22}^{mr}) \\ \mathcal{S}_2^{r3} &= (l_{32}^{mr} \quad m_{32}^{mr} \quad 0; \quad 0 \quad 0 \quad 0 - l_a m_{32}^{mr}) \\ \mathcal{S}_1^{r4} &= (0 \quad 0 \quad 1; \quad 0 \quad 0 \quad 0) \\ \mathcal{S}_2^{r4} &= (l_{42}^{mr} \quad m_{42}^{mr} \quad n_{42}^{mr}; \quad p_{42}^{mr} \quad q_{42}^{mr} \quad r_{42}^{mr}) \end{aligned} \quad (8.69)$$

² If there are no external forces in limbs, Sects. 8.3.2.2 and 8.3.2.3 are not necessary.

Therefore, the twist system of the sub-chain is a two-screw system including the screws in Eqs. (8.70) and (8.71). The reciprocal screws of the system are four main reactions (pink arrows) acting on link a_1b_1 at point a_1 . They are three-time reciprocal as follows

$$\begin{aligned} \mathcal{S}_{a_3}^1 &= (0 \ 0 \ 1; \ 0 \ 0 \ 0) \\ \mathcal{S}_{a_4}^1 &= (1 \ 0 \ 0; \ 0 \ 0 \ 0) \\ \mathcal{S}_{a_5}^1 &= \left(0 \ 1 \ 0; \ \frac{p_{42}^{mr} l_a}{r_{42}^{mr} + l_a m_{42}^{mr}} \ \frac{-p_{42}^{mr} l_a l_R^m}{m_R^m (r_{42}^{mr} + l_a m_{42}^{mr})} \ 0 \right) \\ \mathcal{S}_{a_6}^1 &= \left(0 \ 0 \ 0; \ \frac{p_{42}^{mr}}{A} \ -\frac{p_{42}^{mr} l_R^m + n_R^m l_{42}^{mr} + n_R^m l_a m_{42}^{mr}}{A m_R^m} \ \frac{(r_{42}^{mr} + l_a m_{42}^{mr})}{A} \right) \end{aligned} \quad (8.72)$$

where $\mathcal{S}_{a_3}^1$ and $\mathcal{S}_{a_4}^1$ are reactions passing point m and along axes Z_m and X_m , respectively; $\mathcal{S}_{a_5}^1$ is a constraint force screw, $h \neq 0$, parallel Y_m ; $\mathcal{S}_{a_6}^1$ is a couple normal to \mathcal{S}^M and \mathcal{S}_R^m ; and

$$A = \sqrt{(p_{42}^{mr})^2 + \frac{(p_{42}^{mr} l_R^m + n_R^m r_{42}^{mr} + n_R^m l_a m_{42}^{mr})^2}{(m_R^m)^2} + (r_{42}^{mr} + l_a m_{42}^{mr})^2}$$

Suppose the four screws with their intensities are expressed as $f_{a_3}^1 \mathcal{S}_{a_3}^1, f_{a_4}^1 \mathcal{S}_{a_4}^1, f_{a_5}^1 \mathcal{S}_{a_5}^1$, and $m_{a_6}^1 \mathcal{S}_{a_6}^1$ in the global system. There are also only four unknowns, $f_{a_3}^1, f_{a_4}^1, f_{a_5}^1$, and $m_{a_6}^1$, for the R pair.

(2) Reactions of revolute pair at b_1 .

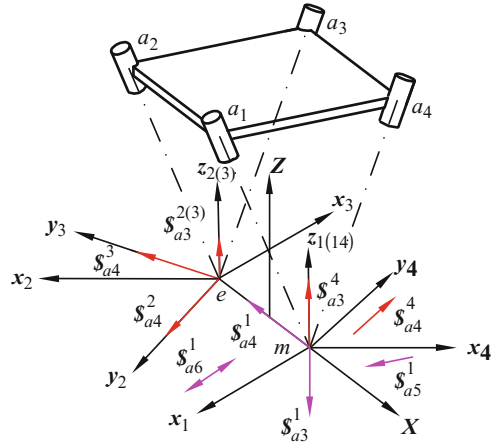
Reactions of the revolute pair at b_1 are determined by analyzing the sub-chain RCR in limb 1, Fig. 8.8a. When the input pair is locked, there are only three basic pairs, whose screws are just the three screws in the middle of Eq. (8.57). Their three reciprocal screws are written as follows

$$\begin{aligned} \mathcal{S}_{b_1}^1 &= (0 \ 0 \ 1; \ 0 \ 0 \ 0) \\ \mathcal{S}_{b_2}^1 &= (0 \ 1 \ 0; \ 0 \ 0 \ 0) \\ \mathcal{S}_{b_3}^1 &= (0 \ 0 \ 0; \ 0 \ -n_9 \ m_9) \end{aligned} \quad (8.73)$$

where $\mathcal{S}_{b_1}^1$ is a reaction force, acting on link a_1b_1 at b_1 , normal to the base and passing through the limb center point; $\mathcal{S}_{b_2}^1$ is also a reaction force passing through that point and along the y_1 -axis; $\mathcal{S}_{b_3}^1$ is a reaction couple in plane Y - Z .

Suppose we use $f_{b_1}^{1t}, f_{b_2}^{1t}$, and $m_{b_3}^{1t}$ to denote their intensities only caused by external force $F_t^1 \mathcal{S}_t^1$ in the global system. The three reactions at b_1 pair acting on link a_1b_1 are $f_{b_1}^{1t} \mathcal{S}_{b_1}^1, f_{b_2}^{1t} \mathcal{S}_{b_2}^1$, and $m_{b_3}^{1t} \mathcal{S}_{b_3}^1$. Since $\mathcal{S}_{a_3}^1$ and $\mathcal{S}_{b_1}^1$ are collinear, $f_{a_3b_1}^{1t}$ is used to denote the resultant intensity of $\mathcal{S}_{a_3}^1$ and $\mathcal{S}_{b_1}^1$.

Fig. 8.9 Free-body diagram of the platform



- (a) *Equilibrium of link a_1b_1 .* As shown in Fig. 8.8a, the reactions of the revolute pairs at a_1 and b_1 of limb 1 can be obtained. The equilibrium equation with six unknowns of link a_1b_1 is

$$f_{a_3b_1}^{1t} \mathcal{S}_{a_3}^1 + f_{a_4}^{1t} \mathcal{S}_{a_4}^1 + f_{a_5}^{1t} \mathcal{S}_{a_5}^1 + m_{a_6}^{1t} \mathcal{S}_{a_6}^1 + f_{b_2}^{1t} \mathcal{S}_{b_2}^1 + m_{b_3}^{1t} \mathcal{S}_{b_3}^1 + F_t^1 \mathcal{S}_{1t}^f = 0 \quad (8.74)$$

In the equation, there are six linearly independent unknowns and the main-reactions are solvable. From Eq. (8.74) $f_{a_3b_1}^{1t}$ is obtained, but it still needs to separate $f_{a_3b_1}^{1t}$ into $f_{a_3}^1$ and $f_{b_1}^{1t}$ by stiffness analysis. Similar to Eq. (8.68), we have

$$f_{a_3}^1 = \eta_3 f_{b_1}^{1t} \quad (8.75)$$

- (b) *The external force acting on link a_1b_1 .* It also brings about the main reactions in limbs 2, 3, and 4. To further analyze the main reactions in limbs 2, 3, and 4, we reconsider the equilibrium of the platform, as shown in Fig. 8.9. $f_{a_3}^{23}$ denotes the resultant force of $f_{a_3}^2$ and $f_{a_3}^3$. Four forces acting on the platform have been solved from Eq. (8.74). Considering the equilibrium equation with five unknowns of the platform, we have

$$-\sum_{i=3}^5 f_{a_i}^1 \mathcal{S}_{a_i}^1 - m_{a_6}^1 \mathcal{S}_{a_6}^1 + f_{a_3}^{23} \mathcal{S}_{a_3}^2 + f_{a_3}^4 \mathcal{S}_{a_3}^4 + \sum_{i=2}^4 f_{a_4}^i \mathcal{S}_{a_4}^i = 0 \quad (8.76)$$

Obtaining $f_{a_3}^2$ and $f_{a_3}^3$ from $f_{a_3}^{23}$ is similar by stiffness analysis.

$$f_{a_3}^2 = \eta_4 f_{a_3}^3 \quad (8.77)$$

Comparing with Eq. (8.68), it is clear that $\eta_4 = \eta_2$, as they correspond to the same situations and have the same proportion.

(c) *Resultant main-pair reactions by superposition principle*

The main reactions brought by the platform force and limb force have been solved by Eqs. (8.67), (8.74), and (8.76). From superposition principle the resultant reaction at point a_1 is

$$f^1 \mathcal{S}_1^R = - \sum_{i=1}^2 f_{ai}^1 \mathcal{S}_{ai}^1 + \sum_{i=3}^5 f_{ai}^1 \mathcal{S}_{ai}^1 + m_{a6}^1 \mathcal{S}_{a6}^1 \quad (8.78)$$

The resultant main reaction at point a_i , where $i = 2, 3, 4$ is

$$f^i \mathcal{S}_i^R = - \sum_{i=1}^4 f_{ai}^j \mathcal{S}_{ai}^j, \quad j = 2, 3, 4 \quad (8.79)$$

8.3.3 Active Moments and Reactions of Other Pairs in Limbs³

When the constraint reactions of the four main pairs are obtained, the four active moments and reactions of other pairs can be easily obtained by solving the equilibrium equations of each links in every limb in descending order, respectively.

8.3.3.1 Reactions of Revolute Pair at b_i

Resultant main-reactions of the revolute pair at a_i have been achieved by Eqs. (8.67), (8.74), and (8.76). To obtain the total unknown reactions at b_i we have to set the equilibrium equation of link $a_i b_i$ once again.

For limb 1, there are ten forces acting on link $a_1 b_1$ including a known external force $F_t^1 \mathcal{S}_{1t}^f$ and six known main-reactions at point a_1 , Eqs. (8.67) and (8.74), and three unknown reactions at b_1 , Eq. (8.73). The equilibrium equation of $a_1 b_1$ is as follows

$$- \sum_{i=1}^2 f_{at}^1 \mathcal{S}_{at}^1 + \sum_{i=3}^5 f_{at}^1 \mathcal{S}_{at}^1 + m_{a6}^1 \mathcal{S}_{a6}^1 + \sum_{j=1}^2 f_{bj}^1 \mathcal{S}_{bj}^1 + m_{b3}^1 \mathcal{S}_{b3}^1 + F_t^1 \mathcal{S}_{1t}^f = 0 \quad (8.80)$$

where f_{bj}^1 , $j = 1, 2$, and m_{b3}^1 are caused by both $F_h \mathcal{S}_h^f$ and $F_t^1 \mathcal{S}_{1t}^f$.

³ If not, there is no need to calculate the constraint reactions of pairs in limbs, and the active forces can be directly obtained by the principle of virtual work. When the forces of the main joints are solved, each limb becomes a serial-chain, and its force analysis would be simpler by directly setting the equilibrium of each body. However, we want to show that, by this method, the unknown number of equilibrium equations will not exceed six.

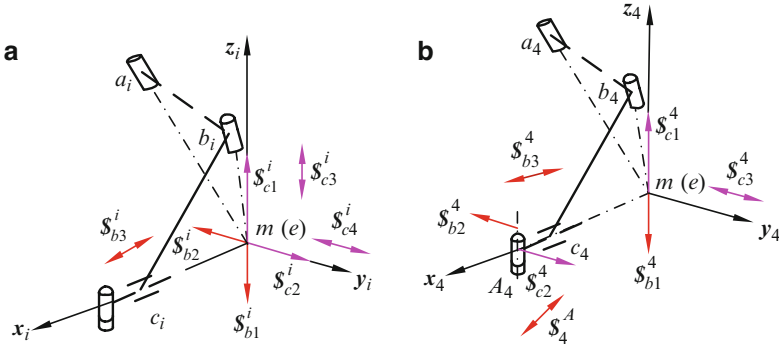


Fig. 8.10 Free body diagram of link $b_i c_i$ in limbs (a) limbs 1, 2, and 3 (b) limb 4

For limbs 2, 3, and 4, considering Eqs. (8.67) and (8.76), the balancing equation with three unknown reactions of link $a_i b_i$ is

$$-\sum_{j=1}^4 f_{aj}^i s_{aj}^i + \sum_{j=1}^2 f_{bj}^i s_{bj}^i + m_{b3}^i s_{b3}^i = 0 \quad i = 2 \sim 4 \quad (8.81)$$

8.3.3.2 Reactions of Cylindrical Pair at c_i

In analyzing the reactions of the cylindrical pair at c_i , we need to consider the kinematic chain RC in each limb.

(1) Limbs 1, 2, and 3.

The first pair at A_i is the active pair, Fig. 8.10a. When the actuated joint is locked, there are only two single-freedom pairs, R and P in chain RC. The twist system includes the second and third screws in Eq. (8.57), and their four unknown reciprocal screws (pink arrows) are in the following forms

$$\begin{aligned} s_{i1}^{Cr} &= (0 \ 0 \ 1; \ 0 \ 0 \ 0) \\ s_{i2}^{Cr} &= (0 \ 1 \ 0; \ 0 \ 0 \ 0) \\ s_{i3}^{Cr} &= (0 \ 0 \ 0; \ 0 \ 0 \ 1) \\ s_{i4}^{Cr} &= (0 \ 0 \ 0; \ 0 \ 1 \ 0) \end{aligned} \quad i = 1, 2, 3 \quad (8.82)$$

where s_{i1}^{Cr} and s_{i2}^{Cr} are two reaction forces passing through the origin of the limb system along z_i and y_i , respectively; s_{i3}^{Cr} and s_{i4}^{Cr} are constraint couples also about axes z_i and y_i .

Assuming that the four reaction screws of the cylindrical pair at c_i in Eq. (8.82) are denoted as s_{cj}^i , $i = 1 \sim 3$, $j = 1 \sim 4$, in the global system, their intensities are

f_{cj}^i , $i = 1 \sim 3$, $j = 1, 2$, and m_{cj}^i , $i = 1 \sim 3$, $j = 3, 4$. Considering the equilibrium of link $b_i c_i$, as shown in Fig. 8.10a, the four unknown reactions of pair C can be obtained by

$$-\sum_{j=1}^2 f_{bj}^i \mathcal{S}_{bj}^i - m_{b3}^i \mathcal{S}_{b3}^i + \sum_{j=1}^2 f_{cj}^i \mathcal{S}_{cj}^i + \sum_{j=3}^4 m_{cj}^i \mathcal{S}_{cj}^i = 0, \quad i = 1 \sim 3 \quad (8.83)$$

(2) Limb 4

For this limb, the single-freedom revolute pair of the cylindrical pair is the actuated joint, and can be locked similarly like the section above. However, here we prefer not to lock the input, and consider that there is an unknown applied force, $m_4^A \mathcal{S}_4^A$. The three-system twist of RC chain consists of the first three screws in Eq. (8.57), and the C pair has three unknown reciprocal screws (pink), as shown in Fig. 8.10b, and is computed as follows.

$$\begin{aligned} \mathcal{S}_{41}^{Cr} &= (0 \quad 0 \quad 1; \quad 0 \quad 0 \quad 0) \\ \mathcal{S}_{42}^{Cr} &= (0 \quad 1 \quad 0; \quad 0 \quad 0 \quad x_{Ai}) \\ \mathcal{S}_{43}^{Cr} &= (0 \quad 0 \quad 0; \quad 0 \quad 1 \quad 0) \end{aligned} \quad (8.84)$$

Considering the equilibrium of link $b_4 c_4$, the four unknowns, one active couple and three reactions, in pair C can be obtained as follows

$$-\sum_{j=1}^2 f_{bj}^4 \mathcal{S}_{bj}^4 - m_{b3}^4 \mathcal{S}_{b3}^4 + \sum_{j=1}^2 f_{cj}^4 \mathcal{S}_{cj}^4 + m_{c3}^4 \mathcal{S}_{cj}^4 + m_4^A \mathcal{S}_4^A = 0 \quad (8.85)$$

where $m_4^A \mathcal{S}_4^A$ is the active moment of limb 4. \mathcal{S}_{cj}^4 , $j = 1 \sim 3$, denote three reaction screws of the cylindrical pair at c_4 in the global system and their intensities are f_{cj}^4 , $j = 1, 2$, and m_{c3}^4 .

8.3.3.3 Active Moments and Reactions of Revolute Pair at A_i

In the limb system, the first R pair for each limb has five constraints, such as

$$\begin{aligned} \mathcal{S}_{i1}^R &= (0 \quad 0 \quad 1; \quad 0 \quad 0 \quad 0) \\ \mathcal{S}_{i2}^R &= (1 \quad 0 \quad 0; \quad 0 \quad 0 \quad 0) \\ \mathcal{S}_{i3}^R &= (0 \quad 1 \quad 0; \quad 0 \quad 0 \quad 0) \\ \mathcal{S}_{i4}^R &= (0 \quad 0 \quad 0; \quad 1 \quad 0 \quad 0) \\ \mathcal{S}_{i5}^R &= (0 \quad 0 \quad 0; \quad 0 \quad 1 \quad 0) \end{aligned} \quad i = 1, 2, 3, 4 \quad (8.86)$$

where \mathcal{S}_{i1}^R , \mathcal{S}_{i2}^R , and \mathcal{S}_{i3}^R are reaction forces passing point A_i and along three coordinate axes, respectively. \mathcal{S}_{i4}^R and \mathcal{S}_{i5}^R are couples about axes x_i and y_i , respectively.

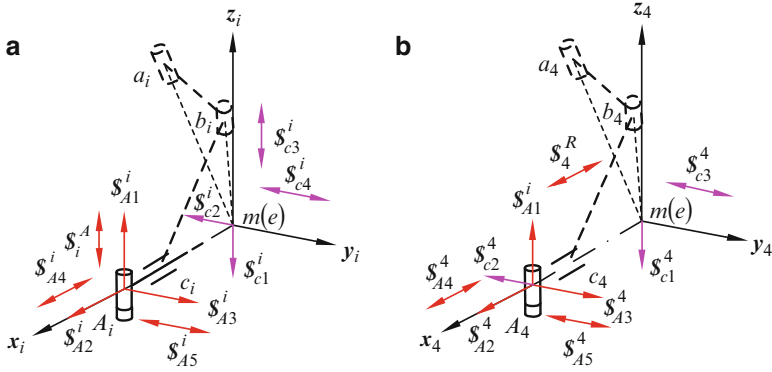


Fig. 8.11 Free body diagram of link u in limbs (a) limbs 1, 2 and 3 (b) limb 4

Assuming that \mathcal{S}_{Aj}^i , $i = 1 \sim 4$, $j = 1 \sim 5$, denote \mathcal{S}_{ij}^R , $i = 1 \sim 4$, $j = 1 \sim 5$ and their intensities are f_{Aj}^i , $i = 1 \sim 4$, $j = 1, 2, 3$, and m_{Aj}^i , $i = 1 \sim 4$, $j = 4, 5$, in the global system, the active couple will be $m_i^A \mathcal{S}_i^A$, $i = 1 \sim 4$.

For limbs 1, 2, and 3 in Fig. 8.11a, the equilibrium equation with six unknowns including the input couple of link $A_i c_i$ is

$$\sum_{j=1}^3 f_{Aj}^i \mathcal{S}_{Aj}^i + \sum_{j=4}^5 m_{Aj}^i \mathcal{S}_{Aj}^i - \sum_{j=1}^2 f_{cj}^i \mathcal{S}_{cj}^i - \sum_{j=3}^4 m_{cj}^i \mathcal{S}_{cj}^i + m_i^A \mathcal{S}_i^A = 0, \quad i = 1 \sim 3 \quad (8.87)$$

For limb 4, Fig. 8.11b, the equilibrium equation with five unknowns of link $A_4 c_4$ is

$$\sum_{j=1}^3 f_{Aj}^4 \mathcal{S}_{Aj}^4 + \sum_{j=4}^5 m_{Aj}^4 \mathcal{S}_{Aj}^4 - \sum_{j=1}^2 f_{cj}^4 \mathcal{S}_{cj}^4 - m_{c3}^4 \mathcal{S}_{c3}^4 - m_4^A \mathcal{S}_4^A = 0 \quad (8.88)$$

where $m_4^A \mathcal{S}_4^A$ is an unknown input couple exerted on link $A_4 c_4$ by the active device.

8.3.4 Numerical Example

Assume the distance Oo is 0.55 m; $l_a = 0.4$ m, $l_A = 0.9$ m; vector mb_4 is $(l_{44}^O \ m_{44}^O \ n_{44}^O)^T$, vector ma_4 is $(0 \ m_{45}^O \ n_{45}^O)^T$, and their values are as follows

$$\left(\frac{22.95}{50}, \frac{13.91}{50}, \frac{42.19}{50} \right)^T \quad \text{and} \quad \left(0, \frac{20}{\sqrt{20^2 + 50^2}}, \frac{50}{\sqrt{20^2 + 50^2}} \right)^T$$

$$F_h \mathcal{S}_h^f = (40, 50, 55; 30, 40, 45)^T \quad (\text{N and N} \cdot \text{m}).$$

a is the distance between point A_i , $i = 1, 4$ and origin point m , or point A_i , $i = 2, 3$ and n .

$$a = \sqrt{\left(\frac{l_A - l_a}{2}\right)^2 + \left(\frac{l_A}{2}\right)^2}$$

The constraint screws in Eq. (8.67) are as follows

$$\mathcal{S}_{a1}^{1(4)} = \left(0 \quad 0 \quad 1; \quad 0 \quad -\frac{l_a}{2} \quad 0 \right)$$

$$\mathcal{S}_{a1}^{2(3)} = \left(0 \quad 0 \quad 1; \quad 0 \quad \frac{l_a}{2} \quad 0 \right)$$

$$\mathcal{S}_{a2}^1 = \left(\frac{l_A}{2a} \quad \frac{l_A - l_a}{2a} \quad 0; \quad 0 \quad 0 \quad \frac{l_A l_a - l_a^2}{4a} \right)$$

$$\mathcal{S}_{a2}^2 = \left(\frac{l_A}{2a} \quad -\frac{l_A - l_a}{2a} \quad 0; \quad 0 \quad 0 \quad \frac{l_A l_a - l_a^2}{4a} \right)$$

$$\mathcal{S}_{a2}^3 = \left(-\frac{l_A}{2a} \quad -\frac{l_A - l_a}{2a} \quad 0; \quad 0 \quad 0 \quad \frac{l_A l_a - l_a^2}{4a} \right)$$

$$\mathcal{S}_{a2}^4 = \left(\frac{-l_A}{2a} \quad \frac{l_A - l_a}{2a} \quad 0; \quad -\frac{(m_{45}^O n_{44}^O - m_{44}^O n_{45}^O)(2l_A^2 - 2l_A l_a + l_a^2)}{4am_{45}^O l_{44}^O} \right. \\ \left. \frac{-n_{45}^O(2l_A^2 - 2l_A l_a + l_a^2)}{4am_{45}^O} \quad \frac{l_A(2l_A - l_a)}{4a} \right)$$

The results of the active moments and reactions are listed in Table 8.2.

8.3.5 Discussion

From the above analysis, we realize that the force analysis of parallel mechanisms is very difficult as it has many unknowns. The 4-R(CRR) mechanism has 13 links, 16 kinematic pairs, and 4 unknown active moments. The number of its unknowns, u , and the number of equilibrium equations, e , are as follows

$$u = 12 \times 5 + 4 \times 4 + 4 = 80$$

$$e = 13 \times 6 = 78$$

Table 8.2 The results of active moments and constraint reactions

Wrench	Limb 1	Limb 2	Limb 3	Limb 4
f_{a1}^i/N	-16.152	-11.348	-11.348	-16.152
f_{a2}^i/N	-60.378	30.403	13.979	1.804
f_{b1}^i/N	-16.152	-11.348	-11.348	-16.152
f_{b2}^i/N	-60.378	-30.403	-13.979	1.804
$m_{b3}^i/N\cdot m$	-22.036	-11.096	-5.102	1.981
f_{c1}^i/N	-16.152	-11.348	-11.348	-16.152
f_{c2}^i/N	-60.378	-30.403	-13.979	1.804
$m_{c3}^i/N\cdot m$	-5.865	2.953	1.358	5.787
$m_{c4}^i/N\cdot m$	6.665	-4.655	-4.674	-
f_{A1}^i/N	-16.152	-11.348	-11.348	-16.152
f_{A2}^i/N	0	0	0	0
f_{A3}^i/N	-60.378	30.403	13.979	1.804
$m_{A4}^i/N\cdot m$	0	0	0	-2.175
$m_{A5}^i/N\cdot m$	-8.346	-5.816	-5.842	-9.180
$m_i^A/N\cdot m$	31.095	-15.649	-7.196	-2.175

This means that it is not only a static indeterminacy issue, but a set system of up to 80 equations is also needed for the solution. As we have mentioned, the unknowns may even be up to 125 for the 5-5R mechanism. To deal with the high-order matrix is quite difficult.

From the above kinetostatic analysis procedure, it is clear that this method based on screw theory can remarkably reduce the number of unknowns and keep the number of simultaneous equilibrium equations not more than six on every occasion. One of the characteristics of this method is the need to solve the main-pair reaction before solving the reaction of others. All the active forces and constraint reactions of kinematic pairs are obtained easily by analyzing the equilibrium of bodies individually in terms of their free-body diagrams.

Evidently, the force-analysis method is decoupled and the method can avoid setting complex high-order matrices.

References

- Huang Z, Zhao Y (1994) The accordance and optimization-distribution equations of the over-determinate inputs of walking machines. *Mech Mach Theory* 29(2):327-332
- Huang Z, Kong L, Fang Y (1997) *Mechanism theory of parallel robotic manipulator and control*. China Mechanical Press, Beijing (in Chinese)
- Huang Z (1985) Modeling formulation of 6-DOF multi-loop parallel manipulators, Part-1: Kinematic influence coefficients. In: *Proceedings of the 4th IFToMM international symposium on linkage and computer aided design methods*, vol. II-1, Bucharest, Romania, pp 155-162
- Huang Z (1985) Modeling formulation of 6-DOF multi-loop parallel manipulators, Part-2: Dynamic modeling and example. In: *Proceedings of the 4th IFToMM international symposium on linkage and computer aided design methods*, vol. II-1 Bucharest, Romania, pp 163-170
- Beyer R (1960) *Statics and dynamics in 3-D mechanisms*. Transactions of the 6th conference on mechanisms, Purdue University, West Lafayette, pp 94-112

6. Yang AT (1965) Static force and torque analysis of spherical four-bar mechanisms. *ASME J Eng Ind Ser* 87(2):221–227
7. Asada H, Slotine JJE (1986) *Robot analysis and control*. Wiley, New York
8. Merlet JP (2006) *Parallel robots*, 2nd edn. Springer, Paris
9. Zhang D, Gosselin CM (2001) Kinetostatic modeling of n-DOF parallel mechanisms with passive constraining leg and prismatic actuators. *Trans ASME J Mech Design* 123(3):375–381
10. Lu Y (2007) Using virtual work theory and CAD functionalities for solving active and passive force of spatial parallel manipulators. *Mech Mach Theory* 42(7):839–858
11. Zhou Y, Liu L, Gao F (2008) Full static solving of 3-DOF spherical parallel mechanism 3-RRR. *Chinese J Mech Eng* 44(6):169–176
12. Zhao Y, Huang Z (2010) Force analysis of lower-mobility parallel mechanisms with over-constrained couples. *J Mech Eng* 46(5):15–21
13. Huang Z, Zhao Y, Liu JF (2010) Kinetostatic analysis of 4-R(CRR) parallel manipulator with overconstraints via reciprocal-screw theory. *Adv Mech Eng*, Article ID 404960:1–11
14. Timoshenko SP, Gere JM (1961) *Theory of elastic stability*, 2nd edn. McGraw-Hill, New York
15. Liu H (2004) *Mechanics of materials*. Higher Education Press, Beijing

Chapter 9

Constraint Screw-Based Method for Type Synthesis

Lower-mobility parallel mechanisms (PMs) are suitable for many tasks requiring less than six DOFs. For instance, 6-DOF PMs currently used in machine tools have a superfluous complexity because only five DOFs are necessary for tool control. Obviously, using 5-DOF PMs to perform such tasks can save on cost. In fact, the machine architecture of lower-mobility PMs is simpler. Consequently, the control system and the manufacturing process are reduced.

The pioneering work on the type or structure synthesis of lower-mobility PMs has been initiated by Hervé [1] in 1978 and Hunt [2] in 1983. Hervé [1] has given a comprehensive list of displacement Lie subgroups, which lay down a solid foundation for the group-based synthesis method. Hunt [2] has presented a table that includes planar, 3-RPS, some 6-DOF, and some 4-DOF or 5-DOF unsymmetrical PMs.

The type or structure synthesis of lower-mobility PMs has been the subject of much research since 1990. Typically, the methods for type synthesis of lower-mobility PMs fall into three classes depending on their starting point.

The first class is called the motion-based method. This method starts from the fact that the motion of the moving platform of a PM is the intersection of the motion of each limb chain. When displacement subgroups are used to represent the motion of the moving platform and limb chains, the method is also called group-based synthesis. The group-based synthesis method is derived from the algebraic properties of a six-dimensional Lie group of the Euclidean displacement set. Based on the pioneering work of Hervé [1], he and his coworkers [3–7] have applied the group-based synthesis method to all kinds of lower-mobility PMs. Other important contributions related to the group-based synthesis method have been proposed by other researchers, such as Angeles [8] and Rico et al. [9]. Meng et al. [10] have also given new accounts of the group-based method using a style borrowed from treatises of mathematics on the Lie group theory and differential geometry. Other synthesis methods based on the single-open-chain [11], the Gf coordinates [12], and linear transforms [13, 14] also belong to this class.

The second class is called the constraint screw-based synthesis method. This method starts from the fact that the constraints acting on the moving platform of a lower-mobility PM is the union of constraints generated by each limb chain.

A screw is used to represent the constraint. Using this method, researchers have obtained important progress in this area [15–22]. The constraint-synthesis method is universally applicable to all kinds of lower-mobility PMs. Considering that a screw is inherently instantaneous, the constraint-synthesis method is a tool at the level of instantaneous motion. However, using more geometrical conditions, the finite mobility of a lower-mobility PM can be further established.

The third class is based on the G-K mobility criterion. In 1999, Tsai [23] has introduced a 3-DOF non-overconstrained PM based on the G-K mobility criterion. However, the application of this method is limited because the geometrical properties of joint axes are not taken into consideration.

It is noted that the type synthesis of symmetrical lower-mobility PMs is a basic and open problem in mechanism theory. Once the method for type synthesis of symmetrical lower-mobility PMs is established, it is easy to be applied to the asymmetrical PM. In this chapter, the type synthesis of symmetrical lower-mobility PMs is systematically performed using the constraint-synthesis method.

9.1 Description of Constraints Acting on a Rigid Body

Consider a rigid body without constraints acting on it. The rigid body has six degrees of freedom, i.e., finite DOF. When a constraint is exerted on the rigid body, the rigid body loses a DOF. When several independent constraints are exerted on the rigid body, the motion of the rigid body is completely determined by the integrative effect of all constraints. Consequently, a mathematical tool that describes and analyzes the constraints need to be find. Naturally, one can turn to the screw theory. The constraints acting on a rigid body can be a force, a couple, or a combination of both. A screw can also be used to represent the combination. For example, for a rigid body with only three translational DOF, the constraints acting on it are three couples:

$$\begin{aligned} \mathcal{S}_1^r &= (0 \ 0 \ 0; \ 1 \ 0 \ 0) \\ \mathcal{S}_2^r &= (0 \ 0 \ 0; \ 0 \ 1 \ 0) \\ \mathcal{S}_3^r &= (0 \ 0 \ 0; \ 0 \ 0 \ 1) \end{aligned} \quad (9.1)$$

When a screw is referred to as a constraint, it is different from the force or couple in the general meaning. The constraint screw is always expressed as a unit screw. There are usually several constraints simultaneously acting on the moving platform of a lower-mobility PM. Hence, the linear dependence or independence of constraint screws is essential. The linear dependence or independence of screws is independent of the location of the frame [17], enabling the fair convenience of the frame selection.

After constraints are described by the screw theory, the combined effects of several constraints need to be investigated. The linear dependence of constraints is

Table 9.1 Constraint couples, maximum linear independence number

Geometrical condition of couples	Maximum linear independence number	Constrained motion of the rigid body
Coaxial	1	Rotation about the axis
Coplanar	2	All rotations about axes parallel to this plane
Non-coplanar	3	Three rotations in space

Table 9.2 Constraint forces, maximum linear independence number and constrained motion of the rigid body

Geometrical condition of forces	Maximum linear independence number	Constrained motion of the rigid body
Coaxial	1	Translation along the forces
Coplanar and parallel	2	Translation along the forces and rotation about the normal of the plane
Coplanar and intersect at a common point	2	Two translations in the plane
Coplanar, non-parallel, and do not intersect at a common point	3	Two translations in the plane and one rotation about the normal of the plane
Parallel in space	3	Translation along the force and two rotations about the axis perpendicular to the force
Intersect at a common point and non-coplanar	3	All three translations in space

determined by the geometrical conditions among them. When the constraints acting on a rigid body are couples, only following three geometrical conditions exist among them. Table 9.1 gives a general description of constraint couples and the corresponding constrained motions of the rigid body under three different geometrical conditions.

For example, the first row in Table 9.1 shows that when all the constraint couples acting on a rigid body are coaxial, they are linearly dependent. Their maximum linear independence number is one. Their combined effect equals one constraint couple in the direction of the axis. The rotation of the rigid body about the axis is constrained.

Given that forces are not free vectors, the maximum linear independence numbers among them are very complicated [24]. However, only the situation when the maximum linear independence number equals one, two, or three for type synthesis of lower-mobility parallel manipulators needs to be considered. Table 2.1 lists the relations, and Table 9.2 gives a concise description of the constraint forces and the corresponding constrained motions of the rigid body under six different geometrical conditions.

For example, the second row in Table 9.2 shows that when all the constraint forces are coplanar and parallel to each other, the maximum linear independence number of the constraint forces is two. Consider three constraint forces parallel to the x axis and lying in the xy plane:

$$\begin{aligned}\$'_1 &= (1 \ 0 \ 0; \ 0 \ 0 \ 0) \\ \$'_2 &= (1 \ 0 \ 0; \ 0 \ 0 \ c_2) \\ \$'_3 &= (1 \ 0 \ 0; \ 0 \ 0 \ c_3)\end{aligned}\tag{9.2}$$

By calculating the screws reciprocal to Eq. (9.2), four linearly independent feasible motions of the rigid body can be obtained:

$$\begin{aligned}\$_1 &= (1 \ 0 \ 0; \ 0 \ 0 \ 0) \\ \$_2 &= (0 \ 1 \ 0; \ 0 \ 0 \ 0) \\ \$_3 &= (0 \ 0 \ 0; \ 0 \ 1 \ 0) \\ \$_4 &= (0 \ 0 \ 0; \ 0 \ 0 \ 1)\end{aligned}\tag{9.3}$$

In other words, the three constraint screws in Eq. (9.2) are linearly dependent, and their total effect is equal to one constraint couple, $(0 \ 0 \ 0; \ 0 \ 0 \ 1)$, and one constraint force, $(1 \ 0 \ 0; \ 0 \ 0 \ 0)$.

9.2 Limb Twist and Limb Constraint Systems

9.2.1 Limb Twist System

Each kinematic pair in a limb chain of a PM can be associated with a unit screw. These unit screws span a screw system, called a limb twist system or limb screw system, which describes the instantaneous motion of the limb kinematic chain. These unit screws form a standard base of the limb screw system. For example, the standard base of a 3R spherical chain is given by

$$\begin{aligned}\$_1 &= (1 \ 0 \ 0; \ 0 \ 0 \ 0) \\ \$_2 &= (0 \ 1 \ 0; \ 0 \ 0 \ 0) \\ \$_3 &= (0 \ 0 \ 1; \ 0 \ 0 \ 0)\end{aligned}$$

To provide the simplest form for a limb screw system, the axes of the frame are assumed to be parallel to or coincident with the direction of kinematic pairs as much as possible. Consequently, the frame is called a limb coordinate frame, which is usually a local frame. In other words, the limb screw system is frame configuration dependent.

9.2.2 Limb Constraint System

The constraints generated by a limb kinematic chain forms a limb constraint system. A limb constraint can be described by a screw reciprocal to the twists associated with all kinematic joints in a limb, namely, the limb twist system. Using the reciprocity between twists and wrenches, the limb constraint system of a limb kinematic chain can be obtained. The limb constraint is often described in the limb coordinate frame.

9.3 Platform Twist and Platform Constraint Systems

9.3.1 Platform Twist System

The instantaneous motion of the moving platform of a PM can be represented by a twist system, called a platform twist system. If the platform twist system is constant in every non-singular configuration of the PM, it also represents the finite mobility of the PM. Usually, the platform twist system is written in a fixed coordinate frame.

For instance, the standard base of the platform twist system of a 3-DOF translational PM is given by

$$\begin{aligned} \mathcal{S}_{m1} &= (0 \ 0 \ 0; \ 1 \ 0 \ 0) \\ \mathcal{S}_{m2} &= (0 \ 0 \ 0; \ 0 \ 1 \ 0) \\ \mathcal{S}_{m3} &= (0 \ 0 \ 0; \ 0 \ 0 \ 1) \end{aligned} \quad (9.4)$$

The platform twist system of a 3-DOF rotational PM is given by

$$\begin{aligned} \mathcal{S}_{m1} &= (1 \ 0 \ 0; \ 0 \ 0 \ 0) \\ \mathcal{S}_{m2} &= (0 \ 1 \ 0; \ 0 \ 0 \ 0) \\ \mathcal{S}_{m3} &= (0 \ 0 \ 1; \ 0 \ 0 \ 0) \end{aligned} \quad (9.5)$$

The platform twist system of a 3R1T 4-DOF PM is given by

$$\begin{aligned} \mathcal{S}_{m1} &= (1 \ 0 \ 0; \ 0 \ 0 \ 0) \\ \mathcal{S}_{m2} &= (0 \ 1 \ 0; \ 0 \ 0 \ 0) \\ \mathcal{S}_{m3} &= (0 \ 0 \ 1; \ 0 \ 0 \ 0) \\ \mathcal{S}_{m4} &= (0 \ 0 \ 0; \ 0 \ 0 \ 1) \end{aligned} \quad (9.6)$$

9.3.2 Platform Constraint System and Classification of Lower-Mobility PMs

Lower-mobility PMs can be classified into 12 subcategories based on the property of mobility. Although such a classification is not mathematically rigorous, it is helpful in the type synthesis of lower-mobility PMs. Hereinafter, T means translation and R means rotation.

The 5-DOF PM can be classified into two subcategories. The first subcategory has two translational DOF and three rotational DOF, called a 3R2T PM. The moving platform of a 3R2T PM loses a translational DOF because of a constraint force acting on the moving platform. The second category has two rotational DOF and three translational DOF, called a 2R3T PM. The 2R3T PM loses a rotational DOF because of a constraint couple acting on the moving platform. The platform constraint system of both the 3R2T and 2R3T PMs consists of one constraint screw.

The 4-DOF PM can be classified into three subcategories. The first subcategory has three rotational DOF and one translational DOF, called a 3R1T PM. The 3R1T PM loses two translational DOF because of two constraint forces independently acting on the moving platform. The platform constraint system of a 3R1T PM belongs to the second constraint screw system. The second subcategory has one rotational DOF and three translational DOF, called a 1R3T PM. The 1R3T PM loses two rotational DOFs because of two constraint couples independently acting on the moving platform. The third subcategory has two rotational DOF and two translational DOF, called a 2R2T PM. The platform constraint system of a 2R2T PM consists of a constraint force and a couple. The effect of the platform constraint system can be equal to two parallel constraint forces. Hence, the platform constraint system of a 4-DOF PM consists of two constraint screws.

The 3-DOF PM can be classified into four subcategories. The first subcategory has three translational DOF, called a 3T PM. The moving platform of the 3T PM loses three rotational DOF because of three constraint couples independently acting on it. The second subcategory has three rotational DOF, called a 3R PM. The moving platform of the 3R PM loses three translational DOF because of three constraint forces independently acting on it. The third subcategory has two rotational DOF and one translational DOF, called a 2R1T PM. The moving platform of the 2R1T PM loses one rotational DOF and two translational DOF because of two constraint couples and one constraint force independently acting on it. The fourth subcategory has one rotational DOF and two translational DOF, called a 1R2T PM. The moving platform of the 1R2T PM loses two rotational DOF and one translational DOF because of two constraint couples and one constraint force independently acting on it.

The 2-DOF PM can be classified into three subcategories, namely, 1R1T, 2T, and 2R. The type synthesis of the 2-DOF PM is generally simple and will not be investigated in this chapter. Table 9.3 demonstrates various constraint screw systems, their geometrical conditions, constrained motions, and corresponding lower-mobility PMs.

Table 9.3 Limb constraint system and platform constraint system of lower-mobility PMs

No.	Lower-mobility PM	Platform constraint system	Limb constraint system	Geometrical condition that all limb constraints satisfy	DOF of limb
1	3R2T	One force	One force	The forces are coaxial	5
2	2R3T	One couple	One couple	The couples are parallel	5
3	1R3T	Two couples	One couple Two couples	The couples are coplanar but not parallel	5 4
4	3R1T	Two forces	One force Two forces	The forces are coplanar and intersect at a common point	5 4
5	2R2T	One couple and one force	One force One couple and one force	The forces are parallel The couples are parallel and the forces are coaxial	5 4
6	3R	Three forces	Three forces Two forces One force	The forces are non-coplanar and intersect at a common point	3 4 5
7	3T	Three couples	Three couples Two couples One couple	The couples are non-coplanar and non-parallel	3 4 5
8	2R1T	One couple and two forces	One force One couple and one force One couple and two forces	The forces are coplanar, non-parallel, and do not intersect at a common point The couples are parallel; the forces are coplanar and intersect at a common point	5 4 3
9	1R2T	Two couples and one force	One force One couple and one force Two couples and one force	The forces are parallel and non-coplanar The couples are coplanar and not parallel; the forces are coaxial	5 4 3

9.4 Constraint-Screw Based Synthesis Method

9.4.1 Procedure of the Constraint-Screw Based Synthesis Method

The idea behind the constraint-screw based synthesis method is reciprocity between the twist and wrench. The lower-mobility PM loses one or several DOF because there are one or several constraints acting on the moving platform.

In a lower-mobility PM, the DOF of the limb has to be equal to or more than the DOF of the moving platform. After the prescribed DOF of the moving platform is given, the standard base of the platform twist system and the platform constraint system becomes available. The standard base of the platform twist system can be used to form a basic limb twist system. There are two ways to construct the limb

kinematic chain. One is by the linear transformation of the twists of the standard base. Before and after linear transformation, the number of screws in the screw system should be invariable. The other way is to select some appropriate twists and add them to the basic limb twist system. The limb kinematic chain can then directly be constructed by the linear transformations of all twists.

After new twists are added to the limb twist system, the linear transformations of the limb twists also produce various limb architectures. The useable architectures need to be identified. From the above Tables, the platform constraint system of different parallel architectures can be obtained. If the platform constraint system remains unchanged, the limb kinematic chain and the parallel architecture are suitable.

The detailed type synthesis procedure is presented in Fig. 9.1. Explanations are provided below.

- Step 1: Write out the standard base of the platform twist system according to the prescribed DOF of the lower-mobility parallel manipulator.
- Step 2: Get the standard base of the platform constraint system.
- Step 3: Take the standard base of the platform twist system as the standard base of the limb twist system.
- Step 4: If other twists are needed in constructing the limb kinematic chain, proceed to Step 5. If not, go to Step 9.
- Step 5: Select appropriate twists and construct the limb kinematic chain by the linear transformations of the twists of the standard base and the selected twists.
- Step 6: Calculate the limb constraint system in the limb frame.
- Step 7: Determine the number of limbs and take the limbs constructed in Step 5 to form a symmetrical PM. Calculate the platform constraint system based on the above Tables in the global frame.
- Step 8: If the platform constraint system has changed after the selected twists are added, proceed to Step 5. If not, go to Step 11
- Step 9: Construct the limb kinematic chain by the linear transformation of the twists of the standard base.
- Step 10: Determine the number of the limbs and take the limbs constructed in Step 9 to form a symmetrical PM.
- Step 11: Check if the mechanism is instantaneous. If yes, proceed to Step 12. If not, go to Step 13.
- Step 12: If the target mechanism is to be used as a micro-motion mechanism, proceed to Step 13. If not, go back to Step 3.
- Step 13: Synthesis is successful.

In Step 1, given the prescribed DOF, the standard base of the platform twist system is easy to write out.

In Step 2, the standard base of the platform constraint system can be obtained by calculating the screws reciprocal to the standard base of the platform twist system.

In Step 3, the DOF of the limb kinematic chain must be equal to or more than the DOF of the PM. Consequently, the standard base of the platform twist system can be taken as the standard base of the limb twist system.

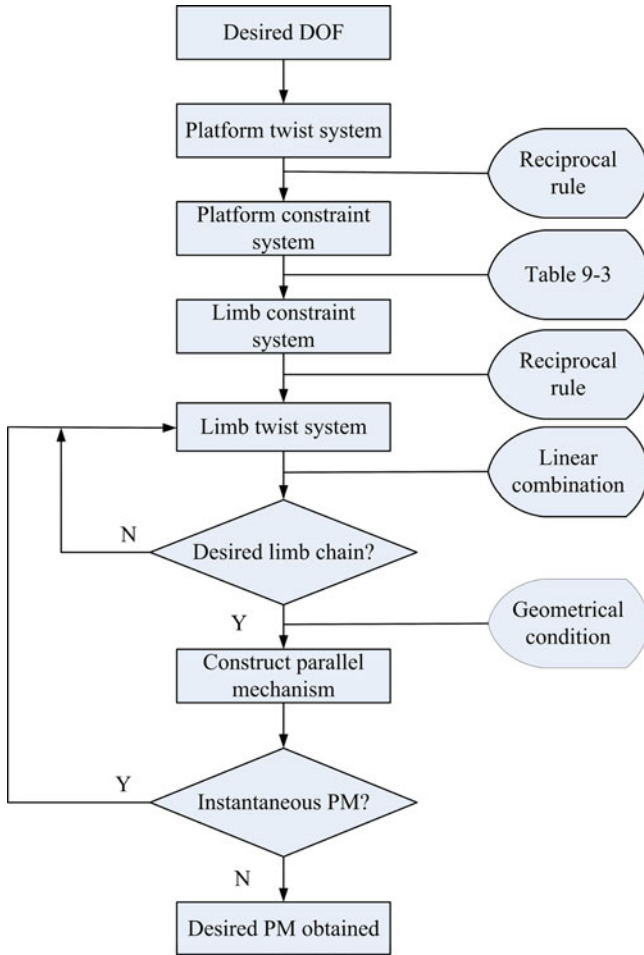


Fig. 9.1 Procedure of type synthesis using the constraint-screw method

In Step 5, the purpose of adding some extra twists is to diversify the structure of PMs. These extra added twists must not change the global constraints on the moving platform; that is, the platform constraint system must remain unchanged. Different limb constraint systems could yield the same platform constraint system.

In Step 7, the number of limbs in a mechanism must first be determined. PMs are then formed by the combination of several limbs. There are various combinations considering the geometrical conditions of all the first pairs of limbs linking the fixed platform. For example, the axes of all the first pairs may or may not intersect at a common point, be coplanar, and be parallel. The different combinations of the same limb may lead to different platform constraint systems such that the mechanism has different mobilities and properties. These operations may also form different mechanisms.

Two basic points need to be considered in Step 5. One is that the extra and former twists must be linearly independent. The other is to avoid the presence of helical pairs.

9.4.2 Generation of Different Architectures of PM

From the above analysis, different architectures of PMs can be obtained by the following methods:

1. Use of limb chains with different DOFs;
2. Changing the types of kinematic pairs by linear transformation; for example, revolute pair into prismatic pair, or prismatic pair into revolute pair;
3. Changing the order of kinematic pairs in a limb;
4. Changing the arrangement of several identical limbs.

9.4.3 Discrimination for Instantaneous PMs

A PM is said to be instantaneous if both its mobility number and corresponding properties cannot remain unchanged after an arbitrary feasible finite motion. If a PM has three translational DOF at a moment, as well as two translational DOF and one rotational DOF at another moment, the mechanism is instantaneous. Instantaneous PMs can also be used as micro-motion mechanisms if necessary.

The mobility number and its properties of a PM are completely determined by the platform constraint system. Consequently, an instantaneous mechanism can be identified by checking the platform constraint system after some finite motions. If the platform constraint system has changed, the PM is instantaneous.

9.5 Examples

Without loss of generality, the XY plane of the global frame, $O - XYZ$, is set to be coincident with the fixed platform plane. Hence, the Z axis of the global frame is perpendicular to the fixed platform plane and is upward. The Z axis of the limb frame, $o - xyz$, is set upward and parallel to the Z axis of the global frame of the mechanism, and the xy plane of the limb frame becomes coincident with the XY plane of the global frame.

9.5.1 Type Synthesis of a 3R2T 5-DOF PM

9.5.1.1 Constraint Synthesis

For simplicity, focus is given on the 5-DOF PM with three rotational DOF and two translational DOF in the XY plane, denoted by 3R2T^{xy}. The standard base of the platform twist system is given by

$$\begin{aligned}
 \$_{m1} &= (1\ 0\ 0; 0\ 0\ 0) \\
 \$_{m2} &= (0\ 1\ 0; 0\ 0\ 0) \\
 \$_{m3} &= (0\ 0\ 1; 0\ 0\ 0) \\
 \$_{m4} &= (0\ 0\ 0; 1\ 0\ 0) \\
 \$_{m5} &= (0\ 0\ 0; 0\ 1\ 0)
 \end{aligned} \tag{9.7}$$

The standard base of the platform constraint system is given by

$$\$_{m1}^r = (0\ 0\ 1; 0\ 0\ 0) \tag{9.8}$$

Using Eq. (9.7) as the standard base of the limb twist system, the limb kinematic chain can be obtained by the linear transformation of the five twists. The linear independence of the five twists must be maintained. In this case, the standard base of the limb constraint system is also given by Eq. (9.8).

9.5.1.2 Generation of Limb Chains

The linear transformation of $\$_{m4}$ and $\$_{m5}$ only yields prismatic pairs parallel to the XY plane. By the linear transformation with $\$_{m3}$, the pairs can also be transformed into revolute pairs whose axes are in z_i axis direction. Hence, the limb kinematic chain can consist of five revolute pairs.

$\$_{m1}$, $\$_{m2}$, and $\$_{m3}$ can represent a spherical pair or three successive revolute pairs whose axes intersect at a common point, namely, a 3R spherical subchain. The common point is called the limb central point. By the linear transformation with $\$_{m4}$ and $\$_{m5}$, $\$_{m3}$ can be transformed into $\$'_{m3} = (0\ 0\ 1; a_3\ b_3\ 0)$, which denotes a revolute pair whose axis is in the z_i axis direction and does not pass the limb central point. Consequently, the remaining $\$_{m1}$ and $\$_{m2}$ form a 2R spherical subchain.

To keep the platform constraint system unchangeable when the mechanism moves, the sixth component in any twist in Eq. (9.7) should be maintained at zero and also unchangeable. Therefore, all the axes of the revolute pairs are divided into two groups. The axes in one group are perpendicular to the base. The axes in the other group successively intersect at a common point, which is selected as the global origin. The number of the axes either normal to the base or intersecting at a common point cannot be greater than three. Otherwise, some pairs in the limb will

Table 9.4 Symmetrical 5-DOF PMs

With 2R spherical subchain	With 3R spherical subchain
$n^{-z}R^zR^zR({}^iR^jR)_N$	$n^{-z}R^zR({}^iR^jR^kR)_N$
$n^{-z}R^zR^xP({}^iR^jR)_N$	$n^{-x}P^yP({}^iR^jR^kR)_N$
$n^{-z}R^xP^zR({}^iR^jR)_N$	$n^{-z}R^xP({}^iR^jR^kR)_N$
$n^{-x}P^zR^zR({}^iR^jR)_N$	$n^{-x}P^zR({}^iR^jR^kR)_N$
$n^{-x}P^yP^zR({}^iR^jR)_N$	
$n^{-z}R^xP^yP({}^iR^jR)_N$	
$n^{-x}P^zR^yP({}^iR^jR)_N$	

be linearly dependent. Therefore, the mechanism must contain a 3R or 2R spherical subchain. The axes of revolute pairs outside the 2R or 3R spherical subchain must be perpendicular to the base plane. For the same reason, the orientation of any translational pair should be parallel to the base.

Force is not a free vector in space; consequently, the position of a point on the force axis is necessary to determine a force vector in space. Several forces are coaxial if, and only if, they pass a common point and are parallel to each other. All the limb central points must coincide such that the limb constraint forces are coaxial because each limb has a limb central point passed through by the constraint force. Such a superposition point is called a mechanism central point. The mechanism central point is fixed relative to the base or the moving platform because of the symmetrical structure.

Given that the center of all spherical pairs in all limbs generally cannot coincide with each other, the limb kinematic chain contains no spherical pairs. All the 2R or 3R subchains must also simultaneously connect either to the base or to the moving platform to avoid being instantaneous.

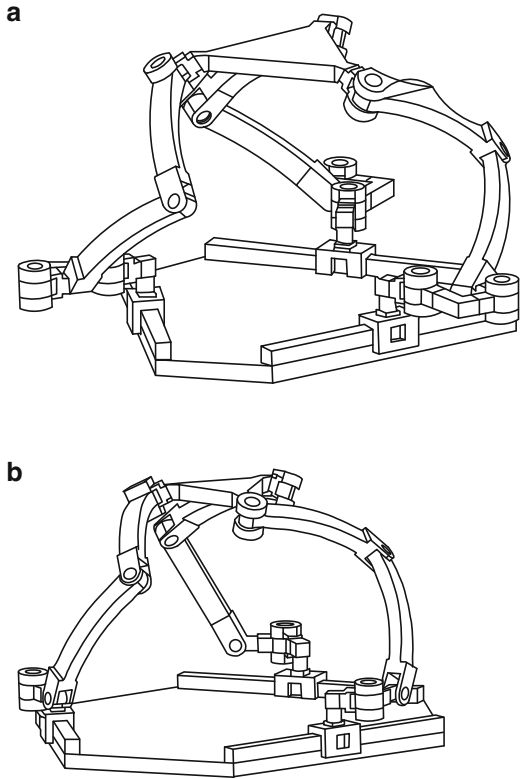
9.5.1.3 Generation of PMs

Based on the above analysis, the usable limb kinematic chains can be obtained by the linear transformation of the five twists in Eq. (9.7). An enumeration of the PMs is given in Table 9.4. n denotes the number of limbs and $2 \leq n \leq 5$. The superscript denotes the direction of the kinematic pair. $({}^iR^jR)_N$ denotes a 2R spherical subchain, and $({}^iR^jR^kR)_N$, a 3R spherical subchain with N as the center.

Cylindrical pairs and universal joints are kinematically equivalent to specific combinations of revolute pairs and prismatic pairs. By setting the first revolute pair axis of the 3R or 2R spherical subchain perpendicular to its anterior revolute pair axis and assuming the intersection of the two axes, a universal joint can be obtained. Similarly, by setting the first revolute pair axis of the 3R or 2R spherical subchain colinear to its anterior prismatic pair, a cylindrical pair can be obtained.

Figure 9.2 shows a $3^{-x}P^zR^zR({}^iR^jR)_N$ PM and a $n^{-x}P^zR({}^iR^jR^kR)_N$ PM.

Fig. 9.2 $3-xP^zR^zR(iR^jR)_N$
 (a) $3-xP^zR^zR(iR^jR)_N$
 (b) $3-xP^zR(iR^jR^kR)_N$



9.5.2 Type Synthesis of 2R3T 5-DOF PMs

9.5.2.1 Constraint Synthesis

The 5-DOF PM with three translational DOFs and two rotational DOFs is denoted by 2R3T. The two rotational axes are assumed to be in the XY plane in the initial configuration. The standard base of the platform twist system is given by

$$\begin{aligned}
 \mathcal{S}_{m1} &= (1 \ 0 \ 0 ; \ 0 \ 0 \ 0) \\
 \mathcal{S}_{m2} &= (0 \ 1 \ 0 ; \ 0 \ 0 \ 0) \\
 \mathcal{S}_{m3} &= (0 \ 0 \ 0 ; \ 1 \ 0 \ 0) \\
 \mathcal{S}_{m4} &= (0 \ 0 \ 0 ; \ 0 \ 1 \ 0) \\
 \mathcal{S}_{m5} &= (0 \ 0 \ 0 ; \ 0 \ 0 \ 1)
 \end{aligned} \tag{9.9}$$

The standard base of the platform constraint system is given by

$$\mathcal{S}_{m1}^r = (0 \ 0 \ 0 ; \ 0 \ 0 \ 1) \tag{9.10}$$

Using Eq. (9.9) as the standard base of the limb twist system, the various limb kinematic chains can be obtained by the linear transformations of the five twists. The new five twists generated by the linear transformation must be linearly independent. The standard base of the limb constraint system is also given by Eq. (9.10) in this case.

9.5.2.2 Generation of Limb Chains

The linear transformation of $\$_{m3}$, $\$_{m4}$, and $\$_{m5}$ yields a prismatic pair that bevels with the base. Obviously, $\$_{m3}$, $\$_{m4}$, and $\$_{m5}$ can be transformed into revolute pairs whose axes are parallel to the XY plane by the linear transformation with $\$_{m1}$ or $\$_{m2}$. Therefore, all revolute axes must be parallel to the XY plane in the initial configuration and the limb kinematic chain contains no spherical pairs.

However, the limb constraint couple is perpendicular to the plane formed by $\$_{m1}$ and $\$_{m2}$. Every limb has such a plane determining the direction of the constraint couple. These planes must always be parallel to each other to guarantee that the constraint couples are in the same direction. To meet this condition, the axes of revolute pairs most adjacent to the base in all limbs must be set parallel, and so must be the axes of the revolute pairs most adjacent to the moving platform.

9.5.2.3 Generation of PMs

Accordingly, the limb kinematic chain can be obtained by the linear transformation of the five twists in Eq. (9.9). The enumeration of such PMs is shown in Table 9.5, in which $2 \leq n \leq 5$. Considering a ${}^xR^uP^xR^yR^yR$ limb where ${}^xR^yR$ can form a universal joint ${}^{xy}U_N$, Fig. 9.3 shows such a 5-DOF $5-{}^xR^uP^{xy}U_N^yR$ PM. The universal joint plane in the i th limb is denoted by U_{34} , which is parallel to the base plane in the initial configuration. The geometrical arrangement of the five limbs guarantees that the five universal joint planes are always parallel.

In this initial configuration, such a single ${}^xR^uP^{xy}U_N^yR$ limb exerts a constraint couple as the one in Eq. (9.10) on the moving platform, and restricts the rotation about the normal of U_{34} . Because the five constraint couples are parallel, they are linearly dependent and form a single system. The platform constraint system is still the same as that in Eq. (9.10).

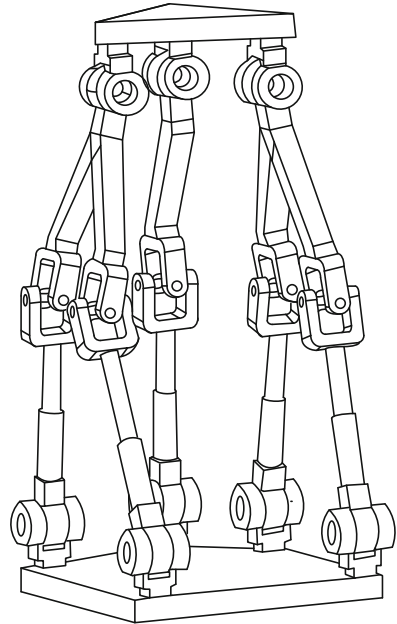
After the moving platform undergoes arbitrary translation or rotation about the y_i axis, the limb twist system remains unchanged, and the plane of U_{34} is always parallel to the base plane. The platform constraint system remains the same as that in Eq. (9.10).

After the moving platform undergoes arbitrary finite rotation about the x_i axis, the limb twist system becomes

Table 9.5 Symmetrical 5-DOF PMs

With no or one prismatic pair	With two prismatic pairs
$n-xR^xR^xR^yR^yR$	$n-uP^uP^vR^xR^yR$
$n-uP^xR^xR^yR^yR$	$n-uP^uP^xR^yR^yR$
$n-xR^uP^xR^yR^yR \dots$	$n-xR^uP^uP^yR^yR \dots$
$n-xR^xR^uR^yP^yR$	$n-uP^vR^uP^yR^yR$
$n-xR^xR^yR^uP^yR$	$n-xR^uP^yR^uP^yR$

Fig. 9.3 $5-xR^uP^{xy}U_N^yR$ PM



$$\begin{aligned}
 \mathcal{S}_{i1} &= (1 \ 0 \ 0 ; \ 0 \ 0 \ 0) \\
 \mathcal{S}_{i2} &= (0 \ 0 \ 0 ; \ 0 \ m_2 \ n_2) \\
 \mathcal{S}_{i3} &= (1 \ 0 \ 0 ; \ 0 \ b_3 \ c_3) \\
 \mathcal{S}_{i4} &= (0 \ m_4 \ n_4 ; \ a_4 \ b_4 \ c_4) \\
 \mathcal{S}_{i5} &= (0 \ m_4 \ n_4 ; \ a_5 \ b_5 \ c_5)
 \end{aligned} \tag{9.11}$$

The limb constraint system becomes

$$\mathcal{S}_{i1}^r = (0 \ 0 \ 0 ; \ 0 \ -n_4 \ m_4) \tag{9.12}$$

\mathcal{S}_{i1}^r denotes a constraint couple perpendicular to U_{34} . Since all five universal joint planes of U_{34} are parallel, the five limb constraint couples are parallel and linearly dependent, thereby equaling one couple, namely, \mathcal{S}_{i1}^r .

In brief, the platform constraint system of the $5\text{-}^x\text{R}^u\text{P}^{xy}\text{U}_N^y\text{R}$ PM only contains one constraint couple along the normal of the plane of U_{34} . Hence, the mechanism loses a rotational DOF about the normal of U_{34} , and has three translational DOFs as well as two rotational DOFs. From the above analysis, the platform constraint system remains unchanged after any finite non-singular displacement. Hence, the mechanism is not instantaneous.

9.5.3 Type Synthesis of 1R3T 4-DOF PMs

9.5.3.1 Constraint Synthesis

For simplicity, focus is given on the 4-DOF PM with three translational DOF and one rotational DOF about the Z axis, denoted by $3\text{T}1\text{R}^z$. The standard base of the platform twist system is given by

$$\begin{aligned} \$_{m1} &= (0 \ 0 \ 1 ; \ 0 \ 0 \ 0) \\ \$_{m2} &= (0 \ 0 \ 0 ; \ 1 \ 0 \ 0) \\ \$_{m3} &= (0 \ 0 \ 0 ; \ 0 \ 1 \ 0) \\ \$_{m4} &= (0 \ 0 \ 0 ; \ 0 \ 0 \ 1) \end{aligned} \quad (9.13)$$

The standard base of the platform constraint system is given by

$$\begin{aligned} \$_{m1}^r &= (0 \ 0 \ 0 ; \ 1 \ 0 \ 0) \\ \$_{m2}^r &= (0 \ 0 \ 0 ; \ 0 \ 1 \ 0) \end{aligned} \quad (9.14)$$

Case 1. *The limb kinematic chain consists of four kinematic pairs and exerts two constraint couples on the moving platform.*

In this case, the standard base of the limb twist system is the same as Eq. (9.14). The limb kinematic chain can be obtained by the linear transformation of the four twists.

Only two prismatic pairs, $\$_{m2}$ and $\$_{m3}$, can be transformed into revolute pairs by the linear transformation with $\$_{m1}$, thereby producing two revolute pairs in the z_i axis direction.

Case 2. *The limb kinematic chain consists of five kinematic pairs and exerts one constraint couple on the moving platform.*

In this case, the limb kinematic chain only exerts one constraint couple on the moving platform. One twist, $\$_{i5} = (1 \ 0 \ 0 ; \ 0 \ 0 \ 0)$, must be added to Eq. (9.13) to eliminate one corresponding constraint. The new limb twist system becomes

$$\begin{aligned}
 \mathcal{S}_{i1} &= (0 \ 0 \ 1; \ 0 \ 0 \ 0) \\
 \mathcal{S}_{i2} &= (0 \ 0 \ 0; \ 1 \ 0 \ 0) \\
 \mathcal{S}_{i3} &= (0 \ 0 \ 0; \ 0 \ 1 \ 0) \\
 \mathcal{S}_{i4} &= (0 \ 0 \ 0; \ 0 \ 0 \ 1) \\
 \mathcal{S}_{i5} &= (1 \ 0 \ 0; \ 0 \ 0 \ 0)
 \end{aligned}
 \tag{9.15}$$

The limb constraint system reciprocal to Eq. (9.15) is

$$\mathcal{S}_{i1}^r = (0 \ 0 \ 0; \ 0 \ 1 \ 0)
 \tag{9.16}$$

which is a constraint couple on the y_i axis. Therefore, all limb constraint couples are parallel to the XY plane.

9.5.3.2 Generation of Limb Chains

\mathcal{S}_{i2} , \mathcal{S}_{i3} , and \mathcal{S}_{i4} can be transformed into revolute pairs by the linear transformation with \mathcal{S}_{i1} or \mathcal{S}_{i5} . Hence, the revolute pairs fall into two groups, namely, those with axes parallel and perpendicular to the base plane. To prevent the mechanism from being instantaneous, the axes of revolute pairs fixed to the base or the moving platform must be perpendicular to the base.

\mathcal{S}_{i1}^r is a couple that is actually perpendicular to the plane formed by \mathcal{S}_{i1} and \mathcal{S}_{i5} , namely, the $x_i z_i$ plane. Given that all z_i axes of the four limbs are parallel, the four x_i axes of the local systems must not be parallel to one another. Hence, the revolute axes parallel to the base plane in each limb must not be parallel to one another.

9.5.3.3 Generation of PMs

The details of the 3TIR^z4-DOF PMs are shown in Table 9.6, where g/p denotes the number of kinematic pairs in a limb, and $2 \leq n \leq 4$. Figure 9.4 shows a 4-zxU_N^u P^{xz}U_M PM.

9.5.4 Type Synthesis of 3R1T 4-DOF PMs

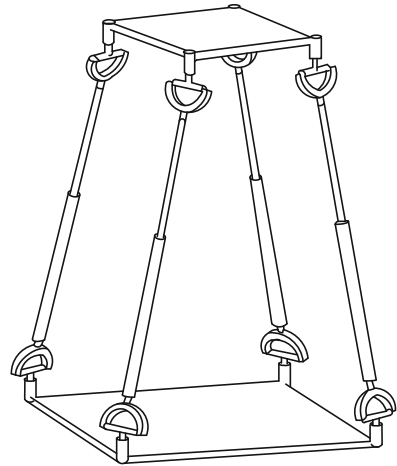
9.5.4.1 Constraint Synthesis

For simplicity, focus is given on the 4-DOF PM with three rotational DOFs and one translational DOF along the Z axis, which is denoted by 3R1T^z. The standard base of the platform twist system is given by

Table 9.6 Symmetrical 4-DOF PMs

g/p	PMs		
4	$n^{-z}R^iP^jP^kP$	$n^{-i}P^zR^jP^kP$	$n^{-z}R^iP^zR^zR$
	$n^{-z}R^zR^iP^jP$	$n^{-z}R^iP^zR^jP$	$n^{-i}P^jP^zR^kP$
	$n^{-i}P^zR^zR^jP$	$n^{-z}R^zR^jP^zR$	$n^{-z}R^iP^jP^zR$
	$n^{-i}P^zR^zR^zR$		
5	$n^{-z}R^zR^zR^xR^xR$	$n^{-x}R^xR^zR^zR^uP$	
	$n^{-x}R^xR^xR^zR^zR$	$n^{-u}P^zR^xR^xR^xR$	
	$n^{-z}R^xR^xR^xR^zR$	$n^{-z}R^uP^xR^xR^xR$	
	$n^{-u}P^zR^zR^xR^xR$	$n^{-u}P^xR^zR^zR^zR$	
	$n^{-z}R^zR^uP^xR^xR$	$n^{-x}R^uP^zR^zR^zR$	
	$n^{-z}R^zR^xR^xR^uP$	$n^{-u}P^xR^xR^xR^zR$	
	$n^{-u}P^xR^xR^zR^zR$	$n^{-x}R^xR^uP^zR$	
	$n^{-x}R^xR^uP^zR^zR$	$n^{-u}P^zR^zR^zR^xR$	
	$n^{-z}R^xR^uP^xR^zR$	$n^{-z}R^zR^zR^uP^xR$	
	$n^{-z}R^uP^zR^xR^xR$	
		$n^{-x}R^uP^xR^zR^zR$	
		

Fig. 9.4 $4^{-zx}U_N^uP^xU_M$



$$\begin{aligned}
 \mathcal{S}_{m1} &= (1 \ 0 \ 0; \ 0 \ 0 \ 0) \\
 \mathcal{S}_{m2} &= (0 \ 1 \ 0; \ 0 \ 0 \ 0) \\
 \mathcal{S}_{m3} &= (0 \ 0 \ 1; \ 0 \ 0 \ 0) \\
 \mathcal{S}_{m4} &= (0 \ 0 \ 0; \ 0 \ 0 \ 1)
 \end{aligned}
 \tag{9.17}$$

The standard base of the platform constraint system is given by

$$\begin{aligned}
 \mathcal{S}_{m1}^r &= (1 \ 0 \ 0; \ 0 \ 0 \ 0) \\
 \mathcal{S}_{m2}^r &= (0 \ 1 \ 0; \ 0 \ 0 \ 0)
 \end{aligned}
 \tag{9.18}$$

Case 1. *The limb kinematic chain consists of four kinematic pairs and exerts two constraint forces on the moving platform.*

In this case, the standard base of the limb twist system is the same as Eq. (9.17). The linear transformations of $\$_{m1}$, $\$_{m2}$, and $\$_{m3}$ can only produce a 3R spherical subchain. The three limb central points must coincide with one another.

Case 2. *The limb kinematic chain consists of five kinematic pairs and exerts one constraint force on the moving platform.*

In this case, adding the twist $\$_{i5} = (0 \ 0 \ 0; 0 \ 1 \ 0)$ to Eq. (9.17) yields a new limb twist system:

$$\begin{aligned}
 \$_{i1} &= (1 \ 0 \ 0; \ 0 \ 0 \ 0) \\
 \$_{i2} &= (0 \ 1 \ 0; \ 0 \ 0 \ 0) \\
 \$_{i3} &= (0 \ 0 \ 1; \ 0 \ 0 \ 0) \\
 \$_{i4} &= (0 \ 0 \ 0; \ 0 \ 0 \ 1) \\
 \$_{i5} &= (0 \ 0 \ 0; \ 0 \ 1 \ 0)
 \end{aligned}
 \tag{9.19}$$

The limb constraint system reciprocal to Eq. (9.19) is

$$\$_{i1}^r = (1 \ 0 \ 0; \ 0 \ 0 \ 0)
 \tag{9.20}$$

which is a constraint force in the x_i direction, passing through the limb central point.

9.5.4.2 Generation of Limb Chains

Similar to the 3R2T^{xy} PMs, the limb kinematic chain must include a 2R or 3R spherical subchain. The revolute axes except those in the 2R or 3R subchain must be parallel to the base plane. The linear transformations of $\$_{i4}$ and $\$_{i5}$ with themselves only lead to a prismatic pair in the yz plane. Therefore, if the limb contains prismatic pairs, they must be perpendicular to $\$_{i1}$.

The limb constraint is a force parallel to the revolute axes outside the spherical subchain, passing through the limb central point. When all the limb constraint forces are coplanar and pass through a common point, they form a desired dual system, as shown in Eq. (9.18).

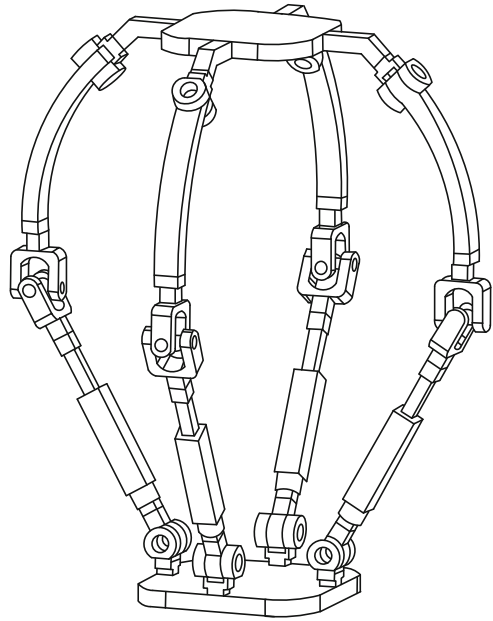
9.5.4.3 Generation of PMs

The enumeration of such 4-DOF PMs is shown in Table 9.7, in which $2 \leq n \leq 4$. Actually, the $4\text{-}^xR^xR(^iR^jR^kR)_N$ PM has first been proposed by [25]. Figure 9.5 shows a $4\text{-}^xR^uP^xiU_N^jR_N$ PM.

Table 9.7 Symmetrical 4-DOF PMs

g/p	PMs	
4	$n-zP(iR^jR^kR)_N$	
5	$n-xR^xR^xR(iR^jR)_N$	$n-xR^xR(iR^jR^kR)_N$
	$n-uP^xR^xR(iR^jR)_N$	$n-xR^uP^xR(iR^jR)_N$
	$n-xP^xR^uR(iR^jR)_N$	$n-uR^xP(iR^jR^kR)_N$
	$n-xR^uP(xR^uR^kR)_N$	

Fig. 9.5 $4-xR^uP^xiU_N^jR_N$



9.5.5 Type Synthesis of 2R2T 4-DOF PMs

9.5.5.1 Constraint Synthesis

The moving platform of a 2R2T PM loses one rotational DOF and one translational DOF because a constraint couple and a constraint force act on the moving platform. Obviously, the platform constraint system of a 2R2T PM consists of a constraint couple and a constraint force, or two parallel constraint forces.

Without loss of generality, focus is given on the $2R^{zy}2T^{xy}$ 4-DOF PMs, where $2R^{zy}$ denotes two rotations around the Z and Y axes, and $2T^{xy}$ denotes two translations along the X and Y axes, respectively. The moving platform is constrained by a force along the Z axis and a couple along the X axis. Hence, the mechanism constraint-wrench system of the $2R^{zy}2T^{xy}$ 4-DOF PM is given by

$$\begin{aligned}
 \mathcal{S}_{m1}^r &= (0 \ 0 \ 1; \ 0 \ 0 \ 0) \\
 \mathcal{S}_{m2}^r &= (0 \ 0 \ 0; \ 1 \ 0 \ 0)
 \end{aligned}
 \tag{9.21}$$

Suppose that the $2R^{zy}2T^{xy}$ 4-DOF PM is symmetrical and consists of four identical limb kinematic chains, the constraint must then be a force. These limbs exert the same constraints on the moving platform. When the limb kinematic chain has five DOFs, it exerts one constraint on the moving platform. Because the combination of four couples of four limbs yields only couples and restricts no translation, the constraint of the limb to the moving platform must be a force.

If each limb exerts a constraint force on the moving platform, there are a total of four constraint forces acting on the moving platform. The four limbs can be arranged following some structural geometrical conditions that classify the four forces into two groups, and the two forces in each group are coaxial. Consequently, two parallel forces that supply the desired constraint effect can be obtained. Hence, the limb constraint-wrench system of a $2R^{zy}2T^{xy}$ 4-DOF PM is given by

$$\mathcal{S}'_{i1} = (0 \ 0 \ 1; \ 0 \ 0 \ 0) \quad (9.22)$$

which is a constraint force being coaxial with the z_i axis.

9.5.5.2 Generation of Limb Chains

Using the reciprocity between twist and wrench, the limb twist system reciprocal to \mathcal{S}'_{i1} can be obtained as follows:

$$\begin{aligned} \mathcal{S}_{i1} &= (1 \ 0 \ 0; \ 0 \ 0 \ 0) \\ \mathcal{S}_{i2} &= (0 \ 1 \ 0; \ 0 \ 0 \ 0) \\ \mathcal{S}_{i3} &= (0 \ 0 \ 1; \ 0 \ 0 \ 0) \\ \mathcal{S}_{i4} &= (0 \ 0 \ 0; \ 1 \ 0 \ 0) \\ \mathcal{S}_{i5} &= (0 \ 0 \ 0; \ 0 \ 1 \ 0) \end{aligned} \quad (9.23)$$

The linear transformation of the above five twists can yield different limb chain structures. The linear transformation of the five twists must keep the linear independency among them. With further inspection, more structural geometrical conditions of the limb chain can be found.

A. Existence of a 2R or 3R spherical subchain and a limb central point

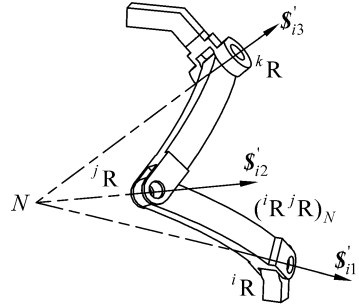
The limb kinematic chain of the $2R^{zy}2T^{xy}$ 4-DOF PM must contain a 2R or 3R spherical subchain. To avoid the presence of helical pairs, \mathcal{S}_{i1} can be linearly combined with \mathcal{S}_{i2} and \mathcal{S}_{i3} . The linear transformation yields

$$\mathcal{S}'_{i1} = (l_{i1} \ m_{i1} \ n_{i1}; \ 0 \ 0 \ 0) \quad (9.24)$$

Similarly, \mathcal{S}_{i2} can be linearly combined with \mathcal{S}_{i1} and \mathcal{S}_{i3} . The linear transformation yields

$$\mathcal{S}'_{i2} = (l_{i2} \ m_{i2} \ n_{i2}; \ 0 \ 0 \ 0) \quad (9.25)$$

Fig. 9.6 2R and 3R spherical subchain



$\$'_{i1}$ and $\$'_{i2}$ represent two revolute pairs with axes intersecting at a common point. The two pairs form a 2R spherical subchain denoted by $({}^iR^jR)_N$, as shown in Fig. 9.6. $\$'_{i3}$ can also be transformed into a revolute pair whose axis passes the limb central point by the linear transformation with $\$'_{i1}$ and $\$'_{i2}$, namely,

$$\$'_{i3} = (l_{i3} \quad m_{i3} \quad n_{i3}; \quad 0 \quad 0 \quad 0) \quad (9.26)$$

The group of $\$'_{i1} - \$'_{i2} - \$'_{i3}$ represents a 3R spherical subchain, $({}^iR^jR^k)_N$, as shown in Fig. 9.6.

B. Arrangement of Prismatic pairs

The prismatic pair in the $2R^z2T^{xy}$ 4-DOF PM must be parallel to the XY plane. $\$_{i4}$ denotes a prismatic pair along the x_i axis, and $\$_{i5}$ denotes a prismatic pair along the y_i axis. The linear transformations of $\$_{i4}$ and $\$_{i5}$ produce a twist in the form of $(0 \quad 0 \quad 0; \quad l_i \quad m_i \quad 0)$, which represents a prismatic pair parallel to the XY plane.

C. Arrangement of revolute pairs not included in the 2R or 3R subchain

By the appropriate linear transformations, a prismatic pair can be transformed into a revolute pair. For instance, the prismatic pair $\$_{i4}$ can be transformed into a revolute pair $\$'_{i4}$ by the linear transformation with $\$_{i3}$ and $\$_{i5}$,

$$\$'_{i4} = (0 \quad 0 \quad 1; \quad a_{i4} \quad b_{i4} \quad 0) \quad (9.27)$$

which represents a revolute pair whose axis is parallel to the z_i axis and passes through any point. The prismatic pair $\$_{i5}$ can be transformed into a revolute pair, $\$'_{i5}$, by the linear transformation with $\$_{i3}$ and $\$_{i4}$,

$$\$'_{i5} = (0 \quad 0 \quad 1; \quad a'_{i5} \quad b'_{i5} \quad 0) \quad (9.28)$$

which represents a revolute pair whose axis is parallel to the z_i axis and passes through any point.

$\$_{i3}$ represents a revolute pair whose axis is parallel to the z_i axis and passes through the origin of the limb frame. However, $\$_{i3}$ can be transformed into a revolute pair whose axis passes through any point by the linear transformation with $\$_{i4}$ and $\$_{i5}$,

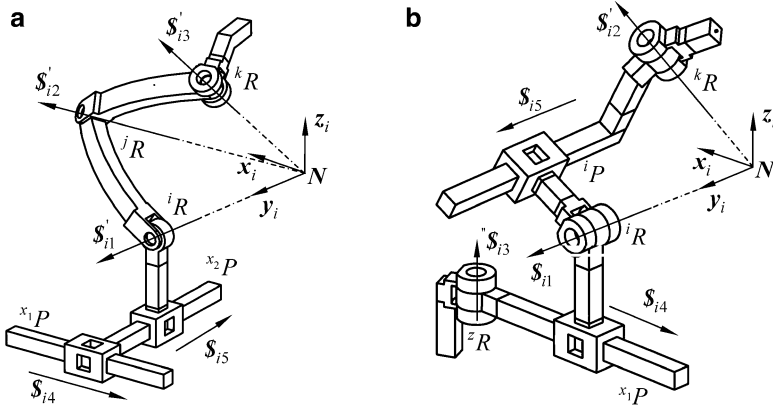


Fig. 9.7 Two limb chains with only R and P pairs (a) $x_1P^x_2P(iR^jR^kR)_N$ (b) $zR^x_1P(x_2R^x_2P^kR)_N$

$$\mathcal{S}''_{i3} = (0 \ 0 \ 1; \ a_{i3} \ b_{i3} \ 0) \tag{9.29}$$

The axes of the revolute pairs not included in the 2R or 3R spherical subchain must be perpendicular to the base. For example, if \mathcal{S}'_{i4} is placed next to \mathcal{S}'_{i5} , they form a 2R parallel subchain ${}^zR^zR$; if $\mathcal{S}''_{i3}, \mathcal{S}'_{i4}$, and \mathcal{S}'_{i5} are placed in succession, they form a 3R parallel subchain ${}^zR^zR^zR$.

A. Limb chains only with R and P pairs

Based on the above analyses, the limb kinematic chains of the $2R^zY2T^{xy}$ 4-DOF PM can be enumerated by the linear transformation of the five twists, as shown in Eq. (9.23). For example, five pairs are placed in the sequence of $\mathcal{S}_{i4} - \mathcal{S}_{i5} - \mathcal{S}'_{i1} - \mathcal{S}'_{i2} - \mathcal{S}'_{i3}$ and are connected by links. A $x_1P^x_2P(iR^jR^kR)_N$ limb chain can then be obtained, as shown in Fig. 9.7a.

Another example is the $zR^x_1P(x_2R^x_2P^kR)_N$ limb chain, as shown in Fig. 9.7b. First, \mathcal{S}_{i3} can be transformed into a revolute pair \mathcal{S}''_{i3} by the linear transformation with \mathcal{S}_{i4} and \mathcal{S}_{i5} , as described by Eq. (9.28), whose axis passes through any point. The five pairs are then placed in the sequence of $\mathcal{S}''_{i3} - \mathcal{S}_{i4} - \mathcal{S}_{i1} - \mathcal{S}_{i5} - \mathcal{S}'_{i2}$ and connected by links.

B. Limb chains with U joints

Two-DOF kinematic joints, such as cylindrical pairs and universal joints, can also be employed using some appropriate combinations. If in a serial arrangement of two revolute pairs and the axes intersect at a point with a right angle, the sequence of two R pairs constructs can then be named a universal joint.

For example, any two of the three revolute pairs $\mathcal{S}_{i1}, \mathcal{S}_{i2}$, and \mathcal{S}_{i3} can yield a U joint. The central point of the U joint is also the limb central joint. However, the limb central joint cannot coincide with each other, which disobeys the structural condition of the $2R^zY2T^{xy}$ 4-DOF PM. Hence, such a generation of U joints can not be used for constructing a $2R^zY2T^{xy}$ 4-DOF PM.

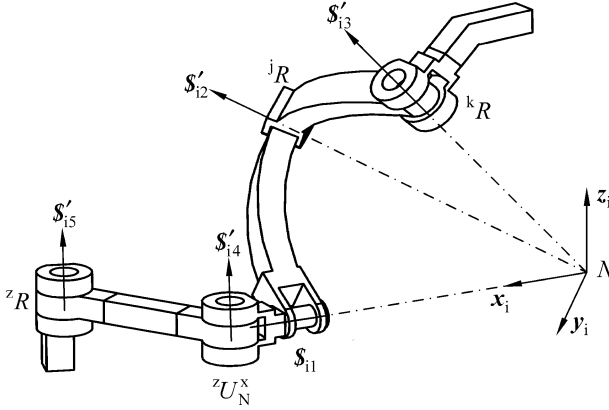


Fig. 9.8 ${}^zR^zU_N^x({}^jR^kR)_N$ limb chain

\mathcal{S}_{i4} and \mathcal{S}_{i5} can also be respectively transformed into revolute pairs \mathcal{S}'_{i4} and \mathcal{S}'_{i5} , which are perpendicular to the base. Hence, \mathcal{S}_{i1} and \mathcal{S}'_{i4} can be used to form a U joint. \mathcal{S}'_{i2} and \mathcal{S}'_{i3} can further form a 2R spherical subchain. Arranging the five pairs in a new sequence of $\mathcal{S}'_{i5} - \mathcal{S}'_{i4} - \mathcal{S}_{i1} - \mathcal{S}'_{i2} - \mathcal{S}'_{i3}$ can yield a ${}^zR^zU_N^x({}^jR^kR)_N$ limb chain (Fig. 9.8).

C. Limb chains with a C pair

A cylindrical pair is the kinematic equivalent of a revolute pair and a prismatic pair coincident to the revolute axis. Because the prismatic pair in a $2R^{zy}2T^{xy}$ 4-DOF PM must be parallel to the base, the C pair must also be parallel to the base. For instance, \mathcal{S}'_{i2} and \mathcal{S}'_{i3} can be used to form a 2R spherical subchain. \mathcal{S}_{i1} and \mathcal{S}_{i4} can then be used to construct a C pair. Arranging the five pairs in the new sequence of $\mathcal{S}'_{i5} - \mathcal{S}'_{i4} - \mathcal{S}_{i1} - \mathcal{S}'_{i2} - \mathcal{S}'_{i3}$ yields a ${}^zR^xC_N({}^jR^kR)_N$ limb chain, as shown in Fig. 9.9.

Based on the above analysis, 30 limb kinematic chains can be enumerated by the linear transformation of the five twists in Eq. (9.23), as listed in Table 9.8.

9.5.5.3 Generation of PMs

Following the structural condition presented in Table 9.3, the limb kinematic chains listed in Table 9.8 can be used to construct various $2R^{zy}2T^{xy}$ 4-DOF PMs. For example, four ${}^zR^zR({}^jR^jR^kR)_N$ limbs can be used to construct a $2R^{zy}2T^{xy}$ 4-DOF PM. The four ${}^zR^zR({}^jR^jR^kR)_N$ limbs can be divided into two groups. In each group, the two limb central points are coincident with each other. When the limbs are connected to the base and moving platform, the two central points of the two groups of limb chains must not be coincident with each other. The $4-{}^zR^zR({}^jR^jR^kR)_N$ 4-DOF PM is depicted in Fig. 9.10. Thirty symmetrical $2R^{zy}2T^{xy}$ 4-DOF PMs can be constructed. Non-symmetrical $2R^{zy}2T^{xy}$ 4-DOF PMs can also be constructed using different limb kinematic chains listed in Table 9.8.

Fig. 9.9 ${}^zR^xC_N({}^jR^kR)_N$ limb chain

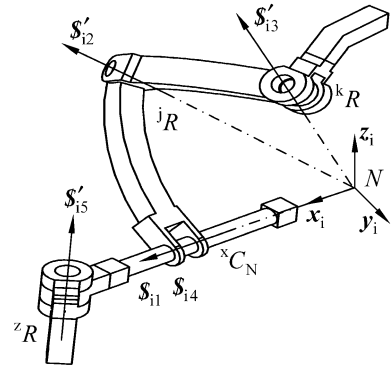


Table 9.8 Limb kinematic chains for $2R^{zy}2T^{xy}$ 4-DOF PM

Type	Limb kinematic chains			
1 Containing only R and P pairs	${}^yP^xP({}^jR^kR)_N$	${}^yP^yR_N^xP({}^jR^kR)_N$	${}^zR^yP^zR({}^jR^kR)_N$	${}^zR^xR_N^xP({}^jR^kR)_N$
	${}^yR^yP^zP({}^jR^kR)_N$	${}^zR^yP^yR_N^xP^kR_N$	${}^yP^zR^zR({}^jR^kR)_N$	${}^zR^zR_N^xP^kR_N$
	${}^zR^yP^yP({}^jR^kR)_N$	${}^yP^zR^xR_N^xP^kR_N$	${}^zR^xP({}^xR^jR^kR)_N$	${}^zR^zR^x({}^xR^jR^kR)_N$
	${}^yP^zR^xP({}^jR^kR)_N$	${}^zR^zR^yP({}^jR^kR)_N$	${}^yP^zR({}^xR^jR^kR)_N$	${}^zR^zR({}^xR^jR^kR)_N$
2 Containing a U joint	${}^zR^zU^x_N({}^jR^kR)_N$	${}^yP^zR^zU^x_NR_N$	${}^zR^zU^x_NP^kR_N$	
	${}^zR^zR^zU^x_NR_N$	${}^yP^zU^x_N({}^jR^kR)_N$	${}^zR^zU^x_NP^kR_N$	
	${}^zR^yP^zU^x_NR_N$	${}^xP^yP^zU^x_NR_N$	${}^zU^x_NP({}^jR^kR)_N$	
3 Containing a C joint	${}^yP^xC_N({}^jR^kR)_N$	${}^zR^yP({}^xC^kR)_N$	${}^yP^zR({}^xC^kR)_N$	
	${}^zR^xC_N({}^jR^kR)_N$	${}^zR^zR({}^xC^kR)_N$		

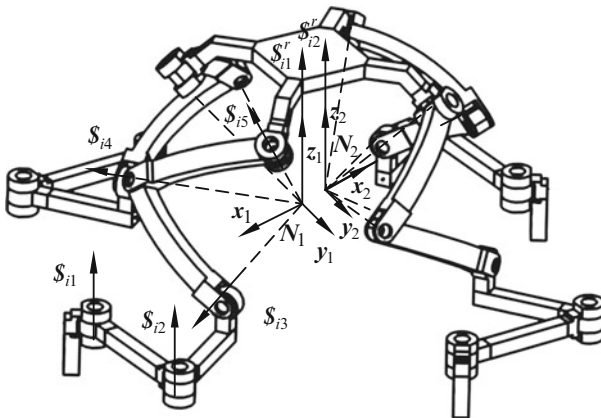


Fig. 9.10 $4\text{-}{}^zR^2R({}^jR^kR)_N$ PM

9.5.6 Type Synthesis of a 2R1T 3-DOF PM

9.5.6.1 Constraint Synthesis

In this case, the platform constraint system must contain one couple and two forces. For simplicity, focus is given on the 3-DOF PM with two rotational DOF in the XY plane and one translational DOF along the Z axis, denoted by 2R1T^z. The standard base of the platform twist system is given by

$$\begin{aligned} \$_{m1} &= (1 \ 0 \ 0; \ 0 \ 0 \ 0) \\ \$_{m2} &= (0 \ 1 \ 0; \ 0 \ 0 \ 0) \\ \$_{m3} &= (0 \ 0 \ 0; \ 0 \ 0 \ 1) \end{aligned} \quad (9.30)$$

The standard base of the platform constraint system is given by

$$\begin{aligned} \$_{m1}^r &= (1 \ 0 \ 0; \ 0 \ 0 \ 0) \\ \$_{m2}^r &= (0 \ 1 \ 0; \ 0 \ 0 \ 0) \\ \$_{m3}^r &= (0 \ 0 \ 0; \ 0 \ 0 \ 1) \end{aligned} \quad (9.31)$$

When the limb kinematic chain consists of five kinematic pairs, it only exerts one constraint to the moving platform. If the constraint is a couple, no translation can be constrained. So the constraint must be a force, and the combined effect of all $p \cdot q$ forces must equal one couple not parallel to the XY plane as well as two forces parallel to the XY plane. Therefore, the constraint force is

$$\$_{i1}^r = (1 \ 0 \ 0; \ 0 \ 0 \ 0) \quad (9.32)$$

9.5.6.2 Generation of Limb Chains

The limb twist system reciprocal to $\$_{i1}^r$ is given by

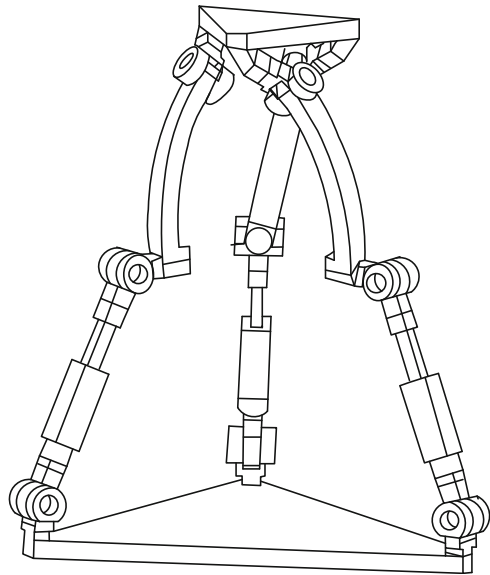
$$\begin{aligned} \$_{i1} &= (1 \ 0 \ 0; \ 0 \ 0 \ 0) \\ \$_{i2} &= (0 \ 1 \ 0; \ 0 \ 0 \ 0) \\ \$_{i3} &= (0 \ 0 \ 1; \ 0 \ 0 \ 0) \\ \$_{i4} &= (0 \ 0 \ 0; \ 0 \ 1 \ 0) \\ \$_{i5} &= (0 \ 0 \ 0; \ 0 \ 0 \ 1) \end{aligned} \quad (9.33)$$

Equation (9.33) is the same as Eq. (9.23). The limb chains generated from Eq. (9.23) can be used in this case.

Table 9.9 Enumeration of 3-DOF PMs formed with a 5-DOF limb

With one prismatic pair	$3-xR^uP(iR^jR^kR)_N$ $3-uP^xR(iR^jR^kR)_{N^3}$	$3-uP^xR^xR(iR^kR)_N$	$3-xR^xR^uP(iR^kR)_N$	$3-xR^uP^xR(iR^kR)_{N^3}$
Without a prismatic pair	$3-xR^xR^xR(iR^kR)_{N^3}$	$3-xR^xR(iR^jR^kR)_{N^3}$		
With a cylindrical pair	$3-xR^{u_1}P^kR_{N^3}^{u_2}C_{N^3}$ $3-xR^uC_{N^3}(iR^kR)_{N^3}$ $3-xR^xR^{u_2}C_{N^3}^kR_{N^3}$ $3-uC_{N^3}^kR_{N^3}^xR^xR$	$3-xR^{u_1}P^{u_2}C_{N^3}^kR_{N^3}$ $3-xR^xR^kR_{N^3}^uC_{N^3}$ $3-kR_{N^3}^{u_1}C_{N^3}^xR^{u_2}P$	$3-xR(iR^kR)_{N^3}^uC_{N^3}$ $3-kR_{N^3}^uC_{N^3}^xR^xR$ $3-kR_{N^3}^{u_1}C_{N^3}^{u_2}P^xR$	
With a spherical joint	$3-u_1P^{u_2}PS_{N^3}$	$3-xR^uPS_{N^3}$ [40]	$3-uP^xRS_{N^3}$	$3-xR^xRS_{N^3}$
With a universal joint	$3-xU_{N^3}^j(iR^kR)_{N^3}^uP$ $3-xR^xU_{N^3}^j(iR^kR)_{N^3}$ $3-xU_{N^3}^jkR_{N^3}^uP^xR$	$3-uP^xU_{N^3}^j(iR^kR)_{N^3}$ $3-xU_{N^3}^jkR_{N^3}^xR^uP$ $3-xR^uP^xU_{N^3}^jkR_{N^3}$	$3-xU_{N^3}^j(iR^kR)_{N^3}^xR$ $3-uP^xR^xU_{N^3}^jkR_{N^3}$ $3-xR^xR^xU_{N^3}^jkR_{N^3}$	

Fig. 9.11 $3-xR^uP^xR(iR^jR)_N$



9.5.6.3 Generation of PMs

The limb chains in Table 9.8 generate a constraint force parallel to $\$_{i1}$ and passing the limb central point. To meet the requirements, the three limb central points can be set not to coincide with one another, and the revolute axis of $\$_{i1}$ can be set not to be parallel. Considering that the limb central points are not coincident, spherical joints can be used, for example, a 3-PRS PM. The architectures of PMs in this category are enumerated in Table 9.9.

Figure 9.11 shows such a 3-DOF $3-xR^uP^xR(iR^jR)_N$ PM. The three limb central points form a triangle, ABC , which is fixed relative to the moving platform. In the initial configuration, as shown in Fig. 9.11, the triangle ABC is parallel to the moving platform plane.

Each limb constraint force is parallel to the first revolute axis and passes through the corresponding limb central point. Obviously, the three forces must not intersect at a common point, and at the origin configuration, the three limb constraint forces lie in the triangle ABC . Therefore, the standard base of the platform constraint system is the same one as Eq. (9.31). The moving platform loses two translational DOF in the base plane and one rotational DOF about the normal of the base plane. Similarly, this mechanism can be confirmed as not instantaneous.

9.5.7 Type Synthesis of a 3T 3-DOF PM

9.5.7.1 Constraint Synthesis

The standard base of the platform twist system is

$$\begin{aligned} \mathcal{S}_{m1} &= (0 \ 0 \ 0; \ 1 \ 0 \ 0) \\ \mathcal{S}_{m2} &= (0 \ 0 \ 0; \ 0 \ 1 \ 0) \\ \mathcal{S}_{m3} &= (0 \ 0 \ 0; \ 0 \ 0 \ 1) \end{aligned} \quad (9.34)$$

The standard base of the platform constraint system is

$$\begin{aligned} \mathcal{S}_{m1}^r &= (0 \ 0 \ 0; \ 1 \ 0 \ 0) \\ \mathcal{S}_{m2}^r &= (0 \ 0 \ 0; \ 0 \ 1 \ 0) \\ \mathcal{S}_{m3}^r &= (0 \ 0 \ 0; \ 0 \ 0 \ 1) \end{aligned} \quad (9.35)$$

To form such a platform constraint system, the limb constraint system only contains couples, and all the limb constraint couples must be non-coplanar. The limb constraint system can contain three, two, or one constraint couple/s.

9.5.7.2 Generation of Translational PMs with 3-DOF Limb Chains

When the mobility of the limb chain is three, the limb imposes three constraint couples on the moving platform. Hence, the platform constraint system is the same as the limb constraint system given by Eq. (9.35). The limb twist system is also the same as the platform twist system given by Eq. (9.34). The three twists in Eq. (9.34) represent three linearly independent prismatic pairs, and form a PPP limb chain. Consequently, 3-PPP translational PM can be constructed.

Table 9.10 Enumeration of 4-DOF limb for a 3-DOF translational PM

Limb chain with two prismatic pairs	${}^uP^u_2P^xR^xR^xR^xR^u_1P^xR^u_2P^u_1P^xR^xR^u_2P$
	${}^uP^xR^xR^xR^xR^xR^uP^xR^uP^xR^xR$
Limb chain with one prismatic pair	${}^uP^xC^xR^uP^xR^xC^xC^uP^xR$
	${}^xR^xC^xR^xR^xR^xC$

9.5.7.3 Generation of Translational PMs with 4-DOF Limb Chains

When the mobility of the limb chain is four, the limb exerts two constraint couples on the moving platform. Without losing generality, the limb constraint system is assumed to consist of two constraint couples. One couple is along the y_i axis, and the other is along the z_i axis:

$$\begin{aligned} \mathcal{S}'_{i1} &= (0 \ 0 \ 0; \ 0 \ 1 \ 0) \\ \mathcal{S}'_{i2} &= (0 \ 0 \ 0; \ 0 \ 0 \ 1) \end{aligned}$$

The limb twist system reciprocal to the two couples is

$$\begin{aligned} \mathcal{S}_{i1} &= (1 \ 0 \ 0; \ 0 \ 0 \ 0) \\ \mathcal{S}_{i2} &= (0 \ 0 \ 0; \ 1 \ 0 \ 0) \\ \mathcal{S}_{i3} &= (0 \ 0 \ 0; \ 0 \ 1 \ 0) \\ \mathcal{S}_{i4} &= (0 \ 0 \ 0; \ 0 \ 0 \ 1) \end{aligned} \tag{9.36}$$

From Eq. (9.36), \mathcal{S}_{i3} can be transformed into a revolute pair by the linear transformation of \mathcal{S}_{i1} and \mathcal{S}_{i4} ; \mathcal{S}_{i4} can be transformed into a revolute pair by the linear transformation of \mathcal{S}_{i1} and \mathcal{S}_{i3} :

$$\begin{aligned} \mathcal{S}'_{i3} &= (1 \ 0 \ 0; \ 0 \ b'_{i3} \ c'_{i3}) \\ \mathcal{S}'_{i4} &= (1 \ 0 \ 0; \ 0 \ b'_{i4} \ c'_{i4}) \end{aligned} \tag{9.37}$$

However, \mathcal{S}_{i2} cannot anymore be transformed into a revolute pair by the linear transformation with the other three twists because this will result in the linear dependence of the new limb twist system. Hence, the limb chain contains at least one prismatic that must not be perpendicular to the x_i axis. The revolute axes in the limb must be parallel. The limb chain can contain a cylindrical pair with an axis parallel to the base. Obviously, there are no spherical and universal joints in the limb chain. Table 9.10 presents an enumeration of 4-DOF limbs for a 3-DOF translational PM.

Considering that z_i is perpendicular to the moving platform, the three constraint couples in the z_i axis must be parallel and form a common constraint. The other three constraint couples in the y_i axis must be coplanar and non-parallel to restrict the translations in the X and Y axes. This condition can be satisfied by setting the revolute axis in different limb chains to be non-parallel. Subsequently, a translational PM with 4-DOF limbs can be constructed, as listed in Table 9.10. For example, Fig. 9.12 shows a $3-{}^xR^uP^xC$ translational PM, and Fig. 9.13 shows a $3-{}^xR^uP^xR^xR$ PM.

Fig. 9.12 $3-xR^uP^xC$

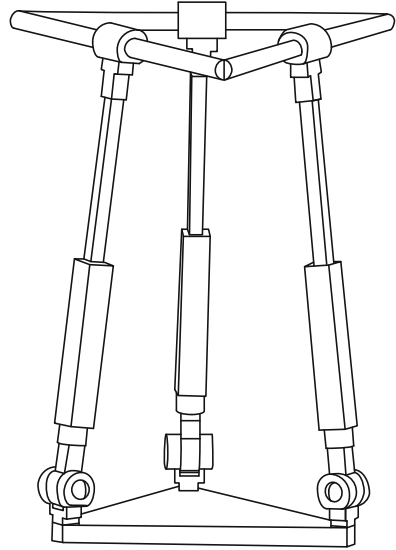
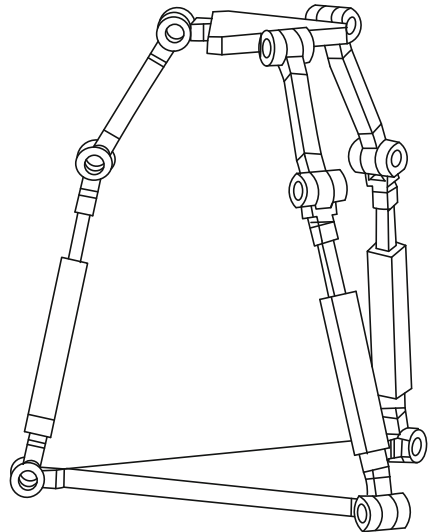


Fig. 9.13 $3-xR^uP^xR^xR$



9.5.7.4 Generation of Translational PMs with 5-DOF Limb Chains

When the mobility of the limb chain is five, the limb exerts one constraint couple on the moving platform. Without losing generality, the limb constraint couple is assumed to be in the $y_i z_i$ plane and askew to the base:

$$\mathcal{S}_{i1}^r = (0 \ 0 \ 0; \ 0 \ m_{i1} \ n_{i1}) \tag{9.38}$$

The limb twist system reciprocal to the constraint couples is

$$\begin{aligned}
 \mathcal{S}_{i1} &= (0 \ -n_{i1} \ m_{i1} ; \ 0 \ 0 \ 0) \\
 \mathcal{S}_{i2} &= (1 \ 0 \ 0 ; \ 0 \ 0 \ 0) \\
 \mathcal{S}_{i3} &= (0 \ 0 \ 0 ; \ 1 \ 0 \ 0) \\
 \mathcal{S}_{i4} &= (0 \ 0 \ 0 ; \ 0 \ 1 \ 0) \\
 \mathcal{S}_{i5} &= (0 \ 0 \ 0 ; \ 0 \ 0 \ 1)
 \end{aligned} \tag{9.39}$$

Equation (9.39) indicates that the limb chain contains at least two revolute pairs. \mathcal{S}_{i1} denotes a revolute pair whose axis is in the $y_i z_i$ plane and askew to the base while passing through the origin of the limb frame. By linear transformations with \mathcal{S}_{i3} , \mathcal{S}_{i4} , and \mathcal{S}_{i5} , \mathcal{S}_{i1} can be transformed into a revolute pair \mathcal{S}'_{i1} , whose axis is in the same direction and passes through any point in space. \mathcal{S}'_{i1} is given by

$$\mathcal{S}'_{i1} = (0 \ -n_{i1} \ m_{i1} ; \ a'_{i1} \ b'_{i1} \ c'_{i1}) \tag{9.40}$$

\mathcal{S}_{i3} , \mathcal{S}_{i4} , and \mathcal{S}_{i5} can be transformed into the following twists by the linear transformation with \mathcal{S}_{i1} :

$$\begin{aligned}
 \mathcal{S}'_{i3} &= (0 \ -n_{i1} \ m_{i1} ; \ a'_{i3} \ b'_{i3} \ c'_{i3}) \\
 \mathcal{S}'_{i4} &= (0 \ -n_{i1} \ m_{i1} ; \ a'_{i4} \ b'_{i4} \ c'_{i4}) \\
 \mathcal{S}'_{i5} &= (0 \ -n_{i1} \ m_{i1} ; \ a'_{i5} \ b'_{i5} \ c'_{i5})
 \end{aligned} \tag{9.41}$$

However, four revolute pairs with parallel axes are linearly dependent, and their rank is three. Consequently, \mathcal{S}_{i3} , \mathcal{S}_{i4} , and \mathcal{S}_{i5} cannot be transformed into parallel revolute pairs whose axes are askew to the base.

\mathcal{S}_{i4} and \mathcal{S}_{i5} can be transformed into revolute pairs whose axes are parallel to the base and passing through any point in space:

$$\begin{aligned}
 \mathcal{S}''_{i4} &= (1 \ 0 \ 0 ; \ 0 \ b''_{i4} \ c''_{i4}) \\
 \mathcal{S}''_{i5} &= (1 \ 0 \ 0 ; \ 0 \ b''_{i5} \ c''_{i5})
 \end{aligned} \tag{9.42}$$

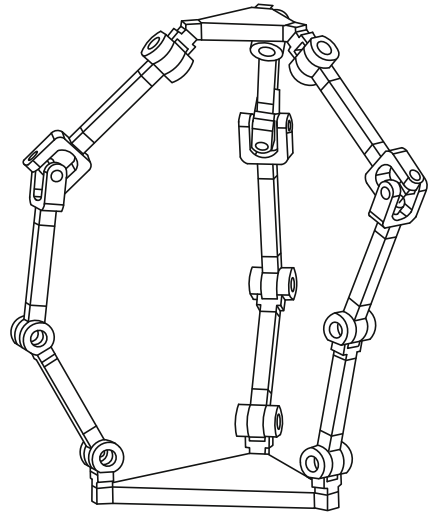
Hence, the revolute pairs in the limb can be divided into two groups. The axes of one group are determined by \mathcal{S}_{i1} and parallel to $(0 \ -n_{i1} \ m_{i1})$. The axes of the other group are determined by \mathcal{S}_{i2} and parallel to the base. The limb constraint couple is perpendicular to the plane determined by \mathcal{S}_{i1} and \mathcal{S}_{i2} . By setting the revolute axes (which are parallel to the base) in different limbs to be not parallel, the three constraint couples can be guaranteed to be non-coplanar and non-parallel. The platform constraint system in Eq. (9.29) can then be obtained.

Subsequently, a translational PM with 5-DOF limbs and the enumeration is listed in Table 9.11. Figure 9.14 shows a $3\text{-}^x\text{R}^x\text{R}^x\text{U}^u\text{R}$ translational PM. Figure 9.15 shows a $3\text{-}^x\text{R}^{u_1}\text{P}^x\text{U}^{u_2 u_2}\text{R}$ translational PM. The limb constraint couple

Table 9.11 Enumeration of 3-DOF translational PMs formed with a 5-DOF limb

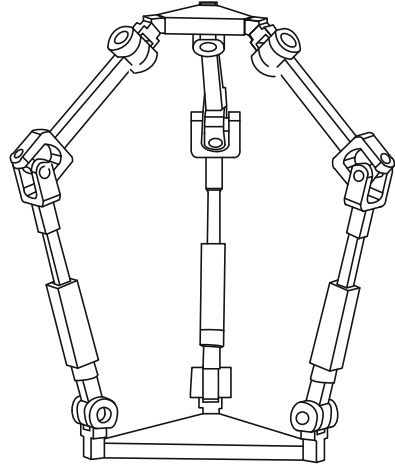
With one prismatic pair	$3_{-u_1} P^{x_1} R^{x_1} R^{u_2} R^{u_2} R$ $3_{-u_1} P^{x_1} R^{x_1} R^{x_1} R^{u_2} R$	$3_{-x_1} R^{x_1} R^{u_1} P^{u_2} R^{u_2} R$ $3_{-x_1} R^{x_1} R^{x_1} R^{u_1} P^{u_2} R$	$3_{-u_1} P^{u_2} R^{x_1} R^{x_1} R^{x_{12}} R$ $3_{-x_1} R^{x_1} R^{x_1} R^{u_1} P^{u_2} R$	
Without a prismatic pair	$3_{-x} R^x R^x U^{u_0} R$	$3_{-x} R^x R^x R^u R^u R$ [26]		
With a cylindrical pair and a universal joint	$3_{-x_1} C^{x_1} R^{x_1} U^u$ $3_{-x_1} R^{x_1} C^{x_1} U^u$	$3_{-u_1} P^{x_1} C^{x_1} U^{u_2}$ $3_{-x_1} R^{x_1} U^{u_{x_1}} C$	$3_{-u_1} P^{u_2} U^{x_1} x_1 C$ $3_{-x_1} C^{u_1} P^{x_1} U^{u_2}$	
With a cylindrical pair	$3_{-x_1} C^u C^{x_1} R$ $3_{-x_1} C^{u_1} P^{x_1} R^{u_2} R$ $3_{-u_1} P^{x_1} C^{x_1} R^{u_2} R$ $3_{-x_1} R^{u_1} P^{x_1} C^{u_2} R$ $3_{-x_1} R^{u_2} R^{u_1} P^{x_1} C$ $3_{-x_1} R^{x_1} R^{x_1} C^u R$	$3_{-x_1} C^{x_1} R^u C$ $3_{-u_1} P^{u_2} C^{x_1} R^{x_1} R$ $3_{-u_1} P^{x_1} R^{x_1} C^{u_2} R$ $3_{-x_1} R^{u_1} P^{u_2} R^{x_1} C$ $3_{-x_1} R^{u_2} R^{x_1} C^{u_1} P$	$3_{-x_1} R^{x_1} C^u C$ $3_{-u_1} P^{x_1} R^{x_1} R^{u_2} C$ $3_{-u_1} P^{x_1} R^{u_2} R^{x_1} C$ $3_{-x_1} R^{x_1} C^{u_1} P^{u_2} R$ $3_{-x_1} C^{x_1} R^{x_1} R^u R$ $3_{-u} C^{x_1} R^{x_1} R^{x_1} R$ $3_{-u_2} C^{u_1} P^{x_1} R^{x_1} R$ $3_{-x_1} C^{x_1} R^{u_1} P^{u_2} R$ $3_{-x_1} R^{x_1} C^{u_2} R^{u_1} P$ $3_{-x_1} C^u R^{x_1} R^u R$	
With a universal joint	$3_{-x_2} R^{x_1} R^{x_1} R^{x_1} U^{x_2}$ $3_{-u_2} R^{u_1} P^{u_2} U^{x_1} x_1 R$ $3_{-u_2} R^{x_1} R^{u_1} P^{x_1} U^{u_2}$ $3_{-x_1} R^{u_1} P^{x_1} U^{u_2} u_2 R$ $3_{-u_1} P^x U^{u_2} U^x$	$3_{-u_1} P^{u_2} R^{u_2} U^{x_1} x_1 R$ $3_{-u_2} R^{u_1} P^{x_1} R^{x_2} U^{u_2}$ $3_{-u_2} R^{x_1} R^{x_1} U^{u_2} u_1 P$ $3_{-x_1} R^{x_1} R^{u_2} R^{u_2} U^{x_1}$ $3_{-x} R^x U^{u_2} U^x$	$3_{-u_1} P^{x_1} R^{u_2} R^{u_2} U^{x_1}$ $3_{-u_2} R^{u_2} U^{x_1} u_1 P^{x_1} R$ $3_{-x_1} U^{u_2} u_1 P^{u_2} R^{u_2} R$ $3_{-x_1} R^{x_1} R^{x_1} U^{u_2} u_2 R$ $3_{-x} U^{u_2} R^u U^x$ [22]	$3_{-u_1} P^{u_2} U^{x_1} x_1 R^{u_2} R$ $3_{-u_2} R^{u_2} U^{x_1} x_1 R^{u_1} P$ $3_{-x_1} U^{u_2} R^{u_1} P^{x_1} R$ $3_{-x_1} U^{u_2} u_1 P^{u_2} U^x$ [22]

Fig. 9.14 $3_{-x} R^x R^x U^{u_0} R$



is perpendicular to the universal joint plane of ${}^x U^u$. One revolute axis that determines the universal joint plane is parallel to the base, whereas the other revolute axis is askew to the base. The universal joint planes in different limbs are not parallel, which guarantees that the three constraint couples are always linearly independent and constraining three translational DOF.

Fig. 9.15 $3\text{-}^xR^{u_1}P^E U^{u_2}u_2R$



9.5.8 Type Synthesis of a 3R 3-DOF PM

9.5.8.1 Constraint Synthesis

The standard base of the platform twist system of a 3-DOF rotational PM is

$$\begin{aligned}
 \$_{m1} &= (1 \ 0 \ 0; \ 0 \ 0 \ 0) \\
 \$_{m2} &= (0 \ 1 \ 0; \ 0 \ 0 \ 0) \\
 \$_{m3} &= (0 \ 0 \ 1; \ 0 \ 0 \ 0)
 \end{aligned}
 \tag{9.43}$$

where $\$_{m1}$, $\$_{m2}$, and $\$_{m3}$ denote three rotational DOF about the X, Y, and Z axes, respectively. Any rotation about the origin of the reference frame can then be obtained by the linear transformation of $\$_{m1}$, $\$_{m2}$, and $\$_{m3}$.

The platform constraint system is given by

$$\begin{aligned}
 \$_{m1}^r &= (1 \ 0 \ 0; \ 0 \ 0 \ 0) \\
 \$_{m2}^r &= (0 \ 1 \ 0; \ 0 \ 0 \ 0) \\
 \$_{m3}^r &= (0 \ 0 \ 1; \ 0 \ 0 \ 0)
 \end{aligned}
 \tag{9.44}$$

where $\$_{m1}^r$, $\$_{m2}^r$, and $\$_{m3}^r$ denote three constraint forces along the X, Y, and Z axes, respectively, and passing through the origin of the reference frame. Hence, any constraint force passing the origin of the reference frame can be obtained by the linear transformation of $\$_{m1}^r$, $\$_{m2}^r$, and $\$_{m3}^r$

9.5.8.2 Generation of Rotational PMs with 3-DOF Limb Chains

When the limb chain has three DOF, the limb chain imposes three constraint forces on the moving platform, and the platform constraint system is the same as the limb constraint system:

$$\begin{aligned} \mathcal{S}_{i1}^r &= (1 \ 0 \ 0; \ 0 \ 0 \ 0) \\ \mathcal{S}_{i2}^r &= (0 \ 1 \ 0; \ 0 \ 0 \ 0) \\ \mathcal{S}_{i3}^r &= (0 \ 0 \ 1; \ 0 \ 0 \ 0) \end{aligned} \quad (9.45)$$

The platform twist system is also the same as the limb twist system. The limb twist system of the i th limb is given by

$$\begin{aligned} \mathcal{S}_{i1} &= (1 \ 0 \ 0; \ 0 \ 0 \ 0) \\ \mathcal{S}_{i2} &= (0 \ 1 \ 0; \ 0 \ 0 \ 0) \\ \mathcal{S}_{i3} &= (0 \ 0 \ 1; \ 0 \ 0 \ 0) \end{aligned} \quad (9.46)$$

where \mathcal{S}_{i1} , \mathcal{S}_{i2} , and \mathcal{S}_{i3} denote three revolute pairs whose axes intersect at a common point and not linearly dependent. Hence, the three revolute pairs can form a $({}^iR^jR^kR)_N$ chain. Setting the limb centers of three $({}^iR^jR^kR)$ limbs to be coincident, a $3 - ({}^iR^jR^kR)_N$ PM, namely, the well-known 3-3R rotational PM, can be constructed. The structural condition that the three limb centers must be coincident guarantees that the platform constraint system be constant.

9.5.8.3 Generation of Rotational PMs with 4-DOF Limb Chains

When the limb chain has four DOF, the limb imposes two constraint forces on the moving platform. Assuming that the limb constraint system consists of one force in the y_i axis and one force in the z_i axis, then

$$\begin{aligned} \mathcal{S}_{i1}^r &= (0 \ 1 \ 0; \ 0 \ 0 \ 0) \\ \mathcal{S}_{i2}^r &= (0 \ 0 \ 1; \ 0 \ 0 \ 0) \end{aligned} \quad (9.47)$$

The limb twist system reciprocal to the above constraint forces is

$$\begin{aligned} \mathcal{S}_{i1} &= (1 \ 0 \ 0; \ 0 \ 0 \ 0) \\ \mathcal{S}_{i2} &= (0 \ 1 \ 0; \ 0 \ 0 \ 0) \\ \mathcal{S}_{i3} &= (0 \ 0 \ 1; \ 0 \ 0 \ 0) \\ \mathcal{S}_{i4} &= (0 \ 0 \ 0; \ 1 \ 0 \ 0) \end{aligned} \quad (9.48)$$

$\$_{i1}$, $\$_{i2}$, $\$_{i3}$, and $\$_{i4}$ cannot anymore be transformed into a revolute pair, whose axis passes an arbitrary point in space. Hence, the limb chain is ${}^xP({}^iR^jR^kR)_N$ and a $3-{}^xP({}^iR^jR^kR)_N$ rotational PM can be constructed following the structural condition. Similarly, a $3-{}^xP({}^iR^jR^kR)_N$ rotational PM can be constructed.

9.5.8.4 Generation of Rotational PMs with 5-DOF Limb Chains

When the limb chain has five DOF, the limb imposes a constraint force to the moving platform. Obviously, the three constraint forces of three limbs must be non-coplanar and intersect at a common point. If the limb constraint forces are parallel or perpendicular to the base, such a condition cannot be satisfied. Therefore, the limb constraint force must be askew to the base and be the form

$$\$'_{i1} = (l_{i1} \ m_{i1} \ n_{i1}; \ 0 \ 0 \ 0) \tag{9.49}$$

where l_{i1} and m_{i1} cannot be simultaneously zero, and n_{i1} is not zero.

The limb twist system reciprocal to the above constraint force is

$$\begin{aligned} \$_{i1} &= (1 \ 0 \ 0; \ 0 \ 0 \ 0) \\ \$_{i2} &= (0 \ 1 \ 0; \ 0 \ 0 \ 0) \\ \$_{i3} &= (0 \ 0 \ 1; \ 0 \ 0 \ 0) \\ \$_{i4} &= (0 \ 0 \ 0; \ -m_{i1} \ l_{i1} \ 0) \\ \$_{i5} &= (0 \ 0 \ 0; \ -n_{i1} \ 0 \ l_{i1}) \end{aligned} \tag{9.50}$$

By the linear transformation of the five twists in Eq. (9.50), a limb chain with 2R spherical subchain can be obtained. For example, one form of linear transformation is

$$\begin{aligned} \$'_{i1} &= (l'_{i1} \ m'_{i1} \ n'_{i1}; \ 0 \ 0 \ 0) \\ \$'_{i2} &= (l'_{i2} \ m'_{i2} \ n'_{i2}; \ 0 \ 0 \ 0) \\ \$'_{i3} &= (l'_{i3} \ m'_{i3} \ n'_{i3}; \ a'_{i3} \ b'_{i3} \ c'_{i3}) \\ \$'_{i4} &= (l'_{i4} \ m'_{i4} \ n'_{i4}; \ a'_{i4} \ b'_{i4} \ c'_{i4}) \\ \$'_{i5} &= (l'_{i5} \ m'_{i5} \ n'_{i5}; \ a'_{i5} \ b'_{i5} \ c'_{i5}) \end{aligned} \tag{9.51}$$

where $a'_{i3} = y_{i1}n'_{i3} - z_{i1}m'_{i3}$, $b'_{i3} = z_{i1}l'_{i3} - x_{i1}n'_{i3}$, $c'_{i3} = x_{i1}m'_{i3} - y_{i1}l'_{i3}$, $a'_{i4} = y_{i1}n'_{i4} - z_{i1}m'_{i4}$, $b'_{i4} = z_{i1}l'_{i4} - x_{i1}n'_{i4}$, $c'_{i4} = x_{i1}m'_{i4} - y_{i1}l'_{i4}$, $a'_{i5} = y_{i1}n'_{i5} - z_{i1}m'_{i5}$, $b'_{i5} = z_{i1}l'_{i5} - x_{i1}n'_{i5}$, and $c'_{i5} = x_{i1}m'_{i5} - y_{i1}l'_{i5}$. The pitches of $\$'_{i3}$, $\$'_{i4}$, and $\$'_{i5}$ are zero.

From the above equation, $\$'_{i1}$ and $\$'_{i2}$ form a 2R spherical subchain, whose limb center is denoted as N_1 . The axes of $\$'_{i3}$, $\$'_{i4}$, and $\$'_{i5}$ intersect at a common point (x_{i1}, y_{i1}, z_{i1}) and form a 3R spherical subchain or a spherical joint, whose center is denoted as N_2 . Obviously, the limb chain contains two centers and can be denoted as $({}^eR^hR)_{N_1} ({}^iR^jR^kR)_{N_2}$ or $({}^iR^jR)_{N_1} S_{N_2}$.

Fig. 9.16
 $3-{}^u_1R^u{}_2P^u{}_1R({}^iR^kR)_N$

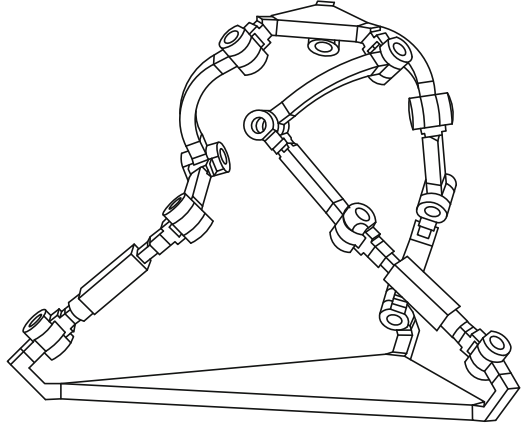


Table 9.12 Enumeration of 3-DOF rotational PMs formed with a 5-DOF limb

With one prismatic pair in a limb	$3-{}^u_1R^u{}_1R^u{}_2P({}^iR^jR)_N$ $3-{}^xP^uR({}^iR^jR^kR)_N$	$3-{}^u_1R^u{}_2P^u{}_1R({}^iR^jR)_N$ $3-{}^u_1R^u{}_1R^u{}_2P({}^iR^jR)_N$	$3-{}^xP^uR^uR({}^iR^jR)_N$ $3-{}^uR^uR^xR_N^xP^jR_N$	$3-{}^u_1R^u{}_2P({}^iR^jR^kR)_N$ $3-{}^uR^uR^xR_N^xP^jR_N$
With no prismatic pair in a limb	$3-{}^uR^uR({}^iR^jR^kR)_N$	$3-{}^uR^uR^uR({}^iR^kR)_N$ [27]	$3-({}^iR^jR)_N S_N^3$ [28]	
With a cylindrical pair in a limb	$3-{}^uP^xC_N({}^iR^kR)_N$ $3-{}^uR^uR^xC_N^kR_N$	$3-{}^uR^xC_N({}^iR^kR)_N$	$3-{}^u_1R^u{}_2P^xC_N^kR_N$	$3-{}^xP^uR^xC_N^kR_N$
With a universal joint in a limb	$3-{}^x_1P^uU_N^x({}^iR^kR)_N$ $3-{}^xP^uR^uU_N^i kR_N$	$3-{}^uR^uU_N^x({}^iR^kR)_N$ $3-{}^uR^uR^uU_N^i kR_N$	$3-{}^uU_N^x xP({}^iR^kR)_N$ $3-{}^uR^uU_N^x xP^kR_N$	$3-{}^uR^xP^uU_N^i kR_N$

Solving the screw reciprocal to the five twists in Eq. (9.31) yields

$$\mathcal{S}_{i1}^r = (x_{i1} \ y_{i1} \ z_{i1} ; 0 \ 0 \ 0) \tag{9.52}$$

where \mathcal{S}_{i1}^r is a constraint force that passes through the two centers of this limb.

Therefore, when constructing a 3-DOF rotational PM with $({}^eR^hR)_{N_1}$ $({}^iR^jR^kR)_{N_2}$ limbs, the center of the 2R or 3R spherical subchain must be set to be coincident. When constructing a 3-DOF rotational PM with $({}^iR^jR)_{N_1}$ S_{N_2} limbs, the center of the 2R subchain must be set to be coincident, such as the $3-({}^iR^jR)_{N_1} S_{N_2}$ rotational PM proposed by Di Gregorio [28].

In Sect. 9.5.5, two categories of limb chains that impose one constraint force on the moving platform have been synthesized. The constraint force passes through the limb center and is parallel to the revolute axis outside the 2R or 3R spherical subchain. When constructing PMs with these limb chains, the revolute axis outside the 2R or 3R spherical subchain must be set to be askew to the base, and the limb centers must be set to be coincident. Consequently, the three constraint forces are non-coplanar and intersect at a common point. The standard base of the platform constraint system is the same as Eq. (9.43) and constrains three translational DOF. Figure 9.16 shows a $3-{}^u_1R^u{}_2P^u{}_1R({}^iR^kR)_N$ rotational PM. Table 9.12 enumerates 3-DOF rotational PMs with 5-DOF limb chains.

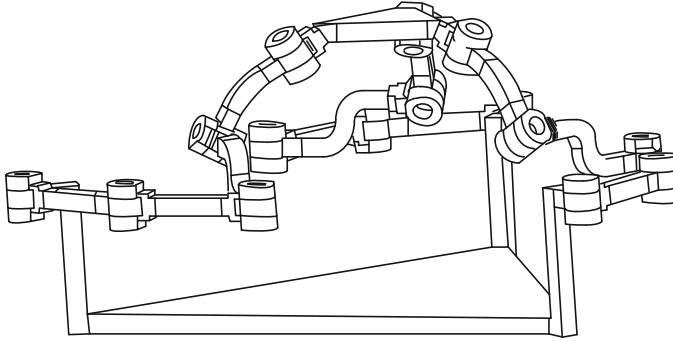


Fig. 9.17 $3^{-z}R^zR^zR(iR^kR)_{N^3}$

9.5.9 Type Synthesis of a 1R2T 3-DOF PM

The most well-known 1R2T 3-DOF PM is the 3-RRR planar PM. Using the limb chains proposed in Sect. 9.5.1, a 1R2T 3-DOF PM with 5-DOF limb chains can be constructed by setting the three limb centers not to be coincident. For instance, consider the $3^{-z}R^zR^zR(iR^kR)_N$ PM in Fig. 9.17, which is a 3R2T 5-DOF PM. After setting the three limb centers of the $3^{-z}R^zR^zR(iR^kR)_N$ not to be coincident, a $3^{-z}R^zR^zR(iR^kR)_{N^3}$ PM can be obtained, as shown in Fig. 9.17. Given that the three limb constraint forces are parallel, their combined effect constrains the two rotations about the X and Y axes, as well as the translation along the Z axis. The moving platform has two rotational DOF about the X and Y axes, as well as one translational DOF along the Z axis.

9.6 Type Synthesis of Non-symmetrical PMs

The above sections deal with the type synthesis of symmetrical PMs. Indeed, the constraint-screw based method is applicable to the type synthesis of non-symmetrical PMs. Using the appropriate optimum design, non-symmetrical PMs can demonstrate very good performances. One of the typical successful applications of non-symmetrical PMs is Tricept. There are two ways for the type synthesis of non-symmetrical PMs, and the constraint-based synthesis method applicable to both.

One way is to add a lower-mobility chain to a six-DOF PM. Such a lower-mobility chain determines the DOF of the mechanism. The lower-mobility chain can be actuated or passive. For example, Tricept is a 3-UPS/UP non-symmetrical PM. The UP chain is passive and only provides constraints, whereas the three UPS chains provide actuation. Another example is the 5-UPS/RPPU parallel kinematic machine developed in the Yanshan University, as shown in Fig. 9.18. The passive RPPU limb exerts one constraint on the moving platform. The five UPS chains provide actuation. Clearly, the type synthesis of such a kind of non-symmetrical PM



Fig. 9.18 5-UPS/RPPU PKM in the Yanshan University

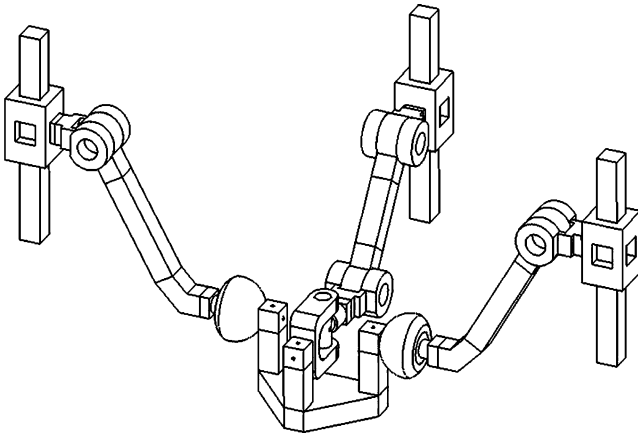


Fig. 9.19 2-PRS/PRRU PM

is simplified to the type synthesis of a serial limb chain with less than six DOF, which is rather straightforward using the constraint-screw based method.

The other way is to use different limb chains synthesized by the constraint-screw based method to construct PMs while obeying the required geometrical conditions. For example, a 2-PRS/PRRU PM can be constructed to replace a 3-RPS PM, as shown in Fig. 9.19.

References

1. Hervé JM (1978) Analyse structurelle des mécanismes par groupe des déplacements. *Mech Mach Theory* 13(4):437–450
2. Hunt KH (1983) Structural kinematic of in-parallel-actuated robot arms. *J Mech Trans Automat Des* 105:705–712
3. Li QC, Huang Z, Hervé JM (2004) Type synthesis of 3r2t 5-dof parallel mechanisms using the lie group of displacements. *IEEE Trans Robot Automat* 20(2):173–180
4. Li QC, Huang Z, Hervé JM (2004) Displacement manifold method for type synthesis of lower-mobility parallel mechanisms. *Sci China Ser E* 47(6):641–650
5. Karouia M, Hervé JM (2005) Asymmetrical 3-dof spherical parallel mechanisms. *Eur J Mech A/Solids* 24(1):47–57
6. Huynh P, Hervé JM (2005) Equivalent kinematic chains of 3-dof tripod mechanisms with planar-spherical bonds. *J Mech Des* 127(1):95–102
7. Lee CC, Hervé JM (2006) Translational parallel manipulators with doubly planar limbs. *Mech Mach Theory* 24(4):433–435
8. Angeles J (2002) The qualitative synthesis of parallel manipulators. In: *Proceedings of workshop on fundamental issues and future research directions for parallel mechanisms and manipulators*, Quebec city, QC, Canada, pp 160–169
9. Rico JM et al (2006) A comprehensive theory of type synthesis of fully parallel platforms. In: *Proceedings of 2006 ASME DETC conference (paper DETC2006-99070)*, Philadelphia, USA
10. Meng J, Liu GF, Li ZX (2007) A geometric theory for synthesis and analysis of sub 6-DOF parallel manipulators. *IEEE Trans Robot* 23(4):625–649
11. Jin Q, Yang TL (2004) Theory for topology synthesis of parallel manipulators and its application to three-dimension-translation parallel manipulators. *J Mech Des* 126(1):625–639
12. Gao F, Zhang Y, Li W (2005) Type synthesis of 3-dof reducible translational mechanisms. *Robotica* 23(2):239–245
13. Gogu G (2004) Structural synthesis of fully-isotropic translational parallel robots via theory of linear transformations. *Eur J Mech A/Solids* 23(6):1021–1039
14. Gogu G (2007) Structural synthesis of fully-isotropic parallel robots with Schönflies motions via theory of linear transformations and evolutionary morphology. *Eur J Mech A/Solids* 26(2):242–269
15. Huang Z, Li QC (2002) General methodology for type synthesis of lower-mobility symmetrical parallel manipulators and several novel manipulators. *Int J Robot Res* 21(2):131–146
16. Huang Z, Li QC (2003) Type synthesis of symmetrical lower-mobility parallel mechanisms using constraint-synthesis method. *Int J Robot Res* 22(1):59–79
17. Huang Z, Kong LF, Fang YF (1997) *Mechanism theory of parallel robotic manipulator and control*. China Mechanical Press, Beijing (in Chinese)
18. Huang Z, Liu JF, Li QC (2008) Unified methodology for mobility analysis based on screw theory. In: Wang L, Xi J (eds) *Smart devices and machines for advanced manufacturing*. Springer, London, pp 49–78
19. Frisoli A, Checcacci D, Salsedo F, Bergamasco M (2000) Synthesis by screw algebra of translating in-parallel actuated mechanisms, *Advances in robot kinematics*. Kluwer, Dordrecht, pp 433–440
20. Kong XW, Gosselin CM (2004) Type synthesis of 3t1r 4-dof parallel manipulators based on screw theory. *IEEE Trans Robot Automat* 20(2):181–190
21. Kong XW, Gosselin CM (2004) Type synthesis of three-degree-of-freedom spherical parallel manipulators. *Int J Robot Res* 23(3):237–245
22. Fang YF, Tsai LW (2002) Structure synthesis of a class of 4-dof and 5-dof parallel manipulators with identical limb structures. *Int J Robot Res* 21(9):799–810

23. Tsai LW (1999) The enumeration of a class of three-Dof parallel manipulators. The tenth world congress on the theory of machines and mechanisms, Finland, pp 1123–1126
24. Merlet J-P (1989) Singular configurationx of parallel manipulators and Grassman geometry. *Int J Robot Res* 8:45–56
25. Zlatanov D, Gosselin CM (2001) A new parallel architecture with four degrees of freedom. In: *Proceedings of the 2nd workshop on Computational Kinematics*, Seoul, Korea, pp 57–66
26. Frisoli A, Checcacci D, Salsedo F, et al.(2000) Synthesis by screw algebra of translating in-parallel actuated mechanisms. J. Lenarčič and M. M. Stanišič, *Advances in Robot Kinematics*, Kluwer Academic Publishers, pp 433–440
27. Karouia M, Hervé JM (2002). A family of novel orientational 3-dof parallel robots. In: *Proceedings of Ro. Man. Sy 2002, 14th CISM-IFTToMM Symposium*, Udine, Italy, pp 359–368
28. Di Gregorio R (2002) The 3-RRS wrist: a new, very simple and not overconstrained spherical parallel manipulator. In: *Proceedings of ASME Design Engineering Technical Conferences*, (paper MECH-34344), Montreal, Canada

Chapter 10

Digital Topology Theory of Kinematic Chains and Atlas Database

This chapter introduces an original theory of loop algebra and its application in isomorphism identification, rigid sub-chain detection, and atlas database of kinematic chains. Introduced first is the unified topology modeling of planar kinematic chains with simple joints, multiple joints, and geared (cam) joints. Based on the array representation of loops in the topological graphs of kinematic chains, basic loop operations are introduced, and the loop algebra is established. The most important problem of isomorphism identification in the automatic structural synthesis of kinematic chains is presented by finding a unique representation of topological graphs. Finally, the digital atlas database for the topological graphs of kinematic chains is also provided.

10.1 Topology Modeling of Mechanisms

10.1.1 Modeling of Simple Joint Kinematic Chains

In the process of structural synthesis and creative design of mechanisms, a mechanism is usually represented by its kinematic chain. The frame of the mechanism is represented by an appropriate link, and all joints are assumed revolute [1–4]. Figure 10.1a shows a heavy-load hydraulic excavator [5], and the upper carriage (arm) of the excavator can rotate 360° around its vertical axis. The upper carriage has four primary links: boom, stick, rocker, and shovel. These primary links perform a planar motion actuated by three pairs of hydraulic cylinders. The kinematic sketch for the mechanism of upper carriage is shown in Fig. 10.1b. Figure 10.1c shows the kinematic chain for the upper carriage.

The topological graph in the graph theory is usually adopted to represent the structures of kinematic chains since the 1960s [6, 7]. That is, the vertices of the topological graph denote the links of the chain, and the edges of the graph denote the joints. The topological graph and the structure of a kinematic chain are correspondent with each other. Thus, the research on the kinematic structure

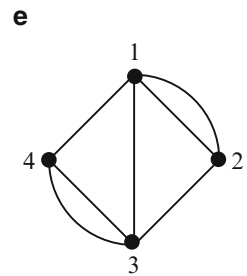
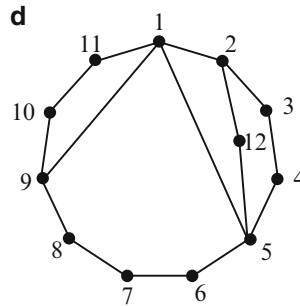
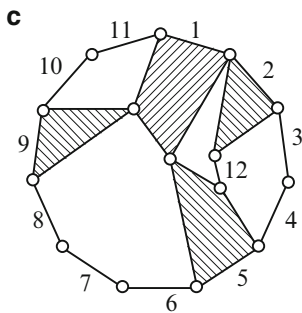
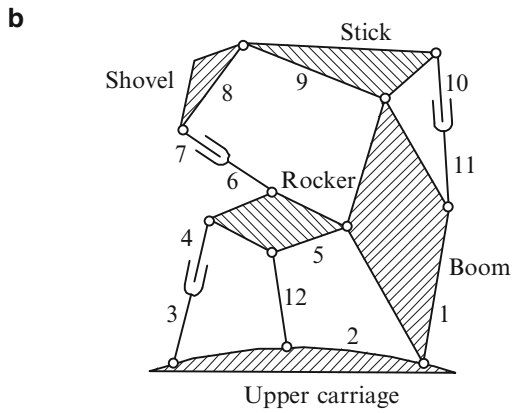


Fig. 10.1 Mechanism and its graph representation (a) a heavy-load hydraulic excavator (b) kinematic sketch of its upper carriage (c) kinematic chain, (d) topological graph, and (e) contracted graph

of a kinematic chain can be converted into the study of its topological graph. For example, Fig. 10.1d shows the topological graph for the chain in Fig. 10.1c.

A topological graph can be represented by its adjacency matrix. The elements of the adjacency matrix are defined as follows:

$$A = [a_{ij}]_{n \times n} = \begin{cases} 1, & \text{if vertices } i \text{ and } j \text{ are adjacent} \\ 0, & \text{otherwise} \end{cases} \quad (10.1)$$

where n is the number of the vertices of the graph.

For the topological graph in Fig. 10.1d, its adjacency matrix is

$$A = \begin{bmatrix} 0 & 1 & 0 & 0 & 1 & 0 & 0 & 0 & 1 & 0 & 1 & 0 \\ 1 & 0 & 1 & 0 & 0 & 0 & 0 & 0 & 0 & 0 & 0 & 1 \\ 0 & 1 & 0 & 1 & 0 & 0 & 0 & 0 & 0 & 0 & 0 & 0 \\ 0 & 0 & 1 & 0 & 1 & 0 & 0 & 0 & 0 & 0 & 0 & 0 \\ 1 & 0 & 0 & 1 & 0 & 1 & 0 & 0 & 0 & 0 & 0 & 1 \\ 0 & 0 & 0 & 0 & 1 & 0 & 1 & 0 & 0 & 0 & 0 & 0 \\ 0 & 0 & 0 & 0 & 0 & 1 & 0 & 1 & 0 & 0 & 0 & 0 \\ 0 & 0 & 0 & 0 & 0 & 0 & 1 & 0 & 1 & 0 & 0 & 0 \\ 1 & 0 & 0 & 0 & 0 & 0 & 0 & 1 & 0 & 1 & 0 & 0 \\ 0 & 0 & 0 & 0 & 0 & 0 & 0 & 0 & 1 & 0 & 1 & 0 \\ 1 & 0 & 0 & 0 & 0 & 0 & 0 & 0 & 0 & 1 & 0 & 0 \\ 0 & 1 & 0 & 0 & 1 & 0 & 0 & 0 & 0 & 0 & 0 & 0 \end{bmatrix} \quad (10.2)$$

The contracted graph can be obtained by replacing each alternating sequence of binary vertices and edges by an edge from its topological graph [8, 9]. For example, Fig. 10.1e is the contracted graph for the graph in Fig. 10.1d.

A contracted graph can also be represented by its adjacency matrix. The elements of the adjacency matrix for a contracted graph are defined as follows:

$$A = [a_{ij}]_{N_m \times N_m} = \begin{cases} k, & \text{if vertices } i \text{ and } j \text{ are adjacent through } k \text{ edges} \\ s, & \text{if vertex } i \text{ has } s \text{ self loops} \\ 0, & \text{otherwise} \end{cases} \quad (10.3)$$

where N_m is the number of the vertices of the contracted graph. The adjacency matrix of the contracted graph in Fig. 10.1e is

$$A = \begin{bmatrix} 0 & 2 & 1 & 1 \\ 2 & 0 & 1 & 0 \\ 1 & 1 & 0 & 2 \\ 1 & 0 & 2 & 0 \end{bmatrix} \quad (10.4)$$

In a contracted graph, two vertices are said to have $k - 1$ multiple-edges if they are connected directly through k ($k > 1$) edges. The number of multiple-edges for a contracted graph is defined as the sum of the numbers of multiple-edges between every pair of vertices. For example, Fig. 10.1e has two multiple-edges.

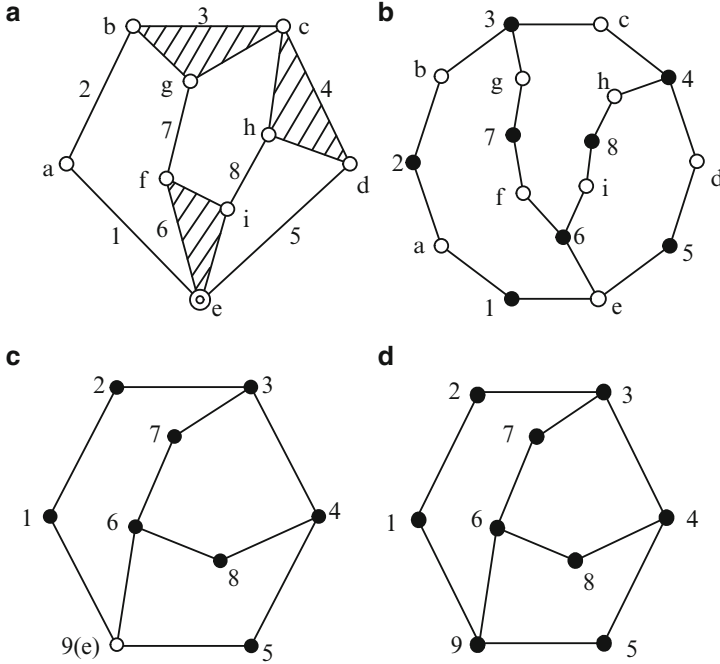


Fig. 10.2 (a) Multiple joint kinematic chain, and its (b) conventional bicolor topological graph, (c) new bicolor topological graph, and (d) basic topological graph

10.1.2 Modeling of Multiple Joint Kinematic Chains

10.1.2.1 Conventional Topological Graph

Many mechanisms contain multiple [8, 10, 11] or compound joints [12] because of the advantages of simplifying kinematic analysis and minimizing the space requirement. Studying simple joint kinematic chains using the above topological graph technique is very convenient. However, this technique cannot be applied directly to multiple joint kinematic chains because the resulting topological graphs contain polygons. Therefore, the topological structure of multiple joint kinematic chains is usually represented by a bicolor topological graph. Conventional bicolor graphs are established as follows: solid (“●”) and hollow (“○”) vertices are used to represent links and joints, respectively, and the corresponding solid and hollow vertices are connected with an edge when a link is connected with a joint [13]. For example, Fig. 10.2a shows an eight-link multiple joint kinematic chain, and Fig. 10.2b shows its conventional bicolor topological graph.

A multiple joint kinematic chain and its conventional bicolor topological graph are also correspondent with each other. However, a conventional bicolor topological graph has too many vertices relative to its number of links (its number of

vertices is equal to the sum of the numbers of links and joints of the chain). Therefore, more storage space is needed in the process of computerized structural synthesis. Moreover, conventional bicolor topological graphs fail to bridge the studies on simple joint chains and multiple joint chains. Thus, the most in-depth study of the structural analysis and synthesis theory of simple joint kinematic chains are hard to employ in studies on kinematic chains with multiple joints.

10.1.2.2 New Topological Graph

Based on the topological graphs of simple joint kinematic chains, a new kind of bicolor topological graph is proposed to represent the topological structures of multiple joint kinematic chains. In the new graph, solid (“●”) and hollow (“○”) vertices denote the links of the chain and multiple joints, respectively. The two corresponding solid vertices are connected with an edge if the two links are connected directly by a simple joint, and the corresponding solid and hollow vertices are connected with an edge if a link is connected with a multiple joint. For example, Fig. 10.2c shows the new bicolor topological graph for the chain in Fig. 10.2a. Obviously, a multiple joint kinematic chain and its new bicolor topological graph are also correspondent with each other.

The new bicolor topological graph can be represented by the adjacency matrix modified from that of the simple joint kinematic chain. The elements of the adjacency matrix are

$$A = [a_{ij}]_{n \times n} = \begin{cases} 1, & \text{if vertices } i \text{ and } j \text{ are adjacent} \\ -d, & \text{if } i = j \text{ and } i \text{ (or } j \text{) is the label of a hollow vertex} \\ 0, & \text{otherwise} \end{cases} \quad (10.5)$$

where n is the number of the vertices of the graph, and d is the pseudo-degree of the hollow vertices (The pseudo-degree of a hollow vertex is equal to the number of edges connected with the hollow vertex).

The adjacency matrix of the topological graph in Fig. 10.2c is

$$A = \begin{bmatrix} 0 & 1 & 0 & 0 & 0 & 0 & 0 & 0 & 1 \\ 1 & 0 & 1 & 0 & 0 & 0 & 0 & 0 & 0 \\ 0 & 1 & 0 & 1 & 0 & 0 & 1 & 0 & 0 \\ 0 & 0 & 1 & 0 & 1 & 0 & 0 & 1 & 0 \\ 0 & 0 & 0 & 1 & 0 & 0 & 0 & 0 & 1 \\ 0 & 0 & 0 & 0 & 0 & 0 & 1 & 1 & 1 \\ 0 & 0 & 1 & 0 & 0 & 1 & 0 & 0 & 0 \\ 0 & 0 & 0 & 1 & 0 & 1 & 0 & 0 & 0 \\ 1 & 0 & 0 & 0 & 1 & 1 & 0 & 0 & -3 \end{bmatrix} \quad (10.6)$$

The characteristics of the new bicolor topological graph for a multiple joint kinematic chain are as follows:

1. In a new bicolor topological graph, the number of vertices is equal to the sum of the numbers of links and multiple joints. This number is reduced noticeably compared with that of the conventional graph.
2. The degree of any solid vertex is equal to the number of joints connected with the corresponding link. The pseudo-degree of a hollow vertex is greater than two, and is one more than the factors of the multiple joint. The factors of a multiple joint are the number of the kinematic pairs that the joint presented.
3. For a multiple joint kinematic chain of N -link and M -kinematic pair (J multiple joints included), the number of vertices and edges of its new bicolor topological graph are $(N + J)$ and $(M + J)$. Both increase by J compared with the number of links and kinematic pairs of its structural diagram.

For example, Fig. 10.2c is the new bicolor topological graph of the eight-link kinematic chain with one multiple joint in Fig. 10.2a. Only one multiple joint exists in this kinematic chain; thus, the numbers of vertices and edges of its new bicolor topological graph (Fig. 10.2c) are 9 and 11, respectively.

If the difference between the solid vertex and the hollow vertex is ignored, then the new bicolor topological graph is converted to the topological graph of simple joint kinematic chains, which is termed the basic topological graph of the multiple joint kinematic chain. For example, Fig. 10.2d is the basic topological graph of the multiple joint kinematic chain in Fig. 10.2a.

For a multiple joint kinematic chain, the DOFs (degrees of freedom) (F_{BG}) of its basic topological graph is

$$\begin{aligned}
 F_{BG} &= 3 \times (N + J - 1) - 2 \times (M + J) \\
 &= [3 \times (N - 1) - 2 \times M] + J \\
 &= F + J
 \end{aligned} \tag{10.7}$$

where N is the number of links, M is the number of kinematic pairs, J is the number of multiple joints, F is the DOFs of the multiple joint kinematic chain, and F_{BG} is the DOFs of the basic topological graph.

Obviously, the DOFs of the basic topological graph increase by J compared with the DOFs of the multiple joint kinematic chain.

The model of the new bicolor topological graph provides a new synthesis method for the topological structures of multiple joint kinematic chains. They may be synthesized in batch directly based on the structural synthesis of the simple joint kinematic chains and their atlas database. For example, in the topological graph of a nine-link, two-DOF simple joint kinematic chain, if a vertex whose degree ≥ 3 is converted to a hollow vertex, then the new bicolor topological graph of an eight-link, one-DOF kinematic chain with one multiple joint is obtained, and the corresponding multiple joint kinematic chain is synthesized.

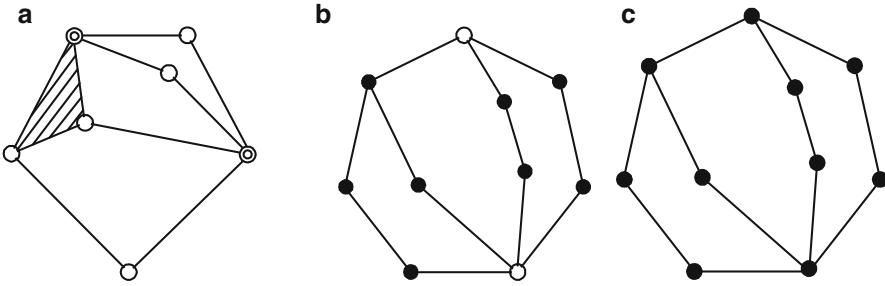


Fig. 10.3 (a) A multiple joint kinematic chain, and its (b) new bicolor topological graph and (c) basic topological graph

Example 10.1. Figure 10.3a shows another eight-link kinematic chain with two multiple joints. Its new bicolor topological graph and basic topological graph are shown in Fig. 10.3b, c, respectively. An eight-link, one-DOF kinematic chain with two multiple joints can be synthesized from the topological graphs of a nine-link, two-DOF chain with one multiple joint, which can be synthesized from a ten-link, three-DOF simple joint kinematic chain.

Example 10.2. Figure 10.2d can also be regarded as the topological graph of a nine-link simple joint kinematic chain. Four vertices (vertices 3, 4, 6, and 9) whose degrees are ≥ 3 exist. As vertices 3 and 9, vertices 6 and 4 are topology symmetrical, and only two different bicolor topological graphs can be obtained from Fig. 10.2d. If vertex 6 (or 4) is converted to a hollow vertex, then the bicolor topological graph of an eight-link one-DOF kinematic chain with one multiple joint is obtained (Fig. 10.4a). The corresponding multiple joint kinematic chain is shown in Fig. 10.4b. If vertex 9 (or 3) is converted to a hollow vertex, another bicolor topological graph and its corresponding eight-link, one-DOF kinematic chain with one multiple joint are obtained, as shown in Fig. 10.4c, d, respectively.

10.1.3 Modeling of Geared (cam) Kinematic Chains

10.1.3.1 Conventional Topological Graph

A geared (cam) mechanism is a complex mechanical system, including simple joints, multiple joints, and high pairs (geared or cam). This system is obtained by adding a series of meshing gears (cams) to a basic kinematic chain of planar or spatial linkages.

Generally, the topological structure of the geared (cam) kinematic chain is represented by a tricolor topological graph. In conventional tricolor topological graphs [13], solid vertices (“●”) represent links, hollow vertices (“○”) represent joints, bicyclic vertices (“⊙”) represent geared (cam) pairs, and vertices are

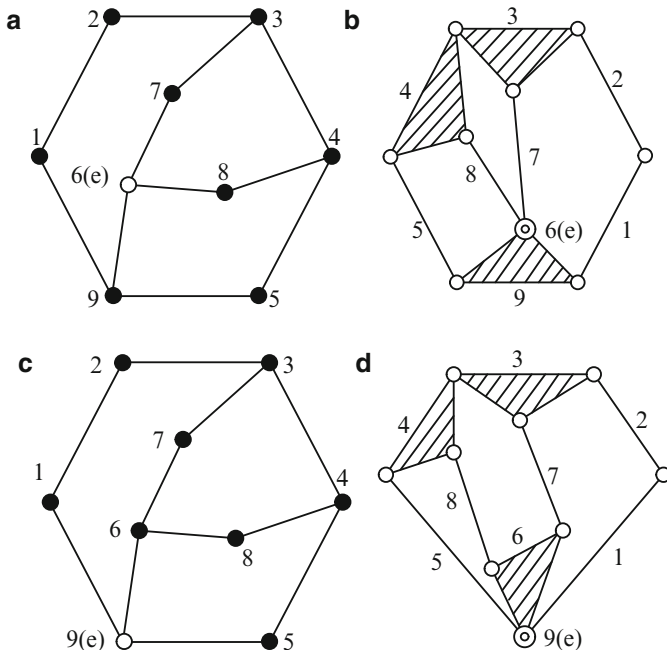


Fig. 10.4 (a) A bicolor topological graph and (b) its corresponding multiple joint chain; (c) another bicolor topological graph and (d) its corresponding multiple joint chain

connected with edges according to the relationship of the corresponding parts in the geared (cam) chain.

Figure 10.5a shows a six-link geared chain with two multiple joints and two gear pairs, which is obtained by adding two pairs of meshing gears to a four-link linkage. Figure 10.5b shows the conventional tricolor topological graph of Fig. 10.5a.

The conventional tricolor topological graph is correspondent with its geared (cam) kinematic chain, but it is too complex, because the number of its vertices is equal to the sum of the numbers of links, joints (simple and multiple joints), and geared (cam) pairs. Moreover, the conventional tricolor topological graph hardly establishes close association with the above two kinds of kinematic chains.

10.1.3.2 New Topological Graph

Based on the topological graph of simple joint kinematic chains and new bicolor topological graph of multiple joint kinematic chains, the new topological graph of geared (cam) kinematic chains is proposed.

1. Solid vertices (“●”) are used to denote links of the chain, and hollow vertices (“○”) are used to denote multiple joints.

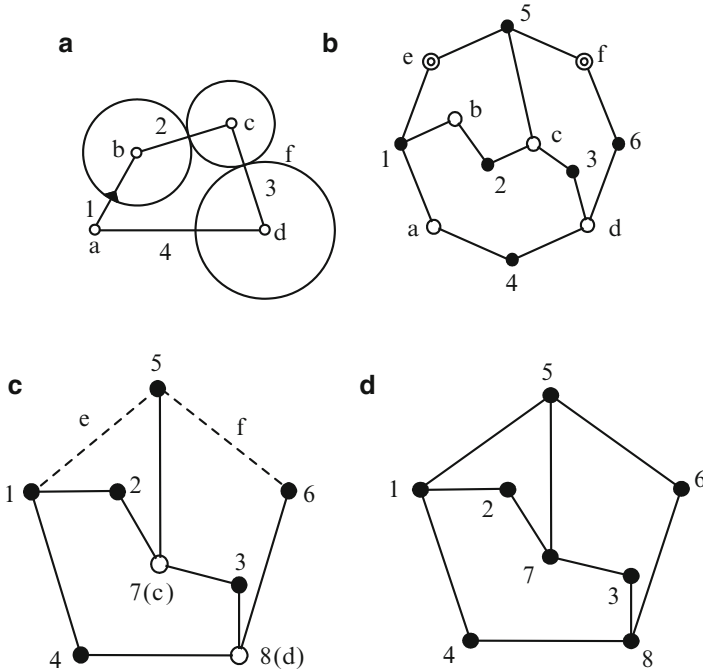


Fig. 10.5 (a) A geared kinematic chain and its (b) conventional tricolor topological graph, (c) new topological graph, and (d) basic topological graph

2. Dash lines (“- -”) are used to denote geared or cam pairs, and solid lines (“-”) are used to denote other joints of the chain.

For example, Fig. 10.5c shows the new topological graph of the geared chain in Fig. 10.5a. Obviously, a geared (cam) chain and its new topological graph are also correspondent.

The new topological graph of the geared kinematic chain can also be represented by the adjacency matrix modified from that of the simple/multiple joint kinematic chain. The elements of the adjacency matrix are

$$A = [a_{ij}]_{n \times n} = \begin{cases} 1, & \text{if vertices } i \text{ and } j \text{ are connected by a solid line} \\ -1, & \text{if vertices } i \text{ and } j \text{ are connected by a dash line} \\ -d, & \text{if } i = j \text{ and } i \text{ (or } j \text{) is the label of a hollow vertex} \\ 0, & \text{otherwise} \end{cases} \quad (10.8)$$

where n is the number of vertices of the graph, and d is the pseudo-degree of the hollow vertices.

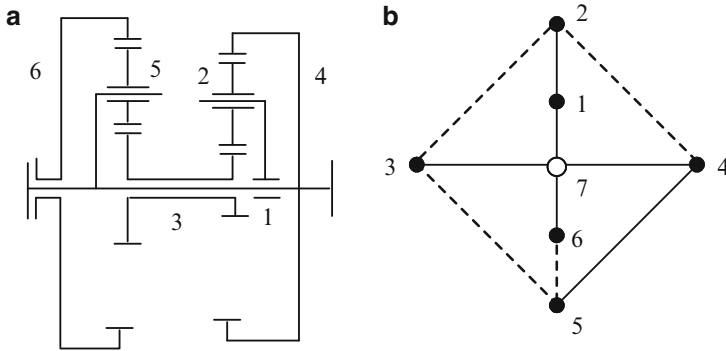


Fig. 10.6 (a) A geared kinematic chain and (b) its new topological graph

For the topological graph in Fig. 10.5c, its adjacency matrix is

$$A = \begin{bmatrix} 0 & 1 & 0 & 1 & -1 & 0 & 0 & 0 \\ 1 & 0 & 0 & 0 & 0 & 0 & 1 & 0 \\ 0 & 0 & 0 & 0 & 0 & 0 & 1 & 1 \\ 1 & 0 & 0 & 0 & 0 & 0 & 0 & 1 \\ -1 & 0 & 0 & 0 & 0 & -1 & 1 & 0 \\ 0 & 0 & 0 & 0 & -1 & 0 & 0 & 1 \\ 0 & 1 & 1 & 0 & 1 & 0 & -3 & 0 \\ 0 & 0 & 1 & 1 & 0 & 1 & 0 & -3 \end{bmatrix} \quad (10.9)$$

Another geared kinematic chain is shown in Fig. 10.6a, and Fig. 10.6b is its new topological graph. The adjacency matrix of the new topological graph is

$$A = \begin{bmatrix} 0 & 1 & 0 & 0 & 0 & 0 & 1 \\ 1 & 0 & -1 & -1 & 0 & 0 & 0 \\ 0 & -1 & 0 & 0 & -1 & 0 & 1 \\ 0 & -1 & 0 & 0 & 1 & 0 & 1 \\ 0 & 0 & -1 & 1 & 0 & -1 & 0 \\ 0 & 0 & 0 & 0 & -1 & 0 & 1 \\ 1 & 0 & 1 & 1 & 0 & 1 & -4 \end{bmatrix} \quad (10.10)$$

The characteristics of the new topological graph of the geared (cam) chain are:

1. The number of vertices of the new topological graph is equal to the sum number of links and multiple joints. This number is reduced remarkably compared with the number of vertices in the conventional tricolor graph.
2. The degree of any solid vertex is equal to the number of joints connected with the corresponding link. The pseudo-degree of every hollow vertex is greater than two, and is one more than the number of the corresponding kinematic pairs.

3. For a geared (cam) kinematic chain with J multiple joints and P geared (or cam) pairs, both the numbers of vertices and edges of its new topological graph increase by J compared with the numbers of links and kinematic pairs of its structural diagram.

For example, the kinematic chain shown in Fig. 10.5a has two multiple joints and two gear pairs. Its new topological graph has 8 and 10 vertices and edges, respectively. Both increase by two compared with the numbers of links and kinematic pairs of its structural diagram.

If the difference between the solid vertices and hollow vertices as well as that between dash lines and solid lines is ignored, then the new topological graph representing the geared (cam) kinematic chain is converted into the topological graph of the simple joint kinematic chain, which is termed the basic topological graph of the geared (cam) kinematic chain. For example, Fig. 10.5d is the basic topological graph of the geared kinematic chain in Fig. 10.5a.

For an N -link geared (cam) kinematic chain, the DOFs of its basic topological graph (F_{BG}) is

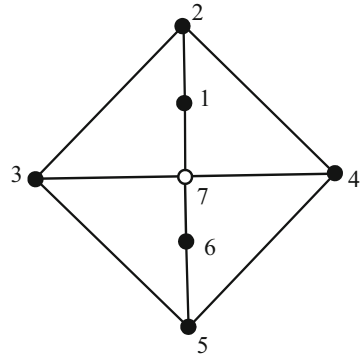
$$\begin{aligned} F_{BG} &= 3 \times (N + J - 1) - 2 \times (M + J - P) \\ &= [3 \times (N - 1) - 2 \times M - P] + J - P \\ &= F + (J - P) \end{aligned} \quad (10.11)$$

where J is the number of multiple joints, M is the number of lower pairs except multiple joints, P is the number of gear pairs, and F is the DOFs of the geared (cam) kinematic chain. The DOFs of the basic topological graph increase by $(J-P)$ compared with the DOFs of the geared (cam) kinematic chain.

The model of the new topological graph inspires us to synthesize the geared (cam) kinematic chain in batch also directly on the structural synthesis of the simple joint kinematic chain and its atlas database. For example, the basic topological graph in Fig. 10.5d has eight vertices and one-DOF because the kinematic chain in Fig. 10.5a has two multiple joints and two gear pairs. Therefore, for the topological graph of an eight-link, one-DOF simple joint kinematic chain, if two vertices whose degrees are greater than two are changed to hollow vertices, and two edges are changed to dash lines, then the topological graph of a six-link, one-DOF geared chain is obtained. In addition, a geared (cam) kinematic chain can be synthesized from the simple joint or multiple joint kinematic chain if the new topological graph representation is adopted.

Example 10.3. For example, Fig. 10.7 shows the new topological graph of a six-link kinematic chain with one multiple joint. Obviously, an edge that is incident with a hollow vertex cannot be changed to a dash line; thus, only six edges can be changed to dash lines. If an edge is represented by the incident vertices, then the six edges are denoted as edges (1, 2), (2, 3), (2, 4), (3, 5), (4, 5), and (5, 6). Edges (1, 2) and (5, 6), edges (2, 3), (2, 4), (3, 5), and (4, 5) are topology symmetrical. Therefore, four non-isomorphic topological graphs (Fig. 10.8a, c, e, g) of geared kinematic

Fig. 10.7 New bicolor topological graph for a multiple joint chain



chains can be derived by eliminating duplicate and invalid graphs (containing rigid sub-chain), and their corresponding geared chains are shown in Fig.10.8b, d, f, h.

Therefore, the structural analysis and synthesis of simple joint kinematic chain is the foundation for multiple joint kinematic chains and geared (cam) kinematic chains.

10.2 Loop Operation Algebra of Kinematic Chains

10.2.1 Loop and Its Representation

In a topological graph, a path consists of an alternating sequence of vertices and edges, where every vertex or edge appears only once, and the starting vertex and ending vertex are different vertices. For example, in a topological graph (Fig. 10.9b) of an eight-link kinematic chain (Fig. 10.9a), successive connecting vertices, 1, 2, 3, and 4 can form a path. Here, a path s is denoted by an n -dimensional array, $P(s)$, where n represents the number of vertices in the topological graph.

When the starting vertex and ending vertex in a path are the same, the path becomes a loop. In Fig. 10.9b, successive connecting vertices, 1, 2, 3, 4, 5, 6, and 1 can form a loop. Loop i in a topological graph is denoted by an n -dimensional array, $L(i)$, where n is the number of vertices of the graph [14].

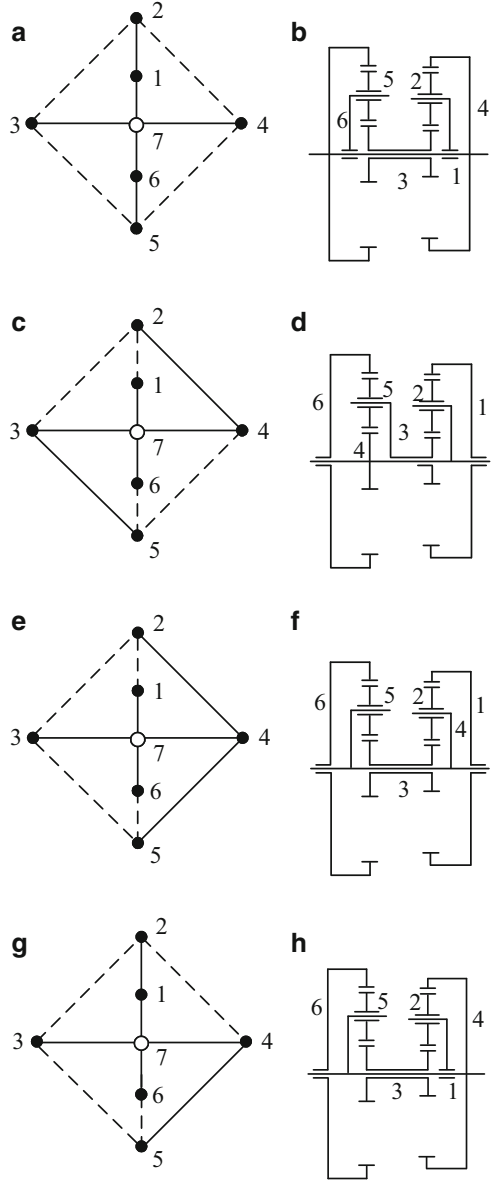
For an n -dimensional array, $P(s)$ or $L(i)$, the j^{th} element (the rightmost element is the first one, and the leftmost element is the last one) indicates the relationship between vertex j and path s or loop i . If vertex j exists in path s or loop i , then the j^{th} element of $P(s)$ or $L(i)$ is “1”; otherwise, it is “0” .

As shown in Fig. 10.9b, loop 1 consists of vertices, 1, 2, 3, 4, 5, and 6. Thus, loop 1 is denoted as

$$L(1) = [0, 0, 1, 1, 1, 1, 1] \tag{10.12}$$

The rightmost element in $L(1)$ is “1”, which indicates vertex 1 in loop $L(1)$. Loop 2 denotes the loop consisting of vertices, 1, 6, 5, 4, 7, and 8; hence,

Fig. 10.8 New topological graphs and their corresponding geared chains



$$L(2) = [1, 1, 1, 1, 1, 0, 0, 1] \tag{10.13}$$

Loop 3 denotes the loop consisting of vertices, 1, 2, 3, 4, 7, and 8; hence,

$$L(3) = [1, 1, 0, 0, 1, 1, 1, 1] \tag{10.14}$$

Fig. 10.9 An eight-link kinematic chain and its topological graph

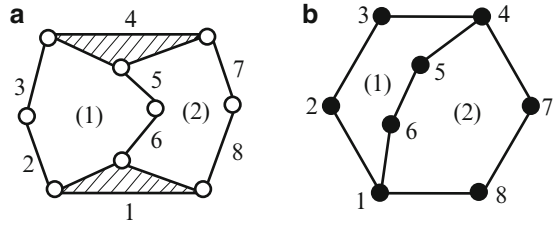
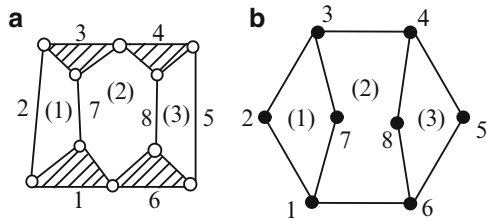


Fig. 10.10 An eight-link kinematic chain and its topological graph



Usually, a kinematic chain has many different loops. For example, the kinematic chain in Fig. 10.10 has six different loops. Generally, if a loop comprises loop a_1 , loop a_2 , \dots , and loop a_k , then the loop can be expressed as $L(a_1 \oplus a_2 \oplus \dots \oplus a_k)$ and is called a combination loop. In Fig. 10.9, loop 3 comprises loop 1 and loop 2, and loop 3 is a combination loop; that is,

$$L(3) = L(1 \oplus 2) \tag{10.15}$$

The number of vertices (or non-zero elements) in a path or loop is defined as the sub-dimension of the path or loop. Here, $N[\cdot]$ is used to denote the sub-dimension of a path or loop. For example, in Fig. 10.9b

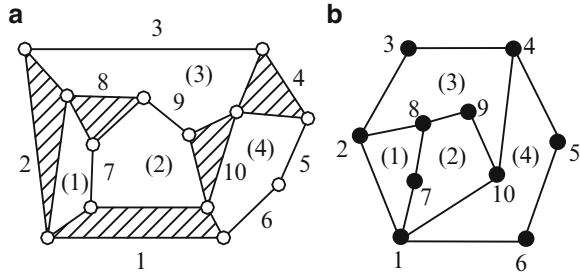
$$N[L(1)] = 6 \tag{10.16}$$

10.2.2 “ Θ ” Operation of Loops

The “ Θ ”operation of two loops is expressed as

$$p(a \Theta b) = L(a) \Theta L(b) \tag{10.17}$$

Fig. 10.11 A ten-link kinematic chain and its topological graph



The algorithm of “ Θ ” operation is

Every element of $L(b)$ is subtracted from its corresponding element of $L(a)$. In each bit of the operation, the result is “1” if the difference is greater than zero; otherwise, it is “0”. That is,

$$p(a \Theta b)_i = \begin{cases} 1, & \text{when } 0 < (b_a(i) - b_b(i)), \\ 0, & \text{otherwise,} \end{cases} \quad (10.18)$$

where $b_a(i)$ is the i th element of loop $L(a)$; $b_b(i)$ is the i th element of loop $L(b)$; and $p(a \Theta b)_i$ is the i th element of $p(a \Theta b)$.

Array $p(a \Theta b)$ denotes the path (paths) consisting of the vertices on loop $L(a)$ but not on loop $L(b)$, and its dimension is the same as the two operated loops.

Example 10.4. For example, in Fig. 10.11

$$\begin{aligned} L(1) &= [0, 0, 1, 1, 0, 0, 0, 0, 1, 1] \\ &\quad \Theta \\ L(2) &= [1, 1, 1, 1, 0, 0, 0, 0, 0, 1] \\ &= \\ P(1 \Theta 2) &= [0, 0, 0, 0, 0, 0, 0, 0, 1, 0] \end{aligned} \quad (10.19)$$

The second bit of $P(1 \Theta 2)$ is not zero, suggesting that vertex 2 is in loop 1 but not in loop 2.

10.2.3 “ \otimes ” Operation of Loops

The “ \otimes ” operation of two loops is expressed as

$$p(a \otimes b) = L(a) \otimes L(b) \quad (10.20)$$

The algorithm of “ \otimes ” operation is

Every element of $L(a)$ is compared with its corresponding element of $L(b)$. In each bit, the result is “1” if they are both equal to “1”; otherwise, it is “0”. That is,

$$p(a \otimes b)_i = \begin{cases} 1, & \text{when } b_a(i) = b_b(i) = 1, \\ 0, & \text{otherwise.} \end{cases} \quad (10.21)$$

where $b_a(i)$ is the i th element of loop $L(a)$; $b_b(i)$ is the i th element of loop $L(b)$; and $p(a \otimes b)_i$ is the i th element of the “ \otimes ” operation result of loops $L(a)$ and $L(b)$.

Array $p(a \otimes b)$ denotes the path (paths) consisting of the vertices that are both on loops $L(a)$ and $L(b)$, and its dimension is the same as the two operated loops.

10.2.4 “ \oplus ” Operation of Loops

The “ \oplus ” operation of two loops is expressed as

$$LP = L(a) \oplus L(b) \quad (10.22)$$

Where LP is an array, and its dimension is the same as the two operated loops.

The algorithm of “ \oplus ” operation is

Every element in $L(a)$ is added to its corresponding element in $L(b)$. In each bit, if the sum is smaller than the *local degree* of the corresponding vertex, then the result is “1”; otherwise, it is “0”. That is,

$$LP(i) = \begin{cases} 1, & \text{when } 0 < (b_a(i) + b_b(i)) < d_l(i) \\ 0, & \text{otherwise} \end{cases} \quad (10.23)$$

where $b_a(i)$ is the i th element of loop $L(a)$; $b_b(i)$ is the i th element of loop $L(b)$; and $d_l(i)$ is the *local degree* of the i th vertices. If LP is a loop, then it can be denoted as $L(a \oplus b)$.

In the “ \oplus ” operation of two loops, the *local degrees* of vertices are the degrees of vertices of the topological graph obtained by modifying the original topological graph according to the following rules:

1. All vertices not in either of the two operated loops and their corresponding connection relationships must be removed from the original topological graph.
2. All inner connection relationships, if any, of the two loops must be removed from the original topological graph.

Example 10.5. For example, in Fig. 10.9b all vertices are either in loop 1 or in loop 2, and loop 1 or loop 2 has no inner connection relationship; thus, the local degrees of vertices are equal to the original degrees of vertices. The “ \oplus ” operation of $L(1)$ and $L(2)$ can be expressed as follows:

$$\begin{aligned}
 L(1) &= [0, 0, 1, 1, 1, 1, 1, 1] \\
 &\quad \oplus \\
 L(2) &= [1, 1, 1, 1, 1, 0, 0, 1] \\
 &\quad = \\
 &= [1, 1, 0, 0, 1, 1, 1, 1]
 \end{aligned}
 \tag{10.24}$$

In the result of this operation: for the rightmost bit, as the sum is two and the local degree of vertex 1 is three, the result is one; for the fifth bit from the rightmost, as the sum is two and the local degree of vertex 5 is two, the result is zero.

Obviously, $L(1) \oplus L(2) = [1, 1, 0, 0, 1, 1, 1, 1]$ is the combination loop $L(1 \oplus 2)$. In a kinematic chain, if the combination loop $L(a \oplus b)$ exists, then it can be obtained through the “ \oplus ” operation of loop a and loop b . That is,

$$L(a \oplus b) = L(a) \oplus L(b) \tag{10.25}$$

Example 10.6. For example, if loop 4 in Fig. 10.10 consists of vertices 1, 2, 3, 4, 8, and 6, then, $L(4) = [1, 0, 1, 0, 1, 1, 1, 1]$. In the “ \oplus ” operation of $L(4)$ and $L(3)$, vertex 7 is neither in loop $L(4)$ nor in loop $L(3)$. Thus, vertex 7 and its corresponding connection relationship must be removed, and the local degrees of both vertices 1 and 3 are two.

For computer realization, the local degrees of vertices can also be obtained by modifying the corresponding adjacency matrix. For Fig. 10.10, the adjacency matrix is given by

$$A = \begin{bmatrix}
 0 & 1 & 0 & 0 & 0 & 1 & 1 & 0 \\
 1 & 0 & 1 & 0 & 0 & 0 & 0 & 0 \\
 0 & 1 & 0 & 1 & 0 & 0 & 1 & 0 \\
 0 & 0 & 1 & 0 & 1 & 0 & 0 & 1 \\
 0 & 0 & 0 & 1 & 0 & 1 & 0 & 0 \\
 1 & 0 & 0 & 0 & 1 & 0 & 0 & 1 \\
 \hline
 1 & 0 & 1 & 0 & 0 & 0 & 0 & 0 \\
 \hline
 0 & 0 & 0 & 1 & 0 & 1 & 0 & 0
 \end{bmatrix}
 \begin{matrix}
 v_1 \\
 v_2 \\
 v_3 \\
 v_4 \\
 v_5 \\
 v_6 \\
 v_7 \\
 v_8
 \end{matrix}
 \tag{10.26}$$

In the “ \oplus ” operation of $L(4)$ and $L(3)$, vertex 7 and its corresponding connection relationship must be removed. That is, the seventh row and the seventh column must be removed from matrix A . The resulting adjacency matrix A_1 is

$$A_1 = \begin{array}{cccccc|c} 0 & 1 & 0 & 0 & 0 & 1 & 0 & v_1 \\ 1 & 0 & 1 & 0 & 0 & 0 & 0 & v_2 \\ 0 & 1 & 0 & 1 & 0 & 0 & 0 & v_3 \\ 0 & 0 & 1 & 0 & 1 & 0 & 1 & v_4 \\ 0 & 0 & 0 & 1 & 0 & 1 & 0 & v_5 \\ \hline 1 & 0 & 0 & 0 & 1 & 0 & 1 & v_6 \\ \hline 0 & 0 & 0 & 1 & 0 & 1 & 0 & v_8 \end{array} \quad (10.27)$$

Two non-zero elements correspond to vertex 3 in matrix A_1 . Thus, the local degree of vertex 3 is no longer three, but two. The local degree of vertex 1 is no longer three, but two. The local degrees of other vertices are the same as their original degrees. Hence,

$$\begin{aligned} L(4) &= [1, 0, 1, 0, 1, 1, 1, 1] \\ &\oplus \\ L(3) &= [1, 0, 1, 1, 1, 0, 0, 0] \\ &= \\ &[0, 0, 1, 1, 1, 1, 1, 1] \end{aligned} \quad (10.28)$$

Example 10.7. For the chain in Fig. 10.11, in the “ \oplus ” operation of $L(3)$ and $L(4)$

$$L(3) = [1, 1, 1, 0, 0, 0, 1, 1, 1, 0] \quad (10.29)$$

$$L(4) = [1, 0, 0, 0, 1, 1, 1, 0, 0, 1] \quad (10.30)$$

vertex 7 is neither in loop 3 nor in loop 4. Thus, vertex 7 and its corresponding connection relationships must be removed. The local degree of vertex 8 is no longer three, but two, and the local degree of vertex 1 is no longer four, but three. The result can also be obtained by modifying the corresponding adjacency matrix. For example, in Fig. 10.11, the adjacency matrix is given by

$$B = \begin{array}{cccccc|c|ccc} 0 & 1 & 0 & 0 & 0 & 1 & 1 & 0 & 0 & 1 & v_1 \\ 1 & 0 & 1 & 0 & 0 & 0 & 0 & 1 & 0 & 0 & v_2 \\ 0 & 1 & 0 & 1 & 0 & 0 & 0 & 0 & 0 & 0 & v_3 \\ 0 & 0 & 1 & 0 & 1 & 0 & 0 & 0 & 0 & 1 & v_4 \\ 0 & 0 & 0 & 1 & 0 & 1 & 0 & 0 & 0 & 0 & v_5 \\ \hline 1 & 0 & 0 & 0 & 1 & 0 & 0 & 0 & 0 & 0 & v_6 \\ \hline 1 & 0 & 0 & 0 & 0 & 0 & 0 & 1 & 0 & 0 & v_7 \\ \hline 0 & 1 & 0 & 0 & 0 & 0 & 1 & 0 & 1 & 0 & v_8 \\ 0 & 0 & 0 & 0 & 0 & 0 & 0 & 1 & 0 & 1 & v_9 \\ 1 & 0 & 0 & 1 & 0 & 0 & 0 & 0 & 1 & 0 & v_{10} \end{array} \quad (10.31)$$

In the “ \oplus ” operation of $L(3)$ and $L(4)$, vertex 7 and its corresponding connection relationships must be removed. That is, the seventh row and the seventh column of matrix \mathbf{B} must be removed. The resulting adjacency matrix is given by

$$\mathbf{B}_1 = \begin{array}{c} \left[\begin{array}{cccccc|ccc} 0 & 1 & 0 & 0 & 0 & 1 & 0 & 0 & 1 \\ 1 & 0 & 1 & 0 & 0 & 0 & 1 & 0 & 0 \\ 0 & 1 & 0 & 1 & 0 & 0 & 0 & 0 & 0 \\ 0 & 0 & 1 & 0 & 1 & 0 & 0 & 0 & 1 \\ 0 & 0 & 0 & 1 & 0 & 1 & 0 & 0 & 0 \\ \hline 1 & 0 & 0 & 0 & 1 & 0 & 0 & 0 & 0 \\ 0 & 1 & 0 & 0 & 0 & 0 & 0 & 1 & 0 \\ 0 & 0 & 0 & 0 & 0 & 0 & 1 & 0 & 1 \\ 1 & 0 & 0 & 1 & 0 & 0 & 0 & 1 & 0 \end{array} \right] \begin{array}{l} v_1 \\ v_2 \\ v_3 \\ v_4 \\ v_5 \\ v_6 \\ v_8 \\ v_9 \\ v_{10} \end{array} \end{array} \quad (10.32)$$

Two non-zero elements correspond to vertex 8 in matrix \mathbf{B}_1 . Thus, the local degree of vertex 8 is no longer three but two. The local degree of vertex 1 is no longer four but three. The local degrees of other vertices are the same as their original degrees. Hence,

$$\begin{aligned} L(3) &= [1, 1, 1, 0, 0, 0, 1, 1, 1, 0] \\ &\quad \oplus \\ L(4) &= [1, 0, 0, 0, 1, 1, 1, 0, 0, 1] \\ &\quad = \\ L(3 \oplus 4) &= [1, 1, 1, 0, 1, 1, 1, 1, 1, 1] \end{aligned} \quad (10.33)$$

1. Conditions of the “ \oplus ” operation

Generally, the “ \oplus ” operation of two loops forms a combination loop. However, $LP = L(a) \oplus L(b)$ cannot constitute a loop sometimes. For example, the result of $L(1) \oplus L(3)$ in Fig. 10.10 cannot constitute a loop. Thus, to ensure that the result also forms a loop in the “ \oplus ” operation of loops a and b , the following conditions must be satisfied:

Condition 1. The two loops must at least have two shared vertices and all these shared vertices constitute only a path. That is,

$$N[L(a) \otimes L(b)] \geq 2 \quad \text{and} \quad p(a \otimes b) \text{ is a path} \quad (10.34)$$

Condition 2. The two corresponding bits of operated loops and their operation result are all “1”, which occurs exactly twice.

For example, in Fig. 10.10, $N[L(1) \otimes L(3)] = 0$, and Condition 1 is not satisfied. The result of $L(1) \oplus L(3)$ cannot form a loop, and is meaningless.

Example 10.8. For example, in Fig. 10.11 where

$$L(1) = [0, 0, 1, 1, 0, 0, 0, 0, 1, 1] \quad (10.35)$$

$$L(4) = [1, 0, 0, 0, 1, 1, 1, 0, 0, 1] \quad (10.36)$$

$N[L(1) \otimes L(4)] = 1$; thus, the result of $L(1) \oplus L(4)$ cannot form a loop.

2. Properties of the “ \oplus ” operation

The properties for the “ \oplus ” operation of any loops $L(a)$, $L(b)$, and $L(c)$ in a kinematic chain are as follows:

1. Commutative Law

$$L(a) \oplus L(b) = L(b) \oplus L(a) \quad (10.37)$$

2. Combination Law

If both $L(a) \oplus L(b)$ and $L(b) \oplus L(c)$ satisfy the existent conditions of the “ \oplus ” operation of loops, then the “ \oplus ” operation satisfies the following combination law:

$$[L(a) \oplus L(b)] \oplus L(c) = L(a) \oplus [L(b) \oplus L(c)] \quad (10.38)$$

3. Self-Vanish Law

$$L(a) \oplus L(a) = \theta \quad (10.39)$$

Where θ denotes an n -dimensional array whose elements are all zeros, and n is the dimension of array $L(a)$.

Proof: the operated corresponding bits are always the same when the “ \oplus ” operation is done on loop $L(a)$ and itself. If both are zero, then the result is zero; if both are one for the local degree of the vertex is two, the result is also zero. Thus, $L(a) \oplus L(a) = \theta$.

4. Absorption Law

$$L(a) \oplus L(a \oplus b) = L(b) \quad (10.40)$$

Proof:

$$\begin{aligned} & L(a) \oplus L(a \oplus b) \\ &= L(a) \oplus (L(a) \oplus L(b)) \\ &= (L(a) \oplus L(a)) \oplus L(b) \\ &= \theta \oplus L(b) \\ &= L(b) \end{aligned}$$

Example 10.9. For example, in Fig. 10.10

$$\begin{aligned}
 L(1) &= [0, 1, 0, 0, 0, 1, 1, 1] \\
 &\oplus \\
 L(1 \oplus 2) &= [1, 0, 1, 0, 1, 1, 1, 1] \\
 &= \\
 L(2) &= [1, 1, 1, 0, 1, 1, 0, 1]
 \end{aligned} \tag{10.41}$$

That is,

$$L(1) \oplus L(1 \oplus 2) = L(2) \tag{10.42}$$

Other examples of the “ \oplus ” operation in Fig. 10.10 are

$$L(1) \oplus L(2 \oplus 3) = L(1 \oplus 2 \oplus 3) \tag{10.43}$$

$$L(3) \oplus L(1 \oplus 2) = L(1 \oplus 2 \oplus 3) \tag{10.44}$$

$$L(1 \oplus 2) \oplus L(1 \oplus 2 \oplus 3) = L(3) \tag{10.45}$$

$$L(2 \oplus 3) \oplus L(1 \oplus 2 \oplus 3) = L(1) \tag{10.46}$$

But

$$L(1 \oplus 2) \oplus L(2 \oplus 3) \neq L(1 \oplus 3) \tag{10.47}$$

The reason is that they do not satisfy the existent conditions of the “ \oplus ” operation of loops, and the result is meaningless.

10.2.5 Loop Analysis

10.2.5.1 Independent Loop Set

The Euler Theorem points out that for a polygon meshwork with n vertices and m edges, the number of its independent loops, v , satisfies the following equation:

$$v = m - n + 1 \tag{10.48}$$

Obviously, the Euler Theorem establishes the basic relationship among the number of vertices, the number of edges, and the number of independent loops of

a topological graph. If a kinematic chain is represented by the corresponding topological graph, then the number of its independent loops can be obtained through the Euler Theorem. For example, the number of the chain in Fig. 10.9 is $v = 9 - 8 + 1 = 2$.

Here, if a loop set in a topological graph satisfies the following two conditions, then the loop set is an independent loop set:

1. Its number of loops is the same as the number of independent loop v determined by the Euler Theorem.
2. All other loops in this topological graph can be obtained through the “ \oplus ” operation of those loops in the loop set.

For example, in Fig. 10.9, the number of loops for the loop set $\{L(1), L(2)\}$ is two. The other loop satisfies the equation $L(1 \oplus 2) = L(1) \oplus L(2)$. Thus, the loop set $\{L(1), L(2)\}$ is an independent loop set. Obviously, the loop set $\{L(1), L(1 \oplus 2)\}$ or $\{L(2), L(1 \oplus 2)\}$ can also serve as an independent loop set.

Generally, selecting the independent loop set for a kinematic chain has many different ways. The selection rule of independent loop set is given as follows:

Theorem 10.1. For the topological graph of a kinematic chain, any loop set $\{L(1), L(2), \dots, L(v)\}$ consisting of v loops is selected, with v determined by the Euler Theorem. For any three different loops in the loop set, $L(i), L(j)$, and $L(k)$ ($i, j, k=1, 2, \dots, v$), if there does not exist

$$L(i) \oplus L(j) = L(k) \tag{10.49}$$

the loop set $\{L(1), L(2), \dots, L(v)\}$ is an independent loop set.

The chain in Fig. 10.10 has six loops in all, namely, $L(1), L(2), L(3), L(1 \oplus 2), L(2 \oplus 3)$, and $L(1 \oplus 2 \oplus 3)$. The independent loop number is $v = 9 - 8 + 1 = 3$. The independent loop set of this topological graph can be selected as follows:

$\{L(1), L(2), L(3)\}$, $\{L(1), L(2), L(2 \oplus 3)\}$, $\{L(2), L(3), L(1 \oplus 2)\}$, or $\{L(1), L(2), L(1 \oplus 2 \oplus 3)\}$, and so on.

However, neither

$\{L(1), L(2), L(1 \oplus 2)\}$ nor $\{L(2), L(3), L(2 \oplus 3)\}$ can be selected as the independent loop set, because $L(1) \oplus L(2) = L(1 \oplus 2)$ and $L(2) \oplus L(3) = L(2 \oplus 3)$.

The usual selection rules for the independent loop set of a plane topological graph and non-plane one are given as follows:

1. For a planar topological graph, that is, a topological graph that can be represented by a planar graph, its mesh loops, within which no other loops are present, can be selected as the independent loop set.

For example, the mesh loop $L(1)$ in Fig. 10.11 consisting of vertices 1, 2, 8, and 7 can be selected as one of the independent loops, the mesh loop $L(2)$ consisting of vertices 1, 7, 8, 9, and 10 can be selected as another independent loop, the mesh loop $L(3)$ consisting of vertices 2, 3, 4, 10, 9, and 8 can be selected as a third independent loop, and the mesh loop $L(4)$ consisting of vertices 1, 10, 4, 5

and 6 can be selected as a fourth independent loop. Obviously, the loop set $\{L(1), L(2), L(3), L(4)\}$ is an independent loop set.

2. For a non-plane graph, that is, a topological graph that cannot be represented by a plane graph, its mesh loops, if any, can also be selected as independent loops. According to the rule for selecting the rest independent loops, every selected loop contains new vertices or edges that are not present in other independent loops.

10.2.5.2 Loop Relationship

In a topological graph, when an independent loop set has been determined, other loops not in the independent loop set are defined as the dependent loops. The concept of dependent loops is different from that of combination loops. A combination loop is not necessarily a dependent loop, and a non-combination loop is not necessarily an independent loop. For example, in Fig. 10.10, when the three loops, $L(1)$, $L(2)$, and $L(2 \oplus 3)$, are selected as independent loops, all other loops, $L(3)$, $L(1 \oplus 2)$, and $L(1 \oplus 2 \oplus 3)$, are dependent loops. In this case, the loop $L(2 \oplus 3)$ is a combination loop and an independent loop, and the non-combination loop $L(3)$ is a dependent loop.

For a kinematic chain, regardless of the different drawing modes and different labeling modes, its loops depend only on its topological structure. The relationship of loops in a topological graph can be summarized in Theorem 10.2.

Theorem 10.2. For a topological graph, when a loop set is selected as its independent loop set, all other loops are dependent loops and can be obtained through the “ \oplus ” operation of the independent loops.

Example 10.10. For example, Fig. 10.10 has six loops in all, $L(1)$, $L(2)$, $L(3)$, $L(4)$, $L(5)$, and $L(6)$, where $L(4) = L(1 \oplus 2)$, $L(5) = L(2 \oplus 3)$, and $L(6) = L(1 \oplus 2 \oplus 3)$.

When the loop set $\{L(1), L(3), L(6)\}$ is selected as the independent loop set, the remaining loops, $L(4)$, $L(5)$, and $L(2)$, are dependent loops and can be obtained using the “ \oplus ” operation of loops $L(1)$, $L(3)$, and $L(6)$. That is,

$$L(2) = L(1) \oplus L(6) \oplus L(3) \quad (10.50)$$

$$L(4) = L(6) \oplus L(3) \quad (10.51)$$

$$L(5) = L(1) \oplus L(6) \quad (10.52)$$

The loop set containing all loops of a topological graph is defined as the maximum loop set, which is denoted as SE_{max} . The number of loops in the

maximum loop set is called its order, which is denoted as $Or(SE_{max})$, which is $\sum_{i=1}^v C_v^i$, i.e., the number of combinations of all the independent loops, subtracted by μ , i.e., the number of operations that do not satisfy the conditions of “ \oplus ” operation. That is,

$$Or(SE_{max}) = \sum_{i=1}^v C_v^i - \mu \quad (10.53)$$

10.2.6 Edge-Based Operations of Loops

In the topological graph of a kinematic chain, a path or loop a can also be denoted by an m -dimensional array, $P(a)$ or $L(a)$, where m is the number of edges of the chain [15]. The j th element in $P(a)$ or $L(a)$ (the rightmost element is the first one, and the leftmost element is the last one) indicates the relationship between edge j and path or loop a . If edge j exists in path or loop a , then the j th element of $P(a)$ or $L(a)$ is “1”; otherwise, it is “0”. The operations of loops established based on the edge-based representation is defined as the edge-based operations of loops. The loops in a kinematic chain have three basis operations:

10.2.6.1 The “ Θ ” Operation of Loops

The “ Θ ” operation of two loops is expressed as follows:

$$p(a \Theta b) = L(a) \Theta L(b) \quad (10.54)$$

The algorithm of “ Θ ” operation is

Every element of $L(b)$ is subtracted from its corresponding element of $L(a)$. In each bit of the operation, if the difference is greater than zero, then the result is “1”; otherwise, it is “0”. That is,

$$p(a \Theta b)_i = \begin{cases} 1, & \text{when } 0 < (b_a(i) - b_b(i)), \\ 0, & \text{otherwise,} \end{cases} \quad (10.55)$$

where $b_a(i)$ is the i th element of loop $L(a)$; $b_b(i)$ is the i th element of loop $L(b)$; and $p(a \Theta b)_i$ is the i th element of $p(a \Theta b)$.

Array $p(a \Theta b)$ denotes the path (paths) consisting of edges on loop $L(a)$, but not on loop $L(b)$.

10.2.6.2 The “ \otimes ” Operation of Loops

The “ \otimes ”operation of two loops is expressed as follows:

$$p(a \otimes b) = L(a) \otimes L(b) \quad (10.56)$$

The algorithm of “ \otimes ”operation is

Every element of $L(a)$ is compared with its corresponding element of $L(b)$. In each bit, if they are both equal to “1”, then the result is “1”; otherwise, it is “0”. That is,

$$p(a \otimes b)_i = \begin{cases} 1, & \text{when } b_a(i) = b_b(i) = 1, \\ 0, & \text{otherwise.} \end{cases} \quad (10.57)$$

where $b_a(i)$ is the i th element of loop $L(a)$; $b_b(i)$ is the i th element of loop $L(b)$; and $p(a \otimes b)_i$ is the i th element of the “ \otimes ” operation result of loops $L(a)$ and $L(b)$.

Array $p(a \otimes b)$ denotes the path (paths) consisting of those edges that are on both loops $L(a)$ and $L(b)$.

10.2.6.3 The “ \oplus ” Operation of Loops

The “ \oplus ” operation of two loops is expressed as follows:

$$LP = L(a) \oplus L(b) \quad (10.58)$$

where LP is an array whose dimension is the same as the two operated loops.

The algorithm of “ \oplus ”operation is

Every element of $L(a)$ is compared with the corresponding element of $L(b)$. In each bit, if they are not equal, then the result is “1”; otherwise, it is “0”. That is,

$$LP(i) = \begin{cases} 1, & \text{when } b_a(i) \neq b_b(i), \\ 0, & \text{otherwise,} \end{cases} \quad (10.59)$$

where $b_a(i)$ is the i th element of loop $L(a)$; $b_b(i)$ is the i th element of loop $L(b)$; and $LP(i)$ is the i th element of the array $LP(i)$.

If LP is a loop, then it can be expressed as $L(a \oplus b)$, which denotes the loop obtained through the combination of loops $L(a)$ and $L(b)$. Obviously, the necessary and sufficient condition for the “ \oplus ” operation result of loops $L(a)$ and $L(b)$ to be a loop is that $p(a \otimes b) = L(a) \otimes L(b)$ is a path (not two or more paths).

10.3 Isomorphism Identification

10.3.1 Perimeter Topological Graph

For a graph with v independent loops, the total number of its loops is TN at most, where

$$TN = \sum_{i=1}^v C_v^i = 2^v - 1 \tag{10.60}$$

For example, as the number of independent loops in Fig. 10.12 is $v = 3$, the total number of loops is seven at most. In fact, the graph has seven loops. That is,

Consist of vertices								
$L(1)$	1	2	3	4	5			
$L(2)$	1	5	4	7	6	2		
$L(3)$	1	8	3	2				
$L(4)$	1	8	3	4	5			
$L(5)$	1	8	3	4	7	6	2	
$L(6)$	1	8	3	2	6	7	4	5
$L(7)$	2	6	7	4	3			

(10.61)

Among all the loops of a graph, the loops with the most number of vertices or edges are defined as the *maximum loops*. For example, the graph in Fig.10.12 has only one maximum loop, which is constituted by vertices 1, 8, 3, 2, 6, 7, 4, and 5.

In a loop, the *degree-sequence* is the degree permutation of vertices sequenced one by one from a starting vertex along the loop in clockwise or in counterclockwise direction. Different starting vertices make different degree-sequences, and different directions make different degree-sequences. These degree-sequences can be viewed as numbers. For a loop, the largest number is defined as its *canonical degree-sequence*. For a graph, the largest number of the canonical degree-sequences of all its maximum loops is defined as the *canonical perimeter degree-sequence*, and the corresponding maximum loops are defined as the *perimeter loops*. Obviously, for

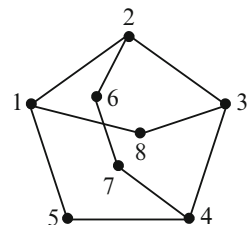


Fig. 10.12 An eight-vertex graph

Fig. 10.13 PTG for Fig. 10.12

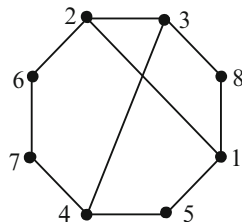
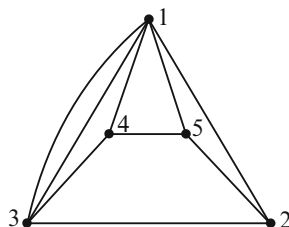


Fig. 10.14 A contracted graph



a graph, the canonical perimeter degree-sequence is unique, although several perimeter loops may exist. For example, the graph in Fig. 10.12 has only one perimeter loop, $L(6)$, and its canonical perimeter degree-sequence is 33232322.

A graph can be drawn in many different ways. The perimeter topological graphs (PTG) of a graph are drawn as follows [16, 17]:

1. Each perimeter loop is drawn as a uniform polygon.
2. The rest of the connections are filled as inner sub-chains.

Obviously, a corresponding perimeter topological graph can be drawn from a perimeter loop. The number of perimeter topological graphs is equal to the number of perimeter loops.

For example, the graph in Fig. 10.12 has only one perimeter loop. From the perimeter loop, the corresponding perimeter topological graph is shown in Fig. 10.13.

For example, the contracted graph in Fig. 10.14 has two maximum loops. The first is constituted by vertices 1, 3, 2, 5, and 4 and the second is by vertices 1, 3, 4, 5, and 2. The canonical degree-sequence for the first maximum loop is 54333, and the canonical degree-sequence for the second is also 54333. Obviously, both maximum loops are perimeter loops. The two perimeter topological graphs corresponding to the two perimeter loops are shown in Fig. 10.15. The forms of the two perimeter topological graphs are the same, but with different labels.

The graph in Fig. 10.16a is a topological graph for a 12-link, one-DOF kinematic chain. It has four perimeter loops: the perimeter loop $L(p_1)$ constituted by vertices 8, 10, 1, 2, 3, 4, 5, 6, and 7; the perimeter loop $L(p_2)$ constituted by vertices 8, 10, 1, 2, 3, 4, 5, 12, and 11; the perimeter loop $L(p_3)$ constituted by vertices 8, 9, 1, 2, 3, 4, 5, 6, and 7; and the perimeter loop $L(p_4)$ constituted by vertices 8, 9, 1, 2, 3, 4, 5, 12, and 11. From each perimeter loop, a corresponding perimeter topological graph can be obtained. The forms of the four perimeter topological graphs are the same, but

Fig. 10.15 Two PTGs for Fig. 10.14

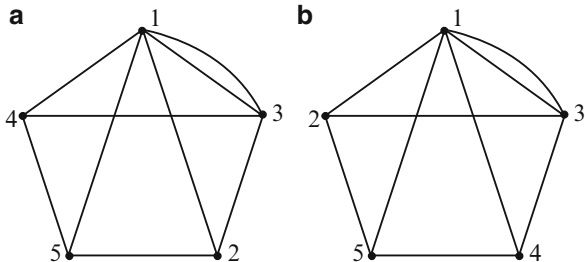
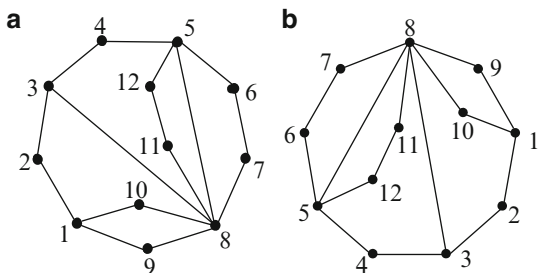


Fig. 10.16 (a) A 12-vertex topological graph and (b) one of its PTGs



with different labels. Figure 10.16b is the perimeter topological graph corresponding to perimeter loop $L(p_3)$.

For the topological graphs of kinematic chains, the forms of the perimeter topological graphs are limited to just several, in most cases only one.

10.3.2 Canonical Perimeter Topological Graph

In a graph, a corresponding perimeter topological graph can be obtained from one of its perimeter loops. The number of its perimeter topological graphs is the same as the number of its perimeter loops. Furthermore, most of the forms of these perimeter topological graphs are the same. Therefore, the perimeter topological graph makes the forms of a graph canonical. To develop a computer-aided method for automatic structural analysis and synthesis, the canonical label of perimeter topological graph is also necessary.

Based on the canonical degree-sequence of perimeter loops, the canonical label of vertices on perimeter loops can be obtained according to the following rules:

1. Each vertex of the perimeter loop is relabeled by the numbering $i = 1, 2, 3, \dots$ in the order of the canonical perimeter degree-sequence.
2. If several canonical perimeter degree-sequences can be obtained, the numbering is started at the vertex connected to the inner sub-chain with the largest number of vertices.

Thus, the canonical label of vertices on the perimeter loop can be obtained.

Here, if an inner sub-chain is a path and is connected with only two vertices on the perimeter loop with the canonical labels m and n , the sub-chain is represented by an array $[m, n]$ ($m \leq n$). The number of vertices on the inner sub-chain is defined as its sub-dimension. For two inner sub-chains $[m_1, n_1]$ and $[m_2, n_2]$, the inner sub-chain with a larger sub-dimension is of a higher rank. When their sub-dimensions are the same, if $m_1 < m_2$, then the rank of sub-chain $[m_1, n_1]$ is higher, and vice versa. When $m_1 = m_2$, if $n_1 < n_2$, then the rank of sub-chain $[m_1, n_1]$ is higher, and vice versa. Their ranks are the same if $m_1 = m_2$ and $n_1 = n_2$.

The canonical label of the vertices on inner sub-chains is obtained according to the following rules:

1. Vertices on inner sub-chains which are not connected with only two vertices on the perimeter loop are relabeled according to their degrees. The vertices with the bigger degrees are relabeled first.
2. Vertices on inner sub-chains which are connected with only two vertices on the perimeter loop are relabeled according to the ranks of inner sub-chains. The vertices on the inner sub-chain with higher rank are relabeled first.
3. For vertices on an inner sub-chain $[m, n]$ $m \leq n$, the vertex connected with vertex m is relabeled first, and the other vertices are relabeled in turn along the sub-chain.

A perimeter topological graph labeled in this manner is termed the *canonical perimeter topological graph*(CaPTG), and the corresponding adjacency matrix is defined as the *canonical adjacency matrix*.

Example 10.11. For example, the canonical labels for the perimeter topological graph in Fig. 10.13 are 1, 2, 3, 4, 5, 6, 7, and 8 for vertices 2, 3, 8, 1, 5, 4, 7, and 6, respectively. The canonical perimeter topological graph is shown in Fig. 10.17, and its canonical adjacency matrix is

$$\begin{bmatrix}
 0 & 1 & 0 & 1 & 0 & 0 & 0 & 1 \\
 1 & 0 & 1 & 0 & 0 & 1 & 0 & 0 \\
 0 & 1 & 0 & 1 & 0 & 0 & 0 & 0 \\
 1 & 0 & 1 & 0 & 1 & 0 & 0 & 0 \\
 0 & 0 & 0 & 1 & 0 & 1 & 0 & 0 \\
 0 & 1 & 0 & 0 & 1 & 0 & 1 & 0 \\
 0 & 0 & 0 & 0 & 0 & 1 & 0 & 1 \\
 1 & 0 & 0 & 0 & 0 & 0 & 1 & 0
 \end{bmatrix} \tag{10.62}$$

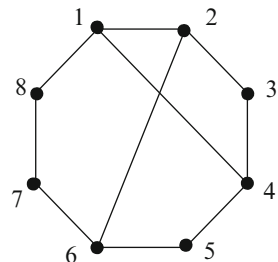
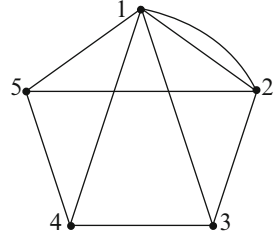


Fig. 10.17 CaPTG of Fig. 10.13

Fig. 10.18 Shared CaPTG for Fig. 10.15



Example 10.12. The canonical perimeter topological graphs for the two perimeter topological graphs in Fig. 10.15a, b are the same, shown in Fig. 10.18. The canonical adjacency matrix is

$$\begin{bmatrix} 0 & 2 & 1 & 1 & 1 \\ 2 & 0 & 1 & 0 & 1 \\ 1 & 1 & 0 & 1 & 0 \\ 1 & 0 & 1 & 0 & 1 \\ 1 & 1 & 0 & 1 & 0 \end{bmatrix} \tag{10.63}$$

Example 10.13. The graph in Fig. 10.16a has four perimeter topological graphs. The canonical perimeter topological graphs for the four perimeter topological graphs are the same, and their shared canonical perimeter topological graph is shown in Fig. 10.19. The canonical adjacency matrix is

$$\begin{bmatrix} 0 & 1 & 0 & 0 & 1 & 0 & 1 & 0 & 1 & 1 & 0 & 1 \\ 1 & 0 & 1 & 0 & 0 & 0 & 0 & 0 & 0 & 0 & 0 & 0 \\ 0 & 1 & 0 & 1 & 0 & 0 & 0 & 0 & 0 & 0 & 0 & 1 \\ 0 & 0 & 1 & 0 & 1 & 0 & 0 & 0 & 0 & 0 & 0 & 0 \\ 1 & 0 & 0 & 1 & 0 & 1 & 0 & 0 & 0 & 0 & 0 & 0 \\ 0 & 0 & 0 & 0 & 1 & 0 & 1 & 0 & 0 & 0 & 0 & 0 \\ 1 & 0 & 0 & 0 & 0 & 1 & 0 & 1 & 0 & 0 & 1 & 0 \\ 0 & 0 & 0 & 0 & 0 & 0 & 1 & 0 & 1 & 0 & 0 & 0 \\ 1 & 0 & 0 & 0 & 0 & 0 & 0 & 1 & 0 & 0 & 0 & 0 \\ 1 & 0 & 0 & 0 & 0 & 0 & 0 & 0 & 0 & 0 & 1 & 0 \\ 0 & 0 & 0 & 0 & 0 & 0 & 1 & 0 & 0 & 1 & 0 & 0 \\ 1 & 0 & 1 & 0 & 0 & 0 & 0 & 0 & 0 & 0 & 0 & 0 \end{bmatrix} \tag{10.64)}$$

Example 10.14. Figure 10.20a is the topological graph of a 22-link, one-DOF kinematic chain. It has two perimeter loops: the first perimeter loop $L(p_1)$ constituted by vertices 13, 12, 11, 16, 5, 4, 3, 2, 1, 15, 17, 21, 20, 19, 14, 8, 9, 10, 18, 7, 6, and 22, and the second $L(p_2)$ by vertices 8, 15, 1, 7, 18, 20, 21, 17, 16, 5, 6, 22, 13, 14, 19, 4, 3, 2, 12, 11, 10, and 9. From each perimeter loop, a corresponding perimeter topological graph is obtained, shown in Fig. 10.20b, c. Their canonical perimeter topological graphs are the same, shown in Fig. 10.20d.

Fig. 10.19 CaPTG of Fig. 10.16

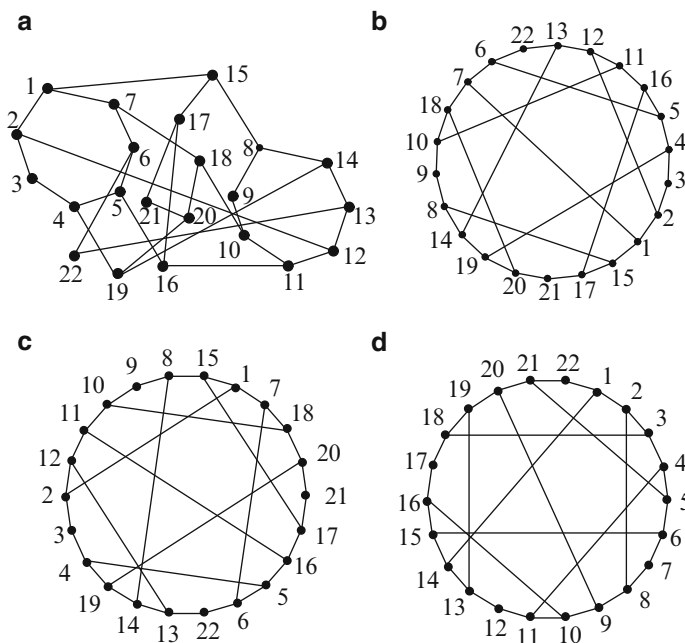
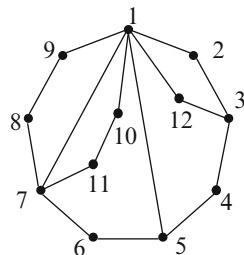


Fig. 10.20 (a) A 22-vertex graph, (b) PTG for perimeter loop $L(p_1)$, (c) PTG for perimeter loop $L(p_2)$, and (d) CaPTG

10.3.3 Characteristic Perimeter Topological Graph

For a graph, the number of its canonical perimeter topological graphs or corresponding canonical adjacency matrices is only few (in most cases, only one). Among the canonical adjacency matrices for a graph, the matrix with the largest value of the number string obtained by concatenating as digits the values of the elements in the upper-right triangle from the first row to the last row is defined as *the characteristic adjacency matrix (CAM)*, and the corresponding canonical perimeter topological graph is defined as the characteristic perimeter topological graph(ChPTG). Obviously, for a graph, its characteristic perimeter topological graph and characteristic adjacency matrix are unique.

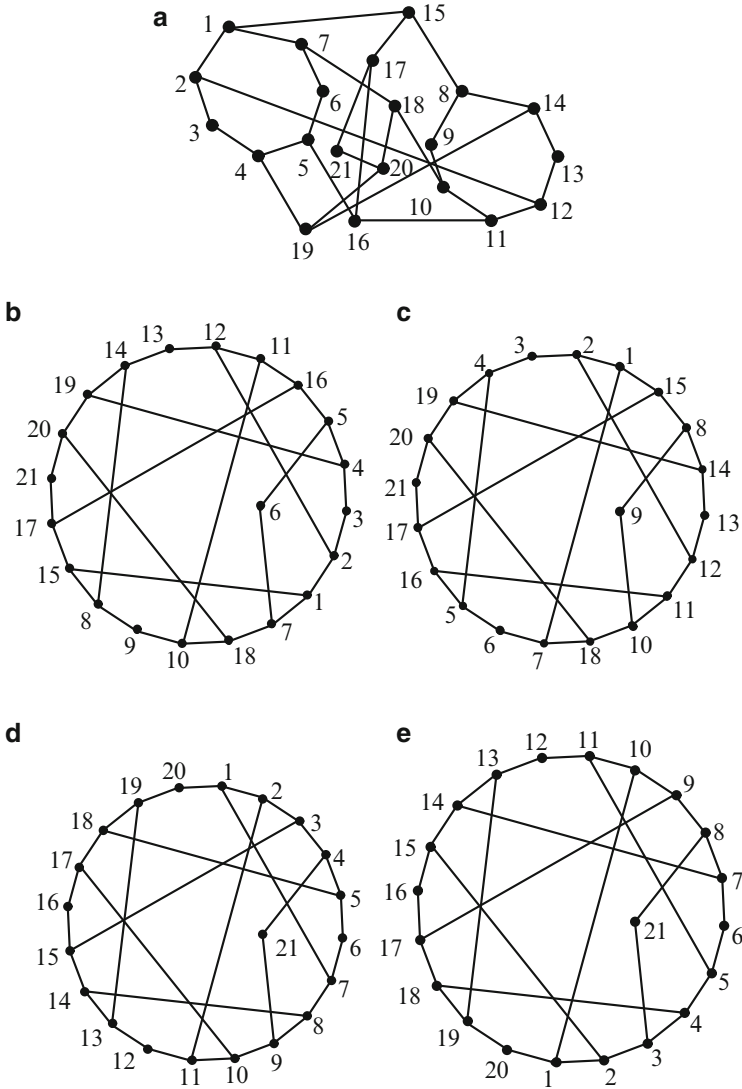


Fig. 10.21 (a) A 21-vertex graph, (b) PTG for $L(p_1)$, (c) PTG for $L(p_2)$, (d) CaPTG of (b), (e) CaPTG of (c)

Example 10.15. Figure 10.21a shows the topological graph of a 21-link, two-DOF kinematic chain. It has two perimeter loops: the first perimeter loop $L(p_1)$ constituted by vertices 10, 18, 7, 1, 2, 3, 4, 5, 16, 11, 12, 13, 14, 19, 20, 21, 17, 15, 8, and 9, and the second perimeter loop $L(p_2)$ constituted by vertices 7, 18, 10, 11, 12, 13, 14, 8, 15, 1, 2, 3, 4, 19, 20, 21, 17, 16, 5, and 6. The perimeter topological graphs corresponding to the first perimeter loop and the second are shown in

Fig. 10.21b, c, respectively. Their canonical perimeter topological graphs are shown in Fig. 10.21d, e, respectively. The characteristic perimeter topological graph is shown in Fig. 10.21d, and its characteristic adjacency matrix is

$$\begin{bmatrix}
 0 & 1 & 0 & 0 & 0 & 0 & 1 & 0 & 0 & 0 & 0 & 0 & 0 & 0 & 0 & 0 & 0 & 0 & 1 & 0 \\
 1 & 0 & 1 & 0 & 0 & 0 & 0 & 0 & 0 & 0 & 1 & 0 & 0 & 0 & 0 & 0 & 0 & 0 & 0 & 0 \\
 0 & 1 & 0 & 1 & 0 & 0 & 0 & 0 & 0 & 0 & 0 & 0 & 0 & 1 & 0 & 0 & 0 & 0 & 0 & 0 \\
 0 & 0 & 1 & 0 & 1 & 0 & 0 & 0 & 0 & 0 & 0 & 0 & 0 & 0 & 0 & 0 & 0 & 0 & 0 & 1 \\
 0 & 0 & 0 & 1 & 0 & 1 & 0 & 0 & 0 & 0 & 0 & 0 & 0 & 0 & 0 & 0 & 0 & 1 & 0 & 0 \\
 0 & 0 & 0 & 0 & 1 & 0 & 1 & 0 & 0 & 0 & 0 & 0 & 0 & 0 & 0 & 0 & 0 & 0 & 0 & 0 \\
 1 & 0 & 0 & 0 & 0 & 1 & 0 & 1 & 0 & 0 & 0 & 0 & 0 & 0 & 0 & 0 & 0 & 0 & 0 & 0 \\
 0 & 0 & 0 & 0 & 0 & 0 & 1 & 0 & 1 & 0 & 0 & 0 & 1 & 0 & 0 & 0 & 0 & 0 & 0 & 0 \\
 0 & 0 & 0 & 0 & 0 & 0 & 0 & 1 & 0 & 1 & 0 & 0 & 0 & 0 & 0 & 0 & 0 & 0 & 0 & 1 \\
 0 & 0 & 0 & 0 & 0 & 0 & 0 & 0 & 1 & 0 & 1 & 0 & 0 & 0 & 0 & 0 & 1 & 0 & 0 & 0 \\
 0 & 1 & 0 & 0 & 0 & 0 & 0 & 0 & 0 & 1 & 0 & 1 & 0 & 0 & 0 & 0 & 0 & 0 & 0 & 0 \\
 0 & 0 & 0 & 0 & 0 & 0 & 0 & 0 & 0 & 0 & 1 & 0 & 1 & 0 & 0 & 0 & 0 & 0 & 0 & 0 \\
 0 & 0 & 0 & 0 & 0 & 0 & 0 & 0 & 0 & 0 & 0 & 1 & 0 & 1 & 0 & 0 & 0 & 0 & 1 & 0 \\
 0 & 0 & 0 & 0 & 0 & 0 & 0 & 1 & 0 & 0 & 0 & 0 & 1 & 0 & 1 & 0 & 0 & 0 & 0 & 0 \\
 0 & 0 & 1 & 0 & 0 & 0 & 0 & 0 & 0 & 0 & 0 & 0 & 0 & 1 & 0 & 1 & 0 & 0 & 0 & 0 \\
 0 & 0 & 0 & 0 & 0 & 0 & 0 & 0 & 0 & 0 & 0 & 0 & 0 & 0 & 1 & 0 & 1 & 0 & 0 & 0 \\
 0 & 0 & 0 & 0 & 0 & 0 & 0 & 0 & 0 & 1 & 0 & 0 & 0 & 0 & 0 & 1 & 0 & 1 & 0 & 0 \\
 0 & 0 & 0 & 0 & 1 & 0 & 0 & 0 & 0 & 0 & 0 & 0 & 0 & 0 & 0 & 0 & 1 & 0 & 1 & 0 \\
 0 & 0 & 0 & 0 & 0 & 0 & 0 & 0 & 0 & 0 & 0 & 1 & 0 & 0 & 0 & 0 & 1 & 0 & 1 & 0 \\
 1 & 0 & 0 & 0 & 0 & 0 & 0 & 0 & 0 & 0 & 0 & 0 & 0 & 0 & 0 & 0 & 0 & 0 & 1 & 0 \\
 0 & 0 & 0 & 1 & 0 & 0 & 0 & 0 & 1 & 0 & 0 & 0 & 0 & 0 & 0 & 0 & 0 & 0 & 0 & 0
 \end{bmatrix}$$

(10.65)

The characteristic perimeter topological graph and corresponding characteristic adjacency matrix make the representation of the topological graph of kinematic chains unique, which is very useful for the computer-aided structural analysis and synthesis of kinematic chains.

10.3.4 Examples of Isomorphism Identification

For any two graphs A and B, if and only if their characteristic adjacency matrices satisfy [17, 18].

$$CAM(A) = CAM(B) \tag{10.66}$$

the two graphs are isomorphic; if not, otherwise.

Example 10.16. Two ten-link kinematic chains A and B are shown in Fig. 10.22a, b, respectively. The kinematic chain shown in Fig. 10.22a has two perimeter loops. The first perimeter loop is composed of links 1, 9, 10, 8, 7, 6, 5, 4, 3, and 2, and the

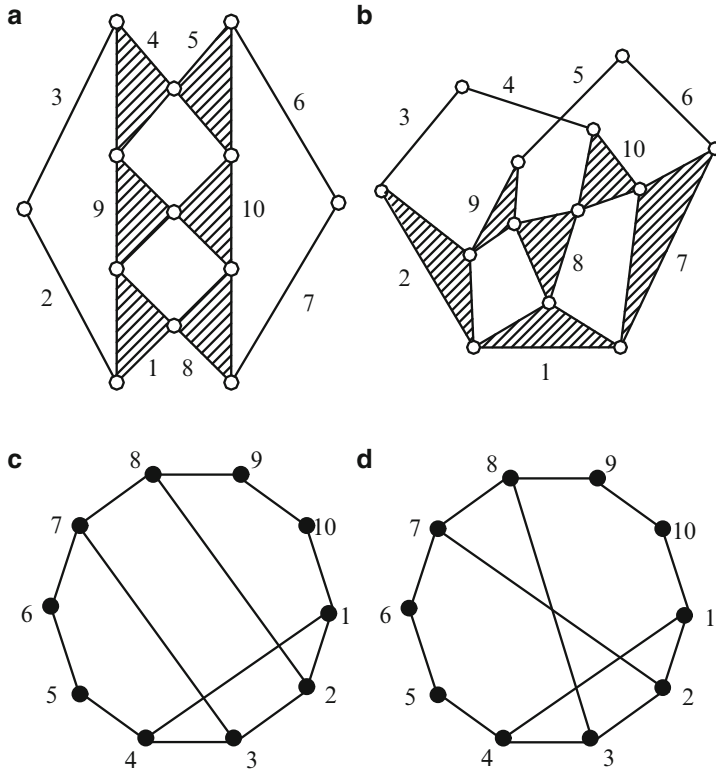


Fig. 10.22 (a) and (b) Two ten-link kinematic chains, (c) ChPTG of (a), (d) ChPTG of (b)

second is composed of links 4, 9, 10, 5, 6, 7, 8, 1, 2, and 3. Therefore, the kinematic chain has two perimeter topological graphs. However, their canonical perimeter topological graphs are the same. Therefore, the characteristic perimeter topological graph for the kinematic chain is just the canonical perimeter topological graph, which is shown in Fig. 10.22c. The characteristic adjacency matrix of this kinematic chain is A_1

$$A_1 = \begin{bmatrix} 0 & 1 & 0 & 1 & 0 & 0 & 0 & 0 & 0 & 1 \\ 1 & 0 & 1 & 0 & 0 & 0 & 0 & 1 & 0 & 0 \\ 0 & 1 & 0 & 1 & 0 & 0 & 1 & 0 & 0 & 0 \\ 1 & 0 & 1 & 0 & 1 & 0 & 0 & 0 & 0 & 0 \\ 0 & 0 & 0 & 1 & 0 & 1 & 0 & 0 & 0 & 0 \\ 0 & 0 & 0 & 0 & 1 & 0 & 1 & 0 & 0 & 0 \\ 0 & 0 & 1 & 0 & 0 & 1 & 0 & 1 & 0 & 0 \\ 0 & 1 & 0 & 0 & 0 & 0 & 1 & 0 & 1 & 0 \\ 0 & 0 & 0 & 0 & 0 & 0 & 0 & 1 & 0 & 1 \\ 1 & 0 & 0 & 0 & 0 & 0 & 0 & 0 & 1 & 0 \end{bmatrix} \quad (10.67)$$

The kinematic chain shown in Fig. 10.22b also has two perimeter loops. The first perimeter loop is composed of links 10, 8, 1, 7, 6, 5, 9, 2, 3, and 4, and the second is composed of links 9, 8, 1, 2, 3, 4, 10, 7, 6, and 5. Therefore, the kinematic chain also has two perimeter topological graphs. The two canonical perimeter topological graphs are the same. The characteristic perimeter topological graph for the kinematic chain is shown in Fig. 10.22d. The characteristic adjacency matrix of this kinematic chain is B_1 , given by

$$B_1 = \begin{bmatrix} 0 & 1 & 0 & 1 & 0 & 0 & 0 & 0 & 0 & 0 & 1 \\ 1 & 0 & 1 & 0 & 0 & 0 & 1 & 0 & 0 & 0 & 0 \\ 0 & 1 & 0 & 1 & 0 & 0 & 0 & 1 & 0 & 0 & 0 \\ 1 & 0 & 1 & 0 & 1 & 0 & 0 & 0 & 0 & 0 & 0 \\ 0 & 0 & 0 & 1 & 0 & 1 & 0 & 0 & 0 & 0 & 0 \\ 0 & 0 & 0 & 0 & 1 & 0 & 1 & 0 & 0 & 0 & 0 \\ 0 & 1 & 0 & 0 & 0 & 1 & 0 & 1 & 0 & 0 & 0 \\ 0 & 0 & 1 & 0 & 0 & 0 & 1 & 0 & 1 & 0 & 0 \\ 0 & 0 & 0 & 0 & 0 & 0 & 0 & 1 & 0 & 1 & 0 \\ 1 & 0 & 0 & 0 & 0 & 0 & 0 & 0 & 0 & 1 & 0 \end{bmatrix} \quad (10.68)$$

$A_1 \neq B_1$; thus, the two kinematic chains are non-isomorphic.

Example 10.17. Three 12-link kinematic chains A, B, and C are shown in Fig. 10.23a, c, e, respectively. These 12-link kinematic chains have the same characteristic polynomial coefficients and eigenvalues. Thus, the characteristic polynomial approach fails to work [19].

Figure 10.23a has two perimeter loops. The first perimeter loop is composed of links 5, 2, 9, 7, 4, 11, 12, 10, 8, 6, and 1, and the second is composed of links 5, 2, 9, 12, 10, 8, 11, 4, 7, 6, and 1. Therefore, the kinematic chain has two perimeter topological graphs. However, their canonical perimeter topological graphs are the same. Therefore, the characteristic perimeter topological graph is the only canonical perimeter topological graph, which is shown in Fig. 10.23b. The characteristic adjacency matrix of this kinematic chain is A_1 , given by

$$A_1 = \begin{bmatrix} 0 & 1 & 0 & 0 & 0 & 0 & 1 & 0 & 0 & 0 & 1 & 0 \\ 1 & 0 & 1 & 0 & 1 & 0 & 0 & 0 & 0 & 0 & 0 & 0 \\ 0 & 1 & 0 & 1 & 0 & 0 & 0 & 0 & 0 & 0 & 0 & 1 \\ 0 & 0 & 1 & 0 & 1 & 0 & 0 & 1 & 0 & 0 & 0 & 0 \\ 0 & 1 & 0 & 1 & 0 & 1 & 0 & 0 & 0 & 0 & 0 & 0 \\ 0 & 0 & 0 & 0 & 1 & 0 & 1 & 0 & 0 & 0 & 0 & 0 \\ 1 & 0 & 0 & 0 & 0 & 1 & 0 & 1 & 0 & 0 & 0 & 0 \\ 0 & 0 & 0 & 1 & 0 & 0 & 1 & 0 & 1 & 0 & 0 & 0 \\ 0 & 0 & 0 & 0 & 0 & 0 & 0 & 1 & 0 & 1 & 0 & 0 \\ 0 & 0 & 0 & 0 & 0 & 0 & 0 & 0 & 1 & 0 & 1 & 1 \\ 1 & 0 & 0 & 0 & 0 & 0 & 0 & 0 & 0 & 1 & 0 & 0 \\ 0 & 0 & 1 & 0 & 0 & 0 & 0 & 0 & 0 & 1 & 0 & 0 \end{bmatrix} \quad (10.69)$$

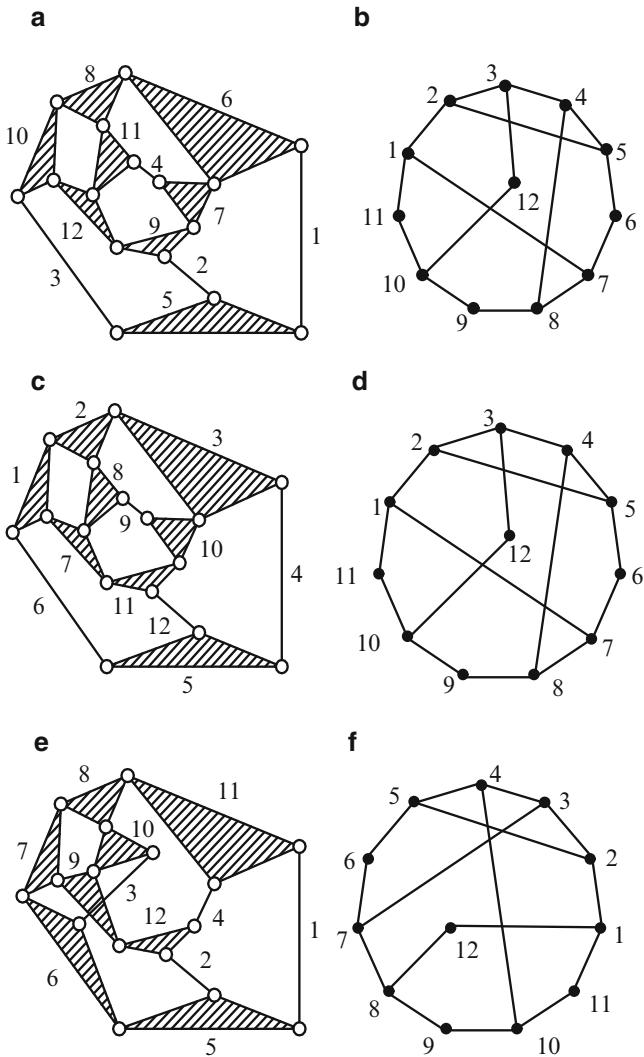


Fig. 10.23 (a), (c), and (e) three 12-link kinematic chains; (b) ChPTG of (a), (d) ChPTG of (c), (f) ChPTG of (e)

Figure 10.23c also has two perimeter loops. The first perimeter loop is composed of vertices 12, 11, 7, 1, 2, 8, 9, 10, 3, 4, and 5, and the second is composed of vertices 5, 12, 11, 10, 9, 8, 7, 1, 2, 3, and 4. Therefore, the kinematic chain has two perimeter topological graphs. However, their canonical perimeter topological graphs are the same. Therefore, the characteristic perimeter topological graph is the only canonical perimeter topological graph, which is shown

in Fig. 10.23d. The characteristic adjacency matrix of this kinematic chain is B_1 , given by

$$B_1 = \begin{bmatrix} 0 & 1 & 0 & 0 & 0 & 0 & 1 & 0 & 0 & 0 & 1 & 0 \\ 1 & 0 & 1 & 0 & 1 & 0 & 0 & 0 & 0 & 0 & 0 & 0 \\ 0 & 1 & 0 & 1 & 0 & 0 & 0 & 0 & 0 & 0 & 0 & 1 \\ 0 & 0 & 1 & 0 & 1 & 0 & 0 & 1 & 0 & 0 & 0 & 0 \\ 0 & 1 & 0 & 1 & 0 & 1 & 0 & 0 & 0 & 0 & 0 & 0 \\ 0 & 0 & 0 & 0 & 1 & 0 & 1 & 0 & 0 & 0 & 0 & 0 \\ 1 & 0 & 0 & 0 & 0 & 1 & 0 & 1 & 0 & 0 & 0 & 0 \\ 0 & 0 & 0 & 1 & 0 & 0 & 1 & 0 & 1 & 0 & 0 & 0 \\ 0 & 0 & 0 & 0 & 0 & 0 & 0 & 1 & 0 & 1 & 0 & 0 \\ 0 & 0 & 0 & 0 & 0 & 0 & 0 & 0 & 1 & 0 & 1 & 1 \\ 1 & 0 & 0 & 0 & 0 & 0 & 0 & 0 & 0 & 1 & 0 & 0 \\ 0 & 0 & 1 & 0 & 0 & 0 & 0 & 0 & 0 & 1 & 0 & 0 \end{bmatrix} \quad (10.70)$$

Figure 10.23e also has two perimeter loops. The first perimeter loop is composed of vertices 12, 9, 7, 8, 10, 3, 6, 5, 1, 11, and 4, and the second is composed of vertices 11, 8, 7, 9, 10, 3, 6, 5, 2, 12, and 4. The two canonical perimeter topological graphs corresponding to the two perimeter topological graphs are the same. The characteristic perimeter topological graph is shown in Fig. 10.23f. The characteristic adjacency matrix of this kinematic chain is C_1 , given by

$$C_1 = \begin{bmatrix} 0 & 1 & 0 & 0 & 0 & 0 & 0 & 0 & 0 & 0 & 1 & 1 \\ 1 & 0 & 1 & 0 & 1 & 0 & 0 & 0 & 0 & 0 & 0 & 0 \\ 0 & 1 & 0 & 1 & 0 & 0 & 1 & 0 & 0 & 0 & 0 & 0 \\ 0 & 0 & 1 & 0 & 1 & 0 & 0 & 0 & 0 & 1 & 0 & 0 \\ 0 & 1 & 0 & 1 & 0 & 1 & 0 & 0 & 0 & 0 & 0 & 0 \\ 0 & 0 & 0 & 0 & 1 & 0 & 1 & 0 & 0 & 0 & 0 & 0 \\ 0 & 0 & 1 & 0 & 0 & 1 & 0 & 1 & 0 & 0 & 0 & 0 \\ 0 & 0 & 0 & 0 & 0 & 0 & 1 & 0 & 1 & 0 & 0 & 1 \\ 0 & 0 & 0 & 0 & 0 & 0 & 0 & 1 & 0 & 1 & 0 & 0 \\ 1 & 0 & 0 & 0 & 0 & 0 & 0 & 0 & 0 & 1 & 0 & 0 \\ 1 & 0 & 0 & 0 & 0 & 0 & 0 & 1 & 0 & 0 & 0 & 0 \end{bmatrix} \quad (10.71)$$

$A_1 = B_1 \neq C_1$; thus, kinematic chains A and B are isomorphic, and both A and B are non-isomorphic with C.

Example 10.18. Two 15-vertex topological graphs A and B are shown in Fig. 10.24a, b. Although each of them has six perimeter loops and six corresponding perimeter topological graphs, each has only one canonical perimeter topological graph. Their characteristic perimeter topological graphs are shown in Fig. 10.24c, d, respectively.

The characteristic adjacency matrix corresponding to Fig. 10.24d is B_1 , given by

$$B_1 = \begin{bmatrix} 0 & 1 & 0 & 1 & 0 & 0 & 0 & 1 & 0 & 1 & 0 & 0 & 0 & 1 & 1 \\ 1 & 0 & 1 & 0 & 0 & 0 & 0 & 0 & 0 & 0 & 0 & 1 & 1 & 0 & 0 \\ 0 & 1 & 0 & 1 & 0 & 0 & 0 & 0 & 0 & 0 & 0 & 0 & 0 & 0 & 0 \\ 1 & 0 & 1 & 0 & 1 & 0 & 1 & 0 & 0 & 1 & 0 & 1 & 0 & 0 & 0 \\ 0 & 0 & 0 & 1 & 0 & 1 & 0 & 0 & 0 & 0 & 0 & 0 & 0 & 0 & 0 \\ 0 & 0 & 0 & 0 & 1 & 0 & 1 & 1 & 0 & 1 & 0 & 0 & 0 & 0 & 0 \\ 0 & 0 & 0 & 1 & 0 & 1 & 0 & 1 & 0 & 0 & 0 & 0 & 0 & 0 & 1 \\ 1 & 0 & 0 & 0 & 0 & 1 & 1 & 0 & 1 & 0 & 0 & 0 & 0 & 0 & 0 \\ 0 & 0 & 0 & 0 & 0 & 0 & 0 & 1 & 0 & 1 & 0 & 0 & 0 & 0 & 0 \\ 1 & 0 & 0 & 1 & 0 & 1 & 0 & 0 & 1 & 0 & 1 & 0 & 1 & 0 & 0 \\ 0 & 0 & 0 & 0 & 0 & 0 & 0 & 0 & 0 & 1 & 0 & 1 & 0 & 0 & 0 \\ 0 & 1 & 0 & 1 & 0 & 0 & 0 & 0 & 0 & 1 & 0 & 1 & 0 & 0 & 0 \\ 0 & 1 & 0 & 0 & 0 & 0 & 0 & 0 & 0 & 1 & 0 & 1 & 0 & 1 & 0 \\ 1 & 0 & 0 & 0 & 0 & 0 & 0 & 0 & 0 & 0 & 0 & 0 & 1 & 0 & 0 \\ 1 & 0 & 0 & 0 & 0 & 0 & 1 & 0 & 0 & 0 & 0 & 0 & 0 & 0 & 0 \end{bmatrix} \quad (10.73)$$

$A_1 \neq B_1$; thus, the two topological graphs are non-isomorphic.

Example 10.19. Two 28-vertex topological graphs A and B are shown in Fig. 10.25a, b, respectively. They have the same characteristic perimeter topological graph, which is shown in Fig. 10.26, and the same characteristic adjacency matrix. Therefore, the two graphs are isomorphic.

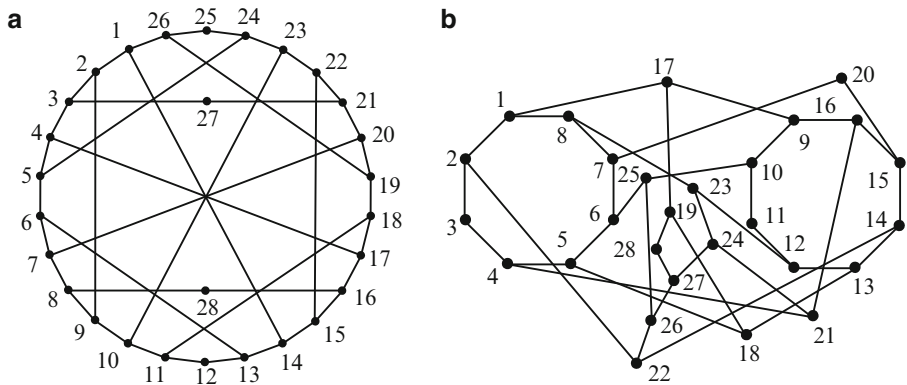


Fig. 10.25 Two 28-vertex topological graphs

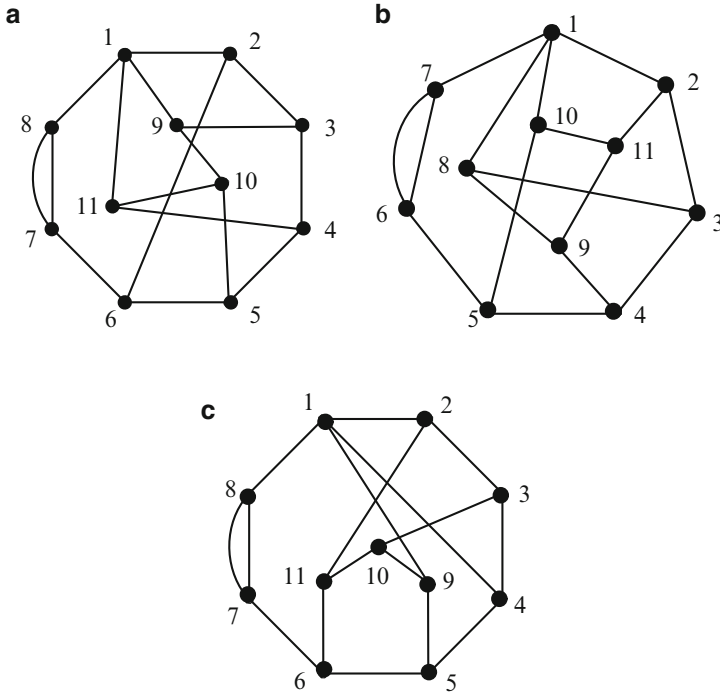


Fig. 10.27 Three contracted graphs

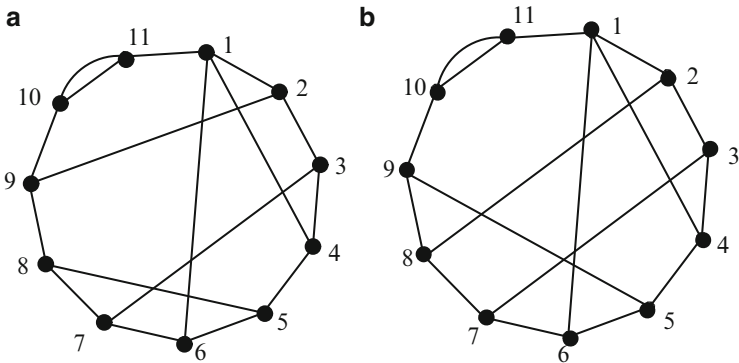


Fig. 10.28 (a) The shared ChPTG of Fig. 10.27a, b, (b) ChPTG of Fig. 10.27c

Example 10.20. Three contracted graphs are shown in Fig. 10.27. The contracted graphs in Fig. 10.27a, b possess the same characteristic adjacency matrix, which is different from that in Fig. 10.27c. Therefore, the graphs in Fig. 10.27a, b are isomorphic, and Fig. 10.27c is a different contracted graph. The shared characteristic perimeter topological graph for Fig. 10.27a, b is shown in Fig. 10.28a, b is the characteristic perimeter topological graph for Fig. 10.27c.

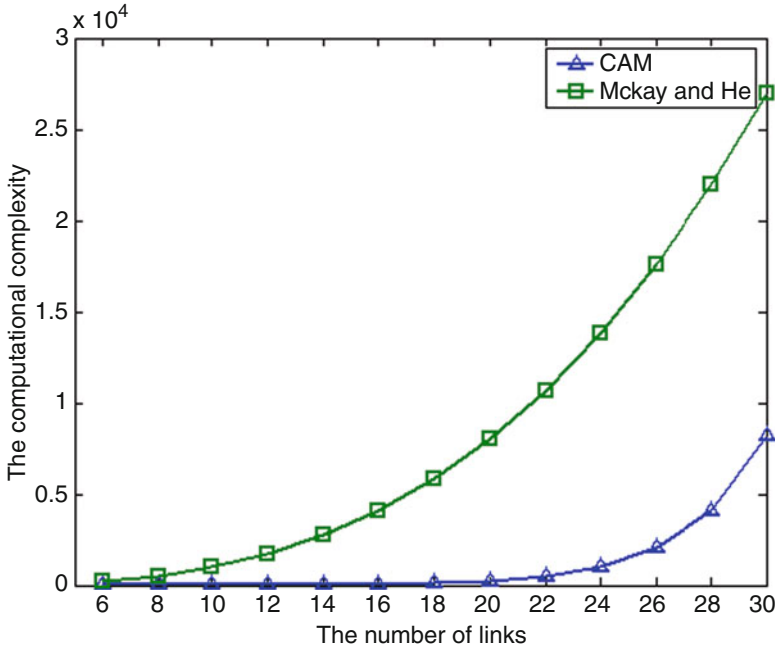


Fig. 10.29 Comparison of computational complexity between the CAM algorithm and the Mckay and He's algorithm

10.3.5 Analysis of Computational Complexity

Although many algorithms exist for isomorphism identification of kinematic chain, the most important problems in applications are effectiveness and computational complexity. In terms of computational complexity, the most efficient algorithm up to now, as far as we know, was proposed by McKay (1981) [20]. The computational complexity of this algorithm is $O(MN^3)$, where N is the number of vertices, and M is the number of levels that a recursive process involves. He (2003) [21] also proposed an algorithm and declared his method has the same computational complexity with McKay's method.

The computational complexity of the algorithm of the characteristic adjacency matrix is $O(2^v)$, where v is the number of independent loops of the graph. A 28-vertex, three-DOF graph has $2^{12} = 4,096$ loops at most. Therefore, the algorithm is very efficient for the topological graphs of kinematic chains (or those graphs that do not have too many independent loops). The comparison of computational complexity with McKay's algorithm for 6–30 links three-DOF kinematic chains (or graphs) is given in Fig. 10.29. The CAM algorithm in the present study remains efficient even when the kinematic chain has as many as 30 links.

10.4 Detection of Rigid Sub-chains

In the structural synthesis of kinematic chains, not all the solutions correspond to proper topological graphs of kinematic chains. Some solutions may correspond to kinematic chains containing rigid sub-chains [22–24]. In the following, based on the edge-based representation of loops an algorithm for the detection of rigid sub-chain is given.

Step 1: The first independent loop $L(1)$ is selected, and its mobility factor w_1 is determined.

The loop with the smallest sub-dimension is selected as the first independent loop $L(1)$. For loop $L(1)$, if its sub-dimension is q , then its mobility factor is $q-3$. The mobility factor w_1 of the loop $L(1)$ is

$$w_1 = N[L(1)] - 3 \quad (10.75)$$

If $Q = w_1 - 1 < 0$, then the topological graph containing rigid sub-chains must be deleted. Otherwise, Step 2 can be implemented.

Step 2: The second independent loop $L(2)$ is selected, and the mobility factor w_2 is determined.

A loop $L(i)$ satisfying the following two conditions in sequence is selected as the loop $L(2)$:

1. Of all the loops of the topological graph, $N\{L(i) \ominus L(1)\}$ is the smallest one.
2. Of the loops satisfying the above condition, loop $L(i)$ is the one with the smallest sub-dimension.

The mobility factor of path w_2 is

$$w_2 = N[P(2)] - 2, \quad \text{and} \quad P(2) = L(2) \ominus L(1) \quad (10.76)$$

If $Q = w_1 + w_2 - 2 < 0$, then the topological graph containing rigid sub-chains must be deleted. Otherwise, Step 3 can be implemented.

Step n : The n th independent loop $L(n)$ is selected, and the mobility factor w_n is determined

A loop $L(i)$ satisfying the following two conditions in sequence is selected as the loop $L(n)$

1. Of all the loops in the topological graph, $N\{L(i) \ominus P(n-1) \ominus \dots \ominus P_1(2) \ominus L(1)\}$ is the smallest one.
2. Of the loops satisfying the above condition, loop $L(i)$ is the one with the smallest sub-dimension.

The mobility factor of path w_n is

$$w_n = N[P(n) - 2], \quad \text{and} \quad P(n) = L(i) \ominus P(n-1) \ominus \dots \ominus P_1(2) \ominus L(1) \quad (10.77)$$

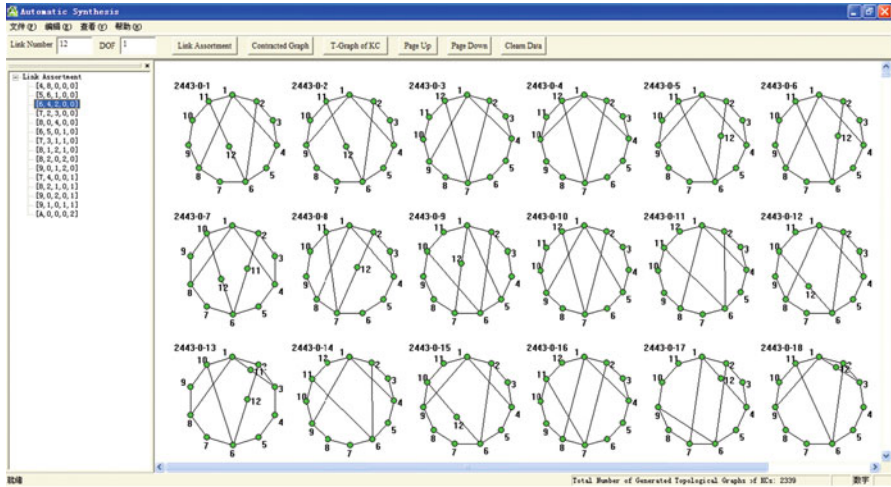


Fig. 10.30 Extract of the complete atlas database for planar 12-link, one-DOF kinematic chains

If $Q = \sum_{i=1}^n w_i - n < 0$, then the topological graph containing rigid sub-chains must be deleted. Otherwise, Step $(n + 1)$ can be implemented.

Step v : The steps above until step v (step v included) are followed, and the last independent loop $L(v)$ and the mobility factor w_v are obtained. If $Q = \sum_{i=1}^n w_i - n < 0$, then the topological graph containing rigid sub-chains must be deleted. Otherwise, the topological graph corresponding to a kinematic chain with proper structure must be stored.

10.5 Digital Atlas Database and Synthesis

For a kind of kinematic chains with specified number of links and degrees of freedom, first synthesize their contracted graphs and then synthesize the topological graphs corresponding to each contracted graph. All valid topological graphs can be synthesized after isomorphism identification and rigid sub-chain detection. As the characteristic perimeter topological graph is a unique representation of the topological graphs of the kinematic chains, in the digital atlas database, the topological graphs are displayed through the forms of their characteristic perimeter topological graphs [25].

As an example, Fig. 10.30 shows an excerpt of the complete atlas database for 6856 planar 12-link, one-DOF kinematic chains. All the topological graphs are displayed in the right window on the forms of the characteristic topological graphs. Displayed in Fig. 10.30 is an excerpt of all 2339 topological graphs corresponding to the link assortment “[6,4,2,0,0]” (in a link assortment $[N_2, N_3, \dots, N_p]$). The digits N_2, N_3, N_4 , and so on denote respectively the number of binary, ternary, quaternary

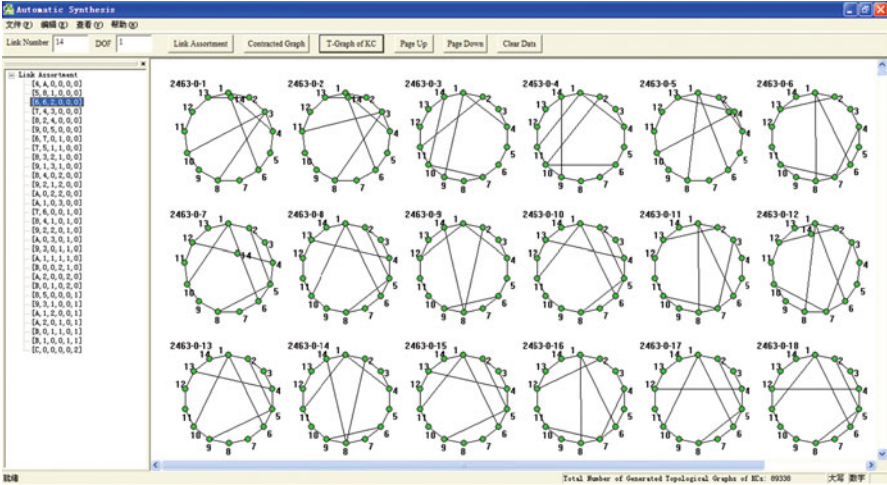
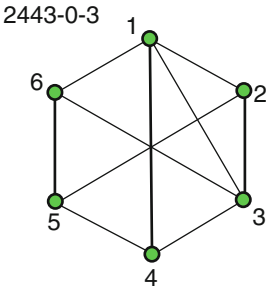


Fig. 10.31 Excerpt of the complete atlas database for planar 14-link, one-DOF kinematic chains

Fig. 10.32 Example of a contracted graph for a 12-link, one-DOF kinematic chain



links, and so on. If the digits are greater than or equal to ten, A, B, C, and so on are used to represent them, i.e., A = 10, B = 11, C = 12, and so on).

Figure 10.31 shows an excerpt of the complete atlas database of 318162 planar 14-link, one-DOF kinematic chains. All the link assortments are shown in the left window. All the topological graphs corresponding to each link assortment can be synthesized automatically and are displayed in the right window. Displayed in Fig. 10.31 is an excerpt of all 89338 topological graphs corresponding to the link assortment “[6,6,2,0,0,0].”

In the complete atlas database, all the valid topological graphs corresponding to a specified contracted graph can also be easily obtained. For example, Fig. 10.32 is a contracted graph for a 12-link, one-DOF kinematic chain. All 157 valid topological graphs are obtained from the complete atlas database, part of which is shown in Fig. 10.33.

Figure 10.34 is a contracted graph for a 14-link, one-DOF kinematic chain. All 1930 valid topological graphs can also be obtained from the atlas database, some of which are shown in Fig. 10.35.

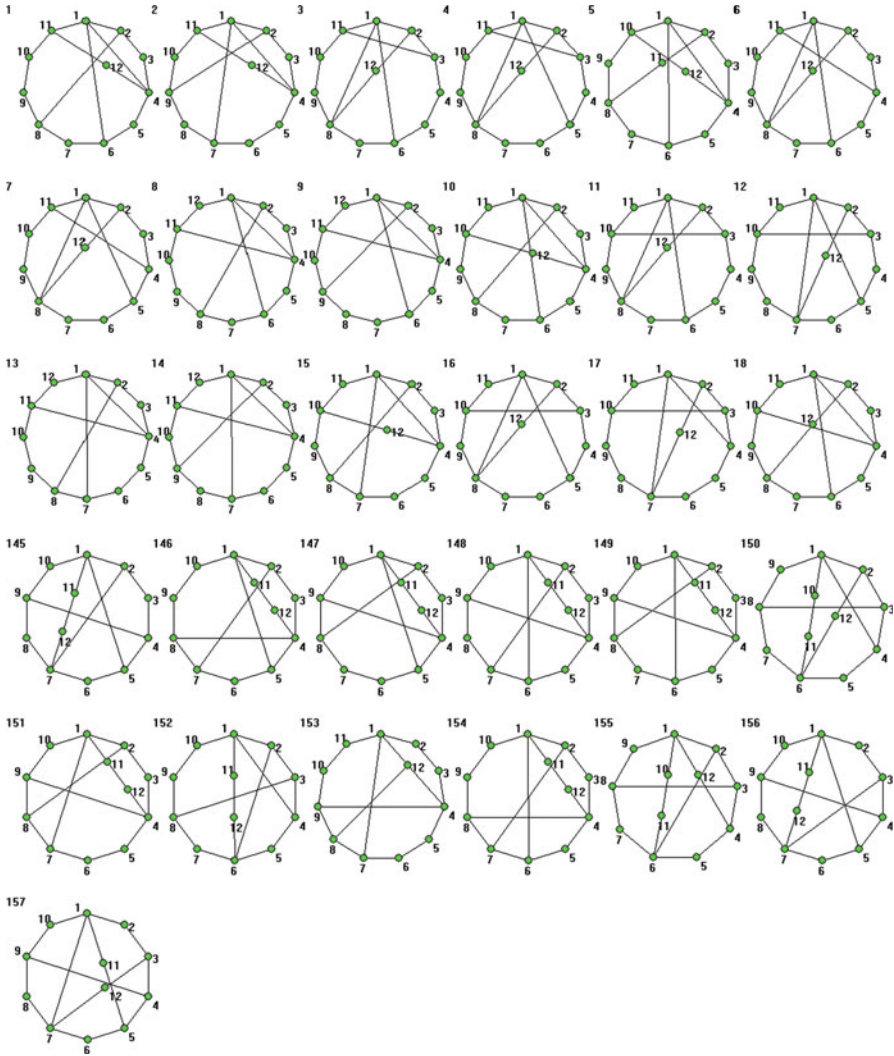
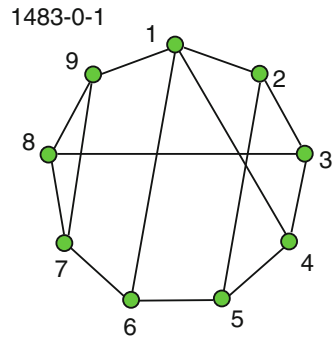


Fig. 10.33 Excerpt of 157 valid topological graphs corresponding to the contracted graph in Fig. 10.32

Fig. 10.34 Example of a contracted graph for a 14-link, one-DOF kinematic chain



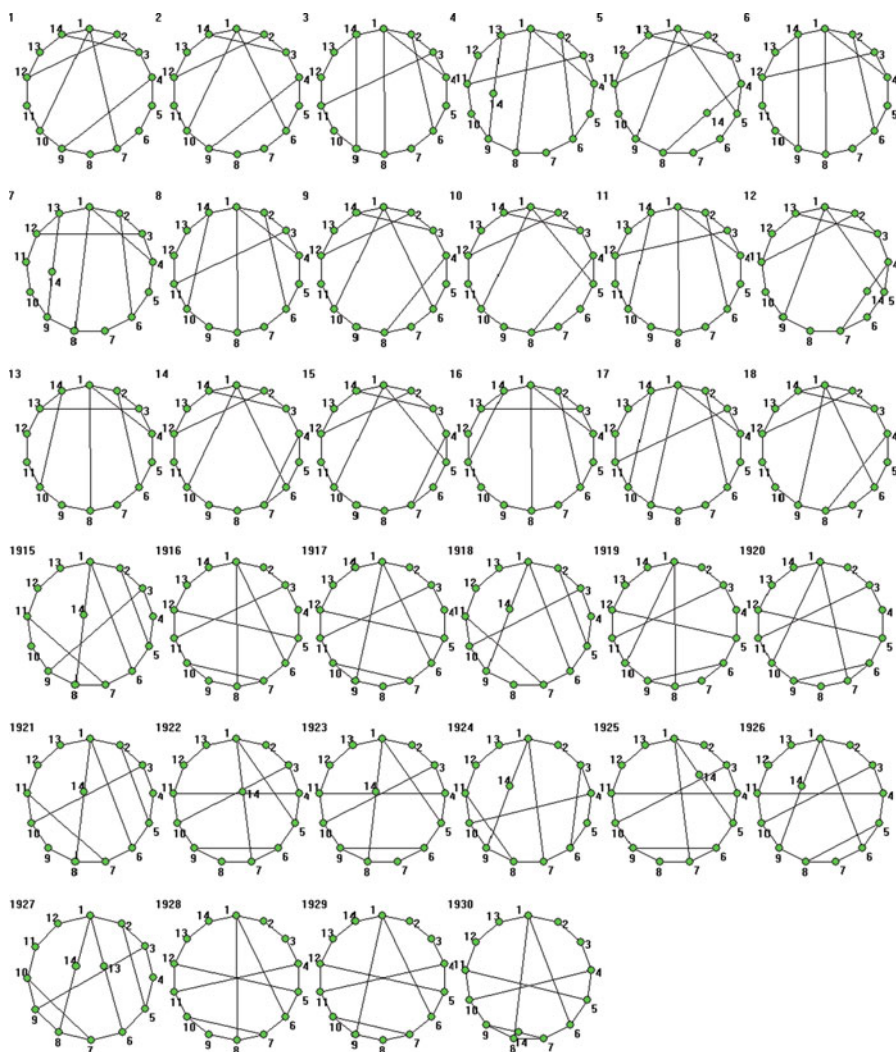


Fig. 10.35 Excerpt of the 1930 valid topological graphs for the contracted graph in Fig. 10.34

Tables 10.1, 10.2, 10.3, 10.4, and 10.5 display the quantitative information for the atlas databases for the one-DOF kinematic chains of 6, 8, 10, 12, and 14 links, respectively. The total numbers of the topological graphs are 2, 16, 230, 6856, and 318162, respectively.

For example, Table 10.3 presents the quantitative information concerning the topological graphs for 10-link, one-DOF kinematic chains. All the contracted graphs and the topological graphs are classified according to their link assortment (column 2). For each link assortment, the numbers of the multiple edges of the contracted graphs are used to classify further both contracted graphs and topological graphs (see columns 3 and 4).

Table 10.1 Numbers of topological graphs for six-link, one-DOF kinematic chains

No	Link assortment	Number of multiple edges	Number of topological graphs	Sum of topological graphs
1	[4,2]	2	2	2

Table 10.2 Numbers of topological graphs for eight-link, one-DOF kinematic chains

No	Link assortment	Number of multiple edges	Number of topological graphs	Sum of topological graphs
1	[4,4,0]	0	6	9
		2	3	
2	[5,2,1]	2	5	5
3	[6,0,2]	3	2	2

Table 10.3 Numbers of topological graphs for ten-link, one-DOF kinematic chains

No	Link assortment	Number of multiple edges	Number of topological graphs	Sum of topological graphs
1	[4,6,0,0]	0	39	50
		1	8	
		2	3	
		3	0	
2	[5,4,1,0]	0	42	95
		1	43	
		2	10	
		3	0	
3	[6,2,2,0]	1	32	57
		2	15	
		3	10	
4	[7,0,3,0]	3	3	3
5	[6,3,0,1]	2	15	15
6	[7,1,1,1]	3	8	8
7	[8,0,0,2]	1	2	2

Table 10.4 Numbers of topological graphs for 12-link, one-DOF kinematic chains

No	Link assortment	Number of multiple edges	Number of topological graphs	Sum of topological graphs
1	[4,8,0,0,0]	0	352	410
		1	52	
		2	6	
		3	0	
		4	0	
2	[5,6,1,0,0]	0	1,282	1,873
		1	536	
		2	55	
		3	0	
		4	0	
3	[6,4,2,0,0]	0	942	2,339
		1	1,059	
		2	308	
		3	30	
		4	0	
4	[7,2,3,0,0]	0	111	648
		1	231	
		2	266	
		3	40	
		4	0	
5	[8,0,4,0,0]	2	28	37
		4	9	
6	[6,5,0,1,0]	0	120	506
		1	311	
		2	69	
		3	6	
7	[7,3,1,1,0]	1	386	716
		2	243	
		3	87	
		4	0	
8	[8,1,2,1,0]	2	74	147
		3	65	
		4	8	
9	[8,2,0,2,0]	2	32	63
		3	21	
		4	10	
10	[9,0,1,2,0]	4	7	7
11	[7,4,0,0,1]	2	40	49
		3	9	
12	[8,2,1,0,1]	3	46	46
13	[9,0,2,0,1]	4	5	5
14	[9,1,0,1,1]	4	8	8
15	[A,0,0,0,2]	1	2	2

Table 10.5 Numbers of topological graphs for 14-link, one-DOF kinematic chains

No	Link assortment	Number of multiple edges	Number of topological graphs	Sum of topological graphs
1	[4,A,0,0,0,0]	0	3,994	4,420
		1	410	
		2	16	
		3	0	
		4	0	
		5	0	
2	[5,8,1,0,0,0]	0	30,510	38,098
		1	7,192	
		2	396	
		3	0	
		4	0	
		5	0	
3	[6,6,2,0,0,0]	0	55,825	89,338
		1	29,270	
		2	4,103	
		3	140	
		4	0	
		5	0	
4	[7,4,3,0,0,0]	0	25,653	62,854
		1	27,516	
		2	8,915	
		3	770	
		4	0	
		5	0	
5	[8,2,4,0,0,0]	0	2,509	12,117
		1	4,900	
		2	3,789	
		3	866	
		4	53	
		5	0	
6	[9,0,5,0,0,0]	0	54	302
		2	182	
		3	56	
		4	10	
		5	0	
		6	0	
7	[6,7,0,1,0,0]	0	8,095	15,215
		1	6,371	
		2	721	
		3	28	
		4	0	
		5	0	
8	[7,5,1,1,0,0]	0	13,766	44,871
		1	23,186	
		2	7,212	
		3	707	
		4	0	
		5	0	

(continued)

Table 10.5 (continued)

No	Link assortment	Number of multiple edges	Number of topological graphs	Sum of topological graphs
9	[8,3,2,1,0,0]	0	3,183	28,242
		1	12,707	
		2	9,831	
		3	2,405	
		4	116	
		5	0	
10	[9,1,3,1,0,0]	1	861	3,320
		2	1,245	
		3	1,076	
		4	138	
		5	0	
11	[8,4,0,2,0,0]	0	309	4,515
		1	1,877	
		2	1,846	
		3	436	
		4	47	
		5	0	
12	[9,2,1,2,0,0]	1	422	3,083
		2	1,452	
		3	1,006	
		4	203	
		5	0	
13	[A,0,2,2,0,0]	3	158	216
		4	36	
		5	22	
14	[A,1,0,3,0,0]	3	37	77
		4	40	
15	[7,6,0,0,1,0]	0	342	2,672
		1	1,588	
		2	692	
		3	50	
		4	0	
16	[8,4,1,0,1,0]	1	2,017	5,120
		2	2,446	
		3	625	
		4	32	
17	[9,2,2,0,1,0]	2	1,078	1,858
		3	600	
		4	180	
		5	0	
18	[A,0,3,0,1,0]	3	39	79
		4	40	
19	[9,3,0,1,1,0]	2	437	857
		3	342	
		4	78	
		5	0	

(continued)

Table 10.5 (continued)

No	Link assortment	Number of multiple edges	Number of topological graphs	Sum of topological graphs
20	[A,1,1,1,1,0]	3	139	306
		4	151	
		5	16	
21	[B,0,0,2,1,0]	5	7	7
22	[A,2,0,0,2,0]	3	32	63
		4	21	
		5	10	
23	[B,0,1,0,2,0]	5	7	7
24	[8,5,0,0,0,1]	2	120	180
		3	60	
25	[9,3,1,0,0,1]	3	211	232
		4	21	
26	[A,1,2,0,0,1]	4	49	49
27	[A,2,0,1,0,1]	4	46	46
28	[B,0,1,1,0,1]	5	8	8
29	[B,1,0,0,1,1]	5	8	8
30	[C,0,0,0,0,2]	1	2	2

References

1. Freudenstein F (1967) The basic concepts of Polya's theory of enumeration with application to the structural classification of mechanisms. *J Mech* 2(3):275–290
2. Yan HS (1998) Creative design of mechanical devices. Springer-Verlag Singapore Pte. Ltd., New York/Singapore
3. Mruthunjaya TS (2003) Kinematic structure of mechanisms revisited. *Mech Mach Theory* 38(4):279–320
4. Ding HF, Hou FM, Kecskeméthy A et al (2012) Synthesis of the whole family of planar 1-DOF kinematic chains and creation of their atlas databases. *Mech Mach Theory* 47(1):1–15
5. Flores FG, Kecskeméthy A, Pöttker A (2007) Workspace analysis and maximal force calculation of a face-shovel excavator using kinematical transformers. In: Proceedings of the 12th world congress in mechanism and machine science, Besancon, France
6. Crossley FRE (1964) A contribution to Gruebler's theory in the number synthesis of planar mechanisms. *J Eng Ind ASME Trans Ser B* 86:1–8
7. Woo LS (1967) Type synthesis of plane linkages. *Trans ASME J Eng Ind* 89B:159–172
8. Ding HF, Zhao J, Huang Z (2009) Unified topological representation models of planar kinematic chains. *ASME J Mech Des* 131(11):114503
9. Crossley FRE (1965) The permutations of kinematic chains of eight members or less from the graph-theoretic view point. In: *Developments in theoretical and applied mechanics*, vol 2. Pergamon Press, Oxford, pp 467–486
10. Chu JK, Cao WQ (1998) Systemics of Assur groups with multiple joints. *Mech Mach Theory* 33(8):1127–1133
11. Cao WQ (2002) The analysis and synthesis of linkage mechanisms, 2nd edn. Science Press, Beijing
12. Wei GW, Dai JS (2010) Geometric and kinematic analysis of a seven-bar three-fixed-pivoted compound-joint mechanism. *Mech Mach Theory* 45(2):170–184
13. Yang TL (1995) Basic theory of mechanical system – structural kinematical dynamics. Mechanical Press, Beijing

14. Ding HF, Huang Z (2007) A new theory for the topological structure analysis of kinematic chains and its applications. *Mech Mach Theory* 42(10):1264–1279
15. Ding HF, Zhao J, Huang Z (2010) The establishment of edge-based loop algebra theory of kinematic chains and its applications. *Eng Comp* 26(2):119–127
16. Ding HF, Huang Z (2007) The establishment of the canonical perimeter topological graph of kinematic chains and isomorphism identification. *ASME J Mech Des* 129(9):915–923
17. Ding HF, Huang Z (2009) Isomorphism identification of graphs: especially for the graphs of kinematic chains. *Mech Mach Theory* 44(1):122–139
18. Huang Z, Ding HF (2007) Theory of loop algebra on multi-loop kinematic chains and its application. *Sci China* 50(4):437–447
19. Uicker JJ, Raicu A (1975) A method for the identification of and recognition of equivalence of kinematic chains. *Mech Mach Theory* 10(5):375–383
20. McKay BD (1981) Practical graph isomorphism. *Congressus Numerantium* 30:45–87
21. He PR, Zhang WJ, Li Q etc (2003) A new method for detection of graph isomorphism based on the quadratic form. *ASME J Mech Des* 125(3):640–642
22. Hwang W, Wang YH (1991) An algorithm for the detection of degenerate kinematic chains. *Math Comp Model* 15(11):9–15
23. Lee H, Yoon Y (1992) Detection of rigid structure in enumerating basic kinematic chain by sequential removal of binary link string. *JSME Int J* 35(4):647–651
24. Ding HF, Huang Z, Mu DJ (2008) Computer-aided structure decomposition theory of kinematic chains and its applications. *Mech Mach Theory* 43(12):1596–1609
25. Ding HF, Huang Z (2007) A unique representation of the kinematic chain and the atlas database. *Mech Mach Theory* 42(6):637–651

Index

A

Accordance equation of input, 294
Adjacency matrix, 367, 369, 373, 374,
381–383, 393, 394, 397–399, 401–404
Amplitude, 11, 36, 156, 171
Applied loads, 293, 294, 296
Atlas database, 408

B

Basic topological graph, 368
Beanpod-like lamina, 114
Bennett mechanism, 49, 53, 55
Bicolor topological graph, 368–372, 376
Bi-directional arrow, 22, 39, 75, 127, 302, 314

C

Canonical adjacency matrix, 393–395
Canonical degree-sequence, 390–392
Canonical perimeter, 390, 392–394, 398, 401
Characteristic perimeter, 395–397
Clifford factor, 312
Closing-constraint method, 59
Combination loop, 378, 381
Common constraints, 33, 54, 77, 79, 81,
83, 90, 91, 100, 119, 125–127,
299, 311
Configuration, 48, 63, 64, 73, 90, 94, 97, 114,
116, 117
Conjugate screw, 21
Constrained motion, 17, 183
Constraint, 17, 37, 42, 44, 323, 325–336,
350–355, 358–362
reaction, 297, 298, 300, 308
screw system, 37, 58, 204, 271, 311, 330

Couple, 1, 8, 10, 15, 22, 24, 75, 87, 97, 108,
111, 118
Cross-head, 63, 64
Cylinder-plane pair, 91, 93
Cylindrical pair, 54, 112, 159, 320, 336, 347,
348, 353

D

Degree of freedom, 39, 48–49
Degree-sequence, 390, 391
Delta robot, 52, 103
D-H parameter, 94
Double arrow, 39, 80
Dual vector, 6, 7, 12, 253, 298

E

End-effector, 17, 18, 58, 61, 164–166, 172,
185, 194
End screw, 21
Equilibrium equation, 258, 289, 305, 306, 308,
313, 314, 317, 321–323
Euler formula, 56

F

First-order screw system, 17
Fixed axodes, 65
Flat pencil, 22, 29, 30
Force-decoupling, 298
Four-screw system, 17
Free-body diagram, 289, 312–314, 323
Free vector, 12, 15, 223, 327
Full-cycle mobility, 55, 63
Full-field mobility, 64

G

General dynamic equation, 293, 294
 Generalized kinematic pair, 110, 130, 132
 G-K formula, 49, 53, 55–57
 Grassmann line geometry, 28–30

H

Half-moon cylinders, 91, 93
 Hessian matrix, 138
 Hexahedron, 123, 125
 High-order matrix, 298, 312
 Hoberman switch-pitch ball, 114–123
 Hollow arrow, 39, 62, 107
 Hollow bi-directional arrow, 39
 Hyperboloid of one sheet, 25, 164, 169, 194, 204, 205

I

Idle freedom, 57
 Imaginary parallel, 56
 Independent loop, 385–388
 Independent loop set, 386
 Infinite-pitch, 54, 60
 Infinitesimal twist, 11
 Input selection, 311, 312
 Isomorphism identification, 390–406, 408

J

Jacobian matrix, 31, 137, 189, 218, 219, 245, 258, 276, 283, 284

K

Kinematic influence, 135–161, 168
 Kinetostatic analysis, 289, 297

L

Laminas, 114, 117
 Linear complex, 217, 223, 225
 Linear congruences, 29, 30
 Linear velocity, 1, 12, 146
 Line vector, 6–10, 28–30
 Local freedom, 57, 73, 103
 Loop operation, 378–383

M

Main kinematic pair, 300
 Main pair, 300, 307, 308, 312

Main-pair reaction, 300, 301, 318, 323
 Maverick mechanism, 49
 Mobility, 18, 28, 38, 41, 47–49
 Mobility open issue (MOI), 49–55
 Modified Grubler-Kutzbach, 54, 90, 100, 309
 MOI. *See* Mobility open issue (MOI)
 Moving axodes, 65
 Mutual moment, 5, 6, 10, 164

N

Nominal mobility, 57, 111
 Non-full-field mobility, 64

O

One-screw system, 17
 Open chain, 17, 120, 130, 146
 Order, 17, 19, 24, 54, 56, 81
 Outer-loop sub-chain, 110
 Output link, 48, 54, 56, 103, 163, 220
 Over-constrained, 47, 49, 52, 203, 298

P

Paradoxical mechanisms, 52
 Parasitic motion, 60, 65, 201
 Passive freedom, 57
 Perimeter loop, 390–391
 Perimeter topological graph, 390–401, 405, 408
 Pitch, 8–11, 13, 19, 21–23, 25, 38, 40, 42, 54, 62, 80, 111, 115, 116, 118, 119, 169, 170, 174, 176, 179, 185, 187, 189, 194, 205, 225, 227–229, 252, 253, 279–281, 283, 284, 304
 Platform constraint system, 58, 337, 338, 340, 342, 344, 355, 357, 358, 360
 Platform twist system, 329, 340, 350, 352, 357, 358
 Principal coordinate system, 20, 21, 25, 169–170
 Principal screw, 20–28, 174, 176, 179, 180, 186, 198, 199, 230
 Principle of d'Alembert, 298

R

Reciprocal product, 10–11, 36
 Reciprocal screw, 17, 36, 43, 71–75, 78–81, 83, 90, 97–102, 104–107, 111, 119, 124, 126, 127, 130, 202, 204, 223, 253, 266, 298, 299, 301, 303, 305, 316, 319, 320

Reciprocal screw system, 37, 90, 99, 102, 110
 Redundant constraint, 55, 123, 202, 309, 311
 Redundant input, 290
 Regulus, 29, 43, 44, 83, 205
 Rigidly closed, 59
 Rotational freedom, 41–44, 48, 103, 105, 111,
 203, 205, 269–271

S

Schonflies motion, 98
 Screw, 1, 6–28, 31, 33, 43, 47, 57–61, 63,
 71–74, 76, 77
 dependency, 17, 31
 pair, 39, 54, 77
 system, 17–28, 31, 35, 37, 57–59, 61, 74,
 76, 77, 87, 98–100, 103, 107, 113
 theory, 1, 28, 47, 52–55, 63, 164, 165, 270,
 289, 298
 Second-order screw system, 17, 19–24, 164
 Second-time reciprocal screw, 61, 62, 73, 105,
 128, 315
 Self-motion, 65, 218
 Serial robot, 17, 18, 61, 71, 73
 Singular, 30, 34, 99, 172, 173, 222, 226, 227,
 229, 231
 Six-screw system, 18
 Slideway, 38, 91
 Sliding pair, 12
 Spatial mechanism, 1, 47–49, 289, 298
 Spherical pair, 54, 103, 109, 278, 290, 291,
 335, 336
 Spherical subchain, 335, 336, 345–348,
 359, 360
 Standard base, 328, 329, 331, 337, 338,
 340–343, 350, 357, 360

Statically indeterminate, 298
 3/6-Stewart, 34, 218, 219, 226
 6/6-Stewart, 34, 217, 219, 256, 269, 270
 Sub-closed-loop, 59
 Superposition principle, 300

T

Tetrahedron, 82
 Third-order screw systems, 17, 167, 169
 Three-screw system, 27, 202
 Topological graph, 366
 Triangular-gait, 290
 Tricolor topological graph, 373
 Trifurcate chain, 122
 Twist, 1, 37, 39, 82, 84, 138
 Twist angle, 5, 37, 82, 84, 138

V

Virtual constraint, 54, 56, 75, 123–124,
 131, 132
 Virtual displacement principle, 293
 Virtual mechanism, 155–158, 187, 189, 191
 Virtual-mechanism principle, 155–161, 165,
 171–173
 Virtual pair, 155, 159, 172, 173, 185, 189, 191

W

Workspace, dexterity, isotropy, 135

Z

Zero-pitch, 41, 42, 53, 60, 62